

**Russian Academy of Sciences
P.P. Shirshov Institute of Oceanology
Atlantic Branch**

**Proceedings of the 2nd International
Conference (school) on**

**DYNAMICS OF COASTAL
ZONE OF NON-TIDAL SEAS**

**Baltiysk (Kaliningrad Oblast, Russia)
26–30 June 2010**

**Kaliningrad
Terra Baltica
2010**

УДК 551.46
ББК 26.89(9).+26.222.5
P93

Conference was supported by the Russian Fund for Basic Researches,
Federal Target Program “The World ocean” (theme No. 1903-17-09)
and BONUS+ Project ECOSUPPORT

Scientific Editor—Dr. Boris Chubarenko

Editorial Board:

Prof. Ruben Kosjan, Dr. Irina Chubarenko, Dr. Tatjana Akivis

Executive Editor—Dr. Natalya Demchenko

Authors are fully responsible for content, style and language of their contributions, which were included in the Proceedings without changes of the main text. Editorial board made only some editor corrections needed to make abstracts, conclusions and figure captions more broadly understandable for wide audience of researchers, managers and students whom these Proceedings are addressed.

P93 Proceedings of the 2nd International Conference (school) on Dynamics of Coastal Zone of Non-Tidal Seas. Baltiysk (Kaliningrad Oblast), 26–30 June 2010 / ed. by B. Chubarenko. — Kaliningrad: Terra Baltica, 2010. — 410 p.
ISBN 978-5-98777-045-0

Proceedings include full-text contributions and abstracts of the presentations given at 2nd International Conference (school) on Dynamics of Coastal Zone of Non-tidal Seas, Baltiysk (Kaliningrad Oblast), 26–30 June 2010.

The purpose of the Conference was to transfer the current knowledge on hydrodynamic and physical aspects of coastal oceanography from senior scientists to young researchers and to provide an opportunity for all participants to share their scientific achievements and ideas to ensure further progress in understanding the physical fundamentals of nearshore and coastal dynamics. The Conference served as a school-seminar, and, therefore, two forms of presentations were used—invited lectures by leading experts and poster sessions for all participants.

The Conference continues the tradition of its first successful predecessor, held in Baltiysk (Russia) in June–July, 2008.

УДК 551.46
ББК 26.89(9).+26.222.5

ISBN 978-5-98777-045-0

© Authors, 2010
© Atlantic Branch of P.P. Shirshov Institute of
Oceanology of Russian Academy of Sciences,
2010
© Terra Baltica, 2010

Contents

Conference program	7
Sessions of poster presentations	11
Topic 1. Hydrodynamics of marine coastal zone and related issues	19
Lectures	21
Akivis T., Kosyan R. Influence of hydrodynamic processes on sediment transport in the coastal zone	21
Badulin S. Statistical theory for forecasting of wind-waves in coastal zone	26
Kabatchenko I., Reznikov M. Simulation of wind waves in coastal shallow zone	40
Kuznetsov S. Irregular waves transformation in a coastal zone	44
Massel S. Wave-induced circulation in porous media	45
Ostrowski R. Hydro- and morphodynamics of a multi-bar coastal zone	53
Poster presentations	65
Alari V., Haran G., Raudsepp U., Kõuts T. Adverse effects of sediment transport in coastal zone	65
Babakov A., Sivkov V. Hydro-lythodynamics of near-bottom layer in coastal area of South-East Baltic	70
Bebieva Y. Beach drifting in the swash area (Baltic Sea)	73
Bobykina V., Boldyrev V. The morphodynamic and technogenic zoning of the shore of the Kaliningrad region	75
Burnashov E., Bednov A., Trashchenkov A. Results of monitoring of the seashore of the Kaliningrad region by GU KO “Baltberegozaschita”	76
Fedorova E., Sviridova E., Marusin K., Khabidov A. Remote and cartographical techniques for estimation of coastal erosion rate in seas and inland water bodies	82
Frydel J., Jeglinski W., Jurys L., Kaulbarsz D., Schiewe M. Monitoring and geohazard assessment of the Polish coastal zone using 3D laser scanning	85
Karmanov K., Domnin D. Analysis of deformation of the bottom relief in the segment of the northern shore of Sambian Peninsula in the vicinity of the Port Pionerskij	86
Kartau K., Soomere T. The evolution of semi-sheltered bayhead beaches: a study for Valgerand in Pärnu Bay	87
Sergeev A. Current mineralogical and petrographic parameters at the coastal zone of the Sambian peninsula (Kaliningrad region)	92
Shishkina A. Geological and geomorphological conditions of the coast of the Sambian Peninsula	96



Szmytkiewicz P. Infragravity waves in the south Baltic dissipative coastal zone	100
Volkova E. Coast protection of artificial territory	105
Zaitseva-Pärnaste I., Räämet A., Soomere T. Comparison between modelled and measured wind wave parameters in Estonian coastal waters	106
Topic 2. Lagoons and estuaries	111
Lectures	113
Cavaleri L. Predictability of historical floods in the Northern Adriatic Sea	113
Chubarenko B. Mixing processes in coastal lagoons	122
Ryabchenko V., Dvornikov A., Haapala J., Myrberg K. Modeling ice conditions in shallow-water estuaries: the case study of the Neva Bay	128
Samolyubov B. Systems of stratified currents and mass-exchange in the near-mouth regions, bays and in the basins with complex bottom relief	140
Tuchkovenko Yu. Influence of hydrological conditions on environment state of lagoons and estuaries	153
Umgiesser G., Bajo M. Numerical modeling of hydrodynamics and sediment transport in coastal lagoons	155
Poster presentations	160
Ambrosimov A., Babakov A. Hydrodynamic conditions in the central part of the Vistula Lagoon	160
Babakov A., Chubarenko B. Dynamics of waters in the Baltiysk Strait	166
Badyukova E., Zhindarev L., Lykianova S., Solovieva G. Marine deposits of the Vistula Spit (Baltic Sea)	169
Bajo M., Umgiesser G. Storm surge forecast in Venice through an hydrodynamic model	173
Domnin D. Hydrological processes of transboundary catchment areas with relationship to coastal zone: modeling and spatial analysis	177
Domnina A. Morphometric characteristics of the lagoons of the World Ocean	183
Gorbunova J. Hydrological regime as one of the factors that determine the phytoplankton productivity in the Volga Delta	186
Grizetskiy A. Estimation of water quality of Pregolia River	187
Ivanova I., Samolyubov B. Wind effected circulations and density flows in the Petrazovodsk Bay	188
Kruk M., Kosakowski J., Rychter A., Mróz M. Project VISLA; coupling environmental and remote sensing research for better understanding of coastal waters behavior and its sustainable management	193
Kurchenko V., Chechko V. On the quantitative evaluation of solid eolian material, entering the Curonian and the Vistula Lagoons (South-East Baltic) in a winter period	198
Kurennoy D. Analysis of wind conditions in the Neva Bay	199
Leitsina L., Chubarenko B. Optimal time-interval for ones-a-day observation of air temperature at the mouth area of the Pregolia River (South-East Baltic)	204
Molchanov M., Eremina T., Neelov I. Modeling of suspended matter transport in the Neva Bay and the Eastern part of the Gulf of Finland	207



Navrotskaya S. Hundred-years dynamics of near-midday water levels in the mouth of the Pregolia River (1901–2009)	212
Pitalskaya O. On the flow vertical structure of shallow strongly stratified basin in summer	218
Plotnikova E., Kuleshov A. Internal waves in shallow water bodies	223
Podgorniy K. Mathematical modeling of spatial-temporal dynamics of current fields in the Neva Bay, the Gulf of Finland	225
Ponomarenko E. Positive and negative setup of water level in the mouth of the Don River: research and prediction	232
Sokolov A., Chubarenko B. Transformation of the wind waves penetrated into a shallow lagoon: Vistula Lagoon case study	236
Sorokina V., Povazhnyy V., Gonsales F. Water transparency, total suspended solid matter and particulate organic carbon of the Azov Sea (field observations in 2008–09 years)	240
Stepantsova V., Alexandrov S. Plankton pigment composition of the Vistula and Curonian Lagoons in condition of salinity variable and algae blooms	244
Topic 3. Interaction between coastal zone and open sea	245
Lectures	247
Chubarenko I. Thermally driven interaction between coastal and open sea areas	247
Diansky N. Numerical simulation of 3-D sea circulation in shelf zone with mesh refinements	264
Lehmann A., Myrberg K. Upwelling in the Baltic Sea	274
Lips U., Lips I., Liblik T., Kikas V., Altoja K., Kuvaldina N., Norit N. Multiparametric in-situ observations in the Gulf of Finland	284
Myrberg K. Coastal and local processes	290
Ostrovskii A. Short period variability in the euphotic zone of the north-eastern Black Sea as inferred from combined acoustic and hydrographic surveys	299
Zatsepin A., Kremenetskiy V., Korzh A., Ostrovskii A. Submesoscale Eddies at the Narrow Shelf: Observations at the Black Sea	305
Poster presentations	311
Ampilogov D., Vasilkin V., Maliy D. Numerical simulation of density inhomogeneity (“spot”) collapse	311
Chubarenko B., Stont Zh., Goushchin O. Changes in hydro-meteorological characteristics for marine coast and lagoons of the South-East Baltic	312
Chubarenko N., Shchuka S., Chubarenko I. Analysis of thermohaline structure of water in coastal zone of the Baltic Sea and of characteristics of its cold intermediate layer	321
Chugaevich V., Sapozhnikova E. Distribution of sea surface temperature in the South-East Baltic by remote sensing and in-situ data	325
Demchenko N., Zatsepin A., Chubarenko I. The temperature front in the rotating fluid: laboratory modeling	326
Elkin D. Laboratory study of sub-mesoscale eddy formation mechanisms at narrow Black Sea shelf	331
Esiukova E. The horizontal water exchange between coastal zone and open sea in the East and South-East Baltic	336



Esiukova E., Chubarenko I., Chubarenko B. Horizontal water exchange through the borders between exclusive economic zones of the Baltic states and sub-basins of the Baltic Sea	341
Fedorov D. Geostrophic currents in the Drake Passage based on the hydrological section in January 2010	346
Gurova E., Ivanov A. Investigations of coastal hydrodynamics features by combining of SAR and SST satellite data	353
Ivonin D., Bakhanov V., Ermoshkin A., Telegin V. Application of nautical X-band radar for measurements of surface currents. Testing. The Black Sea	354
Kileso A. One of the mechanisms of simulation of viscous adhesion at the bottom in numerical model of bottom currents	360
Korosteleva A. About features of autumn cooling of coastal waters in the presence of near-surface currents	363
Kortishko V. Analysis of the velocity gradients and suspension transport in bottom flow at slope	364
Kozlova O. Features of the Baltic Sea cold intermediate layer on the base of mean annual data (1952–2005) of IOW	368
Kremenetskiy V., Korzh A., Ostrovskiy A., Zatsepin A. Short-term water dynamics variability at the narrow Black Sea shelf	373
Maljutenko I. Longterm high resolutional hydrodynamical model simulation for the Gulf of Finland	374
Nizov S. Investigation of evolution of a gravity current with constant inflow on a horizontal bottom (laboratory experiment)	380
Passenko J., Lessin G., Maljutenko I. Analysis of temporal variability of measured and modelled vertical distributions of salinity and temperature in the Gulf of Finland during 10-year period	384
Shishova A. The analysis of mixing and entrainment processes for downslope density currents using Baines' approach	389
Sikharulidze D. Propagation of the denser water on the bottom slope in the stratified fluid	390
Silvestrova K. Structure and dynamics of coastal waters near the Kaliningrad region according to measurements of recent MSU expedition	394
Sineva A. Estimation of oil pollution at the Oil Stones production site in the Caspian Sea using synthetic aperture radar images	395
Värv R. High resolution bathymetry for Gulf of Finland	399
Yurov V. An analytic approach to description of the dissipative effects in 3+1 dimensions	401
Zavyalov I. Physics of spreading of a gravity current on a slanting bottom of the ocean with involving in current solid particles of dredge . . .	405

Conference program

26.06.2010, Saturday Arrival of participants, registration

Arrival of participants to Kaliningrad during the day. Group transfers from airport will be arranged by request. Meeting point—Laboratory Building of the Atlantic Branch of P. P. Shirshov Institute of Oceanology. Address: Kaliningrad, Pionerskaya str, 61. Buses from railway station and airport till the stop “Plostad’ Vasilevskogo” (Vasilevskii’s Square).

16:00–20:00 Group bus transfer from Laboratory Building of ABIORAS (Kaliningrad) to Baltiysk, ferry transfer to Kosa Village, registration and accommodation at the Station

20:00 Welcome BarBQ in the garden, in front of the Station

27.06.2010, Sunday Topic 1. Hydrodynamics of marine coastal zone and related issues

Chairman—Prof. Ruben Kosjan²

Local coordinator—Dr. Alexander Babakov⁶

07:30–08:30 Breakfast, deployment of posters related to **Topic 1**

09:00–09:20 Opening on behalf of Russian Fund of Basic Researches
(*Prof. V. Zhmur*^{9,12}, *Prof. R. Kosjan*^{2,12})

09:20–10:10 Lecture by *Dr. Sci. Iliia Kabatchenko*¹⁴
Modelling of wind waves in the shallow waters

10:10–11:00 Lecture by *Dr. Sci. Sergey Badulin*¹
Statistical theory for forecasting of wind-waves in coastal zone

11:00–11:20 Coffee Break

11:20–12:10 Lecture by *Dr. Sci. Sergey Kuznetsov*¹
Irregular waves transformation in a coastal zone

12:10–13:00 Lecture by *Dr.-hab. Rafal Ostrowski*³
Hydro- and morphodynamics of a multi-bar coastal zone

13:00–14:30 Lunch

14:30–15:20 Lecture by *Prof. Stanislaw Massel*¹⁵
Wave-induced circulation in porous media

15:20–16:10 Lecture by *Dr. Tatyana Akivis*¹
Influence of hydrodynamic processes on sediment transport in the coastal zone

16:10–16:30 Coffee Break



- 16:30–17:20 Lecture (**Topic 3**) by *Dr. Nikolay Diansky*¹⁷
Numerical simulation of 3-D sea circulation with mesh refinements in shelf zone
- 17:20–19:00 **Poster session. Topic 1.**
3-minutes presentations explaining each poster.
Awarding of selected posters by the Scientific Committee.
- 19:00–21:00 Free time
- 21:00 Excursion to eroded sea coast of the Vistula Spit
(*Dr. Valentina Bobykina*⁶, *Mgr. Evgenia Gurova*)
- 28.06.2010, Monday** **Topic 2. Lagoons and estuaries**
Chairman—*Dr. Luidgi Cavaleri*⁷
Local coordinator—*Dr. Julia Gorbunova*⁶
- 07:30–08:30 Breakfast, deployment of posters related to **Topic 2**
- 09:00–09:20 Overview of international activities in lagoon and estuarine researches
(*Dr. Luidgi Cavaleri*, *Dr. Boris Chubarenko*)
- 09:20–10:10 Lecture by *Dr. Boris Chubarenko*⁶
Mixing processes in coastal lagoons
- 10:10–11:00 Lecture by *Prof. Boris Samolyubov*⁵
Systems of stratified currents and mass exchange in the near-mouth regions, bays and in the basins with complex bottom relief
- 11:00–11:20 Coffee Break
- 11:20–12:10 Lecture by *Prof. Yuri Tuchkovenko*⁴
Influence of hydrological conditions on environment state of lagoons and estuaries
- 12:10–13:00 Lecture by *Dr. Luidgi Cavaleri*⁷
Hindcast of historical floods
- 13:00–14:30 Lunch
- 14:30–15:20 Lecture by *Dr. Marco Bajo*⁷
Numerical modeling of hydrodynamics and sediment transport in the coastal lagoons
- 15:20–16:10 Lecture by *Dr. Sci. Vladimir Ryabchenko*¹⁶
Modelling ice conditions in shallow-water estuaries: the case study of the Neva Bay
- 16:10–16:30 Coffee Break
- 16:30–17:20 Lecture (Topic 3) by *Dr. Urmas Lips*¹³
Multiparametric in-situ observations in the Gulf of Finland



-
- 17:20–19:00 **Poster session. Topic 2.**
3-minutes presentations explaining each poster.
Awarding of selected posters by Scientific Committee.
- 19:00–... Free time
- 29.06.2010, Tuesday** **Topic 3. Interaction between coastal zone and open sea**
Chairman—Dr. Andrey Zatsepin¹,
Local coordinator—Dr. Irina Chubarenko⁶
- 07:30–08:30 Breakfast, deployment of posters related to **Topic 3**
- 09:00–09:20 Information on current national projects
(*Prof. L. Zhindarev*^{5, 11})
- 09:20–10:10 Lecture by *Dr. Sci. Andrey Zatsepin*¹
Submesoscale eddies at the narrow shelf: observations at the Black Sea and laboratory modeling
- 10:10–11:00 Lecture by *Dr. Sci. Petr Zavialov*¹
River plumes and their relations with atmospheric forcing and ambient coastal circulations
- 11:00–11:20 Coffee Break
- 11:20–12:10 Lecture by *Dr. Sci. Irina Chubarenko*⁶
Thermally induced interaction between coastal zone and open sea
- 12:00–13:00 Lecture by *Dr. Alexander Ostrovskii*¹
Short period variability of the sea environment over the continental slope and the sea shelf in the north-eastern Black Sea as inferred from combined acoustic and hydrographic surveys
- 13:00–14:30 Lunch
- 14:30–15:20 Lecture by *Dr. Andreas Lehman*⁸
Upwelling in the Baltic Sea
- 15:20–16:10 Lecture by *Dr. Kai Myrberg*¹⁰
Coastal and local processes in the Baltic Sea
- 16:10–16:30 Coffee Break
- 16:30–18:30 **Poster session, Topic 3.**
3-minutes presentations explaining each poster.
Awarding of selected posters by Scientific Committee.
- 19:00 Sport competitions, closing BarBQ
- 30.06.2010, Wednesday** **Excursion to the open coast of the Kaliningrad Oblast**
(Participants, who will depart early at the morning on 01.07.10, will be transferred to Kaliningrad to spend night there just after excursion without returning to the Station at Kosa Village. Please, don't forget to take luggage with you to excursion.)



01.07.2010, Departure

Thursday 09:30–12:00

Transfer of participants to Kaliningrad
(12:00— arrival to Kaliningrad)

- ¹ P.P. Shirshov Institute of Oceanology of Russian Academy of Sciences (IORAS), Moscow, Russia.
- ² Southern Branch of P.P. Shirshov Institute of Oceanology of the Russian Academy of Sciences (IORAS), Gelendzhik, Russia.
- ³ Institute of Hydro-Engineering, Polish Academy of Sciences (IBWPAN), Gdansk, Poland.
- ⁴ Odessa State Hydrometeorological University, Odessa, Ukraine.
- ⁵ Moscow State University (MSU), Moscow, Russia.
- ⁶ Atlantic Branch of P.P. Shirshov Institute of Oceanology of the Russian Academy of Sciences (IORAS), Kaliningrad, Russia.
- ⁷ Institute of Marine Science, National Research Council (ISMAR-CNR), Venice, Italy.
- ⁸ Leibniz Institute of Marine Sciences at Kiel University IFM-GEOMAR), Kiel, Germany.
- ⁹ Moscow Institute (State University) for Physics and Technology (MIPT), Moscow (Dolgoprudnyi), Russia.
- ¹⁰ Finnish Institute of Marine Research, Helsinki, Finland.
- ¹¹ Working Group “Sea Coasts” of the Board of the Russian Academy of Sciences on Problems of the World Ocean.
- ¹² Russian Fund for Basic Research.
- ¹³ Marine Systems Institute, Tallinn University of Technology, Tallinn, Estonia.
- ¹⁴ State Oceanographic Institute, Moscow, Russia.
- ¹⁵ Institute of Oceanology of Polish Academy of Sciences Sopot, Poland .
- ¹⁶ St.Petersburg Branch of P.P. Shirshov Institute of Oceanology of the Russian Academy of Sciences, St. Petersburg, Russia.
- ¹⁷ Institute of Numerical Mathematics (INM) of Russian Academy of Sciences, Moscow, Russia.

Sessions of poster presentations

**27.06.2010, Sunday
16:40–18:30**

Poster session. Topic 1. Hydrodynamics of marine coastal zone and related issues.
3-minutes presentations near each poster.
Awarding of selected posters by Scientific Committee.

Alari Viktor, Urmas Raudsepp, Getli Haran	Marine Systems Institute at Tallinn University of Technology	Adverse effects of sediment transport in coastal zone
Babakov Alexander, Sivkov Vadim	P. P. Shirshov Institute of Oceanology RAS, Atlantic Branch	Hydro-lythodynamics of near-bottom layer in coastal area of south-east Baltic
Bebieva Yana	Moscow Institute of Physics and Technology	Beach drifting in the swash area (Baltic Sea)
Bobykina Balentina, Boldyrev Vadim	P. P. Shirshov Institute of Oceanology RAS, Atlantic Branch	The morphodynamic and technogenic zoning of coasts of the Kaliningrad region
Burnashov Evgeny, Bednov Alexander, Trashchenkov Alexander	GU KO “Baltberegozachita”	Results of monitoring the seashore of the Kaliningrad region according to the GU KO “Baltberegozaschita”
Fedorova Elena, Sviridova Evgeniya, Marusin Konstantin, Khabidov Alexandr	Institute for Water and Environmental Problems SB RAS	Remote methods for the rate of coastal erosion seas and inland water
Frydel Jerzy, Jeglinski Wojciech, Leszek Jurys, Kaulbarsz Dorota, Schiewe Malgorzata	Polish Geological Institute, National Research Institute	Monitoring and geohazard assessment of the Polish coastal zone using 3D laser scanning
Karmanov Konstantin, Domnin Dmitry	P. P. Shirshov Institute of Oceanology RAS, Atlantic Branch	Analysis of deformation of the bottom relief in the vicinity of Port Pionerskij at the Northern coast of Sembian Peninsula



Kartau Katri	Institute of Cybernetics at TUT, Laboratory of Wave Engineering	The evolution of semi-sheltered bayhead beaches; a study for Valgerand in Pärnu Bay
Sergeev Alexandr	A. P. Karpinsky Russian Geological Research Institute (SPB)	Current mineralogical and petrographic parameters at the coastal zone of the Sambian peninsula (Kaliningrad Region)
Shishkina Anna	Southern Scientific Centre RAS	Geological and geomorphological conditions of the Sambian Peninsula coast
Szmytkiewicz Piotr	Institute of Hydro-Engineering of the Polish Academy of Sciences (IBW PAN)	Infragravity waves in the South Baltic dissipative coastal zone
Tribštok Olga, Zaitseva-Pärnaste Inga	Institute of Cybernetics at TUT	Reconsidering wave observation data from Estonian coast waters
Volkova Ekaterina	Branch of Open Society company (Research center "Sea coast")	Coast protection of artificial territory
Zaitseva-Pärnaste Inga, Tarmo Soomere, Andrus Räämet	Tallinn University, Institute of Cybernetics	Seasonal and long-term variations of wave conditions in Estonian coastal waters
28.06.2010, Monday 16:40–18:30	Poster session. Topic 2. Lagoons and estuaries. 3-minutes presentations near each poster. Awarding of selected posters by Scientific Committee.	
Ambrosimov Albert, Babakov Alexander	P. P. Shirshov Institute of Oceanology RAS	Hydrodynamic conditions in the central part of the Vistula Lagoon
Babakov Alexandr, Chubarenko Boris	P. P. Shirshov Institute of Oceanology RAS, Atlantic Branch	Water dynamics in the Baltiysk Strait
Badyukova Elena, Zhindarev Leonid, Lykianova Svetlana, Solovieva Galina	M. V. Lomonosov Moscow State University, Physics Faculty	Marine deposits in Vistula Spit structure.



Bajo Marco, Umgiesser Georg	Institute of Marine Sciences (ISMAR-CNR)	Storm surge forecast in Venice through an hy- drodynamic model
Domnin Dmitry	P. P. Shirshov Institute of Oceanology RAS, Atlantic Branch	Hydrological processes of transboundary catch- ment areas in the re- search on the relation- ship with coastal zone: modeling and spatial analysis.
Domnina Anastasia	P. P. Shirshov Institute of Oceanology RAS, Atlantic Branch	Morphometric charac- teristics of the lagoons of the World Ocean
Gorbunova Julia	P. P. Shirshov Institute of Oceanology RAS, Atlantic Branch	Hydrological regime as one of the factors that determine the phyto- plankton productivity in the Volga Delta
Grizetskiy Alexandr	P. P. Shirshov Institute of Oceanology RAS, Atlantic Branch	Estimation of water quality of Pregolia River
Ivanova Irina, Samolubov Boris	M. V. Lomonosov Moscow State Univer- sity, Physics Faculty	Wind effected circula- tions and density flows in the Petrazovodsk Bay
Kruk Marek, Rychter Agata, Mróz Marek, Kosakowski Janusz	University of Warmia and Mazury in Olsz- tyn	Project VISLA; coupling environmental and re- mote sensing research for better understanding of coastal waters ecosys- tems and its sustainable management
Kurchenko Viktoria, Chechko Vladimir	P. P. Shirshov Institute of Oceanology RAS, Atlantic Branch	On the quantitative evaluation of solid eolian material, entering the coastal zone of South- eastern Baltic in a winter period.
Kurennoy Dmitry	A. P. Karpinsky Rus- sian Geological Re- search Institute	Meteorological and wind-wave conditions in the Neva Bay and the Vistula Lagoon



Leitsina Lidia, Chubarenko Boris	P. P. Shirshov Institute of Oceanology RAS, Atlantic Branch	Optimal time-interval for daily observation of air temperature at the mouth area of the Pregel River (South-East Baltic).
Molchanov Mikhail, Eremina Tatjana, Neelov Ivan	Russian State Hydro- meteorological Uni- versity	Modeling of the sus- pended matter spread- ing in the shallow estu- ary.
Navrotskaya Svetlana	P. P. Shirshov Institute of Oceanology RAS, Atlantic Branch	Dynamics of the near- midday levels at the Pregolja River mouth in 1996–2009
Pitalskaya Olga	Institute of Computa- tional Modeling Sibe- rian Branch of RAS	On the flow vertical structure of shallow strongly stratified basin in summer
Plotnikova Ekaterina, Kuleshov Alexey	Moscow Institute of Physics and Technol- ogy; P. P. Shirshov In- stitute of Oceanology RAS, Atlantic Branch	Internal waves in shal- low water bodies
Podgornyj Konstantin	I. D. Papanin Institute for the Biology of In- land Waters RAS	Mathematical modeling of spatial-temporal dy- namics of current fields in the Neva Bay, Gulf of Finland
Ponomarenko Ekaterina	Southern Scientific Centre RAS	Positive and negative setup of water in the mouth of the Don River: research and prediction
Sokolov Andrei, Chubarenko Boris	P. P. Shirshov Institute of Oceanology RAS, Atlantic Branch	Transformation of the wind waves penetrated into shallow lagoon: Vis- tula Lagoon case study
Sorokina Vera, Povazhnyy Vasiliy, Gonsales Filipp	Southern Scientific Centre RAS	Water transparency, total suspended solids and particulate organic carbon of the Azov Sea (field observations in 2008–09 years)



Stepantsova Vasilina, Alexandrov Sergey	Atlantic Research Institute of Marine Fisheries and Oceanography (AtlantNIRO)	Plankton pigment composition of the Vistula and Curonian Lagoons in condition of salinity variable and algae blooms
--------------------------------------------	-------------------------------------------------------------------------------	---------------------------------------------------------------------------------------------------------------------

**29.06.2010, Tuesday
16:50 – 18:30**

Poster session. Topic 3. Interaction between coastal zone and open sea.

3-minutes presentations near each poster. Awarding of selected posters by Scientific Committee.

Esiukova Elena	P. P. Shirshov Institute of Oceanology RAS, Atlantic Branch	Horizontal water exchange between coastal waters and open part of the South-East Baltic Sea
Ampilogov Dmitry, Vasilkin Viktor, Maliy Denis	Immanuel Kant State University of Russia	Numerical simulation of density inhomogeneity (“spot”) collapse
Chubarenko Boris, Stont Zhanna, Goushchin Oleg	P. P. Shirshov Institute of Oceanology RAS, Atlantic Branch	Variability of hydro-meteorological characteristics for marine coast of the South-East Baltic
Chubarenko Natalya	P. P. Shirshov Institute of Oceanology RAS; Moscow Institute of Physics and Technology	Vertical thermo-haline structure of waters in South-East Baltic Sea based on field data
Chugaevich Vsevolod, Sapozhnikova Elena	Immanuel Kant State University of Russia	Distribution of sea surface temperature in the South-East Baltic by remote sensing and in-situ data
Demchenko Natalya, Zatsepin Andrei, Chubarenko Irina	P. P. Shirshov Institute of Oceanology RAS, Atlantic Branch	The temperature front in the rotating fluid: laboratory modeling
Elkin Dmitriij	P. P. Shirshov Institute of Oceanology RAS	Laboratory modeling of submesoscale eddies at the narrow Black Sea shelf



Esiukova Elena, Chubarenko Irina, Chubarenko Boris	P. P. Shirshov Institute of Oceanology RAS, Atlantic Branch	The horizontal water exchange through the borders between exclu- sive economic zones of the Baltic states and sub- basins of the Baltic Sea
Fedorov Dimitry	P. P. Shirshov Institute of Oceanology RAS	Geostrophic currents in the Drake Passage based on the hydrological sec- tion in January 2010
Golenko Nikolay, Golenko Maria	P. P. Shirshov Institute of Oceanology RAS, Atlantic Branch	Thermohaline structures in South Baltic basins in early spring 2009 and tear associations with major inflow 2003
Gurova Evgenia, Ivanov Alexander	P. P. Shirshov Institute of Oceanology RAS	Coastal hydrodynam- ics features research by combining of SAR and SST satellite data
Ivonin Dmitry, Bakhanov Viktor, Ermoshkin Alexey, Telegin Viktor	P. P. Shirshov Institute of Oceanology RAS	Application of nautical X-band radar for mea- surements of surface currents. Testing. The Black Sea
Kileso Aleksandr	Immanuel Kant State University of Russia	About one of the algo- rithms accounting viscous adhesion on the bottom in the numerical model of bottom currents
Korosteleva Alexandra	Immanuel Kant State University of Russia	Peculiarities of autumn cooling of coastal waters with existing of back- ground undersurface current
Kortishko Vladimir	Immanuel Kant State University of Russia	Velocity gradient analy- sis of bottom slope flow and suspension trans- port
Kozlova Olga	P. P. Shirshov Institute of Oceanology RAS, Atlantic Branch	The analysis of the mini- mum monthly average water temperatures in a cold intermediate layer of Baltic



Kremenetskiy Viacheslav, Korzh Andrey, Ostrovskiy Alexander, Zatsepin Andrey	P. P. Shirshov Institute of Oceanology RAS	Short-term water dynamics variability at the narrow Black Sea shelf
Maljutenko Ilja	Marine Systems Institute at Tallinn University of Technology	Long-term high resolution hydrodynamical model simulation for Gulf of Finland
Nizov Sergey	P. P. Shirshov Institute of Oceanology RAS	Investigation of a gravity current with constant inflow on a horizontal bottom (laboratory experiment)
Passenko Jelena, Lessin Gennadi, Maljutenko Ilja	Marine Systems Institute at TUT	Analysis of temporal variability of measured and modelled vertical distributions of salinity and temperature in the Gulf of Finland during 10-year period
Sapozhnikova Elena, Shaplygin Svetlana	P. P. Shirshov Institute of Oceanology RAS, Atlantic Branch	Mesoscale dynamics of waters in the South-East Baltic by using remote sensing data for September 2007
Shishova Anna	Immanuel Kant State University of Russia	The analysis of mixing and entrainment processes for downslope density currents using Baines' approach
Silvestrova Ksenia	M. V. Lomonosov Moscow State University	Structure and dynamics of coastal waters near the Kaliningrad region according to measurements of recent Moscow State University expeditions
Sineva Anastasia	P. P. Shirshov Institute of Oceanology RAS; Moscow Institute of Physics and Technology	Estimation of oil pollution at the Oil Stones production site in the Caspian Sea using synthetic aperture radar images



Sikharulidze David	P. P. Shirshov Institute of Oceanology RAS; Moscow Institute of Physics and Technology	Propagation of the denser water on the bottom slope in the stratified fluid
Varv Rolf	Tallinn University Of Technology	High resolution bathymetry for gulf of Finland and its purpose
Yurov Valerian	University of Missouri, Immanuel Kant State University of Russia	An analytic approach to description of the dissipative effects in 3+1 dimensions.
Zavialov Ivan	Moscow Institute for Physics and Technology	Physics of spreading of gravity carrying on the slanting bottom of ocean with involving in current solid particles of dredge.

TOPIC 1

Hydrodynamics of marine coastal zone and related issues

Lectures

Influence of hydrodynamic processes on sediment transport in the coastal zone

Tatiana Akivis, Ruben Kosyan

Abstract

Hydrodynamics is the main cause of sediment transport in the coastal zone. Active hydrodynamic processes affecting the coastal zone of non-tidal seas are currents, waves, nearshore anticyclonic eddy, and macro-turbulence in wave breaking zone. In the lecture, an analysis of both field study and modeling of sediment transport in the coastal zone for different spatial and temporal scales is given. Possible mechanisms of fine sediment and pollution transport from the shelf to continental slope are considered too.

Рассматриваются гидродинамические процессы различных масштабов, ответственные за перенос взвешенного вещества в прибрежной зоне и на шельфе бесприливных морей. Показаны закономерности взвешивания и переноса осадочного вещества в волновом донном пограничном слое как для слабдеформированных и неразрушенных волн, так и для интенсивных режимов волнения в прибойной зоне. Рассмотрены также процессы переноса взвешенного вещества квазистационарными течениями и вихрями на внешнем шельфе и их роль в процессах обмена веществом и энергией между шельфом и открытым морем.

1. Introduction

A nearshore zone is a relatively narrow and shallow area of the World Ocean where the most of tremendous hydrodynamic energy of waves and currents transforms and dissipates. Hydrodynamic processes in the coastal zone of non-tidal seas are represented by water motions of various spatial and

Tatiana Akivis (✉)

P. P. Shirshov Institute of Oceanology RAS, Moscow, Russia

e-mail: akivis@yandex.ru

Ruben Kosyan (✉)

P. P. Shirshov Institute of Oceanology RAS, Southern Branch, Gelendzhik,
Russia

e-mail: rkosyan@hotmail.com



temporal scales such as turbulence, waves, along- and cross-shore currents, mesoscale eddies. The complex effect of these processes controls sediment transport in the near-shore zone and, *ultima analysis*, its morphological development and shoreline changes. In recent years much attention has been devoted to challenging environmental problems which are directly connected with sediment transport because human activity in shelf and coastal zone contributes to the contamination of seabed and suspended sediments and has a negative influence on water quality and the functioning of local ecosystems. Both field measurements and modeling are necessary for adequate description and comprehension of sediment transport because the processes under consideration are extremely complex and irregular.

2. Results

2.1. Waves

All significant events of sediment suspending and transfer occur in a bottom boundary layer. When surface waves enter shallow water, oscillatory water motion creates a boundary layer through friction against bottom, so-called wave bottom boundary layer (WBBL). A regime of water flow in the boundary layer can be laminar, turbulent or transitional depending on Reynolds number in terms of bottom roughness. In natural marine conditions the bottom is never smooth but usually covered by micro- and macro-forms of different scales. In this case an equivalent bottom roughness is controlled by bed form types and parameters. A thickness of WBBL is only a few cm above bed that causes serious problems of field instrumental measurements.

Sediment particles can be picked up from the bottom only if near-bottom water velocity exceeds some critical value. For weak wave regime when the velocity only slightly exceeds the threshold for mass transport of bottom sediment two-dimensional ripples are formed. In this case, the mechanism of sediment suspending from the bottom is connected with vortexes formed behind the ripple crests. The laboratory experiments show that the maximum concentration of suspended sediment over ripples occurs at flow reversal moments i.e. has a phase lag of approximately quarter period in relation to the maximum of water velocity. In field conditions the waves are always irregular. Now the group structure of the waves plays the key role in sediment pick up and redistribution. Field measurements revealed that the duration of concentration peaks and their frequency correlate well with periodicity of groups of high waves and a number of waves in a separate group. The pick up of sediment particles from the bottom is the most intensive in deceleration phase of the wave flow when the near-bottom velocity changes its sign.

As height and deformation of surface waves increase, two-dimensional ripples became unstable and are reshaped into three-dimensional ones. In this case sediment pick up from the bottom occurs only once a wave period in deceleration phase of the wave flow. With further intensification of the near-bottom water motion the bed forms are eroded and this is hydrodynamic instability that initiates generation of turbulence in WBBL. Laboratory experiments showed that again, abrupt rise of turbulent kinetic energy (TKE) and bed shear stress take place in the deceleration phase of the wave flow.



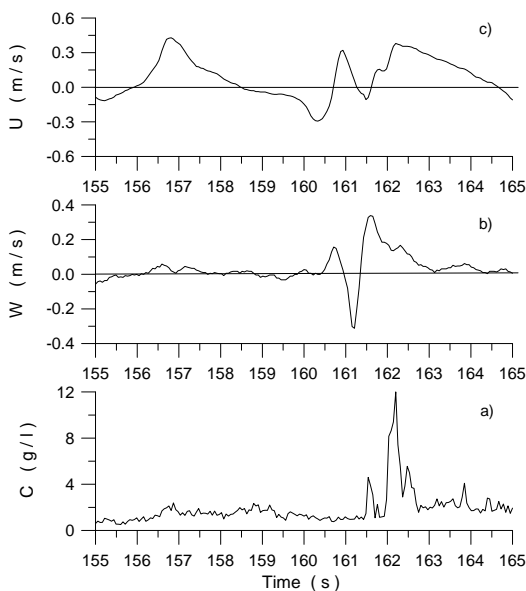
In the wave breaking zone the turbulence is generated by both instability in WBBL and breaking of wave crests near the surface. Macro-eddies which formed near the surface after wave breaking penetrate to the bottom. These eddies are the dominating mechanism of sediment suspending in the wave breaking zone (Fig. 1) (Kosyan et al., 2001). The parameters of the turbulence depend on wave breaking type, i.e. spilling or plunging.

2.2. Quasi-steady flows

The wave and turbulence mechanisms of sediment pick up are typical for relatively shallow part of the coastal zone of the sea (0–15 m) where the seabed is mainly covered by sand sediment. Another hydrodynamic factor of sediment transport acting in deeper part of the coastal zone up to the shelf edge is represented by quasi-steady flows. The well-known example of this kind of hydrodynamic structures is the Black Sea Rim current that encircles cyclonically the whole basin. These large scale currents flow mostly along depth contours due to geostrophic constraints and so contribute to the along-shelf water and sediment transport. But in the same time, there exists clear evidence of the cross-shelf water and sediment transport in the outer shelf and mass and energy exchange between shelf and continental slope zones.

Further of the coastline the bottom is mainly covered by fine sediments rather than by sand. Estimates show that critical bed shear stress for erosion of upper sediment layer should be about 0.1–0.2 Pa that can be reached for water velocities exceeding 20 cm/s at 1 m above bottom. But it is too deep for wind waves to penetrate to the bottom in intermediate and outer shelf. Processes that may be responsible for cross-shelf sediment movement are mesoscale eddies and meanders of along shelf current. Mesoscale eddies are ubiquitous features in the world ocean. However, their influence seems to be particularly important in tideless regions e.g. in semi-enclosed seas like the

Fig. 1. A fragment of the time series of (a) suspended sediment concentration; (b) vertical and (c) cross-shore velocity, which illustrating the sand suspension event under plunging breaker at 10 cm above the bottom under a horizontal eddy passing the measurement point. The Ebro delta'96 experiment.





Mediterranean and Black Seas. The mesoscale eddies have been repeatedly observed both on shelf and continental slope of the Black Sea (Fig. 2).

In this region from 19 to 46 anti-cyclonic eddies a year are detected by long-term observations. The dimensions of near-shore anti-cyclonic mesoscale eddies exceed the shelf width and may transport fine sediment particles and pollutions in the back front from the shelf to the open sea and deliver fresh water to the shelf in its front.

Because of the dimensions of mesoscale eddies (10–30 km) the Earth rotation became an essential factor. This initiates the other mechanism of sediment transport by mesoscale eddies related to Ekman bottom boundary layer (EBBL) which is formed by the balance of pressure gradient, Coriolis force and bottom friction. A thickness of EBBL can be tens of meters. Water velocity veering in EBBL results in counterclockwise deviation of fine SPM and pollutions flow and causes their cross-shelf transport.

Unfortunately there are only scanty field measurements of sediment transport in EBBL. But modeling (Shapiro et al., 2002) shows that SPM capacity of mesoscale eddies is quite substantial. Along-slope current containing an eddy is able to redeposit sediments both off-shore and on-shore. This effect provides a mechanism of suspended matter exchange between the shelf and the open ocean (Fig. 3).

The eddies flush out preferentially fine-grained sediment from the outer shelf, which is more easily accessible to eddies that are formed locally, by instability of the slope current, or are coming onto the shelf from deep water. Frequent propagation of eddies along the coast would result in a sediment grain size being spread uniformly in bands parallel to the shelf break. Geological data provide direct evidence for this on the narrow Black Sea shelf (Shimkus & Evsyukov, 1996).

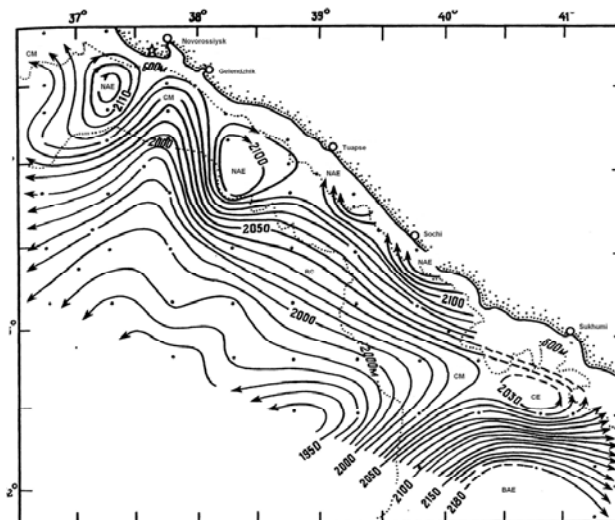
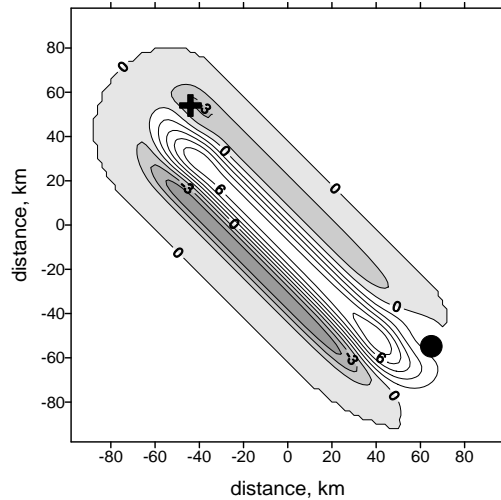


Fig. 2. Surface geostrophic circulation in the north-eastern part of the Black Sea by RV "Yantar" survey with typical mesoscale structures (Krivosheya et al, 1998).

RC—Rim current, CM—cyclonic meander, NAE—near-shore anti-cyclonic eddy, CE—cyclonic eddy, BAE—Batumi anti-cyclonic eddy.



Fig. 3. Modeling of distribution of eroded (positive) and deposited (negative, shaded) sediment per unit area, g/cm^2 by anti-cyclonic eddy travelling from the dot point to the cross point.



Acknowledgements

The authors are grateful to Dr. N. Pykhov for helpful discussions.

References

- Kosyan, R., Kunz, H., Pykhov, N. et al. P. (2001) Physical regularities of suspended sand concentration and transport under irregular waves based on field data. *Die Küste* **64**:161–200.
- Krivosheya, V., Nyffeler, F., Yakubenko, V. et al. (1998) Experimental Studies of Eddy Structures within the Rim Current Zone in the North-Eastern Part of the Black Sea. In: *Ecosystem Modeling as a Management Tool for the Black Sea*, 2:131–144. Netherland: Kluwer Academic Publishers.
- Shapiro, G., Akivis, T., Pykhov, N. (2002) Modeling of Fine Sediment Transport by Eddies and Currents on the Caucasian Shelf of the Black Sea. In: *Multidisciplinary Investigations of the Northern Part of the Black Sea*, 339–357. Moscow: Nauka.
- Shimkus, K. M. & Evsyukov, Yu. D. (1996) Bottom relief and its formation. In: *Anthropogeneous pollution and natural self-cleaning of the near Caucasus zone of the Black Sea*, 13–27. Moscow: Nedra.

Statistical theory for forecasting of wind-waves in coastal zone

Sergei Badulin

Abstract

Theoretical background of statistical description of wind-driven waves is presented. The core of the approach is the kinetic equation for deep water waves obtained by Klaus Hasselmann in 1962. So far description of wave input and dissipation is based on empirical parameterizations while nonlinear transfer is known “from first principles”. The latter implies universality features of wind wave evolution. These features should be respected in wave modeling, especially, in near-shore studies where peculiarities can contaminate essential physics. Examples of application of wind-wave forecasting models for near-shore regions are considered.

В лекции представлены теоретические основы статистического описания морского ветрового волнения. Основой такого описания является кинетическое уравнение, выведенное для волн на воде Клаусом Хассельманном в 1962 г. и описывающее изменение спектральной плотности волнового действия (или энергии волнения), вызванное генерацией волн ветром, диссипацией за счет разнообразных механизмов (турбулентности, взаимодействия с течениями и т. п.) и нелинейными резонансными четырехволновыми взаимодействиями. Генерация и диссипация волнения связаны с множеством физических механизмов, что затрудняет создание соответствующей теории и заставляет широко пользоваться эмпирическими параметризациями. Напротив, нелинейные взаимодействия могут быть теоретически описаны «из первых принципов», что позволяет обнаружить важные черты универсальности развития ветрового волнения, слабо зависящие от конкретных физических условий. Эти свойства необходимо иметь в виду при изучении ветрового волнения в прибрежной зоне.

Sergei Badulin (✉)
P.P. Shirshov Institute of Oceanology RAS, Moscow, Russia
e-mail: badulin@ioran.ru



1. Introduction

The lecture presents the author's vision of the problem of modeling wind-driven waves. It follows consistent theory of weak (wave) turbulence (Zakharov et al., 1992) rather than conventional approaches of wave forecasting (see recent review (Cavaleri et al., 2007)) that combine a variety of methods including empirical physics and purely heuristical findings. In the context of coastal zone dynamics the lecture is seen as a reminder how important and useful general physical principles can be in the very complex and multi-disciplinary studies. The short paper presents just a general scheme of the theoretical vision. Details can be found in the cited works.

§2 gives the basics of the statistical theory. The core of the approach is the kinetic equation for water waves known as the Hasselmann equation (Hasselmann, 1962, 1963a, 1963b). This equation is a limiting case of the quantum kinetic equation for phonons known in condensed matter physics since 1928 thanks to Nordheim (Nordheim, 1928). Properties of the equation known "from first principles" play crucial role in our consideration. Wind forcing and dissipation are traditionally seen as major constituents of wind wave evolution while our knowledge of the terms is quite short. It is based mainly on empirical parameterizations for rather special physical conditions (low winds, weak waves etc.). The shortage of the knowledge and difficulties of calculations of nonlinear transfer remain burning problems of wind-wave modeling.

In §3 we show a way to resolve these problems by introducing a hypothesis of dominating nonlinear transfer (as compared with wave input and dissipation) and, then, demonstrating validity of this hypothesis. The outcome of the resulting asymptotic theory seems very promising: nonlinear transfer determines a quasi-universal shaping of wave spectra, while total energy (or action, or wave momentum) appears to be rigidly linked with corresponding total net fluxes. The approach has shown its efficiency for analysis of experimental data (Badulin et al., 2007) and numerical results (Gagnaire-Renou et al., 2010b).

§4 presents two examples when the statistical approach is used for the wind-wave studies in the near-shore zone. In many cases the validity of this approach is questionable because of relatively short scales of wave development, strong effects of the coast, interference of wind waves and remotely generated swell (mixed sea) *etc.* At the same time, the kinetic equation and our asymptotic theory remain to work quite well for these special cases.

§5 gives a summary of the lecture.

2. Results

2.1. The Hasselmann equation for wind-driven waves

The phenomenon of wind waves is easy to observe but it is not easy to give its consistent physical description. The adequate description is dictated both by our research tools (theoretical and experimental) and by final goals. The nature itself helps us a lot in our efforts to predict sea state: we have, at least, two small parameters. The first one determines a weakness of the coupling and can be introduced as a ratio of air and water densities ρ_a, ρ_w



$$c = \frac{\rho_a}{\rho_w} \tag{1}$$

The second parameter is wave steepness μ that can be expressed in different ways. The “most scientific” (and “less observable”) definition operates with the gradient of sea surface elevation η (angle brackets mean average in wave-vector space here and below)

$$\mu^2 = \langle |\nabla\eta|^2 \rangle \tag{2}$$

Oceanographers prefer another definition that uses surface elevation and wave-number (wavelength or wave frequency) of “typical”, “representative” waves $|\mathbf{k}_p|$

$$\mu_p^2 = \langle \eta^2 \rangle |\mathbf{k}_p| = \langle \eta^2 \rangle \frac{\bar{\omega}_p^4}{g^2} \tag{3}$$

Further we associate $|\mathbf{k}_p|$ and $\bar{\omega}_p$ with a peak of spectral distributions of wind waves.

Wave steepness of wind waves is typically quite small: $\mu_p < 0.1$. In many cases one can use the linear wave theory (Kadomtsev, 1976, Lighthill, 1978, Whitham, 1974) as a well-elaborated tool of theoretical and experimental analysis. It works perfectly, for example, for tsunami problem, or for ship wakes, or in some remote sensing problems but not for prediction of natural wind-driven sea. In absence of the wave-wave coupling the wave field is determined by external forcing and by initial conditions only. This trivial note is conceptual for the problem of wind-wave forecast: poorly determined forcing and boundary conditions makes forecasting itself questionable. To some extent, the problem of unknown (poorly known) boundary conditions is solved by description of wave field in terms of statistical moment. Such description ignores wave phases but requires detailed information on wave forcing due to turbulent wind. Nonlinearity complicates the problem mathematically but gives (somewhat implicitly) a hope that the nonlinearity forces to forget the initial and boundary conditions and, thus, makes the problem of prediction feasible.

Thus, the basic equation of the statistical description of wind waves is written as (Hasselmann, 1962; Zakharov, 1999)

$$\frac{\delta N_{\mathbf{k}}}{\delta t} + \nabla_{\mathbf{k}} \bar{\omega}_{\mathbf{k}} \nabla_{\mathbf{r}} N_{\mathbf{k}} = S_{in}[N_{\mathbf{k}}] + S_{diss}[N_{\mathbf{k}}] + S_{nl}[N_{\mathbf{k}}] \tag{4}$$

Here intrinsic frequency $\bar{\omega}_{\mathbf{k}}$ satisfies linear dispersion equation for gravity water waves

$$\bar{\omega}^2(\mathbf{k}) = g |\mathbf{k}| \tanh(|\mathbf{k}|d) \tag{5}$$

with d —the water depth. Terms in the right-hand side of (4) describe wave input by wind forcing S_{in} , wave dissipation S_{diss} dealing with a number of physical mechanisms and nonlinear transfer due to four-wave interactions S_{nl} that satisfy conditions of spatio-temporal resonance

$$\begin{cases} \bar{\omega}_0 + \bar{\omega}_1 = \bar{\omega}_2 + \bar{\omega}_3 \\ \mathbf{k}_0 + \mathbf{k}_1 = \mathbf{k}_2 + \mathbf{k}_3 \end{cases} \tag{6}$$



The kinetic equation (4) is generally written for two-dimensional wave action spectral density $N(\mathbf{k})$ that has a meaning of a number of waves or quasi-particles. Spectral density of the wave energy and wave momentum are introduced straightforwardly as $E(\mathbf{k}) = \omega(\mathbf{k})N(\mathbf{k})$ and vector quantity $\mathbf{M}(\mathbf{k}) = \mathbf{k}N(\mathbf{k})$. The three physical quantities $N(\mathbf{k})$, $E(\mathbf{k})$, $\mathbf{M}(\mathbf{k})$ are equally important for the statistical description of waves being associated with conservation laws of the kinetic equation in absence of wave input and dissipation ($S_{in} \equiv 0$, $S_{diss} \equiv 0$ in eq. (4)). Strictly speaking, functions $N(\mathbf{k})$, $E(\mathbf{k})$, $\mathbf{M}(\mathbf{k})$ for weakly nonlinear waves are related to their “linear” counterparts by a quadratic transformation (Badulin et al., 2005; Krasitskii, 1994; Zakharov, 1999). Equivalence of the “linear” and “weakly nonlinear” functions can be accepted as an approximation which is valid for deep water waves only.

The collision integral S_{nl} is cubic in spectral density

$$S_{nl}[N_{\mathbf{k}}] = \int_{\mathbf{k}_1} \int_{\mathbf{k}_2} \int_{\mathbf{k}_3} |T(\mathbf{k}, \mathbf{k}_1, \mathbf{k}_2, \mathbf{k}_3)|^2 \{N_2 N_3 (N + N_1) - N N_1 (N_2 + N_3)\} \times \delta(\mathbf{k} + \mathbf{k}_1 - \mathbf{k}_2 - \mathbf{k}_3) \delta(\omega + \omega_1 - \omega_2 - \omega_3) d\mathbf{k}_1 d\mathbf{k}_2 d\mathbf{k}_3 \quad (7)$$

Kernels of four-wave interactions are given by cumbersome expressions that can be found in (Badulin et al., 2005, Zakharov, 1999). In deep water case when there is no specific spatial scale the collision integral S_{nl} has a remarkable property of inhomogeneity that will be used below

$$S_{nl}[vN(v\mathbf{k})] = v^3 v^{19/2} S_{nl}[N(\mathbf{k})] \quad (8)$$

The gradient form of S_{nl} allows one to obtain easily three conservation laws for total energy $E = \int E_{\mathbf{k}} d\mathbf{k}$, wave action $N = \int N_{\mathbf{k}} d\mathbf{k}$ and wave momentum $\mathbf{M}_{\mathbf{k}} = \int \mathbf{k} N_{\mathbf{k}} d\mathbf{k}$ that play an important role in the statistical theory of wind waves. The feature of water waves is the only “true” integral of motion—wave action N . Two other quantities E , \mathbf{M} are formal integrals that exist in principal value sense only.

2.2. The Kolmogorov-Zakharov solutions for water waves

The kinetic equation (4) has stationary solutions that satisfy

$$S_{nl} = 0 \quad (9)$$

One of these solutions appears when

$$N_0 N_1 N_2 + N_0 N_1 N_3 - N_0 N_2 N_3 - N_1 N_2 N_3 = 0$$

i.e. it is balanced at every point of the resonant surface (6). This balance does not depend on interaction kernels that result in thermodynamic solution

$$N_{\mathbf{k}} = \frac{T}{(\omega_{\mathbf{k}} + \mu)} \quad (10)$$

where temperature T and μ are arbitrary parameters. This Rayleigh-Jeans solution appears in a great number of physical problems. However, this solution is physically irrelevant because the corresponding energy spectrum does not decay at $|\mathbf{k}| \rightarrow \infty$.



Stationary kinetic equation (9) has a vast family of exact solutions completely different from the Rayleigh-Jeans spectrum (10). These solutions were found by Zakharov with co-authors (Zakharov, 1966, Zakharov & Filonenko, 1966, Zakharov & Zaslavsky, 1982). The stationarity of these solutions is not provided by vanishing the integrand in the expression (7) but vanishing the whole S_{nl} . The situation can be associated naturally with constancy of spectral fluxes. Two special cases are of interest. The constant flux of energy P gives the Kolmogorov-Zakharov solution for direct cascade (Zakharov & Filonenko, 1966)

$$E(\omega, \theta) = C_p g^{4/3} P^{1/3} \omega^{-4} \tag{11}$$

and the well-known spectral tail ω^{-4} . The constant flux of wave action Q gives the inverse cascade Kolmogorov-Zakharov solution with less exponent 11/3 of frequency spectrum (Zakharov & Zaslavsky, 1982)

$$E(\omega, \theta) = C_q g^{4/3} Q^{1/3} \omega^{-11/3} \tag{12}$$

C_p, C_q are the basic Kolmogorov constants that determine dependence of spectral levels on spectral flux quite like the case of river flow: the flux is higher—the water level is higher.

The stationary solutions (11, 12) seem to be unrealistic. First, they provide a transport between two infinities (from infinitely long to infinitely short waves for direct cascading and in an opposite sense for inverse cascading). Secondly, these solutions are isotropic while wind-sea is strongly anisotropic. At the same time, the power-law tails of these unrealistic solutions are reproduced fairly well in all observations. Further we give an explanation of this fact.

2.3. Wave input

Ocean field experiments give no direct way to discriminate wave generation or dissipation and to quantify experimentally nonlinear transfer term S_{nl} which is coexisting with S_{in}, S_{diss} (Plant, 1982). To resolve this problem, heuristical models for S_{in}, S_{diss} are widely used (Hasselmann, 1974) as work-pieces for further parameterization the observed wave input and dissipation. The Cherenkov-like formula is widely used in a majority of the wave input quasi-linear terms S_{in} (Donelan & Pierson-jr., 1987, Hsiao & Shemdin, 1983, Janssen, 1989, Plant, 1982, Snyder et al., 1981, Soomere, 2005)

$$S_{in} = \beta(\mathbf{k}, N_k) N_k \tag{13}$$

where growth rate $\beta(\mathbf{k})$ takes a form

$$\beta(\mathbf{k}) = c\omega(\mathbf{k})(\zeta - 1)^n \text{ at } \zeta > 1 \tag{14}$$

and has an order of small parameter c in (1). The Cherenkov-like factor

$$\zeta = s \frac{U_h}{C_{ph}} \cos\theta \tag{15}$$



relates a reference wind speed to the phase speed of wave harmonic (s is a coefficient close to 1, angle θ is related to wind direction). Waves moving slower than wind gain energy while waves which are faster than wind do not. Exponent n in (14) usually takes values 1 or 2. Details on parameterizing S_{in} can be found in (Cavaleri et al., 2007) cited above. Here we just refer to fig. 15 as an illustration of high dispersion of results given by different parametric formulas.

2.4. Wave dissipation

Wave dissipation is the most poorly understood term in the kinetic equation (4). The quasi-linear parameterization of whitecapping mechanism by (Hasselmann, 1974) is still the main model implemented in most of the wind-wave forecasting models. Alternative saturation-based whitecapping formulations have been proposed in (Alves & Banner, 2003, Westhuysen et al., 2007). Some other essentially nonlinear parameterizations of the term S_{diss} (Donelan & Pierson-jr., 1987, Phillips, 1985) are discussed predominantly in the context of research models.

Some problems of the original whitecapping parameterization were demonstrated by (Komen et al., 1984) for the balance of fully developed wind-driven sea. Nowadays, spectral wind-wave models use this parameterization in the following form

$$S_{diss}(f, \theta) = -C_{diss} g^{-\beta} \bar{\omega}^{-2\beta+1} m_0^{\beta/2} [\delta (\frac{\bar{\omega}}{\omega})^2 + (1-\delta)(\frac{\bar{\omega}}{\omega})^4] F(f, \theta) \tag{16}$$

where mean frequency $\bar{\omega}$ is defined as

$$\bar{\omega} = E \times \int_0^{+\infty} \int_{-n}^n (\omega^{-1} E(\omega, \theta) d\omega d\theta)^{-1} \tag{17}$$

for total wave energy

$$E = \int_0^{+\infty} \int_{-n}^n E(\omega, \theta) d\omega d\theta \tag{18}$$

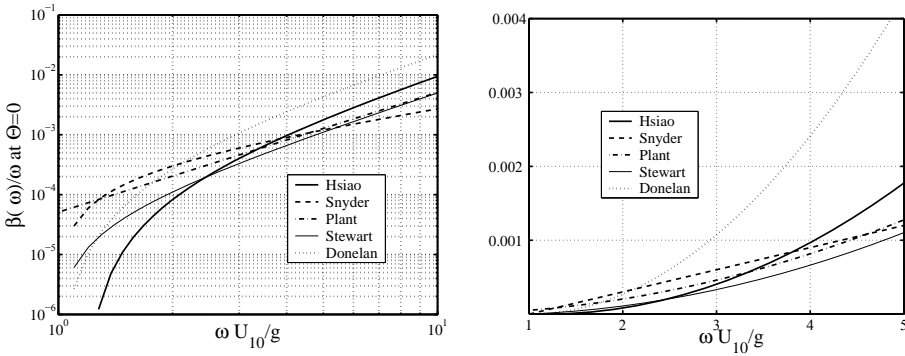


Fig. 1. Dependence of wind-wave growth rate on non-dimensional frequency $\frac{\omega U_{10}}{g}$ in log- and linear scales given by different experimental parameterizations (see legends).



$C_{diss}=4.5$ and $\delta=0.5$ are default values in the WAM-cycle 4 model (Günther et al., 1992, Komen et al., 1995) where the exponent $p=4$ is usually used. Recent studies (Korotkevich et al., 2008, Zakharov et al., 2007) rely on much sharper, threshold-like dependence on wave steepness $\mu=\bar{w}\sqrt{E}/g$, with $p>10$. According to (Zakharov et al., 2007), the whitecapping dissipation is overestimated in the WAM-cycle 3 and WAM-cycle 4 models. They propose the following parameters: $C_{diss}=0.11$, $\delta=0$ and $p=12$. The key message of such revision is high exponent p that models threshold-like dependence of dissipation on wave steepness μ . Note a “non-physical” feature of formula (16): it does not contain explicitly any small physical parameter while, logically, the term S_{diss} should be of the same order of value as other terms of the right-hand side of the kinetic equation (4). In our opinion, the dissipation term (16) should be regarded simply as a tuning formula for poorly determined physical term.

2.5. Self-similarity of wind driven seas

In this section we consider a way to resolve the problem of poorly determined terms S_{in} and S_{diss} . The happy chance is that the term of non-linear transfer S_{nl} appears to be the leading one in the right-hand side of (4).

2.6. On leading role of nonlinear transfer

As mentioned above the nonlinear interaction term S_{nl} can be derived from the first principles. According to (Zakharov, 1999) it can be written as

$$S_{nl} = F_{\mathbf{k}} - \Gamma_{\mathbf{k}} N_{\mathbf{k}} \tag{19}$$

where “nonlinear forcing” $F_{\mathbf{k}}$ and “nonlinear damping” $\Gamma_{\mathbf{k}} N_{\mathbf{k}}$ are

$$F_{\mathbf{k}} = n g^2 \int |T_{0123}|^2 N_1 N_2 N_3 \delta_{\mathbf{k}+\mathbf{k}_1-\mathbf{k}_2-\mathbf{k}_3} \delta_{\omega_{\mathbf{k}}+\omega_1-\omega_2-\omega_3} d\mathbf{k}_1 d\mathbf{k}_2 d\mathbf{k}_3$$

$$\Gamma_{\mathbf{k}} = n g^2 \int |T_{0123}|^2 (N_1 N_2 + N_1 N_3 + N_2 N_3) \delta_{\mathbf{k}+\mathbf{k}_1-\mathbf{k}_2-\mathbf{k}_3} \delta_{\omega_{\mathbf{k}}+\omega_1-\omega_2-\omega_3} d\mathbf{k}_1 d\mathbf{k}_2 d\mathbf{k}_3$$

Kernel $T_{\mathbf{k}, \mathbf{k}_1, \mathbf{k}_2, \mathbf{k}_3} = T_{\mathbf{k}_1, \mathbf{k}, \mathbf{k}_2, \mathbf{k}_3} = T_{\mathbf{k}, \mathbf{k}_1, \mathbf{k}_3, \mathbf{k}_2} = T_{\mathbf{k}_2, \mathbf{k}_3, \mathbf{k}, \mathbf{k}_1}$ is a homogeneous function of order 3, invariant with respect to rotation. Collection of its explicit (and very complicated) expressions can be found in (Badulin et al., 2005). In the most real simulations $F_{\mathbf{k}} \gg |S_{nl}|$ and $|\Gamma_{\mathbf{k}} N_{\mathbf{k}}| \gg |S_{nl}|$. These two great components of S_{nl} almost compensate each other. The Hasselmann equation in the form (19) shows a strong relaxation due to four-wave interactions “by itself” in absence of any external forcing. Thus, one should compare input and dissipation terms not with the total S_{nl} but with its separate components, say, the total source growth rate $\gamma_{\mathbf{k}} = \gamma_{in} - \gamma_{diss}$ with the decrement of nonlinear dissipation $\Gamma_{\mathbf{k}}$.

For infinitely narrow spectrum one can obtain very simple estimate

$$\Gamma_{\mathbf{k}} = 36n\omega(\omega/\omega_p)^3 \mu^4 \cos^2\Theta \tag{20}$$

that includes a huge enhancing factor $36n \approx 113.1$. A representative estimate of wind input increment by (Plant, 1982) gives

$$\gamma_{in} = 5.1 \cdot 10^{-5} \omega \left(\frac{U_{10} \bar{\omega}_p}{g} \right)^2 \left(\frac{\omega}{\omega_p} \right)^2 \tag{21}$$



Where U_{10} —wind speed at standard height 10 m above the sea surface. Two independent parameters—steepness μ_p and wind speed U_{10} determine the answer on relative balance of wave generation and nonlinear transfer. One gets from (20)

$$\Gamma_k / \gamma_{in} \approx 2.26 \cdot 10^5 \left(\frac{\omega}{\omega_p} \right) \mu_p^4 \left(\frac{U_{10} \omega_p}{g} \right)^{-2} \quad (22)$$

Let formally minimal value $\omega/\omega_p=1$ and $U_{10} \omega_p/g=2$. Even for the most aggressive wave input by (Plant, 1982) and rather young wind sea the nonlinear damping appears to be stronger than wind input for rather quiet sea ($\mu_p > 0.0365$).

2.7. Split balance model and weakly turbulent laws of wind wave growth

The fact of leading role of nonlinear transfer allows for constructing quite consistent asymptotic theory of wind-wave growth—the so-called split balance model (Badulin et al., 2005). In the lowest order of the theory the wave evolution is governed by nonlinear transfer only

$$\frac{dN_k}{dt} = S_{nl} \quad (23)$$

The conservative kinetic equation (23) requires a boundary condition to determine a unique solution. The formally small terms of external forcing (wave input and dissipation) allows for formulating such condition in the form of balance of integral quantities

$$d\langle N_k \rangle / dt = \langle S_{in} + S_{diss} \rangle \quad (24)$$

For deep water waves when the collision integral S_{nl} is homogeneous function of wave vector one can construct a family of self-similar solutions for two

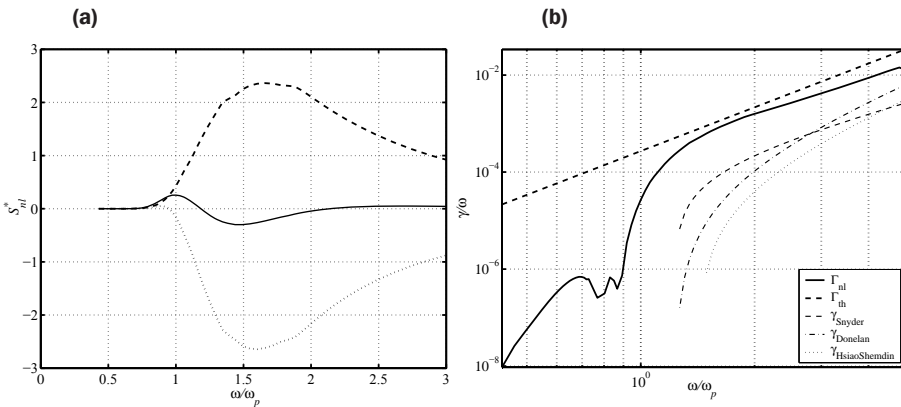


Fig. 2. (a) Decomposition of the collision integral S_{nl} (solid line) for the case by (Komen et al., 1984) into nonlinear forcing F_k (dashed) and damping γ_k (dotted) terms; (b) Nonlinear damping coefficient Γ_k given by theoretical estimate (20) and by the numerical simulation (dashed and solid bold curves, correspondingly). Conventional dependencies of wind growth increments (Donelan & Pierson-jr., 1987; Hsiao and O.H. Shemdin, 1983; Snyder, 1981) are shown by thin curves with authors' names in legend.



particular cases: duration-limited (spatially homogeneous growth) and fetch-limited (stationary spatial growth) when total input $\langle S_{in} + S_{diss} \rangle$ is a power-law function of duration or fetch. These solutions have forms of self-similarity of the second type when spectral shape is determined by an “internal” self-similar variable—non-dimensional frequency ω/ω_p and “external” dependence is specified by a power-law dependence on fetch or duration. Note, that it is consistent with conventional parameterizations, e.g. JONSWAP spectrum (Hasselmann et al., 1973) and its modifications (Donelan et al., 1992). The second self-similar argument in these parameterizations is wave age C_p/U_h , i.e.

$$E(\omega) = (C_p/U_h)^k \Phi(\omega/\omega_p). \tag{25}$$

The self-similar solutions of the split balance model (23, 24) do not contain wind speed explicitly. The key “external” self-similar argument of these solutions is determined by total wave input $\langle S_{in} + S_{diss} \rangle$ —spectral flux at infinitely high frequencies. The relationship between the spectral magnitude (total energy) and the total input appears to be similar to one for the stationary Kolmogorov-Zakharov solutions (11, 12). Thus, the split balance model allows one to propose *weakly turbulent law of wind wave growth* in the following form

$$\frac{E\omega_p^4}{g^2} = \alpha_{ss} \left(\frac{\omega_p^3 dE/dt}{g^2} \right)^{1/3} \tag{26}$$

Self-similarity parameter α_{ss} in (26) is an evident analogue of the Kolmogorov constants C_p, C_q in (11, 12) and depends slightly on exponents of self-similar solutions. Its numerical estimates are close to $\alpha_{ss} = 0.67 \pm 0.1$ (Gagnaire-Renou et al., 2010a). Formally, the law (26) is valid for cases with power-law dependence of total input $\langle S_{in} + S_{diss} \rangle$ on duration or fetch. In general case it can be used as well as an adiabatic relationship. This validity has been demonstrated for more than 20 experimental dependencies of wind wave growth (Badulin et al., 2007).

2.8. Reference cases of wind-wave growth

The split balance model in the form (23, 24) does not consider explicitly wind-wave coupling but operates with total net wave input only. At the same time, important results on the coupling can be obtained using the weakly turbulent law (26). Self-similar solutions of the split balance model predicts a family of power-law dependencies on non-dimensional fetch χ

$$\tilde{E} = E^0 \chi^{p_\chi}; \quad \tilde{\omega}_p = \omega_0 \chi^{-q_\chi} \tag{27}$$

or non-dimensional duration τ

$$\tilde{E} = E^0 \tau^{p_\tau}; \quad \tilde{\omega}_p = \omega_0 \tau^{-q_\tau} \tag{28}$$

Three sets of exponents $p_{\chi(\tau)}, q_{\chi(\tau)}$ in (27, 28) play special role. These exponents correspond to one-parametric dependencies of wave height on wave period

$$H \sim T^z$$



with exponents $z=5/3$ (Hasselmann et al., 1976), $z=3/2$ (Toba, 1972), $z=4/3$ (Dependence... 1983). The most known Toba's 3/2 law (Toba, 1972) being treated within the weakly turbulent law (26) shows stationarity of net energy input $dE/dt=const$. Using the Toba law in the form

$$H_s = B(gu_*^3)^{1/2} T_s^{3/2} \quad (29)$$

one can have from (26) immediately the energy rate

$$\frac{dE}{dt} = \frac{n^9 B^6 u_*^3}{8 \alpha_{ss}^3 g} = 0.16 \frac{\rho_a}{\rho_w} \frac{u_*^3}{\alpha_{ss}^3 g} \quad (30)$$

where $B=0.062$ is the Toba constant (Toba, 1972). Similarly, two other laws correspond to stationarity of wave input of wave momentum (Hasselmann et al., 1976, law 5/3) or wave action (Dependence... 1983, law 4/3). Estimate of energy input give the following result:

$$\frac{dE}{dt} = 7.7 \cdot 10^{-3} \frac{\rho_a}{\rho_w} \frac{C_p u_*^2}{\alpha_{ss}^3 g} \quad (31)$$

for regime of constant in time production of wave momentum. Note, that the wave momentum can be associated quite naturally with turbulent wind stress $\tau_w = \langle u'w' \rangle$.

The evolution of relatively old wind waves is provided by constant production of wave action and is decaying with wave age

$$\frac{dE}{dt} = 1.6 \cdot \frac{\rho_a}{\rho_w} \frac{u_*^4}{C_p \alpha_{ss}^3 g} \quad (32)$$

Summarizing results of the section emphasize fruitfulness of general approach to the wave description. It gives valuable estimates of wave parameters in terms of self-similar solutions and, moreover, allows specify parameters of wind-wave coupling as it is made here for reference cases (30–32).

3. The theory of wave turbulence and wind-wave forecasting

The theory and forecasting of waves develop, to a considerable degree, independently. In addition to theoretical basics the wave forecasting uses extensively advanced technologies of data assimilation, remote and in situ measurements. In many cases, these technologies force out the physically consistent modeling. Two cases given below show how the correct theoretical vision can help in physical analysis and in improvement the wind wave forecasting.

3.1. Example 1: anomalously strong relaxation in the mixed sea

Usually wave field in the ocean is a superposition of waves generated by local wind and of remotely generated swell. This case, the so-called mixed sea, is of special theoretical and practical interest. Special methods are developed for discriminating the observed wave field into two components: wind waves and swell. Theoretical description of the state is also not trivial as far as swell and wind waves evolve at essentially different spatio-temporal scales and the physical mechanisms of their coupling with wind are also quite different. Very interesting effects of the mixed sea state (Kahma & Pettersson, 1994,



Nguy, 1998, Pettersson, 2004, Young, 2006) can be treated adequately within the presented statistical approach and the concept of dominating nonlinear transfer.

In Fig. 3 results of numerical simulation of the mixed wind sea are presented. Initial two-mode spectrum consists of a strong swell with period about 10 s and relatively weak wind component with period 5 s. Anomalously fast relaxation of the wind-driven component is clearly seen at timescales of first hundreds of wave periods. This timescale can be estimated adequately by formula (20): the effect of low frequency swell enhances relaxation by non-dimensional factor ω/ω_p , while steep young wind waves gives additional effect by factor μ_p^4 . As a result, the anomalously fast absorption of wind waves by swell occurs. These effects were reported in (Kahma & Pettersson, 1994, Pettersson, 2004) for Baltic Sea where quite often wind waves follow preferential directions associated with swell.

3.2. Example 2: wind waves in Tallinn Bay

As the second example of adequate use of the statistical approach consider the regional wave model developed for Tallinn Bay in Tallinn University of Technology (Soomere, 2005). This model was created on the basis of

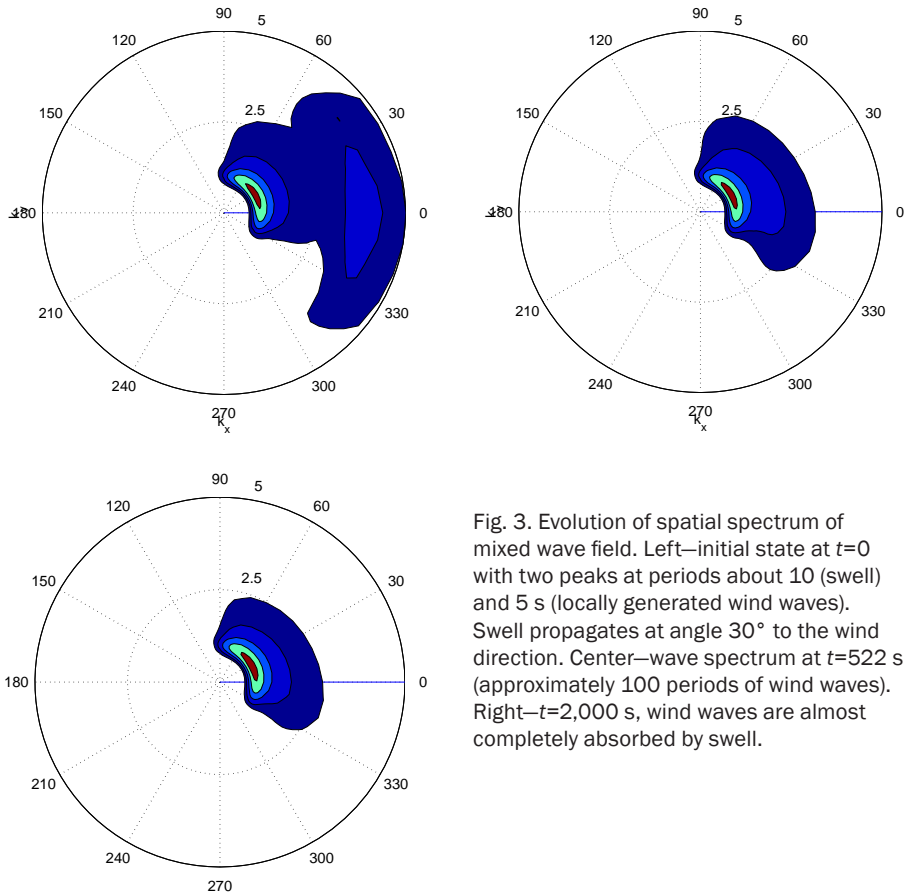


Fig. 3. Evolution of spatial spectrum of mixed wave field. Left—initial state at $t=0$ with two peaks at periods about 10 (swell) and 5 s (locally generated wind waves). Swell propagates at angle 30° to the wind direction. Center—wave spectrum at $t=522$ s. (approximately 100 periods of wind waves). Right— $t=2,000$ s, wind waves are almost completely absorbed by swell.



an international standard of wave forecasting models—WAM (WAve Model) (Komen et al., 1995). The construction of any wave model for such small basin as Tallinn Bay is accompanied by a number of questions. The first one is on adequacy of the statistical approach itself for the case when spatial scales numbers a few hundreds of wavelengths only. Fortunately, it works in a majority of cases quite well. Two assumptions accepted in (Soomere, 2005) take into account specific physics of wind wave field. First, wind field is considered as homogeneous in the bay and local wave field is not affected by remote wave field. The second assumption is not so evident but it allows one to predict wave field quite good at reasonable computational efforts: the wave field is considered as independent on previous history, as a sort of saturated state. The model showed its ability for analysis of long-term and climatic features in the closed basin of Tallinn Bay. Implicitly, the success of this modeling justify our above conclusion: the relaxation of wave field due to nonlinear wave-wave interactions is quite strong. The details of wave input and dissipation appear to be of secondary importance.

4. Concluding remarks

In this lecture we presented ideas rather than ready-to-use recipes and recommendations for modeling wave field in near-shore zone. At the same time, asymptotic split balance model has been given as a tool of transparent physical analysis. Basing on hypothesis of dominating nonlinear transfer we obtained explicit formulas for the rate of nonlinear damping (20) and estimates of wave input due to wind (30–32). Examples of the last section show adequacy of these simple relationships. The list of references is an essential part of this lecture and should be used for further progress in wave studies. Our lecture shows that in the near-shore dynamics is not a collection of a great number of methods, physical factors etc. It can contain, as in case of wave studies, surprisingly transparent physics and, thus, is very attractive for young researchers.

References

- Alves, J. H. G. M. & Banner, M. L. (2003) Performance of a saturation-based dissipation-rate source term in modeling the fetch-limited evolution of wind waves. *JPO* **33**:1274–1298.
- Badulin, S. I., Babanin, A. V., Resio, D., Zakharov, V. (2007) Weakly turbulent laws of wind-wave growth. *J. Fluid Mech.* **591**:339–378.
- Badulin, S. I., Pushkarev, A. N., Resio, D., Zakharov, V. E. (2005) Self-similarity of wind-driven seas. *Nonl. Proc. Geophys.* **12**:891–946.
- Cavaleri, L., Alves, J. H. G. M. et al. (2007) Wave modelling—the state of the art. *Progr. Ocean.* **75**.
- Dependence of wave parameters on the wind velocity, duration of its action and fetch in the weak-turbulence theory of water waves (1983) *Izv. Atmos. Ocean. Phys.* **19**, No. 4:300–306.
- Donelan, M. A. & Pierson-jr., W. J. (1987) Radar scattering and equilibrium ranges in wind-generated waves with application to scatterometry. *J. Geoph. Res.* **92**, No. C5:4971–5029.
- Donelan, M., Skafel, M., Graber, H. et al. (1992) On the growth rate of wind-generated waves. *Atmosphere Ocean* **30**, No. 3:457–478.



- Gagnaire-Renou, E., Benoit, M., Badulin, S. I. (2010a) On weakly turbulent scaling of wind sea. *JFM*, submitted.
- Gagnaire-Renou, E., Benoit, M., Forget, P. (2010b) Ocean wave spectrum properties as derived from quasi-exact computations of nonlinear wave-wave interactions. *JGR*, No. doi:10.1029/2009JC005665.
- Günther, H., Hasselmann, K., Janssen, P. A. E. M. (1992) *The WAM model Cycle 4 (revised version)*, Tech. Rep. 4. Deutsch. Klimatol. Rechenzentrum. Germany: Hamburg, No. 4.
- Hasselmann, K. (1962) On the nonlinear energy transfer in a gravity wave spectrum. Part I. General theory. *J. Fluid Mech.* **12**:481–500.
- (1963a) On the nonlinear energy transfer in a gravity wave spectrum evaluation of the energy flux and swell-sea interaction for a Neumann spectrum. P. 3. *J. Fl. Mech.* **15**:385–398.
- (1963b) On the nonlinear energy transfer in a gravity wave spectrum. P. 2. Conservation theorems; wave-particle analogy; irreversibility. *J. Fl. Mech.* **15**:273–281.
- (1974) On the spectral dissipation of ocean waves due to white capping. *Boundary-Layer Meteorol.* **6**:107–127.
- Hasselmann, K., Barnett, T. P., Bouws, E. et al. (1973) Measurements of wind-wave growth and swell decay during the Joint North Sea Wave Project (JONSWAP). *Dtsch. Hydr. Zeitschr. Suppl.* **12**, No. A8.
- Hasselmann, K., Ross, D. B., Müller, P., Sell, W. (1976) A parametric wave prediction model. *J. Phys. Oceanogr.* **6**:200–228.
- Hsiao, S. V. & Shemdin, O. H. (1983) Measurements of wind velocity and pressure with a wave follower during MARSEN. *J. Geophys. Res.* **88**, No. C14:9841–9849.
- Janssen, P. A. E. M. (1989) Wave-induced stress and the drag of air flow over sea waves. *J. Phys. Oceanogr.* **19**:745–754.
- Kadomtsev, B. B. (1976) *Collective phenomena in plasma*. Moscow: Nauka.
- Kahma, K. K. & Pettersson, H. (1994) Wave growth in a narrow fetch geometry. *Global Atmos. Ocean Syst.* **2**:253–263.
- Komen, G. J., Cavaleri, L., Donelan, M. et al. (1995) *Dynamics and modelling of ocean waves*. Cambridge University Press.
- Komen, G. J., Hasselmann, S., Hasselmann, K. (1984) On the existence of a fully developed wind-sea spectrum. *J. Phys. Oceanogr.* **14**:1271–1285.
- Korotkevich, A. O., Pushkarev, A. N., Resio, D., Zakharov, V. E. (2008) Numerical verification of the weak turbulent model for swell evolution. *Eur. J. Mech. B/Fluids* **27**, No. 361, doi:10.1016/j.euromechflu.2007.08.004.
- Krasitskii, V. P. (1994) On reduced Hamiltonian equations in the nonlinear theory of water surface waves. *J. Fluid Mech.* **272**:1–20.
- Lighthill, J. (1978) *Waves in fluids*. Cambridge University Press.
- Nguy, Dung (1998) *Observations on the directional development of wind-waves in mixed seas*. MSc in Mech. Eng., Univ. of Washington. Tech. Rep. APL-UW-TR9802.
- Nordheim, L. W. (1928) On the kinetic method in the new statistics and its applications in the electron theory of conductivity. *Proc. Roy. Soc. Lond. A* **119**:689–698.
- Pettersson, Heidi (2004) *Wave growth in a narrow bay*, Ph. D. thesis. University of Helsinki.
- Phillips, O. M. (1985) Spectral and statistical properties of the equilibrium range in wind-generated gravity waves. *J. Fluid Mech.* **156**:505–531.



- Plant, W.J. (1982) A relationship between wind stress and wave slope. *J. Geophys. Res.* **87**, No. C3:1961–1967.
- Snyder, R. L., Dobson, F. W., Elliot, J. A., Long, R. B. (1981) Array measurements of atmospheric pressure fluctuations above surface gravity waves. *J. Fluid Mech.* **102**: 1–59.
- Soomere, T. (2005) Wind wave statistics in Tallinn Bay. *Boreal Env. Res.* **10**:103–118.
- Stewart, R. W. (1974) The air-sea momentum exchange. *Bound.-Layer Meteor.* **6**:151–167.
- Toba, Y. (1972) Local balance in the air-sea boundary processes. I. on the growth process of wind waves. *J. Oceanogr. Soc. Japan* **28**:109–121.
- Westhuysen, A.J. van der, Zijlema, M., Battjes, J. A. (2007) Nonlinear saturation-based whitecapping dissipation in SWAN for deep and shallow water. *CE* **454**:151–170.
- Whitham, G. B. (1974) *Linear and nonlinear waves*. New York: Wiley.
- Young, I. R. (2006) Directional spectra of hurricane wind waves. *J. Geophys. Res.* **111**, doi:10.1029/2006JC003540.
- Zakharov, V. E. (1966) *Problems of the theory of nonlinear surface waves*, Ph.D. thesis. Novosibirsk: Budker Institute for Nuclear Physics.
- (1999) Statistical theory of gravity and capillary waves on the surface of a finite-depth fluid. *Eur. J. Mech. B/Fluids* **18**:327–344.
- Zakharov, V. E., Falkovich, G., Lvov, V. (1992) *Kolmogorov spectra of turbulence*. Part I. Berlin: Springer.
- Zakharov, V. E. & Filonenko, N. N. (1966) Energy spectrum for stochastic oscillations of the surface of a fluid. *Soviet Phys. Dokl.* **160**:1292–1295.
- Zakharov, V. E., Korotkevich, A. O., Pushkarev, A. N., Resio, D. (2007) Coexistence of weak and strong wave turbulence in a swell propagation. *Phys. Rev. Lett.* **99**, No. 164501.
- Zakharov, V. E. & Zaslavsky, M. M. (1982) The kinetic equation and Kolmogorov spectra in the weak-turbulence theory of wind waves. *Izv. Atmos. Ocean. Phys.* **18**: 747–753.

Simulation of wind waves in coastal shallow zone

Ilia Kabatchenko, Mikhail Reznikov

Abstract

A numerical simulation of Korteweg-de Vries (KdV) equation for wind waves in coastal seas is proposed. The numerical simulation uses a scheme of “Cabaret” in the version—against the flow. The selected numerical scheme proved to be as stable and dissipation free. The numerical results are in good agreement with well-known analytical KdV solutions. The modelling shows that the evolution of wind waves, described by the KdV equation in shallow coastal zone is generally consistent with predictions of the theory of three-wave interactions in the spectrum of wind waves.

В работе предложена численная реализация уравнения Korteweg-де Вриза (КдВ) для ветрового волнения в прибрежной зоне моря. При численном моделировании использована схема «Кабаре» в варианте — против потока. Выбранная численная схема показала себя как устойчивая и бездиссипативная. Полученные результаты хорошо согласуются с известными аналитическими решениями КдВ. Выполненные численные расчеты показали, что характер эволюции ветрового волнения, описываемый уравнением КдВ, в зоне прибрежного мелководья в целом соответствует характеру, предсказанному теорией трехволновых взаимодействий в спектре ветрового волнения.

1. Introduction

In the deep water in modeling of wind waves traditionally used Hasselman’s kinetic equation (The WAM Model, 1988) for wind wave directional spectrum. Using this equation for the coastal transformation zone encounters well-known difficulties. An alternative spectral approach in the coastal zone is a return to the dynamic equations. This zone is located at depths ranging from 3 to 30 m.

2. Results

In this work, the coastal shallows proposed calculation of wave surface on the model of Korteweg-de Vries (Korteweg, de Vries, 1895):

Ilia Kabatchenko, Mikhail Reznikov (✉)
N.N. Zubov’s State Oceanographic Institute, Moscow, Russia



$$\frac{\partial \xi}{\partial t} + c_0 \frac{\partial \xi}{\partial x} + 1.5 \frac{c_0}{D} \xi \frac{\partial \xi}{\partial x} + \frac{c_0 D^2}{6} \frac{\partial^3 \xi}{\partial x^3} = 0, \quad (1)$$

where ξ —the wave surface elevation, $c_0 = (gD)^{0.5}$ —phase velocity of long waves, D —depth, x —spatial coordinate, t —time.

In the numerical solution of (1) uses “Cabaret” scheme in option “against the flow” (Golovizin et al., 2000).

One possible solution to the KdV equation is a solitary soliton:

$$\xi(x, t) = A \cosh^{-2} \left(\frac{x - At/3}{L} \right), \quad (2)$$

$$L = \sqrt{12\beta/A},$$

where A —amplitude of the soliton, L —effective width of its base. The numerical experiment soliton moved in a circular basin with a length of 1 km. The first and last points of the basin were connected. Fig. 1 shows the two soliton: the original (solid line) and the resulting solutions of the KdV equation after the soliton has passed the basin more than 1.2 km for 1,300 time steps. In the numerical solution used by 100 points on the x -axis in steps of 10 m and discrete time, equal to 0.5.

Along with the solution in the form of a soliton of the KdV equation there is a periodic solution. Fig. 2 shows the elevation of wave surface ξ over the flat bottom with a depth of 10 m. In the numerical solution used 80 points on the x -axis in steps of 10 m and a discrete time, equal to 0.5.

Fig. 3 shows the distortion of the spectrum of wind waves after the passage of wind waves over the bar from the top of the depth equal to 3 m. The calculation is performed by the KdV model. The horizontal dimensions of the bar—400 m, c bottom slope $s=0.035$. Note the strong distortion of the original spectrum and the appearance of a large number of secondary

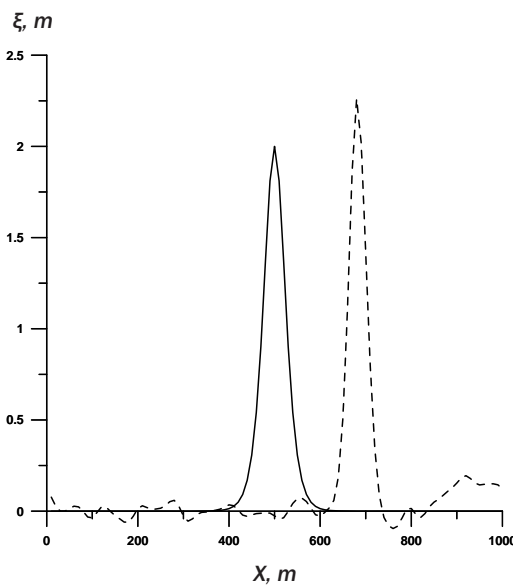


Fig. 1. The distortion of the soliton after the passage of 1,300 time steps (solid line—the original soliton, dotted line—the result of solving KdV).

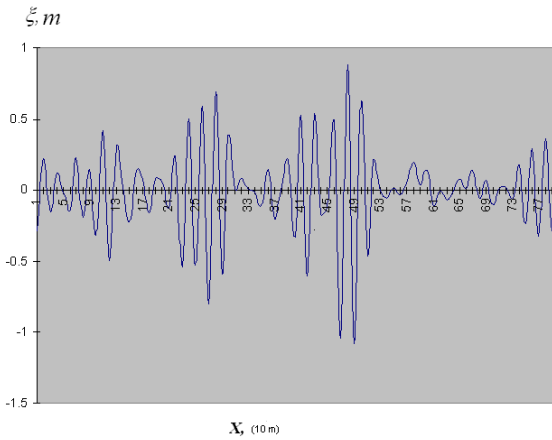


Fig. 2. The ordinates of the wave surface of the flat bottom with a depth of 10 m.

maxima, especially at low frequencies. This type of distortion of the spectrum in shallow water predicted by the theory of three-wave interactions (see, for example (Zaslavsky et al., 1995)). The significant difference solution obtained by the KdV from that obtained by the model (Zaslavsky et al., 1995), is that in (Zaslavsky et al., 1995) three-wave interactions are tied to a specific depth. And if the depth after the bar increases, the secondary maxima were not saved. As part of the KdV equation obtained over the bar distortion of the spectrum are carried on at a relatively deep area of water area.

3. Conclusions

A numerical version of the KdV equation for wind waves is used in the coastal zone of the sea on a “Cabaret” scheme in option “against the flow”. The selected numerical scheme proved itself as a stable and dissipation free.

The evolution of wind waves, described by the KdV equation in shallow coastal zone is generally consistent with the nature, theory predicts the three-wave interactions in the spectrum of wind waves.

This work was supported by RFBR projects No. 09-05-00857.

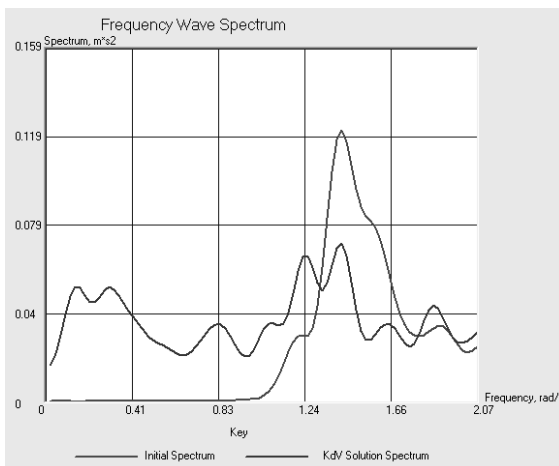


Fig. 3. The distortion of the spectrum of wind waves after the passage of the irregular waves over an underwater bar, obtained by solving the KdV equation.



References

- Golovizin, V. M., Karabasov, S. A., Suhodulov, D. A. (2000) A variational approach to the difference scheme with spatially split time derivative for the equation of Korteweg-de Vries. *Mathematical modeling* **12(4)**:105–116.
- Korteweg, D. J. & de Vries, G. (1895) On the change of form of long waves advancing in a rectangular canal and a new type of long solitary waves. *Phil. Mag.* (5), 39, 422.
- The WAM Model (1988) A third generation ocean wave prediction model. The WAM-DI Group. *J. Phys. Ocean.* Vol. **18**.
- Zaslavsky, M. M. & Krasitsky, V. P. (1995) Relationship of observed and weakly turbulent spatial spectra of surface gravity waves. In: *Problems of research and mathematical modeling of wind waves*, 155–182. St.-Petersburg: Gidrometeoizdat.

Irregular waves transformation in a coastal zone

Sergey Kuznetsov

Abstract

In the lecture the visible phenomena's, arising in result of nonlinear, dissipative and dispersive mechanisms of transformation of individual waves and their group structure in a coastal zone are considered in details by methods of spectral, bispectral and wavelet analysis. By numerical and physical modeling the observed effects (alignment of heights of waves, formation of secondary waves, a periodic exchange of energy between the first and second harmonics, nonlinear expansion of a wave spectrum, paradox of an abnormal dispersion of waves and others) are interpreted and explained from the physical point of view.

В лекции на основе анализа многочисленных экспериментальных данных подробно изложены видимые проявления нелинейных, диссипативных и дисперсионных механизмов трансформации индивидуальных волн и их групповой структуры в береговой зоне моря. Наблюдающиеся эффекты (выравнивание высот волн, образование вторичных волн, периодический обмен энергией между первыми и вторыми гармониками, нелинейное расширение спектра волн, парадокс аномальной дисперсии волн и другие) проинтерпретированы путем численного моделирования и дано их физическое объяснение.

Sergey Kuznetsov (✉)
P. P. Shirshov Institute of Oceanology RAS, Moscow, Russia
e-mail: Kuznetsov@ocean.ru

Wave-induced circulation in porous media

Stanisław Massel

Abstract

Water flow through the beach body is of great importance for introducing water, organic materials and oxygen to the ground environment as well as for sediment transport and coastal structure stability and modern beach nourishment techniques. To explain the nature of the pore-pressure and resulting velocity circulation, an exact close-form solution based on the Biot theory for multiphase flow has been developed. This solution takes into account soil deformations, volume change and pore-water pressure. As the experimental estimation of infiltration into beach sand is very difficult to carry out under real sea conditions, a controlled, almost full-scale experiment was carried out in the Large Wave Channel in Hannover (Germany) on a natural beach sand with the mean diameter of fine grained sand was used and a uniform beach with a 1/20 slope was created in the channel.

Поток воды через пористое тело пляжа играет большую роль для транспорта органического материала и кислорода в грунт. Влияет он также на поток наносов и стабильность береговых сооружений. Для выяснения процесса затухания давления пористых вод и циркуляции, вызванной градиентами давления, была построена теоретическая модель, основанная на теории мульти-фазных сред Бёта. Теоретические результаты были сравнены с результатами эксперимента в большом волновом канале (Ганновер, Германия). Масштаб эксперимента был очень близок натурным условиям. Результаты эксперимента оказались очень похожими на результаты расчета по теории Бёта.

1. Introduction

Permeable sands are most common in the coastal environment and relict sands cover approximately 70 percent of the continental shelves. In particular, large volumes of sea water, driven by wave energy, are filtered by sandy beaches, and during this process the microfauna of the porous sand body

Stanisław Massel (✉)
Institute of Oceanology, Sopot, Poland
e-mail: smas@iopan.gda.pl



mineralize organic materials in the water and recycle nutrients. High nutrient concentrations boost phytoplankton growth to generate about 30 percent of the total oceanic primary production in a zone covering less than 10 percent of the World Ocean (Huettel & Rusch, 2000). Although the biodiversity and biomass of organisms within the beach body are low, it has been shown that marine sands transfer energy very effectively (Węśławski et al., 2000).

The velocity of flow as well as the amount of water circulating within the permeable beach body is important for the biological status of the organisms inhabiting the beach sand. Wave-induced pressure and stresses in seabed are also important with regard to beach protection, design of foundations for gravity-type breakwaters and offshore oil storage tanks. They are the key elements when one considers the problem of flotation of buried pipelines and the burial of rubble mounds, tetrapods and other blocks by waves.

For tideless seas the groundwater flow is governed entirely by the surface wave dynamics on the beach. As waves propagate towards the shore, they become steeper owing to the decreasing water depth and at some depth, the waves lose their stability and start to break. When waves break, wave energy is dissipated and the spatial changes of the radiation stress give rise to changes in the mean sea level (MSL), known as the set-up. Longuet-Higgins (1983) demonstrated that the mean on-shore pressure gradient due to wave set-up drives a groundwater circulation within the beach zone. Water infiltrates into the coastal aquifer on the upper part of the beach near the maximum run-up, and exfiltration occurs on the lower part of the beach face near the breaking point.

As the precise estimation of the extent of run-up, induced infiltration in beach sand, and groundwater table variation are very difficult to carry out under real sea conditions, a controlled large-scale laboratory experiment was performed in the Large Wave Channel (GWK) at the Coastal Research Centre (FZK) in Hannover (Germany). The GWK provides a unique opportunity for such an experiment. The simulation of regular and random waves with prescribed spectra yields a very realistic pattern of the sea surface. Moreover, the excellent testing facilities help substantially in recording the extent of run-up on the beach face, its velocity, and the amount of water infiltrating into the beach body (Massel et al., 2004).

The aim of this paper is to describe the technology used in the experiment and to report some preliminary results. Moreover, a theoretical comprehensive analysis of wave-induced pressure and groundwater circulation based on Biot's linearized theory, which takes into account soil deformations, volume change and pore-water flow, is given.

2. Methods

2.1. Experiments in the Large Wave Channel (LWK)

The experiments reported here were carried out in the largest channel in Europe—the Large Wave Channel (GWK—Grosser Wellenkanal) in Hannover (Germany). The channel is 307 m long, 5 m wide and 7 m (Fig. 1). The installed power of the piston type wave generator combined with an upper flap



Fig. 1. Large Wave Channel in Hannover.



is about 900 kW. The gearwheel driven carrier gives a maximum stroke of ± 2.10 m to the wave paddle.

The stroke can be superimposed by an upper flap oscillating within ± 10 degrees in order to simulate shorter wave kinematics more accurately. As a result, waves (regular and irregular) up to a height of 2.0 m can be simulated.

During the experiment, a water depth of 4 m in front of the beach was assumed. Natural beach sand was used and a uniform beach with a 1:20 slope was created in the channel. To measure the pore water pressure, four systems of pressure gauges were installed along the beach face (Fig. 2).

In each system, four piezoelectric pressure sensors were fixed to a metal rod arranged in the form of a cross. Such an arrangement provides an opportunity to estimate not only the pore pressure, but also the horizontal and vertical water velocities in the beach body. The pore pressure System 1 was located at the waterline, while Systems 3 and 2 were in the run-up and run-down zone, respectively. Additionally, System 4 was placed in front of the breaking zone, where set-up due to radiation stress was not observed.

During experiments two types of pore pressure were distinguished in the observed experimental data. In the zone of non-breaking waves (System 4), only the so-called phase-resolving type of pore pressure exists when the pore pressure responds almost instantaneously to surface wave oscillations (Fig. 3).

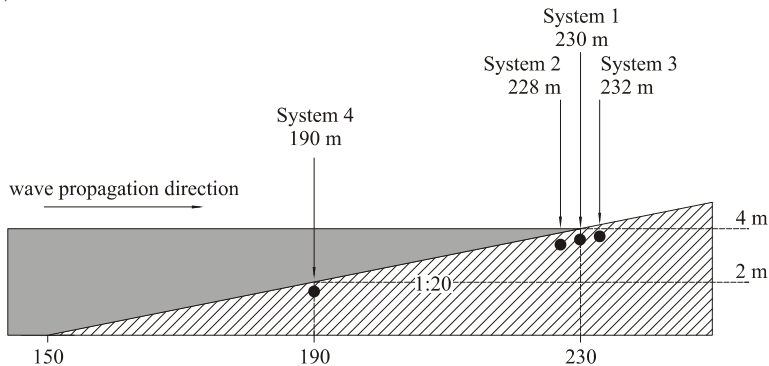


Fig. 2. Location of the pore pressure gauges on the sand beach.

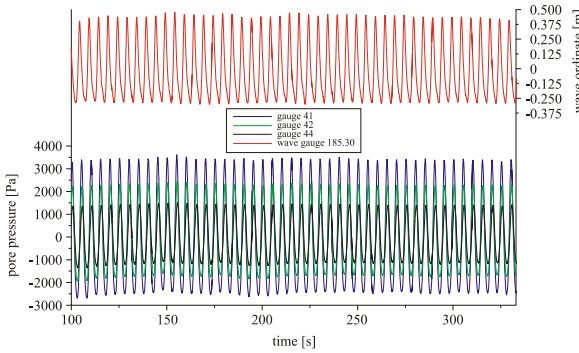


Fig. 3. Wave surface and pore pressure oscillations in System 4 (Test 25 ($H=0.7$ m, $T=5.0$ s)).

On the other hand, two types of pore pressure are generated in the surf zone. Apart from the phase-resolving pore pressure component, a slowly varying pore pressure component is observed. This component is called the phase-averaged pressure when the pressure slowly increases from the initial zero value to some asymptotic value as a result of wave action (Fig. 4).

2.2. Governing equations for wave-induced pressure and groundwater circulation

Let us now summarize briefly the wave-induced flow and stresses in a porous elastic medium using Biot's theory. It is assumed that the sand is isotropic and the flow is two-dimensional in the plane $(0, x, z)$. The origin of the Cartesian coordinates (x, z) is fixed on the mean free surface ($z=0$) and z is positive upwards. The water depth is h and the depth of the nonpermeable bottom is h_n . Thus, the thickness of the permeable layer is $(h_n - h)$. Moreover, that the coefficient of permeability and the porosity of sand are K_f and n , respectively.

We are interested in the small strains in soils, and particular soil grains are assumed to be incompressible, i.e. density of soil $\rho_s = \text{constant}$. However, the soil matrix can still be compressible. In shallow water, due to possible wave breaking and the entrance of gases into the porous media and the production of gases by the organisms living in the sand, the apparent bulk modulus of the pore water E'_w depends on the degree of saturation by water S . In the relationship proposed by Verruijt (1969) we write:

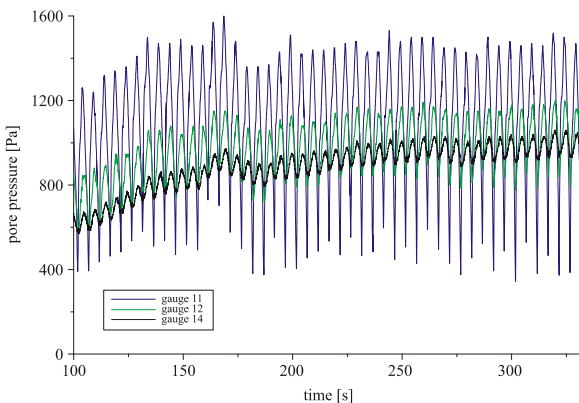


Fig. 4. Pore pressure oscillation in System 1 (Test 25 ($H=0.7$ m, $T=5.0$ s)).



$$\frac{1}{E'_w} = \frac{S}{E_w} + \frac{1-S}{p_0} \quad (1)$$

where E'_w is the true bulk modulus of pore water without air and is equal to 1.9×10^9 N/m², $(1-S)$ is the degree of saturation by air, usually less than one, and p_0 is the absolute pressure.

From the effective stress concept and Hooke's law we obtain the following equations of equilibrium (Massel et al., 2005):

$$G \nabla^2 \xi + \frac{G}{1-2\nu} \frac{\partial \varepsilon}{\partial x} = \frac{\partial p}{\partial x}, \quad (2)$$

$$G \nabla^2 \eta + \frac{G}{1-2\nu} \frac{\partial \varepsilon}{\partial z} = \frac{\partial p}{\partial z},$$

in which ν is the Poisson ratio, ξ and η are the x and z components of the soil displacement, respectively, G is the shear modulus of the soil and ε is the volume strain for the two-dimensional problem. The pore water pressure satisfies the continuity equation:

$$\nabla^2 p = \frac{\gamma}{K_f} \left[\frac{n}{E'_w} \frac{\partial p}{\partial t} + \frac{\partial \varepsilon}{\partial t} \right]. \quad (3)$$

Eqs. (2) and (3) form a system of three partial differential equations for three unknowns: p , ξ and η . To solve them we need to formulate appropriate boundary conditions. At the sea bottom line ($z=-h$), the boundary conditions should express the physical fact that the effective vertical stress is zero, the shear stress is negligible and that wave-induced pressure fluctuations exists. We assume that the bed rock at $z=-h_n$ is impermeable and rigid. Thus, soil displacements at this boundary are zero and no flow across the boundary is allowed, i.e.:

$$\xi = \eta = 0, \quad (4)$$

$$\frac{\partial p}{\partial z} = 0, \quad (5)$$

For the boundary condition, periodic both in time and space, we assume that the soil displacements ξ , η and pore pressure p are also periodic in time and space.

Massel et al. (2005) formulated a close form solution for arbitrary values of the stiffness ratio, G/E'_w of porous media. It was shown that for completely saturated coarse soils ($G/E'_w \rightarrow 0$) the pressure attenuation is very small and independent of the soil permeability, i.e.:

$$\nabla^2 p = 0, \quad (6)$$

In the other extreme case, when dense sand is saturated with a mixture of liquid and gas, the stones of the soil becomes much larger than that of the pore fluid, i.e. ($G/E'_w \rightarrow \infty$). Thus, the equation for pore pressure takes the form:

$$\nabla^2 p - \frac{n\gamma}{K_f E'_w} \frac{\partial p}{\partial t} = 0. \quad (7)$$



Above equation has the following solution:

$$p(x, z, t) = \Re \{ P(z) \exp[i(kx - \omega t)] \}, \quad (8)$$

in which:

$$P(z) = P_0 \frac{\cosh \psi(z+h_n)}{\cosh \psi(h_n+h)}. \quad (9)$$

and

$$\psi^2 \approx \psi_1^2 = k^2 \left[1 - i \frac{n\omega\gamma}{k^2 K_f E'_w} \right]. \quad (10)$$

The general solution for arbitrary soil stiffness takes the form of eq. (8) with the following pressure function $P(z)$:

$$\begin{aligned} P(z) = & c_1 P_0 \frac{\cosh k(z+h_n)}{\cosh kh_n} - c_2 P_0 \frac{\sinh k(z+h_n)}{\sinh kh_n} \\ & - c_3 P_0 \frac{z+h}{h} \frac{\cosh k(z+h_n)}{\cosh kh_n} + c_4 P_0 \frac{z+h}{h} \frac{\sinh k(z+h_n)}{\sinh kh_n} \\ & - c_5 P_0 \frac{\cosh \psi(z+h_n)}{\cosh \psi h_n} + c_6 P_0 \frac{\cosh \psi(z+h_n)}{\cosh \psi h_n}, \end{aligned} \quad (11)$$

in which:

$$\psi^2 = k^2 \left\{ 1 - i \frac{\omega\gamma}{k^2 K_f} \left[\frac{n}{E'_w} + \frac{1}{G} \frac{1-2\nu}{2(1-\nu)} \right] \right\}. \quad (12)$$

3. Results

During a controlled large-scale laboratory experiment carried out in Large Wave Channel in Hannover, an extensive data set was collected. The stiffness ratio G/E'_w varied between 50 and 400. It was shown that for $G/E'_w > 50$, the vertical distribution of the pore pressure was very close to the distribution given by Eq. (7), identical to the solution obtained by Moshagen & Tørum (1975) when the soil is rigid and the fluid is compressible. This is illustrated in Figs. 5 and 6. In Fig. 5 the vertical distribution of the amplitude of the pore-water pressure for both special cases resulting from Eqs. (6) and (7) are shown for short waves (Test 10: period $T=5$ s, incident wave height $H_{in}=0.3$ m). The attenuation of pore-water pressure for the case of fully saturated soils (eq. (6)) is small and independent of the soil permeability. On the other hand the soil is partly saturated with a mixture of water and gas (eq. (9)), pore pressure attenuates very rapidly. In the same figure, the full solution (11) for Test 10 with the stiffness ratio $G/E'_w \approx 78$ is shown. Solution (11) is very close to the solution for a partly saturated soil when $G/E'_w \rightarrow \infty$ and compares very well with the experimental data.

The results for the case of longer waves (Test 2: period $T=8$ s and incident wave height $H_{in}=0.5$ m) is demonstrated in Fig. 6. Now the stiffness ratio $G/E'_w \approx 134$ and the pore pressures resulting from solutions (9) and (11) are almost identical.

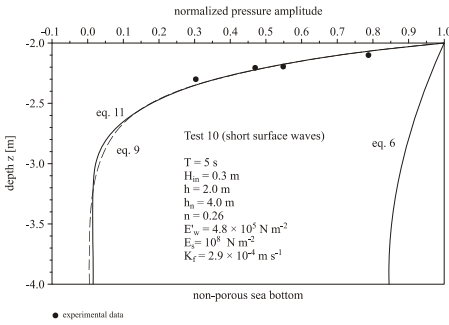


Fig. 5. Comparison between experiment and theory with respect to pore pressure for short surface waves.

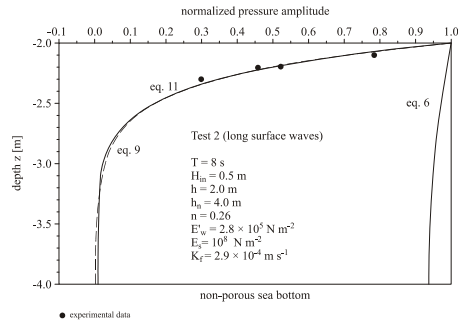


Fig. 6. Comparison between experiment and theory with respect to pore pressure for long surface waves.

4. Discussion

Theoretical results are dependent on the values of coefficient K_f and saturation level S . The filtration coefficient K_f was obtained from the well-known Hazen formula (Massel, 2001):

$$K_f \approx 0.5D_{10}^2, \quad (13)$$

in which K_f is in meters per second and the characteristic diameter D_{10} is in centimeters. Using $D_{10} = 2.1 \times 10^{-2} \text{ cm}$ (Massel et al., 2004), we obtain $K_f \approx 2.2 \times 10^{-4} \text{ ms}^{-1}$, which is very close to the value obtained in the laboratory test.

The degree of saturation of air in the pore water was not measured directly in the experiments, but the apparent bulk modulus of water E'_w was estimated from the best fit of the experimental pore pressures to the theoretical ones. The comparison made for all 23 tests showed that $4 \times 10^5 \text{ Nm}^{-2} \leq G/E'_w \leq 1.6 \times 10^6 \text{ Nm}^{-2}$. Using these values in eq. (1) yields a very high degree of saturation by air. However, sand used in the experiment cannot be regarded exactly as natural sand as was assumed in Verruijt's (1969) formula. It is very probable that during sand layering in the wave channel, some pores within the beach body will be saturated by air/gas microbubbles. From extensive field measurements of wave-induced pore pressure for water depths of approximately 5–10 m and to a depth of approximately 18 m below the sea bottom carried out by de Rouck & Troch (2002), it follows that there was approximately three percent gas in the soil pores. However, in laboratory conditions, the air/gas content can be in the range 3–10 percent.

In the real natural situation, sea bottom is usually covered by the sequence of ripples induced by surface waves. Simple mathematical models are presented for pore water circulation below rippled sea bottom. Two cases of induced flow are considered. First, the circulation induced by bottom current with constant velocity is examined using the conformal mapping technique. Secondly, the circulation of pore water under the system of N sinusoidal ripples is examined (Massel, 2010). In very shallow water depth, the radiation stress mechanism produces some denivelation of the mean water level. Due to this denivelation, some extra stationary pressure is created which induces also the circulation of the pore water in permeable media. Results of the modeling indicate that under waves action, close waterline a vertical “barrier” was formed



with vertical velocity flow only Massel, 2001). This barrier separates sea water from the inland water flowing to the sea which may have substantial ecological consequences.

5. Conclusions

The tests carried out at the Coastal Research Centre provide a substantial amount of very unique experimental data on surface-wave-induced pore pressure. In particular, under controlled and almost full-scale conditions, the dual nature of the pore pressure has been detected. It was found that beyond the breaker zone, only the so-called phase-resolving pressure is observed, while within the surf zone, the phase-resolving component as well as the phase-averaged pressure component are recorded. The pore pressure gradients provide valuable information on the kinematics of groundwater flow in the beach body. The data collected were used for comparison with the theory based on the Biot approach and showed very good agreement.

Acknowledgement

The project was funded by the European Community within the Access to Research Infrastructures Action of the Human Potential Programme (contract HPRI-CT-2001-00157). The staff of the Coastal Research Centre (FZK), as well as Mr. J. Dąbrowski, Mr. K. Wańkiewicz and Mr. M. Wichorowski from the Institute of Oceanology are gratefully acknowledged for their very helpful assistance with experimental observations.

References

- Biot, M.A. (1956) Theory of propagation of elastic waves in a fluid-saturated porous solid. Part 1: Low frequency range. Part 2: Higher frequency range. *J. Acoust. Soc. Am.* **28** (2):168–191.
- De Rouck, J. & Troch, P. (2002) Pore water pressure response due to tides and waves based on prototype measurements. *PIANC Bull.* **110**:9–31.
- Huettel, M. & Rusch, A. (2000) Transport and degradation of phytoplankton in permeable sediment. *Limnol. Oceanogr.* **45** (3):534–549.
- Longuet-Higgins, M.S. (1983) Wave set-up, percolation and undertow in the surf zone. *Proc. R. Soc., Lond.* **A 390**:283–291.
- Massel, S.R. (2001) Circulation of groundwater due to wave set-up on a permeable beach. *Oceanologia* **43** (3):279–290.
- (2010) Circulation of groundwater below a rippled sea bed. In: *6th Study Conference on BALTEX*, Międzyzdroje, June 14–18, 2010 (Abstract).
- Massel, S.R., Przyborska, A., Przyborski, M. (2004) Attenuation of wave-induced groundwater pressure in shallow water. Part 1. *Oceanologia* **46** (3):383–404.
- (2005) Attenuation of wave-induced groundwater pressure in shallow water. Part 2, Theory. *Oceanologia* **47** (3):291–323.
- Moshagen, H. & Tørum, A. (1975) Wave-induced pressures in permeable seabeds. *J. Waterway Div.-ASCE* **101**:49–57.
- Verruijt, A. (1969) Elastic storage of aquifers. In: Deweist, R.J.M., ed., *Flow through porous media*, 331–376. New York: Acad. Press.
- Węśławski, J.M., Urban-Malinga, B., Kotwicki, L. et al. (2000) Sandy coastlines—are there conflicts between recreation and natural values? *Oceanol. Stud.* **29** (2):5–18.

Hydro- and morphodynamics of a multi-bar coastal zone

Rafał Ostrowski

Abstract

Coastal hydrodynamic processes mainly comprise wave transformation in the nearshore zone and appearance of wave-driven currents. At each location of a multi-bar coastal zone, interaction of waves and wave-induced currents (longshore and cross-shore) gives rise to a coupled bed shear stress, which is a driving force for sediment transport. In the longshore direction, motion of sediment is consistent with the resultant wave-induced longshore flux of water. The cross-shore sediment transport rates at individual places of the cross-shore profile are dependent on very delicate imbalances between an onshore flow in the bed boundary layer caused by vertical asymmetry of wave shape and the wave-driven return current (undertow) directed offshore. Evolution of the sea bed and the shoreline depends on spatial variability of the net (resultant) sediment transport rates.

Прибрежные гидродинамические процессы включают главным образом трансформацию волн в прибрежной зоне и появление волновых течений. В каждом участке береговой зоны с множеством подводных валов взаимодействие волн и индуцированных волнами течений (вдольбереговых и поперечных) дает начало придонному сдвиговому напряжению, которое является ведущей силой транспорта наносов. Во вдольбереговом направлении движение наносов направлено в соответствии с результирующим вдольбереговым потоком воды. В поперечном направлении транспорт наносов имеет место на определенных участках подводного профиля и зависит от очень деликатного дисбаланса между направленным на берег потоком в придонном слое, вызванным вертикальной асимметрией волнового профиля, и направленным в сторону моря компенсационным потоком. Эволюция морского дна и береговой линии зависит от пространственной изменчивости результирующего транспорта наносов.

Rafał Ostrowski (✉)
Institute of Hydro-Engineering of the Polish Academy of Sciences (IBW PAN),
Gdańsk, Poland
e-mail: rafal.o@ibwpan.gda.pl



1. Introduction

Coastal zones built of sandy sediments are subject to continuous evolution caused by frequently changing hydrodynamic conditions. This evolution can be observed in many time scales and results in short-term changes (of hours and days) up to long-term morphodynamics (of years and decades). Conventionally, it is assumed that the seabed evolution takes place due to spatial variability of net (resultant) sediment transport rates. In theoretical description, for convenience, the sediment transport is divided into cross-shore and longshore. Similarly, coastal changes in the cross-shore and longshore domains are assumed to result from variability of respective components of the sand motion.

Coastal hydrodynamic processes mainly comprise wave transformation in the nearshore zone and appearance of wave-driven currents. At each location of a multi-bar coastal zone, interaction of waves and wave-induced currents (longshore and cross-shore) gives rise to a coupled bed shear stress, which is a driving force for sediment transport. In the longshore direction, motion of sediment is consistent with the resultant wave-induced longshore flux of water. In the cross-shore direction, the resultant sediment transport is principally dependent on a very delicate imbalance between an onshore flow caused by vertical asymmetry of wave shape and the wave-driven return current directed offshore.

Here, the classical deterministic modelling approach is followed, comprising theoretical description of the physical processes occurring in a coastal zone. Within this modelling system, first the processes of wave transformation and breaking are determined, as well as wave-induced currents, quantitatively much dependent on the features of the multi-bar cross-shore profile. Then the shear stresses at the sea bed are calculated, from which the sediment transport rates are found. Spatial variability of these rates cause changes of the sea bed level and the shoreline position.

2. Results

2.1. Wave transformation and wave-driven currents

A reliable description of the wave-current field is crucial for a precise determination of the sediment transport rates. The set of models developed by Szmytkiewicz (1995) and Szmytkiewicz (2002a, 2002b), enabling calculations of wave transformation and wave-driven currents, has been validated thoroughly using laboratory and field data, both from the literature and the IBW PAN facilities. A brief description of this computational framework is given below.

In the modelling of wave motion, following Battjes & Janssen (1978), it is assumed that the waves are random and that their heights in the entire coastal zone can be described by a Rayleigh distribution. The wave height H is computed from the equation of the energy flux conservation where the roller effect (rotating mass of water, located on the crest of the breaking wave, see Fig. 1) is also taken into consideration:

$$\frac{\partial}{\partial x} (E \cdot C_g \cdot \cos\theta) + \frac{\partial}{\partial x} (E_r \cdot C \cdot \cos\theta) = -D \quad (1)$$



where E is the total wave energy, E_r the kinetic energy of the roller as described by (Svendsen, 1984), C and C_g the phase and group velocity of waves, respectively, θ the wave approach angle (i.e. the angle between the wave crest and the shoreline), and D the wave energy dissipation.

In the above equation, which is a simplified form of the wave action equation, the wave energy dissipation D is calculated on the assumption that the dissipation is related to the wave breaking process only. Under this assumption, the formula of Battjes & Janssen (1978) has been used:

$$D = \frac{\alpha}{4} p_b \cdot f_p \rho g H_m^2 \quad (2)$$

Their approach was successfully adapted to a multi-bar coastal zone and multiple wave breaking (Szmytkiewicz, 1995).

In Eq. (2), g denotes the acceleration due to gravity and ρ is the water density, while the factor p_b , characterising the percentage of broken and breaking waves at a given point in the coastal zone, is described by the relationship:

$$\frac{1-p_b}{\ln p_b} = -\left(\frac{H_{rms}}{H_m}\right)^2 \quad (3)$$

in which α is an empirical coefficient of the order $O(1)$, f_p is the wave spectrum peak frequency ($f_p = 1/T_p$), H_m denotes the maximum possible wave height at the considered location of the coastal zone and H_{rms} is the sought-after root-mean-square wave height.

The wave-driven steady currents in the coastal zone are calculated with the following assumptions:

- (1) isobaths are approximately parallel to the shoreline;
- (2) shear stresses in the water column can be determined according to Boussinesq hypothesis;
- (3) water flow velocities related to circulations of the open sea are negligibly small with respect to the orbital velocities;
- (4) variability of the return flow along the cross-shore profile is much smaller than its variability over depth;
- (5) there is a fully developed roller just in front of breaking wave crest.

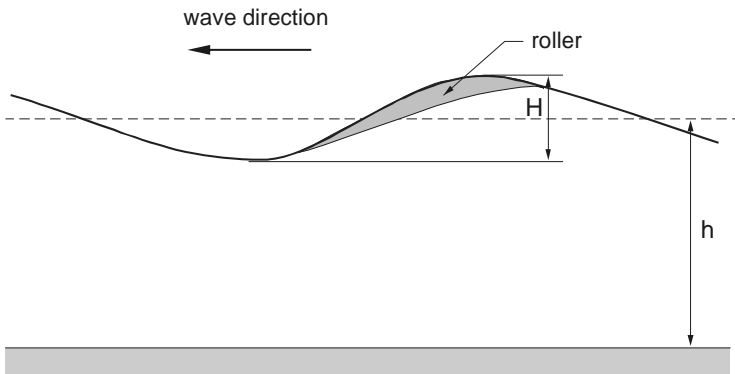


Fig. 1. Concept of a roller generated by the breaking wave.



In the return flow (undertow) model, Szmytkiewicz (2002a, 2002b) follows the classical approach of Longuet-Higgins, in which the momentum equation in the cross-shore direction, integrated over water depth and wave period, describes equilibrium between the derivative of the radiation stress ($\partial S_{xx}/\partial x$) and the spatial change of a free surface slope (resulting from phenomena called the set-down and the set-up, seawards and landwards from the wave breaking point, respectively). On the other hand, these two components of the momentum equation are in local imbalance at individual levels in water column. This is because the component containing water slope is constant over water depth, while the radiation stress S_{xx} is variable, which results from decrease of wave orbital velocities towards the sea bed. The above imbalance, which is particularly significant in the surf zone (at a presence of the roller), is a driving force of the resultant offshore current, called the return flow or the undertow.

In addition, there is an onshore discharge of water between the wave crest and trough, related to a so-called wave drift (or Stokes drift) and the roller-induced flow. This onshore water flow, due to the continuity equation, requires the compensation in a form of the offshore current.

The shear stress resulting from imbalance between the terms with the radiation stress S_{xx} and the water slope in the momentum equation gives rise to a steady (return) current, the velocities of which are found by use of Boussinesq hypothesis.

Following Szmytkiewicz (2002a, 2002b), the mean undertow velocity U_{mean} is determined from the time-averaged (over wave period) momentum equation, having the form:

$$\frac{\partial}{\partial x} [\rho(\bar{u}^2 - \bar{w}^2)] + \frac{\partial}{\partial x} (\rho g \bar{\eta}) + \frac{\partial}{\partial z} (\rho \bar{u} \bar{w}) + \frac{\partial}{\partial x} \left(\frac{M_r}{h} \cos^2 \theta \right) = \frac{\partial}{\partial z} \left(\rho \nu_t \frac{\partial U_{mean}(z)}{\partial z} \right) \quad (4)$$

where:

ν_t —turbulent viscosity in the water column,

\bar{u}, \bar{w} —orbital velocities in the horizontal and vertical direction, respectively,

M_r —roller momentum,

$\bar{\eta}$ —mean elevation of the free surface above still water level.

The wave drift and the roller-induced flow are used to formulate the boundary condition. The other boundary condition is related to a so-called slip velocity at the bottom, which can be determined in a few ways. The details concerning the solution of Eq. (4) can be found in the publications of Szmytkiewicz (2002a, 2002b).

It should be noted, that the vertical distributions of the return current (undertow), obtained from the solution of Szmytkiewicz (2002a, 2002b), have quite different character in front of and behind the wave breaker location (Fig. 2). This is of crucial importance in the modelling of wave-current bed boundary layer and the resultant wave-current bed shear stresses.

In the longshore sediment transport model, the main following assumptions are made:

- ✓ isobaths are approximately parallel to the shoreline;
- ✓ shear stresses inside the liquid in the cross-shore direction play the predominant role;

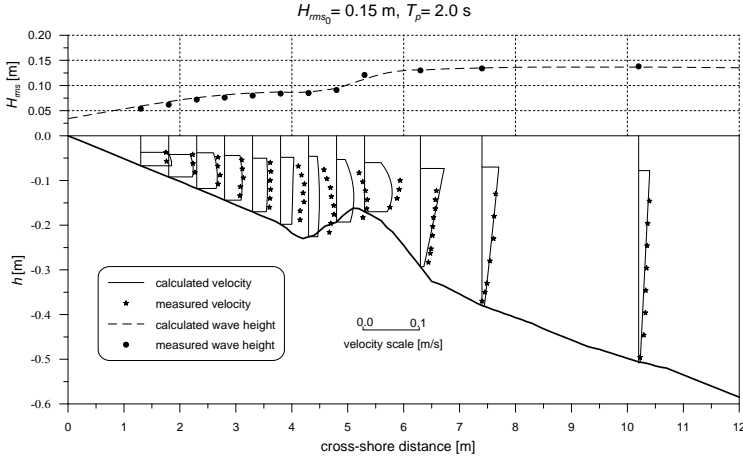


Fig. 2. Wave height and cross-shore currents: model results versus IBW PAN laboratory data.

✓ water flow velocities related to circulations of the open sea are negligibly small in comparison to the wave-induced currents in the nearshore zone.

$$\frac{\partial S_{xx}}{\partial x} + \frac{\partial M_{xx}}{\partial x} + \rho \cdot g \cdot h \frac{\partial \eta}{\partial x} = 0 \quad (5)$$

$$\frac{\partial S_{xy}}{\partial x} + \frac{\partial M_{xy}}{\partial x} = \frac{\partial \tau_{xy}}{\partial x} - \tau_{by} \quad (6)$$

$$\tau_{xy} = \rho v_t \frac{\partial V_{mean}(x)}{\partial x} \quad (7)$$

The time and depth-averaged momentum equations in the cross-shore (x axis) and longshore (y axis) direction, supplemented by Boussinesq hypothesis, have the form:

where: η —mean elevation of the free surface above still water level, τ_{by} —bed shear stress, τ_{xy} —turbulence shear stresses inside the liquid, V_{mean} —longshore velocity averaged over wave period and water depth, S_{xx} and S_{xy} —components of the radiation stress tensor, M_{xx} and M_{xy} —components of the roller momentum tensor.

The above equations enable the computation of the set-up and set-down of sea water level (Eq. (5)) and the distribution of longshore currents, averaged over depth and wave period, as functions of offshore distance (Eqs. (6) and (7)) above a multi-bar bottom and for multiple wave breaking.

The driving factors S_{xy} and M_{xy} of water flow are calculated as the functions of wave energy dissipation:

$$\frac{\partial S_{xy}}{\partial x} = -\frac{\sin \theta}{C} \cdot D \quad (8)$$

$$\frac{\partial M_{xy}}{\partial x} = \frac{\sin \theta}{C} (D - D_r) \quad (9)$$

where D_r is the wave energy dissipation due to appearance of the roller.



2.2. Asymmetric wave free-stream velocities

The ultimate effect of the nearbed interaction between asymmetric wave motion and wave-induced steady flow (e.g. longshore current) depends on the wave shape, in particular the shape of the wave free stream velocity.

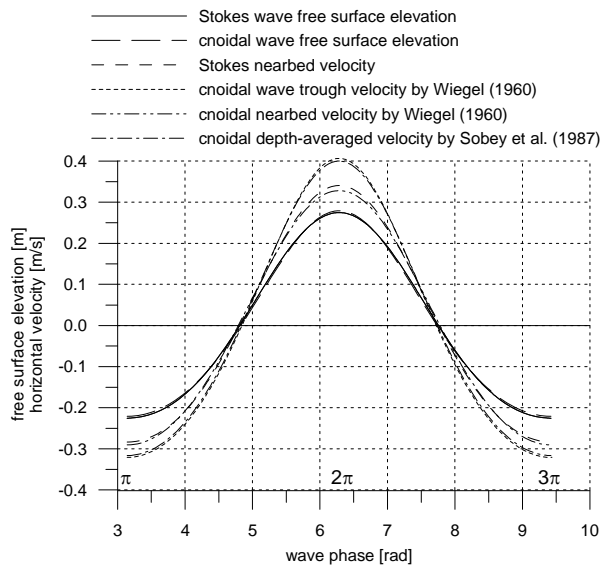
The most elementary description of asymmetrical waves is provided by a classical Stokes theory. This approach, however, can be used in a limited range of wave parameters. Close to the shore, at small water depths, the Stokes approximations are not valid. In this area, the application of the cnoidal wave theory is recommended.

Following conventional classifications, e.g. by Massel (1989), one can assume the rough limit of wave length to water depth ratio $L/h \approx 10$ as the interaction between short and long waves. Wave theories stemming from Stokes approximations can be used for $L/h < 10$, while the theoretical approaches of long waves, namely cnoidal wave theories, should be used for $L/h > 10$. According to Fenton (1979), the above division lies about $L/h = 8$. However, as deduced by Fenton (1979), for smaller waves there is a significant overlap between the areas of validity of Stokes and cnoidal theories. For instance, a wave with height to water depth ratio $H/h = 0.2$ can be solved using either Stokes or cnoidal approximation for L/h between 5 and 12. The above wave conditions yield the value of Ursell parameter $U_r = H/h(L/h)^2$ lying in the range of from 5 to 28.8. This example shows that an arbitrary choice can be made between the two theoretical approaches within quite wide range of wave regimes.

The exemplary results of computations of the free surface elevations and horizontal components of wave-induced orbital velocities (depth-averaged, nearbed and at the wave trough) by use of 2nd Stokes approximation and the cnoidal wave theories of Wiegel (1960) and Sobey et al. (1987) are plotted in Fig. 3.

It can be seen that the cnoidal depth-averaged velocity by Sobey et al. (1987) corresponds to the cnoidal velocity at wave trough found from the cnoi-

Fig. 3. Free surface elevation and wave-induced velocity by various approaches for $h=5$ m, $H=0.5$ m, $T=8$ s; $L/h \approx 11$, $U_r \approx 11$.





dal solution of Wiegel (1960). For the nearbed region, the solution of Wiegel (1960) yields a velocity almost identical to the one obtained using the 2nd Stokes approximation. The latter proves that in the considered wave regime ($L/h \approx 11$, $U_r \approx 11$) both the Wiegel's (1960) cnoidal approximation and Stokes theory can be applied in description of the nearbed wave-induced velocities. More discussion on the applicability of the above wave theories in modelling of nearshore hydrodynamics and lithodynamics can be found in the study of Ostrowski (2002).

2.3. Bed shear stresses and sediment transport

Both longshore and cross-shore sediment transport is assumed to depend on combined wave and current motion. This combined flow of water gives rise to a coupled bed shear stress, which is a driving force for sand movement.

According to the assumptions of many deterministic models, the motion of sediment is caused by the instantaneous bed shear stress ($\tau = \rho u_f^2$), where ρ denotes water density, and u_f is the friction velocity. The instantaneous values and directions of u_f during a wave period can be determined e.g. by the momentum integral method for wave-current flow, proposed by Fredsøe (1984). The solution yields the instantaneous bed shear stresses $\tau = \rho u_f^2(\omega t)$ and the resultant directions of these stresses $\varphi(\omega t)$.

The shear stresses are the driving force of sediment transport rates, which can be determined, for instance, using the model of Kaczmarek & Ostrowski (2002). Successful, thorough testing versus experimental data allow this model to be applied within the framework presented here.

The three-layer sediment transport model comprises the bedload layer (below the theoretical bed level) and two layers of suspension, namely the contact load layer (nearbed suspension of sediment) and the outer layer (suspension in the water column).

The mathematical model of the bedload transport is based on the water-soil mixture approach, with a collision-dominated drag concept and the effective roughness height k_e (necessary for the determination of the bed shear stresses). This roughness is calculated using the approximate formula presented by Kaczmarek & Ostrowski (1996).

From the hydrodynamic input, described by the nearbed wave-induced orbital velocities and the wave-driven steady currents, the instantaneous values of bed shear stresses $\rho u_f^2(t)$ during a wave period are determined by Fredsøe's (1984) model. Then, for known bed shear stresses $\rho u_f^2(t)$, the instantaneous velocities $u(z, t)$ and concentrations $c(z, t)$ of sediment in the nearbed region are found.

The instantaneous values of the sediment transport rate are computed from distributions of velocity and concentration in the bedload layer and in the contact load layer:

$$q(t) = \int_0^{\delta} u(z, t) \cdot c(z, t) dz \quad (10)$$

where δ denotes the upper limit of the nearbed region (the bedload layer and the contact load layer).



Next, using the instantaneous angles φ between the bed shear stresses and the shoreline, the instantaneous sediment transport rates $q(t)$ calculated for all individual locations of the coastal zone are projected on the cross-shore and longshore directions, averaged over wave period and thus the net cross-shore and longshore transport rates q_x and q_y are obtained:

$$q_{x,b+c} = \overline{q(t) \cdot \sin \varphi(t)} \tag{11}$$

$$q_{y,b+c} = \overline{q(t) \cdot \cos \varphi(t)} \tag{12}$$

The net transport rate for sediment suspended in the outer flow (in the water column beyond the nearbed layers) is determined using the following simplified formula:

$$q_s = \int_{\delta}^h \bar{u}(z) \cdot \bar{c}(z) dz \tag{13}$$

where the time-averaged concentration is obtained from a conventional relationship, e.g. that by Ribberink & Al-Salem (1994):

$$\bar{c}(z) = \bar{c}(z=\delta) \left(\frac{\delta}{z} \right)^{\alpha} \tag{14}$$

The quantity $\bar{c}(z=\delta)$ in Eq. (14) plays a key role while determining concentration in the outer region. It is called a reference concentration and in the other theoretical approaches is assumed arbitrarily, assessed from experimental data or simply “guessed”. In the present modelling system, the concentration $\bar{c}(z=\delta)$ is calculated from the solution of the contact load layer, while the velocity $\bar{u}(z)$ is determined from the solution of the bed boundary layer presented by Kaczmarek & Ostrowski (1992). Beyond the bed boundary layer in the water column the velocity $\bar{u}(z)$ is assumed as resulting from the solution of the wave-driven currents model. The concentration decay parameter α is an unknown value which has to be determined, e.g. from experiments. Typically, it has a value of 1.6–2.1.

The net sediment transport in the outer region (q_s) is modelled separately for the cross-shore and longshore directions and added to the respective nearbed components ($q_{x,b+c}$ and $q_{y,b+c}$), yielding the ultimate cross-shore and longshore sediment transport rates q_x and q_y .

2.4. Changes of sea bed level and shoreline position

At sandy coasts, vulnerable to water flows, waves and currents cause a quick response of the littoral system. The seabed is continuously evolving to achieve a state of equilibrium with respect to instantaneous hydrodynamic conditions. In the Baltic Sea, however, these conditions seldom become steady and therefore the above equilibrium cannot be reached. Particularly, the cross-shore profile can never have permanent shape. It changes significantly even in short time scales (of hours and days) and theoretical description of this process, numerical modelling and predictive simulations are very difficult.

Conventionally, the evolution of the sea bed profile is determined on the basis of spatial variability of net sediment transport rates, from the follow-



ing continuity equation for sediment in the direction perpendicular to the shore:

$$\frac{\partial h(x,t)}{\partial t} = \frac{1}{1-n} \frac{\partial q_x(x,t)}{\partial x} \tag{15}$$

where q_x denotes the net sediment transport rate [m^2/s] in the cross-shore direction per unit width, n is the soil porosity while deposited, x stands for the cross-shore coordinate and t is time (in a reasonable time domain of sea bed changes, e.g. hours, days, etc.).

It is very convenient to start the computations from the offshore location, where the sediment transport does not exist as the waves are deep water waves and do not affect the sea bed. Furthermore, there are no wave-driven currents at this location (except for the wave drift between wave crest and trough, which does not cause any sand motion).

While going onshore with the solution of Eq. (15), at smaller water depths, the net sediment transport appears and increases. Simultaneously, the compensative wave-driven return current starts to play more and more important role. This current, called the undertow in the surf zone, can be a predominating factor, locally causing the offshore sand transport. This is all accounted for in determination of $q_x(x, t)$, which is used in Eq. (15), yielding the change of water depth $h(x, t)$, as shown in Fig. 4.

In coastal engineering practice, the detailed distribution of the longshore sediment transport rate $q_y(x, y)$ on the cross-shore profile is not that important as the total (so-called global) longshore sediment transport rates $q_y = \sum q_y(x, y) \Delta x$ at individual longshore locations “ y ”. These rates constitute input data in calculations of the shoreline evolution by use of the one-line theory, in which the shoreline advance or retreat depends on spatial variability of the total longshore sediment transport rates (integrated over the cross-shore transect).

Shoreline evolution in time and space is most often modelled theoretically using the one-line theory. Within this concept, a general assumption is made that a shore can be represented by the shoreline and the cross-shore transects are uniform in the longshore direction.

This means that the cross-shore profile has the same shape at each location of a considered coastal segment. The above assumptions simplify the shore topography very much and are acceptable only in rough large scale modelling.

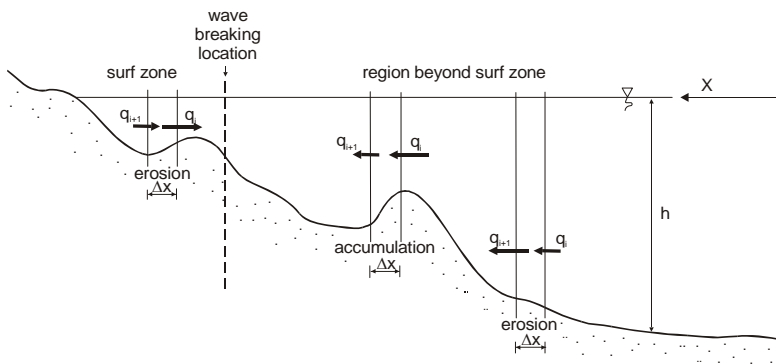


Fig. 4. Definition sketch for calculation of cross-shore profile evolution.



Hence, the one-line approach is generally applied for time domains of a few months up to decades and spatial stretches of a few to tens of kilometres.

In the one-line model, shoreline displacement is accompanied by simultaneous movement of the entire cross-shore profile, with preservation of its shape, as shown in Fig. 5. The shoreline migration in time ($\partial x/\partial t$) is related to spatial variability of the net longshore sediment transport ($\partial q_y/\partial y$) in the following way:

$$\frac{\partial q_y}{\partial y} \pm q_0 + (h_c + h_b) \frac{\partial x}{\partial t} = 0 \tag{16}$$

The above relationship is a continuity equation for sediment. In this equation, h_c is a so-called depth of closure and h_b is a height of the beach berm (a part of the beach subject to wave run-up), while q_0 denotes sediment sources (related to erosion of dunes or cliffs, discharges of river sediment, artificial beach nourishment, etc.) and sinks (e.g. sand mining).

The net longshore sediment transport rate q_y depends on the angle φ between wave crest and the shoreline ($\varphi=90-\gamma$, cf. Fig. 6), which can directly be put into some generalised models, see e.g. a well known CERC formula in Shore Protection Manual (1984). Thus, because $q_y=q_y(\varphi)$, the following relationship is valid:

$$\frac{\partial q_y}{\partial y} = \frac{\partial q_y}{\partial \varphi} \frac{\partial \varphi}{\partial y} \tag{17}$$

For small values of φ it can be assumed that $\partial \varphi = -\partial x/\partial y$ (Fig. 6). Consequently, neglecting the sources/sinks q_0 , one can rearrange Eq. (16) to the following form:

$$\frac{\partial x}{\partial t} = \varepsilon \frac{\partial^2 x}{\partial y^2} \tag{18}$$

where ε stands for $(\partial q_y/\partial \varphi)/(h_c + h_b)$ and is called a diffusivity parameter. This parameter can be easily determined using e.g. the CERC formula for q_y .

Presentation of the one-line theory in the form of Eq. (18) makes sense only if a simple sediment transport model for q_y is engaged and the derivative $\partial q_y/\partial \varphi$ is analytically available. In such a case, an analytical solution of Eq. (18) can be obtained, however, for specific situations in which the shoreline ad-

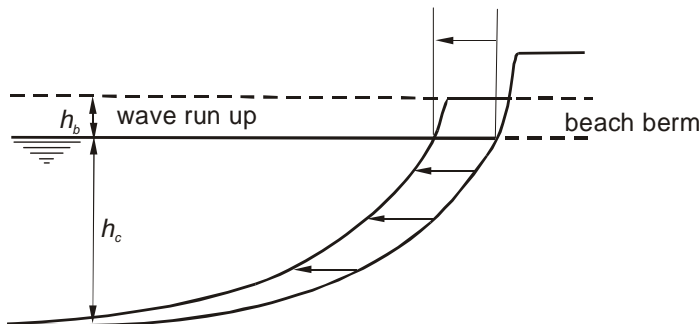


Fig. 5. Cross-shore profile movement in one-line theory.

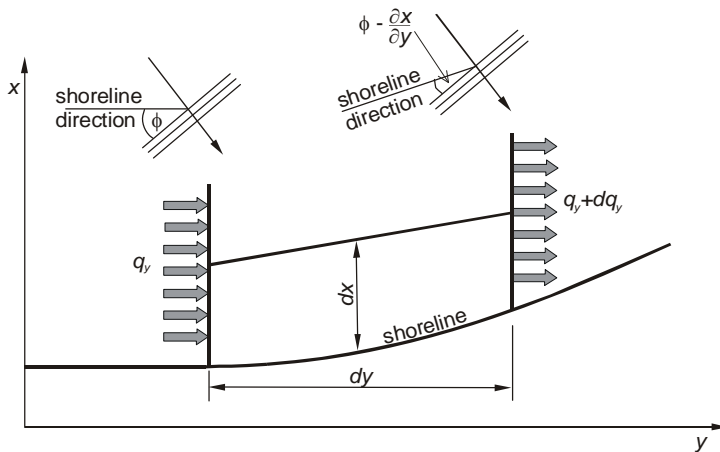


Fig. 6. Plan view of wave approach, shoreline curvature and longshore sediment transport.

vances or retreats (e.g. when the longshore littoral drift is totally interrupted by a single groin perpendicular to the shoreline).

The quantity h_c (a depth “closing” the cross-shore transect) determines the maximum depth at which sea bed remains unchangeable in the assumed time scale. For long periods of time, the value of h_c is related to extreme storms during which sediment motion takes place even at large water depth, far from the shoreline. According to other approaches, the depth of closure h_c could be defined as a function $h_c(t)$, dependent on instantaneous lithodynamic features, estimated in each computational time step. Such ideas, however, have never been tested thoroughly enough and few researchers undertake this way of modelling, being a combination of the very general one-line theory and a detailed sediment transport model.

References

- Battjes, J.A. & Janssen, J.P.F.M. (1978) Energy loss and set-up due to breaking of random waves. *Proc. 16th ICCE.*, Vol. I:569–587.
- Fenton, J.D. (1979) A high-order cnoidal wave theory. *J. Fluid Mech.* **94**(1):129–161.
- Fredsøe, J. (1984) Turbulent boundary layer in combined wave-current motion. *J. Hydraulic Eng.*, ASCE, **110**(HY8):1103–1120.
- Kaczmarek, L.M. & Ostrowski, R. (1992) Modelling of wave-current boundary layer in the coastal zone. *Proc. 23rd ICCE*, ASCE, New York, 350–363.
- (1996) Asymmetric and Irregular Wave Effects on Bedload: Theory versus Laboratory and Field Experiments. *Proc. 25th ICCE*, ASCE, New York, 3467–3480.
- (2002) Modelling intensive near-bed sand transport under wave-current flow versus laboratory and field data. *Coastal Engineering*, Elsevier Science B.V. **45**(1): 1–18.
- Massel, S.R. (1989) *Hydrodynamics of coastal zones*. Elsevier Oceanography Series. Amsterdam.
- Ostrowski, R. (2002) Application of cnoidal wave theory in modelling of sediment transport. *Archives of Hydro-Engineering and Environmental Mechanics*, IBW PAN, Gdańsk **49**(1):107–118.



- (2003) A quasi phase-resolving model of net sand transport and short-term cross-shore profile evolution. *Oceanologia* **45** (2):261–282.
- (2004) *Morphodynamics of a Multi-Bar Coastal Zone*. IBW PAN, Gdańsk.
- Ribberink, J. S. & Al-Salem, A. (1994) Sediment transport in oscillatory boundary layers in cases of rippled beds and sheet flow. *Journal of Geophysical Research* **99**: 12707–12727.
- Shore Protection Manual* (1984) US Army Coastal Engineering Research Center.
- Sobey, R. J., Goodwin, P., Thieke, R. J., Westberg, R. J. (1987) Application of Stokes, cnoidal and Fourier wave theories. *J. Waterway, Port, Coastal and Ocean Engineering* **113**(6):565–587.
- Szmytkiewicz, M. (1995) 2D velocity distributions in nearshore currents. *Proc. Coastal Dynamics'95*, ASCE, New York, 366–376.
- (2002a) Quasi 3D model of wave-induced currents in coastal zone. *Archives of Hydro-Engineering and Environmental Mechanics*, IBW PAN, Gdańsk **49**(1):57–81.
- (2002b) *Wave-induced currents in the coastal zone*. IBW PAN, Gdańsk (in Polish).
- Wiegel, R. L. (1960) A presentation of cnoidal wave theory for practical application. *J. Fluid Mech.* **7**:273–286.

Poster presentations

Adverse effects of sediment transport in coastal zone

Victor Alari, Getli Haran, Urmas Raudsepp, Tarmo Kõuts

Abstract

Lehtma harbour is a cargo and passenger traffic port located in Hiiumaa Island, Estonia. A minimum depth of the fairway in the port is needed for the safe navigation of vessels. In certain storm conditions the fairway is filled with sand, making arrival and departure of ships impossible. Set of numerical models including circulation, surface wind waves, sediment resuspension and transport model is used to study sediment transport in the area. Minimization methods for adverse effects of sediment transport are proposed.

Грузо-пассажирский порт Летма находится на острове Хиiumaa в Эстонии. Глубина подходного фарватера является критической для безопасной навигации. В определенных штормовых условиях подходной фарватер заполняется песком, что препятствует проходу судов по каналу. Для изучения транспорта материала было использовано численное моделирование течений, поверхностного волнения, взмучивания и транспорта донного материала.

1. Introduction

Lehtma harbour is a cargo and passenger traffic port (built in 1914) in north-eastern Hiiumaa Island (Fig. 1), Estonia. A minimum clearance of 5.5 m in the fairway is necessary for the safe navigation of vessels. The fairway is very sensitive to sediment movement and the shipway filled with sand is an ever-lasting problem. Sometimes the fairway is filled with sand just in a result of one storm event. Quite usual is organisation of dredging operations in *ad hoc* methods in weeks, otherwise harbour should be closed to ship traffic.

In order to study the sediment dynamics near the harbour fairway and causing this factor, as well to plan effective mitigation factors of, a modelling study is undertaken. We describe the modelling system and its setup in section 2. The modelling results are presented in section 3. The work is concluded in section 4.

Victor Alari, Getli Haran, Urmas Raudsepp, Tarmo Kõuts (✉)
Marine Systems Institute at Tallinn University of Technology, Tallinn, Estonia
e-mail: victor.alari@phys.sea.ee

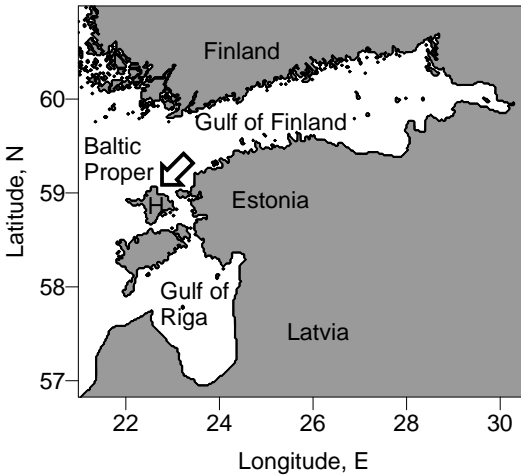


Fig. 1. The area of interest. Arrow indicates the approximate location of Lehtma harbour. H stands for Hiiumaa.

2. Description and setup of models

The resuspension is controlled by shear stress at the sea bed generated by wind waves. When shear stress (or shear velocity) is above critical value, resuspension occurs and deposition occurs when it is lower. SWAN (Booij et al., 1999) wave model was used to model the surface wave fields (significant wave height, peak period and wavelength). From these parameters, shear velocity was calculated (methods described by Jönsson, 2006) which acts of fine sand of grain diameter 0.25 mm. The threshold value for resuspension is 1.4 cm/s. The resuspended sediments are moved with currents. Current fields were calculated with a 2 D circulation model, which is based on non-linear shallow water equations. In order to describe the suspended material movement, Lagrange's transport model, based on so-called tracer equation, was used. In the model, the suspended material is transported to the neighbouring grid point with currents (advection) and the effect of turbulent particle dispersion is also taken into account.

The fairway is usually filled with sand in northern and north-eastern storms, but could be filled in other conditions also. In order to study the dynamics of sediment movement, we here apply constant wind forcing of 15 m/s blowing steadily for 24 h from north. The models are nested consequently, so the 2,000 m model governs the whole Baltic Sea and the most nested 20 m grid the Lehtma harbour area. Sediment resuspension and transport are calculated for 20 m grid. The 20 m grid calculations are made three times. First the situation where safe navigation is possible (Fig. 2a), then when a so called compensation area of 5 m is dredged behind the jetty (Fig. 3a) and thirdly, when a new sediment trap is constructed (Fig. 4a).

3. Results

Under normal hydrographical conditions, when fairway is shippable, the shear velocity does not exceed 1.4 cm/s and sediments are deposited on fairway (Fig. 2b). North to the harbour the shear velocity may exceed 5 cm/s and mostly stays over the threshold value. South to the harbour and in the



Fig. 2 (a) Bathymetry of Lehtma harbour. Water depth are shown in meters. The coordinate system is UTM-34. The arrow indicates so-called underwater sediment trap, constructed in the past to intercept the sediments moving to fairway. The dashed line is the fairway central axis. (b) Wave induced shear velocity (cm/s). (c) Current vectors. (d) Rise of the seabed in cm.

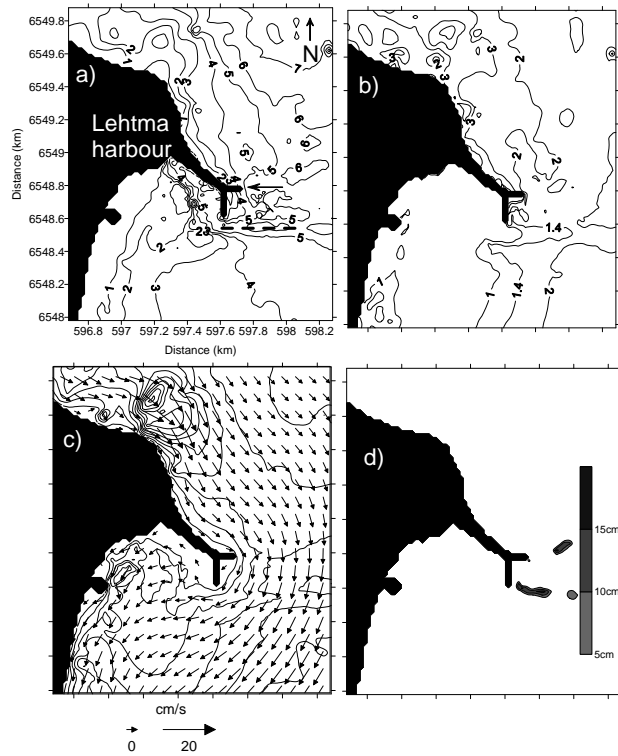
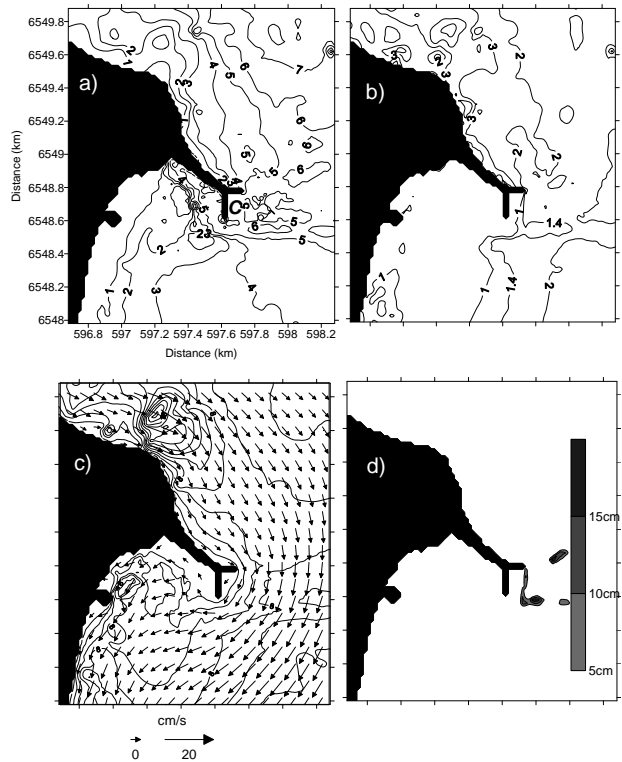


Fig. 3. Same as Fig. 2 but in the case of the compensation area. The letter C on a) marks the compensation area.





aquatorium shear velocity is less than critical value. The current speed stay mostly less than 10 cm/s but may exceed even 20 cm/s on a shallow north of the harbour (Fig. 2c). The current vector is aligned parallel with isobaths in northern part and turns to form an alongshore flow at southern part.

After 24 h the find sand that is accumulated on the fairway increases the seabed elevation 10–15 cm, but at certain points it may reach 17 cm (Fig. 2d). The sediments are deposited on the seaward side of the fairway rather than at the tip of the jetty, since current does not turn parallel to the fairway.

In case of the compensation area, the shear velocity is below the critical value behind the jetty also (Fig. 3b). However, the current does not change its direction enough and sediments are still deposited on the fairway (Fig. 3c). Although the increase in elevation is mostly between 5–10 cm, at certain points it still is over 15 cm (Fig. 3d). Also the area in fairway where sand is accumulated is shorter, but wider. Some sediments are deposited at the boundary of compensation area.

In the case of a new sediment trap and without the compensation area, the area of deposited sediments has decreased compared to previous cases, but the sediments are piled up together forming an elevation increase over 15 cm (Fig. 4d).

4. Conclusion

Lehtma harbour is an area of very intensive sediment transport. Although the minimization methods for sediment accumulation show some improvement, sand deposition on the fairway cannot be obviated. When wind turns from N to NE or E, the current flow reverses its direction and delivers sedi-

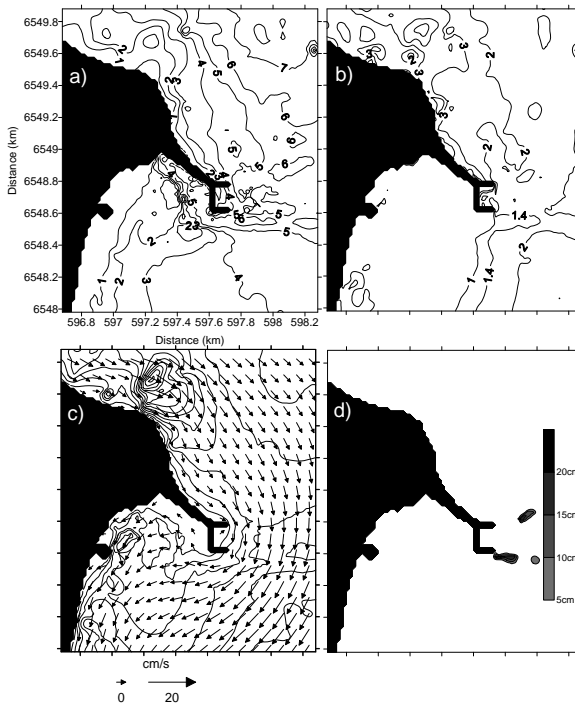


Fig. 4. Same as Fig. 2 but in case of new sediment trap.



ments from the South. In the case the relieving methods would not be effective. Sediment deposition on fairway remains an ever-lasting problem nowadays and in the foreseeable future.

References

- Booij, N., Ris, R.C., Holthuijsen, L.H. (1999) A Third Generation Wave Model for Coastal Regions. 1. Model description and validation. *Journal of Geophysical Research* **C104**:7649–7666.
- Jönsson, A. (2006) A model study of suspended sand due to surface waves during a storm in the Baltic Proper. *Journal of Marine Systems* **63**:91–104.

Hydro-lythodynamics of near-bottom layer in coastal area of South-East Baltic

Alexander Babakov, Vadim Sivkov

Abstract

Stationary research of Atlantic Branch of Institute of Oceanology Russian Academy of Sciences (AO IORAN) in a deep-water part of the Kaliningrad north coast of Baltic sea in 2006–2008 allowed obtaining more accurate conception of temporal and spatial variability of hydro-lythodynamical processes in the near bottom layer (2 m). Diffusion distance, character of distribution and velocity range for storm near bottom currents are estimated for typical storm conditions. The monthly average mass and grain-size composition of suspended sediments are found, a vertical distribution of both horizontal and vertical mass fluxes of suspension and a rate of their weakening along the profile of an underwater coastal slope are estimated.

Стационарные исследования АО ИОРАН в 2006–2008 гг. в глубоководной части калининградского побережья Балтийского моря позволили уточнить представления о пространственно-временной изменчивости гидро-литодинамических процессов в придонном 2-метровом слое. Оценена дальность распространения, характер распределения и диапазон скоростей штормовых придонных течений при типичных штормах. Определена среднемесячная масса и гранулометрический состав взвешиваемых наносов, характер вертикального распределения масс горизонтального и вертикального потоков взвеси и степень их ослабления по профилю подводного берегового склона.

A three-year series of hydro-lythodynamical measurements held on two stations ($H=15$ m and $H=28$ m) in deep-water area of the north Kaliningrad coast showed that conception of massive transfer of sand and siltstone material ($d>0.05$ mm) prevailing in wave break zone essentially narrows an operative range of a stream of deposits and considerably reduces its power.

Investigation results in ascertainment of the prevailing direction of suspended matter transfer as well as intensity of dredging and composition of friable material for horizontal transitional (HF, horizontal flow) and vertically

Alexander Babakov, Vadim Sivkov (✉)

P.P. Shirshov Institute of Oceanology RAS, Atlantic Branch, Kaliningrad, Russia
e-mail: babakov_temp@mail.ru; sivkov@baltnet.ru



precipitated, including saltating suspension flow (VF, vertical flow) in near-bottom layer (0.2–2 m).

Statistical analysis of measurements showed that near-bottom currents in deepwater part of coastal area have velocities up to 5–15 cm/s under moderate winds ($W=7-8$ m/s), and during storms ($W=18-20$ m/s) the velocities vary from 20–25 ($H=28$ m) to 40–60 cm/s ($H=16$ m). Prevailing currents and sediment drift on northern underwater slope of Kaliningrad coast are oriented to northeast quarter, which is due to western winds predominance.

Lythodynamic conditions in the external part of coastal zone ($H>10$ m), where a deficiency of silt are defined by wind and wave activity and by location of friable material fields. Therefore, monthly averaged volumes of coarse siltstone and sand suspension particles ($d>0.05$ mm) differ notably on both stations.

During the period of weak and moderate winds ($W=5-7$ m/s) the HF suspension concentration was about 0.1–0.2 mg/l. However, during the similar wind conditions there were repeatedly recorded periods of abrupt increasing of SM concentration up to 0.6–1 mg/l at $H=28$ m, and up to 6.5 mg/l at $H=15$ m, which exceed average monthly values during the autumn storms period. This can be explained by existing of friable material fields at the bottom of measurement area, and also by episodic drift from the coast. There was noted a case of sanding up a bottom pyramid up to 1.2 m, which has been operated during the winter 2006–2007 at the depth of 15 m.

Monthly averaged VF volume at whole profile is degrees less than HF volume. The part of VF collected sand particles compared to HF increases near bottom and moving away from coast due to intensifying saltation process.

Along the slope (from 15 to 28 m) HF mass decreases in 10–20 times on average, while VF mass decreases slower. For siltstone-sand fractions ($d>0.05$ mm) VF/HF mass ratio is about 1/15–1/30 at $H=15$ m, and 1/10–1/20 at $H=28$ m. In vertical plane VF mass at $Z=2-1.5$ m changes insignificantly; in the low layer ($Z=1-0.4$ m) it increases approaching the bottom on average in 2–3 times at $H=15$ m, and in 3–5 times at $H=28$ m.

In the periods of weak winds fine-particle suspension prevails; thus the VF part decreases, and HF part increases, decreasing the VF/HF ratio to 1/50–1/130. Under moderate winds vertical movements reach maximal activity, and with further increase of wind, precipitation and saltation processes diminish, due to transition of drifts to a stable suspended state. Such a tendency requires more detailed research.

Granulometric composition of suspended particles decreases vertically at both stations when moving away from bottom. In the near-bottom layer (up to 0.4 m) fine sand (0.1–0.25 mm) prevails, and upwards—siltstone and pelite (<0.1 mm). For VF, a tendency of larger particle size than that of HF can be seen, especially at seaward station (28 m).

Along the slope (15–28 m) no regular differentiation of HF suspension by size can be seen, due to dynamic change of bottom sediments composition at $H=15$ m, and its limited carry-over to $H=28$ m, where bottom material and suspension composition near the bottom ($Z=0.2-0.4$ m) is more stable, and is mostly fine sand (0.1–0.25 mm).

According to earlier measurements carried by AB IORAS, with passage from 13–15 m isobath to first wave break area (4–5 m) average suspended



material mass increases vertically nonuniform. Near the bottom ($Z=0.2-0.4$ m) mass about 5–8 times increases, at $Z>1$ m mass raise is minimal (2–5 times), and at $Z=0.4-1.0$ m it is maximal (up to 10–30 times) due to suspension and saltation horizon raise. HF mass compared to VF mass increases faster near the bottom ($Z=0.3-0.4$ m) and slower at $Z=1-1.5$ m near the coast, especially during periods of enhanced storm activity. HF/VF mass ratio is about 12–17 near the bottom, and 38–25 in 1 m from bottom. Near the bottom suspension prevails, and at $Z=1-1.5$ m saltating particles prevail.

The measurements with short exposition period within one typical storm ($W=13$ m/s) confirmed considerable activation of bed sediment suspension during storm period.

The work is carried out under partial financial support of the Russian Foundation of Basic Research grant No. 08-05-01023.

Beach drifting in the swash area (Baltic Sea)

Yana Bebieva

Abstract

An overwash stream zone and a coast dune are considered. The aim of the work is to study the processes changing the shape of the Vistula Spit coastline around Kosa village. The results of field observations of the south-eastern part of the Baltic Sea form a basis for the study. Further trigonometric leveling of the part of the Baltic Sea shore has been carried out. The dynamics of the coast line elements for the period of 2007–09 has been revealed.

В представленной работе рассматриваются зоны потока заплеска волн, а также авандюны. Целью является изучение процессов, изменяющих очертания морской береговой линии Вислинской косы в районе пос. Коса. В основу работы положены результаты полевых наблюдений юго-восточной части Балтийского моря (Вислинская коса, район пос. Коса). Проведены тригонометрические нивелировки части морского побережья Балтийского моря. К настоящему моменту установлена динамика элементов берега за период 2007–2009 гг.

1. Introduction

An overwash stream zone and a coast dune are considered in the work. Urgency of the issue is responsible for assessment of the coast and identification of emergency coastal stations, as the Kaliningrad coast is a subject to destruction nowadays. The work objective is to study the processes changing the shape of the marine coastline of the Vistula Spit around Kosa village.

2. Results

The material for the study was collected from field observations including coastal profiling. Two types of aggradation were recognized, namely. The first one is aggradation by sea current and the second one is aggradation by waves. Analysis of coast line motion relative to rudaceous rock reveals two basic

Yana Bebieva (✉)
Moscow Institute of Physics and Technology, Moscow, Russia
e-mail: yanabebieva@gmail.com



processes. They are inertial movement and gravitational movement. When waves approach obliquely to the shore, these forces operate in a different directions. Therefore, the decelerating water flow circumscribes asymmetrical quasi-parabolic curves on the beach surface and goes back seaward with new acceleration.

The expression for sediment transport rate was suggested to be derived from Pi-theorem. However, this method is not capable of finding the specific type of the function due to arbitrary option of the dimensionless group because there are three independent parameters of five determinants of the problem.

Subsequently exploring the movement of material in the coastal zone, sediment transport rate, based on the method of the dimension and field observations, can be represented as:

$$R=0.2\cdot 10^{-9}h^2\lambda\sqrt{\frac{g}{d}}\sin\beta$$

where h —wind waves height, λ —wind waves length, d —average size of sediment particles, β —an angle between the ray of wave and normal to the shore.

It is known that sediment movement depends on wave energy which is proportional to the squared wave amplitude h^2 . The area covered by the wave depends on the wavelength λ . In the shallow-water theory, $v\propto\sqrt{g}$.

The results of the field observations testified that semi-empirical formula correlated well with experimental data.

Further trigonometric levelings of the part of the Baltic Sea shore have been carried out. The Vistula Spit has ashape of a narrow arc. The beach is covered by sea sandstone. There is a zone of modern anemoarenite or coastal dune extended parallel to the beach. Beach profiling were carried out in 5 typical diameters (benchmarks) established in areas with varying intensity and direction of coastal processes. The comparison between the latest measurements in 2009 with that for the previous period of 2007–08 showed that the width of the beach decreased in 2007–09.

An analysis of dynamics of beach drifting in the swash area, and reveal of interrelation between these processes and the dunes evolution in the selected area is a matter of further study.

The morphodynamic and technogenic zoning of the shore of the Kaliningrad region

Valentina Bobykina, Vadim Boldyrev

Abstract

Results of the divisions into districts of the shore of the Kaliningrad region against prevailing morphodynamical and geodynamic process are presented. Rates of coastal erosion and accretion are given. The sites developing under the anthropogenous (technogenic) influence are allocated as well as segments with coastal protected constructions.

Приводятся результаты морфодинамического районирования берегов Калининградской области по преобладающему геодинамическому процессу, скоростям процесса. Выделяются участки, развивающиеся под влиянием антропогенного (техногенного) воздействия, распределение берегозащитных сооружений.

Valentina Bobykina, Vadim Boldyrev (✉)

P. P. Shirshov Institute of Oceanology RAS, Atlantic Branch, Kaliningrad, Russia
e-mail: bobyval@mail.ru

Results of monitoring of the seashore of the Kaliningrad region by GU KO “Baltberegozaschita”

Evgeny Burnashov, Alexander Bednov, Alexander Trashchenkov

Abstract

GU KO “Baltberegozaschita” realizes annual monitoring of the seashore of the Kaliningrad region since 2007. A unified monitoring system of bench marks for whole Kaliningrad coast was created in 2007. The monitoring system consists of 290 of bench marks, located at 500 m from each other. Step by step the morphological measurements are fulfilling at the shore and at the nearshore zone. In addition, the measurements are also conducted at the traditional monitoring points of AOIORAS, located on the seashore of Kaliningrad. The aerial laser scanning of the entire marine coastline of the Kaliningrad region was carried out in 2007 and 2008. According to the scanning results obtained the one year dynamics of the seashore was analyzed. A comparison of data of air scanning and ground monitoring was made in 2009.

С 2007 г. ГУ КО «Балтберегозащита» проводит ежегодный мониторинг морского берега Калининградской области. В 2007 г. была разработана единая мониторинговая сеть реперов, по створам которых проводились измерения как надводной части берега, так и подводно-берегового склона. Мониторинговая сеть состоит из 290 реперов, расположенных через 500 м друг от друга. Кроме того, измерения также проводятся на мониторинговых реперах АО ИО РАН, расположенных на морском побережье Калининградской области. В 2007 и 2008 гг. было осуществлено воздушное лазерное сканирование всей морской береговой полосы Калининградской области. По результатам сканирования берега была получена динамика всего морского берега в целом. В 2009 г. произведено сопоставление данных воздушного сканирования и наземного мониторинга.

1. Introduction

Since 2007 GU KO “Baltberegozaschita” makes annual monitoring of the sea coast of the Kaliningrad region. A unified monitoring system of bench marks was created in 2007, the range of bench marks was measured as shore

Evgeny Burnashov, Alexander Bednov, Alexander Trashchenkov (✉)
GU KO “Baltberegozaschita”, Svetlogorsk, Russia
e-mail: burnashov_neo@mail.ru

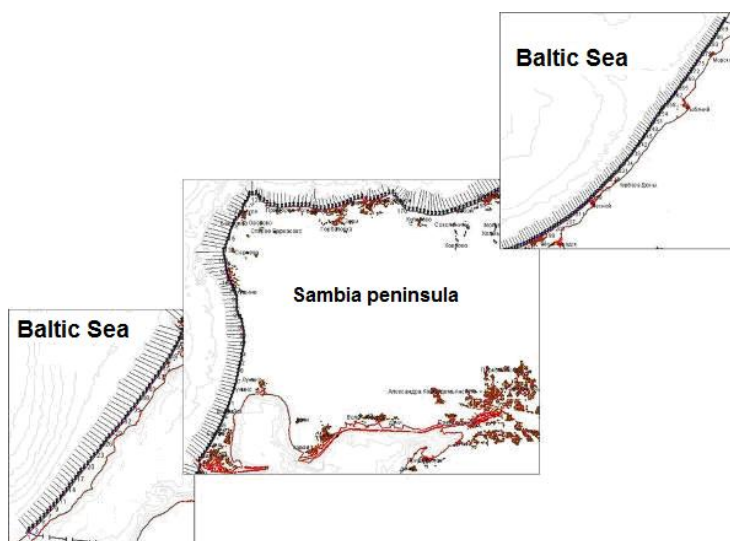


Fig. 1. Locations of 290 traverses and bench marks of the monitoring system of GU KO "Baltberegoshchita" on the coast of the Kaliningrad region.

and nearshore zone. Monitoring system consists of 290 of bench marks, located in 500 m of each other (Fig. 1). Every year is bench mark reconnaissance in coordinate system WGS-84 with reference to their location in the Baltic system of heights BSH-77.

2. Results

As a result, the annual ground-based measurements including trigonometric leveling beach, foredune and bed-rock shore, regular coast fotomonitoring and the measurement of abrasion of coastal escarpments, were constructed profiles of the identified parts of coast and obtained details about their condition and dynamics.

To obtain information on the entire coast in 2007 and 2008 was carried out aerial laser scanning of the entire marine shoreline Kaliningrad region (Fig. 2).

After analyzing the results of the scan using a specific software "Ortolazer" provided information about the various changes of sea coast.

With the application of digital elevation models of shoreline in 2007 and 2008 and the construction of profiles of any parts of coastline are clearly visible the different changes. On the beaches the sea deposited material (pebbles, gravel, sand) forms the beach ridge height of 1 to 2 m. Sand occurs transport under the influence of wind, with the open beaches formed small embryo dune (Fig. 3). As a result of wind erosion on the foredune ridge formed deflation basins (Fig. 4), the transfer of sand in the rear part of the foredune with burial timber and shrub vegetation (Fig. 5). Because of heavy rains and changes in the height of groundwater is leaching of soil on the coastal slopes with landslide processes (Fig. 6). Apart from the above listed, visible signs of the past year storms, which are expressed in foredune erosion (Fig. 7), and collapse of abrasion scarps (Fig. 8).

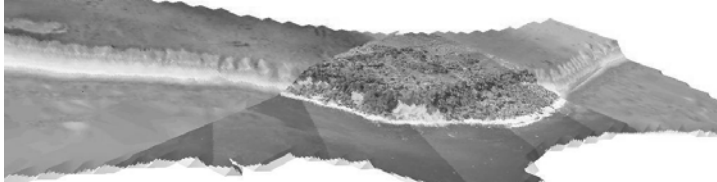
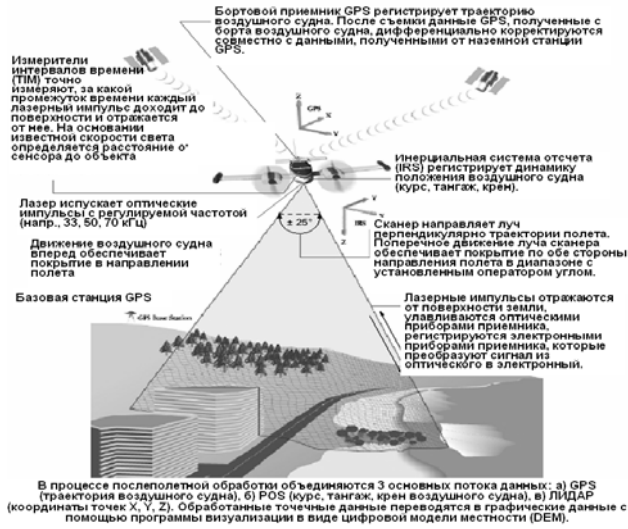


Fig. 2. Methods of aero laser scanning and 3D-model of the coast received after the aero-scanning.

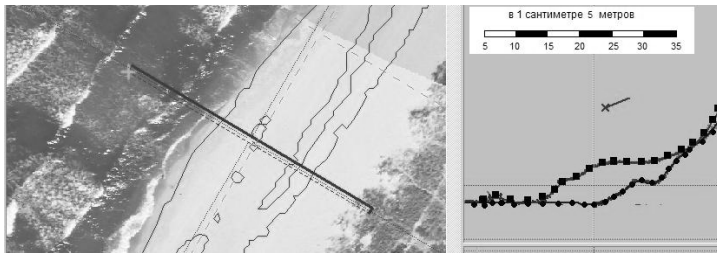


Fig. 3. The appearance of accumulative forms in the beach zone of the Baltic Spit.

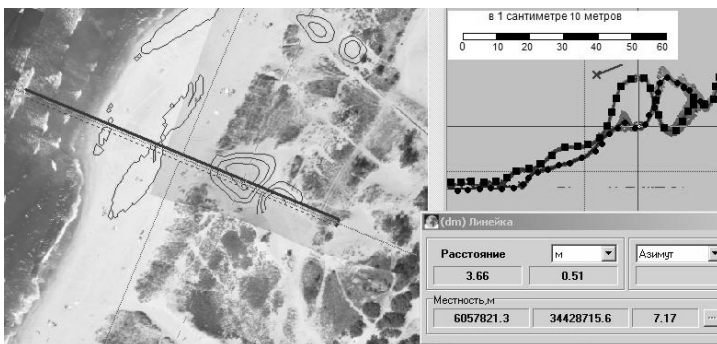


Fig. 4. Moving sand masses and the formation of deflation basins on Curonian Spit.

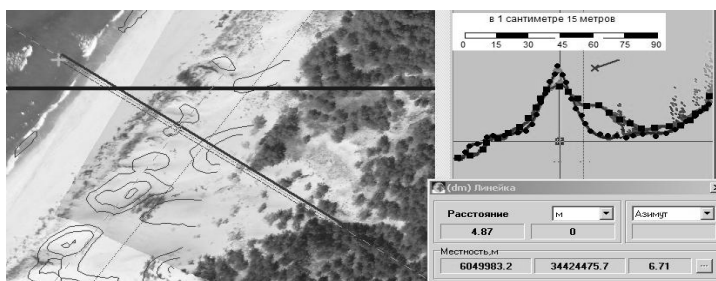


Fig. 5. Moving sand in the back part of the fore dune on Curonian Spit.

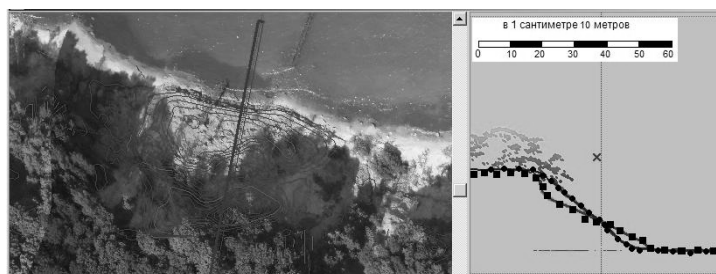


Fig. 6. Landslide abrasive coastal slope near the Otradnoe Village.

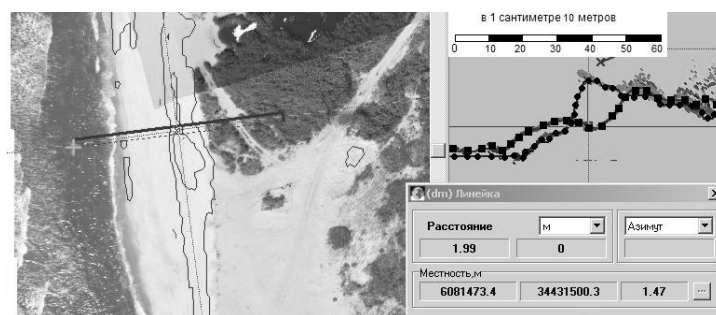


Fig. 8. Coastal scarp retreat near the Pokrovskoe Village.



The following illustrative examples are displayed in the scan data analysis program “Ortolazer”. The line with square points in profile box corresponds to a terrain survey in 2008, with round points—terrain survey 2007.

Foto-monitoring regularly conducted on all monitoring of bench marks (Burnashov et al., 2008). The photos clearly show the changes in the morphological structure of the sea coast (Fig. 9).

In 2009, the comparison of data produced by scanning the air and ground monitoring. Construct the combined profiles of the coast for the period 2007, 2008, 2009 and determined the dynamics of emergency places of coast (Fig. 10).



Fig. 9. Results foto-monitoring for fore dune at the ABIORAS monitoring point Rp51 at the Baltic Spit for (2006–09).

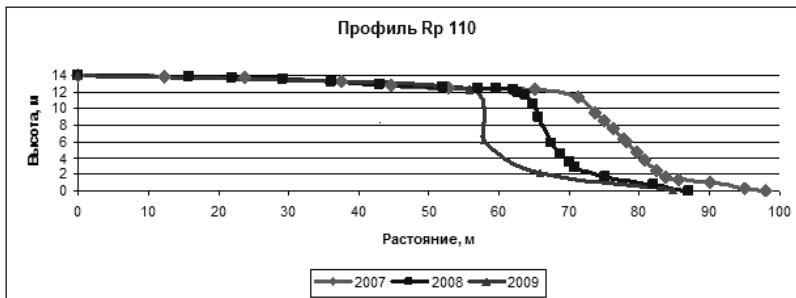


Fig. 10. The negative dynamics of the shore at an emergency places near Sinyavino village.



As a result of the GU KO “Baltberegozaschita” monitoring studies on the coast of the Kaliningrad region for the period from 2007 to 2009 there was accumulated data on 11 previously allocated to an emergency site (Boldyrev, 2006), and generally determine the condition and dynamics of the sea shore. During the monitoring period as a whole all the coast continues to retreat at a speed of 0.7 m per year, and at emergency places a shore for a specified period, the average retreat rates from 0.1 to 6.56 m per year (Table).

Table

The dynamics of the coast at an emergency places (Reports, 2007–2009)

Emergency places	Location	The dynamics of the coast for the period 2007–09 years, m/year
Place 1	Kosa village	-2.19
Place 2	cape Peschanny—Yantarny pumping station	-0.45
Place 3	Sinyavino village	-6.56
Place 4	Donskoe village—cape Taran	-0.10
Place 5	Svetlogorsk, near Moskovskaya st.	-0.36
Place 6	Svetlogorsk, near Vereshchagina st.	-0.10
Place 7	Pionerskiy, embankment	-0.10
Place 8	Pionerskiy, residence	-0.10
Place 9	Zaostrovie village—cape Gvardeyskiy	-0.10
Place 10	Malinovka village—Zelenogradsk	-0.10
Place 11	Zelenogradsk—second km Curonian Spit	-0.36

References

Boldyrev, V. L. (2006) *Emergency places of the coast within the Kaliningrad region*. Morphodynamics coastal zone: IFAS. Kaliningrad.

Burnashov, E. M., Boldyrev, V. L., Bobykina, V. P. (2008) Foto-monitoring as an showing of dynamics of the coastal zone an example of the Kaliningrad region coast. In: *Dynamics of Coastal Zone of Non-tidal Seas*. Mat. of the Int. Conf. (school-seminar), Baltiysk 30 June–5 July, 2008:39–41. Kaliningrad: Terra Baltica.

Burnashov, E. M., Shcherbina, V. V. Modern complex monitoring of a condition of the Kaliningrad region coast. In: *Integrated management, sustainable development indicators, spatial planning and monitoring of the South-East Baltic coastal regions*. Mat. of Int. Conf., Kaliningrad 26–30 March, 2008:53. Kaliningrad: Terra Baltica.

Gogoberidze, G. G., Zhamoida, V. A., Nesterova, E. N. et al. (2008) *Glossary on the coastal zone Cadastre*. St.-Peterburg: RSHU.

Report of the Monitoring department of GU KO “Baltberegozaschita” in 2007 (2007) Kaliningrad.

Report of the Monitoring department of GU KO “Baltberegozaschita” in 2008 (2008) Svetlogorsk.

Report of the Monitoring department of GU KO “Baltberegozaschita” in 2009 (2009) Svetlogorsk.

Remote and cartographical techniques for estimation of coastal erosion rate in seas and inland water bodies

**Elena Fedorova, Evgeniya Sviridova,
Konstantin Marusin, Alexandr Khabidov**

Abstract

With the help of remote sensing and cartographical techniques the rate of erosion and accretion in the coastal zone of the Russian part of Curonian Spit and on the shores of Novosibirsk Reservoir was estimated, and the efficiency of the methods used was evaluated.

С помощью дистанционного и картографического методов произведена оценка скоростей размыва и аккумуляции в береговой зоне российской части Куршской косы и на берегах Новосибирского водохранилища, оценена эффективность метода для морских берегов и берегов внутренних водоемов.

1. Introduction

The use of remote sensing data, maps and GIS-technology allows for the assessment of water objects shores.

We have assessed the extent of the shores for a 50-year period at Novosibirsk Reservoir and for a 92-year period at the Russian part of Curonian Spit (sea side). To carry out the assessment the diverse cartographic material and remote sensing data for the area under study were used.

2. Results

The map supply of investigation included the topographic maps (1:25,000 and 1:50,000 scale) covering the coastline and water for the period before the reservoir impoundment (the year 1953), filling (1958–60) and during 1990–2000. Besides, the state topographic maps of scale 1:200,000 (1987), and Ger-

Elena Fedorova, Evgeniya Sviridova, Konstantin Marusin, Alexandr Khabidov (✉)
Institute for Water and Environmental Problems SB RAS, Barnaul, Russia
e-mail: fedorova@iwep.asu.ru; sviridova@iwep.asu.ru; kat@iwep.asu.ru;
khabidov@iwep.asu.ru



man topographic maps (1908) were used. For the entire area of Novosibirsk reservoir the SPOT-2 panchromatic space images of 10-m resolution (date of survey May–August 2008–09), and multispectral image Iconos for Sosnovka—Burmistrovo site of 4 m resolution (date of survey—July 18, 2004) were applied. For the territory of Curonian Spit the Google Earth images (2007) were used. The comparison of space images and cartographic materials allowed us to determine accurately the current location of the coastline and to estimate its change. Maps and images were processed and georeferenced by ArcGIS software. The works and calculations were carried out in rectangular coordinate system of Pulkovo 1942. A distribution of degraded areas and of accretive sediments in major environments of relief formation and sedimentation in Novosibirsk reservoir is shown in Table.

Table

The extent of abrasion and accumulation in Novosibirsk reservoir during a 50-year period of its operation

	S_{total} , km ²	S_w , km ²	S_t , km ²	S_f , km ²
Degraded territory	31.238	28.786	1.151	1.301
Accumulative territory	40.788	8.265	1.278	31.245

S_{total} —total area of abrasion/accretion; S_w —area of abrasion/accretion in wave-dominated environment; S_t —area of abrasion/accretion in transitional environment; S_f —area of abrasion/accretion in fluvial-dominated environment.

The accretion of solid runoff of Ob river occurs in the fluvial-dominated environment that is similar to delta execution. Most part of this material into the formation of new islands and the advance of coastline. Thus, during a 50-year period of Novosibirsk reservoir operation the number of islands in the wave-dominated environment decreased from 231 to 133 (their total area reduced by 6 km²), in transitional environment their number decreased from 2 to 1 (however the area increased by 0.03 km²), while in fluvial-dominated environment the number of islands increased from 257 to 272, and their total area enlarged by 25 km².

In transitional environment the accretion is associated mainly with the accumulation of fine-grained substances of the sediment runoff, and to a lesser extent due to the coastal erosion products. In wave-dominated environment the sedimentation in the coastal zone takes place mainly due to the entering of small bays followed by the coastline smoothing. Accumulation of alluvium is a result of natural processes and the coastal protection. On the reservoir bottom the sedimentation of silt introduced by the solid runoff takes place.

The most extent coastal erosion for 50 years is observed at Sosnovka village (the right coast of the reservoir), the coastal retreat makes up 535 m; thus, the maximum rate of erosion at Novosibirsk reservoir is 10.7 m/year. At Leninskoye settlement (the left coast of the reservoir), the coast has retreated by 274 m, the rate of erosion is 5.48 m/year. The average rate of erosion in the wave-dominated environment is 1.5–3 m/year. The right bank of the reservoir is eroded more intensely as compared to the left one due to the predominance of west winds. The distribution of erosion areas of Curonian Spit is shown in Fig. 1.

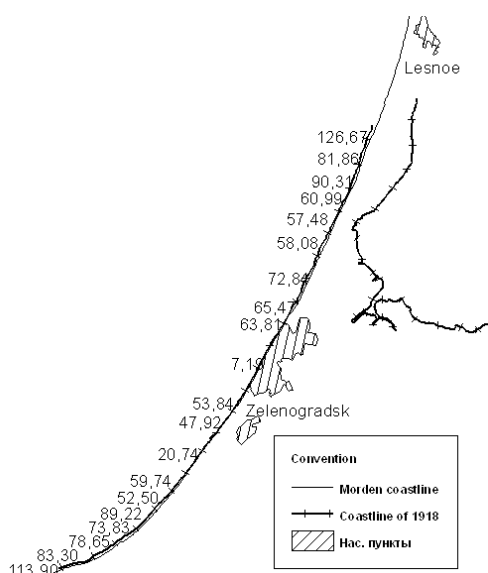


Fig. 1. The distribution of erosion areas of Curonian Spit.

The analysis of cartographic materials was conducted to assess the influence of marine waters on the coast of Curonian Spit. It revealed the most intense erosion in the root part from Zelenogradsk town to Lesnoye settlement. The average rate of coastal erosion decreased from 1.23 to 0.23 m/year; the increase of up to 0.6 m/year was observed in the north-western part of the town. The rate of the coastal erosion at the boundary of Curonian Spit (north-eastern part of Zelenogradsk) varies from 0.69 to 0.79 m per year. Its value increases up to 1.38 m/year between Zelenogradsk and Lesnoye. Further, in the direction Lesnoye → Rybachy → Morskoye → state border of the RF the accumulative processes have a dominant role, and therefore the erosion intensity decreases rapidly from 0.10 to 0.01 m/year.

3. Conclusions

Thus, the application of remote sensing and mapping data allowed accurate assessment of coastal transformation as at Novosibirsk Reservoir as in the Russian part of Kurshskaya Spit. To determine the general state of the coasts and waters the small-scale maps and images with low resolution were used. Large-scale maps and images with high resolution were applied for a detail study of particular sites.

Monitoring and geohazard assessment of the Polish coastal zone using 3D laser scanning

**Jerzy Frydel, Wojciech Jeglinski, Leszek Jurys,
Dorota Kaulbarsz, Malgorzata Schiewe**

Abstract

Coastal zone change is an important issue in northern regions of Poland. It's frequently shaped by geohazard processes such as landslides, falls, slumps, creeps and topples. Monitoring and throughout assessment of these phenomena based on relevant recognition of the coastal zone morphology and geological structure is crucial for successful management of coastal ecosystems. Main factors which trigger denudation are: weathering, mass wasting and erosion. Coastal zone is also subject to abrasion which is responsible for removing, transportation and deposition of fragmented clastic material. Using a 3D laser scanning technique allows to measure the shape of the coast, therefore enables calculation of the exact volume of eroded material. To obtain the surveying recurrence it is essential to determine an accurate geographic location (latitude, longitude and elevation).

Изменение прибрежной зоны является важным вопросом для северных регионов Польши, где происходят процессы опасных геодинамических изменений. Мониторинг и оценка этих явлений начинается с оценки морфологической и геологической структуры, которые сами по себе являются очень важными компонентами существования экосистем. Многие факторы, такие как погода, сброс материала и эрозия ускоряют изменения. Использование трехмерного лазерного сканирования в сочетании с высокоточной географической привязкой позволяет измерять береговые формы и рассчитывать объемные изменения.

Jerzy Frydel, Wojciech Jeglinski, Leszek Jurys, Dorota Kaulbarsz,
Malgorzata Schiewe (✉)
Polish Geological Institute, National Research Institute, Gdansk, Poland
e-mail: jerzy.frydel@pgi.gov.pl

Analysis of deformation of the bottom relief in the segment of the northern shore of Sambian Peninsula in the vicinity of the Port Pionerskij

Konstantin Karmanov, Dmitry Domnin

Abstract

The restructuring of the depths of the study area from 1993 to 2008 is discussed. The change in the amount of bottom sand deposits within the considered section of coast is estimated.

В работе рассмотрено изменение структуры глубин исследуемого района по данным 1993 и 2008 гг. Помимо изменения топографии дна рассматривается изменение количества донных песчаных отложений в пределах рассматриваемого участка побережья.

Konstantin Karmanov, Dmitry Domnin (✉)
P. P. Shirshov Institute of Oceanology RAS, Atlantic Branch, Kaliningrad, Russia

The evolution of semi-sheltered bayhead beaches: a study for Valgerand in Pärnu Bay

Katri Kartau, Tarmo Soomere

Abstract

Valgerand (White Coast) is one of the most beloved sandy beaches in Pärnu Bay, SW of Estonia. During the last 30–40 years, erosion processes in Valgerand have been caused substantial coastal retreat in the entire beach area. Modelling of the evolution of the coastal profile shows that Valgerand is extremely sensitive with respect to strong storms and waves in high water conditions. Simulations of the beach platform and analysis of the morphology indicates that a cafeteria, constructed in the waterline area decades ago and serving as a groin, affects the sediment transport only locally. Therefore it may be concluded that the cafeteria insignificantly affects the functioning of the entire beach and the erosion in Valgerand is mainly due to storms.

Вальгеранд (Белый берег), расположенный в бухте Пярну, известен как один из самых лучших песчаных пляжей юго-восточного побережья Эстонии. В течение последних 30–40 лет процессы эрозии в Вальгеранде привели к значительному отступанию береговой линии. Проведенное численное моделирование показало, что береговая линия Вальгеранда чрезвычайно чувствительна к воздействию штормов и волн большой амплитуды. В результате моделирования динамики и анализа морфологии пляжа было показано, что кафе, построенное несколько десятков лет назад вблизи линии уреза и служащее своего рода волнорезом, влияет только на локальный перенос донных отложений. Таким образом, построенное кафе не оказывает значительного влияния на динамику пляжа в целом, и наблюдаемая в Вальгеранде эрозия берега может быть объяснена воздействием штормов.

1. Introduction

Even though the Estonian coast is experiencing postglacial uplift (1–2.8 mm/year depending on the particular site, Vallner et al., 1988), recession features are often detected in some Estonian beaches. It is thus not unexpected

Katri Kartau, Tarmo Soomere (✉)
Institute of Cybernetics at Tallinn University of Technology, Tallinn, Estonia
e-mail: katri.kartau@gmail.com; tarmo.soomere@cs.ioc.ee



that particularly rapid development of beaches have been reported for the western Estonian archipelago that are widely open to wave fields approaching from the Baltic Proper. Simultaneously, recession of several mostly sheltered bayhead beaches has been also observed in the recent past. While such recession has been mostly caused by human intervention to the development of Pirita Beach (Soomere et al., 2008), natural erosion processes are evident in several other beaches.

In this note, we describe several features of long-term evolution of one of the sandy beaches that suffers from gradual erosion. Valgerand (White Coast, Fig. 1) is one of the main sandy beach areas in Pärnu Bay, in the south-west of Estonia. It is located just a few kilometres west from Pärnu, a few kilometres from a neighbouring village Audru and quite close to Audru River. It is famous for its fine white sand and for a beautiful pine tree forest, but shows gradual retreat and seems to develop under continuous stress.

2. Results

During the last 30–40 years, the erosion processes in Valgerand have dramatically increased which has significantly changed the entire beach area. The performed analysis of historical data, the structure of the beach, and dominant hydrometeorological conditions, reveals that the main cause of erosion in Valgerand apparently is a coincidence of many unfavourable conditions, such as:

- ✓ Strong winds from unfavourable direction (South-West);
- ✓ High storm surge (such as during the January 2005 storm when the water level was 275 cm above the normal sea level and waves attacked unprotected dunes);
- ✓ Mild winters, the lack of sea ice and the presence of non-freezing sediments that can be easily eroded and transported (Tõnisson et al., 2009).

To more understand the beach processes in Valgerand, the modeling software CEDAS—Coastal Engineering Design and Analysis System—was used. CEDAS is an interactive Windows based system that is designed for engineers and scientists in coastal, ocean, and hydraulic engineering; oceanography; and geology fields and it was developed by the Waterways Experiment Sta-



Fig. 1. Valgerand and the cafeteria Doberan today (Estonian Land Board 2009).



tion, Coastal and Hydraulics Laboratory (CHL) in the US Army Corps of Engineers.

CEDAS covers a wide range of software solutions that are designed for the specific situations and locations for modelling. However, programs that were used for analyzing the situation in Valgerand, were SBEACH and GENESIS.

SBEACH (Storm-induced BEACH CHange Model) calculates only cross-shore sediment transport, berm and dune erosion produced by storm waves and water levels. The program operates in the CEDAS graphical user interface designed to facilitate data input, model setup and execution, and analysis of model results. This model can also be used in beach design and fill projects.

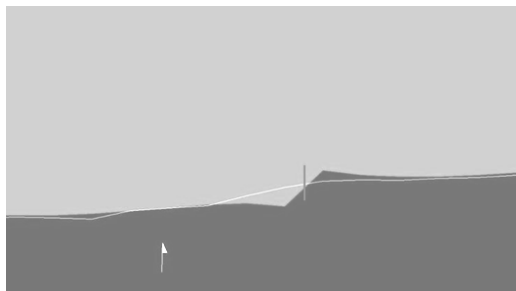
Modelling the evolution of the coastal profile with the use of SBEACH model, shows that Valgerand is extremely sensitive with respect to strong storms and waves in high water conditions. The biggest changes to an actually measured coastal profile occurred in the nearshore area and were accompanied by a certain retreat of the coastline. As the model water level was kept constant, there were no significant changes to the beach and berm. An interesting and quite realistic feature is that sand bars started to form and gradually propagate towards the coast in the nearshore area.

Although the SBEACH model apparently captures the basic features of the cross-shore transport of fine sediment and the erosion processes in the beach, its results should be interpreted with care. Namely, the model assumes that there is always enough sand but in reality sand layer is very thin at some places in Valgerand.

Another module GENESIS (GENERALized Model for SIMulating Shoreline Change) was used to that calculate long-term shoreline changes. The model is mostly designed for coastal engineering and planning communities for predicting the behaviour of shorelines under the assumption that there is insignificant net cross-shore sediment transport and that the cross-shore coastal profiles keep an equilibrium shape. These assumptions evidently satisfactorily match the reality in Valgerand. GENESIS is used to simulate the natural sediment movement on the coast but it also analyzes the effect of groins, detached breakwaters, seawalls, jetties on the beach. It can be used to develop regional sediment budgets and in beach filling projects. Typical longshore extents and time periods of modelled projects can be in the ranges of 1 to 100 months and 1 to 100 km.

An attempt to model the evolution of the planform of Valgerand with the GENESIS model was made starting from a shoreline that was constructed based on the 1970 hydrographical map. As expected, the overall shape of the

Fig. 2. Coastline changes in GENESIS model.





coast showed a tendency to straighten. This process is clearly visible in the nature today. Over the years, the coastline has become smoother and has been considerably straightened as seen in the recent maps.

Exactly at the waterline of Valgerand there is located a cafeteria called Doberan (see Fig. 3). Originally, it was built inland on old dunes but recession of the beach has fully exposed it to the sea since about the year 1990. There have been speculations about the role of this building in the sediment transport and about its potential impact to the coastline. The cafeteria has even been accused to be the major cause for the sediment loss from the entire beach.

In order to simulate the impact of this building on the coastline, a groin was inserted into the planform of the beach at the location of the cafeteria. On the western side of this construction, certain amount sediment is accreting whereas there is relatively fast erosion on its eastern side (Fig. 2). This is due to the fact that the overall sediment movement is to the east (from left to right in Fig. 2). This direction coincides with the direction from the baymouth to the bayhead of Pärnu Bay. When this groin was not present, sediments were divided evenly across the entire coastal area and the coastline gradually straightens. The presence of the groin, as expected, distorts the sediment motion to some extent. There is a certain area of accumulation to the west of the groin whereas there is an almost equal coastline retreat section to the east from the groin where coastal retreat is especially rapid during heavy storms.

Comparison of Figs. 2 and 3 confirms that the performed simulations with the GENESIS model realistically capture the basic disturbances to the coastal evolution caused by the presence of the cafeteria. The construction does have some influence, but it does not essentially contribute to the overall intensity of coastal processes in the beach, except for a small section immediately to the east of it.

There are some adverse effects implicitly caused by this building, a large stone revetment and a seawall have been built (Fig. 3) to avoid further erosion of the foundation of the cafeteria and the beach to the east of the building. Namely, the presence of the relatively large hard structure might fasten both erosion and sediment transport processes in its immediate vicinity. Their presence have apparently increased the local erosion in the vicinity of these



Fig. 3. Valgerand and cafeteria in 1996. (Photo of K. Orviku).



structures as expected from the general experience of the presence of hard structures in a sedimentary beach. They stop the erosion in the protected section but frequently result in overall intensification of coastal processes in the neighbouring areas.

3. Conclusions

In conclusion, simulations with the GENESIS model and analysis of the morphology of the beach with and without an equivalent structure to the cafeteria indicate that its presence affects the sediment transport only locally. The overall sediment budget, however, is almost independent on the presence or absence of this structure. Therefore it may be concluded that this cafeteria insignificantly affects the entire beach. The main cause of erosion in Valgerand is still due to the storms.

However, all the modelling efforts revealed that the deficit of sand is expected to be the overall feature of Valgerand also in the future and sustainable development of the beach needs human intervention. The choice of an adequate beach protection system is an important question in the further development and protection of Valgerand. In general, it should be based on the principle that the method of protection should follow the natural conditions. In a cliff shore, seawall is very good protection method, because the concrete wall acts the same way as the natural beach, but in sandy beach, the best way to protect it, is by filling the beach with sand (Orviku, 2005).

References

- Orviku, K. (2005) Mererand vajab paremat kaitset. [Seaside needs better protection]. *Eesti Geograafia Seltsi aastaraamat [The Society of Estonian Geography]* **35**:111–129.
- Soomere, T., Kask, A., Kask, J., Healy, T. (2008) Modelling of wave climate and sediment transport patterns at a tideless embayed beach, Pirita Beach, Estonia. *Journal of Marine Systems* **74**:S133–S146.
- Tõnisson, H., Jaagus, J., Kont, A. et al. (2009) Damage to coastal nature and society of Estonia by the extreme storm and flooding on January 9, 2005. In: *Climate change impact on Estonian coasts. The Results of the ASTRA Project*:126–127. Institute of Ecology, Tallinn University, Publication 11/2009,
- Vallner, L., Sildvee, H., Torim, A. (1988) Recent crustal movements in Estonia. *Journal of Geodynamics* **9**:215–223.

Current mineralogical and petrographic parameters at the coastal zone of the Sambian peninsula (Kaliningrad region)

Alexander Sergeev

Abstract

Some results on the mineralogical and petrographic analysis are presented in the paper. Testing facilities had been collected from the modern sediment of the coastal zone of the Sambian peninsula. Results contain the information about mineralogical composition of heavy sub fraction from bottom sediments of coastal zone and results of the petrographic analysis from the modern coastal sediment.

В статье приводятся результаты минералого-петрографического анализа современных осадков береговой зоны Самбийского п-ова (Калининградская область). Результаты включают в себя данные по минералогическому анализу тяжелой подфракции донных осадков береговой зоны и результаты петрографического анализа современных отложений приурезовой части пляжа.

1. Introduction

Most integrated mineralogical data related to the seaside and submerged shore slope of the Sambian peninsula take their origin from the second half of last century (Gudelis, Emelyanov, 1976; Stauskaite, 1966).

Seaside zone of Sambian peninsula is a zone, where active erosion shore processes take place. That's the reason for our having updated mineralogical and petrographic parameters of the uppermost shore sediments.

Mezozoic, Cainozoic, Quaternary rocks dominate in the area (Zagorodnyh, 2001). Debris of these rocks is the main source for modern sedimentation.

Mineralogical analysis data of heavy sub fraction from submarine shore slope bottom sediments and petrographic analysis data from soft sediments

Alexander Sergeev (✉)

A. P. Karpinsky Russian Research Geological Institute (VSEGEI), St. Petersburg,
Russia

e-mail: Sergeevau@yandex.ru



are used in this paper. Testing materials were sampled during geological surveying of surface sediment disposition. Surveys were provided by VSEGEI of Karpinskiy during the face of prospecting Kalingrad's shelf zone in the year 2006–07.

2. Results

2.1. Petrographic features of seaward coast sediments.

In general, value of minerals in the coarse and medium size grained sand (1.0–0.25 mm) is not high. However this value grows rapidly in the fine grained sand (0.25–0.1 mm), in the same time value of heavy sub fraction content rises up (Gudelis, Emelyanov, 1976).

According to the petrographic analysis results, middle size grained sand dominates among other coastal sediments. Forming minerals in this sand are quartz, feldspars, carbonates, glauconite.

Quartz grains are clear, well rounded, rarely cracked. Potassium dominates in feldspars in proportion 9/1. Feldspars debris are mean rounded, sometimes they have a tracks cleavage in grains. Carbonates dominate among the sediments. They are exposed mostly by well rounded calcite and dolomite. Glauconite is presented by oval ideally rounded deep green grains with aggregated structure. Glauconite size at all available exposure is 0.2–0.1 mm (fine sand fraction).

According to Shutov diagram, coastal sand sediments have oligomictic and mesomictic compositions (Fig. 1). Depends on the mineral components disposition in sediments three zones were selected.

(1) West side of Sambian peninsula. Here we see most chaotic disposition of mineral components. Consistence of minerals can be low or high in this part of the seaside. Glauconite value is big.

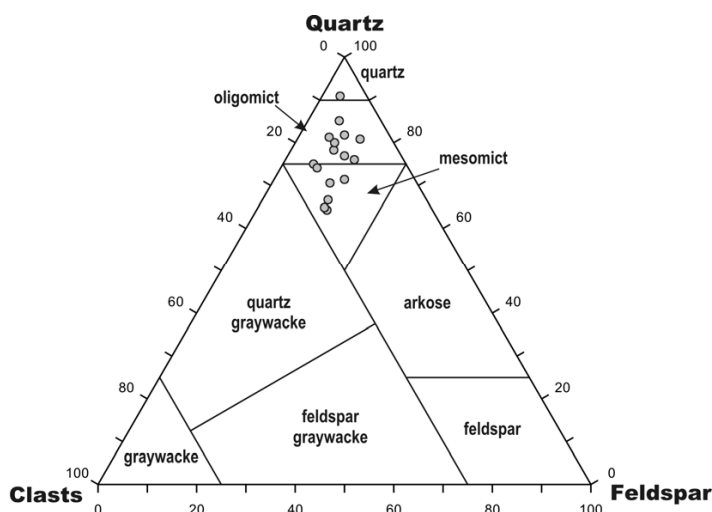


Fig. 1. Diagram of mineralogical and petroclastic sand rocks classification (Shvanov, 1987).



(2) North side of Sambian peninsula. Quartz value exceeds average with its rising to the east. Value of feldspar is high at the west and average at the east. Rocks debris has maximal value at the west (cape Taran) and low value at the east of the zone. Glauconite value is average in the debris of the north seaside accept high value at the west of place.

(3) Attached end of Curonian Spit. Quartz value is high with local minimum in the middle of the zone. Feldspars are opposite. Debris value is high in the sediments of the root part of the Kurshskay spit. Glauconite has a zigzag disposition along the shore. Glauconite does not exist in the root part of the Curonian Spit, high value in the middle, average value in the north-east.

2.2. Mineralogy of heavy sub fraction at the bottom sand sediments

There are 20 minerals in this sub fraction. Most valuable are garnet, amphiboles, pyroxene and other ore minerals. Data for disposition of heavy minerals are in the Table.

Table

Mineral composition of heavy sub fraction in percent

Mineral	West side of Sambian peninsula	North side of Sambian peninsula	Attached end of Curonian Spit
Phosphate	25.7 – 0.5	8.5 – 0.0	7.7 – 2.3
	4.9	2.5	4.4
Glauconite	50.0 – 1.8	6.5 – 0.0	0.0 – 0.0
	14.4	1.8	0.0
Group of epidotes	12.0 – 3.0	14.7 – 2.2	11.1 – 6.5
	6.4	7.7	9.0
Amphiboles	17.7 – 3.2	15.5 – 5.5	22.6 – 4.7
	8.9	7.9	15.6
Group of pyroxenes	9.3 – 3.0	9.5 – 2.2	32.3 – 6.5
	6.4	7.7	9.0
Garnet	12.5 – 0.0	29.4 – 2.4	14.0 – 2.6
	7.0	16.0	6.9
Siderite	4.7 – 0.0	12.2 – 2.1	5.1 – 0.0
	1.3	7.3	3.3
Ilmenite, leucogene	44.4 – 0.0	38.3 – 13.1	16.3 – 0.0
	24.7	21.2	7.2
Marcasite, pyrite	14.9 – 0.0	0.8 – 0.0	0.0 – 0.0
	7.0	0.2	0.0
Heavy minerals content (%)	1.9 – 0.3	1.2 – 0.4	1.7 – 0.5
	0.9	0.9	1.0

Heavy minerals dominate in the modern sediment. They are close in their composition to the minerals from Paleogene and Quaternary periods. This

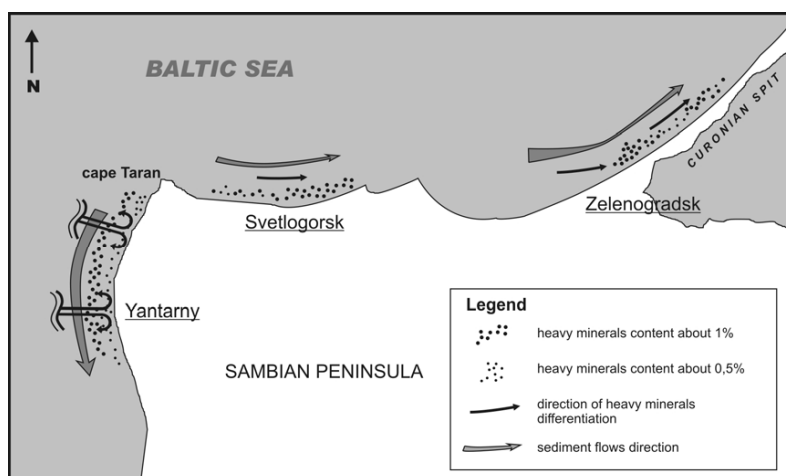


Fig. 2. Scheme of consistence and distribution of the heavy sub fraction from sediment of the submerged shore slope at depth range 1–10 m.

circumstance clearly shows that sediment comes to the shore slope from the erosion of the ancient rocks.

Characteristic of the west shore slope is sediments flow along the coast to south. It caused by natural morphology of the shore and erosion processes. On the western shore slope an enrichment zone heavy minerals are depths of 5–10 m. These depths are area with the maximum wave processing. North shore slope can be divided on 2 zones: west—where erosion process dominates and east which is a kind of transit zone. Submarine slope of the Curonian spit should be divided to the two parts as well. One of them is a root part—zone of transformation for direction of the sediment flow and transformation of hydrodynamics of the environment. Such a changed dynamics leads to the growing of amount of heavy minerals in the sediment and it changes the consistence of heavy materials. Second part which is on the north east—becomes a place of origin for the flow of eroded material shrinking with a slight accumulation of heavy fraction by the less weighted minerals. That shows to the ending of erosion processes (Fig. 2).

Acknowledgements

The author is grateful to its colleagues from VSEGEI and N.A. Kalmykovej for the given analysis date of heavy mineralogy.

References

- Gudelis, V. K. & Emelyanov, E. M., eds. (1976) *Geology of the Baltic Sea*. Vilnius: Mokslas (in Russian).
- Shvanov, V. N. (1987) *Petrography of sandy rocks (composite, systematization and description of minerals)*. Leningrad (in Russian).
- Stauskaite, R. (1966) *Lithology and lithodynamics of modern sediments in the coastal zone of south-east the Baltic Sea*. PhD author's abstract. Vilnius (in Russian).
- Zagorodnyh, V. A., Dovbnya, A. V., Zhamoida, V. A. (2001) *Stratigraphy of Kaliningrad region*. Kaliningrad (in Russian).

Geological and geomorphological conditions of the coast of the Sambian Peninsula

Anna Shishkina

Abstract

Investigations were conducted on the northern coast of the Sambian Peninsula in July 2008. During survey routes from the Filinskoy bay to the Sokolniki village, basic geological sections and shore-composing rocks were described. Besides, beach morphometric profiles were laid for exploration the geomorphological structure and coastal processes of the Semba Peninsula northern coast.

Исследования проводились на северном побережье Самбийского п-ова в июле 2008 г. В ходе обзорных маршрутов, от Фининской бухты до пос. Сокольники, были описаны опорные геологические разрезы, породы слагающие берег, а также заложены морфометрические профили пляжа с целью изучения особенностей геоморфологического строения и развития береговых процессов северного побережья Самбийского полуострова.

1. Introduction

The coast of the Kaliningrad region is an important recreational object. This area suffers strong anthropogenesis influence. Large resort cities are located in the area and amber deposits are developed. All of this results in changes of environment and deterioration of the coastal condition. For understanding of geomorphological processes it is necessary consideration a wide spectrum of influencing factors the coast, in particular an important role of geological conditions. In this connection, a monitoring of the coastal zone is of great value. An activity of Kant State University of Russia contributes considerably to this area study. Annually, survey routes to the coast of Semba peninsula are carried out in the scope of students' practical training. The research helps supervising environmental changes of the coastal zone and making optimal decisions on coastline protection.

Anna Shishkina (✉)
Southern scientific centre Russian Academy of Science, Rostov-on-Don, Russia
e-mail: shishkinaanna@bk.ru



2. Study area

The research was carried out on the northern coast of Semba peninsula, in July 2008. Two routes passed the northern coast of Semba peninsula and covered the territory from the Filinsky bay to the settlement of Sokolniki. A purpose of the work is a study of geological and geomorphological features of the northern coast of Semba peninsula.

3. Results

During the survey routes the sites with resembling geological structures were found and scaled. Within the limits of each site, the reference point was chosen for description of the breeds composing the coastal ledge. Slope processes were described and microrelief forms were located. For the beach study, morphometric profiles were constructed and beachfront sediments were investigated. By means of references the geological history of the region, peculiarities of the coastal zone development, factors influencing formation of coast shape and basic tendencies of modern development of a coastal zone have been studied.

In coastal breakages the breeds are neozoic bared, the most ancient of them are palaeogene. Quaternary sediments are presented by all four departments: bottom, average and top Pleistocene and Holocene. Preholocene sediments in overwhelming majority have glacial genesis. The bottom department is presented by the sediments genetically connected with the most ancient quaternary glaciations. Holocen on conditions of sedimentation is a postglacial epoch. Its sediments are presented by the diversified continental phase of various genesis: lake-marsh, sea, lake-sea and aeolian. Coast formation is directly connected with the history of development of the Baltic sea which has appeared as a modern reservoir only in postglacial epoch. The sea level change, connected with approach and melting of a glacier, was the basic relief-forming factor. The coast is the a complex of friable breeds. The characteristic is interlaying clay and sand.

During a survey route from the settlement Rybnoye to the Filinsky bay 5 sites have been allocated. Criterion of allocation was the change of the it complex of radical breeds bared in the coastal ledge. The height of coastal ledges from Svetlogorsk to settlement Lesnoye varied from 10 to 45 m from the West to the east. During the description of geological cuts the basic composing breeds have been revealed. The profiles constructed near Svetlogorsk (700 m to the east from the termination of the promenade and the western extremity of the promenade), have been formed by sand. On advancement from the east to the West there was a change of breeds of the top horizon. In the east from the promenade of Svetlogorsk in the top horizon sand with gravel and pebble layers (15 cm), and in the west—brown loams lie down. On further advancement to the West in coastal ledges we allocated small capacity (to 2 m) Layers of black clay (lignite) which carry out the water protection role. Near the settlement Lestnoye on sand and clay the layer of black loams (5) and higher—sandy loams (15) lie.

Various coastal sediment have different genesis, clay and loams—marsh, sand—costal-sea or lake, sandy loams—glacial.



On the coast of Semba peninsula there is a unique formation—the Earth of Kranta. These sediments finish cut the palaeogene. They are formed of brown sandstone, a basis of its mineral structure is glauconitic-quartz sand, strongly cemented iron hydroxides. In a slope there is set of fossils (moves of mud-eaters and of minerals mollusks). Sandstone is covered by glaukanito-quartz sand. The genesis is coastal-sea.

On a site of coast from settlement Rybnoye to settlement Sokolniki 5 profiles have been constructed. In this area the height of coastal ledge varied from 9 to 5 m, then the shaft gradually decreases, and the beach takes a form of a full profile. The profile put on cape Gvardejsky, is combined of loams with inclusion of boulders. To the east of the stream the Spokojny coastal ledge is combined of a pebble and loams with inclusion of lenses sand-gravel-pebble material. To the west of the river the Zabava the slope is combined by loams, the presence of boulders in the top part of the coastal ledge shows transportation activity of a glacier. Near the settlement Kulikvo in a coastal slope we see clay and sand. The origin of breeds is mainly glacial and leke-glacial.

Geological a condition, characterized by prevalence of easily destructed friable breeds, in a combination with increasing level of the ocean, strengthening of storm activity and intervention of human civilization, promote development of abrasive and landslide processes on the northern coast of Semba peninsula. Widespread of such slope processes, as formation of taluses, sailings and erosive furrows are observed.

The process of destruction of the coast has become more intensive last years because of increase in quantity of storm excitements, increase in anthropogenous loading and reduction of width of beaches. Speed of washing out of abrasive makes coast is from 0.1–0.7 on capes (capes Kupalniy, Gvardeyskiy) to 0.6–1.5 m/year on boards of bays from settlement Filino to Svetlogorsk, to the east of cape Gvardeyskiy. In storm rates of destruction of the coast is ten times above mid-annual values.

Along coastal ledges lean-to beach is formed. The width of such beach is from 5–7 on capes and up to 40–50 m in bays and concavities. On capes where waves can easily reach the coastal breakages, beaches are combined of a bollder-clumpy material. In bays where the coast is protected from the impact of waves by a wide beach, in a structure of beaches sandy accumulation with a pebble and gravel impurity in the serf strip prevails.

Now the tendency of reduction of beaches width of the Kaliningrad region is marked. The narrowest beaches are located on the northern coast of Semba peninsula this is connected with deficiency of deposits, washing out of an underwater raincoat and disturbance of natural lithological mode. On the northern coast of Semba peninsula there are mainly beaches less than 15 (27 percent) in width and 15–30 m (61 percent), beaches in width. Beaches of more than 50 m in width are not found, while in 1984 they were stretched 1 km along of coast.

During the expedition it has been noticed that on Capes Kupalniy, Gvardeyskiy the beach is composed of boulder-pebble material. In the rear part as a rule pebbles with sand prevail, and the quantity of rough fragments increases in the front part. On the site of Cope Gvardeyskiy it is possible to observe a beach of an incomplete profile: in a rear part sandy with a considerable quantity of gravel, pebble, boulders, in the front part the quantity rough



fragments increases and the quantity of sand decreases. The width of the beach is of 8 m.

On the northern coast of Semba peninsula, near the settlement of Sokolniki the accumulative type of coast is presented. The beach of a full profile with accurately expressed shaft is observed. The rear part of a beach is adjoin by the eolian-accumulative forms: foredune ridge and sandy spits generated by the transportation and accumulation of sand, grasped by a wind stream on the beach. The width of the beach up to the foredune ridge 20 m, the height of the dune is 5 m.

Reduction of width of a beach worsens an ecological condition of coast. The reason of reduction of beaches is deficiency of the overburden, formed as result of regulation of abrasion slopes. On the one hand, the destruction of the coast from erosion is a serious problem for recreational facilities, on the other hand, is a natural process that plays a key role in the supply of sediment to build such accumulative forms like scythes and beaches.

4. Conclusions

Summarizing the knowledge received as a result of the research, it is possible to draw following conclusions on geologo-geomorphological conditions of northern coast of Semba peninsula. Coastal ledges are combined of a complex of friable breeds (sandstones, sand, loams, sandy loams) and clays. Geological conditions in a combination to wave activity, are the reason of distribution of abrasive processes on the coast of Semba peninsula. As a result of abrasion coastal ledges up to 45 m. high are formed. Abrasive material goes on construction of the beaches which width on the northern coast of Semba peninsula reaches 20 m. There are sandy beaches and the beaches combined formed of rough fragments (a pebble, gravel, boulders). The width of the beaches is reducing that negatively affects the an ecological condition of the coast.

Acknowledgements

I express my gratitude to the managing chair the geography of ocean of the Russian State Kant University of the Edging to the doctor of physical and mathematical sciences to the professor Vladimir Gritsenko and the senior teacher of chair geography of ocean Galina Mihnevich.

Infragravity waves in the south Baltic dissipative coastal zone

Piotr Szmytkiewicz

Abstract

It is a widely accepted assumption that infragravity waves are generated by complex of nonlinear mechanisms: time-varying breakpoint position, surf zone wave groupiness effect, shoreline reflection, and refractive trapping. The study done at IBWPAN Coastal Research Station at Lubiatowo suggested existing infragravity waves can develop at a dissipative, multiple bar south Baltic system. At the beginning of the analysis the observations obtained with alongshore oriented string wave gauges have been previously used to identify concentrations of wave energy. This was done by using wavelet and Fourier analysis. Deployment of the 2nd wave gauge in close shoreline proximity confirmed the hypothesis on the presence of infragravity waves at the studied dissipative beach.

Широко принято предположение, что инфрагравитационные волны генерируются комплексом нелинейных механизмов, зависящих от положения точки разрушения, фактора групповитости в прибойной зоне, отражения от берега и рефракционного улавливания. Исследование, проведенное на IBWPAN береговой исследовательской станции в Любятово предположило, что существующие инфрагравитационные волны могут развиваться в диссипативной береговой системе южной Балтики с множеством подводных валов. В начале анализа наблюдения получали с помощью ориентированных вдоль берега струнных волнографов, до сих пор использовавшихся для определения концентраций волновой энергии. Это было сделано с использованием вэвлет и Фурье анализа. Разрушение второго источника волн в близости к урезу подтвердило гипотезу существования инфрагравитационных волн на изученном диссипативном берегу.

Piotr Szmytkiewicz (✉)
Institute of Hydro-Engineering of the Polish Academy of Sciences (IBW PAN),
Gdańsk, Poland
e-mail: P.Szmytkiewicz@ibwpan.gda.pl



1. Introduction

It is a widely accepted assumption that infragravity waves are generated by complex non-linear mechanisms: time-varying breakpoint position, surf zone wave groupiness effect, shoreline reflection, and refractive trapping. In general, there are two concepts concerning generation of the infragravity waves. The first one defines them as secondary waves, namely the waves generated by wave breaking and mutual nonlinear interaction between two or more series of wind waves. Within the second theory, the infragravity waves appear as a result of reflection of long waves from the coast. Height of this type of waves strongly decreases with the distance offshore. Generally, these waves can be both progressive and standing. Recently, more and more theories based on the concept of the so-called self organization processes occurring in the coastal zone become popular. As yet, there are no systematic observations of infragravity waves. Due to a high level of complexity, the randomness of a highly non-linear processes associated with the generation of infragravity waves is not fully recognized. The most realistic assessment of these phenomena should be expected from analyses carried out on the basis of observations in natural conditions.

2. Study area

The study done at IBWPAN Coastal Research Station at Lubiatowo suggested existing infragravity waves can develop at a dissipative, multiple bar south Baltic beach system. Initially the observations obtained with alongshore oriented string wave gauges were used to identify concentrations of wave energy. This was done by using wavelet and Fourier analysis. The experimental work was done at the IBW PAN Coastal Research Station (CRS) in Lubiatowo in 2006. CRS is located at Lubiatowo on the Polish coast in the southern part of the Baltic Sea. The beach usually exhibits 4 multiple bars (Fig. 1 bottom)

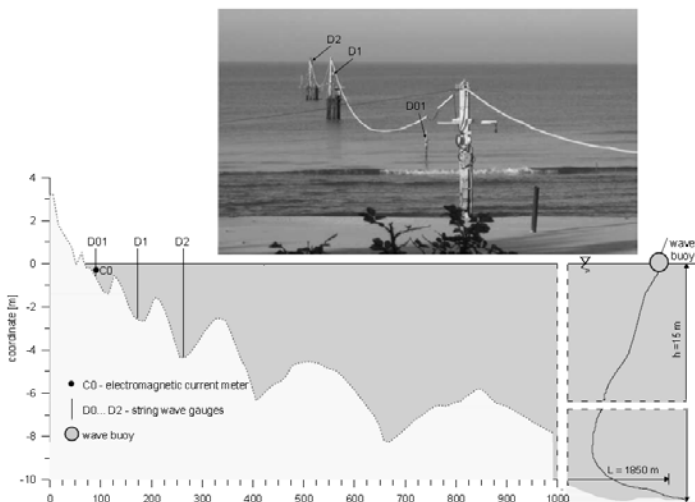


Fig. 1. Layout of measuring equipment during field campaign 2006.



and has a mild mean slope of $m=\tan\alpha=1-1.5\%$ with a median grain size of $D_{50}=0.22$ mm. A predominant west to east littoral drift and multiple breakers are observed. Long term observations show that during average storms the significant wave height outside the surf region, for water depth h of about 20 m usually reaches $H_s=2-2.5$ m with a mean period of $T=5-7$ s. The Lubiatowo beach is a highly dissipative system (Różyński, 2005).

In 2006 field experiments two steel rods were positioned some 30 m offshore, where the average depth of seabed is in the range of 0.6 m (D01, D02 at Fig. 2). In this way it became possible to study cross-shore properties of nearshore hydrodynamics within the surf zone, making use of simultaneous records from two cross-shore locations.

3. Methods and results

The possession of long (time) series describing random variability of the studied physical parameters allows for application of various signal processing tools. In this study two complementary techniques were incorporated, that is conventional spectral analysis and Discrete Wavelet Transform (DWT). DWT was employed to extract key components that may account for the presence of infragravity waves. The wave climate data containing 52 days of registered parameters in close shoreline proximity at two positions: point D01 and D02, *cf.* Fig. 2, were examined using the Discrete Wavelet Transform to extract slow varying components T_h of the wave spectrum. It possesses an important property of locating various oscillations during measurements with the wavelet functions. The resulting multi-resolution analysis performed in this study was based on near-symmetrical *coif5* wavelet function.

We obtained the details which best reflected individual hydrodynamic processes (Figs. 3, 4). From both Figures we can see that the 2nd harmonics and wind waves are captured by period contents: $2 < T < 8$ s. Likewise, most information on infragravity waves are contained in $T \in (32 \text{ s}, 64 \text{ s})$ and on periodic content $T \in (64 \text{ s}, 128 \text{ s})$. Incidental remaining energy are contained by $T \in (128 \text{ s}, 1,024 \text{ s})$.

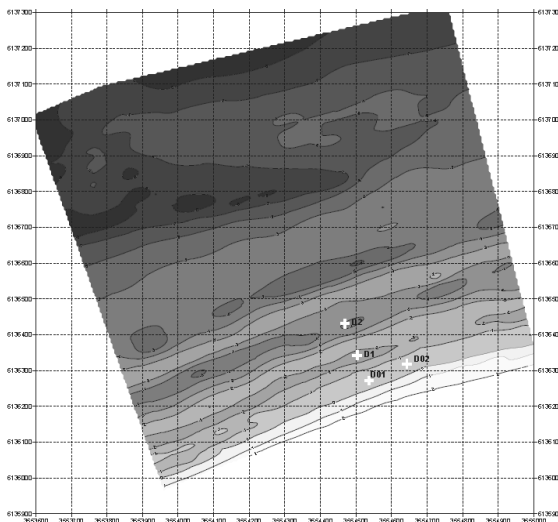


Fig. 2. Measuring equipment, bathymetry of 19.09.2006. D2—string wave gauge at $h=4.2$ m, D1 at $h=2.8$ m, D01 and D02 at $h=0.6$ m.



On the basis on Figs. 3, 4 we could also find moments where in the both places (D01 and D02) long waves occurred on the exactly the same time. Only this part of data was used for further analysis of the presence of infragravity waves at a dissipative multiple bar system.

Wavelet decomposition of both wave records is targeted toward identification of a phase shift in each pair of slow-varying components, from which the associated wavelengths will be extracted. The knowledge of these parameters will then allow for computation of the concomitant modal number for each slow-varying component. In this way the existence of infragravity waves at a dissipative beach will either be confirmed with very strong evidence (existence of relatively stable phase shift between records from two near locations) or rejected (lack of such phase shift). Fig. 5 shows that for $T=32\div 64$ s the phase shift is about 45° , whereas for $T=64\div 128$ it is close to zero.

4. Conclusions

(1) The study provided knowledge on offshore range of slow varying components of the wave spectra, recorded in the surf zone of the overwhelmingly dissipative beach system with multiple bars. Rapid offshore decay of these components allowed for inferring about reflective properties of this system only in close shoreline proximity.

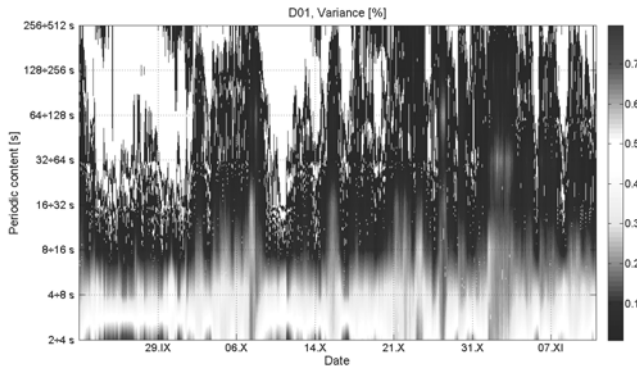


Fig. 3. Various oscillations of variance at string wave gauge D01 at depth 0.6 m.

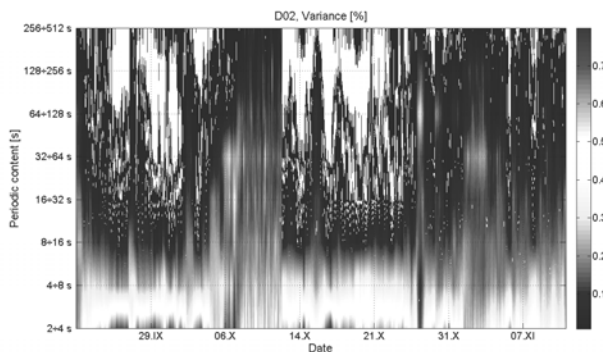


Fig. 4. Various oscillations of variance at string wave gauge D01 at depth 0.6 m.

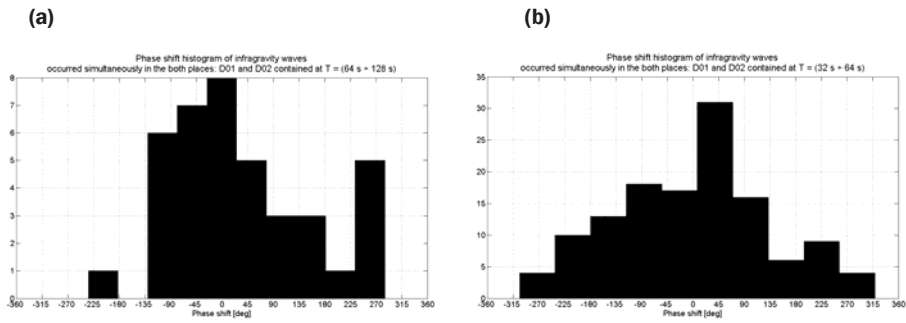


Fig. 5. Infragravity waves phase shifts at D01 and D02; (a) $T=32\div 64$ s, (b) $64\div 128$ s.

(2) Deployment of the 2nd wave gauge in close shoreline proximity confirmed the hypothesis on the presence of infragravity waves at the studied dissipative beach.

(3) Analysis shows that for infragravity waves ($T=32\div 64$ s) the phase shift is about 45° , whereas for infragravity waves ($T=64\div 128$) it is close to zero.

References

- Pruszk, Z., Szymtkiewicz, P., Ostrowski, R. et al. (2008) Shallow-water energy dissipation in a multi-bar coastal zone. *Oceanologia* **50**(1):43–58.
- Różyński, G. (2007) Infragravity waves at a dissipative coast; evidence upon multi-resolution analysis. *Coastal Engineerin* **54**(3):217–232.
- (2005) Long term shoreline response of a non-tidal, barred coast. *Coastal Engineering* **52**:79–91.
- Schaffer, H.A. & Jonsson, I.G. (1992) Edge waves revisited. *Coastal Engineering* **16**:349–368.
- Webb, S.C., Zhang, X., Crawford, W. (1991) Infragravity waves in the surf zone. *Journal of Geophysical Research* **96**:2723–2736.

Coast protection of artificial territory

Ekaterina Volkova

Abstract

Over the last years, creation of beaches over artificial territories has become a common practice. In this way, the artificial territory is protected with the help of creating beaches. Beaches are among the most attractive recreation areas. Simultaneously they carry out protection functions, providing during storm coast protection, and located in shoreline constructions and communications. The beaches are important element of protection of environment coastline zones of the sea. The aim of investigation is protecting artificial territories and artificial islands with the help of creating beaches. Results of experimental research, design and parameters of protection construction were analyzed.

В последние годы обычной практикой стало создание искусственных пляжей на вновь создаваемых территориях для их защиты. Пляжи сами по себе являются очень притягательными для отдыха. Кроме того они обеспечивают защиту во время штормов и самого берега и конструкций, расположенных в непосредственной близости от воды. Пляжи являются также важнейшим элементом защиты береговой зоны моря. Целью работы является защита вновь создаваемых территорий и островов с помощью пляжей. Проанализированы результаты экспериментальных исследований, технические характеристики защитных конструкций.

Ekaterina Volkova (✉)
Branch of Open Society Company, Sochi, Russia
e-mail: brovko.e@mail.ru

Comparison between modelled and measured wind wave parameters in Estonian coastal waters

Inga Zaitseva-Pärnaste, Andrus Räämet, Tarmo Soomere

Abstract

Historical visual observations and numerical hindcasts are merged to reveal the basic features of the wave properties and to identify their changes in the western and northern coastal waters of Estonia. Wave conditions, their seasonal cycle, interannual and long-term variations are established based on visual observations at Vilsandi on the western coast of Estonia (1954–2008), at Pakri (1954–85) and at Narva-Jõesuu on the southern coast of the Gulf of Finland (1954–2008). The observed data are compared against numerically simulated wave data for 1970–2007. The typical wave periods in the coastal areas are 3–4 s. The monthly mean wave height follows the seasonal variation in wind speed with a maximum in October–January and with a substantial variability on weekly scales. The annual mean wave heights reveal nearly synchronous interannual variations along the entire coast of Estonia until the mid-1980s after which this coherence is lost. The shortening of the ice season apparently has led to an increase of the annual mean wave height at the coastal areas of the northern Baltic Proper but has insignificantly affected the wave properties along the southern coast of the Gulf of Finland.

На основе данных визуальных наблюдений проведен анализ долгосрочных изменений волновой активности в прибрежных водах Эстонии в Вилсанди (1954–2008), Пакри (1954–1985) и Нарва-Йыэсуу (1954–2008). Проведено сравнение этих данных, полученных с 1970 по 2007 г., с результатами численного моделирования в рамках пакета WAM. Показано, что до середины 1980-х гг. в изменениях высот волн прослеживается ярко выраженная согласованность краткосрочных изменений с характерным временным масштабом в 1–3 года. Позднее эта согласованность про-

Inga Zaitseva-Pärnaste (✉)
Institute of Cybernetics at Tallinn University of Technology, Tallinn, Estonia
e-mail: inga.zaitseva@gmail.com
Andrus Räämet, Tarmo Soomere (✉)
Tallinn University of Technology, Faculty of Civil Engineering,
Department of Mechanics, Tallinn, Estonia
e-mail: andrus.raamet@ttu.ee



падает. Также с 1980-х гг. в данных визуальных наблюдений в Нарва-Йыэсуу выявлены значительные изменения в направлениях распространения волн, которые не подтвердились в численных прогнозах.

1. Introduction

Studies of properties of complex wave fields in different sea areas and research towards the understanding of both the status of and changes to the wave climate form one of the key elements of physical oceanography and coastal science. This is not only because surface waves are a major driver of processes in the surface layer, nearshore and coastal area, but also because the wave climate is one of the most robust indicators of the changes in wind regime in semi-enclosed sea areas. An accurate picture of typical and extreme wave properties and their potential changes is, thus, of great value for a wide variety of research topics and engineering applications.

In this study we focus on the properties of the waves and their variations along the coasts of north-eastern Baltic Sea. The analysis relies on a comparison of long-term variations of visually observed wave properties at the eastern part of the northern Baltic Proper and the Gulf of Finland (Vilsandi, Pakri, Narva-Jõesuu) and on numerical hindcast of wave properties over the last 38 years in this region calculated using the wave model WAM. Finally, we discuss changes in the directional distributions of wave fields according to measurements and simulations.

2. Methods

The analysis is based on three visually observed wave data sets recorded at (i) the western coast of the island of Vilsandi (58°22'59" N, 21°48'55" E, Fig. 1), (ii) Pakri in the western part of the Gulf of Finland (59°23'37" N 24°02'40" E) and (iii) Narva-Jõesuu in the eastern part of this gulf (59°28'06" N, 28°02'42" E, Fig. 1) in Narva Bay. Systematic wave observations at these sites started in 1954 and have been carried out until today (until 1985 at Pakri).

Data from Vilsandi reflect well waves coming from the westerly directions (Soomere & Zaitseva, 2007) but owing to a small water depth at the observation sites the largest waves may be distorted. Pakri is the only deep-water wave observation site on the southern coast of the Gulf of Finland that is largely open to waves generated in the northern Baltic Proper (Zaitseva-Pärnaste et al., 2009). Waves at Narva-Jõesuu are frequently locally generated and usually stem from the Gulf of Finland. The site is fully open to waves approaching from the north-west and almost open for waves approaching from the south-west to the north. The height of the observation platform is 12.8 m above the mean sea level. This allows even better wave observation conditions than at Vilsandi. The measurement routine was identical for all observation sites (Soomere & Zaitseva, 2007).

The properties of wave fields were calculated using the third generation spectral wave model WAM (Komen et al., 1994). The calculation was done for a regular rectangular grid (a resolution of about 3×3 nautical miles, 239×208 points, 11,545 sea points) based on the bathymetry prepared by Seifert et al. (2001) that extends over ice-free sea from 09°36' E to 30°18' E



Fig. 1. Location of wave observation sites.

and from $53^{\circ}57' \text{ N}$ to $65^{\circ}51' \text{ N}$ (Soomere, 2003). At each sea point, 1,008 components of the two-dimensional wave spectrum were calculated. The model uses 24 evenly spaced directions. Differently from the standard configuration of the WAM (that ignores waves with periods $< 2 \text{ s}$), an extended frequency range from 0.042 to about 2 Hz (wave periods 0.5–23.9 s, 42 frequencies with an increment of 1.1) was used to ensure realistic wave growth rates in low wind conditions after calm situations (Soomere, 2005).

The wind forcing at a 10 m level was derived from geostrophic winds as recommended by Bumke and Hasse (1989): the geostrophic wind speed was multiplied by 0.6 and the direction turned by 15° to the left. This approximation is used in many contemporary studies into the Baltic Sea dynamics (Myrberg et al., 2010).

3. Results

The almost perfect match of short-term variability (1–3 years) of the annual mean wave heights (Fig. 2) and a high correlation coefficient (0.58) between these values in 1957–85 at Vilsandi and Pakri once more confirms that the visual wave observations reproduce well the basic properties of wave fields and their changes.

Although the Pakri data exist only until 1985, the high correlation suggests that the drastic variations of wave properties at Vilsandi reflect real changes in wave fields in the Baltic Proper. All data sets show almost perfect match of years of relatively high and low wave intensity at all measurement sites within the time interval of 1958–1990 (Fig. 2).

This feature shows that the short-term interannual variability with time scales of 1–3 years has the same appearance along the entire coast of Estonia from the Baltic Proper to Narva Bay. This coherence in the long-term variation in wave heights ends abruptly at the end of the 1980s (Fig. 2). While wave activity reveals drastic decadal-scale increase and decrease in the Baltic Proper during the latter two decades, a gradual decrease of the annual mean

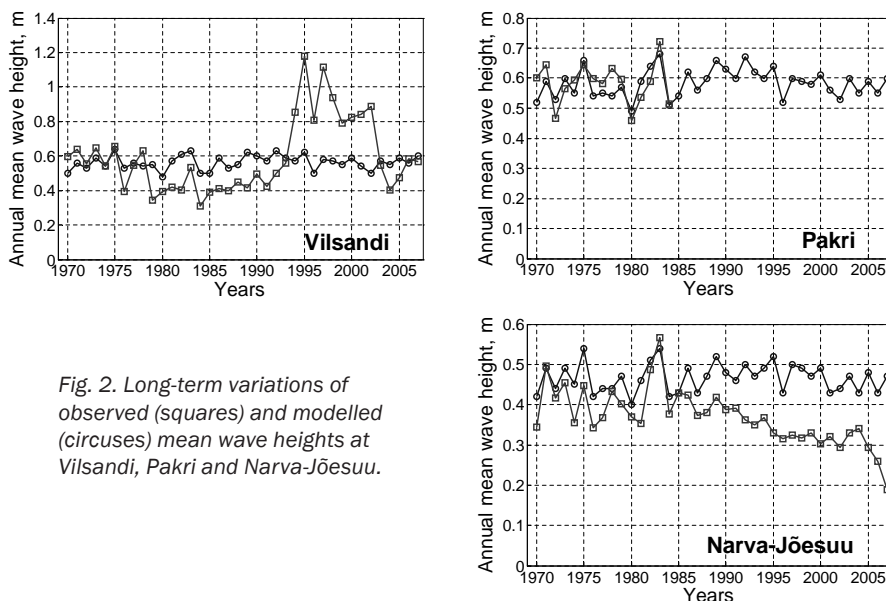


Fig. 2. Long-term variations of observed (squares) and modelled (circuses) mean wave heights at Vilsandi, Pakri and Narva-Jõesuu.

wave height is observed at Narva-Jõesuu. Moreover, differently from the period before the 1980s, years with relatively high wave intensity at Vilsandi correspond to relatively calm years in Narva Bay and *vice versa*.

Long-term variations of simulated mean wave heights match well the observed ones for all measurement sites until 1993. However, the drastic increase of mean wave height at Vilsandi in the turn of millennium and the subsequent decrease are not represented in the numerical hindcast. A similar mismatch happens at Narva-Jõesuu. Although visual observations show rapid decrease in wave activity from 1990, the model does not reflect any strong long-term variations (Fig. 2).

The direction of wave propagation in visual observation diaries was interpreted as the direction from which the waves approach, similarly to the definition of the wind direction. The opposite interpretation in the WAM model is reversed below so that all figures reflect the wave approach direction.

The annual directional distributions of wave approach for Vilsandi and Pakri show a certain interannual and decadal variability but reveal no substantial long-term changes of the predominant direction. Substantial changes in the predominant wave direction have occurred in Narva Bay during the half-century of observations (Fig. 3). Waves mostly approached from the W-NW direction in the 1950s and until about 1965. The predominant approach direction turned almost to the north for the 1970s. Further on, it turned considerably, from the north-west to south-west (for some years even almost to the south) over the 1980s. Then it switched between the W-SW and the south and has been mostly to the south within the latter decade. The most frequent observed propagation direction, therefore, has changed by more than 90° over the half-century of the observations. The second most frequent wave direction (S-SE) has turned in a similar manner but to a lesser extent. Interestingly, none of these changes are reflected in simulated wave propagation directions.

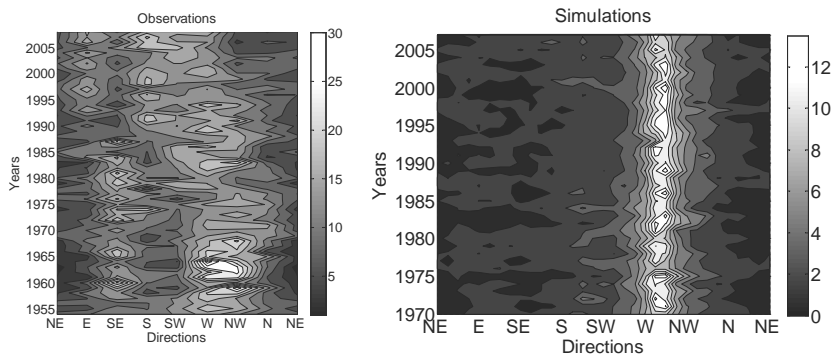


Fig. 3. Observed (left panel, 1954–2008) and modelled (right panel, 1970–2007) directional distribution of wave approach at Narva-Jõesuu. The scale shows the frequency of occurrence (%) of waves from a particular direction.

4. Conclusions

Although the WAM model with the used wind forcing does not replicate certain features of long-term changes in wave properties, short-term variations of observed and simulated wave parameters match well each other.

A highly interesting feature, however, is the substantial turn of the predominant observed wave propagation direction in Narva Bay. Even though the visual observations may contain systematic errors and are strongly observer-dependent, the systematic rotation by more than 90° over a half-century can be interpreted as an evidence of certain changes in the wind fields over the entire Gulf of Finland, possibly connected with the overall increase in the role of SW winds over Estonia (Kull, 2005).

References

- Bumke, K. & Hasse L. (1989) An analysis scheme for determination of true surface winds at sea from ship synoptic wind and pressure observation. *Boundary-Layer Meteorol.* **47**:295–308.
- Komen, G.J., Cavaleri, L., Donelan, M. et al. (1994) *Dynamics and Modelling of Ocean Waves*. Cambridge: Cambridge University Press.
- Kull, A. (2005) Relationship between interannual variation of wind direction and wind speed. *Publicationes Instituti Geographici Universitatis Tartuensis* **97**:62–73.
- Myrberg, K., Ryabchenko, V., Isaev, A. et al. (2010) Validation of three-dimensional hydrodynamic models in the Gulf of Finland based on a statistical analysis of a six-model ensemble. *Boreal Env. Res.* **15**, in press.
- Seifert, T., Tauber, F., Kayser, B. (2001) A high resolution spherical grid topography of the Baltic Sea. In: *Proc. of Baltic Sea Science Congress*, Stockholm, 2, Poster No. 147, www.io-warnemuende.de/iowtopo.
- Soomere, T. (2003) Anisotropy of wind and wave regimes in the Baltic Proper. *J. Sea Res.* **49**:305–316.
- (2005) Wind wave statistics in Tallinn Bay. *Boreal Env. Res.* **10**:103–118.
- Soomere, T. & Zaitseva, I. (2007) Estimates of wave climate in the northern Baltic Proper derived from visual wave observations at Vilsandi. *Proc. Estonian Acad. Sci. Eng.* **13**(1):48–64.
- Zaitseva-Pärnaste, I., Suursaar, Ü., Kullas, T. et al. (2009) Seasonal and long-term variations of wave conditions in the northern Baltic Sea. *J. Coastal Res.*, Special Issue **56**, 1:277–281.

TOPIC 2

Lagoons and estuaries

Predictability of historical floods in the Northern Adriatic Sea

Luigi Cavaleri

Abstract

The predictability of the most severe storms and floods in the Adriatic Sea, and in particular in its northern section where they lead to the flooding of Venice. In 1966 the most damaging flood took place, greater by over 40 cm than any previous record. Given the lack of predictability at the time, I discuss if this was due to the lack of sufficient data or to that of suitable methods and computer power. At this aim I report the a posteriori forecasts done for this storm and a similar one in 1979, forecasts done starting from the simple information that was available at the time. The results show that, even with the relatively few data available 30 or 40 years ago, it would have been possible to forecast the storms several days in advance. This is reassuring for the present forecasts, should similar events happen again. This paper is a compact version of a more extensive one (Cavaleri et al., 2010) recently published, to whom the interested reader is referred for a complete information on the subject.

Обсуждается предсказуемость наиболее жестоких штормов и наводнений в Адриатическом море, особенно в его северной части, где эти явления приводят к наводнениям в Венеции. Наиболее разрушительное наводнение имело место в 1966 г., когда вода поднялась на 40 см выше ранее фиксируемого максимума. Имея в виду, что это наводнение не было предсказано, обсуждаются причины — отсутствие необходимых данных или отсутствие соответствующих методов и компьютерных ресурсов. Для этой цели проведен апостериорный прогноз для этого явления, а также для аналогичного, имевшего место в 1979 г. Прогноз сделан на базе упрощенной информации, имевшейся на тот момент. Результат показал, что даже те немногочисленные данные, имевшиеся 30–40 лет назад, позволяют предсказать наводнение с заблаговременностью в несколько дней. Это обнадеживает в случае, если аналогичное может случиться сейчас. Эта статья является укороченной версией статьи (Cavaleri et al., 2010), к которой и отсылается заинтересовавшийся читатель.

Luigi Cavaleri (✉)

Institute of Marine Sciences—CNR, Castello 1364/A, 30121 Venice, Italy
e-mail: luigi.cavaleri@ismar.cnr.it



1. Introduction: the reasons for the study

In the early November 1966 the central and north-eastern part of Italy were affected by an exceptional storm that brought very intense precipitation over large areas and strong winds over the Adriatic Sea, east of the Italian peninsula. Fig. 1 shows the area I refer to and the meteorological map at the peak of the storm, as it was derived in the aftermath of the event. The storm caused the flood of two of the greatest historical towns of Italy, Florence and Venice, and strong damages and many fatalities in small towns and villages in central and north-eastern Italy. Because of its exceptional character and consequences, the storm has been deeply studied, see, among others, Fea et al. (1968), Warner & Hsu (2000), Bertò et al. (2005), De Zolt et al. (2006), Malguzzi et al. (2006).

Here I report a different approach, focused not only on the characteristics of the storm, but on their predictability. At the time there was hardly any forecast of what was going to happen, and it is natural to wonder what we could do should similar events happen today. The limitations to the quality of a forecast may derive from a lack of sufficient data or from the limited accuracy of the numerical models we use to predict the storm. If the main reason turns out to be associated to the lack of data, this may be considered as an encouraging result for the present conditions. In fact nowadays we enjoy a wealth of data, both on land (at least in Europe) and on the sea, the latter thank to the steady flow of information from the various meteorological satellites circling the globe. To clarify this matter I consider the data available in November 1966 to the forecasters and apply to them the sophisticated numerical models presently used for the daily forecast. For a better reliability of the conclusions the approach is repeated for a storm happened in December 1979, that ranked second, just after the 1966 one, in the list of the heaviest events in the northern Adriatic and the Venice lagoon.

The paper begins, section 2, with a short description of the morphological characteristics of the area of interest and of the conditions present during the two storms. In 3 I outline the methodology followed during the study. The main results are provided in section 4, then discuss in the final section 5.

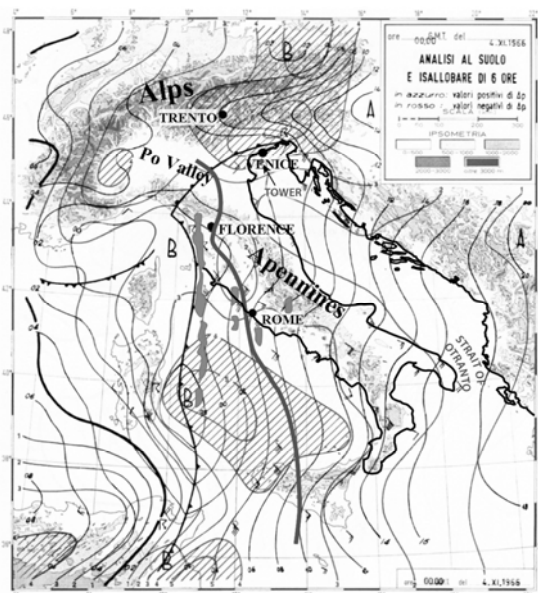
2. The characteristics of the area and of the analysed storms

The Adriatic Sea (Fig. 1) is an elongated basin to the East of Italy, enclosed between the Italian peninsula and the Balkans. It is about 750 km long, 200 km wide, aligned in the north-west to south-east direction. At its southern end it is connected with the Mediterranean Sea via the narrow Otranto strait. The sea is shallow in its northern part, the bottom sloping down from the northern coast at a 1/1,000 rate. Beyond the 200 m isobath the bottom deepens suddenly, remaining so until Otranto except for the narrow strip of shallow water along the Italian peninsula.

The orography bordering the sea on both its sides strongly affects the local winds. For our present purposes the relevant wind is the sirocco, often associated to slanting isobaths with respect to the main axis of the basin, but channelled along its main direction by the bordering mountain ridges. The long fetch and the strong wind lead to heavy sea conditions in the Northern Adri-



Fig. 1. Weather map re-elaborated from handmade analysis published in Fea et al. (1968). The basic meteorological fields refer to November 4, 1966, 00 UTC. Continuous black lines: mslp, (contour interval 2 hPa). Coloured thin lines: pressure tendency in 6 h (blue: positive; red: negative; contour interval hPa/6h). Wind barbs in knots. Low pressure centres: B; high pressure: A. The green spots reproduce reflectivity maxima of the meteorological radar in Rome Fiumicino, at 00:40 UTC, same day). The thick line indicates the position of the cold front at 12 UTC of the same day (after Malguzzi et al., 2006). The highlighted coastline borders the Adriatic Sea. The open circle shows the position of the oceanographic tower (see Fig. 5), 15 km off the coast of Venice.



atic and to strong storm surges that peak in front of the Venice littoral. (upper left in Fig. 1). The reader is referred to Pirazzoli & Tomasin (2003) for a more detailed description of the main types of flow conditions that affect the Adriatic area.

Indeed this was the case in the first days of November 1966 when, following a deep tropospheric trough positioned over Spain, this started intensifying very rapidly leading to cyclogenesis and consequently, as the cyclone moved to the Western Mediterranean, to strong southerly flow over the Adriatic, that on the surface veered to sirocco all along this sea. Very few marine data is available, also because the storm waves destroyed the final part of the jetties bordering the three inlets to the lagoon with all the associated instruments. The only tidal records locally available were in Venice itself. Compared to the statistics derived from the previous data, recorded since 1872, the 1966 event stands out dramatically, and it was variously judged (see Cecconi et al., 1999) to have a return period between 150 and 300 years. Another remarkable detail that highlights even further the exceptional character of the 1966 storm is that the flood was entirely due to the storm surge, with actually a negative contribution (−11 cm with respect to the present mean sea level) coming from the astronomical tide.

3. The methodology followed during the study

All meteorological simulations have been started from ERA-40 data (ERA is the ECMWF Re-Analysis, see Uppala et al., 2005), or have been produced using the tools developed by the ECMWF ERA group. Aiming at a better resolution than the related T159 truncation level corresponding to about 125 km resolution, Cavaleri et al. (2010) have repeated the analysis with T511, corresponding to about 40 km resolution. They have used the 31R1 version of

the ECMWF meteorological model, operational at the time when the experiments were carried out. For both the considered storms, a sequence of analyses was done at 12 h intervals, beginning ten days before the date of the storm peak. Starting from each analysis, Cavaleri et al. (2010) have generated a series of ten day forecasts, still with T511, saving the model output fields at 3 h intervals. Including the initial analysis fields, these forecast fields provide the meteorological forcing to drive the surge and wave oceanographic models.

The surface wind fields thus obtained were typically underestimated. An extensive discussion on the reasons for it is given by Cavaleri & Bertotti (1997, 2006), who have developed a objective method, based on extensive comparisons with satellite and buoy data, to correct the ECMWF wind speeds. The procedure is independent on the specific storm and it is regularly applied in the daily forecast operations.

The general circulation and sea level distribution on the whole Mediterranean Sea, and in particular the surge in the Adriatic Sea, were estimated using SHYFEM, a 3D finite elements model developed at ISMAR and used here in its 2D version. SHYFEM is a shallow water, hydrostatic, primitive equation model that runs on an unstructured grid. A complete description of the model is given by Umgiesser et al. (2004). For the estimate of the wave conditions the WAM model was used (WAMDI Group, 1988; Komen et al., 1994), a well established third generation spectral model amply described in the literature. For the purposes of this paper the tide results are reported at the Salute tide gauge at the border of the Venice area. The wave results correspond to the position of the oceanographic tower (Fig. 1), 15 km offshore, on 16 m of depth.

4. Results for the storms of November 1966 and December 1979

Fig. 2 shows the 10 m wind fields over the Adriatic Sea at 12 and 18 UTC of November 4. The intense sirocco wind blowing over the whole basin is clearly represented, with peak wind speeds at 12 UTC, in front of Venice, higher than 28 m/s. The wave conditions follow accordingly, and their peak is

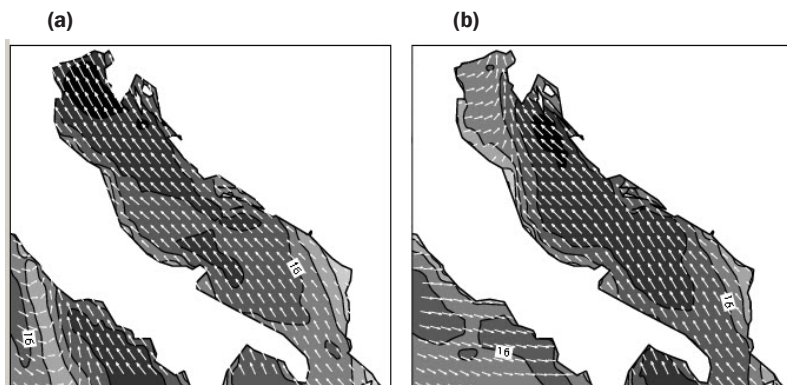
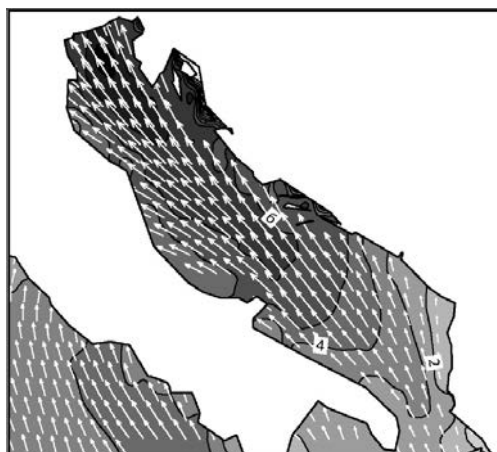


Fig. 2. Wind speed distribution at 10 m over the Adriatic Sea at (a) 12, (b) 18 UTC November 4, 1966 according to the T511 ECMWF analysis. Isotachs at 4 m/s interval (after Cavaleri et al., 2010).



Fig. 3. The distribution of the wave heights on the Adriatic Sea at 12 UTC November 4, 1966 according to the T511 ECMWF analysis. Isolines of significant wave height at 1 m interval. The maximum values are above 8 m, just offshore Venice at the north-western end of the basin (after Cavaleri et al., 2010).



shown in Fig. 3. Offshore the northern coast, in the area with the highest wind speed, the significant wave height H_s was estimated to exceed 8 m. This value is fully consistent with the damage inflicted by the storm to the jetties.

Concerning the evolution of the storm, Fig. 2b shows the passage of the cold front, as represented by the ECMWF analysis, over the northern part of the basin, indicated by a sudden shift of the wind direction, associated with a speed drop in the cold sector where the direction is from W–SW.

Fig. 4 shows the measured evolution of the sea level in Venice throughout the storm, the modelled evolution using the ECMWF analysis wind fields and the corresponding ECMWF forecasts, initialized using the 12 UTC data from one, two, three, up to six, days in advance (for clarity I have not included in this figure the results of the intermediate 00 UTC forecasts). Although underestimated in the early phases of the surge and anticipated of a few hours on the day of the peak, all the forecasts show clearly the expected surge,

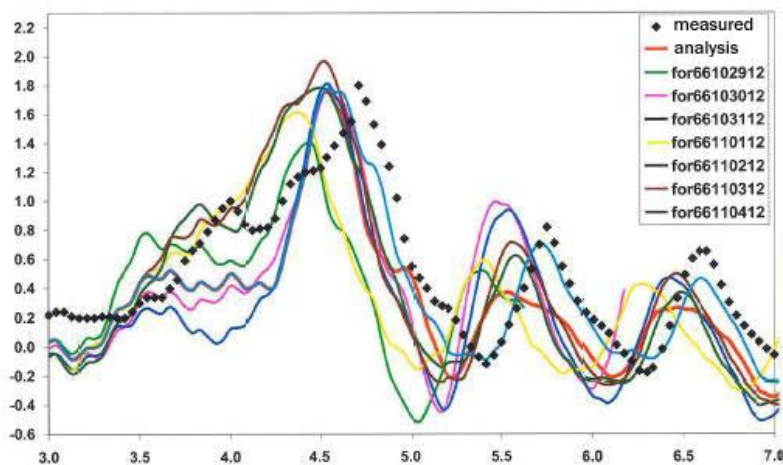


Fig. 4. Time history of the sea level in Venice according to recorded and model data, the latter both as analysis and forecasts initialized at the indicated times. Input wind fields according to the T511 ECMWF analysis. Time scale: days of November 1966. Height scale in metre (after Cavaleri et al., 2010).



usefully quantified up to day 5 in advance, with only a partial underestimation from day 6. Note that Fig. 4 shows sea levels, which implies, for the mentioned phase difference between astronomical and surge peaks, that also the timing of the peak of the storm was, for most forecasts, remarkably correct.

All this is highly positive and, as hinted in the Introduction, leads us to believe that presently our forecast capability of floods is rather good, also in case of a very severe or extreme storm. However, a careful analysis of the data suggests some caution in such conclusion. In Fig. 4 I have shown the forecasts issued on the base of 12 UTC data. Similar forecasts have been issued also on the base of 00 UTC data, and in general they provide similar results. However, there is an exception, and it is the forecast issued the day before the storm. The tidal forecast issued at 00 UTC 3 November 1966 does not provide any indication of a flood. This was a result of concern and it deserved a devoted analysis.

To understand better the origin of this miss we need first to understand the crucial role of the wind conditions in the upper part of the basin. The difficulty of a surge forecast is well exemplified in Fig. 5, where we see a section of the sea level distribution along the main axis of the Adriatic at the time of the peak of the surge. For a given surface stress, the increased spatial gradient with decreasing depth leads to the surge just in front of the Venice coast. It follows that even limited differences of the wind field in this area, e.g. a shift of the location of its maximum strength with a decrease of the wind speed in the shallower area, can alter substantially the surge.

Having clear in mind the role of the wind in the upper part of the basin, we can now go back to the wrong forecast issued 36 h before the 1966 event. The interpretation of the nature—not of the cause—of the meteorological forecast error is shown in Fig. 6. Here I compare the analysis wind field of 12 UTC November 4, the peak of the storm, with the corresponding forecast started 36 h in advance. Clearly the forecast has anticipated the passage of the cold front. A comparison with its actual position six hours later in Fig. 2b suggests a time shift of about nine hours. The matter becomes clear when we look at the distribution of the surge in Fig. 5. Due to the mentioned increase

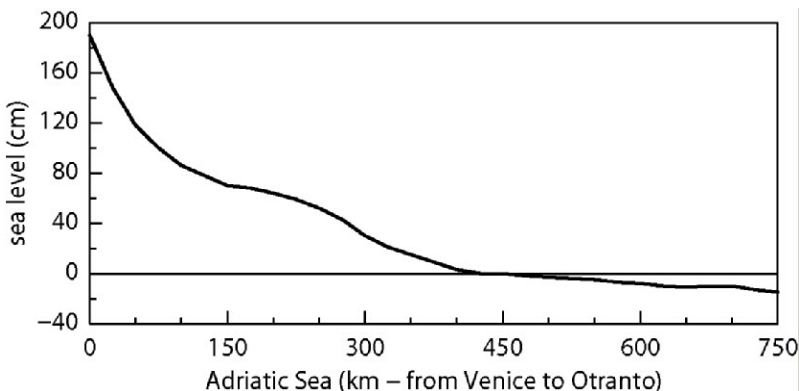


Fig. 5. Longitudinal section, along its main axis, of the sea level distribution in the Adriatic Sea (see Fig. 1) at the peak of the flood at 12 UTC November 4, 1966 (after Cavaleri et al., 2010).

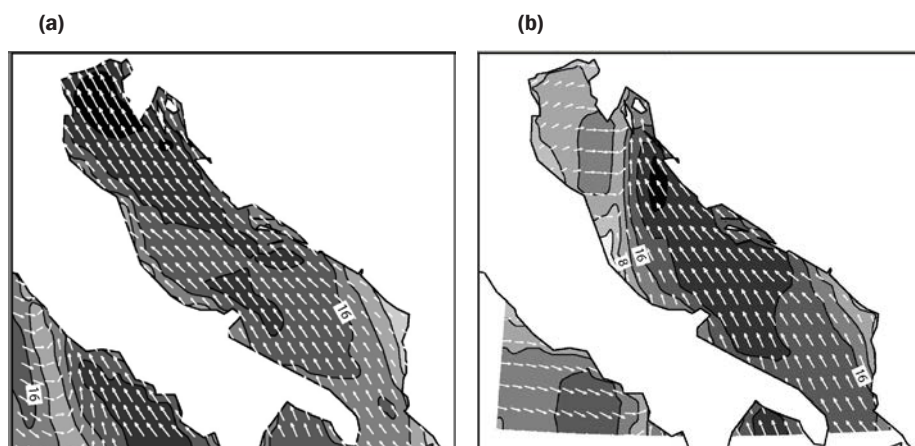


Fig. 6. Left panel: distribution of the 10 m wind field (analysis) over the Adriatic Sea at 12 UTC November 4, 1966 (see Fig. 6a). Right panel: corresponding field according to the forecast initialized 36 h in advance (after Cavaleri et al., 2010).

of the sea level spatial gradients with decreasing depth, and because of the wind distribution (Fig. 2a), most of the surge was concentrated in the upper part of the basin, in practice in front of Venice. The anticipation of the frontal passage changed completely the wind speed and direction in this area at the crucial moment when the surge was mounting. The result is the mentioned drastic underestimate of the peak of the flood. This highlights how critical the surge forecasts can be depending on small shifts in time and position of the forcing fields. To a lesser extent because of their stronger dependence on the overall field, also the wave heights showed locally a substantial decrease. This was probably associated with the local breaking (steep waves moving in shallower depths) and absence of direct forcing by wind.

The results for the storm of December 1979 are very similar, in that (Fig. 7) there is a very good predictability of the flood till several days before the event, without any example of wrong forecast.

5. Discussion and conclusions

The exercises described in the previous sections have shown that the present state-of-the-art meteorological and oceanographic numerical systems can predict the surge and the sea state in the Adriatic Sea during intense storms till several days in advance. The positive results obtained in the case of past storms, when the amount of data available was much lower than today, is a strong support to such conclusion. Two pieces of evidence, and the results discussed in this work, support this statement. The first piece of evidence comes from Canestrelli & Zampato (2005), see also Bajo et al. (2007), who discussed statistics of the tide forecast system operational in Venice, and showed that operational forecasts of “average” sea-state conditions issued two days in advance are, in general, reliable. The second piece of evidence comes from a study of the predictability of severe weather events that affect the Italian peninsula. In fact, Grazzini (2006) showed that exceptional events as those of 1966 and 1979 are associated with large-scale synoptic conditions that are

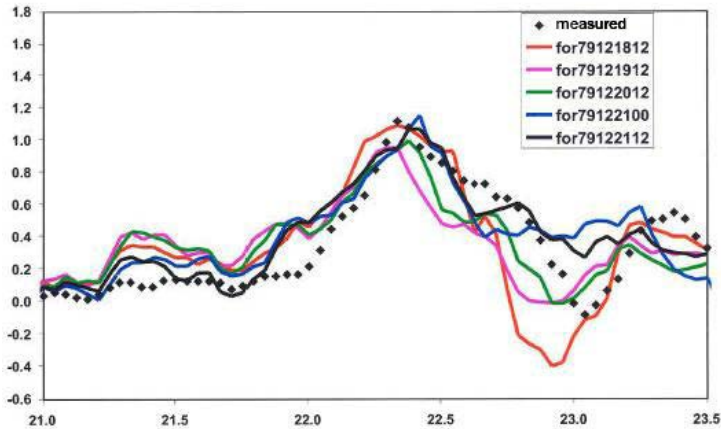


Fig. 7. Time history of the sea level in Venice according to recorded and model data, the latter as forecasts initialized at the indicated times. Time scale: days of December 1979. Height scale in metre (after Cavaleri et al., 2010).

easier to predict. The two cases discussed in this work support this conjecture. Thus, although less intense sea conditions might be predictable only for up to few days in advance, extreme cases associated with larger-scale synoptic forcing, could be predictable with longer lead times.

Given the meteorological predictability, the corresponding oceanographic one depends on the specific situation. In the case of the Adriatic Sea, and also in a more general case, waves depend on the wind distribution over the overall basin of interest. Therefore limited changes in the wind distribution are likely not to have drastic consequences. This is not the case with storm surges, the more so the shallower the water. Because most of the surge is concentrated in the lower depth areas, also limited variations of the wind field in this zone could lead to large differences in the results.

An example is given by the wrong forecast issued on the base of the data available on November 3, 1966. Comparing this situation to a similar miss happened on the French-English coasts in October 1987, Cavaleri et al. (2010) have tried to trace back the origin of the mistake. However, the kind and structure of the data available for 1966 did not allow any conclusion. The relevant question is if such a miss could happen also today, 44 years after the Venice flood and 20 years after the failure of 1987. Cavaleri et al. (2010) tend to think that the present enormous amount of data and the keen analysis of their consistency done before and during the assimilation should exclude that one or a few isolated wrong data can affect drastically the analysis, hence the forecast.

References

- Bajo, M., Zampato, L., Ungiesser, G., Canestrelli, P. (2007) A finite element operational model for storm surge prediction in Venice. *Estuar. Coast. Shelf Sci.* **75**:236–249.
- Berto', A., Buzzi, A., Nardi, D. (2005) A warm conveyor belt mechanism accompanying extreme precipitation events over north-eastern Italy. Proceedings of the



- 28th ICAM, The annual Scientific MAP Meeting, 2005, Zadar, Extended Abstracts, *Hrv. Meteorol. Casopis* (Croatian Meteorological Journal) **40**:338–341.
- Canestrelli, P., & Zampato, L. (2005) Sea level forecasting at the Centro Previsioni e Segnalazioni Maree of the Venice Municipality. In: Fletcher, C., Spencer, T., eds., *Flooding and Environmental Challenges for Venice and its Lagoon: State of Knowledge*, 85–97. UK, Cambridge: Cambridge University Press.
- Cavaleri, L., & Bertotti, L. (1997). In search of the correct wind and waves in a minor basin. *Monthly Weather Review* **125**(8):1964–1975.
- (2006) The improvement of modelled wind and wave fields with increasing resolution. *Ocean Engineering* **33**(5–6):553–565.
- Cavaleri, L., Bertotti, L., Buizza, R. et al. (2010) Predictability of extreme meteorological events in the Adriatic Sea. *Q.J. Roy. Met. Soc.* **136**(647), Part B: 400–413.
- Cecconi, G., Canestrelli, P., Corte, C., Donato, M. Di. (1999). Climate Record of Storm Surges in Venice. In: *Impact of climate change on flooding and sustainable river management*, RIBAMOD Workshop, 149–156. Wallingford.
- De Zolt, S., Lionello, P., Nuhu, A., Tomasin, A. (2006) The disastrous storm of 4 November 1966 in Italy. *Nat. Hazards Earth Syst. Sci.* **6**:861–879.
- Fea, G. A., Gazzola, A., Cicala, A. (1968) Prima documentazione generale della situazione meteorologica relativa alla grande alluvione del novembre 1966, CNR-CEN-FAM PV, 32, 215 pp.
- Grazzini, F. (2006) Predictability of a large-scale flow conducive to extreme precipitation over the western Alps. *Meteorol. Atmos. Phys.* **95**:123–138.
- Komen, G. J., Cavaleri, L., Donelan, M. et al. (1994) *Dynamics and Modelling of Ocean Waves*. Cambridge University Press.
- Malguzzi, P., Grossi, G., Buzzi, A. et al. (2006). The 1966 “century” flood in Italy: a meteorological-hydrological revisitation. *J. Geoph. Res.* **111**, D24106:1–15.
- Pirazzoli, P. A., & Tomasin, A. (2003) Recent near-surface wind changes in the central Mediterranean and Adriatic areas. *Int. J. Climatol.* **23**:963–973.
- Ungiesser, G., Melaku-Canu, D., Cucco, A., Solidoro, C. (2004) A finite element model for the Venice Lagoon. Development, set-up, calibration and validation. *Journal of Marine Systems* **51**:123–145.
- Uppala, S. M., Kallberg, P. W., Simmons, A. J. et al. (2005) The ERA-40 Reanalysis. *Quart. J. Roy. Meteorol. Soc.* **131**:2961–3012.
- WAMDI Group (1988) The WAM model—a third generation ocean wave prediction model. *Journal of Physical Oceanography* **18**:1775–1810.
- Warner, T. & Hsu, H.-M. (2000) Nested-model simulation of moist convection: the impact of coarse-grid parameterized convection on fine-grid resolved convection. *Mon. Wea. Rev.* **128**:2211–2231.

Mixing processes in coastal lagoons

Boris Chubarenko

Abstract

Different mechanisms of water mixing in coastal non-tidal lagoons are presented. Main attention is paid to estuarine lagoons where mixing of marine and river waters occurs. Baltic lagoons are used as examples.

В работе представлены различные механизмы перемешивания, существующие в непреливных береговых лагунах. Основное внимание уделено эстуарным лагунам, как месту смешения морских и речных вод. В качестве примеров используются примеры лагун Балтийского моря.

1. Introduction

Estuarine lagoons are the arenas of permanent mixing of the marine and river originated waters. Salinity and partly temperature are the main characteristics of waters in a lagoon, which combination determine water density. The transformation of these characteristics we may consider due to both mechanical steering/mixing of waters of different density (marine and fresh-water intrusions, wave mixing, night convection, Langmuir circulation) and heat exchange processes caused a change a water characteristics without mechanical motion (evaporation and ice formation leading to an increase of salinity, surface and internal heating, surface cooling lead to change in temperature).

The mixing process as the process leading to originating of waters with intermediate characteristics we may consider in two aspects: (i) mechanical exchange (steering) of considerable amount of water with given characteristics by another one due to external forcing leading to formation of intermediate spatially averaged characteristics, and, further, the (ii) proper mixing as a final act of steering, when a water volume with individual characteristics becomes less than the sensor measured it (e.g. CTD sensor).

Boris Chubarenko (✉)

P.P. Shirshov Institute of Oceanology of Russian Academy of Sciences, Atlantic Branch, Kaliningrad, Russia

e-mail: chuboris@mail.ru



Considering that all processes listed above lead to lose of initial characteristics of water, all the time we have to remember that originally it were two types of water (marine and river ones) which are experienced permanent transformation within the lagoon. This approach is based on experimental fact that water characteristics in a lagoon vary not continues (liner change between marine and fresh waters), but stepwise. And those compartments in a lagoon with individual characteristics bordered by local frontal zone.

2. Horizontal steering

Horizontal or isopycnal movement of water occur in a lagoon under forcing of external factors. Increase of water level outside a lagoon in an adjacent sea area due to water level variations of different origin (local storm surges, seiches, boundary waves, seasonal variations) leads to marine water intrusion inside a lagoon volume. Permanent river discharge brings to lagoon volume fresh waters, which usually less dense that lagoon waters and spread over them.

2.1. Intrusions of saline waters into the lagoon

A lagoon and adjacent marine area is a typical system of linked volumes connected with relatively narrow inlet. Due to natural inertia level rise outside the lagoon immediately initiates marine water intrusion into the lagoon volume. The duration and intensity of this intrusion directly depends on duration and amplitude of level rise. Usually no-tidal level variations are of 1–24 h and have an amplitude of an order of 10–100 cm. Smooth and weak intrusions goes into the lagoon at the bottom layer, fast and intensive intrusion fills whole volume of the inlet, pushes the lagoon water deep inside a lagoon and occupy considerable area within the lagoon near its outlet. As level rise turns to drop, the pressure gradient is disappeared, and lagoon more light water comes over the dense and saline intruded water.

2.2. Freshwater input

Freshwater river discharge usually has no such fast variations as water level. Only in case of huge local rain storm the discharge may increase dramatically for short period. Usually seasonal variations of freshwater discharge cause extension or shrinking of fresh water plume spreading over the more dense lagoon water. This river water is a subject of gradual mixing near the river mouth.

2.3. Horizontal circulation

Horizontal circulation in lagoon is caused by the wind influence. Some parts in the lagoon volume are “more attractive” to originating of gyres because of favorable peculiarities of lagoon shape (widening of lagoon area or local deepening). Existence of non-uniform currents field and gradients in horizontal velocity originate significant velocity sheer stress producing horizontal turbulence, which considerably ensure horizontal mixing.



3. Vertical mixing

While horizontal mechanical motion (except horizontal turbulence) produces steering effect mostly, the proper mixing of water in a lagoon is ensured by vertical exchange of momentum. Marine and fresh waters every time tends to be in balance in terms of stratified structure. And, even the water within this structure moves, the motion is isopycnal without tendency to mix, and turbulence generated due to shear stress makes the mixing at the narrow intermediate interface between stratified layers only.

The only active vertical mixing caused by wind waves and other mechanisms indeed produces the waters of intermediate characteristics.

3.1. Wind-waves mixing

A lagoon as an open area is usually a subject of intensive wind influence. Wind waves develop along the fetch and usually became limited by depth. It means that whole water column is involved in wave motion, waves interact with the bottom, and, that is the reason of wave breaking and producing of turbulence, as well as the turbulence producing due to wave-bottom interaction. The highest level of turbulence in the shallow environment is the main reason of homogenization of water volume and vertical mixing.

3.2. Sheer stress turbulent mixing

Even the lagoon is a shallow water environment, the current structure is usually 3-dimensional (Chubarenko & Chubarenko, 2003). Typical situation (as in any limited volume water body) is that the compensative currents are developed near the bottom while strong wind forces the upper layer water to move in windward direction. As, the two layers vertical current structure occur, a velocity sheer stress in between these two layers is an internal source of turbulence, which intensify the erosion of pycnocline if it is exist.

3.2. Night convection

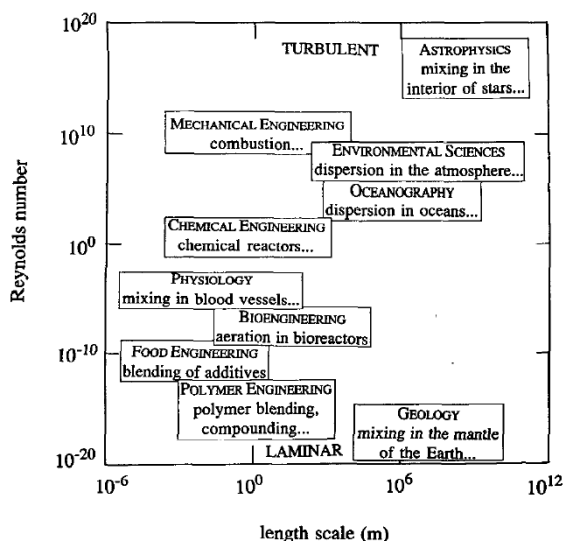
Day-night cycle of heating and cooling is an important driving force for the lagoon. While in an open sea daily thermocline is developed and eroded during day-night cycle within the upper layer of order of 10 m, a lagoon which typical depth varies within the range of 2–5 m is usually fully undergo to this influence. This thermo-induced convection as much develop as salinity stratification is weak. For example, for the conditions of the Vistula Lagoon (average salinity is 3–4 psu) the change of temperature between day and night of 5–10 degrees equivalent to a change of salinity of 1–2 percent, that is obviously may destroy the salinity vertical stratification in the lagoon.

3.3. Salinity increase due to ice formation

It is known that when water freezes most part of the salt remains in the liquid water, while the very formed ice is almost fresh. The salt appears in the upper layer make it more dense than down water, and intensive vertical



Fig. 1. Spectrum of problems studied in various disciplines in which mixing is important (Ottino, 1990).



convection has to be develop. Estimations for the Vistula lagoon show, that for the typical winter conditions (water level is 5–10 cm below the mean climatic level; the thickness of the ice is 30–40 cm), the ice formation may cause vertical mixing and total *increase of the lagoon water salinity up to 9–11 percent on average*. For the extreme year (the lowest observed water level and the thickest 60 cm strong ice cover) it can makes up to 18 percent. Moreover, this effect theoretically may lead to formation of more heavy water in the lagoon, than in adjacent sea area, and gradient near-bottom outflows of the lagoon waters in opposite to situation of upper layer outflow.

4. Langmuir circulations (Chubarenko I. et al., 2010)

The Langmuir circulation (LC) is the phenomenon widely observed both in the ocean and in shallows. This process induces the vortical currents, which grow in size, amalgamate into bigger and bigger rolls, occupying all the space (depth) allowed by input energy. In shallow areas, the LC is limited by the bottom depth, so, some equilibrium state is reached soon, with the diameter of rolls prescribed by the local water depth. Observations show, that the picture of windrows in shallow area becomes fully developed soon after the beginning of the wind action (5–10 min). However, even in fully developed structure, the rolls continue amalgamation/destruction process, which causes the formation of the Y-junctions of 4 kinds at the water surface.

In the fully-developed picture of the windrows in a shallow basin, the most probable are the rolls of regular circular shape (what is in full agreement with Thorpe (2004), who termed them to be of “square shape”). The distribution of the roll’ diameters has other obvious peaking values, where the ratio of the horizontal roll’ diameter to the roll’ depth is 0.75, 1.2 and 1.4. In a whole, 78 percent of the roll’ diameters in shallow basin are in range 0.65–1.5 of water depth.

Analysis of the motion of particles of different buoyancy in the LC showed that they experience different forcing in the flow, get different accelerations

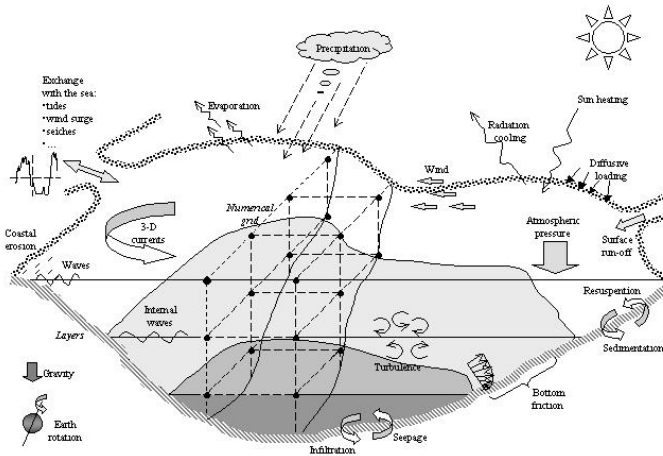


Fig. 2. Sketch of a lagoon and schematic indication of physical processes in it. (Chubarenko I., 2007).

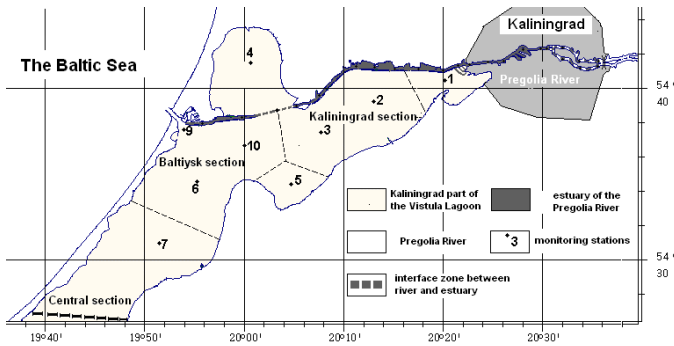


Fig. 3. Compartments within the Northern (Russian) part of the Vistula Lagoon, the Baltic Sea (Chubarenko B., 2007)

and velocities, and finally describe different trajectories. Thus, the existence of LC not just maintains sediments in suspended state and entrains the floating material into the water body, but really mixes different fractions of them by forcing different particles to follow different paths.

To sum up, we conclude that LC is a very important environmental phenomenon, because it essentially influences the dispersion and transportation of dissolved and suspended matter, especially in shallow basins.

Conclusions

Mixing mechanisms listed above are acting in the estuary lagoon permanently. Its intensity depends on external forcing caused mostly by direct or indirect wind action.

As the wind is the main reason of mixing, the synoptic and seasonal variability are the main scales of time variations of steering and mixing within a lagoon.



Action of different mixing mechanisms doesn't fully mixed water within the lagoon area. Usually, there are several compartments with quasi-homogeneous characteristics within them, which are bounded by frontal zone with sharp gradients of characteristics.

Those compartments are attributes to the variations of morphometric characteristics, like widening of the lagoon area, or deepening of it.

Existence of compartments in the lagoon area with quasi-uniform hydrologic structure is the basis of optimization of monitoring activity. Monitoring stations should be located in the center of such a compartment.

Regionalization of a lagoon area, based on a compartment structure, helps in development of simplified ecological models for a lagoon using the spatial approximation considering these compartments.

Acknowledgements

Preparation of this overview was partly supported by grants Nos. 08-05-01023 and 08-05-92421 of the Russian Foundation of Basic Researches. Author appreciates very much to Prof. Irina Chubarenko for her valuable advises.

References

- Chubarenko, B. (2007) Zoning of Kaliningrad Bay and mouth of the Pregolia River on hydro-ecological parameters aiming to monitoring optimization. In: *"Integrative study of processes, characteristics and resources of Russian seas of the North-Eastern Basin"* (results of the Federal Targeted Program "World Ocean". Issue 2, Apatity, Kolsk Sci.Center of Russian Academy of Sciences, 2007, 591–602 (in Russian).
- Chubarenko, B. V. & Chubarenko, I. P. (2000) The field study of the frontal area between the coastal zone and the Vistula lagoon (South-Eastern Baltic). *Intergovernmental Oceanographic Commission. Workshop report No. 159*. Proc. of Int. Symp. on Oceanic Fronts and Related Phenomena (Konstantin Fedorov International Memorial Symposium), Pushkin, Saint-Petersburg, Russian Federation, 18–22 May, 1998, UNESCO, 2000, 71–76.
- (2003) The transport of Baltic water along the deep channel in the Gulf of Kaliningrad and its influence on fields of salinity and suspended solids. In: Dahlin, H., Dybern, B., Petersson, S., eds., *ICES Cooperative research report*, 257, 151–156.
- Chubarenko, I. (2007) Physical processes in lagoons. In: Gonenc, I. E., Koutitonsky, V. G., Rashleigh, B., Ambrose, R. B., Wolflin, J., eds. *Assessment of the Fate and Effects of Toxic Agents on Water Resources*, 57–84. Springer.
- Chubarenko, I., Chubarenko, B., Esiukova, E., Baudler, H. (2010) Mixing by Langmuir circulation in shallow lagoons. Submitted to *the Baltica* Int. Journal.
- Chubarenko I. P., Esiukova E. E., Hutter K. (2004) Impact of the ice formation on seasonal salinity increasing the Vistula Lagoon. In: *Proceedings of the VI scientific Workshop on High Resolution Operational Model of the Baltic Sea.*, 8–10 September, 2003, Saint-Petersburg, Russia, 58–68. St. Petersburg: MORZASCHITA and Russian State Hydrometeorological University.
- Ottino, J. M. (1990) Mixing, chaotic advection and turbulence. *Annu. Rev. Fluid Mech.*, **22**:207–53. www.anualreviews.org/aronline.
- Thorpe, S. A. (2004). Langmuir Circulation. *Annual Review of Fluid Mechanics* **36**: 55–79.

Modeling ice conditions in shallow-water estuaries: the case study of the Neva Bay

**Vladimir Ryabchenko, Anton Dvornikov,
Jari Haapala, Kai Myrberg**

Abstract

To model ice conditions in the eastern Gulf of Finland a high-resolution three-dimensional hydrodynamic model is coupled with the advanced sea ice model HELMI (Haapala et al., 2005). To test the model in extreme situations the ice pattern in the eastern Gulf of Finland was simulated for a mild ice-winter (2007–08) and a moderate one (2003–04). To study the physical processes responsible for the ice regime, the following runs have been performed for each year: (i) the run on the assumption that the ice in the model domain is fast ice if the sea depth is less than 10 m, (ii) the run with non-prescribed fast ice region, (iii) the run with snow on ice surface in the case (ii). As shown, the model solution in the case (iii) shows the best agreement with the ice thickness derived from ice charts.

С целью воспроизведения ледовых условий в восточной части Финского залива трехмерная гидродинамическая модель высокого разрешения объединяется с современной моделью морского льда ХЕЛМИ (Хаапала и др., 2005). Для испытания модели ледовая обстановка воспроизведена в двух экстремальных ситуациях: мягкой зимы 2007–2008 гг. и умеренной зимы 2003–2004 гг. Для выяснения роли различных процессов в формировании льда, выполнены следующие расчеты для каждой из зим: (i) расчет в предположении о существовании припайного льда для областей моря с глубиной меньше 10 м; (ii) расчет, в котором область припая не предписывается заранее, (iii) расчет со снегом на поверхности льда для случая (ii). Показано, что модельное решение в случае (iii) согласуется наилучшим образом с толщинами льда, оцененными из карт ледовой обстановки.

Vladimir Ryabchenko, Anton Dvornikov (✉)
P. P. Shirshov Institute of Oceanology RAS, St. Petersburg Branch,
St. Petersburg, Russia
e-mail: vladimir_ryabchenko@VR584I.spb.edu
Jari Haapala (✉)
Finnish Meteorological Institute, Helsinki, Finland
Kai Myrberg (✉)
Finnish Environment Institute/Marine Research Centre, Helsinki, Finland



1. Introduction

Located at the north-eastern extremity of the Baltic Sea, the Gulf of Finland (GoF) is an elongated estuary (length c. 400 km, width from 48 to 135 km) with a mean depth of 37 m. The Neva Bay is an inner estuary of the Neva River situated between the river mouth and Kotlin Island in the easternmost part of the GoF (Fig. 2). The shallow-water Neva Bay (the mean depth is 3.6 m) is separated from the GoF by the St.Petersburg flood protection barrier (FPB). The salinity in the Neva Bay is almost always zero, and water masses are more or less homogeneous with the exception of flood situations. Circulation in the Neva Bay is driven by a strong river run-off with direct wind forcing and water elevation gradient at the open sea boundary playing a key role in flood situations (Voltzinger et al., 1990). The hydrodynamic regime in the eastern GoF is strongly changed when ice appears. The average freezing date is December 1 in the Neva Bay, and the last drift ice floes have typically melted by May 1. Ice formation and melting influence the stratification of water masses. Thick ice damps the momentum transfer from the wind to the water body. Circulation becomes weak as it is forced only by the boundary fluxes at the ice edge (Leppäranta, 2005).

The first modelling studies of the circulation in the Neva Bay were based on the two-dimensional shallow-water approach (Rukhovets, 1982, Andrejev & Sokolov, 1989, Voltzinger et al., 1990, Klevanny & Smirnova, 2002). Despite the Neva Bay being a shallow basin, the shallow-water approach does not describe the vertical structure of currents and stratification during storm surges. The first 3-D studies of the Neva Bay circulation (Menshutkin, 1997, Korpinen et al., 2003) were based on simplified circulation models and implemented on coarse grids with resolution of 250 and 500 m, respectively. The restrictions were overcome in a 3-D model of the Neva Bay developed by Ryabchenko et al. (2006) and based on the σ -coordinate model of Princeton University (Blumberg & Mellor, 1987).

None of the above-mentioned models have any snow-ice cover model, and therefore they cannot be used in winter conditions. A further development of the Neva Bay model of Ryabchenko et al. (2006) was undertaken to couple it with an ice cover model. The coupled water circulation and sea-ice model will be described here. The sensitivity of the model solution will be studied relative to the assumption of existence of fast ice, presence of snow on the ice, presence of heat sources (warm waste waters) in the Neva Bay, and the temperature of the Neva River.

2. Model, simulations and validation data

2.1. Sea-ice and snow models

The Neva Bay model described in (Ryabchenko et al., 2006) was modified in two main respects. Firstly, it was coupled with the multicategory sea ice model HELMI (Haapala et al., 2005), and secondly, snow cover was introduced in the model HELMI. *The sea-ice model HELMI* resolves ice thickness distribution, i.e. ice concentrations of variable thickness categories, redistribution of ice thickness due to deformations, thermodynamics of sea ice, hori-



zontal components of ice velocity, and internal stress of the ice pack. The redistribution function of ice categories due to deformations is dependent on ice thickness, concentration and the strain rates (Thorndike et al., 1975). The following assumptions of the deformation processes have been made: (i) deformed ice is generated only from undeformed ice categories, i.e. rafted ice is not deformed further, (ii) cross-over thickness determines whether the undeformed ice is rafted or ridged. This assumption is based on the Parmeter (1975) law and on field observations. It is also assumed that the thinnest 15 percent of the ice categories experience deformation (Thorndike et al., 1975). Further assumptions based on field observations (Kankaanpää, 1997) are that shear deformations are not taken into account, and that the shape and porosity of the ridges are constant. Ice motion is determined by the time-dependent momentum balance equation, which takes into account the Coriolis acceleration, wind and water stresses, the sea surface tilt term, and the internal stress. The internal stress of pack ice is calculated according to the viscous-plastic rheology (Hibler, 1979), but in contrast to two-level approach, ice strength is parameterized according to dissipation of kinetic energy in ridged ice build-up (Rothrock, 1979).

Snow cover model. The snow cover on the ice category j is introduced as a layer of thickness h_j . According to Leppäranta & Myrberg (2009), the thickness of snow increases by precipitation and decreases for three different reasons: surface melting, compaction, and the formation of slush, which further transforms into snow ice. Taking into account that snow ice thickness does not exceed 20–25 percent of congelation ice, we neglect here the processes of snow compaction and slush formation and consider that changes in snow thickness are due to the processes of precipitation and surface melting. It is also assumed that precipitation in the form of rain falling on the ice cover flows down into the sea water. Changes in snow thickness due to melting as well as the temperature of the snow cover are determined from the surface heat balance equation. The heat flux in ice is determined using the assumption that changes of temperature in the snow-ice cover are quasi-stationary. The freezing point temperature is calculated as a function of sea water salinity at the sea surface using an empirical formula. The shortwave radiation, the outgoing long-wave radiation, sensible and latent heat fluxes are parameterized according to Parkinson & Washington (1979) as functions of cloudiness, the difference between near-surface air temperature and ice cover surface temperature, near-surface relative humidity and wind velocity.

2.2. Model configuration and forcing

Model domain and grid. The model domain covers the Neva Bay itself as well as a part of the external estuary from the FPB to the meridian of the Zelenogorsk (Terijoki). A curvilinear grid was built in such a way that the maximal resolution would be situated within the Neva Bay. The steps in X-direction (from west to east) and in Y-direction (from south to north) were from 75 to 990 m and from 60 to 440 m, respectively. The number of σ -levels was 7. The configuration of the FPB is set in the model as it existed in the investigated periods of 2003–04 and 2007–08: all water-way gates are open,



the southern navigation pass is open, and the northern navigation pass is closed.

Atmospheric forcing. The coupled model is driven by atmospheric forcing and boundary conditions for hydrodynamic and ice characteristics at the lateral and bottom boundaries of the model domain. Prescribing *atmospheric forcing* at the open water/ice surface principally follows recommendations by Parkinson & Washington (1979). The heat flux at the ice-sea boundary is proportional to the difference between the seawater temperature at the top level of the model and the freezing temperature at the lower edge of ice, and to the magnitude of the difference between ice drift and current velocities. The salt flux at this boundary is calculated from the rate of ice growth or melt. The sea ice salinity is taken to be equal to zero.

Open boundary conditions. *At the eastern boundary* of the model domain, the current velocities are prescribed in the branches of the Neva River using the total river transport and its relative distribution over the branches. Constant temperature over the river cross-section is also prescribed using available observation data, salinity is taken to be equal to 0, and a non-flux condition is used for ice mass. *At the western boundary*, water level changes are assumed to be zero. Current velocity as well as velocity and mass of ice are calculated from the radiation condition of Orlanski (1976). For temperature and salinity the radiation condition is used for outflow currents, and distributions typical for the winter are prescribed for inflow currents.

Solid boundary conditions. *At the sea bottom* the vertical component of current velocity is equal to zero and no-flux conditions are specified for heat and salt. The bottom friction stress is parameterized as a function of the horizontal velocity at a model level nearest to the bottom. *At the solid lateral boundaries* no-slip condition for horizontal current velocity, slip condition for ice velocity and no-flux conditions for heat and salt fluxes are specified.

2.3. Reference simulations

The coupled water circulation and sea-ice model with exclusion of snow on ice was used to simulate two wintertime situations: the moderate ice winter 2003–04 and the mild ice winter 2007–08. The present set-up of the ice model predicts the evolution of five undeformed and two deformed ice categories. Deformed ice is divided into separate categories of rafted and ridged ice types. Fast ice is solid ice and it remains immobile apart from very early and late stages of the ice season. On average, the outer boundary of the fast ice zone lies at the 10 m isobath in the Baltic Sea (Leppäranta & Myrberg, 2009). In the reference runs the ice is always considered as fast ice if the sea depth is less than 10 m.

The meteorological forcing (wind speed and direction, air temperature, relative humidity and cloudiness) was assumed to be uniformly distributed with values taken from the station “Saint-Petersburg”. Data on precipitation were not available. Precipitation was therefore taken from NCEP reanalysis (Kalnay et al., 1996). The model starts from zero current velocities, the absence of ice in the region, and with initial temperature and salinity taken from available observations. Because of lack of detailed data on the inter-annual variability of temperature and salinity, it is assumed that the initial fields of



them are the same for the winters of 2003–04 and 2007–08. Distributions of temperature and salinity at the open western boundary were constructed from their initial distributions.

The discharge of the Neva River and its temperature during the wintertime period were taken from 10-day means of climatological data for 1980–2000, being the same for the winters of 2003–04 and 2007–08. According to the data above, the temperature of the Neva became less than 0.2 °C in the last ten-day period of November and became greater than 0.2 °C in the first ten-day period of April. In reference runs the temperature of the Neva during the winter period (December–March) was set as 0.0 °C.

2.4. Ice observations

The comparison between the model and data as well as the description of the changes in ice conditions in the Neva Bay are based on an analysis of ice charts produced daily by the North-West Hydrometeorological Centre, Russia. The charts describe various ice types. The source information for manually produced contouring is the SAR-images of NOAA satellites. In addition, the maximum and minimum values of ice thickness for different regions occupied by ice are given on the charts. Within the Neva Bay, as a rule, only one such region can be distinguished. In the next section these estimates will be compared with model ice thickness averaged over the Neva Bay.

3. Results

3.1. Reference runs

The model simulates well the appearance of ice in the mild winter of 2007–08, but in the moderate winter of 2003–04 an ice appears in the model 10 days earlier than shown by observations (Fig. 1). In the period of ice growth (December to mid-March) the model fits well the maximal observed ice thickness in 2003–04, but overestimates them in 2007–08 by 15–20 cm. In the model, ice disappeared by April 28, 2008 and by May 8, 2004, whereas in reality the disappearance of ice occurred almost 3 weeks earlier for both winters. The above discrepancies can be explained by the absence of snow on the ice surface in the model, while in reality there was snow on the ice, which made the ice growth relatively slow. Additionally, according to ice charts, there was practically no fast ice at all in the Neva Bay during the mild winter, but the ice drifted due to the existence of polynyias. When there is no fast ice, the assumption of fast ice may also lead to an incorrect description of the periods of ice formation in the autumn and ice melting in the spring. One more reason for the discrepancy between modelled and observed ice thicknesses is the non-representativeness of the climate data on the Neva River water temperature during the mild winter 2007–08. Finally, there are heat sources within the Neva Bay, which can also influence the ice formation. The above reasons will be studied in Section 3.2.

Modelled sea ice thickness distributions in 2004 and 2008 are shown in Figs. 2a and 2b, respectively, for the period when sea ice thickness was maximal in the Neva Bay. In the fast ice region, the maximal difference of the sea



ice thickness is about 25 cm in both cases, and it is regionally rather uniform with a decrease in the vicinity of the Neva mouth. The difference in sea ice thickness is due to the differences in the surface energy balance, and since the atmospheric data were assumed to be regionally uniform over the model domain, the sea ice thickness in the fast ice region is also rather uniform.

In the drift ice region the situation is rather different when the years 2004 and 2008 are compared. In the winter 2004 the thickest ice was located near the northern coast of the GoF, but in the winter 2008 the thickest ice was also found on the south-eastern side of the drift ice region (Fig. 2). This can be explained by differences in the wind direction during these two winters. In the winter 2007–08 the frequency of winds from western directions during the period of ice formation (December 15–January 10) favoured increasing

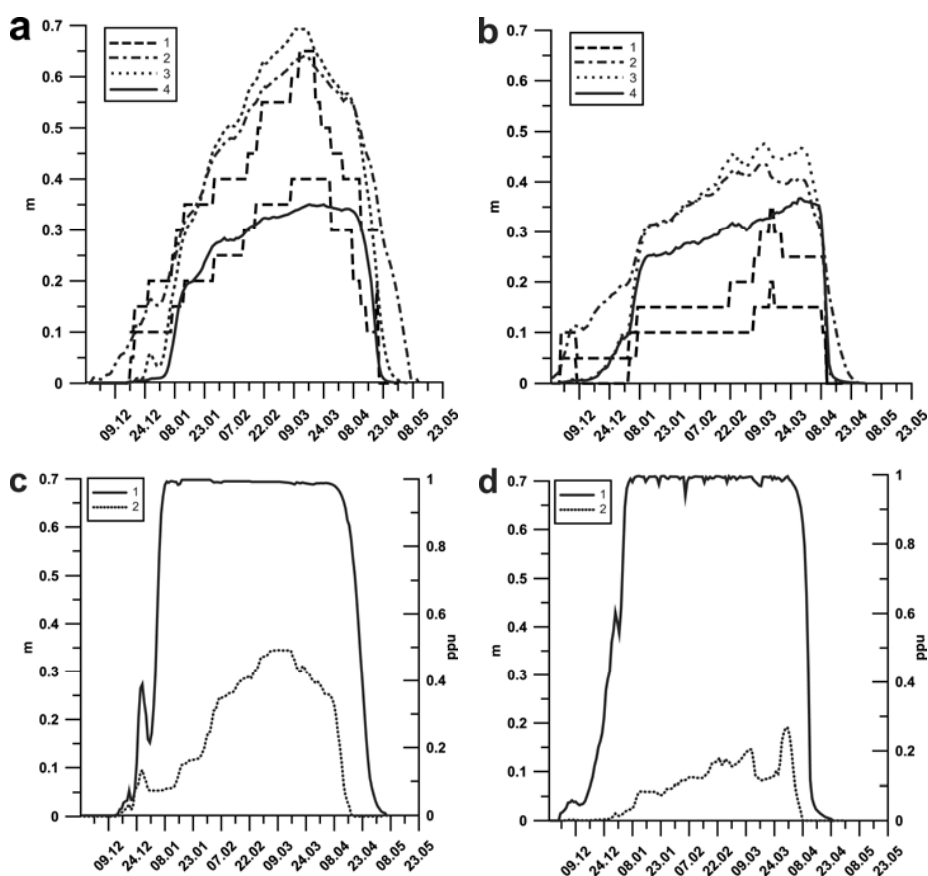


Fig. 1. Ice characteristics averaged over the Neva Bay in different runs: (a) ice thickness in the winter 2003–04 in the cases of fast ice assumed (the reference run, curve 2), without the assumption of fast ice and ice without snow cover (curve 3), without the assumption of fast ice and with snow cover on ice (curve 4), curves 1 are estimates of maximum and minimum ice thickness from ice charts (see Section 2.4), (b) ice thickness in the winter 2007–08 for the same cases, (c) snow thickness (curve 1) and ice concentration (curve 2) in the winter 2003–04 in the case without the assumption of fast ice and with snow cover on ice, (d) the same as fragment c but for the winter 2007–08.



ridged ice on the south-eastern side of the drift ice region. In the winter 2007–08 the frequency was 61 percent, whereas in the winter 2003–04 it was only 45 percent. As a result, by the end of December near the northern coast of the GoF ridged ice was formed in both winters at the boundary between the fast ice and drift ice regions, but on the south-eastern side of the drift ice region ridged ice appeared only in the winter 2007–08. During the both winters winds were weak ($0\text{--}4\text{ m s}^{-1}$) in the period of January 11–March 15. In this period the frequency of winds from western directions was 69 percent in the winter 2008, and only 32 percent in the winter 2004. This favoured the further growth of ridged ice on the south-eastern side of the drift ice region in 2008, but did not lead to the formation of ridged ice there in 2004.

The thick ridged ice production in the model is related to non-uniform ice motion, and the largest ice motion gradients and ridged ice production rates are usually located between the fast ice and drift ice regions. However,

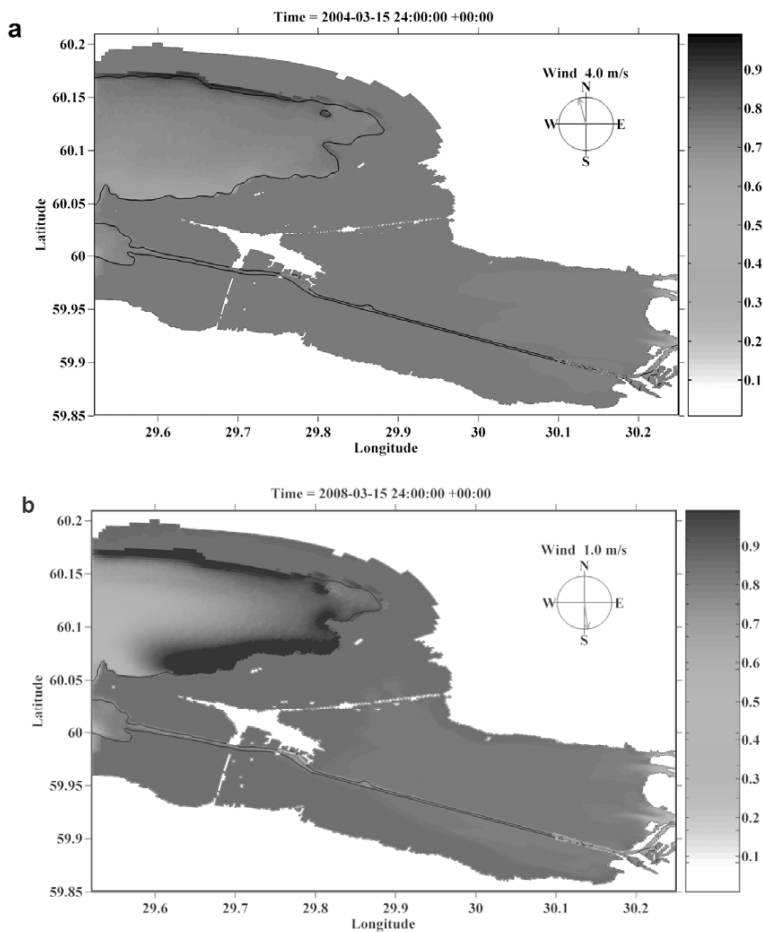


Fig. 2. The modelled ice thickness (m) distributions in the model domain in the case of fast ice assumed without the allowance for heat sources within the Neva Bay: (a) on March 15, 2004 and (b) on March 15, 2008. Dark line is the boundary between fast and drift ice. Ice drift velocities (not shown) did not exceed 0.1 mm s^{-1} .



the easternmost part of the GoF, cannot be considered to be a fast ice region during the entire winter since, according to the ice charts, rafted and ridged ice types are observed in these areas. A description of mechanism of ridged ice production in the case of removing the assumption of a fast ice region will be given in the next section.

3.2. Sensitivity studies

Sensitivity runs have been carried out to study the effects of different factors on the ice cover: removing the assumption of fast ice, snow cover on ice, heat sources in the Neva Bay, and changes in the water temperature of the Neva River.

Removing the assumption of fast ice. In reference runs the ice in the model domain was assumed to be fast ice if the sea depth was less than 10 m. According to this assumption, the ice was fast ice during the whole ice season everywhere within the Neva Bay, with the exception of a narrow zone above the shipping canal, where the bottom depths exceed 10 m. Without this assumption the modelled ice thickness is in a better agreement with the data during the periods of ice formation and ice melting. The modelled ice thickness (averaged over the Neva Bay) in this case turned out to be smaller than in the reference runs during the period of ice formation (Figs. 1a, 1b). During the rest of the ice period the ice thicknesses are rather close to each other in the runs compared. The ice disappears completely 5 days earlier than in the reference runs during both the winters. Without the assumption of a fast ice region, heat exchange with the atmosphere happened through both the ice cover and open water, leading to a decrease in the ice growth. When this assumption is used, initial ice formation leads immediately to a fully ice-covered region with the transfer of atmosphere-sea momentum flux disabled, and reduced vertical mixing and strengthened vertical stratification reducing ice-sea heat flux. Although ice in the Neva Bay is immobile for most of the winter, the ice will drift in the early winter when it is thin, and hence the model without the assumption of fast ice more realistically simulates the evolution of the ice.

Effects of snow cover. Introducing snow on ice in the model—without the assumption of fast ice—significantly decreases the modelled ice thickness in both the winters (Figs. 1a, 1b), this effect being stronger in the moderate winter 2003–04 because of a thicker snow cover (Cf. Figs. 1c, 1d). The modelled ice thickness fits well the observed minimum values in the winter 2003–04, excepting 5 cm underestimation of the observed maximal value of ice thickness (h_{imax}) in March. This underestimation may be connected with the fact that in our snow model the snow ice is not allowed for. According to Leppäranta & Myrberg (2009), the snow ice thickness can be as much as 30 percent of snow thickness so that in our case the total ice thickness could be $35+10=45$ cm at the maximum, this fitting well with observations. In the winter 2007–08, the model overestimated ice thickness in January–March by 10 cm, the modelled h_{imax} and complete disappearance of ice being reached 2 weeks later than shown by observations. Possible reasons for these discrepancies are connected with regular thaws in 2008. They favoured decreasing of snow thickness, the minima of which were reached on January 30, February 22, March 9 and 24 (Fig. 1d). During these thaws the temperature in the



Neva River could be higher than its climatic values used in the model, and this, as will be shown later, would lead to decreasing ice growth.

The modelled spatial distributions of ice thickness on March 15, during the period of its maximal values, are different in moderate and mild winters (Fig. 3). In the moderate winter, the southern winds in mid-March led to ice drift to the north, and increased ice thicknesses. Rafted and ridged ice occur along the northern coast of the model domain in both the Neva Bay itself and outside of it, before the northern part of FPB, near the southern coast of Kotlin Island. The increased ice thickness regions along the southern coast of the model domain are absent. In the mild winter, weak winds from northern directions prevailed in the same period (mid-March) and the increased ice thicknesses occurred along the northern and southern coasts in the Neva Bay, near the southern coast of Kotlin Island, behind the northern part of the

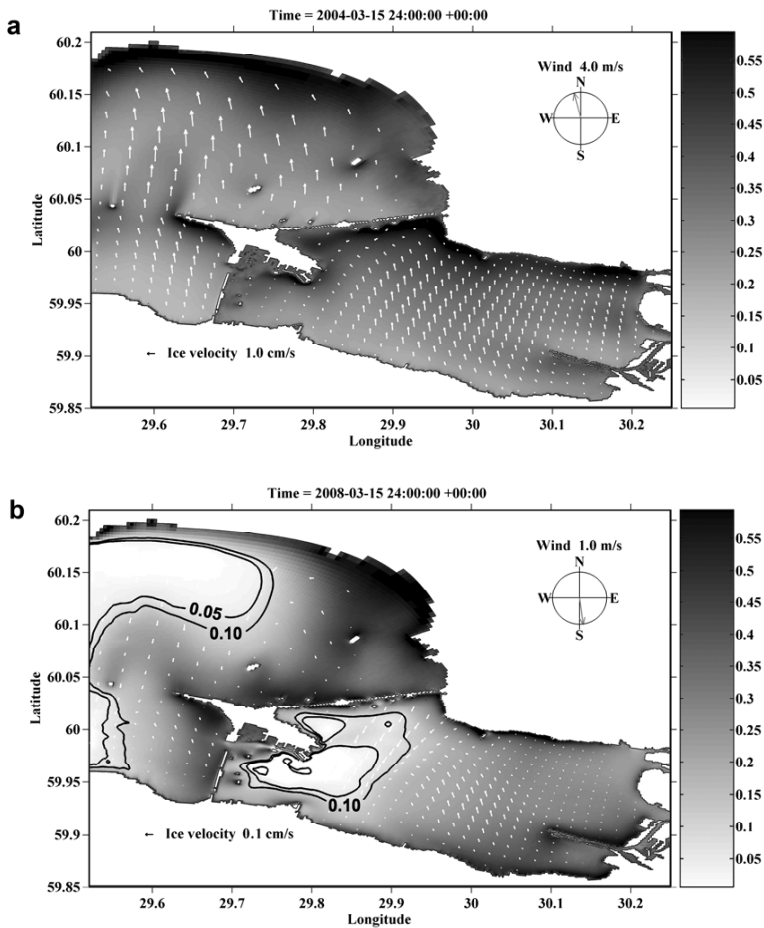


Fig. 3. The modeled ice thickness (m) distributions and ice drift velocity fields in the model domain in the case without the assumption of fast ice and with allowance for snow on ice surface: (a) on March 15, 2004 and (b) on March 15, 2008. Isolines are ice thicknesses of 0.5 and 10 cm. White arrows are ice drift velocities. The scale of ice velocity in fragment a is 10 times greater than in fragment b.



FPB in the GoF. Near the northern and easternmost coasts of Kotlin Island within the Neva Bay, there were regions of thin ice (less than 5 cm thickness) looking like polynyas. It is notable that ridged ice was produced in the model by the redistribution process of thin ice to thicker ice categories. Redistribution depends on the ice velocity gradients. The gradients are largest in the coastal zone. In the GoF, sea ice drifts towards to the coast in almost all wind conditions, and hence any variations in wind direction and speed have a large impact on the spatial distribution of ridged ice production.

Effects of heat sources. Heat sources in the modelled area consist of warm waste waters coming into the Neva Bay at release points. The total waste water discharge at release points was $28 \text{ m}^3 \text{ s}^{-1}$, i.e. only 2 percent of the river discharge of $1,500 \text{ m}^3 \text{ s}^{-1}$. The temperature of waste waters, as measured at waste water treatment plants (WWTPs), was about $16 \text{ }^\circ\text{C}$ in the winter seasons. However, temperatures at the release points, located at the distance of several kilometers from WWTPs, are not measured. In this situation reasonable values of the temperature were assumed at the release points: $16 \text{ }^\circ\text{C}$ in the mild winter, when mean winter air temperature was about $+1 \text{ }^\circ\text{C}$, and $3 \text{ }^\circ\text{C}$ in the moderate winter, when air temperatures reached $-20 \text{ }^\circ\text{C}$. If all the heat were spent on ice melting, the heat sources acting for a month could lead to a melting of 80 and 15 km^2 of ice with a thickness of 20 cm (24 and 4.5 percent of the Neva Bay area of 329 km^2) at heat source temperature of 16 and $3 \text{ }^\circ\text{C}$, respectively. In the case of heat sources in the Neva Bay, polyniyas arise in the vicinity of release points, the sizes of these polyniyas being larger in the winter 2007–08. Allowing for heat sources weakly affected the mean ice thickness in the Neva Bay with maximal changes of 2 and 7 cm, respectively, in the winter 2003–04 and 2007–08.

Changes in the Neva River temperature. The temperature in the Neva River in winter periods is usually about the fresh water freezing temperature of $0 \text{ }^\circ\text{C}$. The Neva River is typically covered by ice, and thus there are no temperature measurements. At the same time, in the beginning of ice growth as well as during the period of ice melting, the water temperature may differ from $0 \text{ }^\circ\text{C}$. An increase of $0.1 \text{ }^\circ\text{C}$ in the river temperature is equal to a heat flux of $630 \cdot 10^6 \text{ W}$ at the winter river discharge of $1,500 \text{ m}^3 \text{ s}^{-1}$, so that the heat flux averaged over the area (329 km^2) of the Neva Bay is only 2 W m^{-2} . This value is small in comparison with heat fluxes averaged over the ice cover surface, which can reach values of 80 W m^{-2} during the winter period and average $20\text{--}30 \text{ W m}^{-2}$. Nevertheless, in periods when the difference between air and water temperatures is not great, heat fluxes due to river water warming can significantly influence the ice growth locally, especially near the river mouth. Such changes reaching 10 cm were obtained in the model run performed on the assumption of a specified fast ice region, and differing by $0.1 \text{ }^\circ\text{C}$ in the assumed river temperature.

4. Summary

To model ice conditions in the eastern Gulf of Finland a high-resolution three-dimensional hydrodynamic model is coupled with the advanced sea ice model HELMI (Haapala et al., 2005). To test the model in extreme situations the ice pattern in the eastern Gulf of Finland was simulated for a mild



ice winter (2007–08) and for a moderate one (2003–04). The reference runs were performed on the assumption that the ice in the model domain is fast ice if the sea depth is less than 10 m. Using this assumption, the ice thickness averaged over the Neva Bay (the easternmost part of the Gulf of Finland) is overestimated by the model for almost the entire wintertime in the mild winter and during the ice formation and melting periods in the moderate winter, as compared with the thickness reported in ice charts.

For both winters, the model solution without the assumption of a fast ice region is in better agreement with averaged ice thicknesses from ice charts during the ice formation and ice melting periods. The addition of snow on the ice surface in the model without a fast ice region led to a significant decrease of ice thickness during the entire wintertime period for the moderate winter, so that the model agrees well with the ice thickness estimated from observations. At the same time, the decrease of ice thickness in the mild winter turned out to be not strong enough, and the model overestimated the observed ice thickness in the Neva Bay in January–March by about 10 cm. We will show that possible reasons for this are heat sources (warm waste water) within the Neva Bay and uncertainties in the assumed river temperature.

In the case of no fast ice region and snow on ice, the model correctly simulates the spatial distribution of ice thickness seen on ice charts for the mild winter. Despite the absence of irregularities in wind forcing—which was assumed to be homogeneous over the model domain—the modelled ice thickness distributions included meso-scale features such as the ridged and rafted ice regions with increased ice thickness, and the regions of small ice thicknesses having a resemblance to polynyias.

Acknowledgements

All data used in this study were kindly given us by Yury Liberman from the North-West Hydrometeorological Centre, Russia. We also thank Polina Soloshchuk from the same Centre for her assistance with ice charts.

References

- Andrejev, O.A. & Sokolov, A.V. (1989) Numerical modelling of the water dynamics and passive pollutant transport in the Neva Bay. *Meteorology and Hydrology* **12**:75–85 (in Russian).
- Blumberg, A.F. & Mellor, G.L. (1987) A description of a three-dimensional coastal ocean circulation model. In: Heaps, N., ed., *Three-dimensional Coastal Ocean Models*. Am. Geoph. Union.
- Haapala, J., Lönnroth, N., Stössel, A. (2005) A numerical study of open water formation in sea ice. *Journal of Geophysical Research* **110**:C09011.
- Hibler, III, W.D. (1979) A dynamic thermodynamic sea ice model. *J. Phys. Oceanography* **9**:815–846.
- Kalnay, E. et al. (1996) The NCEP/NCAR 40-year reanalysis project. *Bull. Amer. Meteor. Soc.* **77**:437–470.
- Kankaanpää, P. (1997) Distribution, morphology and structure of sea ice pressure ridges in the Baltic Sea. *Fennia* **175**(2):139–240.
- Klevanny, K.A. & Smirnova, E.V. (2002) Simulation of current and water pollution changes in the Neva Bay after completion of St. Petersburg flood Protection Barrier. *Envir. and chem. physics* **24**(3):144–150.



- Korpinen, P., Kiirikii, M., Rantanen, P. et al. (2003) High resolution 3D—ecosystem model for the Neva Bay and Estuary—model validation and future scenarios. *Oceanologia* **45(1)**:67–80.
- Leppäranta, M. (2005) *The Drift of Sea Ice*. Heidelberg: Springer-Verlag.
- Leppäranta, M. & Myrberg, K. (2009) *The Physical Oceanography of the Baltic Sea*. Berlin-Heidelberg-New York: Springer-Verlag.
- Menshutkin, V. V., ed. (1997) *The Neva Bay: experience of modeling*. St.-Peterburg: Borey Print (in Russian).
- Orlanski, I. (1976) A simple boundary condition for unbounded hyperbolic flows. *J. Comp. Physics* **21**:251–269.
- Parkinson, C. L. & Washigton, W. M. (1979) A large-scale numerical model of sea ice. *J. Geoph. Res.* **84(C1)**:311–337.
- Parmeter, R. R. (1975) A model of simple rafting in sea ice. *J. Geoph. Res.* **80**:1948–1952.
- Rothrock, D. A. (1979) Modeling sea-ice features and processes. *Journal of Glaciology* **24(90)**:359–375.
- Ruchovetz, L. A. (1982) Mathematical modelling of water exchange and tracer distribution in the Neva Bay. *Meteorology and Hydrology* **7**:78–87 (in Russian).
- Ryabchenko, V. A., Konoplev, V. N., Kondratyev, S. A. et al. (2006) Assessment of water quality changes in the Neva Bay after opening of the South-Western Wastewater Treatment Plant in St. Petersburg (results of modeling). *Izvestiya Russian Geogr. Soc.* **138(5)**:48–57.
- Thorndike, A. S., Rothrock, D. A., Maykut, G. A., Colony, R. (1975) The thickness distribution of sea ice. *J. Geoph. Res.* **80**:4501–4513.
- Voltzinger, N. E., Zolnikov, A. V., Klevanny, K. A., Preobrazhensky, L. Yu. (1990) Calculation of hydrological regime of the Neva Bay. *Meteorology and Hydrology* **1**:70–77 (in Russian).

Systems of stratified currents and mass-exchange in the near-mouth regions, bays and in the basins with complex bottom relief

Boris Samolyubov

Abstract

This report includes the results of theoretical and natural investigations of the systems of stratified currents developed at different depths and interacting to each other. The goal of the investigations is extraction of such systems types and revelation of mass-exchange mechanisms between the flows in the system. On the base of analysis of many years measurements in 11 lakes and reservoirs there were revealed 8 types of systems of stratified currents. The results of these systems investigations are considered for the near-mouth regions, bays and for the basins with complex bottom relief.

Работа включает результаты теоретических и натуральных исследований систем стратифицированных потоков, развивающихся на разных глубинах и взаимодействующих между собой. На базе анализа данных измерений в 11 озерах и водохранилищах выявлено 8 типов систем стратифицированных течений. Результаты исследований этих систем рассматриваются применительно к процессам, характерным для приустьевых областей, заливов и бассейнов со сложным рельефом дна.

1. Introduction

Water dynamics and diffusion of admixtures in coastal zone, lakes and reservoirs are extensively determined by the development of systems of stratified currents. System of currents is a complex of flows moving at different depths from the bottom up to the open surface and interacting with each other. These systems consist of near bottom flows, jets, and other streams (Fig. 1). They are studied for the solution of several fundamental and applied problems of geophysical dynamics, including ecological ones (Boegman et al., 2008, De Cesare & Boillat, 2003, Michioku, 1993; Samolyubov, 2007). The

Boris Samolyubov (✉)
M. V. Lomonosov Moscow State University, Moscow, Russia
e-mail: samolyubov@phys.msu.ru



purposes of this study are: (1) extraction of types of such systems of currents, (2) exploration of the peculiarities of the transformations of velocity distributions and the parameters of the water composition; (3) revelation of mass-exchange mechanisms between the flows in the system; (4) the advancement of mathematical models of systems of currents and of the transport of admixtures in these currents.

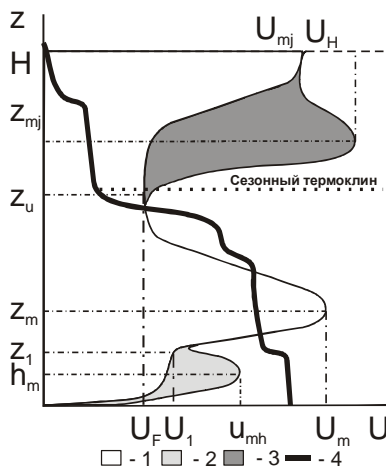
2. Classification of systems of currents

On the base of analysis of many years measurements in 10 lakes and reservoirs there were revealed 8 types of systems of stratified currents. Classification of such systems was made taking into account their composition. There were discovered that this classification was possible only by types of the currents. This is stipulated by the wide diapasons of the hydrodynamic parameters of the flows ingressed in the system (including stratification stability; admixture activity; water exchange intensity; extent, power and velocity of current propagation). Thus, the distance of propagation of the investigated currents differs between 3–64 km, current velocity—3–40 cm/c, water density difference in the flow and above it—from $2 \cdot 10^{-5}$ – $5 \cdot 10^{-3}$ g/cm³, flow height—3–30 m.

There were singled out 8 types of the systems of stratified currents. These systems were registered at 20 crossings and temporal stations in different hydrological and meteorological conditions at the lakes Teletskoe, Onega, Imandra and at the reservoirs Mozhai, Ruza, Ozerna, Istra, Vazuza, Ivankovo and Nurek. The systems are introduced on the basis of the frequency of appearance.

- (1) Density current—intermediate jets—flowing and drift currents.
- (2) Density current—flowing and drift currents.
- (3) Circulating current (in plain and in depth) induced by the wind—intermediate jets—currents, induced by internal seiches in the presence of the density current and without it.
- (4) Density current—circulation induced by the wind.
- (5) Near-bottom density current—currents, induced by internal seiches.
- (6) Jet in thermocline—circulating current—density current.

Fig. 1. The overview of profiles of current velocity U —1, 2, 3 and water density difference $\delta\rho$ —4 in the system of currents over the entire depth H from the bottom up to the open surface. Symbols: 1—density current U_g at $z \leq z_u$ and flow-drift current at $z = z_u \div H_L$, 2—near-bottom reversing current $u(z)$ at $z \leq z_1$, 3—intermediate jet U_j . Heights h_m , z_m , z_{mj} , H correspond to maxima of current velocities u_{mh} , U_m , U_{mj} ; z_1 —the level of lower boundary of the jet-type part of density current (height of reversing current). Here $U_F = U(z_u)$, $U_1 = U(z_1)$.





- (7) Density current—the flow caused by water surface level changes.
(8) Circulating current—flow ascending along the bottom slope, generated by gravity jet down-warded from the cupola-shaped thermocline.

There were established the following mechanisms of energy- and mass-exchange between the flows in the revealed systems of currents. 1. The direct and stepped transfer of pulse induced by internal wave from near-bottom current to intermediate jet. This mechanism is typical for the systems of types 1, 3, 6, 2. Turbulent transfer of the pulse from the near-surface current to the near-bottom flow through the high stable thermocline due to the valve gear (Ozmidov, 1997) in combination with the wave energy transfer (Samolyubov, 2007). This mechanism is typical for the systems of types 2, 4, 5, 7. 3. Turbulent entrainment, leading to the confluence of the jets and near-bottom currents. This mechanism is typical for the systems of types 1, 5. 4. The amplification of the current in the near-bottom branch of circulation under the near-bottom stratified current action. This mechanism is typical for the systems of types 4, 6, 7, 8.

3. Systems of currents above a complex bottom relief

One of the most complex systems of currents was discovered in our investigations at the Teletskoye Lake in 2003–06. With application of gaging equipment the detailed profiles of current velocity, temperature, concentrations of suspended sediments, dissolved salts; oxygen and chlorophyll-“a” were drawn at the crossings and at the term stations. There were revealed mechanisms of the near-bottom and intermediate current development including the underwater jets lowering along the dome of the thermocline (Fig. 2) (Samolyubov, 2007, Samolyubov & Kirillov, 2005).

The stratification of waters is mainly thermal (Selegei & Selegei, 1978). The development of systems of near-bottom, jet, and flow-drift currents and the transport of admixtures from the underwater threshold that divides the deepwater (depth up to 325 m) and shallow (depth up to 38 m) parts of the lake was examined.

The range of currents propagation towards the Biya River source in the shallow part (right at Fig. 3) is characterized by a complex bottom relief. On the crossings with a distance of 11.5 km and a step by depth of 0.5 m, profiles of velocity, temperature, and concentrations of salts and oxygen, as well as the velocity and direction of the wind were recorded at this part of the lake. The velocity U profiles from the first underwater sill on the left (Fig. 3), above it, and behind it, contain near-bottom flows, intermediate jets, and flow-drift currents. The measurements at the crossing introduced at Fig. 4 were carried out on August 8, 2006. The profiles of water density are characterized by basic maxima of gradient $\partial_z \rho$ in pycnoclines at depths of 7 ± 1.5 and 12 ± 2.4 m.

These results, compared with those from July 22, 2003 and July 27, 2004, are characterized by stratification stability (De Cesare & Boillat, 2003). According to the data of 2003, 2004, and 2006 the average, along the crossing, differences of densities of surface and near-bottom waters and Richardson numbers $Ri_u = g \overline{\Delta \rho} z_u / \rho \overline{U}^2$ for the near-bottom flow at station I were $\overline{\delta \rho_{xa}} = 2, 4.4,$ and 5.2×10^{-4} g/cm³ and $Ri_{u0} = 0.4, 0.8,$ and 1.3, where g is gravity, z_u is flow thickness, $\overline{\Delta \rho}$ is the difference of densities of waters within and above the flow,

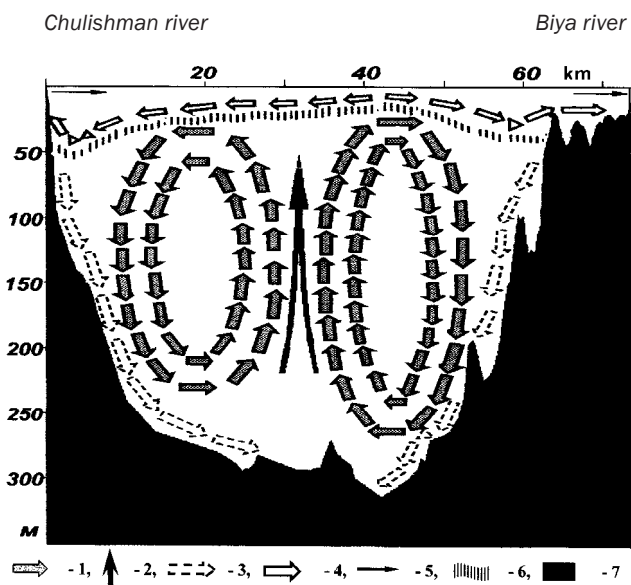


Fig. 2. The scheme of stratified currents at the longitudinal crossing of the Teletskoye Lake. Designations: 1–5—vectors of velocities: (1) circulations, generated by the development of the longitudinal thermobar; (2) upwelling in region of the circulations convergence; (3) gravity thermally stratified currents, especially active at the spring season, previous the time of our measurements; (4) inclined stratified jets, streaming down along the dome of the thermocline to the southward and northward (towards the Chulishman river mouth and Biya river source); (5) The main inflow in the lake and outflow from it; (6) seasonal thermocline; (7) bottom relief.

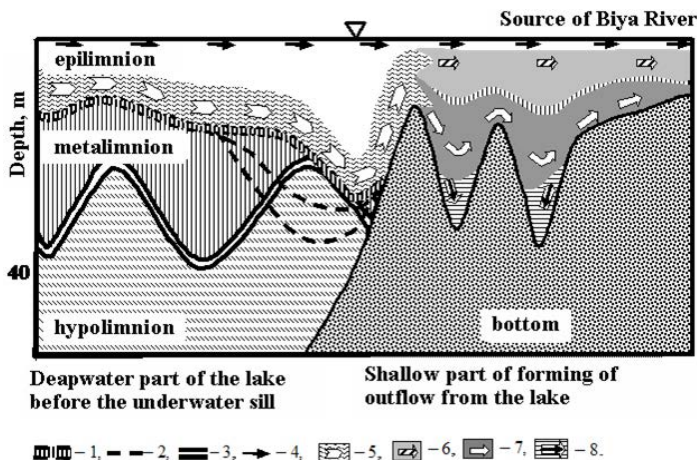


Fig. 3. Schematic distribution of water masses and currents in Teletskoye lake in region of transfer from the deep part to the source of Biya river. Symbols: (1), (2) thermocline and its oscillations under the action of internal seiches; (3) oscillations of isotherms $T=4-5$ °C under the action of internal seiches; (4) flow-drift current; (5), (6) slope stratified, intermediate jets; (7) near-bottom density current; (8) reverse gravity flow by the density current incomplete detachment from the bottom.



and \bar{U} is the vertically average current velocity. The recorded currents were transformed in relation to the heterogeneity of the field structure of the water density and bottom relief. The main transformations are the gravity of the near-bottom current on the slopes, the confluences and divisions of two intermediate jets in the thermocline region, and also an intensification of the flow current in the final part of the section near the source of the Biya River.

The curves $U(z)$ in Fig. 4 are plotted using a modification of the theory from (De Cesare & Boillat, 2003) by the averages of the superposition of velocity profiles of currents, which are a part of the system.

The characteristic levels conforming to the height of the near-bottom currents, maximums of velocity of flow, and the jets are recorded on the first vertical (at $x=0$). The theoretical velocity distribution was obtained using the regularities that determine several key parameters of the near-bottom, jet, and flow-drift currents. For the near bottom current there were obtained the expressions of the entrainment function and of current velocity on its upper boundary. The proportionality of current thickening $\partial_x z_u$ and bed slope common for gravitational streams occurs only at precritical slopes (with a slope less than 0.016).

At extra-critical slopes, the relationship $\partial_x z_u$ and is acquired a weaker logarithmic character. This is explained by a velocity decrease and, accordingly, the intensity of turbulent exchange on the steep slopes. A corresponding expression for flow thickening $\partial_x z_u$, analogous to that entrainment function $En = \bar{U}^{-1} \partial_x(z_u \bar{U})$ at $z_u \bar{U}^{-1} \partial_x \bar{U} \ll \partial_x z_u$ appears

$$\partial_x z_u \cong \begin{cases} 0,044i_s, & |i_s| < 0,016 \\ 0,08 \ln(i_s + 0,02), & 0,016 < |i_s| < 0,024 \end{cases} \quad (1)$$

The velocity of the upper boundary of the density flow $U_F = U(z_u)$ depends on the velocity profile of the flow current (from the lake to the Biya River), which in turn is under the influence of the stratification stability.

According to the measurement data analysis, the main factor resulting in changes of the value U_F is the stability of the water mass to wind influence.

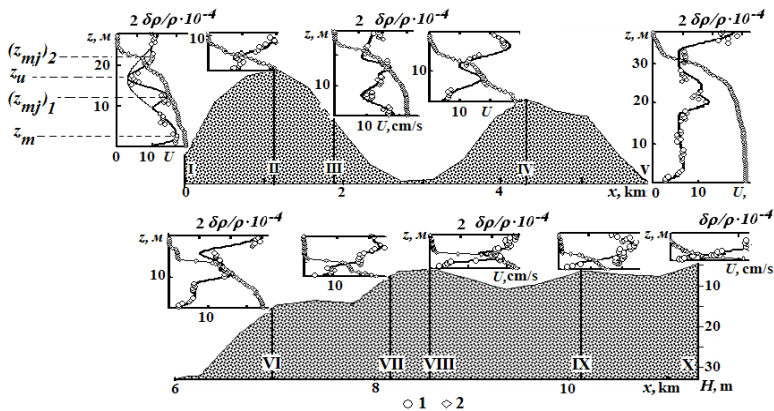


Fig. 4. Vertical distributions of current velocity U —1 and water density changes with depth from the water surface toward the bottom $\delta\rho/\rho$ —2 on the longitudinal-axial section in the latitudinal part of Teletskoe Lake (August 8, 2006).



This stability is characterized by the full Richardson number $Ri_H^* = g\Delta\rho_H H / \rho U_*^2$ where $\Delta\rho_H = |\rho_{z=0,5M} - \rho_{z=H-0,5M}|$, H is the depth, $U_* = (\tau_{*w} / \rho)^{1/2}$ is the friction speed at the water-air interface, $\tau_{*w} = \rho_A C_{DA} U_w |U_w|$ is the friction stress, $\rho_A = 1.2 \times 10^{-3} \text{ g/cm}^3$ is the air density at $T = 20^\circ \text{C}$ and atmospheric pressure, $C_{DA} = 1.7 \times 10^{-3}$ is the friction coefficient, and U_w is the wind speed at 2 m above the water surface. Variations of $U_F = U(z_u)$ are defined as

$$U_F \cong U_{F0} \exp(1 - (Ri_H^* / Ri_{H0}^*)) \quad (2)$$

according to which an increase of the stratification stability to the wind influence leads to an energy exchange decline in the flow-current and its velocity decrease near the bottom. Here and below, the subscript 0 indicates a parameter value at the first station (at $x=0$). Taking into account (1) and (2), the distribution of the average velocity of the density flow $\bar{U}(x)$ by the model from (Samolyubov, 2007) was obtained. By the theoretical values of \bar{U} the maximal velocity of the near-bottom current U_m the main part of the crossing the approach of the quasi-invariance of the velocity defect $D_u = U_m / \bar{U} = 1.2$ was satisfied. This regularity was disturbed in the final part of the section only ($x=9-11.4 \text{ km}$), when the jet current passed ahead the near-bottom current so strongly that the vertical velocity gradient in the layer of near-bottom flow mixing $z_m - z_u$ reversed its sign. The maximal flow velocity was on the level z_u . At the level of the previous maxim, the ratio $U(z_m) / \bar{U}$ was equal 0.4.

The velocities of jets $U_j(x, z)$ were obtained using the model from (Samolyubov, 2007) added by expressions for the trajectory (positions of maximal velocity) $z_{mj}(x)$ and thickness Δz_{mj} of every jet. A quasi-linear relationship to depth was discovered for jets in the regions of the lower and upper thermocline as $(z_{mj})_1 \cong 0,46H(x)$ and $(z_{mj})_2 \cong 0,66H(x)$. The thicknesses of jets were

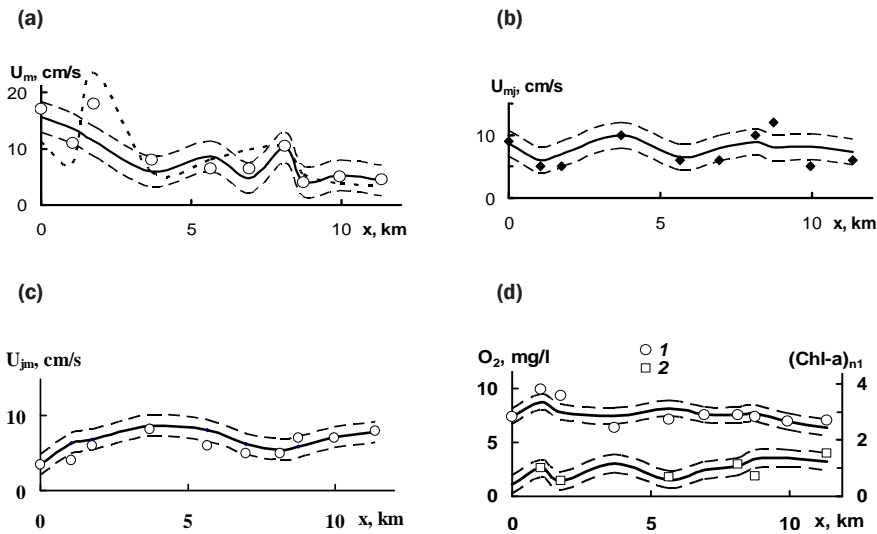


Fig. 5. Measured and theoretical longitudinal distributions of (a), the velocity of the near-bottom flow; (b) and (c), the velocities of the lower and upper jets; and (d), the oxygen concentrations within density flow and chlorophyll-a concentration at the upper boundary of the flow.



determined based on the typical, for gravity flows, relationship involving the function with slopes i_{sj} by the trajectories of the lower and upper jets:

$$(\Delta z_{mj})_1 \cong (\Delta z_{mj})_1 \Big|_{x=0} + \int_0^x (i_{sj})_1 dx \quad \text{and} \quad (\Delta z_{mj})_2 \cong (\Delta z_{mj})_2 \Big|_{x=0} + 0,35 \int_0^x (i_{sj})_2 dx$$

The distributions of the velocities of jets according to the model from (Samolyubov, 2007) taking these expressions into account are presented in Figs. 2b, 2c. A correlation between near-bottom flow velocities and overlaying ones in the system of currents is revealed by the dependence of the ratio of the velocities of these flows on the bottom slope:

$$U_m / U_{mj} \cong (95 |i_s| + 0,3) \quad (3)$$

This dependence is caused by the following factors. On the one hand, the velocity of the near-bottom flow U_m can increase not only on positive slopes due to gravity, but on negative ones under the influence of a pressure gradient related to the decrease of the flow thickness and water density along a stream. On the other hand, jet velocity U_{mj} is inversely proportional to slope, since together with depth increase, water density is redistributed and the difference of water densities within a jet and above it decreases. As a result, the ratio U_m / U_{mj} is proportional to $|i_s|$. The curve $U_m(x)$ from (3) is presented in Fig. 5a (dotted line).

The velocity of the flow-drift current necessary for the use of the model is estimated in approximations of the constancy of the water rate at all depths and the proportionality of the velocities of the drift current and wind. A suitable velocity expression for the flow-drift current at a depth of 3 m has the form

$$U_{H-3} \cong 0,8(q_{H0} / H) + 4 \cdot 10^{-3} \cdot U_w \quad (4)$$

Here, $q_{H0} = U_{FD} H$ is the water rate at $x=0$, U_{FD} is the velocity averaged over the depth, and $4 \cdot 10^{-3}$ is the wind coefficient for a depth of 3 m. The use of (1)–(4) in the model shows the conformity between the calculated and measured velocity distributions (Figs. 4, 5).

Among distributions of admixtures the most dynamic ones are the dependencies of concentrations of dissolved oxygen and chlorophyll-a on the distance along the crossing (Fig. 2d). The decrease in the oxygen concentration in a near-bottom flow with distance x is caused by the gradual water mixing within this current transporting oxygen from the deep-water part of the lake to the shallow one with overlying waters. The satisfactory fit of theoretical and measured longitudinal distributions of oxygen concentrations confirms the shape of the model from (Samolyubov, 2007), by which the curve at Fig. 5d was calculated.

The distribution of chlorophyll-a (Fig. 5d) was graphed using the deduced dependence of its concentration on the coefficient of turbulent exchange for a near-bottom flow K_u (Fig. 6a):

$$(Chl-a)_u = (Chl-a)_{u1} (K_{u1} / K_u)^{0,5} \quad (5)$$



The parameters for the station II in Fig. 3 located over the first underwater threshold are marked with the sign 1. Samples for spectrometry analysis on chlorophyll-a content were taken at the crossings in 2004 and 2006 at the stations II, III, V, VII, VIII, X at heights $z=H-0.5$ m and $z_{prob}=(0.85-1.45)z_u$. The K_u value was calculated using the expression $K_u \cong 1 \cdot \sigma_w \cong 14.4 \cdot 10^{-4} z_u \bar{U} / (1+0.4 Ri_u)^{3/4}$, where $1 \cong 0.036 z_u / (1+0.4 Ri_u)^{1/4}$ and $\sigma_w \cong 0.04 / (1+0.4 Ri_u)^{0.5}$ are the average, by the current thickness, offset, and average standard of the vertical component of the velocity pulsation (Anisimova et al., 1992).

As follows from (5), the intensification of the vertical exchange in density flow leads to a decrease of the chlorophyll-a concentration at $z=z_u$. This is explained by water dilution at was determined (solid line at Fig. 5a) and utilized for the calculation of the current velocity profiles (Fig. 4). On the upper boundary of the current by the waters from its near-bottom layer with a low chlorophyll concentration. According to dependence of the chlorophyll-a concentration in the upper boundary of the current on the entrainment function of ambient waters (Fig. 6b), the concentration is inversely proportional to the $\partial_x z_u$ and maximal by the negative entrainment.

4. Systems of stratified currents and mass-exchange in the near-mouth regions and bays.

The detailed analysis of systems of currents in the near-mouth regions was performed on the base of the results of our complex investigations carried out in 7 reservoirs. These materials are eliminated in [book]. The main characteristics of the observed processes are the following: (1) forming of systems of currents of types 1–4; (2) bifurcations and confluences of intermediate and near-bottom currents; (3) mutual transformation of the flows inside the system into each other.

The mechanism of energy transfer, induced by the internal wave, from the near-bottom current into the intermediate jet, specific for the systems of types 1, 3, 6 was revealed during the analysis of the results obtained in August 2008 at the Petrozavodsk Bay of the Onega Lake by the expedition

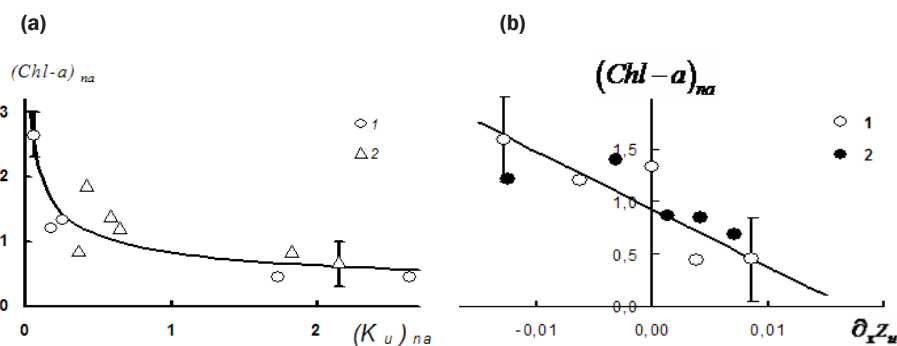


Fig. 6. Dependences of chlorophyll-a concentration on average by crossing, a, on similarly normalized coefficient of turbulent exchange which were found on two crossings in latitudinal part of the lake and b, on the entrainment function of the overlying waters in the density current (July 27, 2004–1 and August 8, 2006–2).



of MSU. The investigations were carried out from the board of the scientific Vessel “Ecolog” of IWP of the North Karelian Research Center of RAS. Measurements were performed using the Doppler Current Profiler RDCP600 (Aanderaa) and some probes (CTD and others). There were carried out the 36-h temporal station in central part of the bay. Current velocity profiles were measured every 10 min with step 0.5 m.

The wind velocity (mainly south-west direction) changed from 4 up to 12 m/c. Maximum of water density gradient in thermocline was located at depth 7–9 m. Water temperature difference at the epi- and hypolimnion reached 10 °C. The near-surface current velocity reached 30 cm/s. Under the level of maximum of water density gradient the current direction changed its sign. The near-bottom current height was equal to 3–6 m while its velocity was about 10–29 cm/s. Intermediate jet was located in the depth 7–15 m (Figs. 7a, 7b). In current velocity field there were registered jet accelerations while wave surge of the near-bottom current height under the action of the internal seiches (Fig. 7a). Amplitudes of wave disturbances of the current velocity were proportional to the velocity of the near-bottom flow.

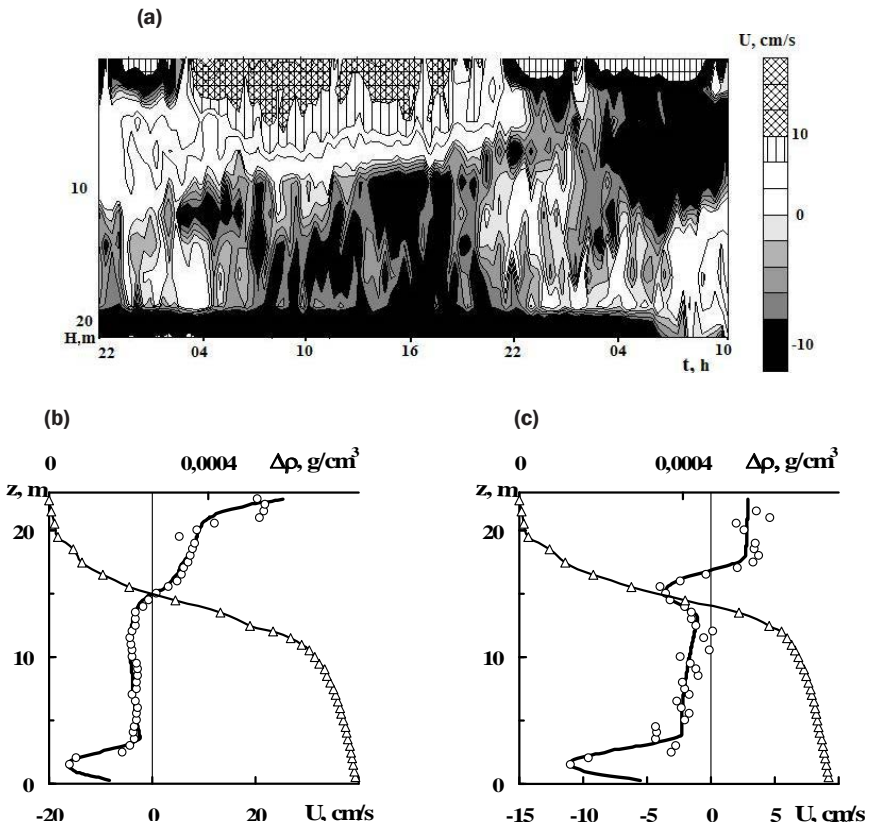


Fig. 7. Distributions of (a) current velocity on depth and in time during the 36-h temporal station, (b) current velocities and water density changes with depth averaged on 90 profiles during the period of intermediate jet development, (c) current velocities and water density profiles typical for formatted jet. Curves $U(z)$ are computed by the model of circulating and near-bottom density currents.



The probability of such pulse transfer grows with increase of wave height up to the values relevant to area of the intermediate jet. This probability also increases with lowering of stratification stability. Height of the standing internal wave (with seiche origin) is proportional to the value of the interval between the bottom and the level of maximum of water density gradient. Effectiveness of the interaction of near-bottom current and jet grows while wave approaching of current boundaries due to the entrainment. There were also observed two-stage pulse transfer under the influence of spreading antiphase waves of high-order modes. There was found and analytically expressed the relationship of velocities of the near-bottom current and of the jet situated in the thermocline. The corresponding semi-empirical expression includes not only the mentioned velocities, but also the following parameters. (1) Depth of thermocline. (2) Integral Richardson number that defines the stability of current over the entire depth to the wind action (Michioku, 1993). (3) The function of the internal wave profile with taking into account the superposition of two modes with periods 2 and 3 h, that dominated in the near-bottom layer. These periods are in agreement with the results from (Filatov, 1983). The obtained expression is useful for the evaluation of the jet velocity taking into account its interaction with the near-bottom flow by simulation of the systems of the currents.

In August 2008 at the Petrozavodsk bay and at the nearest open part of the Onega lake there was discovered system of currents with the jet in thermocline in occurrence of circulation flows, currents caused by the internal seiches and weak near-bottom flow. The near-bottom flow appeared at the slopes and detached from the bottom at the depths more than 40 m (Fig. 8a). The revealed thermally stratified jet, that propagated at the intermediate depths transported waters with heightened mineralization from the bay into the open lake (Fig. 8b). In the bay this current was supplied by the wind induced local water circulation.

Outside the bay the jet-type current was caught into the zone of action of large scale lake circulation that was close to the direction of the jet at the mouth of the bay. The Richardson number Ri_j defining the jet stability increased from 3 up to 43 before the current going out of the bay. Then $Ri_j = g\Delta\rho_i \cdot \Delta z_j / \rho U_{mj}^2$ lessened twice and further was practically invariable after the jet submerging by the wind velocity changing from 4 up to 8 m/s.

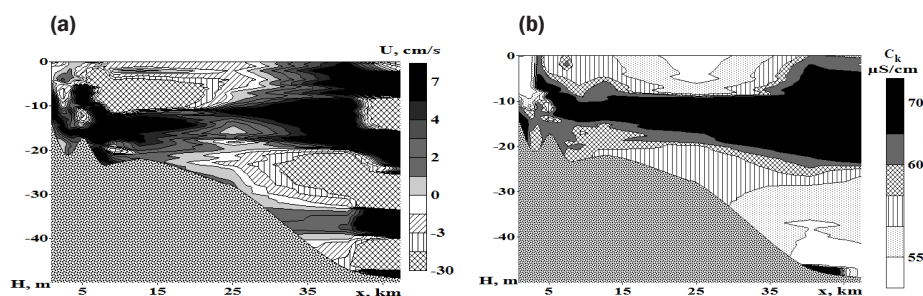


Fig. 8. The distributions of (a) current velocity, (b) water conductivity over the depth and along the crossing from the Petrozavodsk bay toward the open Onega lake (August 11, 2008).



The measured current velocity profiles (Fig. 9) are in whole conformed to the theoretical ones.

The circulation flow velocity profile was obtained from the dynamic equation for the gradient current stipulated by the water level rising due to the wind action. There was used the profile of the turbulent viscosity coefficient K_u found in this work taking into account specific of turbulent transfer at the shear layers and at the core of the current. The profile $K_u = K_u(z, N, \tau_w, u_{*s}, l)$ was calculated on the base of the data about the changings of the wind stress τ_w , shear velocity u_* , buoyancy frequency N and turbulent scale l . As it follows from the solution of the current dynamic equation the lessening of the exchange coefficient gives the local increase of the current velocity. By such a way there appeared the velocity maximum changed by the acceleration of the jet at the slope isopycnical surface (Figs. 9, 10b).

For this and other similar jets the height of the current velocity maximum above the bottom z_{mj} is proportional to the depth H and is determined as $z_{mj} = 0.76(H - H_0) + (z_{mj})_0$. Expressions of z_{mj} and Δz_j where utilized in models of the jet propagation and suspended sediment transfer. The jet thickness Δz_j expressed as $\Delta z_j = \Delta z_{j0} + a_{Ej} \int_{x_0}^x i_{sj} dx$ corresponds to that obtained using the current velocity profiles (Fig. 10a) where $\Delta z_{j0} = \Delta z_j(0)$, $i_{sj} = \partial_x z_{mj}$, $a_{Ej} = 0.76$. The velocity U_j of the jet moving along the slope isopycnical surface under the action of the gravity force is found taking into account changing the sign of the slope along the jet trajectory i_{sj} . The corresponding expression of the U_j is $U_{jg} = \alpha_{wj} (g \Delta \rho_j \Delta z_j |i_{sj}|^{1/3} / (\rho C_{Dj}))^{1/2} i_{sj}^{1/3}$ in approach of local quasi-stationarity and horizontal quasi-homogeneity of the flow (Samolyubov, 2007). The jet velocity change under the wind action is evaluated as $k_w U_w$ with wind coefficient $k_w = 0.01$.

The whole evaluation of the jet velocity under the action of the mentioned above factors is introduced in first approximation as $U_{mj} = U_{jg} + k_w U_w$. The comparison of the values $U_{mj}(x)$ found by this expression with the measurement data (Fig. 10b) indicate about the domination of gravity component in the summary distribution. The inclinations from the curve $U_{mj}(x)$ are stipulated by the internal waves and by the discrecity of the wind velocity registration at the crossing. The suspended sediments concentration S along the jet (Fig. 10c)

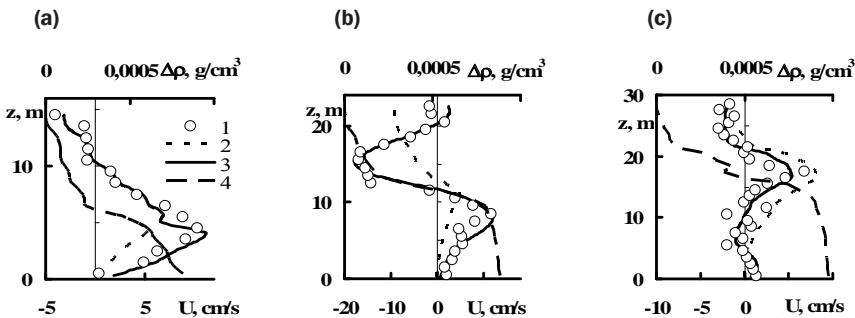


Fig. 9. The profiles of the current velocity U (1 corresponds to the measured values, 2, 3 are noted to the theoretical velocity distributions for the circulation and whole currents) and density difference $\Delta \rho$ (4). Figures (a), (b), (c) correspond to the results obtained at the upper part, mouth of the bay and at the open lake (curve 3 corresponds to the sum of the profiles of the circulation wave and density currents).

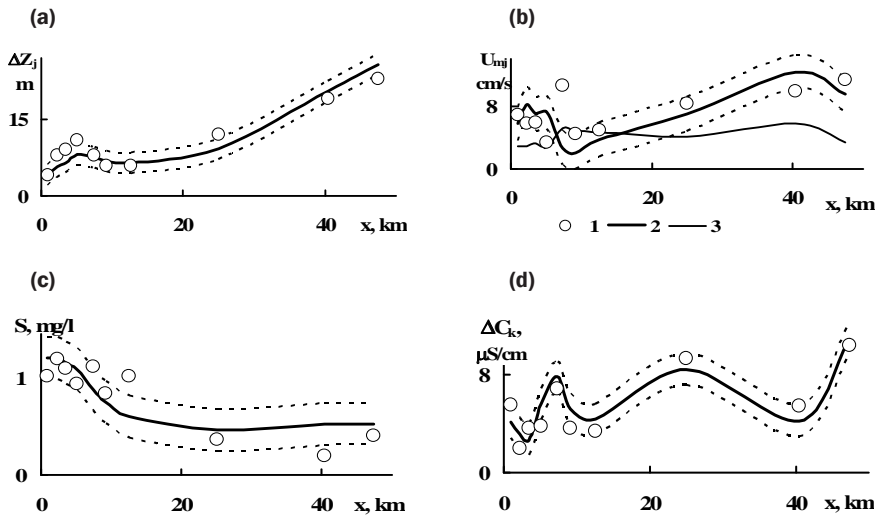


Fig. 10. The longitudinal distributions of (a) of the jet thickness Δz_j and (b) of its velocity U_{mj} (1, 2, 3 specify the measured, theoretical and wind induced velocities), (c) of the suspended sediments concentration S and (d) of the excess water conductivity ΔC_k .

is in compliance with the theoretical one obtained by the model similar to that elaborated for the density current (Samolyubov, 2007).

The mineralization, determined by the conductivity C_k (Figs. 8c, 10d), is reduced at the upper boundary of the jet simultaneously with exchange amplification at the near-surface water layers due to the wind velocity growth. This process is followed by the increase of the excess salts concentration in the core and at the jet boundaries ΔC_k . The increase of the exchange intensity at the lower part of the jet leads to the entrainment of the underlying waters with higher mineralization into the jet body. These considerations were verified by the obtained relationship ΔC_k on the standard of the vertical component of the current velocity turbulent pulsations σ_w and on the wind velocity U_w in form $\Delta C_k = \Delta C_{k0} (k_{c1} \cdot \sigma_w / \sigma_{w0} + k_{c2} (U_w / U_{w0})^2)$. Corresponding curve is shown at Fig. 10d. Here $\sigma_w = 0.04 U_{mj} / (1 + 0.4 Ri_j)^{0.5}$, $k_{c1} = 0.44$, $k_{c2} = 0.086$.

4. Conclusions

The observed systems of stratified currents are of great interest because they are widespread in coastal zone, lakes and reservoirs. Suggested classification and generalization are necessary for the elaboration of theory of interacting stratified currents. The concrete results introduced above enable us to reveal some interesting mechanisms of development of such systems and to suggest some modification of mathematical models of interacting stratified currents.

Acknowledgements

This work was supported by the Russian Foundation for Basic Research (project No. 08-05-00574).



References

- Anisimova, E. P., Petrov, V. V., Speranskaya, A. A. (1992) *Vestn. Mosk. Un-Ta. Fiz. Astron.* 5, 63.
- Boegman, L., Loewen, M. R., Hamblin, P. F. (2008) Vertical mixing and weak stratification over zebra mussel colonies in western Lake Erie. *J. Limn. & Oceanogr.* **53**(3):1093–1110.
- De Cesare G. & Boillat J.L. (2003) Intrusive and Bottom Density Currents and Induced Vertical Exchanges in a Stratified Lake. In: *Proc. of the 30th IAHR Congress*, AUTH, Greece, 1, THEME, 381.
- Filatov, N. N. (1983) *Dynamics of lakes*. Leningrad: Hydrometizdat.
- Michioku, K. (1993) Hydrodynamics in Lakes and Reservoirs Res. and Practice in Hydraulic Engineering in Japan. *Spec. Iss. JHHE SI* **19**:17.
- Ozmidov, R. V. (1997) Vertical exchange through the layers with high water density gradients in the ocean. *Oceanology* **37**(4):492–496.
- Samolyubov, B. I. (2007) *Density Flows and Diffusion of Impurities*. Moscow: URSS (in Russian).
- Samolyubov, B. I. & Kirillov, W. W. (2005) *Proc. of the Intern. Conf. on Fluxes and Structures in Fluids*, Moscow, 96.
- Selegei, V. V. & Selegei, T. S. (1978) *Lake Teletskoe*. Leningrad: Gidrometeoizdat (in Russian).

Influence of hydrological conditions on environment state of lagoons and estuaries

Yuriy Tuchkovenko

Abstract

The overview and typology of lagoons of the North-East coast of the Black Sea are presented. There are 21 lagoons located in between the Danube River and Dnepr River mouths. All of them may be divided into three groups: open, periodically open and closed. Hydraulic management, namely stabilization and adaptive regulation of the water exchange with the sea, is proposed as a main effective measure to stabilize the state of the lagoon environment for second and third groups of lagoons. The scientific basis of this idea is examined by an application of 3-dimensional numerical dynamic model to some of them.

Дан обзор и описана типология лагун северо-западной части Черного моря. На участке побережья в междуречье Дуная и Днепра расположен 21 лиман. Их можно разделить на 3 типа: открытые, периодически изолированные, полностью закрытые. Наиболее эффективным способом стабилизации гидрологического и гидрохимического режимов лиманов 2-й и 3-й группы, управления их экологическим состоянием с целью сохранения и восстановления ресурсного потенциала является обеспечение и регулирование искусственного водообмена с открытым морем. Научные основы решения этой проблемы рассмотрены на примере Дофиновского лимана и Тузловской группы лиманов. Используется численная трехмерная нестационарная модель.

There are 21 lagoons located in between the Danube River and Dnepr River mouths. All of them may be divided into three groups: open, periodically open and closed.

The Dniester, Bug and Dnepr estuarine lagoons (the local name is “liman”) are typical representatives of first group, as well as lagoons “Sukhoi liman” and “Malyi Adzhalykский (Grigorievskiy) liman”, which are artificially deepened and modified into big sea ports. These estuarine lagoons have free

Yuriy Tuchkovenko (✉)
Odessa State Environmental University, Odessa, Ukraine
e-mail: tuch2001@ukr.net



connections with the sea through straits, which are dredged for navigation. River discharge and wind-induced water level variations in lagoons and in the adjacent marine area are the main driving forces for lagoon hydrology. Penetration of colder saltwedge near the bottom into the lagoon, sedimentation and resuspension, summer hypoxia in the deep fairways are of the main interest from the hydro-ecological point of view.

The lagoons of Tusla, “Dofinovka”, “Budakskiy”, “Dzhantsheiskiy”, “Malyi Sasyk” limans represent the second group. They separated from the sea by sandy barrier, which have artificial or naturally formed temporary active inlets. The water quality in these lagoons is determined by balance between positive and negative terms of water budget for different years, by water quality of incoming river waters, by intensity of water exchange and seepage. Reduction of water volume due to intense evaporation leads to increase of salinity and concentration of all substances, development of eutrophication. Drying of lagoon and instability in water level make unfavorable conditions for recreation and fishery. The similar problems are typical for closed lagoons, like “Kuyalnik”, “Hadzhibey”, “Tiligul” limans.

Hydraulic management, namely stabilization and adaptive regulation of the water exchange with the sea, is proposed as a main effective measure to stabilize the state of the lagoon environment for second and third groups of lagoons. The scientific basis of this idea is examined by application of 3-dimensional numerical dynamic model to lagoons like “Dofinovka liman” and Tusla lagoons. This model simulates water quality of shelf marine systems and is based on hydrodynamic model MECCA—Model for Estuarine and Coastal Circulation Assessment (Hess, 1989, Tuchkovenko & Ivanov, 2007), which advantage is a resolving of processes in elongated sub-grid areas (as canals, channels or river mouths). The complete number of thermo-hydrodynamics equations in Byssinesk, incompressibility and hydrostatic approaches are solved in curvilinear in vertical direction frame. To resolve the motion in small channels of sub-grid scale, the equations is averaged across the stream.

References

- Hess, K. W. (1989) *MECCA Programs documentation*, NOAA Technical Report NESDIS 46. Washington, D.C.
- Tuchkovenko, Yu. S., & Ivanov V. A. (2007) Modelling of processes of water quality formation for North-East part of the Black Sea. In: *Ecological security for shore and shelf zones and integrative use of shelf resources*, Vol. 15, 304–325. Sevastopol: Marine Hydrophysical institute of National Academy of Ukraine.

Numerical modeling of hydrodynamics and sediment transport in coastal lagoons

Georg Umgiesser, Marco Bajo

Abstract

An overview over various numerical techniques, different approaches for structured and unstructured meshes is given. Various applications of numerical model SHYFEM are shown, ranging from lagoon environments in the Mediterranean and the Baltic Sea to the coastal zone and the open sea. Ecological models and sediment transport models are discussed. Finally the possibility to apply these models in the coastal zone management is shown.

Дан обзор различных численных методов, подходов для структурированных и неструктурированных численных сеток. Показаны примеры применения численной модели SHYFEM, начиная от лагун Средиземного и Балтийского морей, и кончая прибрежной зоной и открытым морем. Обсуждаются экологическая модель и модель транспорта осадка. Также показана возможность применения этой модели при управлении прибрежной зоной.

1. Introduction

1.1. Models as a complement to observations

Measurements are the primary source of information on the coastal ocean, its ecosystem and its variability. There is no point of attempting to model a coastal zone without having data. However, we have seen that data are difficult to obtain because of the technology of sensing instruments and platforms and the costs of using existing platforms over long durations and large domains. For these reasons models can complement observations in coastal management. They can interpolate in 4 dimensions (time and space) the observations and predict the future evolution of the system. Moreover it is possible also to simulate the impacts of non-observed forcing scenarios.

Georg Umgiesser, Marco Bajo (✉)
Institute of Marine Sciences (ISMAR-CNR), Venice, Italy
e-mail: georg.umgiesser@ismar.cnr.it



1.2. Modelling applications

Models can be used for management of coastal zones or in an operational context. They can simulate the coastal erosion and the variations of morphology. The study of the current dynamic and of the sediment transport can be useful also for the harbour construction.

Their main operational applications are the prediction of waves, tides and storm surges. In coastal areas this information can be useful both for the navigation and for the populations that live near the sea.

1.3. Description of a coastal system

Different aspects of a coastal system can be analysed by means of models. Physical, chemical and biological features can be investigated. However to have a good description of the last two groups, the first one, that is the hydrodynamic investigation, is necessary.

The hydrodynamic model is the “engine” that transports and mixes all ecosystem constituents, including the water itself. In a model the hydrodynamic equations of conservation of mass and momentum are solved numerically, in every cell of a computational grid, taking into account the information present in adjacent cells.

The hydrodynamic engine is then coupled to appropriate numerical models that transport some ecosystem constituents. There are three major classes of transport models:

- ✓ Sediment transport models;
- ✓ Water quality models;
- ✓ Ecosystem models.

The sediment transport models deal with cohesive (e.g. mud) sediment transport and non-cohesive (e.g. sand) sediments transport.

The water quality transport models deal with interactions between:

- ✓ Organic matter;
- ✓ Dissolved oxygen;
- ✓ Nutrients;
- ✓ Chlorophyll-a;
- ✓ Bacteria;
- ✓ Pollutants.

Finally, ecosystem models deal with interactions between some or all of the following:

- ✓ Nutrients;
- ✓ Bacteria;
- ✓ Phytoplankton;
- ✓ Zooplankton;
- ✓ Detritus;
- ✓ Oxygen

as a function of hydrodynamics and light.

1.4. Model grids

Depending on the method used to discretise the spatial domain of the equations governing the system, different grids are used.

In Fig. 1 a grid of a model based on finite differences is reported, while in Fig. 2 a grid of a finite element model is represented.



2. Case study: the Venice lagoon

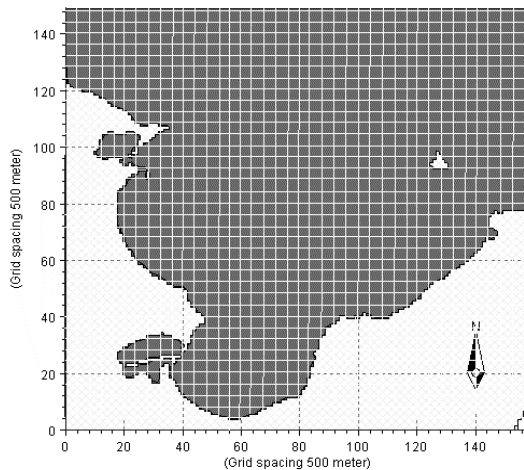
In the past a consistent effort has been put into the modelling of the physical, chemical and biological aspects of the Venice Lagoon. Due to its complicated bathymetry, the Venice lagoon is one of the most complex coastal systems in Italy, and due to this difficulty, along with extensive field campaigns, modelling techniques must be used if some understanding of this system wants to be achieved. Finite difference hydrodynamic models have been applied in the past to the Venice lagoon by Chignoli & Rabagliati (1975), Volpi & Sguazzero (1977) and Sguazzero et al. (1978).

In 1987 the Danish Hydraulic Institute set up an operational model for the Venice Lagoon that was used in planning the sluice gates that were to be built in the lagoon (Marchi et al., 1992). All these models used the finite difference method with a grid size of 300 m or more. Recently a higher resolution model with a grid size of 100 m was implemented by Casulli & Cheng (1992), Casulli & Cattani (1993). This model can describe the channel network faithfully, but the computational demand of such a high resolution model is quite high. However, all finite difference models have suffered all from the same problem: the need of a small grid size to resolve the narrow channels inside the lagoon that has to be imposed everywhere. A compromise between accuracy and computer time has to be made.

The finite element or finite volume method, on the other hand, allows for more flexibility with its subdivision of the system into triangles varying in form and size. One such approach has been used by Casulli & Zanolli (1998), where a model with an unstructured grid has been presented. This finite volume approach was then extended to the resolution of the non-hydrostatic equations and has also been applied by Casulli & Zanolli (2002) to the Venice Lagoon with promising results.

The lagoon of Venice has been a case study for ecological models too. Contributions in the peer review literature started to appear in the eighties, with a number of contributions on modelling the macroalgae blooms, first by using a 0-dimensional representation (Bocci et al., 1997), and then within a 3D coupled model (Solidoro et al., 1997). Subsequent contributions have dealt not only with the growth, fishing and rearing of clams (Solidoro et al.,

Fig. 1. Example of a finite differences grid.



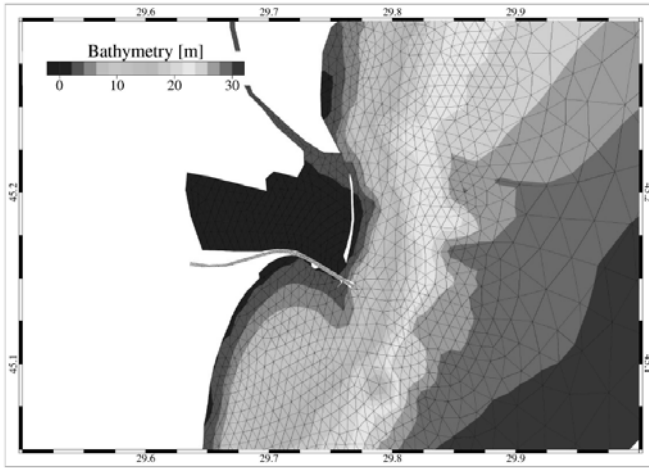


Fig. 2. Example of a finite elements grid.

2000, Pastres et al., 2001), but also using a methodology for the identification of Maximum Permissible Load compatible with a predefined Water Quality Target (Pastres et al., 2003). More recent contributions include the definition of VEELFEM, a finite element ecological model for the lagoon of Venice and the first applications of this coupled model (Melaku Canu et al., 2001).

At the Venice institute of the CNR (National Research Council) a finite element model (SHYFEM) has been developed that was conceived as a model suitable for the application to basins with the characteristics of the Venice Lagoon. This model has been enhanced with modules that treat wave, sediment and ecological processes. This model has been applied not only to the Venice lagoon, but also to other Italian and Mediterranean lagoons, showing its general suitability for shallow water basins.

The model presented here is freely available to the scientific community. The source code has been released under the GPL (Gnu Public License) and is free to use for everybody who wants to use it. The model can be downloaded under the web page <http://www.ve.ismar.cnr.it/shyfefem>, where not only the source code for the general model can be found, but also the set-up for the Venice lagoon (numerical grid, data, input files), in order to serve as a reference implementation of a numerical model of the Venice lagoon for other scientists that work on these topics.

In the following sections the model framework is presented and its application to the Venice lagoon and other shallow basins described. The main focus in this paper is on the hydrodynamic modelling, where most of the results are available.

References

- Bocci, M., Coffaro, G., Bendoricchio, G. (1997) Modelling biomass and nutrient dynamics in eelgrass (*Zostera marina* L.): applications to the Lagoon of Venice (Italy) and Øresund (Denmark). *Ecol. Model* **102**:67–80.
- Casulli, V. & Cattani, E. (1993) Stability, accuracy and efficiency of a semi-implicit method for three-dimensional shallow water flow. *Computer Mathematics and its Applications* **27**(4):99–112.



- Casulli, V. & Cheng, R.T. (1992) Semi-implicit finite difference methods for three-dimensional shallow water flow. *International Journal for Numerical Methods in Fluids* **15**:629–648.
- Casulli, V. & Zanolli, P. (1998) A three-dimensional semi-implicit algorithm for environmental flows on unstructured grids. In: *Conference on Numerical Methods for Fluid Dynamics*, 57–70. Oxford: University of Oxford.
- (2002) Semi-implicit numerical modeling of nonhydrostatic free-surface flows for environmental problems. *Mathematical and Computer Modelling* **36**:1131–1149.
- Chignoli, C. & Rabagliati, R. (1975) Un modello delta idrodinamica lagunare. In: *Venezia e i problemi dell'ambiente*, Il Mulino, Bologna, 225–297.
- Marchi, E., Adam, A., Caielli, A., Cecconi, G. (1992) Water flow modelling of the Venice Lagoon. *Coastal Engineering* **20**:1869–1878.
- Melaku Canu, D., Umgiesser, G., Solidoro, C. (2001) Short-term simulations under winter conditions in the lagoon of Venice: a contribution to the environmental impact assessment of temporary closure of the inlets. *Ecol Model.* **138**:215–230.
- Pastres et al. (2001) Managing the rearing of *Tapes philippinarum* in the lagoon of Venice: a decision support system. *Ecological Modelling* **138**:231–245.
- Pastres et al. (2003) Sensitivity analysis as a tool for the implementation of a water quality regulation based on the Maximum Permissible Loads policy. *Reliability Engineering and System Safety* **79**:239–244.
- Sguazzero, P., Chignoli, C., Rabagliati, R., Volpi, G. (1978) Hydrodynamical modelling of the Lagoon of Venice. *IBM Journal of Research and Development* **22**(5):472–1180.
- Solidoro, C. et al. (1997) Modelling macroalgae (*Ulva rigida*) in the Venice lagoon: model structure identification and first parameters estimation. *Ecological Modelling* **94**:191–206.
- Solidoro, C., Pastres, R., Melaku Canu, D. et al. (2000) Modelling the growth of *Tapes philippinarum* in Northern Adriatic lagoons. *Marine Ecology Progress Series* **199**:137–148.
- Umgiesser, G. (2000) Modeling residual currents in the Venice Lagoon. In: Yanagi, T., ed., *Interactions between Estuaries, Coastal Seas and Shelf Seas*, 107–124. Tokyo: Terra Scientific Publishing Company (TERRAPUB).
- Volpi, G. & Sguazzero, P. (1977) La propagazione della marea nella Laguna di Venezia: un modello di simulazione e il suo impiego nella regolazione delle bocche di porto. *Rivista Italiana di Geofisica e Scienze Affini* **IV** ½:67–74.

Poster presentations

Hydrodynamic conditions in the central part of the Vistula Lagoon

Albert Ambrosimov, Aleksandr Babakov

Abstract

The paper present the results of the field measurements of wind waves and currents executed in the central part of the Vistula Lagoon. Hypothesis is made on deep penetration of waves from the Baltic Sea area into the Vistula Lagoon.

В статье представлены результаты измерений ветровых волн и течений в центральной части Вислинского залива. Выдвинута гипотеза о глубоком проникновении морских волн в залив.

1. Introduction

The aim of this work is to study experimentally the waves and currents in the central part of the Vistula Lagoon. The experiment was performed for the more general problem of assessing the impact of flow and surface waves on the resuspension, transport and re-deposition of sediment in the Vistula Lagoon.

2. Measurement procedure

Measurement of anxiety, level and flow in the bottom layer in the Vistula Lagoon was carried out using the wave recorder LGU-2 (SDB GMF Obninsk), where the pressure sensor in the device use frequency strain gauge transducer “silicon on sapphire”, included in one arm of the measuring bridge. If you change the water level above the device varies the pressure recorded by the

Albert Ambrosimov (✉)

P. P. Shirshov Institute of Oceanology RAS, Moscow, Russia

e-mail: ambrosimov@ocean.ru

Aleksandr Babakov (✉)

P. P. Shirshov Institute of Oceanology RAS, Atlantic Branch, Kaliningrad, Russia

e-mail: babakov_temp@mail.ru



sensors, which resulted in a change in its frequency. In addition to measuring the pressure fluctuations, the unit provides measurement of the average hydrostatic pressure for a given time of measurement equivalent to measuring the level of the sea, and is thus, and a tide gauge. The flow was measured using a current meter “flow”.

Experimental setup for the integrated study of transport processes of matter consisting of a metal pyramid height of 2.3 m, which was installed at a depth of 4.7 m in the Vistula Lagoon, abreast of the Baltiysk Strait—cape Severny near island Nasypnoy. Wave recorder was fixed to the pyramid on depth of 2.6 m from the surface of the lagoon and at a depth of 2.1 m from the bottom. Register excitement produced in the beginning of every hour for 10 min with increment 0.25 s. The flow was measured with a flow recorder “FLOW-3M” is fastened inside the pyramid from the bottom brace, which the impeller was located at 0.9 m from the bottom. The device was installed in such a way that the impeller device was in the bottom of the lagoon. Fixing the parameters of currents occurs with increments of 30 min. During this period, summed up the current meter speed impeller and gave the averaged value of current speed and direction for 0.5 h.

To convert the pressure fluctuations induced at a depth of 2.6 m surface waves in the characteristics of waves on the sea surface and bottom, was the method of calculating wave elements, based on the findings of the spectral theory of sea waves, developed by Hasselman (Hasselman, 1962). The main the complexity of solving equations for the spectral density of the wave of accounting is a member of the nonlinear interactions of waves of various heights and periods, which was resolved in the framework of the “sharply focused” approach developed by V. E. Zakharov, Academician of RAS (Zakcharov et al., 1999).

At moments of the frequency spectrum $(m_i = \int_0^\infty S(\omega)\omega^i d\omega)$ can be calculated main parameters of wind waves: the average height and average period. Based on the moments of the frequency spectrum is determined, the five most important parameters of wind waves: the characteristic wave height h_s , the peak of the spectrum of T_p , the average period of waves \bar{t} , the wavelength range of peak L_p , the average wave length \bar{L} . For the average height, we have:

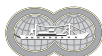
$$\bar{h} = \sqrt{2nm_0},$$

where— m_0 zero point frequency spectrum. The average period \bar{t} defined through the moments of the frequency spectrum as the time interval between the intersections at lowering the level of the middle line for implementation:

$$\bar{t} = 2n \sqrt{\frac{m_0}{m_2}}.$$

where m_0 and m_2 —zero and second moments of the frequency spectrum, respectively.

The average height of waves are strongly correlated with the heights, a lower or higher average. For example, the most probable value of the largest wave height of a thousand successive waves passing through a fixed point on the surface of the sea, about three times greater than average height, five



hundred of the biggest waves of the successive waves of more than twice the average height, etc. Thus, you can get a pretty comprehensive description of the unrest in the test area of the sea on the known values of the average heights by multiplying them by the corresponding coefficients.

3. Waves

As the results of observations of the excitement at a depth of 2.6 m recorded virtually no wind disturbance occurring in the Lagoon with a wavelength of less than one meter and a height less than 0.2 m, whose impact on the depth of wave recorder installed 2.6 m, as shown by spectral analysis completely decays. Impact on the resuspension of bottom sediments, as shown by field experiments have long waves with periods of ~ 3.5 s, and the lengths of 12–19 m. The source of these waves may be a wave of marine origin, fallen into the lagoon through his neck. Check the characteristics of waves in the experiment was carried out wave recorder at the beginning of each hour for 10 min with the discreteness of readings equal to 0.25 s.

Fig. 1 shows the temporal variability of wave heights in the lagoon and as an example of the frequency spectrum of a realization of emotion, it can be seen that for the period from May 16 to June 17 there are 12 periods of increasing wind waves up to 0.45 m length from a few hours to several days were recorded in the Vistula Lagoon. There are 12 wind and wave samples, where the maximum wave height greater than 5 cm, were selected for analysis, and energy spectrum shows that at the entrance to the lagoon of long waves shatter on the high-frequency components, which are stored for a long time.

Fig. 2 shows one of the 12 wind-wave amplification of surface wind waves in the lagoon, observed in the period from June 20 (06:00) to June 8 (24:00),

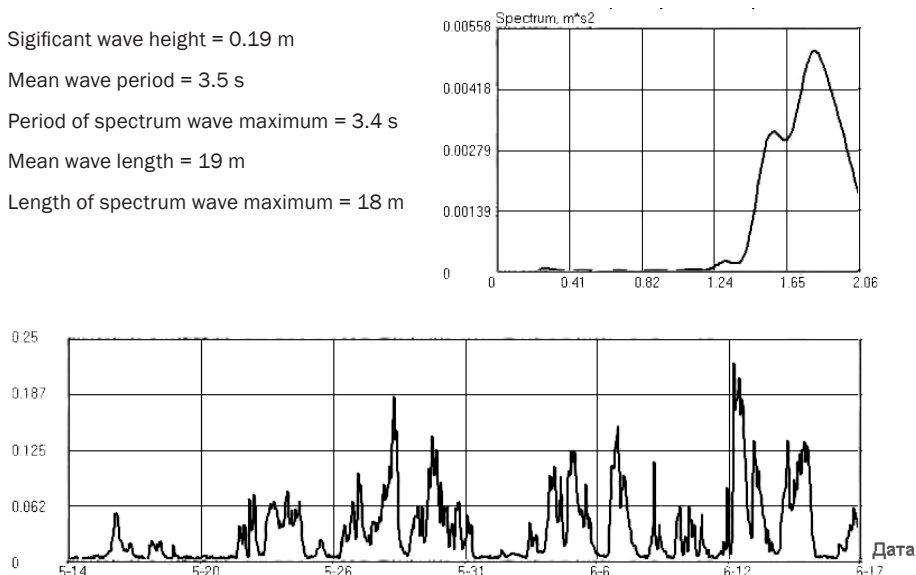


Fig. 1. The frequency spectrum of waves in the Vistula Lagoon and temporal variability of waves in the lagoon during the observation period from May 15 to June 17, 2009.



2009. Fig. 2a shows the maximum (solid line) and average height (dotted line) surface waves throughout the entire wind-wave amplification, and Fig. 2b shows the maximum and average (solid and dashed lines, respectively), amplitude of water at the bottom of induced surface waves. Maximum wave—this is one of the maximum 10-min sample. Average wave is a wave averaged in 10 min interval wind-wave disturbance.

The spectra calculated from the excitement of observational data (Fig. 1) are clearly visible overtones waves fallen into the lagoon through its inlet. Fluctuations of water particles at the bottom of induced surface waves, is reciprocal in nature and occurs in an ellipse, thus there is the involvement of sediments in the aquatic environment, which are then carried by currents to other lagoon area.

4. Currents

During the experiment, the dominant water transport was directed in the NE quarter (NNE–E, 54.3 percent) and to the south (SSE–SSW, 28.4 percent), with a maximum frequency of occurrence in the ENE (19.0 percent) and S (13.6 percent). The dominance of flow in the NE quarter (to the mouth of the river. Pregolya and Baltiysk Strait) persisted for a range of velocities $V=0-10$ cm/s and $10-20$ cm/s, and only if $V>20$ cm/s began to dominate the south-west transport over the north-east (0.7 vs 0.35 percent) (see Fig. Roses flows). However, the rate of more than 20 cm/s occurred only one percent of the cases were of short duration and are usually recorded during periods of increasing input or output flows and a sharp rise or decline in sea-level canal and the Straits. This relationship suggests a close connection of hydrodynamic regime in the studied area with a level regime in the channel and marching in the investigated area Vistula Lagoon, adjacent to the Baltic

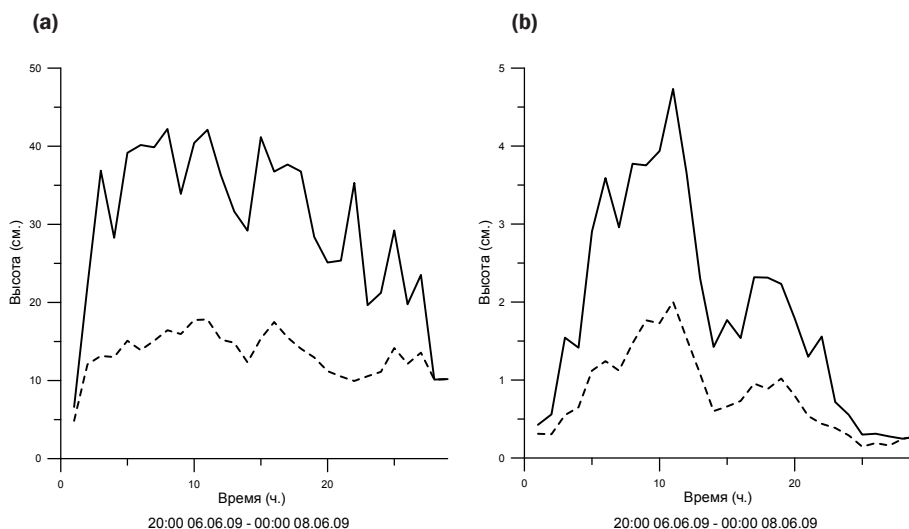


Fig. 2. Example of maximum and average heights of waves on the surface of the lagoon and induced oscillations of water at the bottom (depth 4.7 m) in the observation period from 8:00 p.m. June 6 to 12 p.m. June 8, 2009.

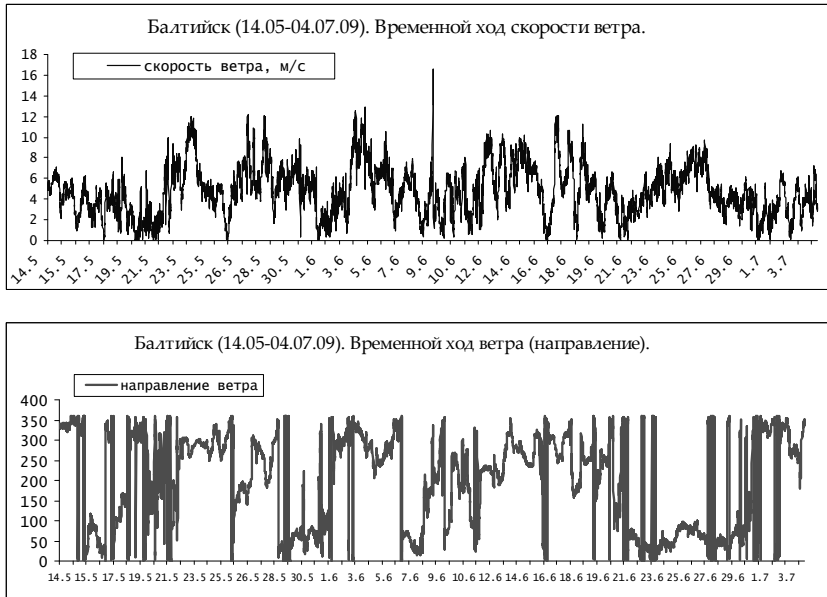


Fig. 3. Time variations of speed and direction of wind during the field experiment in the Vistula Lagoon.

Strait. It is in times of storm surge the wind-level fluctuations are activated by the flow capacity when the joint impact of the wave to the transfer of particulate matter, mainly in the NE and SW quarters to the top of the Vistula Lagoon (estuary Nogat and region Pregolya) and in the direction of the Baltiysk Strait, the Gulf of Gdansk.

5. Wind

Time variation of wind direction during the period of full-scale hydro-litodynamic experiment (15.05–05.07.09) in the Baltic is characterized by a regular change of stability and long-winds from the NW and NE quarters horizon. In the period of validity of the rate increases to 10–13 m/s, and in three cases—in W–NW winds—up to 15–16 m/sec. Between the period of validity of the wind direction was unstable and, as a rule, the rate of less than 5 m/s (Fig. 3).

6. Conclusion

Dynamic effects on the resuspension of bottom sediments, as shown by field experiments have long waves with periods of ~ 3.5 s, and the lengths of 12–19 m. The source of these waves may be a wave of marine origin, fallen into the lagoon through his neck. Excitement at the wave perturbations roil precipitation, and currents carry them into the deeper parts of the lagoon.

When reaching into the lagoon, the waves of the Baltic Sea decay and are transformed by reflection from the coast, that are clearly visible on the frequency spectra of disturbances.



Bottom fluctuations in water depths of about 5 m induced by long surface waves, approximately one order of magnitude smaller than the amplitude of surface waves.

Acknowledgements

The work was partly supported by Grant No. 08-05-01023 of the Russian Foundation for Basic Research. Authors thank their colleagues B. Chubarenko and I. Kabatchenko for support in planning/organization of field measurements and discussion of results.

References were not provided by the author.

Dynamics of waters in the Baltiysk Strait

Aleksandr Babakov, Boris Chubarenko

Abstract

The analysis of long-term measurements of currents (2003–2009) in the Baltiysk Strait is carried out. Schemes of currents are received at various hydrometeorological conditions. Time variability and statistical distributions (histograms, roses) for near bottom currents at the core and at the end of the northern pier is analyzed. Essential change of behavior of currents between piers and outside is shown. Water level variations defines a water dynamics between the piers, as wind and waves define water dynamics of waters outside of piers.

Проведен комплексный анализ данных инструментальных измерений течений, проводимых в Балтийском проливе в период 2003–2008 гг. Получены схемы течений при различных гидрометеорологических условиях, а также графики временного хода и статистические распределения (гистограммы, розы) для придонных течений у корня северного мола и на полигоне у оголовков молв. Показана существенная смена поведения течений между входными молами и на выходе в открытое море. В проливе главным фактором, определяющим динамику вод является уровеньный режим, за пределами молв — ветер и волнение.

The Baltiysk Strait is the only connection between the Vistula Lagoon and the Baltic Sea. Three measuring data sets are analyzed in the paper. First is a result of direct measurements of currents in the Strait by floating drifters (0 and 7 m depth) at different situations of wind forcing. Second is the data from permanently installed current meter at the depth of 6 m at the point of traffic control. The third one is the two-months data-series of measurements of bottom currents at 4 points near the outer end of piers bounded the Baltiysk Strait (Fig. 1).

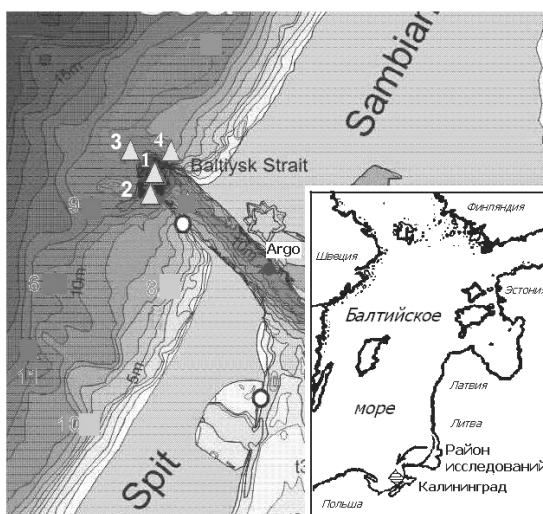
The analysis of the received data has shown that the dynamic regimen of the Baltiysk Strait is defined mainly by wind and gradients currents, and rare by long waves—seiches.

Aleksandr Babakov, Boris Chubarenko (✉)

P. P. Shirshov Institute of Oceanology RAS, Atlantic Branch, Kaliningrad, Russia
e-mail: babakov_temp@mail.ru, chuboris@mail.ru



Fig. 1. Locations of current measurements (i) at the traffic control point (round mark), and (ii) at the outer end of piers (triangle marks).



The amplitude of level fluctuations in the Strait is of 25–40 cm. Currents averaged through upper 7 m is in the range of 20–30 cm/s (Fig. 2), it may reach 50–70 cm/s during stormy weather. Maximum value for inflow current was of 1.3 m/s, and for outflow current is of 1.5 m/s. The amplitude of seiche induced level fluctuations is of 5–8 cm with the period from several hours to about one day.

Current averaged through upper 7 m direct toward the sea (outflow) at 51.5 percent and toward the lagoon (inflow) a 48.5 percent. The current velocity usually was in a range of 5–30 cm/s (Fig. 3).

The near bottom currents are within the range of 10–30 cm/s, the maximum of probability is for the range of 0–10 cm/s (60–80 percent of cases), more 20 cm/s—9–14 percent (Fig. 4).

The most intensive currents were regularly fixed at the end of the Southern pier. Current velocity decreases slightly (at 1.2–1.5 time) with depth; sometimes an amplifies in the middle of a water column was found.

Currents at different section of the Strait were of 20–25 cm/s at the upper layer and of 23–30 cm/s at the 5–7 m depth. Different current directions for the same wind direction (Fig. 5) evident about grater influence of the level variations on the current at the Strait. Characteristic time scale of level changes is of 4–8 h.

At a moderate wind (6–9 m/s) and stable level (+28–30 cm) seiches induced currents with the period nearby 12–24 h is fixed. The single-layered inflow stream was of 18–36 cm/s, outflow stream of 33–52 cm/s.

The work is partly carried out under financial support of the Grant No. 08-05-01023 from the Russian Foundation of Basic Research.

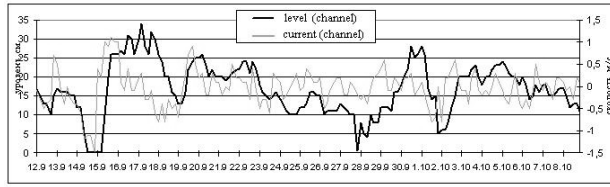


Fig. 2. Example of temporal variations of current and level in the Baltiysk Strait.

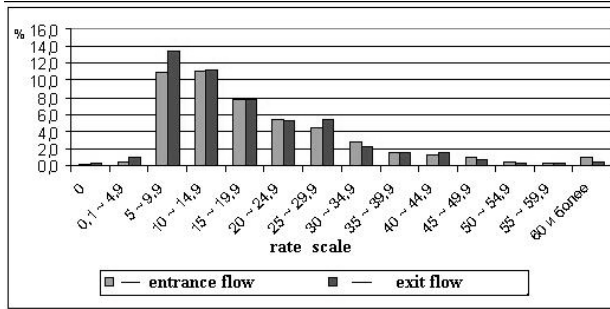


Fig. 3. Percentage of repetition of inflow (entrance flow) and outflow (exit flow) currents in the Baltiysk Strait.

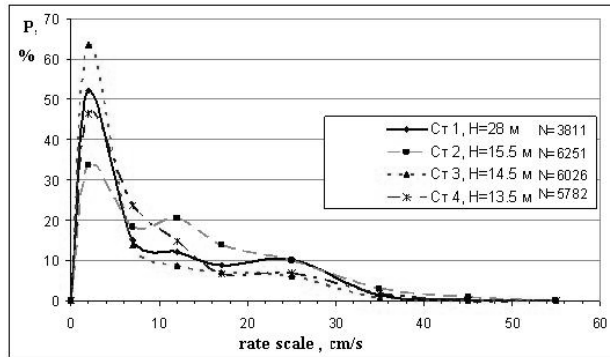


Fig. 4. Repetition of the near bottom currents near the ends of piers bounded the Baltiysk Strait.

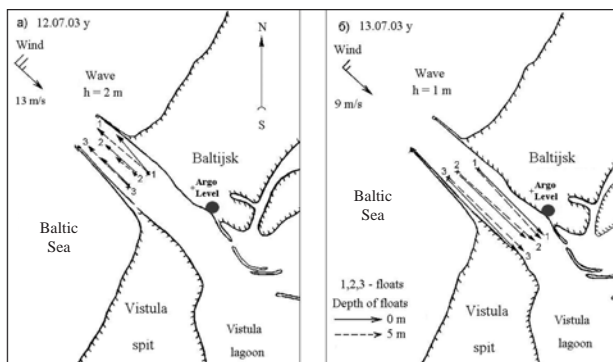


Fig. 5. Floats displacement under NW storm wind.

Marine deposits of the Vistula Spit (Baltic Sea)

**Elena Badyukova, Leonid Zhindarev,
Svetlana Lykianova, Galina Solovieva**

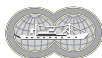
Abstract

Geological-geomorphologic structure of the Vistula Spit evident that a body of the Spit (except for beaches, a fragment of deltaic plain on 23 km of the Spit, and also those sites where former lagoon inlets existed, e.g. at the 23 km of the Spit) consist from eolian sand which form upper layer down to 1–2 m below modern sea level. The subsequent fluctuations of the Baltic Sea water level resulted in formation of the Vistula Spit. Low terrace (height up to 1–1.5 m abs.), which fix the rise of sea level, have been revealed and described on the lagoon coasts of both, the Vistula and Curonian Spits, The similar terrace is located on sea coast of a settlement Kosa (Vistula Spit) under eolian foredune deposits. Thus rise of a sea level during Littorina and Limnea exceeds contemporary level only on 0.5 m.

Исследования геолого-геоморфологического строения Вислинской косы позволили сделать вывод о том, что тело косы, за исключением пляжей, призаливной террасы и фрагмента дельтовой равнины на 23 км тела косы, в значительной степени состоит из эоловых песков, которые залегают не только с поверхности, но и на 1–2 м ниже современного уреза. На заливных берегах как Вислинской, так и Куршской косы авторами ранее были закартированы и описаны низкие призаливные террасы (высотой до 1–1,5 м абс.), фиксирующие один из последних подъемов уровня Балтийского моря. Фрагмент аналогичной террасы выявлен на морском берегу у пос. Коса под эоловыми отложениями авантюны и дюнного вала. Таким образом, уровень моря за все время развития косы (литорина и лимнея) превышал современный только на 0,5 м.

The geomorphologic structure of the accumulative barrier forms bordering significant parts of sea coasts does not leave doubts in close connection of the reasons and stages of their formation with changes of a sea level. Such

Elena Badyukova, Leonid Zhindarev, Svetlana Lykianova, Galina Solovieva (✉)
M. V. Lomonosov Moscow State University, Moscow, Russia
e-mail: badyukova@yandex.ru



dependence is traced and in the structure of sandy barriers of southeast Baltic—Curonian and Vistula spits. Analyzing relief of these spits it is necessary to note, that now the most part of their surface is consist of the eolian sand (Badyukova et al., 2008), marine genesis has a modern sea beach, and marine-lagoon genesis have a beach and low terraces in the Curonian and Vistula gulfs. Terraces fragmentary frames the lagoon coasts of both the spits and have height not more than 1.5 m.

Most widely low young lagoon terrace is distributed on the Vistula Spit, forming in its northern part, in area of capes Tikhi and Peschanyi. The capes Taran located to the south, the Duga, Krainyi and Glavnyi are bordered by low, narrow lagoon terraces. Their surfaces are complicated with low coastal bars and colonize, as a rule, cane or shrubbery.

On sea coast of the spit there are the layers of pebbles in the bottoms of some blow-outs. These layers can serve as age analogue of lagoon terrace. The blow-outs strip is situated in the zone of the most active deflation of the coastal sand and located directly behind the avandune or foredune. The pebble layers fix, apparently, position of an ancient coastal bar, which was primary burred by sand, and then excavated by the modern processes of a deflation. The present pebble layers position exceeds a modern sea level on 1.5–2 m.

In area of the Curonian barrier-lagoon system low lagoon terrace is traced by narrower fragments both along the spit, and on the other coasts of a gulf. So, on the southern coast it is submitted by well expressed coastal bar. It consists of coarse-grained quartz sand, pebbles and mollusk shells. Bar height above lagoon level is 1.6 m. The similar form of a relief is fixed and on the spit along a southern part of lagoon coast where a low swamp terrace surface extends on the north almost to the settlement Lesnoe.

As to the marine coast of Curonian Spit, here just as on Vistula Spit the pebbles appear behinds the foredune. One of such sites—area of settlement Khvoinoe where in 80–100 m from the foredune top, among sand, on the depth about 0.5 m presence of pebbles and gravel material is revealed. Further, drilling in area of settlement Morskoe let to find out some pebbles in the size 3–4 cm at once under a soil layer. The pebble is also found out by a bore-hole located to the west of Morskoe on seaside of the spit, behind the foredune at absolute height of 1.5 m.

Beach pebbles among eolian deposits allow assuming the presence along spit seaside an ancient coastline. On the Curonian Spit the presence of an ancient coastline proves to be true also character of Muller dunes relief. The dune slopes inverted to sea are abnormal abrupt, that obviously it is not peculiar windward slope of eolian forms on the sea coasts. Presence of an ancient coastline specifies also archeology researches (Kulakov et al., 2003), authors connect it with an epoch of Vikings.

The most obvious proof of presence along Vistula Spit the ancient coastline connected to a sea-level rise is the coastal bar traced in the cliff foot in area of settlement Kosa. Inside part of a bar is buried under eolian deposit and another one is opened in cliff extended in this part of the spit on some kilometers. The cliff height varies from 2 up to 4.0 m above sea-level, the beach joint borders on the cliff foot at the height about 1.5 m abs. Above the beach it is exposed about 1 m in cliff it consists of light grey coarse-grained layered sands with pebbles, mollusk shells and gastropods (Fig. 1, layer I). The char-



acter of sand, occurrence and bedding does not leave doubts in their marine genesis.

Above sand there is a thin interlayer (about 10 cm) of chocolate-brown sandy loams with numerous inclusions of pebbles and gravels. Its roof settles down at height of 2.5 m abs. Contact of this interlayer to underlying deposits is distinct. Visually these sandy loams remind hydromorphic palaeosoil, formed in a coastal zone.

The top part of the section consists of eolian sand which thickness in a place of a described outcrop composes 1 m. Contact of the eolian sand with the roof of chocolate-brown sandy loams is distinct too. In an average part of a sandy layer the interlayer grey-black palaeosoil is observed (Fig. 1, a layer II). Despite of its insignificant thickness (about 2–3 cm), the interlayer in cliff is traced on large distance along the sea, gradually rising in a southwest direction.

On the basis of radiocarbon dating ^{14}C of the mollusk shells from the marine sediments composing the bottom part of a cliff their absolute age 1,270+60 cal BP (LU-6129) has been received. According to opinion of a lot of competent researchers, authors of World Ocean and Baltic sea-level curves in Holocene (Badyukova et al., 2007), by this time one of last peaks of Limnea transgression exceeded. Sea level was on 0.5 m higher than contemporary one.

The exposure of an ancient coastal bar in the cliff of a northeast part of the spit was promoted by active erosion observed here and by the retreat the coastline. The beach is steep, incomplete profile, joint borders on the cliff foot. There is no avandune or foredune sand in some places as they are eroded completely. Chocolate-brown sandy loams under a small inclination fall on the south, to settlement Kosa and wedging out there. The settlement is located on typically marine deposits exposed by numerous dikes and gutters. As a rule, it is bedded sandy thickness of grey and olive-grey color with black interlayer in which on depth about 1 m numerous slices of amber are found out. At some sandy interlayer there is the coarse-grained material which alongside with amber inclusions specifies littoral genesis of deposits. Probably, on a place of settlement flat offshore contributed to the formation of shoal, extending to the Vistula gulf.

Similar marine sand is found out and on other sites of Vistula Spit sea coast. To tell the truth, frequently their presences at the foot of cliff are hid under eolian deposits. In particular in 2 km to southwest from the settlement Kosa behind a rearward of a modern beach, under eolian deposits of foredune the layer of beach deposits with pebble and mollusk shells was found. Sometimes in these deposits thin interlayer of heavy minerals observe, that unequivocally speaks about their formation on the berma surface of an ancient beach. So in one of points of supervision, after extensive dig the beach deposits under the foredune were opened. These deposits contain interlayer

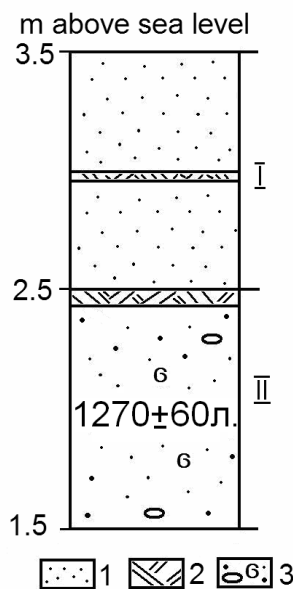
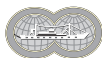


Fig. 1. Outcrop near the settlement Kosa (the Vistula Spit). (1) eolian sand; (2) palaeosoil; (3) beach deposits.



of garnets (2–3 cm) and glauconite (1–2 cm) appreciably inclined aside the sea.

Apparently, the coastal bar clearly enough traced in a cliff in northeast part of Vistula Spit sea coast, is stretched along this accumulative form. In a southwest direction there is an attenuation of erosion process, the roles of modern marine sand and eolian deposits in a coastal zone increase. It creates conditions for an ancient bar burial. Apparently, its age is the same as lagoon terrace which frame fragmentary the coasts of Vistula and Curonian gulfs.

Interesting data on Vistula Spit structure can be received from the article of the Polish researchers (Uściniowicz, 2006) in which results of borehole drilling on profile across the spit are submitted. One of the boreholes is on nearshore in the spit seaside; another one is located actually in a zone of a modern sea beach. It opens the beach deposits—coarse-grained sand with pebbles up to depth about 7 m. Marine deposits discover below too. These are fine-grained sand, with interlayer of medium-grained sand, with a rare pebble and mollusk shells (*Cerastoderma sp.*, *Macota sp.*). The age of sand on depth 4 m, determined on shells, is $2,920 \pm 60$ cal ^{14}C BP. General thickness of the marine beach deposits is 14 m. The deposits of low delta plains—clay, silty clay, silt, olive-grey silty sand and peat—lie beneath the marine sand. Age of this alluvial layer is $8,040 \pm 70$ cal ^{14}C years BP (Uściniowicz, 2006). The transgressive overlapping by marine sand was the result of Littorina transgression of the Baltic Sea.

The analysis of geological profiles through the Vistula Spit shows, that the marine sand composing in a basis its body, approached on alluvial-deltaic deposits, being gradually replaced by marshes. This transition, apparently, fixes a stage of fast development and formation of bars surrounded the delta coast. Sea-level rise promoted flooding of delta plain was accompanied by peat formation and accumulation of marsh and oxbow lakes deposits directly behind bars. Proceeding transgression strengthened promotion of bars inland, intensified active eolian processes and marshes overlapping, and also has led to the further flooding of the rivers mouths.

Thus, along the sea coast of the Vistula Spit the ancient coastline corresponding to one of the last sea-level rise is traced. This rise not exceed, apparently, 0.5 m above its contemporary position. Depending on character of modern coastal processes geomorphologic attributes of this coastline are expressed to a greater or lesser extent. On the erosion sites the coastal bar fixing high position of a sea-level, exposes in the cliff bottom. On the accumulative coasts accompanying with the development modern and ancient eolian forms of a relief, marine deposits substantially burred under eolian sand.

References

- Badyukova, E. H., Zhindarev, L. A., Lykianova, S. A., Solovieva, G. D. (2007) Geological structure of the Curonian Spit (of the Baltic Sea) and its evolution history (revised). *Oceanology* **47**(4):594–604.
- (2008) Barrier-lagoon systems in the south-east of the Baltic Sea. *Oceanology* **48**(4):37–48.
- Kulakov, V. I., Zhindarev, L. A., Volkova, I. I. (2003) Korallenberg: palaeogeographic reconstructions of the Viking settlement. In: *Problems of investigations and protections of nature environment*, 95–107 (in Russian).
- Uściniowicz, S. (2006) A relative sea-level curve for the Polish Southern Baltic Sea. *Quaternary international*, 145–146, 86–105.

Storm surge forecast in Venice through an hydrodynamic model

Marco Bajo, Georg Umgiesser

Absract

An overview over various numerical techniques in hydrodynamic modeling is given. In particular, different approaches to solve the hydronamic equations on structured and unstructured meshes are shown. The complications of applying these models to very shallow systems and the complicated coastal zone is discussed.

Дан обзор различных численных подходов в гидродинамическом моделировании. Основное внимание уделено различным методам решения уравнений гидродинамики на структурированных и неструктурированных сетках. Обсуждаются сложности применения моделей для мелководных водоемов со сложной береговой линией.

1. Introduction

Since the end of 2002 a numerical model, named SHYFEM, runs daily at the Centre for sea level forecasting and flood warning (ICPSM) of the Venice municipality. It is the second deterministic model operational at the Centre. The other one is a finite difference model that runs with an assimilation scheme (Lionello et al., 2006). SHYFEM model forecasts the hourly sea level at the “Acqua Alta” platform near the Venice Lagoon for five days in advance. The model has been validated and improved during the last years. Though the model provides the storm surge forecast on each node of the domain, which is extended on the whole Mediterranean Sea, the results near Venice are mostly taken into account. Consequently, several methods to improve the local forecast has been developed. A post-processing routine based on a MOS system (Kalnay, 2003) was implemented first, to correct the surge forecast at the “Acqua Alta” platform, located near Venice (Bajo et al., 2007). Later a more complex post-processing procedure based on an Artificial Neural

Marco Bajo, Georg Umgiesser (✉)
Institute of Marine Sciences (ISMAR-CNR), Venice, Italy
e-mail: marco.bajo@ve.ismar.cnr.it



Network (ANN) has been developed (Bajo & Umgiesser, 2010). A free ANN library named Fast Artificial Neural Network (FANN), has been used (Nissen, 2003). The network has 51 inputs and is calibrated with observed data, but can be adapted to accept other input variables correlated with the forecast surge.

2. Methods

The hydrodynamic model used, named SHYFEM, was developed at CNR-ISMAR in Venice. The code is freely downloadable from the web page: www.ve.ismar.cnr.it/shyfem. The SHYFEM model solves the following vertically integrated shallow-water equations:

$$\begin{aligned} \frac{\partial U}{\partial t} - fV + gH \frac{\partial}{\partial x} \left(\zeta + \frac{p}{\rho_0 g} \right) - A_H \left(\frac{\partial^2 U}{\partial x^2} + \frac{\partial^2 U}{\partial y^2} \right) - \frac{1}{\rho_0} (\tau_{sx} - \tau_{bx}) &= 0, \\ \frac{\partial V}{\partial t} - fU + gH \frac{\partial}{\partial y} \left(\zeta + \frac{p}{\rho_0 g} \right) - A_H \left(\frac{\partial^2 V}{\partial x^2} + \frac{\partial^2 V}{\partial y^2} \right) - \frac{1}{\rho_0} (\tau_{sy} - \tau_{by}) &= 0, \\ \frac{\partial \zeta}{\partial t} + \frac{\partial U}{\partial x} + \frac{\partial V}{\partial y} &= 0, \end{aligned}$$

where ζ is the water level, U and V the vertically-integrated velocities (total or barotropic transports), t the time, g is the gravitational acceleration, p the atmospheric pressure at the mean sea level, ρ_0 is the water density, $H=h+\zeta$ the total water depth, h the undisturbed water depth, f the variable Coriolis parameter, τ_s is the wind stress, τ_b is the bottom stress, A_H is the horizontal diffusion coefficient.

The model uses finite elements for spatial integration and a semi-implicit algorithm for integration in time. The terms treated semi implicitly are the water level gradients and the Coriolis term in the momentum equations and the divergence term in the continuity equation, the bottom friction term is treated fully implicitly. All other terms are treated explicitly.

The model domain is reproduced by means of a staggered finite element grid made up of 18,626 triangular elements varying in size and shape and covers the whole Mediterranean Sea. The grid elements describing the Adriatic Sea vary in size between 1.5 and 10 km, whereas in the Mediterranean region the spatial resolution is less than 35 km (Fig. 1).

At the closed boundaries only the normal velocity is set to zero and the tangential velocity is a free parameter. This corresponds to a full slip condition. At the open boundary in the Gibraltar Straits, a water level equal to zero is imposed, since it is unknown. Wind and atmospheric pressure data used by the model are provided by the European Centre for Medium-Range Weather Forecasts (ECMWF). The Centre supplies mean sea level pressure and surface wind fields over the Mediterranean area, at synoptic hours 00, 06, 12, 18 UTC, with a resolution of 0.5 degree both in latitude and longitude. Only the storm surge component is computed by the dynamic model, the total sea level is computed simply by adding the astronomical tide, obtained by means of harmonic analysis.

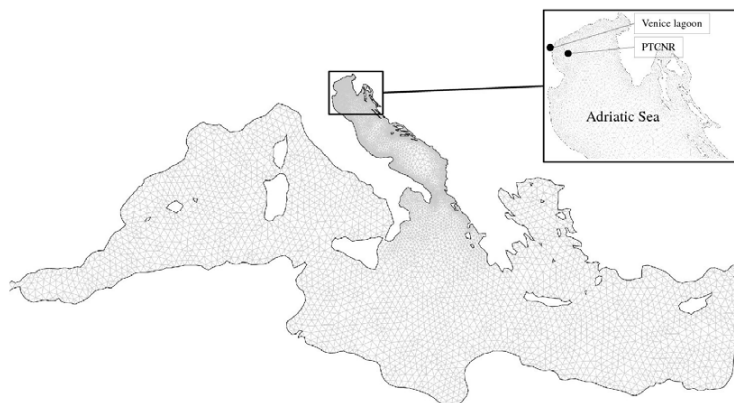


Fig. 1. Computational grid of the Mediterranean Sea.

In order to set up the ANN, the surge forecast of the model and the observed level of 5 years, collected at the CNR platform, have been used. These values were organised in inputs and desired output of the ANN. The available data have been split into three parts. Data from years 2003, 2004 and 2005 were used for the training phase. Data from 2006 were used for the testing phase and data from 2007 were used for the validation phase.

3. Results

After the ANN calibration through the training and testing phases, the ANN was executed with the data of the year 2007 to validate the system and check its general functioning. In Fig. 2 is reported a comparison between the model performances with (FANN) and without (Mod) the neural network correction for the validation phase (year 2007). The standard deviation (Std) and the mean of the differences (Mean) between model and observed data are plotted against the forecast hour. The original model results (Mod) have a mean of the differences that oscillates with a period of about 24 h and has an amplitude of about 0.02 m not centred around zero. This periodicity is explained by the fact that each surge level is predicted five times, for subsequent days, using different but similar, meteorological forcing.

The mean value of the post-processed data (Mean FANN) is considerably reduced to less than a half and is now centred around zero. For the first forecast day it is almost completely removed and for the next days it keeps acceptable values, lower than ± 2 cm.

The standard deviation shows periodic variations during each forecast day, but its trend is nearly constant until the 60-forecast hour, then it rises linearly. For the post-processed data, the standard deviation of the differences (Std FANN) is considerably lower. It increases almost linearly after the low values of the first hours and rises from a value of less than 3 cm to an average value of about 5 cm for the first 24 h. In the second day of forecast (from 25th till 48th forecast hour) the standard deviation is almost constant, with a value of about 6 cm. This represents a strong improvement with respect to the results

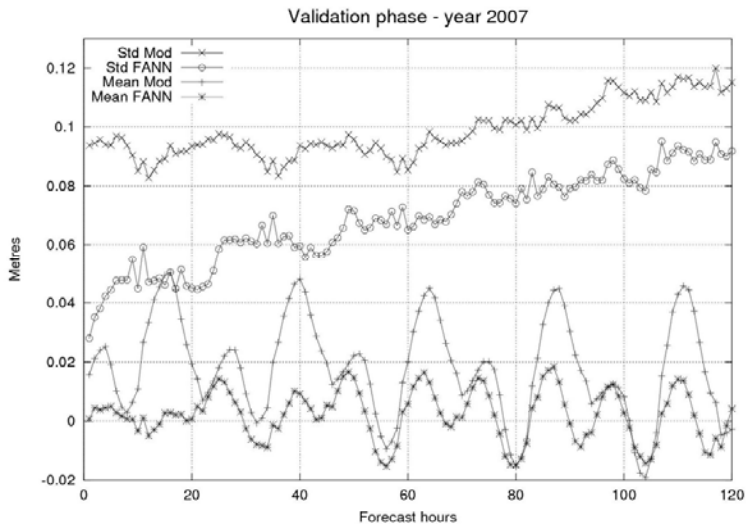


Fig. 2. Comparison between the model performances with (FANN) and without (Mod) the neural network correction. The standart deviation (Std) and the mean of the differences (Mean) between model and observed data are plotted against the forecast hour.

of the hydrodynamic model (Std Mod). For lags longer than 48 h, the standard deviation has an average improvement of about 2 cm, without increase the rate of losing accuracy.

4. Conclusions

A mean standard deviation of the differences of 4.7 cm was obtained for the first forecast day and a value of 8.9 cm for the fifth day. The accuracy of the fifth day of forecast is now higher than the one of the first day of the model without the ANN correction. Further improvements will be a new training of the ANN with more inputs and with longer databases.

References

- Bajo, M., Zampato, L., Umgiesser, G. et al. (2007) A finite element operational model for the storm surge prediction in Venice. *Estuarine, Coastal and Shelf Science* **75(1-2)**:236-249.
- Bajo, M. & Umgiesser, G. (2010). Storm surge forecast through a combination of dynamic and neural network models. *Ocean Modelling* **33(1-2)**:1-9.
- Kalnay, E. (2003) *Atmospheric Modeling, Data Assimilation and Predictability*, first ed. Cambridge: Cambridge University Press.
- Lionello, P., Sanna, A., Elvini, E., Mufato, R. (2006). A data assimilation procedure for operational prediction of the storm surge in the northern Adriatic Sea. *Continental Shelf Research* **26(4)**:539-553.
- Nissen, S. (2003) *Implementation of a Fast Neural Network Library (FANN)*. Technical report, Department of Computer Science, University of Copenhagen (DIKU), Copenhagen.

Hydrological processes of transboundary catchment areas with relationship to coastal zone: modeling and spatial analysis

Dmitry Domnin

Abstract

This article discusses the structure of transboundary watershed in the South-East Baltic, taking into account their impact on the coastal zone. A quantitative assessment of individual morpho-hydrological parameters of the catchments is performed by tools of spatial analysis and modeling of hydrological processes.

В статье обсуждается структура трансграничных водных бассейнов в Юго-Восточной Балтике, принимая во внимание их влияние на прибрежную зону. Количественная оценка морфо-гидрологических параметров бассейнов выполнена методами пространственного анализа и моделирования.

1. Introduction

Kaliningrad Region (Kaliningrad Oblast) together with the Klaipeda County (Lithuania), Pomeranian and Warmia-Masurian Voivodeships (Poland) belongs to the sub-region of South-East Baltic. This catchment area includes a watershed of the Vistula and the Curonian Lagoons, the Vistula River, and small rivers basins that flow into the Gulf of Gdansk (Fig. 1). Rivers of the Kaliningrad Region are transboundary watercourses. This situation requires the development of new concepts for management of neighbors' interests in catchment (Khublaryan et al., 2005). Currently, the basin approach is a common methodological basis for water resources management in Russia and in Europe. Since 2006, it was enshrined in Article 3 of the Water Code of the Russian Federation (Water Code, 2006), and in Article 28 stipulates that "basin districts are the basic unit for use and protection of water bodies..."

Transboundary issues of interstate or national level (catchment are divided among administrative unit) always contains the potential "conflict" for the

Dmitry Domnin (✉)

P. P. Shirshov Institute of Oceanology RAS, Atlantic Branch, Kaliningrad, Russia
e-mail: dimanisha@rambler.ru



interests of water users, this leads to some restrictions on the activities and the need to registration the interests of basin neighbors. Water consumer in the bottom of the basin is determined by the quality of water that comes with its upper part, and at the top—it is regulated by the amount of water used in the lower reaches. In these circumstances, regulatory authorities, economic managements and territorial governments need a clear idea of their location in the river basin, and they need information about the upstream and downstream neighboring. Water quality in the Vistula and the Curonian Lagoon, as well as in the coastal zone of the sea is completely determined by economic activities in the watershed. Even the administrative units that don't have outlet to the sea or lagoons, have close connection with them through the waterways, they transfer to the receiving water body everything that falls into river basin.

2. Methodology

Atlas of transboundary river basins of Kaliningrad Oblast was issued in 2007 (Domnin & Chubarenko, 2007). It reflects the relative position of river basins and administrative-territorial units of the Oblast. It contains illustrative schemes that show the spatial intersection of the basin and administrative entities, parts of the basin area within the administrative units. However, to assess the impact of administrative structures in coastal waters of the sea and lagoons require data on average annual runoff from parts of the territories of municipalities within the boundaries of a single catchment. This information can be obtained by using the tools of drainage models. The main incoming parameters for the model are the data on precipitation, evaporation, surface and underground runoff (Fig. 2).

The calculations were used application MIKE11 DHI Software (MIKE11, 2004), which provides information about the runoff from a certain area and

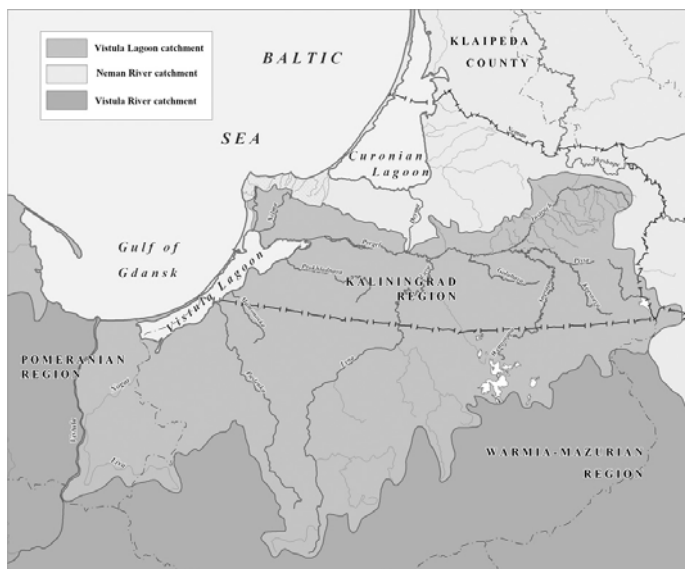


Fig. 1. Kaliningrad Region and watershed of the Vistula Lagoon, South-East Baltic (Chubarenko & Domnin, 2008).



for a given time-series. To calculate the water discharge used NAM-model, which uses time-series of precipitation, evaporation and temperature, and for calibration—consumption in the outlet of the basin. The NAM model is a deterministic, lumped and conceptual Rainfall-runoff model accounting for the water content in up to 4 different storages. NAM can be prepared in a number of different modes depending on the requirement. As default, NAM is prepared with 9 parameters representing the Surface zone, Root zone and the Ground water storages (MIKE11, 2004). Internal factors of the defaults were used for the assessment analysis of expenditure from the territory of municipalities.

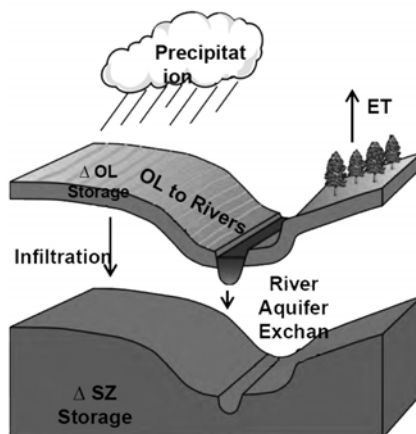


Fig. 2. The main components accounted for in the drainage models (Modelling... 2006).

The period, for which it was simulated, covering 1995–2000 (this is due to the presence of data for water discharge from catchment). Rainfall and temperature were observed at meteorological stations in Kaliningrad Oblast (Chernyakhovsk, Gusev, Gvardeysk, Ulianovo, Sovetsk, Zheleznodorozhny). Evaporation is a calculated parameter. It was obtained by multiplying the amount of precipitation on the index of its relationship with evaporation. This relationship is calculated for each meteorological point for months of the calendar year (Barinova, 2006). Daily water discharge is known for every day in the control hydrological point of the basin. The total consumption of the pool determined the amount of expenditure which is received in the administrative parts of the basin (Fig. 3).

Meteorological data from weather stations of Gusev, Chernyakhovsk, Sovetsk used for administrative units Instruch river catchment in accordance with the location of the municipalities. Value of discharge calculation by use flow models listed in Table. The total value of water discharge from the catchment area is 0.21 km³ per year.

Table

The values of the area and water discharge from the territories of municipalities, which are located in the Instruch river basin

Municipalities	Area, km ²	Discharge, km ³ per year
Gusev district	250	0.05
Krasnoznamensk district	510	0.11
Neman district	200	0.04
Nesterov district	30	0.01
Chernyakhovsk district	260	0.06
Total for catchment	1,250	0.21

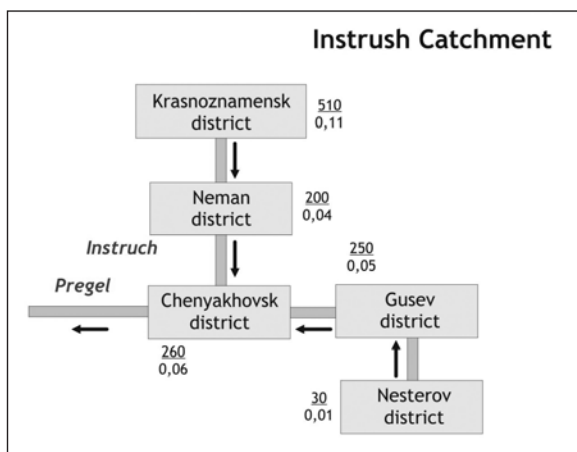


Fig. 3. Administrative structure of the Instrush River Catchment. The numbers in the picture indicate: in numerator—area of municipality in the catchment (km²), in denominator—discharge from municipality area (km³ per year).

Time after which the stock water gets into the receiving water body, determined by isochrone map of the Kaliningrad Oblast. The most rapid effect of internal parts of the region on the coastal zone is carried out by river streams. The calculation of this influence is defined distance before outlet and the time of discharge. For each node of the river network (point of merging streams) by tools of spatial analysis (module ArcGIS) was determined the distance from it to the mouth (confluence with the sea or lagoon). Next, all points are grouped by river basins, to which they belong. For the points assessed runoff time, this based on the seasonal average annual flow velocity.

Next, the whole area was divided into zones depending on the time flow (Fig. 4). Data on the rate of flow during flood, low water and the average for the year were taken from the hydrological yearbooks.

3. Results and discussion

The structure of the ratio of administrative division and river basin in the Kaliningrad Oblast is a complex. Any catchment (both international and domestic) belongs to at least two administrative units, maximum number of subjects within the basin may be up to 9, and any administrative unit of the Kaliningrad region includes from 3 to 20 parts of the catchment area of different river basins, depending on their size. Each part of the municipalities located in the catchment area contributes to the hydrological components of the entire watershed and, consequently, it affects the chemical and biological indicators of water quality and determines the water balance.

If we look at a map of isochrones, we can see that the most rapidly drain water from municipalities with access to the sea and bay, and most of the time required for water to flow from the south-eastern part of the Kaliningrad Oblast. During the “high” water runoff of the minimum time in the Kaliningrad Oblast is 6 days, during low water period is 2 weeks, and in an average year is about 8 days. Runoff from the coastal areas occurs within 3 days in the period of low water, at an average rate of long-term value of it is 2 days, and during a flood—for one day.

Thus, the assessment of hydro-morphological parameters is an integral part of the administration of the territory. From this point of view in the

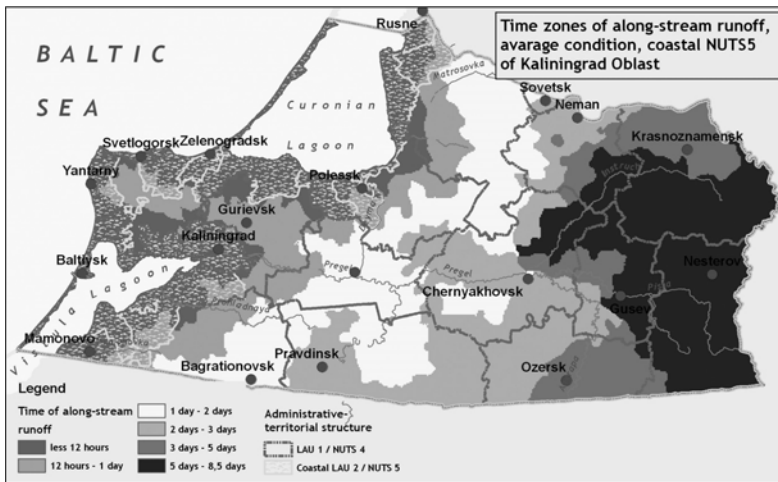


Fig. 4. Time zone of along-stream runoff, average condition, coastal NUTS4 and NUTS5 of Kaliningrad Oblast.

catchment area of the Kaliningrad Oblast, the most vigorous efforts must be applied in the municipalities near shore. The influence of more deeply situated municipalities of the Kaliningrad Oblast significantly, but it is tantamount to the influence of catchment area, located in Poland. The relatively small size of the catchment and the high rate of runoff water cannot solve the problem of improving water quality in the coastal zone separately from the neighbors on the catchment—the border municipalities of Poland and Lithuania. Significant part of the catchment Vistula and the Curonian Lagoon are located here.

It should be noted that the presented results are preliminary and require further verification and correlation. To clarify the discharge is necessary to introduce the internal model coefficients, which are based on indicators of soil properties, the state of groundwater, as well as the necessary information on the reclamation area. In addition, it is desirable to perform simulation of water consumption with the use of other models Mike 11. Isochrones of the Vistula Lagoon catchment should be expanded over the whole catchment, and isochrones of Curonian Lagoon catchment should be allocated to the territory of the municipalities of Lithuania, which border with the Kaliningrad Oblast.

Acknowledgements

The work was partly supported by Grant No. 08-05-92421 of the Russian Foundation for Basic Research.

References

- Barinova, G. (2006) *Klimat. Kaliningradskaya oblast*. Kaliningrad: Yantarny Skaz (in Russian).
- Chubarenko, B. & Domnin, D. (2008) International and Inner Transboundary River Basins in the Kaliningrad Oblast, South-Eastern Baltic. In: *Integrated Water Management: Practical Experiences and Case Study*, 309–321, Springer.



- Domnin, D. & Chubarenko, B. (2007) *Atlas transgranichnyh rechnyh basseynov Kaliningradskoy oblasti*. Kaliningrad: Terra Baltica. (in Russian).
- Khublaryan, M., Kovalevskiy, V., Bolgov, M. (2005) Koncepciya upravleniya vodno-resursnymi sistemami na osnove sovmestnogo ispolzovaniya poverhnostnyh i podzemnyh vod. *Vodnye resursy* **32(5)**:617–624 (in Russian).
- MIKE 11 (2004) A Modelling System for Rivers and Channels. Reference Manual. DHI Software.
- Modelling the World of Water (2006) DHI Software.
- Water Code of Russian Federation from June 3, 2006. N 74-FZ. Was passing by State Duma 12.04.2006. Was approving by Upper chamber 26.04.2006 (in Russian).

Morphometric characteristics of the lagoons of the World Ocean

Anastasia Domnina

Abstract

Research of morphometric characteristics of the lagoons of the World Ocean was made. Measurements were carried out by satellite photographs LandSat7. Such parameters as alongshore and cross-shore lengths and square of lagoons were estimated.

Было проведено исследование морфометрических характеристик лагун мирового океана. Измерения были сделаны по космическим снимкам LandSat 7. Определялись такие параметры как протяженность лагуны вдоль и поперек береговой линии, а также площадь лагун.

Lagoons are shallow inland marine waters, usually oriented parallel to the coast, separated from the ocean by a barrier, and connected to the ocean by one or more restricted inlets (Phleger, 1969).

Morphometric characteristics of 175 lagoons all over the World Ocean were considered. Data was taken from satellite photographs of 2000–09 years. As the shape of lagoons varies significantly, and to unify the description of a lagoon morphometry, the principal “rectangle” shape was attributed to any real lagoon (Chubarenko, 2004). First, a characteristic alongshore size was estimated for a lagoon, than, a cross-shore size was selected to keep equivalence between both a real lagoon area and area of attributed rectangle (alongshore and cross-shore lagoon sizes). Lagoons with the square of 10 km² were not considered.

The greatest number of lagoons are found along the coastline of Eurasia and North America, less number of lagoons are along the Australian and South American coasts. The biggest lagoon in Australia has an area of 1,050 km², the biggest one in Eurasia, the Kara-Bogaz-Gol lagoon, has an area of 18,092 km². The biggest lagoon in North America has an area of 9,918 km².

There is an irregular distribution of lagoons along coasts of continents. Lagoons in Africa (Fig. 1), Australia and Eurasia are almost equally distrib-

Anastasia Domnina (✉)

P. P. Shirshov Institute of Oceanology RAS, Atlantic Branch, Kaliningrad, Russia
e-mail: annasta_sea@mail.ru

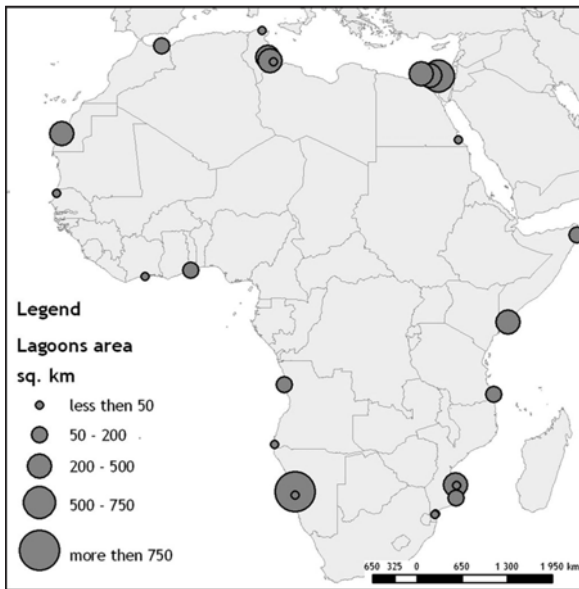


Fig. 1. Lagoons locations along the African coast ranked according to lagoon surface water area.

uted along a shore. Maximum number of lagoons is along the eastern coast of the North America, but lagoons are almost absent along western coast of the South America.

Alongshore size of lagoons is several times bigger than cross-shore one, the minimum alongshore/cross-shore ratio is for Eurasia and equals to 2.5. Average alongshore length of lagoons is 34.4 km, whereas average cross-shore one is 9 km. The biggest alongshore size is found for lagoon system Albemarle-Pamlico Sound (261 km). Kara-Bogaz-Gol has the biggest cross-shore length (108 km).

Lagoons in the Baltic Sea are located along the southern and western shores (Fig. 2). All lagoons, except, Puck Lagoon (Poland), are oblong to coastline. Average alongshore/cross-shore ratio is of 5.2 (Fig. 3). The Curonian lagoon is the longest and biggest lagoon in the Baltic. Also it is the closest lagoon of the Baltic Sea.

The work was partly supported by RFBR Grant 08-05-01023. Author thanks to Dmitry Domnin for his help in applications of the GIS tools.

References

- Chubarenko, B. V., Koutitonski, V. G., Neves, R., Umgiesser, G. (2004) Modelling concept (Chapter 6). In: Gonenc, I. E., Wolflin, J., eds. *Coastal Lagoons: Ecosystem Processes and Modelling for Sustainable Use and Developmemnts*, 231–306. Boca Raton, London, New York, Washington D.C.: CRC Press.
- Continent. Krugosvet—Online encyclopedia.
URL: http://www.krugosvet.ru/enc/Earth_sciences/geografiya/MATERIK.html
- Phleger, F.B. (1969) Some general features of coastal lagoons. In: Ayala-Castañeres, A., ed. *Lagunas Costeras, un Simposio*, 5–26. México D.F.: Universidad Nacional Autónoma de México.

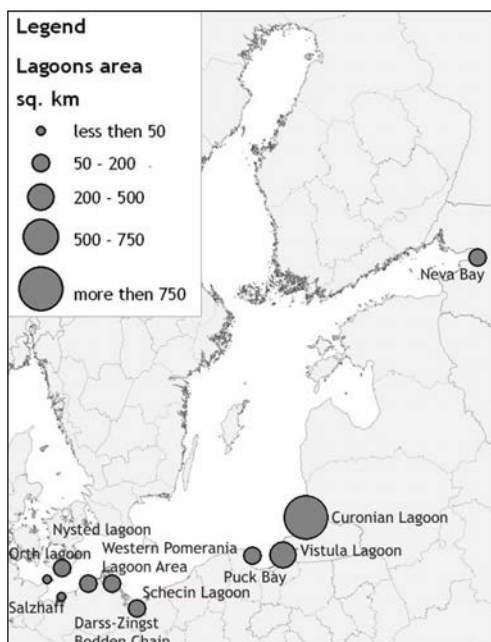


Fig. 2. Baltic Sea lagoons ranked according to lagoon surface water area.

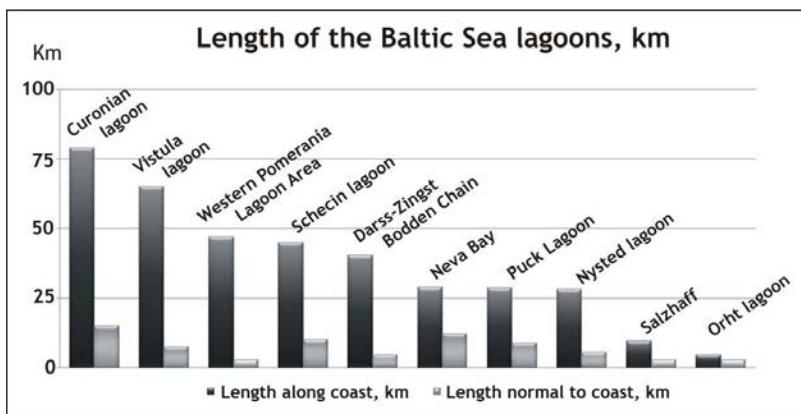


Fig. 3. Alongshore and cross-shore lengths of the Baltic Sea lagoons (km).

Hydrological regime as one of the factors that determine the phytoplankton productivity in the Volga Delta

Julia Gorbunova

Abstract

Volga River delta is one of the largest in the world. Hydrologic regime in the Volga River delta is one of the determinants of ecosystem functioning. At present the Volga River flow regime is characterized as regulated. Parameters of the hydrological regime to a large extent determine the productivity of phytoplankton in the delta. Usually phytoplankton productivity is high when river discharge is medium or temperately high and phytoplankton productivity is low when river discharge is low or extremely high.

Дельта реки Волги является одной из наиболее крупных в мире. Гидрологический режим в дельте Волги является одним из факторов, определяющих характер функционирования экосистем. В настоящее время режим стока Волги характеризуется как зарегулированный. Параметры гидрологического режима в большой степени определяют продуктивность фитопланктона дельты. Более высокая продуктивность фитопланктона приурочена, как правило, к средним по водности и умеренно многоводным годам, а более низкая — к маловодным и экстремально высоким по водному стоку годам.

Julia Gorbunova (✉)

P. P. Shirshov Institute of Oceanology RAS, Atlantic Branch, Kaliningrad, Russia
e-mail: julia_gorbunova@mail.ru

Estimation of water quality of Pregolia River

Alexandr Grizetskiy

Abstract

Study of hydrological peculiarities and quality of the Pregolia River water is actual for Kaliningrad Region for solving of ecological problems. Investigation of the surface layer of the Pregolia River by seasonal meteorological, hydrological measurements and hydrochemistry analysis is presented. These studies were made during expeditions of the Laboratory for Coastal System Study of the Atlantic Branch of P. P. Shirshov Institute of Oceanology in Spring 2007, 2008. The aim was to study geoeological peculiarities of Pregolia River from its source (beginning) to Kaliningrad.

Изучение гидрологических особенностей и качества воды реки Преголи очень актуально для Калининградской области и необходимо для решения многих экологических проблем. Представлены результаты метеорологических и гидрологических измерений, а также гидрохимических анализов проб воды поверхностного горизонта реки Преголи. Работы проводились в рамках экспедиций лаборатории прибрежных систем Атлантического отделения Института океанологии им. П. П. Ширшова РАН весной 2007 и 2008 г. с целью изучения геоэкологических особенностей р. Преголи от ее истока до г. Калининграда.

Alexandr Grizetskiy (✉)

P. P. Shirshov Institute of Oceanology RAS, Atlantic Branch, Kaliningrad, Russia
e-mail: minorinfo@mail.ru

Wind effected circulations and density flows in the Petrazovodsk Bay

Irina Ivanova, Boris Samolyubov

Abstract

The results presented in this report were obtained in periods of the wake water density stratification in September 2007 in Petrozavodsk Bay of the Onega Lake. It was shown that the interaction of the wind effected circulation with the density current is enhanced with growth of stability of the currents over the entire depth to the wind action. It was discovered that the near-bottom density current plays the main role in the suspended sediment transfer in the bay at the indicated conditions.

Результаты, представленные в данной работе, получены в период слабой плотностной стратификации вод в сентябре 2007 г. в Петрозаводской губе Онежского озера. Показано, что взаимодействие циркуляции, индуцированной ветром, с плотностным течением усиливается по всей глубине с ростом устойчивости течений к ветровому воздействию. Установлено, что плотностное течение играет основную роль в транспорте взвеси в заливе в указанных условиях.

1. Introduction

The interacting circulations and density currents propagated under the low-density water layers in the oceans, seas, lakes and reservoirs excite continuously increased scientific and practical interest. In spite of the sharp necessity of the similar systems of currents evolution prediction methods the mechanisms of many phenomena determining these flows propagation regularities are not discovered yet. Physical problems of these flows study are connected with the multifamily of these currents structures and energy-exchange types. The turbulent transfer and internal waves determine mass-exchange in the near-bottom boundary layers and in the mixing layers of currents. At the interaction of these exchange types the vortex-wave structures are formed in the current shear layers. This article includes the results of such system of currents natural investigations and simulation.

Irina Ivanova, Boris Samolyubov (✉)
M. V. Lomonosov Moscow State University, Moscow, Russia
e-mail: ivair@yandex.ru



2. Study area and methods

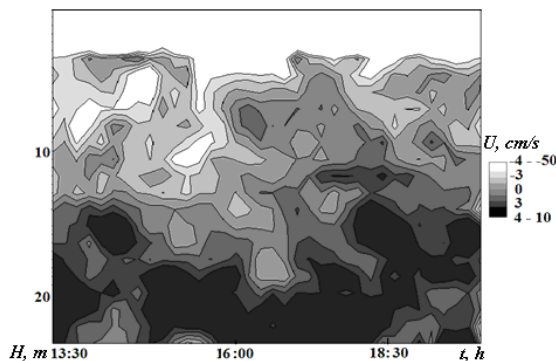
The results discussed below obtained in period of the wake density stratification in September 2007 in Petrozavodsk bay of Onega Lake. Hydrophysical measurements were performed by the expedition of M.V. Lomonosov Moscow State University from the board of the scientific Vessel “Ecolog” of Institute of Water Problems of the North, Karelian Research Center, Russian Academy of Sciences. The registrations at the temporal station were made every 10 min with vertical step 0.5 m by the Doppler Current Profiler RDCP600 (Aanderaa) in mode of autonomous bottom station. At the same time there were performed the measurements of the profiles of current velocity, temperature, conductivity and turbidity by the multiparameter platform RCM 9 LW (Aanderaa). In the course of plane survey through the 29 stations with utilizing RCM9, conductometer, oxymeter “Expert” and transmissiometer (MSU) there were obtained detail distributions of the parameters of currents and water composition. These investigations enable us to obtain the unique information about the development of the systems of stratified currents with the wind effected circulations, jets and density flows.

3. Results

In period of measurements the hydrodynamical conditions in the bay were stipulated by the wind effected current caused by south-east wind with velocity 7–12 m s⁻¹ directed toward the bay from open lake. The investigations were performed at the temporal station. During the data analysis there were revealed some peculiarities of the exchange in the discovered system of currents. This system included the wind effected and density flows (Fig. 1). In the current velocity field there were registered the drift flow up to the head of the bay and the compensating and near-bottom currents directed out of the bay (Fig. 1). The mean velocities were equal to 30 cm s⁻¹ и 3–10 cm s⁻¹ for the drift, compensating and density currents.

The oscillations of isotaches at the Fig. 1 correspond to the transformations of the current velocity field under the action of the internal waves with height up to 3 m and with period about 1 h. Such period is close to that of the peer seiche of the Petrozavodsk bay (Palshin, 1999, Filatov, 1983). The theoretical distribution of the wind effected current (Fig. 2a) was calculated by the numerical solution of the Reynolds equation for the gradient turbulent

Fig. 1. Current velocity versus depth and time at the station located at the central part of the Petrozavodsk Bay (19.09.2007).





current (Rukhovets et al., 2006, Boegman et al., 2008, Samolyubov et al., 2008). There was taken into account the influence of the exchanges of the stratification stability and of the turbulence scale vertical distribution on the profile of the exchange coefficient K_u .

The suspended sediments concentration profile $\partial S_{nm}(z)$ includes maxima in zones of the drift, compensating and density currents.

The picks of $\partial S_{nm}(z)$ in compensating current at the levels about $z=5-18$ m are related to the turbidity clouds migrating on the depth (Fig. 2b). The integral Richardson number for density current $Ri_u = g \cdot \Delta \rho \cdot z_u / \rho \bar{U}^2$ was equal 0.5–2 for the theoretical velocities of the current. The evaluations of Ri_u gave 0.2–1.5 by the measured velocities. Other Richardson numbers took place only at two cases: at $t=15:30$ when Ri_u fall up to 0.1 and at $t=19:00$ when Ri_u raised up to 14 in the stage of decay of the current by its detachment from the bottom (Fig. 1).

The distributions of the current velocity were measured in the interval from the height $z=1.5$ m up to the surface. At the layer $z < 1.5$ m the current velocity profiles were reconstructed by the model from (Samolyubov, 2007). By the verification of the model of the density current propagation there were performed the comparison of theoretical curve \bar{U}_{th} with the evaluations of the current velocity in approach of local quasi-stationarity and horizontal quasi-homogeneity of the current by the expression $\bar{U}_{sg}(t) = (2g\bar{\Delta\rho} \cdot z_u i_s / \rho C_D)^{1/2}$. Here g , $\bar{\Delta\rho}$, z_u , i_s and C_D specify correspondingly the gravity acceleration, the vertically averaged water density difference between the waters in the flow and above it, the height of the current, the bottom slope and the friction coefficient at the boundary flow-bottom. The height of the current z_u was determined with taking into account the proportionality of the entrainment function to the bottom slope.

The distribution of $\bar{U}_{th}(t)$ at Fig. 3 was obtained by the one-dimensional dynamic equation of the current. In contrast to the previous models there were taken into account not only the influence of the tangential component of the gravity force $F = \bar{\Delta\rho} g z_u i_s$, of the baroclinic pressure gradient $(\partial_x p)_\rho = \partial_x (\bar{\Delta\rho} g z_u^2 / 2)$ and of the force of the turbulent stress $F_D = \rho \cdot C_D \cdot \bar{U}^2 / 2$, but also

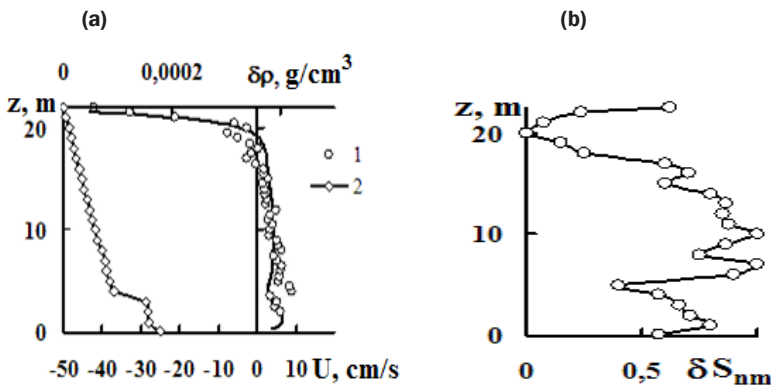


Fig. 2. (a) profiles of current velocity U and water density change $\delta\rho$ against the depth; (b) depth profile of the change of the suspended sediments concentration δS_{nm} normalized relatively to their maximal at the water column.

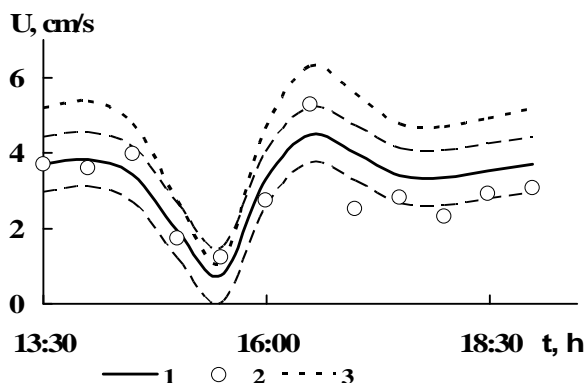


Fig. 3. The time variations of the velocity U of the density current: (1) the theoretical vertically averaged velocity by the model of horizontally heterogeneous current U_{ht} , (2) the velocity U_{sg} determined in text, and (3) the maximum velocity at the each profile. The dashed line corresponds to the boundaries of standard deviation.

the action of the pressure gradient due to the wind effected flow on the near-bottom current $(\partial_x p)_\zeta = 0,4g\rho(z_u^2/H)\partial_x \zeta$. The contributions of the forces moving the current into their sum were 20, 64 и 17 percent, correspondingly, for F_g , $(\partial_x p)_\rho$ and $(\partial_x p)_\zeta$.

The interaction of the near-bottom density current and compensating flow related to the wind effected circulation was determined by the expression $\bar{U}/\bar{U}_{com} \cong 0,63(\bar{U}/\bar{U}_{com})_0 1n[0,14 \cdot R_{iw}^*(1+2\bar{U}_{sg}/(\bar{U}_{sg})_0)]$. In accordance with this expression the relation of the vertically averaged velocities of these currents increases with the growth of the hydrodynamic stability of the currents over the entire depth to the wind action. This increase is also connected with the mentioned above parameters $\bar{\Delta\rho}$ and z_u determining value of \bar{U}_{sg} .

Here $R_{iw}^* = g\Delta\rho_H H/\rho U_{tw}^2$ is the integral Richardson number characterizing the hydrodynamic stability of the currents over the entire depth to the wind action, $\Delta\rho_H$ is the density difference of waters near the surface and near the bottom, $U_{tw} = (\tau_w/\rho)^{1/2}$ is shear velocity at boundary water-air, τ_w —the wind friction stress at the water surface (Michioku, 1994).

The distribution of the vertically average suspended sediments concentration in the near-bottom current $\bar{S}(t)$ in time is characterized at this station by the decay in the period of the wind amplification. It is stipulated by the suspended particles entrainment in the compensating current that is related to the wind effected circulation. The shape of a curve $\bar{S}(t)$ is in accordance with the theoretical distribution obtained by the model from (Michioku, 1994).

4. Conclusions

The near-bottom density current amplified by the wind effected circulation played the main role in the suspended sediment transfer in the bay at the indicated conditions.

The interaction of the wind effected circulation with the density current is enhanced with growth of stability of the currents over the entire depth to the wind action.



The turbidity clouds migrating under the action of internal waves were discovered at the middle depths and at the near-surface layer.

The mathematical models of the wind effected stratified current and of the near-bottom density current were modified and verified with taking into account the interaction of these currents and influence of the vortexes originated in region of current velocity direction change on the opposite one.

Acknowledgements

This work was supported by the Russian Foundation for Basic Research (grant No. 08-05-00574).

References

- Boegman, L., Loewen, M. R., Hamblin, P. F. (2008). Vertical mixing and weak stratification over zebra mussel colonies in western Lake Erie. *J. Limnol. and Oceanogr.* **53**(3):1093–1110.
- Filatov, N. N. (1983) *Dynamics of lakes*. Leningrad: Hydrometizdat.
- Michioku, K., Tsujimoto, G., Miyamoto, H. (1994) Wind-Driven Density Currents in a Semi-Enclosed Basin. In: *Proc. Chine-Japan Bilateral Simp. on Fluid Mech. and Manag. Tools for Environ.*, Beijing, 11, 19, 96–105.
- Palshin, N. I. (1999) *Thermal and hydrodynamic processes in lakes during the freezing-over*. Petrozavodsk: NWPI KarRC RAS.
- Rukhovets, L. A., Astrakhantsev, G. P., Mal'gin, A. N. et al. (2006) Modeling Climatic Circulation of Onega Lake. *Vodnye Resursy* **33**(5):511–522.
- Samolyubov, B. I. (2007) *Density currents and diffusion of admixtures*. Moscow: LKI, URSS.
- Samolyubov, B. I., Ivanova, I. N., Budnikov, A. A. (2008) The action of the circulation current induced by the wind and density flow on the suspended sediment transport. *Physical problems of ecology* **15**:335–343.

Project VISLA; coupling environmental and remote sensing research for better understanding of coastal waters behavior and its sustainable management

Marek Kruk, Janusz Kosakowski, Agata Rychter, Marek Mróz

Abstract

The project aims at the implementation of the innovative internet service for the management of environmental resources and the space of Vistula Lagoon. Prognostic of the status of this area by the use of marine research, satellite remote sensing and mathematical modelling should be an obligatory requirement for carrying out of any investment or revalorization activity in such a complex ecosystem. The detailed objectives of the second project are as follows: (i) to use and improve the remote sensing technique for extraction of spatial variability of physical, chemical and biological water parameters, (ii) to adopt the environmental and remote sensing research results into input-output of simulation model, (iii) to implement the internet service for diagnostic and prediction of environmental changes in Vistula Lagoon as useful management tool.

Целью проекта является внедрение инновационных интернет средств для управления природными ресурсами и пространством Вислинского залива. Прогноз состояния среды с использованием морских исследований, спутниковых методов и математического моделирования должен быть обязательным требованием при реализации инвестиций или стоимостной оценке компонент этой комплексной системы. Конкретными задачами проекта являются: (i) использовать и улучшить методы спутникового дистанционного зондирования для выделения пространственных вариаций физических, химических и биологических параметров водной среды, (ii) адаптировать результаты спутникового зондирования в качестве входных-выходных данных численной модели, (iii) внедрить интернет средства как полезный инструмент управления для диагноза и прогноза изменений в Вислинском заливе.

Marek Kruk, Marek Mróz (✉)
University of Warmia and Mazury in Olsztyn, Poland
e-mail: mkruk@uwm.edu.pl, marek.mroz@uwm.edu.pl
Janusz Kosakowski, Agata Rychter (✉)
State Higher School for Vocational Education in Elbląg, Poland
e-mail: jkosak@uwm.edu.pl, agata.rychter@pwsz.elblag.pl



1. Introduction

The article aims on presentation the project “System of the environmental and spatial information as the background for the sustainable management of the Vistula Lagoon ecosystem (VISLA)” funded by Polish-Norwegian Reaserch Fund. The beneficiary and coordinator of the project is University of Warmia and Mazury in Olsztyn, Poland, which have a following partners: Norwegian Institute for Water Research, Oslo–Bergen, Norway and The State Higher School of Vocational Education in Elbląg, Poland. The duration of the project is from 07/2008 to 12/2011. The most important part of this complex and multidisciplinary project in the stage of its running is the management system. The important aim of the paper is to demonstrate the usefulness of the information system approach for the environmental project. The most important feature of such an approach is the treatment of the project as composition of the elements, able to describe using abstractive formal measures. The structural analysis method and UML language were used (Penker & Eriksson, 2000).

2. Description of the project

The overall aim of the project is to improve the control, diagnosis and prediction of environmental status and changes of coastal, shallow marine waters, i.e. Vistula Lagoon (Baltic Sea, N Poland). The project proposes a new and complex tool for the sustainable management of this water body, which faces several investment activities. The project is focused also on establishing fundamental frames for improving water quality and revitalization of wildlife in the Vistula Lagoon. These objectives are concordant with the requirements of Water Framework Directive and NATURA 2000. The project is planned for the period from May 2008 till December 2010.

Presented project aims at the implementation of the innovative internet service for the management of environmental resources and the space of Vistula Lagoon. Precise and repetitive diagnostic of the status of this area by the use of marine research, satellite remote sensing and mathematical modeling should be an obligatory requirement for carrying out of any investment or revalorization activity in such a complex ecosystem.

The major scientific aim of the project is the construction of a mathematical model as formulas allowing the prediction of the environmental consequences of various human interventions in the spatial system of the Vistula Lagoon and also more long-term climate change scenarios. The fundamental tool applied to create a spatial model will be a satellite remote sensing technique combined with GEMSS modeling of hydrodynamic and processes control water quality (Edinger, 2001). The connection of the mathematical modeling using biogeochemical and hydrobiological data with satellite imaging is the most important innovative value of the project. It is widely accepted in applied environmental sciences that spatial modeling of ecosystem modifications is the most effective approach conducted to elaboration of ecological engineering effective tools for the management of natural resources in the Global Change conditions.

The objectives of the project, which are concordant with the main tasks are listed here:



- (1) To develop an ecological research and GIS documentation directed on the better understanding of ecosystem processes as causes of high primary productivity and biodiversity loss in Vistula Lagoon.
- (2) To use and improve the remote sensing technique for extraction of spatial variability of physical, chemical and biological water parameters.
- (3) To adopt the environmental and remote sensing research results into input-output simulation model.
- (4) To implement the internet service for diagnostic and prediction of environmental changes in Vistula Lagoon as useful management tool.

The target group consists of the units of local government of communes situated along Vistula Lagoon, management staff of civil shipping and ports, services of environmental protection, managers of treatment stations in the surrounding towns and villages, fishery enterprises, managers of nature preserve areas, high schools.

3. Management system of the project

Project VISLA consists of three subsequent phases. In the first analysis stage, the collection of data was conducted, namely *in situ* water quality data, measurements of water optical features, GIS frames were established, hydro- and meteorological data from COAMPS model and satellite images from mainly CHRIS-PROBA and MERIS missions. In the second phase the synthesis of data was planned, and it is realized using GEMSS modeling, GeoDataBase and WebMapService, all located in the project GeoServer (Fig. 1).

The functional mock-up of the project VISLA include five boxes: GIS Area, Remote Sensing (RS) Area, Eco Area and two Internet Areas, GeoServer for data collection and processing and Service area with portal and map service for external users. These areas are connected each other by several linkages constitutes management flow system of the project (Fig. 2).

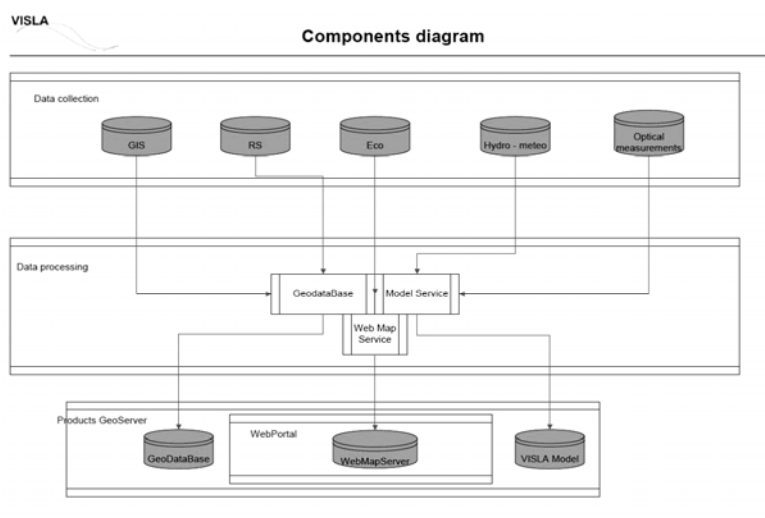


Fig. 1. Three phases of the project VISLA data collection, data processing and GeoServer products.



VISLA project – funkcjonalny mock - up

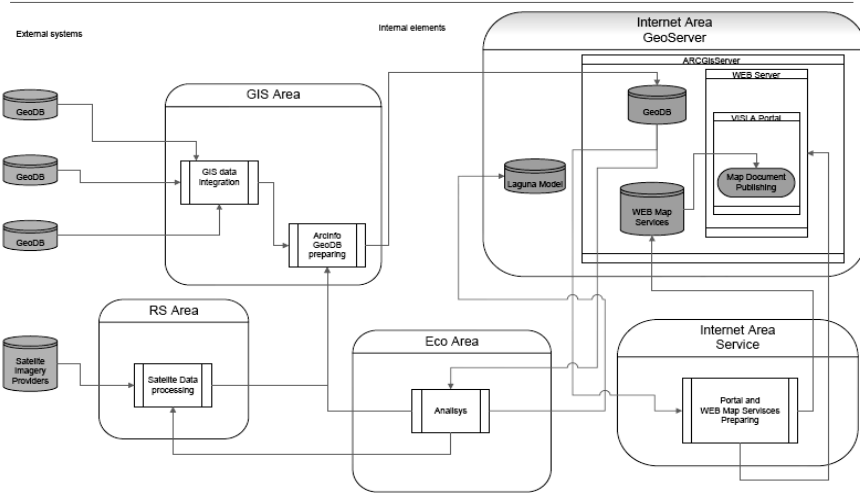


Fig. 2. Functional flow system of the project VISLA.

Every area included in the functional mock-up system of the project covered its internal flow diagram and functional connections with external areas. It can be seen for example in Eco area, in which components constitutes biological, hydro-chemical, hydro-meteorological data collection and optical measurements. These elements are directly related with hydrodynamic and water quality GEMSS modeling and they all feed GeoServer and its modeling and data base functions and services. Eco Area participate also in remote sensing data processing directed into production of satellite images of water parameters (Fig. 3).

VISLA Project – Eco Area mock-up

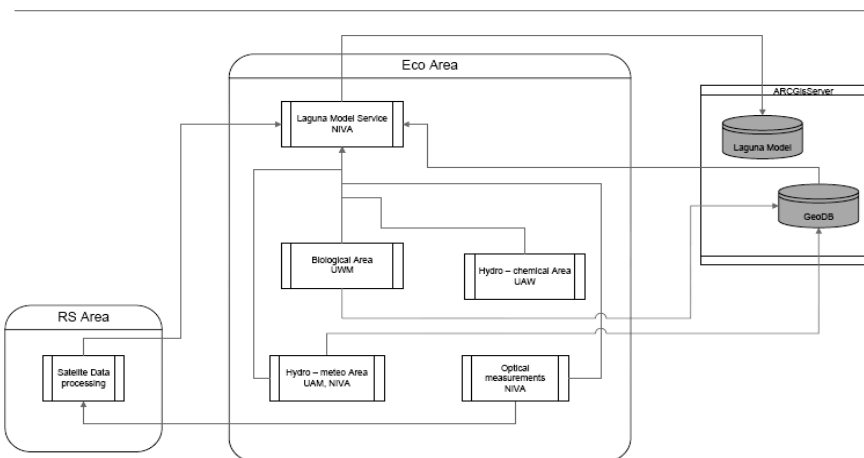


Fig. 3. The example of the Area flow system: Eco Area within internal boxes and external linkages.



4. Conclusions

It should be concluded that structural analysis method and UML language used in the project VISLA as the fundamental management tool have very fruitful consequences in organization of activities and achievement of planned objectives of the project.

References

- Edinger, J. E., ed. (2001) *Waterbody Hydrodynamic and Water Quality Modeling: An Introductory Workbook on Three Dimensional Water Body Hydrodynamics and Water Quality Modeling including Modeling Software*. Reston: ASCE Press.
- Penker, M. & Eriksson, H. E. (2000) *Business Modeling with UML*. John Wiley & Sons.

On the quantitative evaluation of solid eolian material, entering the Curonian and the Vistula Lagoons (South-East Baltic) in a winter period

Victoria Kurchenko, Vladimir Chechko

Abstract

The results of winter study of eolian matter coming into the coastal zone of south-eastern Baltic Sea during winter period are presented. The quantitative composition of aerosol particulate matter, accumulating in snow cover was studied. It is found out that, on the average of 2 years, 2.2 mg/m² a day of solid eolian matter arrives from the atmosphere into the coastal zone during the winter period.

Представлены результаты зимних исследований эолового материала, поступающего в береговую зону Юго-Восточной Балтики в зимний период. Изучался количественный состав твердых аэрозольных частиц, накапливающихся в снежном покрове. Выяснено, что в береговую зону в зимний период поступает из атмосферы (в среднем за 2 года) 2,2 мг/м²/сутки твердого эолового материала.

A snow cover is an effective trap, capable of accumulating and keeping of particles deposited from the atmosphere. A study of the snow cover gives reliable quantitative and qualitative characteristics of eolian matter arriving from the atmosphere. Snow samples have been collected from the surface of ice in the Vistula and Curonian lagoons in the end of winter 2009 and 2010. The snow was sampled from a platform 1×1 m by a plastic scoop into clean polyethylene packages and delivered to the laboratory. In the laboratory, the snow was melted at a room temperature, and the water obtained was filtered through membrane filters with diameter of a time 0.45 microns. On the average, for the winter period of 2009, 1.6 mg on 1 m² of eolian material per day and 2.63 mg on 1 m² of eolian material per day was besieged from the atmosphere onto the water areas of the Vistula Lagoon and Curonian Lagoon, respectively. In 2010 these figures have made 1.9 mg/m² per day for the Vistula Lagoon, and 2.6 mg/m² per day for the Curonian Lagoon.

Victoria Kurchenko, Vladimir Chechko (✉)
P.P. Shirshov Institute of Oceanology RAS, Atlantic Branch, Kaliningrad, Russia
e-mail: piwis@mail.ru

Analysis of wind conditions in the Neva Bay

Dmitry Kurennoy

Abstract

Analysis of the distributions of wind speeds and directions in the Neva Bay has been conducted on the basis of the data obtained from the observation sites for 2004–09. Average and extreme seasonal values were estimated. The durations of the storms were determined. In general, wind climate may be characterized as calm, but sometimes wind speed may reach >25 m/s. Strong storms may occur in the autumn-winter period. Most of the storms are induced by the western winds. Results of this study may be used for the modeling of a wave fields in the Neva Bay within typical and extreme meteorological conditions.

По данным с гидрометеорологических станций проведен анализ скорости и направления ветра в Невской губе за период с 2004 по 2009 гг. Оценены среднесезонные и экстремальные значения. Определены продолжительности штормов, которые могут достигать нескольких суток. Ветровой климат спокойный и носит сезонный характер, максимумы скорости ветра наблюдаются в осенне-зимний период и могут превышать 25 м/с. Большинство штормов порождаются ветрами западных румбов. Результаты могут быть использованы как исходные данные при моделировании волновых полей в Невской губе при типичных и экстремальных метеорологических условиях.

1. Introduction

Coastal erosion is already a widespread and serious problem in the Baltic Sea region. Water impact on the coastal zone has been observed in many sections of the eastern Gulf of Finland for a long time (Orviku et al., 2003). The high rate of coastal erosion results from the specific features of this water area: morphology, shallowness and local wave field (Ryabchuk et al., 2009). The most vulnerable are areas that may be affected by both direct storm-induced surge and long, basin-scale waves (e.g., seiches) reinforced by other factors. A classical example of that situation is the eastern end of the Gulf of Finland, Baltic Sea. There are several factors that may cause long waves in

Dmitry Kurennoy (✉)

A. P. Karpinsky Russian Geological Research Institute, Russia

e-mail: D.Kurennoy@gmail.com



the joint basin of the Baltics and the Gulf of Finland, such as, cyclones the prevalence of westerly winds, which may cause a “slow” Kelvin waves that move towards Neva Bight. Such long waves meet the voluminous, oppositely directed Neva River flow in the St. Petersburg area. The water level rise is further amplified by the joint influence of the shallowness of Neva Bight and the narrowing of the bight near the delta of the Neva River. The long waves approaching the mouth of the Gulf of Finland increase in height by 40–50 percent propagating across this gulf in the absence of wind (Averkiev & Klevanny, 2007). During the windstorm *Gudrun* (January 2005) an early forecast for the maximum surge height in St. Petersburg was 3.7 m, but owing to a more favourable trajectory and speed of the cyclone, the water level reached only 2.39 m (Averkiev & Klevanny, 2007). While the pressure change resulted in the sea level increase for approximately 0.7 m, the additional increase was caused by the combination of wind surge and long wave. Interestingly, this event almost did not cause high rates of coastal erosion in the Eastern Gulf of Finland (Ryabchuk et al., 2009).

A high water level alone is dangerous only when it exceeds a certain threshold, whereas a combination of unusually high water levels and rough seas presents acute danger to depositional coasts (Orviku et al., 2003). However, relatively moderate surges combined with high waves may cause a large impact on coastal processes. Even the floods that did not exceed 1.9–2.2 m in the vicinity of St. Petersburg accompanied by strong wind waves caused extensive coastal erosion and sediment resuspension processes in many coastal sections. Sequences of such events are particularly dangerous for the coastal zone, as they do not allow the recovery of beaches and may lead to destruction of buildings at the coast and to unrecoverable dune erosion which are observed in the eastern part of Gulf of Finland (Ryabchuk et al., 2009).

Knowledge of wave fields is important for the development and construction in the coastal zone. However, wave measurements in the Eastern Gulf of Finland had not been conducted regularly. Therefore, there is almost no information about wave fields in this area, particularly in the Neva Bay.

Detailed measurements of wind parameters in several sites around the bay could help to estimate the local wind wave fields. This information can be used for the detection of typical wind conditions within different seasons and to estimate duration of the strong storm events.

The main goal of this study is to prepare data for the Neva Bay for the following implementation in the SWAN wave model developed at the Delft University of Technology. Results may be used in the comparison of wind wave fields during typical and extreme weather conditions and, combined with a spatial distribution of bottom sediments to complete estimation of sediment transportation due to wind waves in the bay.

2. Study area

The Neva Bay is the shallowest water area located in the eastern end of the Gulf of Finland (Fig. 1). It is 21×15 km stretched from west to east. The average depth in the bay is around 3.6 m. The maximum depths of 5–6 m are observed at the central western part of the bay. There are few underwater sand-mining careers with a depth of around 10–12 m.



Neva Bay is separated from the Gulf of Finland by Kotlin Island and a Flood Protection Dam which was constructed in 1979–2008. The Dam is 25.4 km long and includes six slice gates and two navigation passages which do not allow strong storm waves from the Gulf of Finland to enter the bay. Therefore, Neva Bay is able to be considered as a lagoon with a local wave field.

Moreover, this area has been an extensive constructing site for the several last years. The largest in Europe Passenger Terminal has been constructing at the eastern end of the bay. With the shallowness of the bay, some signs of erosion of the artificial areas were observed after strong storms. The fairways located in the bay need to be served almost every year owing to sediment accumulation. It shows the importance of the profound study of the local wind wave climate in the bay.

3. Data and processing

Wind speed and direction are recorded by means of an anemohumbometer (M-63) using a traditional scheme which gives the wind direction with a resolution of 10° and averages the wind speed over a 10-min time interval with a resolution of 1 m/s. The averaging time of an estimate of the wind direction is 2-min within each 3-h period (Keevallik et al., 2007). The device fixes gusts (maximum wind speed) during each observation, but it is skipped in this study due to a lack of this information into the data.

Data obtained during 2004–09 at three observation stations located around the Gulf of Finland and Neva Bay were selected for the present analysis. Ozerki site is the westernmost meteorological station located at the northern coast of the Gulf of Finland. This site is open to the dominating wind directions and reflects the wind properties of incoming marine winds. The mean wind speed is around 3 m/s within the all data set—the highest value for all

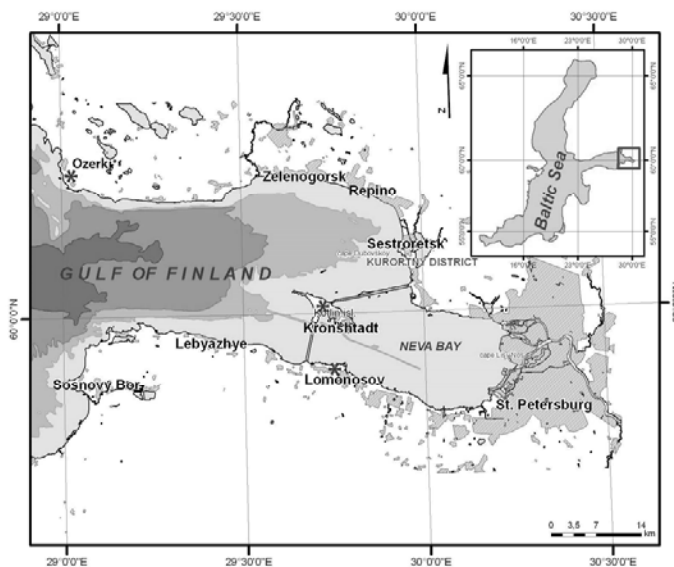


Fig. 1. The Neva Bay and the locations of wind measurement sites (stars).



three sites. Kronshtadt site is situated in Kotlin Island in the westernmost centre of the Neva Bay. This site represents the wind properties at the entrance to the bay. Mean wind speed here is also about 3 m/s. Lomonosov observation site is located at the southern coast of the gulf at south-west edge of the Neva Bay. Mean wind speed at this site is smaller than at Ozerki and is about 2.4 m/s. Data from the last two sites show that wind speed does not decrease significantly during propagation along the Gulf of Finland to the Neva Bay. Data from the observation sites located in St. Petersburg were not considered due to distortion of wind properties caused by influence of buildings and constructions in the city.

Monthly average wind speed for the different observation sites are shown in Fig. 2. It reveals that in general a calm season starts in February and lasts till August. The highest wind speeds are observed from September till January at all observation sites. Wind speed at Lomonosov station is significantly smaller than at Ozerki and Kronshtadt stations, which may be explained by the site location. During calm (spring) season, Kronshtadt and Lomonosov stations observe a higher wind speeds, whereas Ozerki completely dominates in autumn.

Analysis confirms that an average wind speeds in the Eastern Gulf of Finland and the Neva Bay are not large, however storm surges and wind waves are able to erode the coasts in this area. The most devastated impact to the coast happened during the autumn-winter 2006–07 (Ryabchuk et al., 2009). Fig. 3 shows the wind speed in January 2007 at Kronshtadt observation site. It shows that there were 3 situations-when wind speed exceeded 5 m/s. The events on January 10 and 17 developed gradually manner and ended rapidly. Therefore the storm attenuation stage was very short which usually results in high damage for a coastal zone. This situation caused one of the highest rate of coastal erosion ever fixed in the study area (Ryabchuk et al., 2009). Frequency distribution for different wind speeds in January 2007 is presented in Fig. 4.

The results show that in general wind direction varies insignificantly and most of the storms come from SW–W–NW. The maximum constant wind duration may reach approximately 4–5 days.

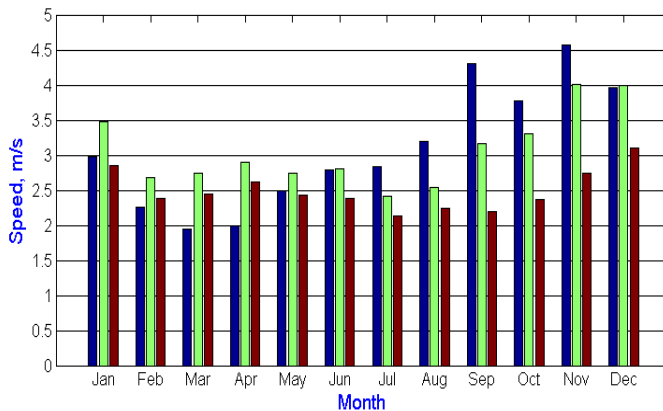


Fig. 2. Monthly average wind speed respectively at the Ozerki (first), Kronshtadt (second), Lomonosov (third).

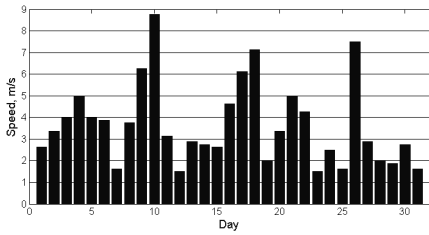


Fig. 3. Wind speed, Kronstadt, January 2007.

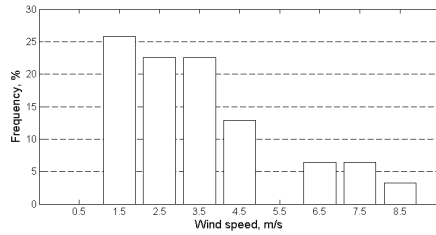


Fig. 4. Frequency of occurrence of different wind speed in January 2007 (Kronstadt).

4. Conclusions

This study determines wind properties in the Neva Bay area based on data obtained from the local observation sites. On average, the wind climate in the Neva Bay is mild. Typical and extreme properties were detected. The dominant storm winds come from the West, the highest wind speed reached 26 m/s for several times. The longest intervals of constant wind directions were determined (approximately 5 days). Obtained information can be used as an initial data for the further investigations of wind wave fields using the SWAN model for the Neva Bay.

Acknowledgements

Present study was supported by RFBR (grant No. 10-05-90700). Great thanks Dr. Darya Ryabchuk for useful and friendly comments and Dr. A. Kolesov who provided wind data for the analysis.

References

- Averkiev, A. & Klevanny, K. (2007) Determining cyclone trajectories and velocities leading to extreme sea level rises in the Gulf of Finland. *Russian Meteorology and Hydrology* **32**(8):514–519.
- Keevallik, S., Soomere, T., Pärj, R., Žukova, V. (2007) *Outlook for wind measurement at Estonian automatic weather stations.*
- Orviku, K., Jaagus, J., Kont, A. et al. R. (2003) Increasing activity of coastal processes associated with climate change in Estonia. *Journal of Coastal Research* **19**(2): 364–375.
- Soomere, T., Behrens, A., Tuomi, L., Nielsen, J. W. (2008) Wave conditions in the Baltic Proper and in the Gulf of Finland during windstorm Gudrun. *Natural Hazards and Earth System Sciences* **8**:37–46.
- Ryabchuk, D., Spiridonov, M., Kurennoy, D. et al. (2007) Lithodynamics of the northern coastal zone of eastern Gulf of Finland. In: *Materials of the XVII International Scientific Conference on Marine Geology*, November 12–16, Geology of Seas and Oceans 4, 167–169 (in Russian, English Abstract).
- Ryabchuk, D., Sukhacheva, L., Spiridonov, M. et al. (2009) Coastal processes in the Eastern Gulf of Finland—possible driving forces and the connection with near-shore development. *Estonian Journal of Engineering* **15**(3):151–167.

Optimal time-interval for ones-a-day observation of air temperature at the mouth area of the Pregolia River (South-East Baltic)

Lidia Leitsina, Boris Chubarenko

Abstract

The data set of measurements of air temperature (every half an hour) in the mouth of the Pregolia River (South-East Baltic) for the period from November 2007 to January 2010 (27 months) was analyzed. The data registered by an automatic meteorological station of the Museum Ship “Vityaz”. The purpose of this study was to identify the time-interval within a day, when the observed temperature as close to the average air temperature. Both observations in the interval 10:30–11:30 a.m. (for the months corresponding to winter time) and 10:00–11:00 a.m. (for the months corresponding to summer time in Kaliningrad) allow to achieve highest reliability of estimation of the mean temperature by individual observation.

Проанализированы массивы данных измерений температуры воздуха (каждые полчаса) в устьевой части р. Преголи (Юго-Восточная Балтика) за период времени с ноября 2007 по январь 2010 (27 месяцев), зарегистрированных автоматической метеостанцией музейного судна «Витязь». Целью исследования являлось выявление такого интервала времени в сутках, в который наблюдаемая температура максимально близка к среднесуточной температуре воздуха. Наибольшая достоверность оценки среднесуточных температур по единичным наблюдениям достигается при проведении этих наблюдений в интервале 10:30–11:30 для месяцев, соответствующих зимнему калининградскому времени, и 10:00–11:00 для месяцев, соответствующих летнему калининградскому времени.

The air temperature data of automatic meteorological station of the Museum Ship “Vityaz” (every half an hour) for the period from November 2007 to January 2010 (27 months) was analyzed (Vityaz, 2009, 2010). MS “Vityaz” is located in Kaliningrad, 7 km upstream the mouth of the Pregolia River entering the Vistula Lagoon (South-East Baltic).

Lidia Leitsina, Boris Chubarenko (✉)

P. P. Shirshov Institute of Oceanology RAS, Atlantic Branch, Kaliningrad, Russia
e-mail: lvleitsina@mail.ru



The initial matrix of measured temperature deviation from the daily average (48 measurements per day, 822 days) was compiled for analysis. Elements in the matrix are the absolute differences between the actual temperature at time of measurements and the mean value for the current day:

$$\delta_{ij} = |T_{ij} - \bar{T}_j|,$$

where T_{ij} —the air temperature in the i -th moment ($i=1\div 48$) of measurement and the j -th day ($j=1\div 822$), \bar{T}_j —the average temperature for j -th day.

To estimate the time interval within a day-time when deviation of daily average temperature from the measured temperature is minimal (Fig. 1), deviations for the fixed moment of measurements was averaged through all days of a period November 2007 to January 2010, i.e. matrix δ_{ij} was converted to vector Δ_i ($i=1\div 48$). Months relating to winter time (November–March) and to summer time (April–October) are considered separately (Fig. 2).

In the months corresponding to the local winter time the deviation ranged between 0.4 and 0.8 °C with local minimum at the period 10:30–11:30 a.m. (Fig. 2a). Deviations during summer time are much higher, from 0.6 up to 1.9 °C. There are two well pronounced minimums—at the periods of 10:00–11:00 a.m. and 09:30–11:00 p.m.

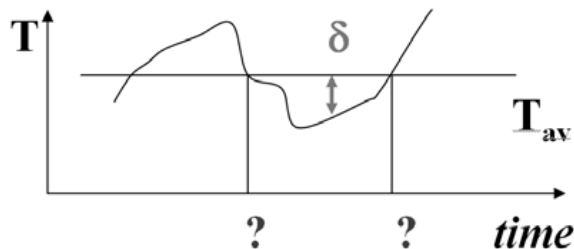
Nowadays man-made instrumental control measurements are conducted once a day at the MS “Vitiaz” at the time of 9:00 GMT. It gives 11:00 a.m. local time during November–March, the winter time, and 12:00 a.m. local time during April–October, summer time.

Due to natural daily variations of air temperature, there are two possible time intervals when real temperature “crosses” the level of its daily average value (Fig. 1). It usually happens before noon and before midnight.

The deviation between once-a-day measured air temperature and its daily average value very much depends on season, namely, on daily amplitude of temperature variations. The deviations in winter time are much less then ones for the summer time.

The time intervals, when deviations between once-a-day measured air temperature and its daily average value are minimum, could be calculated for each month or week, But, from practical points of view, it is recommended to make once-a-day measurements at 11:00 a.m., at the winter time, and 10:30 a.m., at the summer time. This recommendation is valid exactly for the point of measurements at the mouth of the Pregolia River. For any other locations, considerably remote from this point, an optimal time interval could be slightly different.

Fig. 1. What time during the day is the most favorable to measure air temperature to obtain the temperature value more close to the daily averaged temperature?



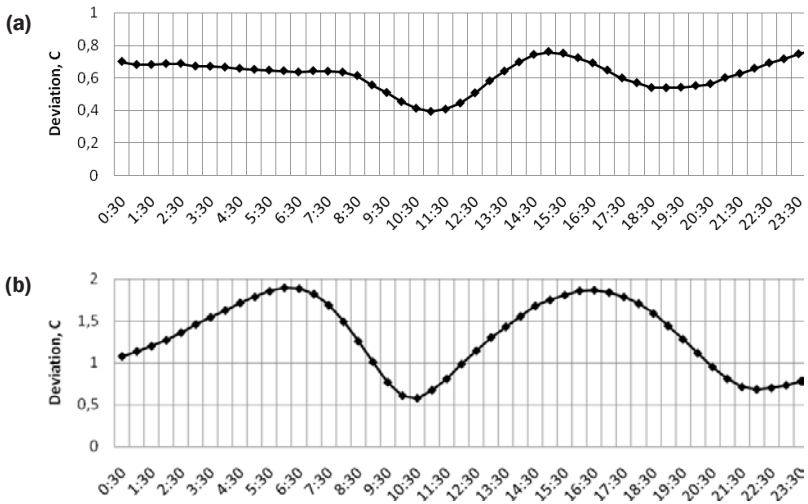


Fig. 2. The deviation of the measured temperature from the daily average for each period of measurement averaged over the months of winter (a) and summer (b) time for the interval of November 2007–January 2010. Automatic station at the Museum Ship “Vityaz”, Kaliningrad. The Pregolia River mouth, South-East Baltic.

References

- Vityaz'2008 (2009) *Hydro-meteorological observations*. Atlantic Branch of the Shirshov Institute of Oceanology of the Russian Academy of Sciences. Museum of World Ocean.
- Vityaz'2009 (2010) *Hydro-meteorological observations*. Atlantic Branch of the Shirshov Institute of Oceanology of the Russian Academy of Sciences. Museum of World Ocean.

Modeling of suspended matter transport in the Neva Bay and the Eastern part of the Gulf of Finland

**Mikhail Molchanov, Tatjana Eremina,
Ivan Neelov**

Abstract

The aim of research is to study of the suspended matter spreading in the shallow estuary using mathematical modeling. For carrying out of calculations was used high resolution 3D hydrodynamic model, developed by RSHU (Neelov et al., 2003). Calculation area of the model includes the Neva Bay and the Eastern part of the Gulf of Finland. The model has spatial and vertical resolution of 250 and 2 m accordingly. The substances have been conditionally divided into three fractions with the different gravitation speed. The period of May–September 2007 was chosen as calculation period because the hydrotechnical works in the Neva Bay was carried out at that time. The comparison of modeling results with the satellite images and field data gives a good agreement of the suspended matter fields in the investigated area.

Целью исследования является изучение распространения взвешенных веществ в мелководном эстуарии на основе математического моделирования. Для проведения расчетов была использована 3-мерная гидродинамическая модель высокого разрешения, разработанная в РГГМУ (Neelov и др., 2003). Расчетная область модели охватывает Невскую губу и восточную часть Финского залива с шагом по пространству 250 м и вертикальным разрешением 2 м. Моделирование проводилось для трех фракций взвеси, имеющих различные скорости оседания. Расчеты проводились с мая по сентябрь 2007 г., в период интенсивных гидротехнических работ в Невской губе. Результаты моделирования верифицировались с использованием спутниковых снимков и экспедиционных измерений. Сравнение результатов моделирования со спутниковыми снимками и данными наблюдений показало их хорошее согласование.

Mikhail Molchanov, Tatjana Eremina, Ivan Neelov (✉)
Russian State Hydrometeorological University, St.-Petersburg, Russia
e-mail: mol4anoff@gmail.com



1. Introduction

Since mid-1960s the Neva Bay and the Eastern part of the Gulf of Finland have been under continuous anthropogenic impact due to active hydrotechnical works carried out in the Neva Bay, such as: land build-up of the western territories of Vassilievsky and Dekabristov islands, bottom dredging, construction of the Flood Protection Barrier (FPB), dumping.

Presently, starting from summer 2006 the build-up of a territory near Vassilievsky Island has been one of the most urgent problems affecting the investigated water ecosystem.

In summer 2007 a catastrophic situation occurred behind the dam in the Neva Bay and the Eastern Gulf of Finland due to pollution and the increase of water turbidity. Active dredging, land build-up and ground transfer to make new territories in the area of Vassilievsky Island have been carried out in the Neva Bay in front of Vassilievsky Island near the Lahta settlement. At the same time there was a high bottom dredging activity in the navigational channels near Lomonosov and Kronshtadt. There was a large-scale extraction of sand from the bottom and its loading on barges behind Kronshtadt on the Kronshtadt road near the London shoal. These works resulted in water turbidity in the Neva Bay to reach its critical values. For many decades all possible suspended matter and sediments carried by the Neva River have been settling down here. The works on bottom ground transfer caused high amounts of silt, sediments and suspended matter to be lifted (Rumyantsev & Drabkova, 1999).

Determination of the range of suspended matter distribution and time-space variability of suspended matter content in water and areas of matter sedimentation is possible only on the basis of methods of mathematical modeling.

Modeling of suspended matter transfer and distribution in the Neva Bay and the Eastern part of the Gulf of Finland was carried out by several researchers (Rukhovets, 1982, Andrejev, 1982, Afanassiev, 1982, Afanassiev & Vorobyev, 1980). Most part of mathematical models is based on the admixture transport equation with corresponding boundary and initial conditions which are determined by a specific task setting. For example, in (Rukhovets, 1982) besides the calculation of steady flows the numerical experiments to study passive admixture transfer in natural conditions and conditions of FPB construction were conducted. Pollution sources were located at the mouth of the Great Neva, in the Morskoy channel route and in the north of the Neva Bay, calculation was performed in conventional units. Modeling results showed that there are significant differences in the distribution of admixture over the Neva Bay area; however, the value of background concentration coming from pollution sources is very important.

A calculation of passive admixture transfer by the flow circulation from one source is presented in (Andrejev, 1982). A pollution source was located in the east of the area and wind was set spatially homogenous. Average long-term discharge at the Neva mouth was distributed along the branches proportionally to their sections. Resting state was taken as the initial condition.

(Afanassiev & Vorobyev, 1980, Afanassiev, 1982) are devoted to the model investigation of suspended matter fields' formation in the Neva Bay under the



effect of the Neva flow in various hydrometeorological situations. The model developed by the author was applied to study the impact of the Flood Protection Barrier on suspended matter distribution with the account for gravitational sedimentation and particle stirring.

This model was also used to study the distribution of suspended matter in the Neva Bay and the adjacent part of the Gulf of Finland accounting for FPB in modern conditions, i.e. with no pollution sources present (due to dredging works) for flow and flow-surge situations. Model experiments showed that when there are no suspended matter sources of anthropogenic origin, the determining factors of its fields' formation are the Neva flow and hydrometeorological conditions in the region. In conditions of increasing flow and wind impact the stirring processes cause a rise of suspended matter concentration in coastal shallow areas of the Neva Bay and the Eastern Gulf of Finland. In conditions of decreasing flow and no wind the predominant factor is the gravitational sedimentation of particles.

In all listed models wind conditions were set as spatially homogenous and temporally constant that in its turn made a relatively homogenous picture of flows and suspended matter distribution. Besides, these models considered particles belonging to one size fraction with the set constant rate of sedimentation.

The present work investigates the features of distribution of suspended matter on the basis of a mathematical model with high spatial resolution and atmospheric forcing set according to the data of reanalysis of European Centre for Medium-Term Weather Forecast (NCEP).

2. Methods and materials

A modified 3D hydrodynamic model of the Baltic Sea developed by I.A. Neelov (Neelov, 1982, Neelov et al., 2003) was used to simulate the distribution of a suspended matter spot coming to the Neva Bay as a result of dredging works.

The model is based on full hydrothermodynamics equations in the Boussinesq and hydrostatics approximations including the equation of sea water state in the form suggested by UNESCO. Vertical turbulence is described on the basis of the original turbulence b-l model. The original iteration scheme of free sea surface calculation is used for numerical simulations. Advection members are described by the scheme of the second order of accuracy for spatial coordinates.

The system of equations supplemented by corresponding boundary conditions is solved by the finite difference method. The numerical scheme is based on the implicit iteration scheme of liquid free surface calculation that allows to significantly increase the time step. The implicit scheme (run) is also used for the calculation of vertical turbulent flows of impulse, heat and salt. To solve the turbulent energy balance equation the implicit scheme is also used—a run with iterations. Advection members and members describing horizontal diffusion are calculated according to the explicit scheme. Spatial derivatives are approximated at the disperse Mesinger-Arakava grid (B-grid), i.e. velocity vector is calculated at the grid nodes and temperature, salinity and free surface—in the centre. Advection members are calculated using the



directed differences against the flow with addition of anti-diffusion member that compensates calculating viscosity.

The advection-diffusion equation that is realized together with hydrothermodynamic model was used to study the process of suspended matter transfer.

The following conditions were set for numerical experiments: the total Neva discharge was set as average monthly long-term values and proportionally distributed over the branches. The amount of emission from a local continuous source was 10 million tons which were distributed evenly over the entire period of dredging works (7 months).

The NCEP data of reanalysis with 6-h time step and 2-degree resolution were used for the calculation that included data on air temperature, atmospheric pressure, wind rate, absolute humidity, cloud cover and precipitation.

The calculation of suspended matter transport has been carried for the period of June–November 2007. The horizontal resolution was 250 m, vertical resolution—2 m, time step—120 s. Particles have been conditionally divided into fractions with different gravitational speed.

3. Discussion

The calculations made it possible to analyze the time-space variability of suspended matter transport in the investigated water area.

Absence of authors' access to data of observations of suspended matter content during the period of dredging and land build-up works made it impossible to carry out a quantitative comparison of modeling results. Thus, the comparison was held only on the basis of satellite images. The comparison results are presented on Figs. 1, 2 and show their relatively good agreement.

It is evident that the main suspended matter flow was spreading along the northern coast of the Neva Bay; then suspended matter passing through the FPB North Gate was filling in almost the entire resort zone and was spreading further north-westwards reaching Berezoyve Isles. Further calculations showed that the pollution by suspended particles of small fractions was remaining and spreading during a very long time in the large part of the water area even after the dredging works have been finished.

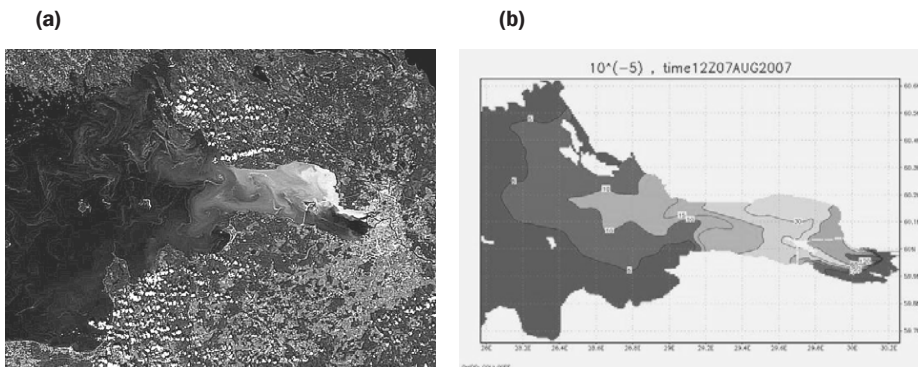


Fig. 1. Satellite image taken on August 7, 2007 (a) and suspended matter concentrations (mg/l) in the 2-meter surface layer, simulated by the model for the calculation date, August 7, 2007 (b).

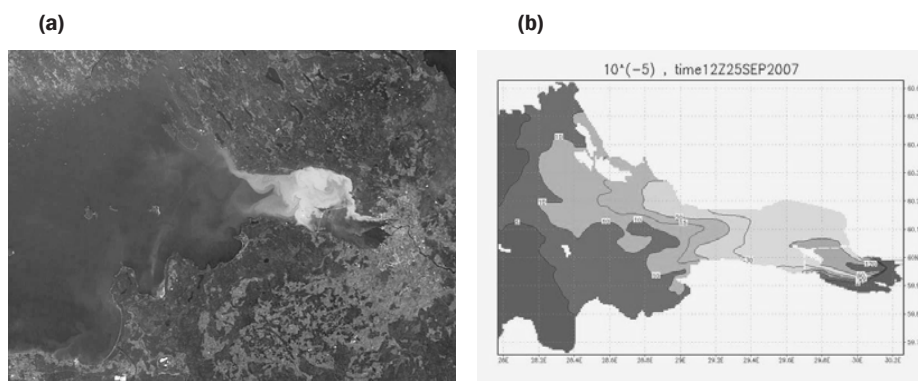


Fig. 2. Satellite image taken on September 25, 2007c (a) and suspended matter concentrations (mg/l) in the 2-meter surface layer, simulated by the model for the calculation date, September 25, 2007 (b).

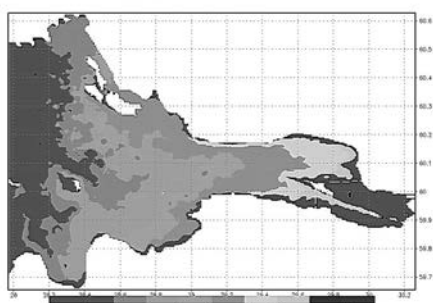


Fig. 3. Thickness of settled sediment (mm) at the end of simulation period (November 30, 2007).

An assessment of settled sediment thickness was performed on the basis of the calculations made (Fig. 3). The maximum thickness of suspended particles with grain size of less than 0.01 mm was 40 mm. The main part of suspended matter settled down in the Morskoy channel, in the Neva Bay and the adjacent shallow area of the Gulf of Finland.

References

- Afanassiev, S. V. (1982) Results of numerical modeling experiments of admixture transfer in the Neva Bay. In: *Systems and methods of automatization of research and management*, 30–34. Moscow: Nauka.
- Afanassiev, S. V. & Vorobyev, V. I. (1980) Algorithmic modeling of admixture sedimentation in problems of water rational use. In: *Algorithmic models in research automatization*, 57–60. Moscow.
- Andrejev, O. A. (1982) Numerical modeling of water dynamics and passive admixture transfer in the Neva Bay. *Meteorologiya i gidrologiya* **12**:78–86.
- Neelov, I. A. (1982) Mathematical model of synoptic eddies in the ocean. *Okeanologiya* **22**(6):875–885.
- Neelov, I. A., Eremina, T. R., Isaev, A. V. et al. (2003) A simulation of the Gulf of Finland ecosystem with 3-D model. *Proc. Estonian Acad. Sci. Biol. Ecol.* **52**(3):346–359.
- Rukhovets L. A. (1982) Mathematical modeling of water exchange and admixture distribution in the Neva Bay. *Meteorologiya i gidrologiya* **1**:78–87.
- Rumyantcev, V. A. & Drabkova, V. G., eds. (1999) *The Gulf of Finland in conditions of anthropogenic impact*. St.-Petersburg.

Hundred-years dynamics of near-midday water levels in the mouth of the Pregolia River (1901–2009)

Svetlana Navrotskaya

Abstract

The time variations of the water level at the mouth of the Pregolia River at Kaliningrad are investigated. Daily near-midday observations (1996–2009) fulfilled by the Atlantic Branch of P. P. Shirshov Institute of Oceanology of Russian Academy of Sciences at the Museum Vessel “Vityaz” located in the center of Kaliningrad are used. For comparison Annual data from the beginning of the last century (1901–2006) at the point Kaliningrad–Rybachyi (former Königsberg) is involved. The tendency of growth of an average level in South East Baltic Sea has been proved: the steady positive linear trend for average and minimal levels and weak trend—for maximal levels. Variation in amplitudes between extreme levels is characterized by a negative trend. It testifies to the greater contribution of increase of minimum levels to the rise of an average level. To last years this process goes more intensively.

Исследован временной тренд уровня воды в устьевой части реки Преголи в Калининграде. Используются ежесуточные околополуденные наблюдения (1996–2009 гг.) Атлантического отделения института океанологии им. П. П. Ширшова РАН на Музейном судне «Витязь». Для сравнения привлечены данные с начала прошлого века (1901–2006 гг.) в пункте Калининград–Рыбачий. Подтверждается многолетняя тенденция роста среднего уровня в Юго-Восточной Балтике. Положительная динамика более явно выражена для средних и минимальных уровней и менее явно — для максимальных. Размах колебаний между экстремальными уровнями характеризуется отрицательным трендом. Это свидетельствует о большем вкладе роста минимальных уровней в подъем среднего уровня. Процесс этот в последние годы идет более интенсивно.

Study of the water level regime of coastal reservoirs has the big practical significance for the population and its economic activities in these regions. Forecasts of increase of a water level which can occur in connection with

Svetlana Navrotskaya (✉)

P. P. Shirshov Institute of Oceanology RAS, Atlantic Branch, Kaliningrad, Russia



warming of a climate observable in last years are especially important: growth of precipitations causes increase of a river drain. On change of a water level in the river mouths significant influence also wind-driven processes which are caused by strong winds above a coastal zone of the seas. Such object is the mouth of the Pregolia River running in Vistula Lagoon. Unfortunately, now the number of hydroposts on the river is reduced. Therefore it is valuable, that with 1996 of supervisions over a level are conducted in the center of Kaliningrad by Atlantic Branch of P.P. Shirshov Institute of Oceanology of Russian Academy of Sciences (ABIORAS) at the former vessel-museum “VITYAZ”. She anchored at 9 km upstream of the river mouth. The width of the river is up to 90 m. Regular observations over a water level, and also wind and rainfall, were fulfilled every day in near-midday time (09 h World (UTC)/Greenwich), in the winter in 11 h, in the summer in 12 h of local decretive time. By the end 2009 of observations over a level have made a number of daily readings for 14 years, it’s analyzing possible to draw conclusions on features of river regime for this period and on tendency of a development.

Variations of the mouth river level measured in 1996–2009 in the center of Kaliningrad near vessel-museum “VITYAZ” are individual for every year. Nevertheless the intra-annual course of a mean level generalized for 14 years reflects some seasonal rhythm (Fig. 1, 2). The long-standing intra-annual dynamics of level is characterized by quite precise seasonal maxima close to values (February—19 cm, July—18 cm and November—22 cm), they correspond to the peculiar to a local climate periods of winter gales and long thawing period, maximum in rainfall and autumn strong set-up winds. But the spring minimum is swept especially in annual level dynamics: in the Pregolia

Fig. 1. Intra-annual dynamics of variations of the monthly maximal (2), mean (3) and minimal (4) water levels, as well as amplitude between monthly maximal and minimal levels (1).

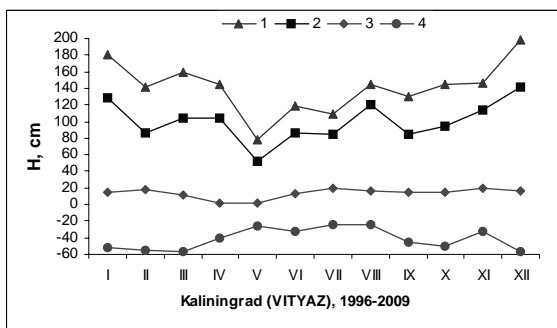
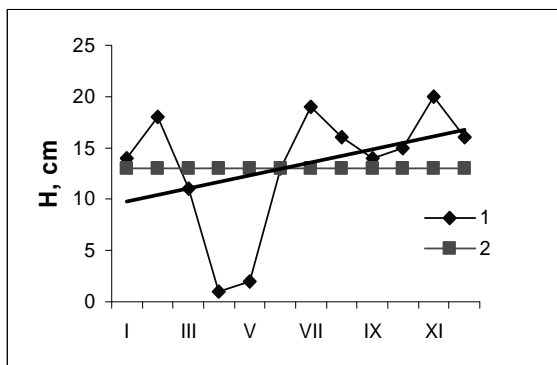


Fig. 2. Intra-annual dynamic of monthly mean water level (1) for the mouth of the Pregolia River, Kaliningrad (MV “Vityaz”), 1996–2009. Mean annual level marled by (2).





River mouth site the biggest recession (April–May—up to 1 cm) is observed. It is influenced by the spring weak zone wind component, also reduction of quantity precipitations influencing a drain—its minimum is fall for February–April. Intra-annual dynamic of level in 1996–2009 is characterized by the positive linear trend. The overall annual mean level estimated for 14 years is of 13 cm.

The atmospheric processes play the principal role in the occurrence of such conditions, especially action of the western winds: they can cause flooding and spreading of salt waters from shallow Vistula Lagoon up to the river stream. Strengthening of the western circulation to last years increases quantity of rainfall within the drainage basin, leads to increase of frequency and magnitude of surge storms. Well positive and statistically significant linear trend of average level, zone component of wind and rainfall confirm that (Fig. 3; Tables 1, 2).

Table 1

Trend rates for rainfall and latitude (zone) component of wind for 1996–2008 and Student's coefficient (t_{st})

Parameter	Rainfall, mm/year	Zone wind, $ms^{-1}/year$
Trend	17.50	0.02
t_{st}	1.40	Insignificant

Well expressed linear tendency in dynamics of annual levels 1996–2009 (“Vityaz”) shown on Fig. 3 and Table 2. It concerns to both an average level and measured extreme values. H_{mean} and H_{min} have small, but significant positive trends. H_{max} and amplitude of level monthly fluctuations show a negative trend. It is possible to consider, that steady positive growth of average water level during 1996–2009 caused mostly by an increase in minimal levels.

In the mouth Pregolia River at the point Kaliningrad–Rybachyi (Königsberg), we have annual level data in 1901–1980 (Extreme values of level... 1982) and in 1977–2006 (Atlas... 2007). The tide gage Rybachy (now does not exist)

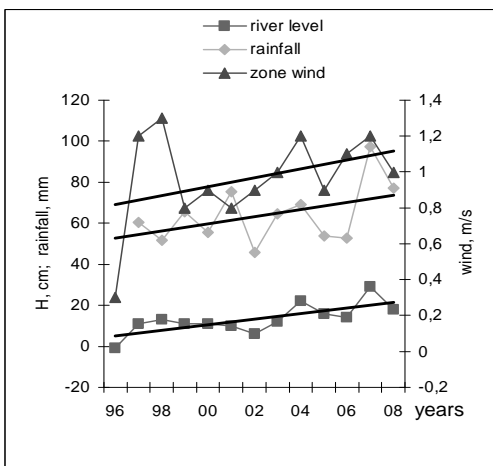
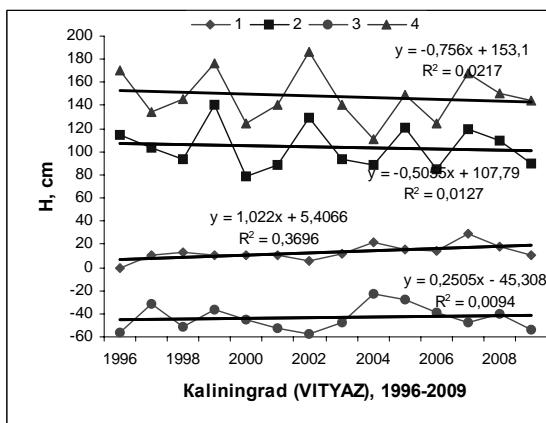


Fig. 3. Variations and trends for monthly averaged values of water level, rainfall and latitude (zone) component of wind for 1996–2008, Kaliningrad (“Vityaz”). Note: the values of rainfall are reduced in 10 times to be expressed by the same axis as water level.



Fig. 4. Inter-annual dynamics of mean (1) maximal (2) and minimal (3) levels, as well as amplitude of water level monthly variations (4) and their linear trends. The mouth of the Pregolia River, Kaliningrad (“Vityaz”), 1996–2009.



is located of 3.5 km down stream from the “Vityaz”. The variations of annual mean and extreme levels according these data are in the Fig. 5.

The appreciable rise of mean water levels is evident for the last century. It is seen in all periods, that trend for maximal levels are weaker than one for minimal level. All the calculated variants of trends on these data are collected in the Table 2. Obviously, rise of a minimum level have the greater effect on growth of average level during the considered periods. For Kaliningrad–Rybachyi (Königsberg) a growth of an average level for 100 years has made in general nearby 20 cm (Tables 2, 3; Fig. 6), especially in last years (1977–2006) when the increase of the level equals to 11 cm. The greatest growth is noted for the mean annual water levels at “VITYAZ” in short period 1996–2009: by the end of the period the level has risen by 14 cm. During 100 last years maximal amplitude of water level variations for Kaliningrad–Rybachyi is 316 cm (Table 3).

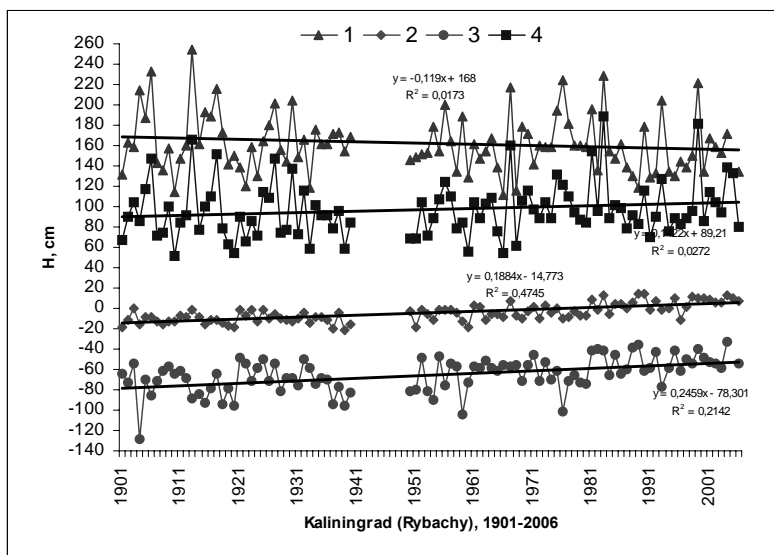


Fig. 5. Inter-annual dynamics of amplitude of monthly variation of water level (1) and maximal (2), mean (3) and minimal (4) water level values and their linear trends.



Table 2

Long-term water level trends in 1901–2009 and their Student’s coefficient (t_{st})

Years	Increase of mean level, cm/pr	H _{mean}		H _{max}		H _{min}		Amplitude	
		Trend, mm/year	t_{st}	Trend mm/year	t_{st}	Trend mm/year	t_s	Trend mm/year	t_{st}
“VITYAZ”									
1996–2009	14	10.2	2.41	-5.1	insign.	2.5	insign.	-7.6	insign.
Rybachy									
1901–1980	8	1.0	3.30	0.5	insign.	1.2	1.55	-0.7	insign.
1901–2006	20	1.9	6.71	1.4	1.61	2.5	4.49	-1.2	1.27
1977–2006	11	3.8	2.45	1.4	insign.	3.4	insign.	-3.8	insign.

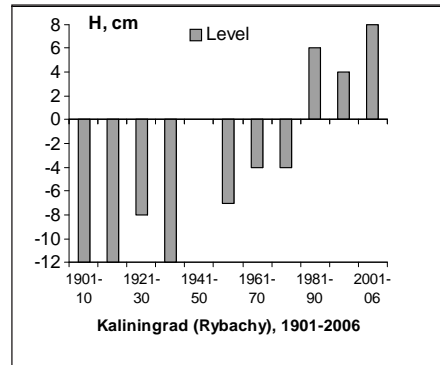
Table 3

Average annual and extreme levels, maximal amplitude for annual variations of water level (cm) for 1901–2006 by decades, Kaliningrad–Rybachyi

Years	Annual mean	$\pm\sigma$	Maximal	Date	Minimal	Date	Max. amplitude, year
1901–10	-12	5.29	147	30.XI.06	-128	25.XII.04	233 (1906)
1911–20	-12	5.29	166	27.XII.13	-96	4.XI.20	254 (1913)
1921–30	-8	7.74	147	26.IV.27	-82	25.III.28	205 (1930)
1931–40	-12	6.09	116	12.IX.32	-95	5.XI.39	176 (1934)
1941–50							
1951–60	-7	7.14	125	26.VIII.56	-104	6.XII.59	200 (1956)
1961–70	-4	5.99	160	18.X.67	-72	22.I.69	217 (1967)
1971–80	-4	4.65	132	8.I.75	-102	17.X.76	224 (1976)
1981–90	6	6.90	188	29.I.83	-66	26.III.84	229 (1983)
1991–2000	4	7.41	182	4.XII.99	-77	11.XI.93	222 (1999)
2001–06	8	2.73	138	18.XI.04	-58	7.III.03	171 (2004)
1901–2006	-5	8.76	188	29.I.1983	-128	25.XII.1904	316



Fig. 6. Average annual levels (H, cm) for 1901–2006 on decades, Kaliningrad (Rybachy).



The water level increase at the mouth of the Pregolia River during 1996–2009 is the continuation of the tendency of level growth marked in previous years behind 1901 in the Vistula Lagoon and the South-East Baltic (Dailidienė et al., 2006, Jamalavičius et al., 2007, Gilbert, 2008). Climatic changes, both regional, and global could be the cause of this tendency. It is important to watch for—does the water level increase create threat to low coastal areas in the center of Kaliningrad?

References

- Atlas “Klimat morey Rossii i kluchevyh rayonov Mirovogo okeana” (2007) Baltijskoe more. Obninsk, <http://data.oceaninfo.ru/atlas/Balt/5-1.html>.
- Dailidienė, I., Davulienė, L., Tilickis, B. et al. (2006) Sea level variability at the Lithuanian coast of the Baltic Sea. *Boreal Environment Research* **11**:109–121.
- Extreme values of the level at coast and river mouths of Baltic Sea* (1982) Tables. Leningrad (in Russian).
- Gilbert & Drukamia, W. L., eds. (2008) *State of the Coast of South East Baltic: an indicators-based approach to evaluating sustainable development in the coastal zone of the South East Baltic Sea*. Gdansk.
- Jamalavičius, D., Žilinskas, G., Dubra, V. (2007) Pattern of long-term seasonal sea level fluctuation in the Baltic Sea near the Lithuanian coast. *Baltica* **20(1–2)**:28–34.

On the flow vertical structure of shallow strongly stratified basin in summer

Olga Pitalskaya

Abstract

We conducted measurements at Lake Shira in order to determine its hydro-physical characteristics. The measurements were made using Acoustic Doppler Current Profilers (ADCPs) 600 and 1,200 kHz. These current profilers make it possible to identify three-dimensional velocity along the liquid column up to a depth of 14 (ADCP 1200) and 60 m (ADCP 600). Also we used SonTek Acoustic Doppler Velocimeter (ADV) 16 Hz, which measures the three components of velocity at the point. After field data processing, we have compared these data with data obtained by mathematical modeling of wind flows using the Ekman's model. These results clarify some important characteristics used in the numerical calculations.

Проведены натурные измерения на озере Шира с целью определения его гидрофизических характеристик. Измерения проводились с помощью акустических доплеровских профилографов течений ADCP 600 и 1200 кГц, способных определять трехмерную скорость вдоль всего столба жидкости на глубину до 14 м (ADCP 1200) и 60 м (ADCP 600), и при помощи прибора SonTek 16 Гц, который измеряет три компоненты скорости в точке.

1. Introduction

Acoustic Doppler Current Profiler (ADCP) is device of a new technology for hydrometric observations and now is widely used to measure the velocity field in the cross section of the flow in rivers, in lakes and marine waters (Admiraal & Demissie, 1996, Wewetzer et al., 1999, Simpson, 2001, Best et al., 2001, Kostaschuk et al., 2005). It has found application in conducting hydrometric surveys, monitoring of water surface and in the scientific research.

At the present time ADCP is produced abroad by firms SonTek, R. D. Instruments, Nortek. ADCP has many significant advantages over traditional

Olga Pitalskaya (✉)
Institute of Computational Modeling SB RAS, Krasnoyarsk, Russia
e-mail: olga.pitalskaya@gmail.com



methods of hydrometric observations, for example, with hydrometric current meters, though there are some restrictions on its usage.

In July 2009 measurements of hydrodynamic characteristics of wind movement of a liquid have been conducted at Lake Shira (Hakasiya). The importance of this problem lies in the fact that these data are as initial data, and as verification of numerical models used for determining hydrophysical characteristics of Lake Shira and for estimation of biological substances distribution in the lake.

The unique therapeutic salt lake is part of the resort “Lake Shira”. The increase in recent years, anthropogenic pressures on the lake created a threat to reduce the healing properties of water and, accordingly, has set a target of complex study of the ecological state of the lake. Investigations continued in the direction of the study of biological and chemical properties of water, and on mathematical simulation of hydrophysical regime.

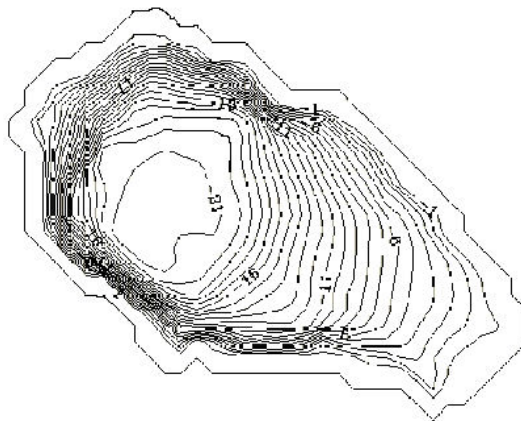
The Shira is an inland lake, without islands. The Son River flows into the lake from the south. As the inflow is very little, river only influences the part of the lake near its mouth. The bathymetry of the lake is presented in Fig. 1. The lake has an oval shape and is 9.4 km long and about 5 km width. The water area of the lake is 34.7 km², average depth is 11.2 m and the maximum depth over the past few decades has changed from 21 to 24 m (at this time—24 m).

2. Results

Temperature measurement has shown that in the observation period (July 11–20, 2009) in the lake thermocline is formed. The upper boundary of thermocline is 5 m, the bottom is 10 m. These data are been presented by D. Y. Rogozin, PhD, the Institute of Biophysics. The horizontal temperature gradient is virtually absent. Water salinity varies in the direction of decreasing (from 18–22 g l⁻¹ according to the observations in 1958 to 11–13 g l⁻¹ on observations in 2004).

In-situ measurements were made with instruments ADCP of firm RD Instruments (RDI) 600 and 1,200 kHz and the company SonTek 16 Hz. RDI are capable to determine the three-dimensional velocity along the entire column of liquid to a depth of 14 m (RDI 1200) or up to 60 m (RDI 600). This liquid

Fig. 1. The bathymetric map of Lake Shira (depth indicated in meters).



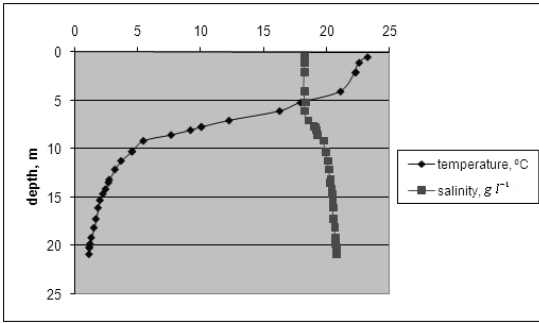


Fig. 2. The typical temperature distribution and salinity over depth in July 2009.

column is broken into sections (depth cell), each of which is measured by the average speed. The size of the depth cell determines the depth at which the device starts the measurement and the distance from the bottom or surface on which the measurements are acceptable. The device SonTek 16 Hz measured three components of velocity at the point. We used adjunct software packages for configuring, data collection and review. All the devices used in standalone mode. Fig. 3 shows the format of the output values of the time series for the velocity and correlation of data obtained using the device SonTek in ViewHydra program. The measurements were carried out with following parameters: the north-east wind is 2.3 m s^{-1} , depth is 1.5 m, the velocity range is from -2.5 to $+2.5 \text{ m s}^{-1}$ and the total depth at the point is 24 m. The program also allows you to conduct minimal processing and smoothing data.

The data were processed as follows: first discarded the values for which the correlation was less than 50 percent, then the velocity in all directions averaged over time. Fig. 4 shows the data after some preliminary processing. Measurement results of RDI 600 at the depth of 24 m with depth resolution of 2 m are shown. The transducers are directed downward. Wind is north-eastern, $3\text{--}4 \text{ m s}^{-1}$, u is the east component of velocity, v is the north component of velocity.

After field data processing, we have compared these data with data obtained by mathematical simulation for wind-induced flow of homogeneous

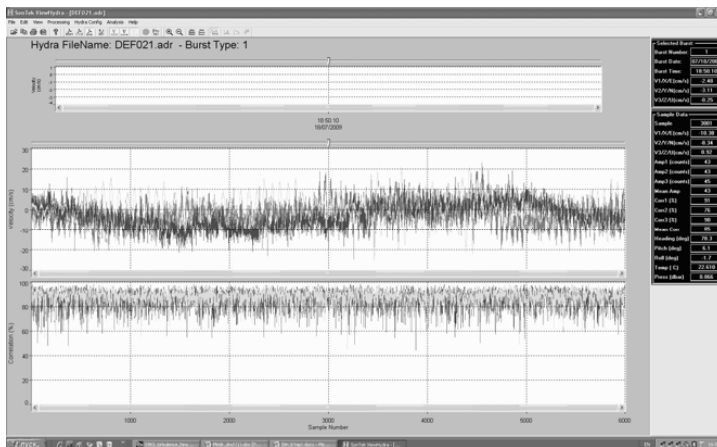


Fig. 3. The changing of velocity value by time.



liquid. Fig. 5 shows the velocity hodographs for the four cases. Hodograph depicted by diamonds is made by in-situ measurements (1). The dotted line (2) is hodograph, constructed by the formula of drift component with constant coefficient of vertical turbulent exchange and with condition of adhesion (Welandar, 1968):

$$W = u + iv = \frac{\tau^w}{\rho_0} \cdot \frac{\text{sh}\left(\sqrt{\frac{il}{K_z}}(z+H)\right)}{\sqrt{ilK_z} \text{ch}\left(\sqrt{\frac{il}{K_z}}H\right)},$$

the wind stress:

$$\tau^w = \tau_x + i\tau_y, \tau_x = 1.25 \cdot 10^{-3} \cdot \rho_a w_x |\bar{W}|, \tau_y = 1.25 \cdot 10^{-3} \cdot \rho_a w_y |\bar{W}|.$$

Calculations have been made with the following parameters: $H=24$ m, $l=0.00015$ s⁻¹, $\rho_0=1000$ kg m⁻³, $\rho_a=1.225$ kg m⁻³, $|\bar{W}|=6.5$ m s⁻¹, $K_z=3 \cdot 10^{-5}$ m² s⁻¹.

In the case of the variable coefficient of the vertical turbulent exchange $K_z=cz+d$, for model with taking into account horizontal viscosity ($K_x=K_y=1$ m² s⁻¹), we can write the solution of its equation in the form of series with the modified Bessel functions $I_0(\xi), K_0(\xi), \xi=cz+d$ (Witten, 1976, Kompaniets et al., 2009). This solution is shown on Fig. 5 by dotted line (3).

When $K_z=\delta e^{\lambda z}$, the solution has the similar form and its can be written through $I_1(\xi), K_1(\xi), \xi=e^{\lambda z}$. This solution is shown on Fig. 5 by solid line (4). We have considered these cases when $c=1.5 \cdot 10^{-6}, d=4.8 \cdot 10^{-5}$ and $\lambda=2 \cdot 10^{-2}, \delta=3.8 \cdot 10^{-5}$ for linear and exponential distribution respectively.

3. Conclusions

The simple models of homogeneous fluid, starting from the depth of 3 m to the upper boundary of thermocline, can be used for estimation of the flow in the upper quasi-homogeneous layer. The results in the near-surface layer are very much different and can be explained by the fact that we consider

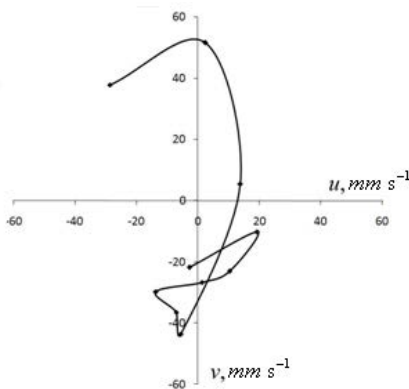


Fig. 4. The velocity hodograph.

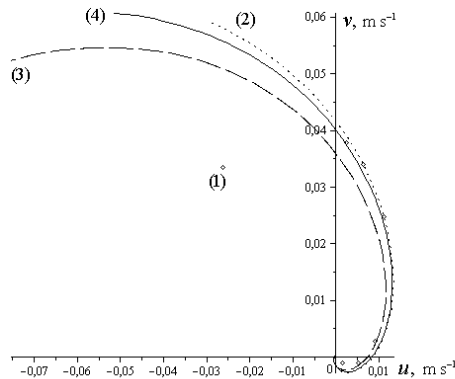


Fig. 5. The comparison of the velocity hodograph from $H=-8$ m to $H=-1.7$ m.



analytical solutions without taking into account geostrophic component. In-situ data may correspond to the restructuring of the flow in accordance with the changing wind, while the analytical solutions are dealt with the stationary case.

References

- Admiraal, D. & Demissie, M. (1996) Velocity and discharge measurements at selected locations on the Mississippi River during the great flood of 1993 using an acoustic Doppler current profiler. *Water Int.* **21**(3):144–151.
- Best, J.L., Kostaschuk, R.A., Villard, P.V. (2001) Quantitative visualization of flow fields associated with alluvial sand dunes: results from the laboratory and field using ultrasonic and acoustic Doppler anemometry. *J. Vis.* **4**:373–381.
- Kompaniets, L.A., Yakubylik, T.V., Gavrilova, L.V., Gurevich, K. Yu. (2007) *Models of Ekman's type in hydrodynamics problems*. Novosibirsk: Nauka.
- Kompaniets, L.A., Yakubylik, T.V., Pitalskaya, O.S. (2009) About the analytical solution of a single model of wind-induced flow of a viscous fluid. *Computational Technologies* **14**(4):46–55.
- Kostaschuk, R., Best, J., Villard, P. et al. (2005) Measuring flow velocity and sediment transport with an acoustic Doppler current profiler. *Geomorphology* **68**:25–37.
- Simpson, M.R. (2001) *Discharge measurements using a broad-band Acoustic Doppler current profiler*. Sacramento: U. S. Geological Survey.
- Welander, P. (1968) Wind action on a shallow sea: some generalisations of Ekman's theory. *Tellus* **XX**(1):1–16.
- Wewetzer, S., Duck, R.W., Anderson, J.M. (1999) Acoustic Doppler current profiler measurements in coastal and estuarine environments: examples from the Tay Estuary, Scotland. *Geomorphology* **29**(1):21–31.
- Witten, A. (1976) Steady wind-driven currents in a large lake with depth-dependent eddy viscosity. *J. Phys. Oceanogr.* **6**:85–92.

Internal waves in shallow water bodies

Ekaterina Plotnikova, Aleksey Kuleshov

Abstract

Study of internal waves is very important problem of oceanography. These waves have gravity nature therefore they are formed in the region of vertical density stratified water. Disturbance of the stratified medium causes the restoring mass force, therefore the medium oscillates. Internal waves are of practical importance. They influence on the physical, chemical, biological processes happening in the seas and oceans. For example they further sound scattering, cause erosion of port installations and are very dangerous for submarines.

Одной из актуальных проблем современной океанологии является проблема исследования внутренних волн. Эти волны имеют гравитационную природу и формируются поэтому в области вертикально неоднородного профиля плотности морской воды — в области пикноклина. Возмущение стратифицированной жидкости приводит к возникновению возвращающих массовых сил, в результате действия которых среда осциллирует. Значение внутренних волн довольно велико. Они оказывают существенное влияние на физические, химические и биологические процессы, происходящие в океанах и морях. Так, например, внутренние волны способствуют рассеянию звука, участвуют в размыве оснований портовых сооружений, представляют большую опасность для подводных лодок.

1. Methods and results

Our aim was to measure characteristics of the internal waves in Vislinsky bay. Special feature of the experiment is that medium adaptation to the gravity force is explored in shallow water bodies (the maximum depth is about 12 m) in contrast to the biggest part of the same researches. Theoretical frequency of internal waves can be calculated using formula for Brunt–Väisälä frequency:

Ekaterina Plotnikova (✉)

Moscow Institute of Physics and Technology, Moscow, Russia

e-mail: e.m.p.tow@gmail.com

Aleksey Kuleshov (✉)

P. P. Shirshov Institute of Oceanology RAS, Atlantic Branch, Kaliningrad, Russia



$$\omega = \sqrt{\frac{g}{\rho} \frac{d\rho}{dz}},$$

where g —gravitational acceleration, ρ —potential density, $d\rho/dz$ —density gradient at the given depth.

As usual, the water column stratification in the sea is not too big therefore internal waves are characterized by big periods—from few minutes to several hours. The task given in this research was to visualize internal waves in the Vislinsky bay using CTD-zond. At first we made vertical probing to define density.

Then we had to detect depth where the gradient of the density $d\rho/dz$ is ultimate and carry out time profiling. Two measurements lasted one hour each other were made at the depth of 4.4 and 7.8 m and formula evaluated frequencies are 0.015 and 0.0001 Hz.

Time-base sweep of oscillation processes appears to be complex wave pattern including a lot of unnecessary noises. Because of its small self-descriptiveness we had to get and analyze energetic spectrums. At the depth of 7.8 m there were no neat waves therefore I eliminate results of this experiment.

On the Figs. 2–3 you can see spectrums for temperature, salt and oxygen content oscillations at the depth of 4.4 m. Maximum of intensity is observed on the small frequencies. Corresponding to frequencies less than 0.001 Hz periods are bigger than 20 min but measurement time was about one hour consequently data about such small frequencies should be eliminated. Thus value of measured frequency is about 0.002 Hz which is in a rather good correspondence with theoretical magnitude. The underlying cause of this deviation is dependence of frequency on the way of linear approximation on Fig. 1. Thereby the significant peculiarities of internal waves in the Vislinsky bay were researched and perspectives for the nearest researches were outlined.

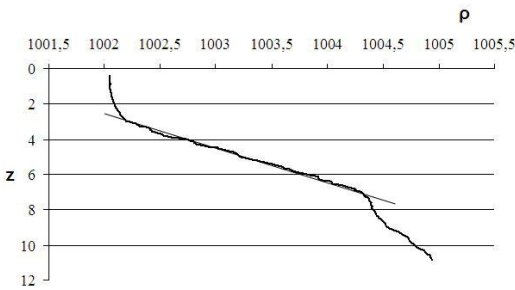


Fig. 1. Vertical density profile.

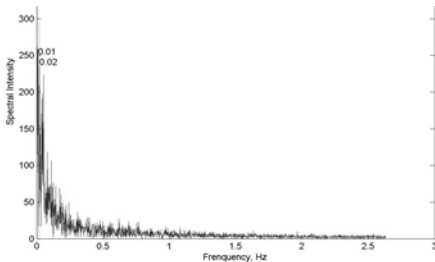


Fig. 2. Spectrum of the temperature oscillation.

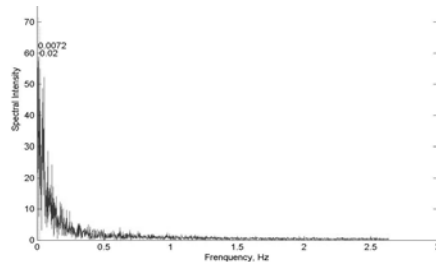


Fig. 3. Spectrum for salinity oscillations.

Mathematical modeling of spatial-temporal dynamics of current fields in the Neva Bay, the Gulf of Finland

Konstantin Podgornyj

Abstract

Flow regime in the Neva Bay is formed in the result of interactions of processes of different temporal scales, and characterized by high spatial-temporal variability. Values of water current velocities components averaged over depth were determined in the result of numerical integration of Saint-Venan system equations without considering turbulent mixing. In order to build the numerical solution an implicit differential scheme straddling in space and time utilizing method of alternated directions was used. Modeling was performed during the whole period of open water for natural as well as project conditions i.e. in the presence of Saint-Petersburg flood control facilities' complex. It was shown that modeling data are in good correspondence with all observed characteristics of flow structure formation in the water body.

Режим течений в Невской губе формируется в результате взаимодействия процессов различных временных масштабов и отличается большой пространственно-временной изменчивостью. При моделировании значения средних по глубине составляющих скорости течения определялись в результате численного интегрирования системы уравнений Сен-Венана без учета турбулентного перемешивания. Для построения численного решения использовалась неявная, разнесенная по пространству и времени разностная схема с применением метода переменных направлений. Моделирование проводилось на весь период открытой воды для естественных, а также для проектных условий, то есть при наличии комплекса водозащитных сооружений города Санкт-Петербурга от наводнений. Показано, что данные моделирования хорошо соответствуют всем наблюдаемым особенностям формирования структуры течений в водоеме.

Konstantin Podgornyj (✉)

I. D. Papanin Institute for the Biology of Inland Waters of the Russian Academy of Sciences, Borok, 152742 Yaroslavl region, Russia

e-mail: kap@ibiw.yaroslavl.ru



1. Introduction

1.2. Object of the study

Hydrological regime of the Neva Bay including its current regime is formed as the result of interactions of processes of varying spatial-temporal scales. The most important ones are: river drainage and its irregular distribution over the bay's width, wind impact upon the water surface, long waves of storm onsets, seiches, inertial currents (Baidin, 1965, 1997, Belyshev & Preobrazhenskii, 1988, Rumyantsev & Drabkova, 1999, Menshutkin, 1997). Of all these processes only river Neva drainage may be considered as a quasistationary process although it is also subject to both intra- and interannual fluctuations. Mean annual value of river Neva drainage is around 2,500 m³/s (Baidin, 1965, Nezhikhovskii, 1981). All other processes bear either accidental or polycyclic character with complex structure of frequency energy distribution. All these factors lead to strong spatial-temporal variability of current regime present in the Neva Bay and make finding circulation schemes hard.

Data of long-time observations carried out using floating beacons and autonomous buoy stations (Belyshev & Preobrazhenskii, 1988) and subsequent spectral analysis of this data allowed selecting ranges of main energy-bearing zones: seasonal, with characteristic periods of variability of year and half a year; synoptic, with periods from 2–3 to 5–7 days; daily, with periods 24–26 h; intradaily, with periods 12–14 and less than 10 h (Belyshev & Preobrazhenskii, 1988, Rumyantsev & Drabkova, 1999, Klevannyi, 2002, Menshutkin, 1997). Seasonal variability of currents in the Neva Bay is rather sharply pronounced and linked with fluctuations of river drainage and ice phenomena, mostly. River flow determines the intensity of circulation's drainage component. Uni-layer structure of currents is characteristic of the Neva Bay as its waters are almost always mixed from the surface to bottom. Exceptions are observed when overall change of currents occurs and in cases of brackish waters under-run from the west (Rumyantsev & Drabkova, 1999).

An idea of the spatial structure of currents considering its variability and statistical parameters is given in (Rumyantsev & Drabkova, 1999) based on the materials collected during field observations. Data analysis allowed authors to give a general characteristic of currents as well as carry out zoning of the Neva Bay. It is noted that characteristic feature of field current is its instability, with the size of pulse component usually exceeding the average (residual) value of current speed vector, which is determined after relevant averaging using time scale of averaging from two weeks to six months. This is clearly seen on dispersion ellipses (Fig. 1) built for the Neva Bay using data of immediate observations of speed values and current directions (Rumyantsev & Drabkova, 1999).

Character of current mean vectors in the Neva Bay allows concluding that their spatial structure is determined by river Neva drainage. On average, drainage component is directed from the east westwards and deflections are conditioned by the bottom relief and shoreline. In natural conditions 60 percent of Neva's discharge flows through the North Gate and 40 percent through the South Gate (Rukhovets, 1982). Maximum value of drainage component of current speed is up to 10 cm/s in the central part of the Neva Bay. In this part

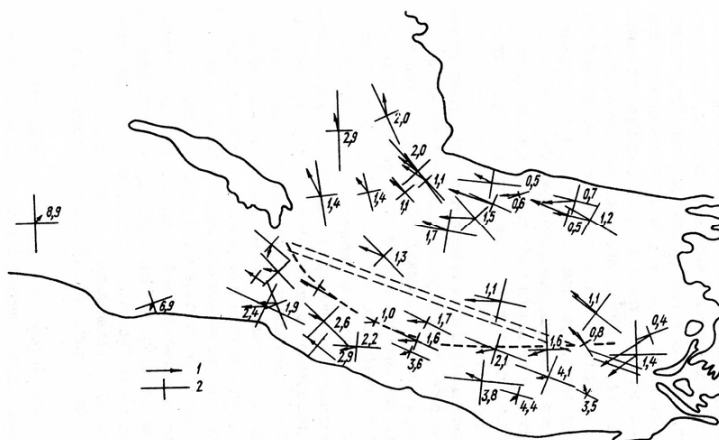


Fig. 1. Scheme of currents in the Neva Bay during the navigation period according to the data of perennial observations (Belyshev & Preobrazhenskii, 1988): (1) vector of "average current" velocity; (2) main axes of current variability ellipse. Digits denote the factor by which pulse values of speed exceed its average values.

of the bay large axis of dispersion ellipse exceeds the small one by 3–5 times. Probability of motions in different directions increases in the vicinity of the shore. To the south of Marine Canal dikes and close to the north shore general direction of drainage component is preserved but value of the backwards speed decreases significantly.

Variable (pulse) component of current vectors is extremely changeable and determined by wave oscillations of large period and wind impact upon water surface (Belyshev & Preobrazhenskii, 1988, Rumyantsev & Drabkova, 1999). Situations when winds promote rundown (east points' winds) or onset (west points' winds) effects are especially important. Onset winds may stop drainage and turn the currents eastwards. Observations show that speeds of east currents do not exceed 10 cm/s in 60–70 percent cases and reach 25 cm/s only in 3–4 percent.

Analysis of data gathered during observations using multi-day stations shows that transversal circulation may be formed in the Neva Bay in addition to longitudinal circulation as well as cyclonic and anticyclonic vortex formations. They create conditions needed for waters flow to the northern, southern shores of the bay or to its central longitudinal axis (Baidin, 1997).

Spectral analyses of currents as well as combined study of spatial-temporal variability of current structure, local wind and level fluctuations allow finding several characteristic zones in the Neva Bay (Belyshev & Preobrazhenskii, 1988, Rumyantsev & Drabkova, 1999):

- ✓ zone of Neva waters transit with stable currents and high speed of average transfer. This zone is located in the central part of the Neva Bay;
- ✓ zone of slowed water cycle with relatively developed transversal relocations of water masses. This zone encompasses southern part of the bay (southwards of the Marine Canal) and narrow coastal zone. Current speeds in this zone do not exceed 2–6 cm/s usually;
- ✓ area of the North and South gates of the Neva Bay with hydrodynamic regime transitional towards typically marine regime of currents of the eastern



part of the Gulf of Finland. Their own, local zones of intensive currents are formed here in the openings of water discharge and navigational facilities of dikes;

✓ narrow littoral zone contacting with mainland limited by 1 m isobath. The main factor determining current structure here is the wind impact upon water surface;

✓ zone of slow water cycle in the south-eastern, shallow part of the Neva Bay. This zone is characterized by small current speeds (1–2 cm/s) and high variability of currents.

Speeds of drainage current were 4–10 cm/s in the zone of Neva waters west transit with a decrease towards the north and south coasts before the St.-Petersburg flood control facilities' complex was built. The least motile was south-eastern region of the Neva Bay adjacent to the Marine Port. Construction of protective facilities has not lead to significant change of neither the structure of drainage currents nor structure of wind currents in the Neva Bay (Belyshev & Preobrazhenskii, 1988). These changes bear local character and may be seen within 3–4 km on both sides of protective facilities. In project conditions distribution of the Neva River drainage through the North and South gates of the Neva Bay change slightly unlike natural conditions as shown by the model evaluations. Now 54 percent of discharge passes through the North gate and 46 percent through the South gate (Rukhovets, 1982).

2. General description of the hydrodynamic model and utilized digital methods.

Saint-Venan equations system was used to model hydrodynamic regime of the Neva Bay (not considering the effect of turbulent mixing) (Podgornyj, 2003):

$$U = \frac{1}{h+\zeta} \int_{-h}^{\zeta} u dz, \quad V = \frac{1}{h+\zeta} \int_{-h}^{\zeta} v dz, \quad H = h + \zeta, \quad (1)$$

$$\frac{\partial U}{\partial t} + U \frac{\partial U}{\partial x} + V \frac{\partial U}{\partial y} + g \frac{\partial \zeta}{\partial x} - fV + g \frac{U \sqrt{U^2 + V^2}}{C^2 H} - \frac{1}{\rho H} \tau_x^s = 0, \quad (2)$$

$$\frac{\partial V}{\partial t} + U \frac{\partial V}{\partial x} + V \frac{\partial V}{\partial y} + g \frac{\partial \zeta}{\partial y} + fU + g \frac{V \sqrt{U^2 + V^2}}{C^2 H} - \frac{1}{\rho H} \tau_y^s = 0, \quad (3)$$

$$\frac{\partial \zeta}{\partial t} + \frac{\partial(HU)}{\partial x} + \frac{\partial(HV)}{\partial y} = 0, \quad (4)$$

where U , V is the projections of vector of speed average over depth on coordinate axis, with OX axis directed eastwards, OY axis—northwards, OZ axis—up; ζ is the displacement of the free surface from the equilibrium state; h is the distance from horizontal reference plane to bottom; H is the temporal flow depth; f is Coriolis parameter; g is the acceleration due to gravity; τ_x^s , τ_y^s is the wind shear stress along axis OX and OY respectively; ρ is density of water; C is Chezy coefficient for bed resistance.



In case of active turbulence of the current for calculation of the shearing stress components of the wind according to Van-Dorn law the following ratios are taken (Podgornyj, 2003):

$$\tau_x^s = \theta \rho_a W_a^2 \cos \alpha_w, \quad \tau_y^s = \theta \rho_a W_a^2 \sin \alpha_w, \quad (5)$$

where W_a —speed of wind over the waterbody, α_w —wind direction, ρ_a —air density, θ —coefficient of hydraulic resistance on the water surface. Chezy coefficient accounts for energy loss needed to overcome friction forces dependant of degree of roughness and transversal sizes of the bed (or waterbody depth). In order to determine Chezy coefficient we used Manning’s formula.

Let’s expand the system by the following boundary conditions (1)–(4):

- ✓ for closed (coast) boundaries, the boundary condition is that the normal component of the vertically integrated velocity vanishes: $\bar{U}_n = 0$;
- ✓ at the open-sea boundary, the normal component of the velocity cannot vanish and so radiation type of boundary condition is generally used (condition of the gravity waves radiation):

$$\bar{U}_n = \zeta \sqrt{\frac{g}{H}}, \text{ if } \bar{U}_n \geq 0 \quad \text{and} \quad \begin{cases} \bar{U}_n = \zeta \sqrt{\frac{g}{H}}, \text{ if } \bar{U}_n \leq 0, \\ \bar{U}_t = 0, \end{cases} \quad (6)$$

where \bar{U}_t is the tangential component of the vertically integrated velocity;

- ✓ at the river boundary energy condition was used:

$$U_n^2 + g\zeta = \frac{Q_{river}^2}{W_{river}^2 h_{river}^2}, \quad (7)$$

where Q_{river} is the intensity of flow, W_{river} is the width of the river station, h_{river} is the average depth in the river station.

Arakawa’s C-grid and implicit, staggered in space and time finite-difference scheme with using of the alternate direction technique were used for digital integration of system equations (1)–(4) at chosen bounding conditions. Algorithm of solving the task was thoroughly described in (Podgornyj, 2003). Zero values of speeds and level (quiescent state) were used as initial conditions. Calculations have been performed on a uniform rectangular grid 500×500 m. Calculations have started from the moment of clearing of the Neva Bay from ice and continued until October 31. Change of hydrometeorological situation over the water body took place every day of the model time. Speeds and directions of the wind were given according to the daily-averaged data of immediate meteorological observations and were equal in each point of the grid area. Time increment for numeric integration was taken as equal to 30 s. During the change of wind situation over the waterbody initial fields were values of current speed and level elevation obtained in the preceding step.

Modeling was performed both for natural and project conditions i.e. with the flood control facilities’ complex of St.-Petersburg. In the project conditions North and South gates of the Neva Bay are blocked by dikes with six water discharge (B1–B6) and two navigation (C1, C2) openings. According to project conditions 54 percent of discharge passes through the North gate and



46 percent—through the South gate (Rukhovets, 1982). Current speeds in the grid's nodes corresponding to water discharge and navigational openings were calculated according to these data. Areas of these openings are given according to (Baidin, 1965). Water discharge of Neva (1,900 m³/s on average), Discharges for the rivers Small Neva (400 m³/s on average) and the Small Nevka (300 m³/s on average) were taken from the data of perennial observations (Baidin, 1965, Menshutkin, 1997).

3. Results

Modeling data confirm conclusions obtained earlier from results of immediate measurements and combined study of spatial-temporal variability of current structure, local wind and level fluctuations. Calculations show that several characteristic zones may be allocated in the Neva Bay according to the development of hydrodynamic processes: zones of Neva waters transit in the central part of the bay; zones of slow water cycle south of the marine canal and in the south-eastern part of the bay; shallow coastal zones. It is also shown that few zones of cyclonic and anticyclonic circulations may be formed at rather strong winds (more than 4 m/s on average) of corresponding direction. At winds of any direction with speeds of less than 3.5 m/s the influence of the Neva River drainage is the determining factor in current structure formation. No circulation zones are formed and currents in the Neva Bay conform to drainage regime of water transfer, virtually. Exceptions are only seen in the shallow south-eastern part of the Neva Bay where current formation depends on the wind speed, elevation gradients of free surface and friction forces and virtually non-dependent of drainage component. That is why circulation formations in this part of the bay are present even at small wind speeds and water transfer direction (cyclonic or anticyclonic) depends on the wind direction and morphometric features of this area. Examples of current field calculations for natural and project conditions are shown on Fig. 2.

Calculations show that current field structure and their quantitative indices for projects conditions are insignificantly different from current fields in natural conditions. These changes bear local character and are seen within

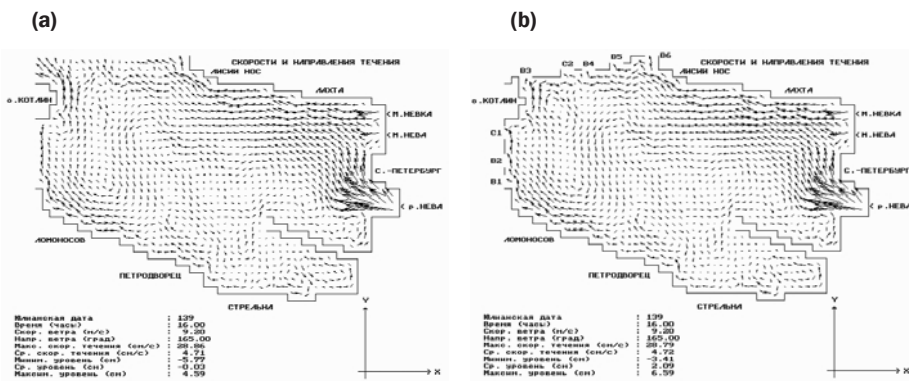


Fig. 2. Examples of current field calculations for natural (a) and project conditions (b).



3–4 km from flood control facilities. They are mainly manifested in appearance and more pronounced structure of cyclonic and anticyclonic vortexes. Zones with such vortexes are most frequently formed near Kotlin island and water discharge opening B3.

References

- Baidin, S. S. (1965) *Hydrology of Neva's mouth area*. Moscow: Gidrometeoizdat (in Russian).
- (1997) Unstudied types of currents in bays. *Wat. Resources* **24(4)**:413–416 (in Russian).
- Belyshev, A. P. & Preobrazhenskii, L. Yu. (1988) Structure of the Neva Bay and east part of the Gulf of Finland currents. Study of waterbodies' system Lake Ladoga—river Neva—Neva Bay and east part of the Gulf of Finland. In: *Proc. GGI*, 321, 4–16 Leningrad: Gidrometeoizdat (in Russian).
- Klevannyi, K. A. (2002) Floods in Saint-Petersburg at unfinished flood control facilities complex. *Proc. AS. Geographical series* **2**:80–88 (in Russian).
- Menshutkin, V. V. (1997) *Neva Bay—experience in modeling*. St.-Peterburg: Borey Print (in Russian).
- Nezhikhovskii, R. A. (1981) *River Neva and Neva Bay*. Leningrad: Gidrometeoizdat (in Russian).
- Podgorniy, K. A. (2003) *Mathematical modeling of freshwater ecosystems of unstratified waterbodies (algorithms and numerical methods)*. Rybinsk: Rybinsk Press House (in Russian).
- Rukhovets, L. A. (1982) Mathematical modeling of water cycle and additives' distribution in the Neva Bay. *Meteorology and hydrology* **7**:78–87 (in Russian).
- Rumyantsev, V. A. & Drabkova, V. G., eds. (1999) *Gulf of Finland in conditions of anthropogenic impact*. St.-Peterburg (in Russian).

Positive and negative setup of water level in the mouth of the Don River: research and prediction

Ekaterina Ponomarenko

Abstract

Since 2007 year in Southern Scientific Center of Russian Academy of Sciences water level observations were carried out in the mouth of the Don River to study hydrological regime. Measurements are performed by standard hydrological equipment (depth-gauge, float level indicator) and hardware-software system of the data gathering. The conditions of level rises and recessions and dependence of these phenomena on synoptic conditions are discovered. Level dynamics forecast is made according to this dependence by analog method. This method predicts the scenario of positive and negative level setup development (time duration of level rises and recessions, time of coming of extreme values, value of level rise and recession).

В Южном научном центре Российской академии наук с целью изучения гидрологического режима с 2007 г. ведутся наблюдения за уровнем воды в дельте Дона. Измерения проводятся с помощью стандартного гидрологического оборудования (гидрологической рейки, поплавкового уровнемера), а также специально разработанного программно-аппаратного комплекса сбора данных. По результатам наблюдений выявлена степень зависимости стонно-нагонных явлений от метеоусловий (направления и скорости ветра), на основании которой делается прогноз динамики уровня по методу аналогов, который позволяет предсказать сценарий развития стонно-нагонных явлений (время начала и продолжительность сгона или нагона, время наступления экстремумов уровня, величину подъема или спада уровня).

Hydrological processes in the delta region and estuary are extremely complex. Level regime is formed under the influence of long-term fluctuations of river flow that create standing of the high or low levels, against which there are fluctuations caused by seasonal changes in river flow. Short-term (a few

Ekaterina Ponomarenko (✉)
Southern Scientific Centre Russian Academy of Science, Rostov-on-Don, Russia
e-mail: katarina777787@mail.ru



hours or days) level fluctuations are caused by winds (wind with a westerly component causes an influx of water from the Taganrog Bay and rising of level, winds with an eastern component causes an eviction of water and falling of level). Delta hydrological regime has no heavy seasonal fluctuations because of sea influence. Level extremum in coastal zone (positive and negative setup) are caused by wind.

Since 2007 year in Southern Scientific Center Russian Academy of Sciences water level observations were carried out in the mouth of the Don River to study hydrological regime. Measurements are performed by standard hydrological equipment (depth-gauge, float level indicator) and hardware-software system of the data gathering (HSSDG). Using HSSDG allows to realize continuous remote monitoring of the level. Data are transmitted via DAC/ADC to SSC RAS. Level measurement are carried out using a pressure sensor at intervals of 5 min, to trace the changes of the water surface and level in the delta area for a full cycle of rises and recessions phenomena. To date time we have accumulated data of 6,896 measurements by depth-gauge, 92,766 measurements by float level indicator, 51,885 measurements by HSSDG.

The analysis of the accumulated data is carried out, the periods of water rises and recessions are defined. Situation, when the level was raising during more than 10 h under condition of westerly winds and low pressure was defined as positive setup of level (Fig. 1). Situation, when the level was falling during more than 10 h under condition of easterly winds and high pressure was defined as negative setup of level (Fig. 1).

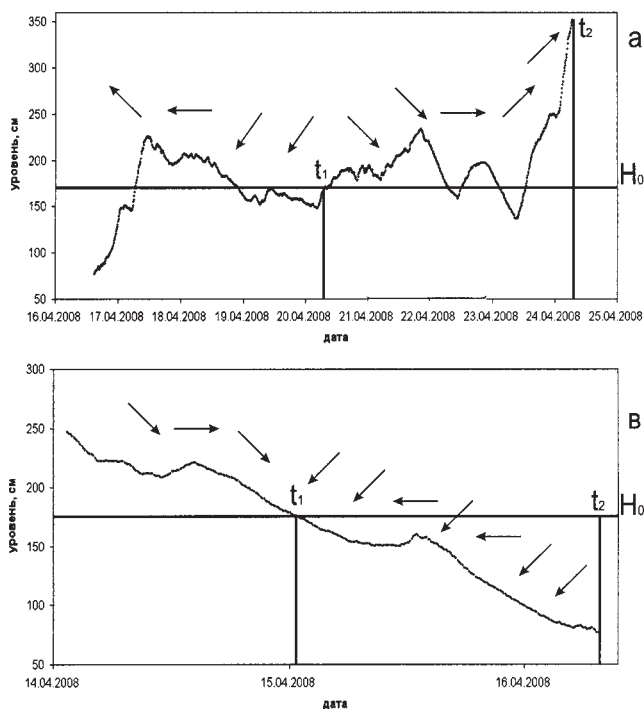


Fig. 1. Example of situations: (a)—positive water level setup, (b)—negative water level setup (recession). H_0 —average level, t_1 —beginning of the phenomenon, t_2 —ending of the phenomenon, the arrows show the direction of the wind.



During the monitoring period (from May 31, 2007 to July 23, 2009) share of positive setup was 55 percent, negative setup—45 percent. The increase of positive setup quantity was caused by decrease of eastern winds and increase of western winds during the year due to increase in frequency of the western and northern forms of atmospheric circulation.

For positive and negative setup periods information about a meteorological situation in the area of research was analyzed (analysis of sea level pressure, wind speed and direction). The conditions of rises and recessions phenomena formation and the degree of dependence on synoptic conditions were discovered.

Positive setup of level (Fig. 2) is characterized by low pressure (average 1,007 hPa) and westerly wind. The wind changes direction at an average of 1–3 h before level rising, the pressure falls by an average of 11 hPa just before the level rising. Duration of phenomenon is an average of 33 h (from 10 to 78 h) and the level rise value is an average of 88 cm (40 to 214 cm).

Negative setup of level (Fig. 3) is characterized by increased pressure (average 1,015 hPa) and eastern wind. The wind changes direction for on average 1 h before the fall of the level, pressure increased by on average 8 hPa. Duration of phenomenon is an average 44 h (from 12 to 88 h) and the magnitude of the level recession is an average of 86 cm (from 27 to 150 cm).

Statistical treatment of the positive and negative setup characteristics was carried out. In the most cases (18.8 percent) magnitude of level rise is up

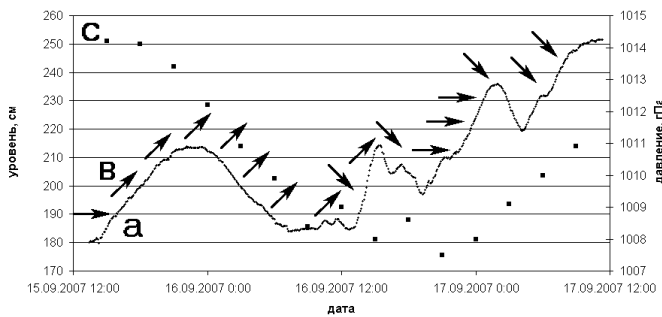


Fig. 2. Example of positive level setup for the period of 15.09.2007(12 a.m.)–17.09.2007(12 a.m.): (a) level; (b) wind direction; (c) pressure. Left axis—level in cm, right axis—pressure, gPa.

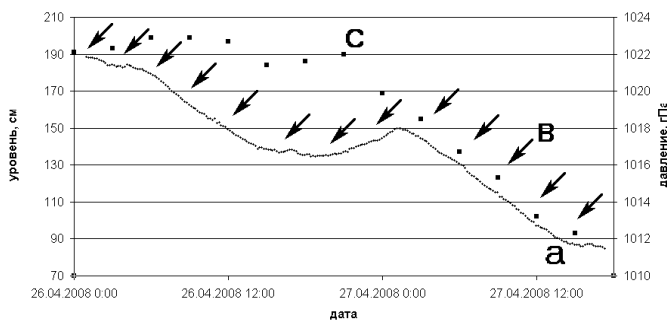


Fig. 3. Example of negative level setup for the period of 26.04.2008(12 p.m.)–27.04.2008(12 a.m.): (a) level; (b) wind direction; (c) pressure. Left axis—level in cm, right axis—pressure, gPa.



to 90 cm, the maximum magnitude (214 cm) occurs in 3 percent of cases. In the most cases (15.6 percent) the value of the maximum level is in the range 230–260 cm, in 3 percent of cases the level reaches 360 cm. In the most cases (31.3 percent) duration of phenomenon is from 30 to 40 h, the maximum duration (80 h) meets in 6.3 percent of cases. In the most cases (46.9 percent) rate of level rise is 0.0005–0.001 m/s, maximum level rise rate (up to 0.0035 m/s) occur in 3 percent of cases. The most common (28.01 percent) are situation when the average wind speed is from 3 to 4 m/s, maximum average wind speed—6 m/s observes in 6 percent of cases.

In the most cases (18.8 percent) magnitude of level drop is from 80 to 90 cm, the maximum magnitude (150 cm) occurs in 3.8 percent of cases. In the most cases (19.2 percent) the value of the minimum level is in the range 120–110 cm, in 7.7 percent of cases the level reaches 75 cm. In the most cases (26.9 percent) duration of phenomenon is from 30 to 40 h, the maximum duration (80–90 h) meets in 11.5 percent of cases. In the most cases (34.6 percent) rate of level fall is 0.0006–0.0008 m/s, maximum level fall rate (up to 0.0014 m/s) occur in 3.8 percent of cases. The most common (30.8 percent) are situation when the average wind speed is from 5 to 6 m/s, maximum average wind speed—9 m/s observes in 7.7 percent of cases.

Distribution of positive and negative level setup during the year corresponds with the distribution of east and west winds. Situations, during which the level reaches extremes in a short period of time, were attributed to the extreme.

During the monitoring period one extreme positive setup of level was marked in April 2008. Level increased on 215 cm during 21 h and 40 min. Level rise speed was of 0.0027 m/sec. Extreme negative setups of level were not registered in the observation period.

Level dynamics forecast (Fig. 4) is made according to level dependence from synoptic conditions (wind speed and direction, the pressure at sea level) by analog method. This method allows to predict the scenario of positive and negative level setup development (time of rises and recessions beginning, duration, extremum time on, rises and recessions value).

Statistical processing of results of forecasting was made. The average correlation coefficient of real value and the projected level is 0.86. In 14 percent of cases for falling, and 10 percent for the raising of level forecast was executed without error. The average prediction error is from –24 to –5 cm. Prediction errors are bound up with the quality of meteorological data.

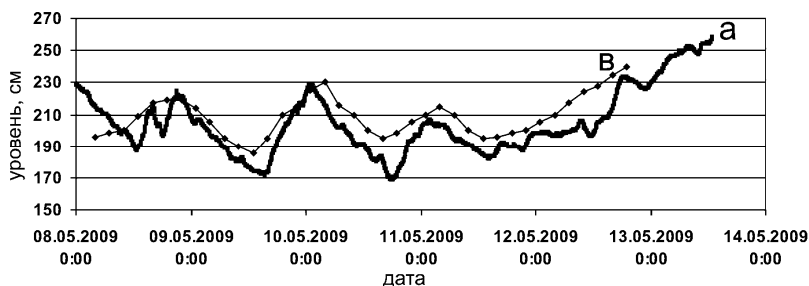


Fig. 4. Example of level forecast. (a) real value; (b) projected level.

Transformation of the wind waves penetrated into a shallow lagoon: Vistula Lagoon case study

Andrey Sokolov, Boris Chubarenko

Abstract

Using numerical modeling the option of penetration of wind waves from the opens sea into the Vistula lagoon is discussed.

Возможность проникновения морских волн в Вислинский залив обсуждается на основе данных численного моделирования.

1. Introduction

Baltiysk Strait connects the Baltic Sea with the Vistula Lagoon (Fig. 1). It is continuing by Kaliningrad Marine Canal, the navigation route passing along the northern shore of the Vistula Lagoon towards the Kaliningrad port located 43 km to the East in the Pregolya River. The Strait is bounded by concrete piers, which are almost parallel and directed from the south-east to the north-west direction. A distance from an outer end of the breakwater to arc-like moles, which cover Baltiysk port from the lagoon side, is about 2 km. A width of the strait is about 400 m and its depth changes from 13–14 m near the entrance (a deep depression in front of the outer end of the breakwater is not taken into consideration) to 10–12 m near the arc-like moles.

There are different opinions about the marine waves influence on a wind-wave situation in the lagoon. According to (Lasarenko & Majewski, 1971) wave field in the lagoon is affected by internal factors only. Wave measurements in the strait (Chepikova & Chubarenko, 2000) have shown, that wave amplitude monotonically damps to some fixed value during wave propagation along the channel. In the other hand, automatic wave measurements near the Nasypnoi Island (Ambrosimov, 2009) show signals in the wave records, which can evident about sea waves penetration into the lagoon.

Andrey Sokolov, Boris Chubarenko (✉)
P.P. Shirshov Institute of Oceanology RAS, Atlantic Branch, Kaliningrad, Russia
e-mail: ans@sntp.ru



Fig. 1. Baltiysk strait is the only strait that connects Vistula Lagoon and Baltic Sea. It is the entrance to the fairway from Baltic Sea to Kaliningrad.

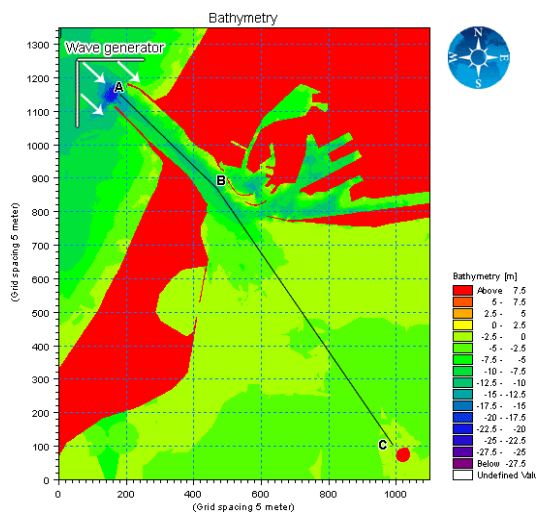
2. Study area and methods

The aim of study was a numerical simulation of a penetration of marine wind waves into the Vistula Lagoon. A Mike 21 BW (Mike 21 BW, 2005) module (DHI software environment) was used for simulations.

The source of waves (1 m significant wave height, JONSWAP spectrum) was placed near the outer end of the Baltiysk Strait breakwaters. The waves propagate from the north-west direction. The direction was chosen to obtain the best conditions for the penetration into the lagoon. The model domain (with spatial grid step of 5 m) covers the area of 5,500×6,750 m, from outer end of the Baltiysk Strait to the Nasipnoi Island in the middle of the Vistula Lagoon. The bathymetry is shown on Fig. 2.

According to an analysis (Riabkova, 1987) of the experimental data (GMS Baltiysk, 1975–84) a period of waves with maximum height near the outer end of the breakwater is about 9 s. Sometimes we can see ripple waves with a period of 13 s. And one time in a century an appearance of 20 s period waves is possible.

Fig. 2. The computational area bathymetry from the outer end of the breakwater to the Nasipnoi Island in the middle of the lagoon.



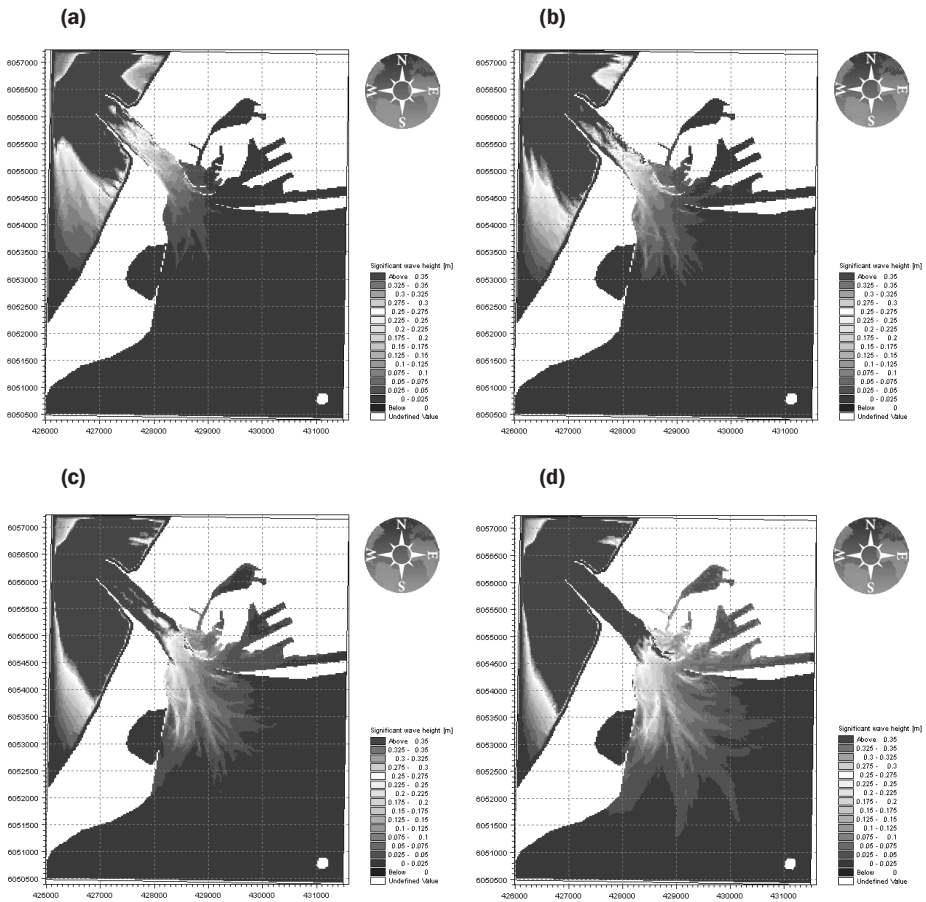


Fig. 3. Steady state wave fields in the study area for waves with periods of 7 (a), 9 (b), 13 (c) and 20 s (d).

Modeling simulations of waves with the periods of 7, 9, 13 and 20 s shows detect dependence between the waves period and waves propagation into the lagoon. Fig. 3 represents wave fields and Fig. 4 dependences of significant wave height along the ABC profile (Fig. 2).

3. Conclusions

Simulation shows that amplitude of waves with the period of 9 s spreading through the strait decreases by 60 percent at 1 km distance from their source. At the distance of 2 km from the entrance (just before the arc-like moles) the wave height is less than 20 percent of incoming waves. In the middle of the lagoon, near the Nasipnoi Island the wave is dumped by 100 times. The waves reach the Island in about 20 min. Thus we can suppose that the influence of marine waves with the period of 9 s or less on the wave climate in the lagoon may be neglected.

On the other hand, long-period waves can penetrate into the lagoon much more efficient. In Figs. 4c and 4d we can see, that long-period waves damp

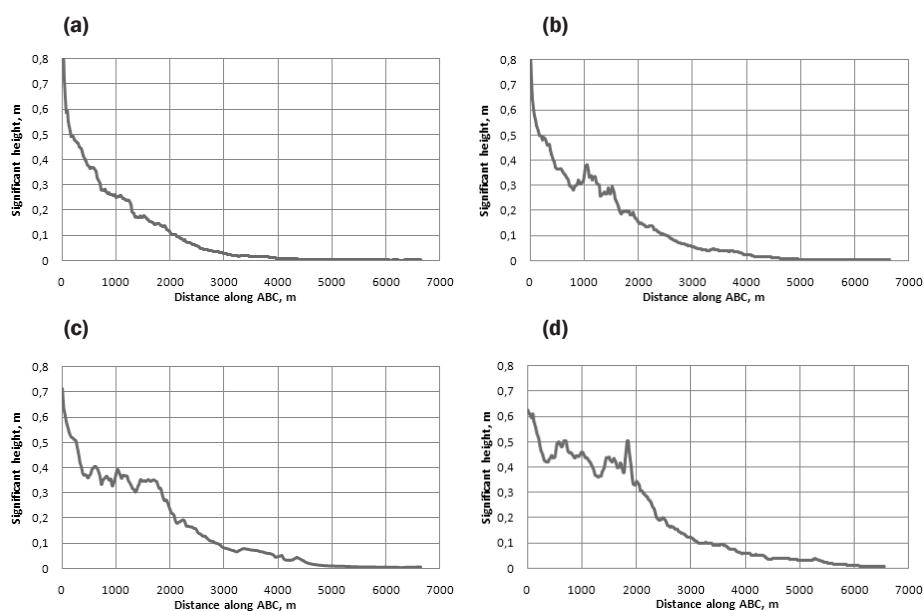


Fig. 4. Dependences of significant wave height along the ABC profile for waves with periods of 7 (a), 9 (b), 13 (c) and 20 s (d).

in the strait considerably weaker than short-period waves. This is especially true for waves with the period of 20 s. We can see that at a 2 km distance (just before arc-like moles) the wave damping is about only 2 times (in comparison with the incoming wave height). Comparing the significant wave height near the Nasipnoi Island for waves with different periods, we obtained that waves with the period of 20 s has the height of about 3–4 cm there, and therefore they can be detected by instrumental measurements. At the same time, waves with the period of 9 s have amplitude less than 1 cm.

Anyway simulation shows that an influence of marine waves on the wave climate in an internal part of the lagoon is not essential.

Study was partly supported by grants Nos. 08-05-01023 and 08-05-92421 of the Russian Foundation of Basic Researches.

References

- Ambrosimov, A. K. (2009) *The characteristics of wind waves in the Vistula Lagoon for the period of 15 of May till 17 of June 2009*. Technical report. Atlantic Branch of P.P. Shirshov Institute of Oceanology of Russian Academy of Sciences. Kaliningrad.
- Chepikova, I. S. & Chubarenko, B. V. (2000) *About surface waves parameters in the Baltijsk Strait (Vistula Lagoon, Baltic Sea)*. Technical report on field expedition. Atlantic Branch of P.P. Shirshov Institute of Oceanology of Russian Academy of Sciences. Kaliningrad.
- Lazarenko, N. N. & Majewski, A., eds. (1971) *Hydrometeorological regime of the Vistula Lagoon*. Leningrad: Hydrometeoizdat (in Polish and Russian).
- MIKE 21 BW (2005) Boussinesq Waves Module User Guide. DHI Software.
- Riabkova, O. I. (1987) *Dynamics of the coast of Sambian Peninsula and Curonian Spit in a view of the coastal protection problems*. PhD Thesis. Moscow State University, Geographical Faculty.

Water transparency, total suspended solid matter and particulate organic carbon of the Azov Sea (field observations in 2008–09 years)

Vera Sorokina, Vasiliy Povazhnyy, Filipp Gonsales

Abstract

The results of field observations carried out in 2008–09 in the inner part and the coastal zone of the Azov Sea are given. A linear regression between the transparency (x , m) and the total suspended solids concentration (TSS) (y , mg l⁻¹) in the surface water (0–0.3 m) is established: $y=13.02 \cdot x^{-1.22}$. Seasonal dynamics of TSS and particulate organic carbon (POC) is shown: the lowest values are typical for winter and early-spring period; in summer the concentration of TSS becomes higher and the relative share of organic component is increases, due to phytoplankton activity; in autumn there is a tendency of TSS to increase, basically because of increase of hydrodynamics and a tendency of POC to decrease. In general the decrease of suspended solids and particulate organic matter from the Taganrog Bay to the Black Sea. The average TSS for the whole period of field observations varied insignificantly (around 125–281 mg l⁻¹) in the coastal waters of the Taganrog Bay.

В работе приведены результаты экспедиционных исследований прозрачности и содержания взвешенных веществ в водах Азовского моря, выполненных в 2008–2009 гг. Установлена связь прозрачности (x , м) и концентрации взвешенного вещества в воде (TSS) (y , мг л⁻¹) поверхностного горизонта (0–0.3 м) Азовского моря: $y=13.02 \cdot x^{-1.22}$. Показана сезонная динамика TSS и взвешенного органического углерода (POC): их относительно низкие значения характерны для зимнего (средняя концентрация TSS — 5 мг л⁻¹, POC — 0,66 мгC_{орг} л⁻¹) и ранневесеннего периодов (TSS — 11 мг л⁻¹, POC — 1,3 мгC_{орг} л⁻¹); в летний сезон концентрация TSS увеличивается (20–27 мг л⁻¹) и в его составе возрастает относительная до-

Vera Sorokina, Vasiliy Povazhnyy (✉)
Southern Scientific Centre of Russian Academy of Science, Rostov-on-Don, Russia
e-mail: sorokina@ssc-ras.ru
Filipp Gonsales (✉)
Southern Federal University, Rostov-on-Don, Russia



ля органики (ПОС 2,5–2,8 мгС_{орг} л⁻¹) вследствие активного развития фитопланктона. Осенью наблюдается тенденция увеличения TSS (средняя концентрация — 21–36 мг л⁻¹) в основном из-за увеличения гидродинамики и уменьшения ПОС (2,4 мгС_{орг} л⁻¹). Наблюдалось общее уменьшение взвеси и ее органической составляющей по ходу движения от Таганрогского залива в Черное море. В прибрежных водах Таганрогского залива средние значения TSS за весь исследуемый период изменялись незначительно (в пределах 125–281 мг л⁻¹).

1. Introduction

Data on the turbidity and dynamics of the sea water masses can be very important in the research of production and sedimentary processes. Unfortunately, the data on the turbidity of the Azov Sea available are very poor now. Measurements of the transparency of the water are outnumbering those on turbidity. D. G. Panov and M. K. Spichak tried to determine regression between the transparency and the turbidity in the waters of the Azov Sea (Panov & Spichak, 1961). To do this, they used transparency maps for the period 1952–59 as the source data. Then the total suspended solid matter concentration in the sea water was determined according to the graphical relation between the transparency and the turbidity of the water for the same period. The authors do not give coefficients of equation in their work. We managed to find only one transparency and turbidity regression for the area of Kerch Strait in the reference book (Mankovskiy et al., 2009).

2. Study area

The data on the total suspended solid matter concentration (TSS), concentration of the particulate organic carbon (POC) and the transparency of the Azov Sea were taken from the field observations carried out by the Southern Scientific Center of RAS (SSC RAS) for the period 2008–09.

3. Methods

The measurements of the transparency of the water were made with the Secchi disk. The particulate organic carbon concentration was estimated in accordance with the manual “Methods of hydrochemical studies of the ocean” (Bordovskiy & Ivanenkov, 1978). Water samples were taken with Molchanov water sampler and filtered through fiberglass filters GMF 5 (pores size 0.7 μm), after that the makeweight (suspended solids) on the filter and the total suspended solids concentration in the sampler were determined in the interdisciplinary analytical laboratory of the SSC RAS. The particulate organic carbon was determined with “wet oxidation” of potassium dichromate.

4. Results and Discussion

The linear regression between the transparency and the total suspended solid matter concentration in the water (Fig. 1) was determined on the basis of the expedition research and can be described by the formula:



$$y = 13.02x^{-1.22}$$

where x —transparency, m; y —the TSS in the surface water (0–0.3 m) of the Azov Sea, mg l^{-1} .

The dynamics of TSS и POC in the Azov Sea was researched from June 2008 till December 2009. For this period during 20 expeditions 235 samplers were made: 91—in the Taganrog Bay from the research vessel (r/v) “Professor Panov” during different seasons; 58 samplers—during spring and autumn expeditions on the r/v “Deneb” in the Azov Sea and in the north-eastern area of the Black Sea; 26 samplers—from icebreaker “Captain Demidov” for the period January–February; 60 samplers—during coastal expeditions.

The average concentration of TSS under the ice field of the Taganrog bay and in the north-eastern area of the Azov Sea was the lowest (5 mg l^{-1}) because of the absence of vertical interfusion. The concentration of POC fluctuated between $0.23\text{--}1.69 \text{ mgC}_{\text{org}} \text{ l}^{-1}$, when the average values— $0.66 \text{ mgC}_{\text{org}} \text{ l}^{-1}$.

The Taganrog Bay and the inner part of the sea differ from each other in hydrological and hydrochemical regimes, organic life, and by the main sources of sediment material etc. The factors mentioned affect the concentration of TSS as they are interacting and the influence of every factor changes at every moment that leads to fluctuations of the scores and of the substance structure of the suspended solids. In the Taganrog Bay TSS and POC changed during the year in the wide range ($5\text{--}120 \text{ mg l}^{-1}$ и $0.26\text{--}6.92 \text{ mgC}_{\text{org}} \text{ l}^{-1}$). The lowest values were observed in winter (TSS— $1.5\text{--}15 \text{ mg l}^{-1}$; POC— $0.23\text{--}1.69 \text{ mgC}_{\text{org}} \text{ l}^{-1}$) and in March (TSS— $5.4\text{--}16 \text{ mg l}^{-1}$; POC— $0.26\text{--}1.96 \text{ mgC}_{\text{org}} \text{ l}^{-1}$) with insignificant vertical interfusion and phytoplankton activity. For the period spring–summer the relative concentration both TSS and POC increases, reaching in June–July $20\text{--}27 \text{ mg l}^{-1}$ и $2.5\text{--}2.8, \text{ mgC}_{\text{org}} \text{ l}^{-1}$. In autumn (September–October) the concentration of TSS remains high (on the average $21\text{--}36 \text{ mg l}^{-1}$), basically because of increase of hydrodynamics, and there is a tendency of POC to decrease ($2.4 \text{ mgC}_{\text{org}} \text{ l}^{-1}$).

The similar mechanisms of seasonal changes of the suspended solids are also typical for the inner part of the sea. The difference was a total decrease

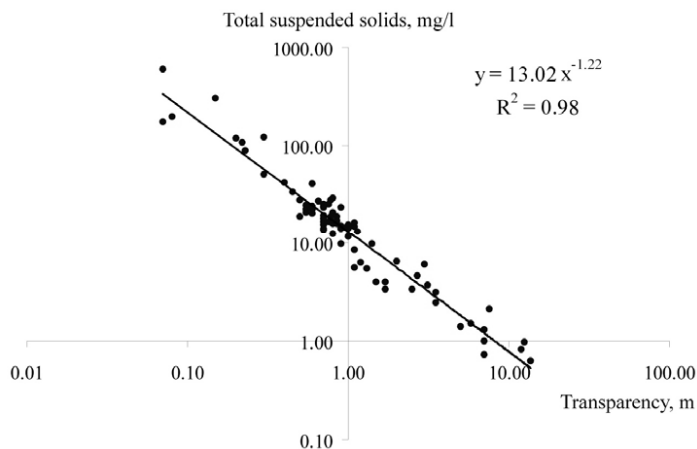


Fig. 1. A linear regression between the transparency (x , m) and the TSS (y , mg/l) in surface water (0–0.3 m) of the Azov Sea.



of the suspended matter level and its organic components from the Taganrog Bay to the Black Sea. For example, in April 2009, the average TSS and POC concentrations in the Azov Sea were 16.5 mg l^{-1} and $0.79 \text{ mgC}_{\text{org}} \text{ l}^{-1}$, while in the north-eastern area of the Black Sea— 1.8 mg l^{-1} и $0.1 \text{ mgC}_{\text{org}} \text{ l}^{-1}$.

Together with the marine expeditions, the study of the coastal area of the Taganrog Bay was performed. The average TSS values changed considerably for the period of the investigation, fluctuating from $125\text{--}281 \text{ mg l}^{-1}$, with the extreme values 2.4 and 851 mg l^{-1} .

5. Conclusions

A linear regression between the transparency and the total suspended solid matter concentration in the surface water (0–0.3 m) of the Azov Sea is established on the basis of field observations carried out in 2008–09. Seasonal dynamics of TSS and POC is shown. The lowest values are typical for winter (average concentration of TSS— 5 mg l^{-1} , POC— $0.66 \text{ mgC}_{\text{org}} \text{ l}^{-1}$) and early-spring period (TSS— 11 mg l^{-1} , POC— $1.3 \text{ mgC}_{\text{org}} \text{ l}^{-1}$); in summer the concentration of TSS becomes higher ($20\text{--}27 \text{ mg l}^{-1}$) and the relative ratio of organic component increases (POC $2.5\text{--}2.8 \text{ mgC}_{\text{org}} \text{ l}^{-1}$), due to phytoplankton activity. In autumn there is a tendency of TSS to increase (average concentration— $21\text{--}36 \text{ mg l}^{-1}$, basically because of increase of hydrodynamics) and a tendency of POC to decrease ($2.4 \text{ mgC}_{\text{org}} \text{ l}^{-1}$). In general the decrease of suspended solids and particulate organic matter from the Taganrog Bay to the Black Sea is observed.

Acknowledgements

The research was carried out in the Southern Scientific Center of RAS in the frame of the Grant of the Russian Federation President MK-1355.2009.5 “The research of the reasons of organic carbon increase in the Azov Sea ecosystem”, Presidium program of RAS “Fundamental problems of oceanology: physics, geology, biology, ecology” the project “Organic carbon in the Azov Sea ecosystem as a possible indicator of contemporary climate change and anthropogenic activities” and the Federal Target Program “Scientific and scientific-pedagogic staff for the innovative Russia in 2009–2013” (reference No. 2009-1.1-155-070-008).

References

- Bordovskiy, O. K. & Ivanenkov V. N., eds. (1978) *Methods of hydrochemical studies of the ocean*. Moscow: Nauka.
- Mankovskiy, V. I., Soloviov, M. V., Mankovskiy, E. V. (2009) *Hydrooptical characteristics of the Black Sea*. Reference book. Sevastopol: MHI NASU.
- Panov, D. G. & Spichak, M. K. (1961) About sedimentation conditions of the Azov Sea. In: Strakhov, N. M., ed., *Contemporary sediments of the seas and oceans*, 512–520. Publishing house of AN USSR.

Plankton pigment composition of the Vistula and Curonian Lagoons in condition of salinity variable and algae blooms

Vasilina Stepanitsova, Sergey Alexandrov

Abstract

Curonian and Vistula Lagoons are the largest lagoons of the Baltic Sea. Lagoon ecosystems are strongly influenced by hydrological conditions (varying salinity of the interaction of sea and river waters), “blooming” of water. Information about the spatial and temporal variability of phytoplankton pigments is an indicator of eutrophication and water pollution. Pigments of phytoplankton were studied monthly from April to October 2009 at 9 stations in the Vistula Lagoon and 9 stations in the Curonian Lagoon. Concentration of pigments (chlorophyll *a*, *b*, *c*) was determined by spectrophotometry. The seasonal and spatial variations of pigments in the lagoon ecosystems have been caused by seasonal succession of phytoplankton (including “algae blooms”) and changes in hydrologic conditions (salinity, temperature).

Куршский и Вислинский заливы — крупнейшие лагуны Балтийского моря. Экосистемы лагун находятся под сильным воздействием гидрологических условий (изменяющаяся соленость в результате взаимодействия морских и речных вод), «цветения» воды. Информация о пространственно-временной изменчивости содержания пигментов фитопланктона служит индикатором эвтрофирования и загрязнения вод. Пигменты фитопланктона изучались ежемесячно с апреля по октябрь 2009 г. на 9 станциях в Вислинском заливе и 9 станциях в Куршском заливе. Содержание пигментов (хлорофилл *a*, *b*, *c*) определялось спектрофотометрическим методом. Показаны сезонные и пространственные изменения пигментов в лагунных экосистемах, обусловленные сезонной сукцессией фитопланктона (в т. ч. «цветением» воды) и изменением гидрологических условий (соленость, температура).

Vasilina Stepanitsova, Sergey Alexandrov (✉)
Atlantic Research Institute of Marine Fisheries and Oceanography (AtlantNIRO),
Kaliningrad, Russia
e-mail: v.stepanitsova@yandex.ru

TOPIC 3

Interaction between coastal zone and open sea

Lectures

Thermally driven interaction between coastal and open sea areas

Irina Chubarenko

Abstract

Increase or decrease of water temperature with the off-shore distance, often called a differential costal heating, is a typical feature of natural water bodies. It results in large-scale horizontal water exchange: if coastal waters become heavier than the open-sea ones, they sink along underwater slopes down to approximately the level of their density; if they become lighter—they are pushed out of the coastal zone by heavier open-sea waters. The mechanism of the formation of horizontal temperature/density gradients above underwater slopes due to heating/cooling from the surface is considered. It is shown that the time required for formation of the gradients is rather small (tens of minutes for a thermocline depth of tens of meters), but the development of the corresponding flows may not be accomplished even in a day long cycle. The time dependence of the horizontal water exchange between the shallow and deep areas is analytically treated. The spatial scale of the problem is the main parameter that defines the resulting quasi-stationary value of the flow rate. The joint analysis of the published field, laboratory, and numerical data of many authors in the range of the above-slope depths of $10^{-2} < d < 3 \cdot 10^2$ m ($d \leq D$, where D is the thickness of the upper thermally active layer of a basin) indicates that the relation between the value of the horizontal quasi-stationary volumetric flow rate and the local depth looks like $Q = 0.0013d^{1.37}$ ($R^2 = 0.96$). The horizontal convective water exchange is shown to be generally two-layered, ageostrophic, and exhibits its maximum flow rate at the deepest part (end) of the slope. The process is illustrated by various field examples, laboratory experiments and numerical modeling results.

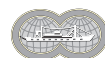
Irina Chubarenko (✉)
P. P. Shirshov Institute of Oceanology RAS, Atlantic Branch, Kaliningrad,
Russia
e-mail: irina_chubarenko@mail.ru



Падение или рост температуры воды по мере приближения к берегу (дифференциальный прибрежный прогрев) — типичная черта прибрежной зоны любого водоема. Исследуется крупномасштабный горизонтальный водообмен, вызываемый этим фактором: если прибрежные воды в процессе теплообмена становятся тяжелее вод открытого моря — они опускаются вдоль прибрежных подводных склонов до уровня своей изопикнической поверхности, если легче — вытесняются ими. Рассматривается механизм формирования горизонтальных градиентов температуры/плотности. Показано, что время их возникновения достаточно коротко (десятки минут при глубине залегания термоклина в десятки метров), но установление соответствующих течений может не достигаться даже в суточном цикле. Основным параметром, определяющим величину объемного расхода в квазистационарном состоянии Q , оказывается линейный масштаб задачи. Совместный анализ натуральных данных, результатов лабораторных и численных экспериментов многих авторов в диапазоне глубин над склоном $10^{-2} < d < 3 \cdot 10^2$ м ($d \leq D$, D — толщина верхнего теплоактивного слоя водоема) указывает на зависимость Q от локальной глубины вида $Q = 0.0013d^{1.37}$ ($R^2 = 0.96$). Горизонтальный конвективный водообмен двухслоен, агеострофичен и имеет максимум расхода над концом склона. Приводятся примеры из натуральных наблюдений, лабораторные эксперименты, результаты численного моделирования.

1. Introduction

Differential coastal heating or cooling is just an ordinary routine of any natural basin. The viewpoint concerning the role of horizontal convective flows that arise within the coastal zone of lakes, seas, and oceans due to this feature has considerably changed during the last decades (see, for instance, (Farrow, 2004, Fer et al., 2002, Ivanov et al., 2004)). It was previously believed that such temperature gradients are local, unstable, and can be formed merely in the absence of wind, and any considerable motions emerge only in the close vicinity of sources or sinks of heat (Huang, 1999). However, the field data accumulated to date do not corroborate this viewpoint. Differential coastal heating (of various intensity, of positive or negative sign) frequently occurs on a daily scale (Adams & Wells, 1984, Farrow, 2004, Fer et al., 2002, James & Barko, 1991, Monismith et al., 1990), is persistently traceable at synoptic averaging (Tikhomirov, 1982, Chubarenko et al., 2007a, 2007b, Ivanov et al., 2004), and is explicitly available in the seasonal cycle (Filippov, 1968, Shimaraev, 1977, Tikhomirov, 1982, Titov, 2006). The horizontal temperature gradients result in horizontal gradients of the density and pressure that generate the mesoscale water exchange between the coastal and deepwater basin areas. This way, field data indicate that the horizontal temperature gradients above the underwater slopes cause the “cascading” (Fer et al., 2002, Ivanov et al., 2004), thermal bar (Shimaraev, 1977, Tikhomirov, 1982), and day/night circulation (Farrow, 2004). To date, different types of water motion caused by temperature difference at the horizontal boundary of a basin (be it the surface or the bottom) or by the difference in the flow of heat across the boundary are termed the “horizontal convection”, how was introduced by Stern in 1975 in his course of physical oceanography (Stern, 1975).



The coastal zones where the natural bed slope provides conditions for the origination and maintenance of horizontal temperature gradients at daily, synoptic, and seasonal scales turn out to be a substantial source of convective exchange currents (Adams & Wells, 1984, Farrow, 2004, Fer et al., 2002, Horsch & Stefan, 1988, Ivanov et al., 2004, James & Barko, 1991, Monismith et al., 1990, Sturman et al., 1999). In total, this water exchange is of a two-layer structure (Gershuni et al., 1989, Farrow, 2004, Fer et al., 2002): the coastal waters, becoming lighter (heavier) against the open sea waters as a result of the heat exchange, move off-shore in the upper(lower) layer, being replaced by the open basin waters in the lower (upper) layer. The emerging motions are quite difficult object for investigation since they are governed by the distributed field of pressure in the region above the slope, exhibit inherently non stationary behavior (even at a constant heat flux through the surface) (Horsch & Stefan, 1988, Horsch et al., 1994, Mullarney et al., 2004, Sturman et al., 1999), develop with a considerable time lag relative to the external conditions (Farrow, 2004, Sturman et al., 1999), and are characterized by strong entrainment (Fer et al., 2002). In addition, the time lag of the currents' response to changes in surface conditions increases with the distance along the slope so that the water motion is not simply out of phase in reference to the external forcing but the phase shift increases downwards (Farrow, 2004, Horsch & Stefan, 1988). Field measurements in lakes and man-made reservoirs (Adams & Wells, 1984, Monismith et al., 1990, Sturman et al., 1999) demonstrate the occurrence of convective currents that develop at night (day) but survive even after changing of the sign of the external forcing and remain directed against the actual pressure gradient for a while. All of this tells, on the one hand, that the interpretation of the concrete data on the water temperature field and the current velocity requires one to know the time scales needed for the stabilization of the currents and their space structure above the given slope. On the other hand, it is obvious that the basic interest is in the assessment of the overall efficiency of such water exchange; and this implies the forecasting of the value of the resulting quasi-stationary water exchange potentially possible under the given conditions, and the degree of approach to it of the concrete dynamic pattern rather than an analysis of the instantaneous values of the gradients of the temperature, density, or current velocities.

This lecture, prepared on the base of paper (Chubarenko, 2010), is arranged in the following way. Section 2 is devoted to a detailed examination of the mechanism of the origination of horizontal gradients of temperature and density above a bottom slope. The analytical treatment of the process of the convective horizontal water exchange development in time is given in Section 3. Next, Section 4 is devoted to the substantiation of change from the description of the process in terms of the heat flux through the surface and of the horizontal water temperature gradient to the description in terms of the buoyancy flux and density gradients; the characteristic scales of the process are introduced. Based on the latter, Section 5 considers the field and laboratory data of many authors in an attempt to establish a linkage between the value of the resulting horizontal quasi-stationary water exchange through a cross section with its local depth. For short, the expression "differential coastal heating" is understood as both an increase and a decrease in the temperature towards the shore.



2. Mechanism of generation of horizontal water temperature gradients above sloping bottom

Exchange currents of a convective nature between the coastal zone and the deep-water aquatic areas of a basin arise because of the difference in the rates of their response to the external conditions of the heat exchange (Chubarenko, 2010): the shallower areas exhibit faster responses, while the deeper ones are more inertial. Breezes and monsoons are the direct analogs of these processes in the atmosphere. If the coastal waters become denser than the open waters due to the external heat exchange, they sink down the slope to the bottom or to the level of their isopycnal surface. If the former become lighter, they are displaced by the latter, but, in any case, the motion is caused by the interaction of waters that occur above the *entire slope* with waters of deeper basin areas. Since the occurrence of an external heat exchange is a common feature of any natural water basin and, additionally, horizontal motions in a fluid arise at the slightest pressure gradients, the more or less intensive circulation of direct or reverse direction has to occur virtually always, thus leading to the general more or less intensive down- or upwelling of waters within the domain over the slope.

In the context of the present problem, the *slope* domain is defined by the physical mechanism itself: this is a coastal area where the conditions of the heat exchange through the surface are perceptible down to the bottom. Under conditions of the autumn cooling, these are the regions whose depths are less than the thickness of the upper mixed layer (UML). For instance, these are the depths down to 250–300 m in the Caspian Sea, Lake Baikal, or the ocean. On the scale of the basin, the areas occupied by such slopes may be quite significant. The Baltic Sea in November gives an illustrative example to this end (Fig. 1). Here, the areas where vertical convection reaches the bottom (and further cooling results in the formation of waters denser than the surface waters of the deep sea regions) exceed 50 percent (respectively, the deeper areas that “receive” these waters occupy less than 50 percent). Under the summer heating conditions, the end of the slope is defined by the depth where the slope contacts the daytime/seasonal thermocline. In this case, the areas occupied by the slopes are somewhat diminished. They made up about 34 percent of the total area of the Baltic Sea with the thermocline depth at about 30 m. The calculations are based on the bottom topography available at <http://www.io-warnemuende.de> from the Leibniz Institute for Baltic Sea Research of Warnemuende (Germany).

In the deep basin region, where the heating/cooling does not reach the bottom, the heat flux through the surface is distributed over the depth in the neighboring water columns in a similar way. If the *autumn cooling* generates the vertical convection, the depth D of the upper mixed layer (Figs. 1 and 2) will be the same everywhere (assuming uniform initial stratification); the heat will be drawn off the water column whose length equally grows with time over the entire area. However, as the convection reaches the bottom at specific sites, the further water entrainment from below ends and the heat continues to be drawn off the same mass of water. The smaller the mass is (i.e., the less the depth d , $d < D$), the faster the temperature decreases, and its horizontal gradients are generated exactly in this way: the smaller is the depth, the lower is the temperature and the faster its latter decrease.

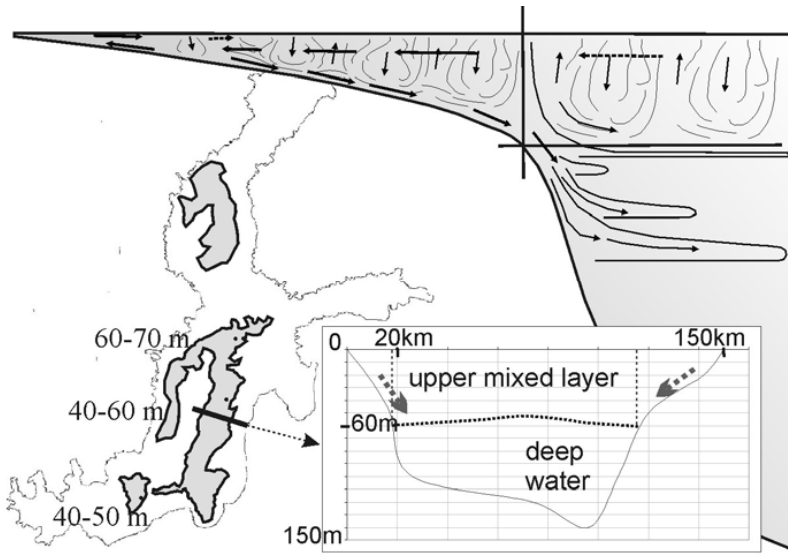


Fig. 1. Map of the Baltic Sea, showing the regions (in dark), where winter vertical convection does not reach the bottom (numbers show the maximum depth of the upper mixed layer). Upper right scheme illustrates the mechanism of seasonal horizontal convective exchange between littoral area, where vertical convection reaches the bottom, and the open sea. The inset shows the bathymetry cross-section from Liepaja to Gotland with two 20–30 km long littoral slopes, where vertical convection reaches the bottom, separated by about 100 km-long deep-water portion (from Chubarenko & Demchenko, 2010).

A similar pattern takes place under the conditions of the summer heating caused by the absorption of solar radiation. The daytime thermocline appears in the deep-water part of the basin at about the same depth level D over its whole area. If transparency of coastal and open waters is similar, the solar radiation is equally attenuated with the depth everywhere in the basin according to the Bouguer–Lambert–Beer law: $I(z) = I_0 e^{-\eta z}$ ($z \geq 0$). Here, I_0 , $I(z)$ are the radiation intensity at the surface and at the depth z , and η (m^{-1}) is the light attenuation coefficient. Hence, this mechanism by itself (as well as the heat diffusion from the surface) does not result in the generation of horizontal temperature gradients (Farrow, 2004). However, a fraction of the light energy is able to warm up the coastal waters from below at locally shallow depths d ($d < D$) where the radiation is partially backscattered from the bottom and returns into the water. Indeed, the water temperature profiles observed in the coastal zone are usually not as steep as those in the open sea areas (see, for instance, (Tikhomirov, 1982, Chubarenko et al., 2007a, Adams & Wells, 1984, Farrow, 2004, Monismith et al., 1990). From the physical viewpoint, this heat flux destabilizes the water column. If the heating intensity at the surface is $H_0 = I_0 / (\rho_0 c_p)$, where ρ_0 is the water density and c_p is the specific heat of the water at a constant pressure, then the heat coming to the bottom at the depth d is $H_d = H_0 e^{-\eta d}$. A fraction of this heat is wasted for the bottom warming, but the rest returns into the water due to reflection or reemission:

$$H = \delta H_0 e^{-\eta d}. \tag{1}$$

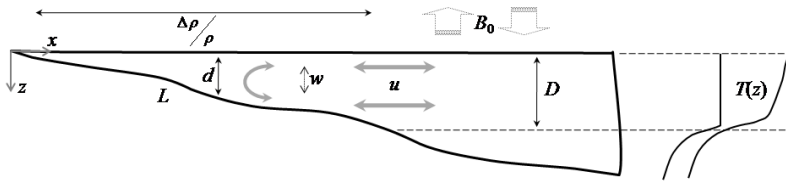


Fig. 2. Characteristic scales for the process of horizontal convective water exchange. Right: the vertical profiles of the temperature in the deep area for the conditions of destabilizing and stabilizing buoyancy flux through the surface, structure of which is the base for determination of the vertical spatial scale D .

Here, δ ($0 < \delta < 1$) is the proportionality factor indicating the fraction of the radiation energy that is returned in the water after the interaction with the bottom. Hence, expression (1) gives an estimate of the destabilizing heat flux in the case of the summer warming from the surface.

As a rule, higher turbidity is inherent to the coastal waters, which may be an important factor of the generation of horizontal inhomogeneities of the water temperature. This mechanism will not be elaborated in what follows because it substantially depends on the particular characteristics of the spatial distribution of the suspended matter and its ability to absorb the solar radiation.

3. Beginning of the water exchange

In both the foregoing situations, the origination of the horizontal water temperature gradients was controlled by strictly local factors, namely, by the conditions of the heat exchange at the surface and by the response of the water column of some local depth to these conditions. Consequently, the differences in the temperature field appear quite rapidly during the time period just needed for the response (Fig. 3). In the beginning, the emerging horizontal density gradient is vanishingly small. In spite of the fact that there is no critical value of the Raleigh number for horizontal convective flows and exchange motions begin immediately, the temperature changes caused by the heat exchange in the vertical occur much faster than the emerging horizontal currents are able to smooth them. Indeed, the field data provide evidence that differential coastal warming is confidently observed in the coastal zone. The horizontal temperature gradient continues to grow for some time, but the currents develop with a certain delay that increases with the distance to the shore (Farrow, 2004).

For instance, it was shown in (Monismith et al., 1990) that the settling time of the currents is at least of the same order of magnitude as that of the daily variations of the heat flux even for a shallow (down to 15 m depth) bay of a lake. Under conditions of a permanent external heat flux, the system tends to achieve a quasi-stationary state (Fig. 3) characterized by the (quasi-)constancy of the horizontal temperature gradient with the latter being determined by the balance of the heat flux through the surface and the horizontal heat transport with the currents (Farrow, 2004). Under laboratory conditions, the settling process is easy to identify; it takes tens of minutes in a basin of 15–20 cm

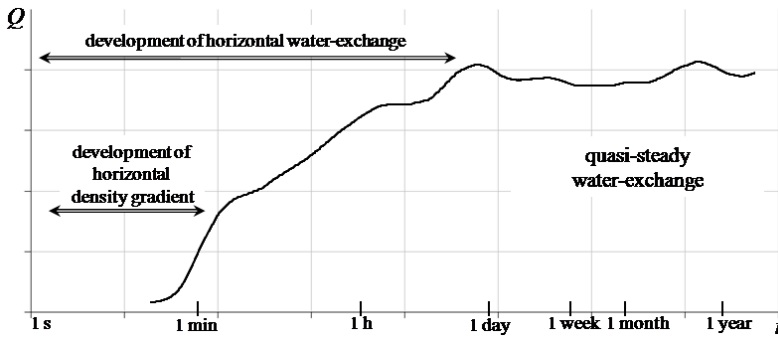


Fig. 3. Development of the horizontal convective water exchange in time at a constant mean buoyancy flux through the surface. The time scales are given for typical conditions of a coastal zone of a sea or lake at middle latitudes (see the text).

depth (for example, (Chubarenko et al., 2007a)). However, there are no permanent external conditions in nature and, for instance, deeper areas of lakes or reservoirs frequently fail to achieve the final stationary state during the daily cycle (Farrow, 2004). Even more, the development of convective circulation is so inertial that the currents sometimes flow in the opposite direction in reference to the currently existing pressure gradient. As was measured in (Monismith et al., 1990), the “night type” circulation in a bay was maintained for seven hours after the switching of the surface conditions from cooling to heating. Thus, both the final quasi-stationary state and the transition process are of interest.

4. Characteristic scales of the process

Thus, as the heating and cooling take place above the bottom slope, the horizontal water temperature gradients arise and grow with time; the respective gradients of the density and pressure appear; and, consequently, the currents begin to develop. Physically important for the fluid motion is not the temperature difference ΔT by itself, but the corresponding density difference $\Delta\rho = \alpha\rho_0\Delta T$ (and the hydrostatic pressures Δp). Due to the nonlinear dependence of the water density on the temperature, equal changes of the latter within different temperature ranges result in different changes of the density $\Delta\rho$. In addition, the coefficient of thermal expansion of water $\alpha = -1/\rho_0 \cdot d\rho/dT$ is an alternating quantity. At atmospheric pressure, the change of sign of α takes place in fresh water at the temperature of the maximum density (T_{md}) equal to 3.98 °C, in the brackish waters of the Baltic Sea (3 to 8 psu at the surface) at 3.3–2.3 °C, in the Caspian Sea (6 to 12 psu) at 2.7–1.4 °C, and in the Black Sea (6 to 18 psu) at 2.7–0.1 °C.

Hence, both heating and cooling occur in many lakes and seas of middle latitudes at both $\alpha > 0$ and $\alpha < 0$. So, the total heat balance of the surface layer is negative while the coefficient of thermal expansion of the water is positive during the *autumn cooling* in the coastal zone. Therefore, the buoyancy flux into the upper layer $B_0 = gaH/\rho_0 c_p$ [m^2/s^3] is negative (here, g is the gravitational acceleration), the surface waters become denser due to cooling, and



vertical convective mixing begins to form UML. However, $B_0 < 0$ corresponds to a combination ($\alpha < 0, H > 0$) too, i.e., to water heating at a temperature lower than T_{md} (the early spring heating). Similarly, $B_0 > 0$, which corresponds to the enhancement of the vertical stratification that takes place both during the warm water heating (at a temperature $T > T_{md}$) and during the further cooling of the cold water (at a temperature $T < T_{md}$) (Chubarenko & Demchenko, 2008). Hence, the most universal is the process description in terms of the buoyancy flux through the surface B_0 [m^2/s^3] and the resulting horizontal density difference $\Delta\rho$ [kg/m^3] (as is adopted in studies on convection, see, for example, (Hughes & Griffiths, 2008) rather than in terms of the heat flux through the surface H [W/m^2] and the horizontal temperature difference ΔT [$^\circ\text{C}$] at differential coastal heating. The negative buoyancy flux through the surface corresponds to the generation of the down-slope “cascading”, while the positive one points to the water upwelling regardless of the heat exchange conditions under the specific circumstances.

Let us introduce the scales characteristic of the problem. Different scales are needed because both the vertical and horizontal processes are equally substantial and distinguished by their physical nature. As the *spatial scales*, it is convenient to choose (Fig. 2) the horizontal length of the slope L and the depth of the layer D in the deep basin area that responds to changes in buoyancy flux across the surface. The characteristic temperature difference between the coastal and deep water basin area ΔT is quite suitable as the temperature scale. This defines the scale of the horizontal difference of the pressure as $\Delta p = \Delta\rho g D = \rho_0 \alpha \Delta T g D$. An additional discussion is needed to introduce the remaining scales, namely, the scales of the time and velocities of the vertical and horizontal currents, since the physical basis of the situation changes with the process’s evolution.

The time of the occurrence of the horizontal density gradients. The response of the local vertical water columns above the different depths d to the buoyancy flux through the surface B_0 is the first stage of the development of the horizontal water temperature gradients. The destabilizing buoyancy flux B is of physical importance in all the cases. Therefore, the time of the convective mixing of the water column of depth D (the maximum depth above the slope, Fig. 2) represents the characteristic time period after the lapse of which the entire slope is influenced by the external heat exchange. Considering the rate of the convective turbulent mixing $w \sim (Bd)^{1/3}$ (Maxworthy & Narimuoosa, 1994) as the scale of the vertical velocity under the given circumstances, we obtain the time scale through the division of the total depth D by this velocity:

$$\tau_1 \sim D / (BD)^{1/3} = (D^2/B)^{1/3}. \quad (2)$$

If the destabilizing buoyancy flux comes directly through the surface (as in the case of the autumn cooling), then $B = B_0$ and $\tau_1 = (D^2/B_0)^{1/3}$. If the buoyancy flux through the surface is of a stabilizing nature (the case of the summer coastal heating), then the destabilizing buoyancy flux (see expression (1)) makes up $B = \delta B_0 e^{-\eta d}$. Assuming, in this case, that the e-folding depth of the light intensity represents a measure of the maximal depth D above the slope, we obtain $\eta D = 1$ and the respective time of the mixing



$$\tau_1 \sim \left(\frac{D^2}{B_0} \cdot \frac{e}{\delta} \right)^{1/3} \tag{3}$$

In the context of the present problem statement, this time appears to be independent on the water transparency. So, the higher the transparency, the longer the “working” slope length is (and $\eta D=1$ holds). If the bottom is such that all the heat reaching the bottom returns into the water (i.e., $\delta=1$), then the time of the horizontal temperature gradients origination is only $e^{1/3} \sim 1.4$ times larger than in the case of the destabilizing buoyancy flux directly from the water basin surface.

Let us estimate the time scales (2) and (3) for the conditions of the coastal zone of a natural water basin: at $D=10$ m, $B_0 \sim 10^{-6}$ m²/c³, it makes up about 10 min when the destabilizing buoyancy flux comes from the surface and about 50 min when the flow comes from the bottom that absorbs 50 percent of the energy. In other words, the scales are of the same order of tens of minutes in the both cases, which is a very short response time for natural basins. Thus, formation of horizontal gradients above the bottom slope begins already *in minutes or in tens of minutes* after the initiation of the heating/cooling (Fig. 3) both with the stabilizing and destabilizing buoyancy flux through the surface. By that time, the *entire domain above the slope has already sensed* the external buoyancy flux, and the density difference has started to form but there is no mean current yet.

Time of settling of the currents. The horizontal currents begin to develop under the action of the growing horizontal density gradient. The speed of the settled current, which corresponds to the settled horizontal density gradient, can be estimated from the balance of the inertial member and the horizontal pressure gradient $u \partial u / \partial x = -1/\rho_0 \partial p / \partial x$ in the equation of motion if we neglect the viscosity and the rotation of the Earth.

Accepting the foregoing scales of the respective quantities, we obtain for the horizontal component of the velocity under quasi-stationary conditions:

$$\frac{u^2}{L} \sim \frac{1}{\rho_0} \cdot \frac{g \cdot \Delta \rho \cdot D}{L}, \text{ or } u \sim [g \cdot \Delta \rho / \rho_0 \cdot D]^{1/2} \tag{4}$$

The convective currents’ velocities measured in lakes relate to scales of centimeters per second (Farrow, 2004, Fer et al., 2002, Monismith et al., 1990). The winter cascading in Lake Geneva is an example of detailed published evidence (Fer et al., 2002) obtained at $D \sim 50$ m, $\Delta T \sim 0.2$ °C, and $\alpha \sim 10^{-4}$ (°C)⁻¹, which yielded $u \sim 0.05$ m/s for the measured velocity of the flow down the slope. In this case, the proportionality coefficient in (4) equals 0.5.

Let us consider the time necessary to achieve the “settled” current velocity (4) as the settling time. Based on the same consideration and on the balance $\partial u / \partial t = -1/\rho_0 \partial p / \partial x$, we obtain the scale for the settling time:

$$\tau_2 \sim \left[\frac{L}{g \cdot \Delta \rho / \rho_0 \cdot A} \right]^{1/2}, \tag{5}$$

where $A=D/L$ is the bottom inclination. The dependence (5) indicates that the settling time increases with the slope length, which agrees well with the



observations. The product $\Delta\rho/\rho A$ in the denominator changes not so strongly: the lesser density gradients occur at steep slopes (large A) and vice versa. This approach underestimates τ_2 because of the use of the settled value of the horizontal density difference while the real process proceeds at $\Delta\rho(t)$ growing from 0 to $\Delta\rho$. In view of this fact, let us introduce the multiplier 1/2 and estimate the value of the settling time for the case of $L \sim 10$ km, $\Delta T \sim 1$ °C, $\alpha \sim 10^{-4}$ (°C)⁻¹ (from 7.5 to 40 °C), and $A \sim 0.001$. Expression (5) gives $\tau_2 \sim 1.4 \cdot 10^5$ s, or one and a half days, which agrees well with the field data.

Thus, the horizontal convective currents have, apparently, no time to settle at daily oscillations of the heat flux over the marine aquatic areas, but it appears quite reasonable to think about the quasi-stationary convective water exchange at synoptic and, all the more, at seasonal scales of the oscillations.

Time of the water renewal in the coastal zone. Considering $u \sim (g\Delta\rho/\rho_0 D)^{1/2}$ as the velocity scale and assuming that the water flows out of the coastal zone as a layer half of the depth D thick, we estimate the time of the complete renewal of the coastal zone water due to the mechanism of convective water exchange:

$$\tau_3 \sim \frac{V}{ud} = \frac{1/2 \cdot LD}{u \cdot 1/2 \cdot D} = \frac{L}{u} \sim \frac{L}{[g \cdot \alpha \cdot \Delta T \cdot D]^{1/2}}. \quad (6)$$

Although expression (6) has exactly coincided with (5), they differ in their physical meaning: initially, the exchange currents settle for the time τ_2 and, next, the regular renewal of the coastal zone water proceeds at the level of the settled water exchange. It is important that the renewal scale is of the order of a few days for coastal zones of closed seas and large lakes, which is particularly substantial from the viewpoint of aquatic ecology.

5. The value of the horizontal quasi-stationary water exchange

The characteristic feature of the structure of the horizontal convective exchange is its two-layer nature on any scales: in a laboratory (Chubarenko et al., 2005, Chubarenko & Demchenko, 2008, Gershuni et al., 1989, Mullarney et al., 2004, Rossby, 1965, Sturman et al., 1999), in a small bay (Adams & Wells, 1984, James & Barko, 1991, Monismith et al., 1990), in a lake (Farrow, 2004, Fer et al., 2002, Horsh & Stefan, 1988, Sturman et al., 1999), in a sea (Filippov, 1968, Ivanov et al., 2004), or in an ocean (Hughes & Griffiths, 2008, Ivanov et al., 2004). This allows us to suppose that the spatial scale is to the most important characteristic of the process. The foregoing analysis indicates that the dependence of the resulting quasi stationary horizontal flow rate of the exchange current at the depth d above the slope looks like

$$Q \sim u \cdot d \sim [\Delta\rho/\rho \cdot g \cdot d]^{1/2} \cdot d \sim d^{3/2}. \quad (7)$$

Following the idea of (Sturman et al., 1999), the data of many authors from field and laboratory studies of the horizontal convection above the bottom slope have been collected to check this dependence. Fig. 4 in a log-log scale represents the flow rate (in m³/s per one running meter of the shore line) and the depth of the layer at site of the measurement (in meters). The use has been

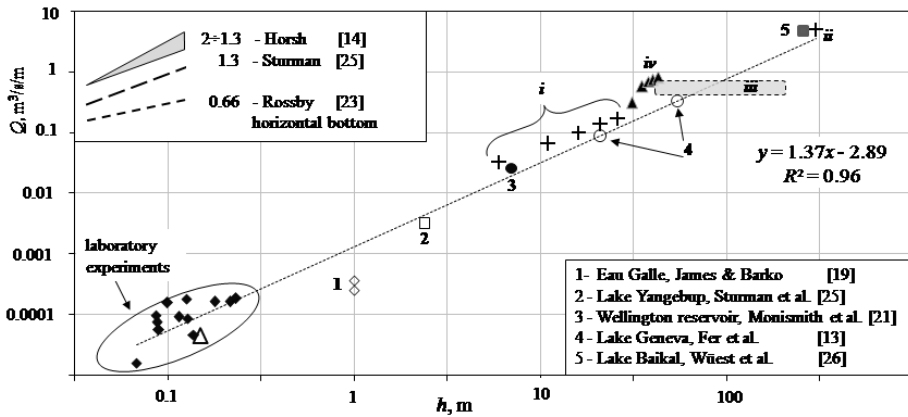


Fig. 4. Dependence of the horizontal convective volumetric flow rate in a basin with a sloping bottom upon the thickness of the thermally active layer according to laboratory and field data. The latter are exhaustively described in the text.

made of the following data. The oval-enclosed cluster of dots in the range of the smallest scales (~0.1 m) represents the data of laboratory experiments (Chubarenko et al., 2005, Chubarenko & Demchenko, 2008) on heating and cooling of a basin with sloping bottom. The same cluster involves the results of similar laboratory experiment on cooling, namely, five points from (Sturman et al., 1999): a basin with sloping bottom 10 cm deep and the quasi-stationary flow rate $(2-7) \cdot 10^{-5} \text{ m}^2/\text{s}$ (these points are omitted in Fig. 4).

In (James & Barko, 1991), the data was obtained in a small shallow flat-bottomed bay about 1 m deep of the water reservoir in Galle, USA when studying the water exchange at night on July 25–26 and September 12–13, 1988. The water exchange value was calculated from the propagation of a rhodamine patch from 10 p.m. to 10 a.m. and is meant to be the estimate of the mean over the cascading phase rather than the quasi-stationary value. The flow rate during the nighttime cooling made up $\sim(2-4) \cdot 10^{-4} \text{ m}^2/\text{s}$, being larger in July ($\sim(2-3) \cdot 10^{-4} \text{ m}^2/\text{s}$) than in September ($\sim(3-4) \cdot 10^{-4} \text{ m}^2/\text{s}$).

The measurements in (Sturman et al., 1999) were performed on September 3–5, 1996, in the small lake of Yangebup (Australia) where the intensive daily heating, clear night sky, and seasonally weak wind create conditions for the permanent presence of a convective circulation component in the daily rhythm in the shallow bays. The bowl-shaped lake of 3 m maximum depth features about one degree of bottom inclination in the coastal area. The measurement at a site 1.8 m deep resulted in the estimate of the horizontal flow rate of the convective circulation close to $\sim 3 \cdot 10^{-3} \text{ m}^2/\text{s}$.

The measurement data for Anna Lake (Adams & Wells, 1984)—flow-rate close to $\sim 2.3 \cdot 10^{-2} \text{ m}^2/\text{s}$ are given according to a reference in (Sturman et al., 1999).

The field measurement data above the shelf and slope of Lake Geneva (the maximum depth is 315 m) were collected during 38 days in the winter of 1999–2000 (Fer et al., 2002) (Table 1). The dots in Fig. 4 represent the flow rates at the depths of 21 $((8.6 \pm 4.4) \cdot 10^{-2} \text{ m}^2/\text{s})$ and 55 m $((32 \pm 20) \cdot 10^{-2} \text{ m}^2/\text{s})$ obtained by the authors as a result of averaging over 25 individual “slugs”, or masses of cold water slipping down the slopes.



The upper-most dot (the dark square symbol) corresponds to the flow rate of the cold near-bottom intrusions in Baikal Lake (Wüest et al., 2005) that originate during the spring heating ($T < T_{md}$); the estimate of the thickness of the upper thermally active layer is set by the depth level of the meso-thermal maximum (~ 250 m, see Fig. 2 in (Wüest et al., 2005)). The authors have not identified the specific origination mechanism of these intrusions, but they unequivocally relate the intrusions with the thermal processes at the lake surface as the heating proceeded and the temperature tended to reach T_{md} . The specific features of the deep-water mixing in Lake Baikal (the occurrence of a potential barrier for the sinking of heavier waters) prevented most of the intrusion from reaching the bottom (Wüest et al., 2005). Therefore, from the viewpoint of the exchange mechanism in question, the foregoing flow rate estimates characterize the mean of the most intensive cases rather than the quasi-stationary exchange.

The linear approximation of the foregoing data points to the dependence of type $Q \sim d^{1.37}$ at trustworthiness of $R^2 = 0.96$ (Fig. 4). It is substantial that this experimental evidence. Fig. 3 involves other dots too that were ignored when constructing the linear trend. These are the data from a numerical simulation with the help of the non-hydrostatic MIKE3-FlowModel (DHI Water & Environment): the symbol (i) marks the values of the horizontal flow rate of the cooling above the slope through the sections at the depths of 6, 11, 16, 21, and 26 m (Chubarenko et al., 2007b), while the dot (ii) for the 300 m depth designates the cooling in the basin that reproduces the scales of the northern shelf and slope of the Caspian Sea. The rectangle (iii) corresponds to the range of features of 61 cases of “cascading” of various nature observed under oceanic conditions (see (Ivanov et al., 2004)); their mean flow rate was estimated by the authors as 0.05–0.08 Sv per 100 km, or 0.5–0.8 m³/s/m, and the depth range made up 40–200 m. Unfortunately, the flow rate estimates for individual cases of “cascading” of said nature are unavailable.

Five dark triangle markers (iv) were obtained on the basis of study (Titov, 2006) concerning the depth of the UML and the volume of the cold intermediate layer (CIL) in the Black Sea for winters of different types (bottom-up): anomalously warm, warm, normal, cold, and anomalously cold. The “advection hypothesis of origination of the Black Sea CIL” due to waters that trickle down the slopes in the winter has been known since the 1950–1960s (Filipov, 1968), and its details are still being discussed thus far. The estimates of the flow rate in the plot have been obtained through dividing the CIL volume during the respective winter by the duration of the cooling period (five months) and the total length of the shore line of the sea (not only the northwestern sector). According to the present day evidence, the origination of the cold waters due to similar mechanisms is possible in the center of the sea too (Titov, 2006): because of the domelike shape of the pycnocline in the Black Sea, the vertical convection reaches the layer of discontinuity and the horizontal water temperature gradients appear in the surface layer. This fact can be taken into account if one increases “the length of the shore line”, which will shift the dots (iv) closer to the line of the general trend.

The resulting plot generalizes the data in the range of vertical scales (the thickness of the upper thermally active layer) from few centimeters to 300 m



and shows that the quasi-stationary convective water exchange varies meanwhile from 10–5 to 5 m³/s per one meter of the shore line. The bottom inclination range makes up 0.001–0.1 (the slopes were as steep as 0.4 at segments of the Lake Geneva slopes (Fer et al., 2002)). The same dependence describes the data on the horizontal flow rate under the “cascading” conditions caused by the autumnal–winter cooling (at $T > T_{md}$), during the daily heating ($T > T_{md}$), and during the heating under a temperature below T_{md} . We failed to find published evidence on the values of the horizontal water exchange at cooling of the waters at temperature below T_{md} . The linear equation $y = 1.37x - 2.89$ (Fig. 4), being rewritten in explicit form, gives the dependence $Q = 0.0013 d^{1.37}$, where all of the involved quantities are expressed in SI, the flow rate in m³/s/m, and d in m.

5. Discussion

Comparison with other authors’ results. The work of Rossby (Rossby, 1965) is considered as one of the first studies aimed at the evaluation of the quasi-stationary convective water exchange. He accomplished a laboratory experiment in a rectangular flume with a horizontal differentially heated bottom. Rossby’s experiments and analysis based on the introduction of scales for the arising boundary layer, along with later experiments of other authors (for instance, (Mullarney et al., 2004)), have shown that the volumetric rate of the flow (per unit of the basin’s width) is proportional to the Rayleigh number: $Q \sim Ra_F^{1/6}$, where $Ra_F = \frac{agHh^4}{\rho_0 c_p \nu k_T^2}$. Here, h is the spatial scale, ν is the kinematic viscosity, and k_T is the coefficient of the thermal diffusion. Therefore, according to Rossby’s (1965) results, the dependence of the water exchange value on the spatial scale looks like $Q \sim h^{4/6} = h^{0.66}$.

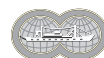
It was shown for basins with a sloping bottom (Farrow, 2004, Horsh & Stefan, 1988, Sturman et al., 1999) that, while the arising horizontal exchange is complicated and differently structured under heating and cooling, it is allied to the currents observed by Rossby (1965): they are caused by the gradients of the temperature/density at the horizontal boundary; they are distinguished by the “always non-stationary” behavior of the exchange and its two-layer structure with the maxima of the current velocity distant from the boundary. The numerical and laboratory data (Horsh & Stefan, 1988, Horsh et al., 1994) for basins with a sloping bottom have demonstrated a substantially stronger dependence: $Q \sim Ra^{1/n}$, where $2 < n < 3$, which yields $Q \sim h^{1.3 \pm 2}$. Sturman et al. (1999) have generalized the numerical, laboratory, and field data of several authors (for lakes and small bays) and obtained the dependence $Q \sim h^{1.3}$ by means of interpolation. All these dependences are given in Fig. 4 in the upper left corner as lines of the respective slopes. It is evident that results of the present work agree well with the inferences of other authors. The “independence” of the foregoing results upon the bottom tilting and the external buoyancy flux through the surface is no more than an outward appearance. First, both parameters substantially influence the value of the emerging horizontal density gradient. The laboratory experiments (Chubarenko et al., 2005, Chubarenko & Demchenko, 2008) allow us to qualitatively indicate the cause of this “independence”: large temperature/density gradients that appear above



gentle slopes and are accompanied by powerful buoyancy fluxes generate more intensive currents but within a thinner layer. In contrast, at steeper slopes and weaker buoyancy fluxes, the density gradients decrease and the currents become slower but their velocity profile broadens (Chubarenko et al., 2005, Chubarenko & Demchenko, 2008), so that the total flow rate falls short of being considerably changed. In addition, the effect of the buoyancy flux strength is actually exhibited through the change in the thickness D of the thermally active layer. The duration of the water exchange process's stabilization is changing too: small B and $\Delta\rho$ result in a longer time of the slope response τ_1 and the time of the current stabilization τ_2 (see expressions (2) and (5)). This is corroborated by study (Sturman et al., 1999): the analysis of a series of numerical solutions has revealed that the currents are insensitive to changes in value of the external buoyancy flux (the occurrence of the latter is of importance only) and quite moderately sensitive to changes in the angle of the bottom slope. Thus, the spatial scale dependence becomes the most important indeed.

The comparison of the results obtained in basins with inclined and horizontal bottoms shows that the occurrence of a bottom slope considerably intensifies the horizontal convective water exchange. This is confirmed by the well known engineering fact of faster cooling of tilted bottom basins (laboratory experiments, for example, (Chubarenko et al., 2005, Chubarenko & Demchenko, 2008)). Such a conclusion appears useful when discussing the quantitative contribution of the temperature difference between the equator and the Pole in the thermohaline circulation of the ocean: it is known (Hughes & Griffiths, 2008, Mullarney et al., 2004, Rossby, 1965) that the horizontal convection in an ocean with a horizontal bottom is insufficient to explain the intensity of the observable circulation. Indeed, one of the latest estimates of the flow rate value of the global thermohaline circulation is ± 5.6 Sv (or $5.6 \cdot 10^6$ m³/s) at 26.5 N (Cunnindham et al., 2007), which is approximately equivalent to 2–2.5 m³s⁻¹/m (see the vertical axis in Fig. 4). At a certain depth $D \sim 1$ –3 km corresponding to the ocean scales, this point occurs markedly higher in reference to the dependence obtained by Rossby but lower than that obtained by the author. This apparently means that the availability of bottom inclinations in the polar regions plays a certain role in the ocean too.

The influence of other factors on the water exchange. The problem of wind, waves, and the Earth's rotation effects on the convective water exchange has virtually not been examined until now. It is evident that a strong wind is able to completely block the water exchange of this nature for some time, but it is evident too that the differential coastal heating is persistently observable both at synoptic and seasonal averaging. At that, the stability of the isotherms when going in parallel to the shore line and isobaths is not an indication of a lack of motion but results from the permanently renewable balance of the vertical and horizontal heat fluxes. There are reasons to believe that the above mechanism continues to operate at moderate winds too and adds its contribution to the general circulation. Most of the field measurements aimed at convective water exchange were conducted in lakes and at weak winds. Nevertheless, observations of winter cascades in seas and oceans are well known. The CIL of the Black Sea is special evidence of the persistent operation of this mechanism: its advective (nonlocal) origination in the open Black Sea was proved



(Filippov, 1968), and the significant role of the shelf in the CIL formation has been shown.

Two factors complicate the analysis of the Earth's rotation effect: first, the currents of this nature are always non-stationary and, second, the bottom availability is of basic importance, which entails the effects of the bottom friction. It is possible to anticipate that the rotation has no time to influence the development of the daytime/nighttime circulation and shorter events. However, it is evident that the seasonal water exchange has to be adopted to the rotation even though separate down-slope tongues or convective jets are non-stationary in nature. If there is a permanent pressure gradient down the slope, the Earth's rotation leads to the generation of the along-shore current and the Ekman bottom layer remains to be the only space for water exchange between the deep and shallow areas. The thickness of the layer is $h=(2K_z/f)^{1/2}$, where K_z is the coefficient of the turbulent exchange, and f is the Coriolis parameter. At typical $K_z\sim 10^{-4}$ m²/s, and $f\sim 10^{-4}$ s⁻¹, the bottom layer thickness containing the down-slope current component turns out to be small (about 1.4 m) regardless of the local depth. This contradicts the field observations: Fer et al. (2002) have shown that the estimation of the Ekman transport in the boundary layer $v(2K_z/f)^{1/2}$ yields less than one-tenth of the observed transport under the conditions of "cascading" at slopes of Lake Geneva down to the 56 m depth. Thus, the application of the classic version of the Ekman theory results in the substantial underestimation of the water exchange value. However, the problem in question admits the application of a somewhat generalized Ekman approach. According to the physical meaning, the value of the coefficient of the turbulent exchange in this context depends on the destabilizing buoyancy flux and the local depth. Based on the dimensionality, we have for K_z [m²/s] the following:

$$K_z \sim \frac{d^2}{\tau_1} = d^{4/3} B^{1/3},$$

i.e., the coefficient of turbulent exchange depends on the spatial scale. In this case, we have $h\sim d^{2/3} B^{1/6} f^{1/2}$ for the thickness of the bottom friction layer. This yields tens of meters for the thickness of the friction layer at $B\sim 10^{-6}\div 10^{-8}$ m²/s³, $f\sim 10^{-4}$ s⁻¹, and a local depth of $d\sim 27$ m. Thus, the entire exchange current occurs substantially within the boundary layer, and the Earth's rotation is not a limiting factor. The friction layer's thickness and many other parameters of this problem turn out to be much more strongly dependent on the spatial scale rather than on the external buoyancy flux.

Acknowledgements

The work is supported by the Russian Foundation for Basic Research, project Nos. 10-05-00540, 10-05-00472, 09-05-00446, and 08-05-92421-BONUS.

References

- Adams, E. E., & Wells, S. A. (1984) Field Measurements on Side Arms of Lake Anna. *J. Hydraul. Engng.* **110**:773–793.
- Chubarenko, I. P. (2010) Horizontal Convective Water Exchange above a Sloping Bottom: The Mechanism of Its Formation and an Analysis of Its Development. *Okeanologiya* **50**(2):184–193 (in Russian), *Oceanology* **50**(2):166–174 (in English).



- Chubarenko, I. P. & Demchenko, N. Yu. (2010) On contribution of horizontal and intra-layer convection to the formation of the Baltic Sea cold intermediate layer. *Ocean Sci.* **6(1)**:285–299.
URL: <http://www.ocean-sci.net/6/285/2010/os-6-285-2010.html>.
- (2008) Laboratory Modeling of the Structure of a Thermal Bar and Related Circulation in a Basin with a Sloping Bottom. *Okeanologiya* **48(3)**:349–361 (in Russian), *Oceanology* **48(3)**:327–339 (2008) (in English).
- Chubarenko, I. P., Afon, V. V., Demchenko, N. Yu. (2007a) On the Hypothesis of Convective Formation of Summer Coastal Upwelling. In: Trukhin, V. I. et al., eds., *Collected Scientific Papers. Physical Problems in Ecology (Ecological Physics)*, 402–410. Moscow: MAKS Press (in Russian).
- Chubarenko, I., Esiukova, E., Koutitonsky, V. (2007b) Simulation of Horizontal Convection Induced by Surface Cooling Over Sea Slope. In: *Proc. Int. Conf. BSSC*. Rostock, 35. Warnemünde, Germany.
- Chubarenko, I., Demchenko, N., Hutter, K. (2005) Horizontal Convection Induced by Surface Cooling Over Incline: Laboratory Experiment. In: *Proc. Int. Conf. Fluxes and Structures in Fluids*, 89–95. Moscow: Moscow University Press.
- Cunnindham, S. A., Kanzov, T., Rayner, D. et al. (2007) Temporal Variability of the Atlantic Meridional Overturning Circulation at 26.5°N. *Science* **317**:935–938.
- Farrow, D. E. (2004) Periodically Forced Natural Convection over Slowly Varying Topography. *J. Fluid Mech.* **508**:1–21.
- Fer, I., Lemnin, U., Thorpe, S. A. (2002) Winter Cascading of Cold Water in Lake Geneva. *J. Geophys. Res.* **107**:2236–2569.
- Filippov, D. M. (1968) *Circulation and Structure of Water in the Black Sea*. Moscow: Nauka (in Russian).
- Gershuni, G. Z., Zhukhovitskii, E. M., Nepomnyashchii, A. A. (1989) *Stability of Convective Flows*. Moscow: Nauka (in Russian).
- Horsch, G. M. & Stefan, H. G. (1988) Convective Circulation in Littoral Waters due to Surface Cooling. *Limnol. Oceanogr.* **33(5)**:1068–1083.
- Horsh, G. M., Stefan, H. G., Gavali, S. (1994) Numerical Simulation of Cooling-Induced Convective Currents on a Littoral Slope. *Int. J. Num. Meth. in Fluids* **19**:105–134
- Huang, R. X. (1999) Mixing and Energetics of the Oceanic Thermohaline Circulation. *J. Phys. Oceanogr.* **29**:727–746.
- Hughes, G. O. & Griffiths, R. W. (2008) Horizontal Convection. *Annu. Rev. Fluid Mech.* **40**:185–208.
- Ivanov, V. V., Shapiro, G. I., Huthnance, J. M. et al. (2004) Cascades of Dense Water around the World Ocean. *Prog. Oceanogr.* **60(1)**:47–98.
- James, W., & Barko, J. (1991) Estimation of Phosphorus Exchange between Littoral and Pelagic Zones during Nighttime Convective Circulation. *Limnol. Oceanogr.* **36(1)**:179–187.
- Maxworthy, T., & Narimuosa, S. (1994) Unsteady, Turbulent Convection into a Homogeneous, Rotating Fluid, with Oceanographic Applications. *J. Phys. Oceanogr.* **24**:865–887.
- Monismith, S., Imberger, J., Morison, M. (1990) Convective Motions in the Sidearm of a Small Reservoir. *Limnol. Oceanogr.* **35(8)**:1676–1702.
- Mullarney, J. C., Griffiths, R. W., Hughes, G. O. (2004) Convection Driven by Differential Heating at a Horizontal Boundary. *J. Fluid Mech.* **516**:181–209.
- Rossby, H. T. (1965) On Thermal Convection Driven by Non-Uniform Heating from Below: An Experimental Study. *Deep-Sea Res.* **12**:9–16.



- Shimaraev, M. N. (1977) *Elements of the Thermal Regime of Lake Baikal*. Novosibirsk: Nauka (in Russian).
- Stern, M. E. (1975) *Ocean Circulation Physics*. Int. Geophys. Ser. Academic. Vol. 19.
- Sturman, J. J., Oldham, C. E., Ivey, G. N. (1999) Steady Convective Exchange Flow down Slopes. *Aquat. Sci.* **61**:260–278.
- Tikhomirov, A. I. (1982) *Thermics of Large Lakes*. Leningrad: Nauka (in Russian).
- Titov, V. B. (2006) Zones of Formation and Volume of Waters of the Cold Intermediate Layer in the Black Sea with Allowance for Winter Severity. *Meteorol. Hidrol.* **6**:62–68 (in Russian).
- Wüest, A., Ravens, T. M., Granin, N. G. et al. (2005) Cold Intrusions in Lake Baikal: Direct Observational Evidence for Deep-Water Renewal. *Limnol. Oceanogr.* **50**(1):184–196.

Numerical simulation of 3-D sea circulation in shelf zone with mesh refinements

Nikolay Diansky

Abstract

Efficient numerical technique for the numerical simulation of the ocean/sea circulation and applying it to the simulation of the Japan/East Sea (JES) dynamics with high spatial resolution (<5 nm) with mesh refinements in shelf zone is presented. To solve model equations the splitting method by physical processes and space coordinates is used. The main parts of the model operator are selected to perform their numerical treatment independently of one another. The general methodology and some special aspects of this approach are described. Numerical simulation of the JES circulation is performed on the basis of the sigma-coordinate primitive equation model, which was developed at the Institute of Numerical Mathematics of Russian Academy of Sciences. Analysis of the results of the numerical experiment is presented. It was shown strong eddy activity of the JES circulation which is confirmed by observations. This eddy activity has substantial contribution to the formation of JES large-scale climatic circulation.

Представлена эффективная методология для численного моделирования океанической или морской циркуляции и ее применение для расчета динамики Японского моря (ЯМ) с высоким пространственным разрешением (<5 миль) со сгущением сетки в шельфовой зоне. Для решения уравнений модели применяется расщепление по физическим процессам и пространственным координатам, выделяются главные части оператора модели, которые численно решаются отдельно друг от друга. Описывается общая методология и некоторые специальные аспекты такого подхода. Численное воспроизведение циркуляции ЯМ выполнено на основе сигма-координатной модели в примитивных уравнениях, разработанной в Институте вычислительной математики Российской академии наук. Представлен анализ результатов численного эксперимента. Показана сильная вихревая активность циркуляции ЯМ, которая подтверждается данными наблюдений. Такая вихревая активность дает существенный вклад в формирование крупномасштабной климатической циркуляции ЯМ.

Nikolay Diansky (✉)

Institute of Numerical Mathematics, Russian Academy of Sciences (INM RAS)
e-mail: nikolay.diansky@gmail.com



1. Introduction

The aim of this work is to present efficient numerical methods of predicting the ocean or sea dynamics. These methods are used for calculating the circulation in the Japan/East Sea (JES) or the Sea of Japan, which is characterized by the strong annual cycle and complex spatial and temporal variability. For the adequate simulation of the complex dynamics of the JES and the peculiarities of its eddy structure it is necessary to use models with high spatial resolution highest then 5 nm, which are physically complete and numerically efficient. Such models are based on nonlinear differential equations describing the evolution of 3D velocity, temperature, salinity fields as well as pressure and density.

Numerical treatment of the JES circulation is performed on the basis of one version of the model of ocean dynamics, which was developed at the Institute of Numerical Mathematics (INM) (Zalesny, 1996, Diansky et al., 2002). The global version of the INM ocean model (INMOM) is used as the oceanic component of the IPCC climate model INMCM3 which developed also at the INM and is presented in the IPCC Fourth Assessment Report (Solomon et al., 2007).

2. Description of Institute of Numerical Mathematics Ocean Model (INMOM)

The Institute of Numerical Mathematics Ocean Model (INMOM) is a so-called “terrain following” σ -coordinate ocean model. The model is based on the primitive equations of ocean dynamics in the Boussinesq and hydrostatic approximations, written in a generic spherical system. Prognostic variables of the model are the horizontal components of velocity, potential temperature, salinity and SSH. The global version of the INMOM with coarse spatial resolution is used as the oceanic component of the IPCC climate model INMCM presented in the IPCC Fourth Assessment Report (Solomon et al., 2007).

2.1. Specificities of the model

The main feature of the model, which distinguishes it from such other well-known ocean models as the z-coordinate Modular Ocean Model (Pacanovsky & Griffies, 2000) based on the pioneering work (Bryan, 1969), the OPA ocean model (Madec et al., 1998), the σ -coordinate Princeton Ocean Model (Mellor, 1998), and other models, is that the numerical implementation of the model uses splitting with respect to physical processes and spatial coordinates (Marchuk, 1968, 1988). This technique eliminates much of the difficulties associated with the approximation of the terms involving gradients of pressure, density, and bottom topography in the σ -coordinate system. Biharmonic viscosity is used for the momentum.

Governing equations. The Institute of Numerical Mathematics Ocean Model (INMOM) is so-called σ -coordinate ocean model. Its vertical coordinate σ is the dimensionless variable defined by the relation:

$$\sigma = \frac{z-\zeta}{H-\zeta}, \quad \sigma \in [0,1], \quad (1)$$



where H is the total ocean depth, ζ is sea surface height (SSH) deviation from undisturbed state and z is the physical vertical coordinate in depth downward directed. An advantage of this coordinate system is that the bottom topography can be smoothly represented and that currents are well described in deep ocean layers, on the continental shelf, and the continental slope.

The model is based on the primitive equations of ocean dynamics in the Boussinesq and hydrostatic approximations, written in a generic spherical system (x, y) , where x and y are longitude and latitude in particular case. The prognostic variables in the model are the horizontal components of velocity, potential temperature, salinity and SSH. The equations are:

momentum:

$$D_t u - (f + \xi)vH = -\frac{H}{r_x} \left(\frac{1}{\rho_0} P_x + \frac{1}{\rho_0} \frac{\partial p_a}{\partial x} - g \frac{\partial \zeta}{\partial x} \right) + \frac{\partial}{\partial \sigma} \frac{v}{H} \frac{\partial u}{\partial \sigma} + Fu, \quad (2)$$

$$D_t v + (f + \xi)uH = -\frac{H}{r_y} \left(\frac{1}{\rho_0} P_y + \frac{1}{\rho_0} \frac{\partial p_a}{\partial y} - g \frac{\partial \zeta}{\partial y} \right) + \frac{\partial}{\partial \sigma} \frac{v}{H} \frac{\partial v}{\partial \sigma} + Fv, \quad (3)$$

continuity:

$$\text{div}_h \mathbf{u} + \frac{1}{H} \frac{\partial w}{\partial \sigma} = \frac{1}{H} \frac{\partial \zeta}{\partial t}, \quad (4)$$

heat:

$$\bar{D}_t \theta = \frac{\partial}{\partial \sigma} \frac{v_\theta}{H} \frac{\partial \theta}{\partial \sigma} + D\theta + \frac{\partial R}{\partial \sigma}, \quad (5)$$

salt:

$$\bar{D}_t S = \frac{\partial}{\partial \sigma} \frac{v_s}{H} \frac{\partial S}{\partial \sigma} + DS, \quad (6)$$

intended specially for ocean circulation models, the equation of state from (Bryden et al., 1999) makes allowance for water compressibility:

$$\rho = \hat{\rho}(\theta, S + 35 \text{psu}, \rho_0 g \sigma H). \quad (7)$$

Here $\mathbf{u}=(u, v)$ is horizontal velocity vector, u and v are zonal and meridional velocity components; w is vertical velocity in σ -coordinate, that is related with vertical velocity w in z -coordinate by:

$$w = w - \left(\frac{u}{r_x} \frac{\partial Z}{\partial x} + \frac{v}{r_y} \frac{\partial Z}{\partial y} + \frac{\partial Z}{\partial t} \right), \quad (8)$$

where $Z = \sigma(H - \zeta) + \zeta \equiv \sigma h + \zeta$, $r_x = a \cos y$ and $r_y = a$ are metrical coefficients, where a is earth mean radius; θ is potential temperature; R is penetrative radiation flux; S is salinity deviation from the constant 35PSU; ρ is density deviation from a mean profile, depending on water column pressure $\rho_0 g z$ with average ocean density $\rho_0 = 1.025 \text{ g/cm}^3$ at the depth $z = \sigma h$; $f = 2\Omega \sin y$ is Coriolis parameter, where Ω is Earth angular velocity; $\xi = \frac{1}{r_x r_y} \left(\frac{\partial r_y}{\partial x} v - \frac{\partial r_x}{\partial y} u \right)$ is momentum change in curvilinear coordinate system; v_θ, v_s and v_σ are vertical viscosity



(for u and v) and diffusion (for θ and S) coefficients; p_a is sea level pressure. The coefficients ν , ν_θ and ν_s are calculated by Pacanovsky and Philander (1981) parameterization.

Horizontal pressure gradient components P_x and P_y in (2) and (3) are written in the form:

$$\begin{aligned}
 P_x &= \frac{1}{2} g \left(\frac{\partial}{\partial x} \left(H \int_0^\sigma \left(\rho - \sigma \frac{\partial \rho}{\partial \sigma} \right) d\sigma \right) - \sigma \left(\frac{\partial H}{\partial x} \rho - H \frac{\partial \rho}{\partial x} \right) \right), \\
 P_y &= \frac{1}{2} g \left(\frac{\partial}{\partial y} \left(H \int_0^\sigma \left(\rho - \sigma \frac{\partial \rho}{\partial \sigma} \right) d\sigma \right) - \sigma \left(\frac{\partial H}{\partial y} \rho - H \frac{\partial \rho}{\partial y} \right) \right),
 \end{aligned}
 \tag{9}$$

that reduces approximation error in σ -coordinates.

The momentum transport operator in (2) and (3) is used in semi-divergent symmetrized form:

$$\begin{aligned}
 D_i \varphi &= \frac{1}{2} \left(h \frac{\partial \varphi}{\partial t} + \frac{\partial h \varphi}{\partial t} \right) + \frac{1}{2 r_x r_y} \left[r_y H u \frac{\partial \varphi}{\partial x} + \frac{\partial}{\partial x} (r_y H u \varphi) + \right. \\
 &\quad \left. + r_x H v \frac{\partial \varphi}{\partial y} + \frac{\partial}{\partial y} (r_x H v \varphi) \right] + \frac{1}{2} \left(\omega \frac{\partial \varphi}{\partial \sigma} + \frac{\partial \omega \varphi}{\partial \sigma} \right),
 \end{aligned}
 \tag{10}$$

that allows us to reduce 3-dimensional transport problem to 3 one-dimensional ones, and each of them can be solved by using implicit time integration methods.

Temperature and salinity transport operator is used in divergent form:

$$D_i \varphi = \frac{\partial h \varphi}{\partial t} + \frac{1}{r_x r_y} \left[\frac{\partial}{\partial x} (r_y H u \varphi) + \frac{\partial}{\partial y} (r_x H v \varphi) \right] + \frac{\partial \omega \varphi}{\partial \sigma},
 \tag{11}$$

that provides heat and salt conservation.

The second-order lateral diffusion operator for heat and salinity is represented in universal form in order to provide adequate description of ocean dynamic processes:

$$\begin{aligned}
 D \varphi &= \frac{1}{r_x r_y} \frac{\partial}{\partial x} \left[K^x H \frac{r_y}{r_x} \left(\frac{\partial \varphi}{\partial x} - \kappa_x \frac{\partial \varphi}{\partial \sigma} \right) \right] - \frac{1}{r_x r_y} \frac{\partial}{\partial \sigma} \left[K^x H \frac{r_y}{r_x} \kappa_x \left(\frac{\partial \varphi}{\partial x} - \kappa_x \frac{\partial \varphi}{\partial \sigma} \right) \right] + \\
 &\quad + \frac{1}{r_x r_y} \frac{\partial}{\partial y} \left[K^y H \frac{r_x}{r_y} \left(\frac{\partial \varphi}{\partial y} - \kappa_y \frac{\partial \varphi}{\partial \sigma} \right) \right] - \frac{1}{r_x r_y} \frac{\partial}{\partial \sigma} \left[K^y H \frac{r_x}{r_y} \kappa_y \left(\frac{\partial \varphi}{\partial y} - \kappa_y \frac{\partial \varphi}{\partial \sigma} \right) \right],
 \end{aligned}
 \tag{12}$$

where φ is either θ or S , $K^x(x, y, \sigma H)$ and $K^y(x, y, \sigma H)$ —lateral diffusion 2nd order coefficients. The terms κ_x and κ_y define one or more directions for diffusion. For instance:

$$\begin{aligned}
 \kappa_x &= \alpha \frac{\partial Z / \partial x}{\partial Z / \partial \sigma} + \beta \frac{\partial \rho_p / \partial x}{\partial \rho_p / \partial \sigma}, \\
 \kappa_y &= \alpha \frac{\partial Z / \partial y}{\partial Z / \partial \sigma} + \beta \frac{\partial \rho_p / \partial y}{\partial \rho_p / \partial \sigma}.
 \end{aligned}
 \tag{13}$$



If $\alpha=0, \beta=0$, the diffusion occurs along σ -surfaces; if $\alpha=1, \beta=0$ —along z -surfaces; if $\alpha=0, \beta=1$ —along ρ -surfaces.

The velocity equations use the plain (for σ -coordinate models) form of lateral viscosity acting along σ -surfaces, which is completed by the 4th order viscosity operator.

$$F\varphi = F^1\varphi + F^2\varphi, \tag{14}$$

where φ is either u or v , F^1 and F^2 are:

$$F^1 = H \operatorname{div}_h(\mathbf{A} \operatorname{grad}_h), \tag{15}$$

and

$$F^2 = -H (\operatorname{div}_h(\mathbf{B}^{\frac{1}{2}} \operatorname{grad}_h))^2. \tag{16}$$

\mathbf{A} and \mathbf{B} in (16) and (17) are 2nd order diagonal tensors:

$$\mathbf{A} = \begin{pmatrix} A^x & 0 \\ 0 & A^y \end{pmatrix}, \quad \mathbf{B} = \begin{pmatrix} B^x & 0 \\ 0 & B^y \end{pmatrix}, \tag{17}$$

An approximation $\partial Z / \partial(x, y, \sigma) \approx \partial(\sigma H) / \partial(x, y, \sigma)$ is used in these equations because it is assumed that $\zeta = H$.

Hunke & Dukowicz (1997) elastic-viscous-plastic model for sea ice dynamics is used in the INMOM.

The mathematic boundary conditions for ocean model are:

At sea surface $\sigma=0$:

✓ for horizontal velocity components:

$$-\frac{\nu}{H} \frac{\partial \mathbf{u}}{\partial \sigma} \Big|_{\sigma=0} = \frac{(\tau_x, \tau_y)}{\rho_0}, \tag{18}$$

where (τ_x, τ_y) is wind stress vector at sea surface;

✓ for vertical velocity:

$$\omega \Big|_{\sigma=0} = 0, \tag{19}$$

corresponding to the linearized kinematic condition $w = \partial \zeta / \partial t$ in z -system;

✓ for temperature and salinity:

$$\begin{aligned} & \left[\frac{1}{r_x^2} K^x H \kappa_x \left(\frac{\partial \varphi}{\partial x} - \kappa_x \frac{\partial \varphi}{\partial \sigma} \right) + \frac{1}{r_y^2} K^y H \kappa_y \left(\frac{\partial \varphi}{\partial y} - \kappa_y \frac{\partial \varphi}{\partial \sigma} \right) - \frac{\nu_\varphi}{H} \frac{\partial \varphi}{\partial \sigma} \right]_{\sigma=0} \equiv \\ & \equiv -\frac{\nu_\varphi}{H} \frac{\partial \varphi}{\partial \sigma} \Big|_{\sigma=0} = q_\varphi, \end{aligned} \tag{20}$$

where φ is either θ or S , q_θ and q_S are normalized heat and salt fluxes at ocean surface, which can depend on the model solution at sea surface.

At the ocean bottom $\sigma=1$:

✓ no normal current condition:

$$\omega \Big|_{\sigma=1} = 0, \tag{21}$$



corresponding to the condition $w|_{z=H} = u|_{z=H} \frac{1}{r_x} \frac{\partial H}{\partial x} + v|_{z=H} \frac{1}{r_y} \frac{\partial H}{\partial y}$ in z-system;
 ✓ quadratic bottom friction:

$$-\frac{\nu}{H} \frac{\partial \mathbf{u}}{\partial \sigma} \Big|_{\sigma=1} = C_D \sqrt{u^2 + v^2 + e_b^2} \mathbf{u} \Big|_{\sigma=1}, \quad (22)$$

where $C_D = 2,5 \times 10^{-3}$ and $e_b = 5$ cm/s;

No heat and salt flux conditions

$$\left[\frac{1}{r_x^2} K^x H \kappa_x \left(\frac{\partial \varphi}{\partial x} - \kappa_x \frac{\partial \varphi}{\partial \sigma} \right) + \frac{1}{r_y^2} K^y H \kappa_y \left(\frac{\partial \varphi}{\partial y} - \kappa_y \frac{\partial \varphi}{\partial \sigma} \right) - \frac{\nu}{H} \frac{\partial \varphi}{\partial \sigma} \right]_{\sigma=1} = 0, \quad (23)$$

where φ is either θ or S .

At the lateral boundary Σ no normal current and free-slip conditions are set for velocity:

$$\mathbf{n} \cdot \mathbf{u} \Big|_{\Sigma} = 0, \quad (24)$$

$$\mathbf{n} \cdot (\mathbf{A} \text{grad}_h u_i + \mathbf{B}^{\frac{1}{2}} \text{grad}_h u_i) \Big|_{\Sigma} = 0, \quad (25)$$

$$\mathbf{n} \cdot \text{grad}_h (\text{div}_h (\mathbf{B}^{\frac{1}{2}} \text{grad}_h u)) \Big|_{\Sigma} = 0, \quad \mathbf{n} \cdot \text{grad}_h (\text{div}_h (\mathbf{B}^{\frac{1}{2}} \text{grad}_h v)) \Big|_{\Sigma} = 0. \quad (26)$$

where \mathbf{n} is a vector of normal to the lateral boundary Σ , u_i is velocity component tangential to Σ .

At the solid walls of Σ_S the isolation conditions are set for θ and S :

$$\mathbf{n} \cdot (\mathbf{K} \text{grad} \theta) \Big|_{\Sigma_S} = 0, \quad \mathbf{n} \cdot (\mathbf{K} \text{grad} S) \Big|_{\Sigma_S} = 0. \quad (27)$$

If there are open boundaries, observed values of temperature θ_{obs} and salinity S_{obs} are set at liquid boundaries:

$$\theta \Big|_{\Sigma_l} = \theta_{obs}, \quad S \Big|_{\Sigma_l} = S_{obs}. \quad (28)$$

The initial conditions by $t=t_0$ are set as:

$$u = u_0, \quad v = v_0, \quad \theta = \theta_0, \quad S = S_0, \quad \zeta = \zeta_0. \quad (29)$$

2.2. Numerical realization

Splitting methodology with respect to geometric coordinates and time are constructed to derive simpler evolution equations. The model uses spatial approximations on a staggered C-grid (Arakawa & Lamb, 1977). The splitting method allows implementing efficient implicit time-integration schemes for transport and diffusion equations for elements (the Crank-Nicholson approximation is used for transport processes, and an implicit scheme is used for diffusion and second-order viscosity). The shallow water linear equations are integrated by iterative or direct method without splitting. In the geostrophic adjustment problem, the Coriolis terms are also approximated implicitly by (Delecluse et al., 1998).



2.2.1. Boundary conditions in numerical realization

Land-ocean interface. The major flux between continental margins and the ocean is a mass exchange of fresh water through river runoff. Such an exchange modifies the sea surface salinity especially in the vicinity of major river mouths. It has to be taken into account for long term integrations as it influences the characteristics of water masses formed (especially at high latitudes). It is required for closing the water cycle of the climate system. It is usually specified as a fresh water flux at the air-sea interface in the vicinity of river mouths. Year climatic runoffs are used from the CORE data (forcing for Common Ocean-ice Reference Experiments) (Large & Yeager, 2004). Main rivers are spread and coastal runoffs are applied along the coast.

Solid earth-ocean interface. The boundaries are set to no flux conditions of heat and salt across the solid boundaries. For the moment, there is no flow across the solid boundaries, i.e. the velocity normal to the ocean bottom and coastlines is zero. The free-slip conditions are used at the lateral boundary and non-linear bottom friction.

Open boundary. All open boundaries are buffer zones where temperature and salinity fields are damping toward the climatic monthly mean from Levitus.

Atmosphere-ocean interface (the forcing of the model): the kinematic surface condition plus the mass flux of fresh water PE (the precipitation minus evaporation budget). The atmospheric conditions from the CORE data are transformed into surface fluxes with the bulk formulae for latent and sensible heat fluxes and wind stresses. The heat, salt and momentum fluxes at the sea surface are calculated using 6hr atmospheric wind, pressure, temperature and humidity, daily shortwave and longwave radiation and monthly precipitation.

2.2.2. The closure equations and the dissipation terms

The vertical viscosity and diffusion coefficients are calculated by Pacanovsky & Philander (1981) parameterization. Laplace operator along the geopotential surface is used for the lateral diffusion on the tracers and a bi-Laplacian along σ -surface is used for the lateral viscosity on momentum.

2.2.3. Type of computation/configuration

The geographical domain is the full JES basin. The bathymetry is processed from ETOPO2 2-min bathymetry. Spatial resolution is changed from 5 near Japan islands to 0.5 nm in the Bay of Peter the Great and the Strait of Tartary. The Tsushima Strait, Tsugaru Strait, Laperouse Strait and Strait of Tartary are buffer zones where temperature and salinity fields are damping toward the climatic monthly mean from Levitus.

The non-uniform distribution of the levels is such that, for the ocean depth equal to 3,500 m and for the number of levels equals to 25, the upper 150-m layer contains 10 levels. A higher concentration of model levels in the upper layer is required for a better treatment of stratification and mixing in that layer, as well as for a better representation of the structure of surface and subsurface currents.



3. Results of experiments

At first the experiment have been performed to reproduce the annual cycle of climatic circulation in the JES. The model was run from Levitus data for 5 years with the so-called normalized annual cycle in atmospheric forcing from the CORE data. Then several runs for years 1976, 1983 and 2003 were performed. Fig. 1 shows the surface climatic currents simulated in (cm/s) for winter (left panel) and summer (right panel). These results have good resemblances with observed data (see, for example, (Naganuma, 1973)).

One can see that well reproduced surface currents, forming main cyclonic gyre, which is composed of warm Tsushima Current in the east and the cold Primorskoe Current in the west. The last change its length to the south during the year. It is mesh refinements in shelf zone which permit to reproduce well Primorskoe current.

Fig. 2 shows strong mesoscale eddies in the JES. This eddy structure of JES currents is well reproduced in model results shown in Fig. 3. This figure shows that mesoscale eddies have strong impact on current field formation in the JES.

4. Summary

Efficient numerical technique for the numerical simulation of the ocean/sea circulation is presented. The its application to the solution of the problem of the Japan/East Sea (JES) circulation with high spatial resolution demonstrated that this numerical technique works well in reproducing velocity field

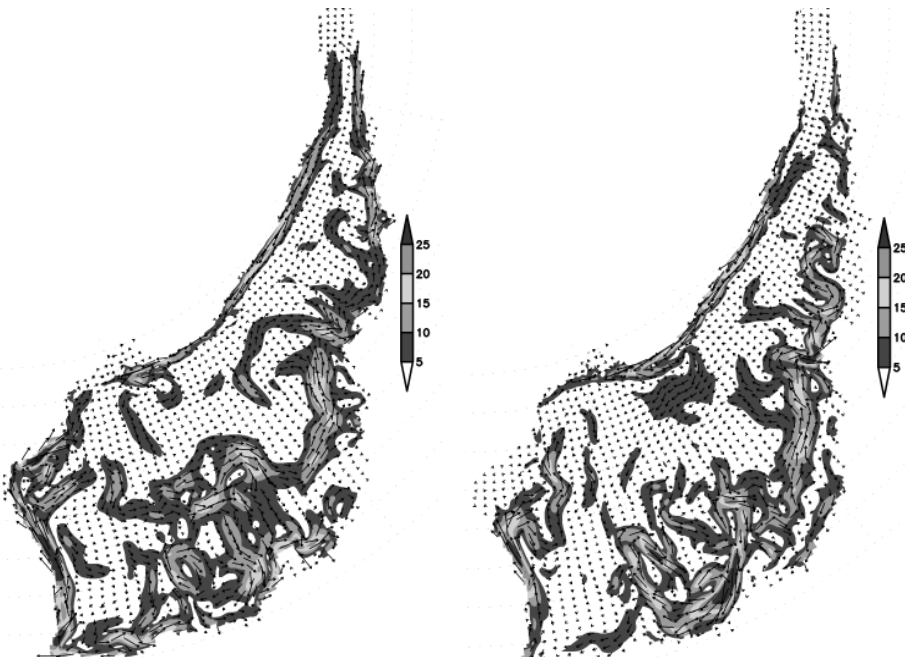


Fig. 1. Simulated surface climatic currents (cm/s) for winter (left panel) and summer (right panel).

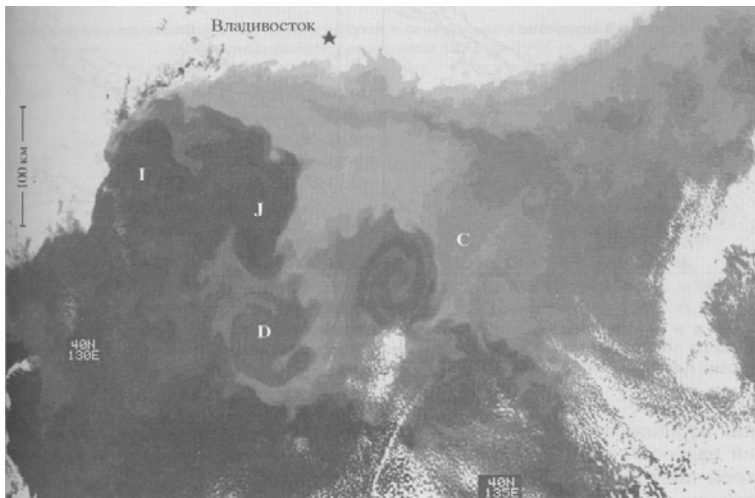


Fig. 2. Anti-cyclonic eddies in the northwestern Sea of Japan on the satellite image in the infrared range for January 11, 1997 (satellite NOAA-14). The dark tone of the image corresponds to the warmer waters.

in the JES. Simulation of the time evolution of the circulation of the JES was performed.

The calculations show the high eddy activity of the JES. Mesoscale eddies can modify the structure of basin scale currents. With high spatial resolution which is accompanied by the high eddy activity, requirements for the observational data are greater.

It is shown that for the simulation of the circulation of the seaward part of the JES it is necessary to use the 3D circulation model with high spatial resolution to adequately reproduce the structure of the eddy circulation, since the eddy activity may have strong impact on the spatial and temporal variability of currents.

Acknowledgements

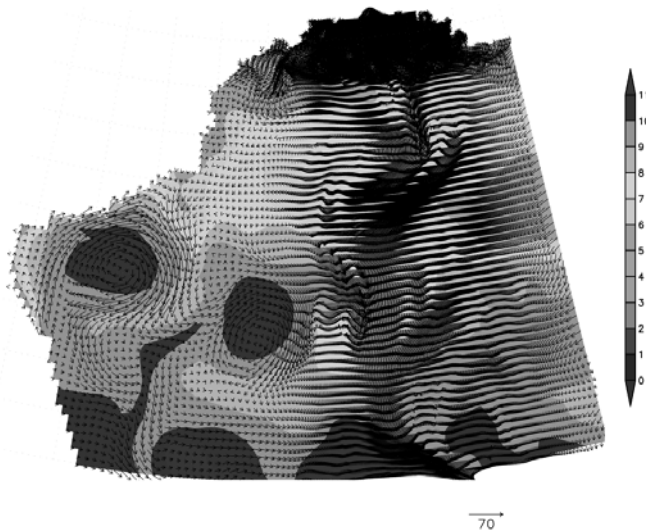
The work was supported by the Russian Foundation for the Basic Research, the Project No. 09-05-01231.

References

- Arakawa, A. & Lamb, V.R. (1977) Computational design of the basic dynamical processes of the UCLA general circulation model. In: Chang, J., ed., *Methods in computational Physics*, 17, 173–265. New York: Academic Press.
- Bryan, K. (1969) A numerical method for the study of the circulation of the World Ocean. *J. Computational Physics* 4:347–376.
- Bryden, D., San S., Bleck, R. (1999) A new approximation of the equation of state for seawater, suitable for numerical ocean models. *J. Geoph. Res.* 104(C1):1537–1540.
- Delecluse, P., Davey, M.K., Kitamura, Y. et al. (1998) Coupled general circulation modeling of the tropical Pacific. *J. Geoph. Res.* 103(C7):14357–14373.
- Diansky, N.A., Bagno, A.V., Zalesny, V.B. (2002) Sigma Model of Global Ocean Circulation and Its Sensitivity to Variations in Wind Stress. *Izvestiya Rossiiskoi Akademii Nauk Fizika Atmosfery i Okeana [Izvestiya Atmospheric and Oceanic Physics]* 38(4):477–494.



Fig. 3. Surface temperature (SST) (shaded, °C) and surface currents (arrows, cm/s) on the first of January 1983. Dark areas are from concentration of the arrows in mesh refinements zones.



- Hunke, E.C & Dukowicz, J.K. (1997) An elastic-viscous-plastic model for sea ice dynamics. *J. Phys. Oceanogr.* **27**:1849–1867.
- Large, W.G. & Yeager, S.G. (2004) *Diurnal to Decadal Global Forcing for Ocean and Sea-Ice Models: The Data Sets and Flux Climatologies*. Climate and Global Dynamics Division, National Center for Atmospheric Research, Colorado: Boulder.
- Madec, G., Delecluse, P., Imbard, M., Levy, C. (1998) *OPA 8.1 Ocean General Circulation Model Reference Manual*. Institut Pierre Simon Laplace des Sciences de l'Environnement Global. Notes du Pole de Modelisation.
- Marchuk, G.I. (1968) Some application of the splitting-up methods to the solution of mathematical physics problems. *Applik. mat.* **13**(2).
- (1988) *Splitting-up methods*. Moscow: Nauka.
- Meehl, G.A., Stocker, T.F., Diansky, N.A. et al. (2007) Global climate projections. In: *Climate change 2007. The physical science basis*, 748–845. Cambridge: Cambridge University Press.
- Mellor, G.L. (1998) *Users Guide for a Three-Dimensional, Primitive Equation, Numerical Ocean Model*. Program in Atmospheric and Oceanic Sciences Princeton University, Princeton, NJ 08544–0710.
- Naganuma, K. (1973) On the discussion on the existence of the third branch of the Tsushima current. *Ann. Rep. Japan Sea Reg. Fish. Res. Laboratory* **266**:1–3.
- Pacanovsky, R.C. & Philander, G. (1981) Parametrization of vertical mixing in numerical models of the tropical ocean. *J. Phys. Oceanogr.* **11**:1442–1451.
- Pacanovsky, R.C. & Griffies, S.M. (2000) *The MOM 3.0 Manual*. Geophysic Fluid Dynamics Laboratory. Princeton: NOAA.
- Solomon, S., Qin, D., Manning, M., eds. (2007) *IPCC Fourth Assessment Report. Climate Change 2007: the Scientific Basis (Chapter 10)*. Cambridge, New York: Cambridge University Press.
- Zalesny, V.B. (1996) Numerical Simulation and Analysis of the Sensitivity of Large-scale Ocean Dynamics. *Russ. J. Numer. Anal. Math. Modelling* **11**, 6:421–443.

Upwelling in the Baltic Sea

Andreas Lehmann, Kai Myrberg

Abstract

Up- and downwelling are typical phenomena in the Baltic Sea. Because of the complex coastline and many islands, winds from any direction cause up- and downwelling near the coast. The extent of upwelling is scaled by the internal Rossby radius which is about 2–10 km in the Baltic Sea. During summer and autumn when the sea surface is warm, upwelling can be observed by infrared satellite images as a local drop in temperature of several degrees. Upwelling is forced by sudden storms or strong wind events from different directions, with typical time scales ranging from a few days up to weeks. Satellite data indicate that the horizontal scales of coastal upwelling are of the order of 100 km along-shore and some 10–20 km off the coast. A general introduction of the upwelling process will be presented, but also recent results of a comprehensive analysis of satellite data for the period 1990–2009, as well as results of numerical model simulations from which the upwelling process can be studied with respect to transports and fluxes.

Ап- и даунвеллинги — типичные явления на Балтике. Поскольку береговая линия изрезана и имеется множество островов, ветер практически любого направления вызывает прибрежные ап- или даунвеллинг. Пространственный масштаб апвеллинга связан с инерционным радиусом Россби, имеющим для Балтийского моря порядок 2–10 км. Летом и осенью, когда воды на поверхности теплые, апвеллинг проявляется на инфракрасных спутниковых снимках как локальное понижение температуры на несколько градусов. Апвеллинг вызывается штормами или сильными ветрами с различных направлений и обычно имеет временной масштаб от нескольких дней до нескольких недель. Спутниковые данные указывают, что пространственные масштабы прибрежного апвеллинга имеют порядок 100 км вдоль берега и 10–20 км поперек него. В лекции

Andreas Lehmann (✉)

Leibniz Institute of Marine Research, Kiel, Germany

e-mail: alehmann@ifm-geomar.de

Kai Myrberg (✉)

Finnish Environment Institute/Marine Research Centre, Helsinki, Finland

e-mail: Kai.Myrberg@ymparisto.fi



представлены как общее введение в процесс формирования апвеллинга, так и новые результаты комплексного анализа спутниковых снимков за период 1990–2009 гг., а также результаты численного моделирования, позволяющего исследовать вопросы транспорта и потоков вещества при апвеллинге.

1. Introduction

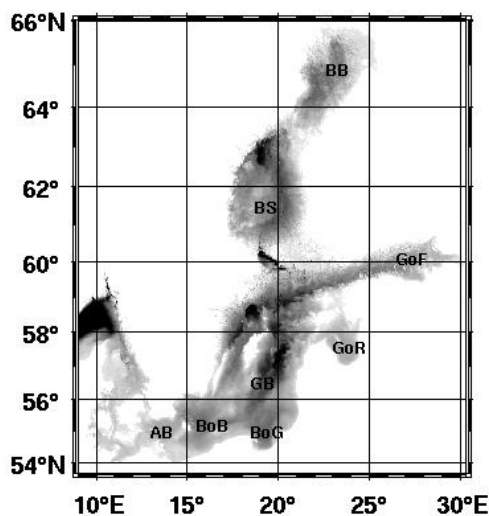
In general, upwelling is the result of horizontal divergence in the surface layer of the ocean. It involves wind-driven motion of dense, cooler and usually nutrient-rich water towards the ocean surface, replacing the warmer, mostly nutrient-depleted surface water. Upwelling is an important process in the Baltic Sea. As the Baltic Sea is a semi-enclosed basin with a small size (Fig. 1), upwelling become frequently visible all along the coast depending on prevailing wind conditions (for details see Lehmann & Myrberg, 2008).

2. Early studies of upwelling

The first documented scientific observation of upwelling in the Baltic Sea was carried out by Alexander von Humboldt (Kortum & Lehmann, 1997). During August 1834 von Humboldt was traveling with a Russian steam boat from Szczecin to Kaliningrad and back to Szczecin. While the boat was traveling at about 2–3 nm off the coast, Humboldt measured a strong drop in sea-surface temperature of about 10 °C near the 18° longitude off the Polish coast (Fig. 2), while eastward of Hel Peninsula, the temperature again increased to values of about 20 °C. Von Humboldt speculated that in deeper layers of the Baltic Sea cold water exists which reach the surface in a similar manner like katabatic winds that blow down a topographic incline but in opposite vertical direction (anabatic winds).

A first comprehensive explanation of the upwelling process could be given by the application of Ekman's theory (1905). It provided a basis for understanding the effect of wind stress on ocean circulation, and showed that due

Fig. 1. Topographic map of the Baltic Sea and its sub-basins:
 (AB) Arkona Basin,
 (BoB) Bornholm Basin,
 (BoG) Bay of Gdansk,
 (GB) Gotland Basin,
 (GoF) Gulf of Riga,
 (GoF) Gulf of Finland,
 (BS) Bothnian Sea,
 (BB) Bothnian Bay.



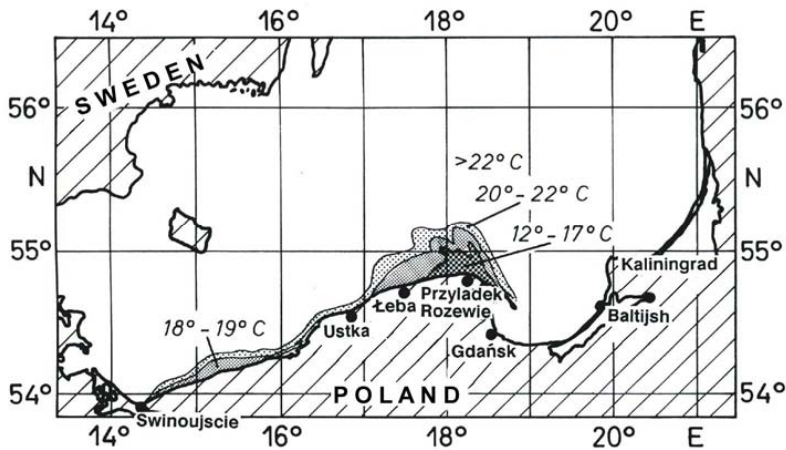


Fig. 2. Sea-surface temperature in the beginning of September 1997 redrawn from infrared satellite data. A similar upwelling situation has been observed in August 1834 by A. v. Humboldt when traveling from Szczecin to Kaliningrad (Kortum & Lehmann, 1997).

to the effect of Earth's rotation and frictional forces, the net transport of water due to the wind stress is directed 90° to the right of the wind in the Northern Hemisphere.

Further studies of Baltic Sea upwelling were carried out by Palmén & Laurila (1938), Hela (1946), Sjöblom (1967), Walin (1972a, 1972b) and Svansson (1975). These results were based on analyses of measurements. Their work has been summarized by Hela (1976). Palmén & Laurila (1938) described the change in surface temperature after a strong wind event. Additionally, Hela (1946) and Sjöblom (1967) argued that certain sub-regions of the Baltic Sea coast are more favorable for upwelling and that these regions are also favorable as fishing areas. Svansson (1975) discussed a possible relation between upwelling and the generation of Kelvin waves.

3. Observations (from traditional methods to remote sensing)

3.1. Detection

Before satellite data were available upwelling could only be detected on the basis of temperature measurements during the thermal stratified period (Hela, 1976). Among those studies an important early founding was the one by Palmén & Laurila (1938). In the transition from September to October 1936, hydrographic sections across the Gulf of Finland were carried out which documented strong changes in temperature and salinity distributions due to upwelling at the Estonian coast. Even if first results were already published before World War II, upwelling as a process itself remained poorly understood for a long while. So, the measurements of upwelling were in some extent random in character and not results of well-prepared measurement campaigns. Only in the 1970's more comprehensive results were obtained. Walin (1972a) detected upwelling at the Swedish east coast and found that temperature fluctuations extended only 5–10 km offshore. He also proposed



these fluctuations to have a tendency to propagate along the coast as internal Kelvin waves. Svansson (1975) also found upwelling in the Hanö Bight, as Wallin (1972a). Svansson also took up the question of the biological significance of upwelling in the coastal regions where nutrients may be transported to the uppermost, euphotic layer of the sea. This fact has been later found to be an important element of the upwelling phenomenon.

One of the main areas where upwelling has been observed in temperature measurements, is the northern coast of the Gulf of Finland (Hela, 1976, Niemi, 1979, Kononen & Niemi 1986, Haapala, 1994). All these papers confirm that upwelling is especially favored by south-westerly winds. In such cases, sea-surface temperatures can drop by 10 degrees in 1–2 days during stratified periods. During such conditions, when the surface layer can be depleted of nutrients, upwelling plays a key role in replenishing the euphotic zone with the nutritional components necessary for biological productivity. Consequently, upwelling favors fishing in the area (Sjöblom, 1967). Niemi (1979) found out that in such areas where upwelling lifts phosphorus-rich deep water to the surface, the N/P ratio becomes low which favors the blooming of nitrogen-fixing blue-green algae.

3.2. Analysis

The utilization of satellite measurements started in the early 1980's and since then space borne measurements of various kinds (AVHRR radiometers in NOAA satellites etc.) have been utilized by numerous authors (e.g. Siegel et al., 1994, Kahru et al., 1995, Lass et al., 2003, Kowalewski & Ostrowski, 2005). Among the most comprehensive studies is the one by Horstmann (1983) where the author studied upwelling at the southern coast of the Baltic Sea from AVHRR satellite data for the year 1982. Sequences of satellite pictures documented the development of upwelling during south-east and easterly winds at the western coast of Rügen, along the Polish coast between the Pommeranian Bight and Ustka, and from Leba to Hel Peninsula. Gidhagen (1987) did an analysis based on AVHRR data and concluded that upwelling at the Swedish coast takes place up to 10–20 km offshore and about 100 km alongshore. According to Gidhagen (1987) water is lifted to the surface from depths of 20–40 m which is somewhat larger than previously estimated. He also found that in some areas upwelling exists even one-fourth to one-third of the time. Bychkova & Viktorov (1987) found 14 upwelling cases around the Baltic with different scales and life-times. In the southwestern Baltic, at the German and Polish coasts, satellite observations of upwelling were analyzed by Siegel et al. (1994).

4. Basic physical principles of upwelling

4.1. Ekman transport

The work of Ekman (1905) provided a basis for understanding the effect of wind stress on an infinite non-stratified ocean. Due to the effect of the Earth's rotation and frictional forces the net transport due to the wind stress is directed 90° to the right of the wind in the northern hemisphere. Thorade



(1909) first applied Ekman's theory to an upwelling situation. He showed that coastal winds blowing parallel to the coast were sufficient to induce an off-shore transport of surface water.

The wind stress on the sea-surface is based on the following formula

$$\tau = C_D \rho_a |U_a| U_a \quad (2)$$

with C_D the drag coefficient, ρ_a density of air and U_a the wind velocity at 10 m height. The effect of the driving force is limited to a small surface boundary layer, the Ekman boundary layer of depth $D_E = n(2\mu_v/f)^{1/2}$ within which the current rotates and decreases with depth. μ_v denotes the vertical eddy viscosity and f the Coriolis parameter. This depth, D_E , called the depth of the frictional influence or the depth of the wind current. This depth coincides not necessarily with the depth of the mixed layer. Although the transport of water within the Ekman layer is in different directions at different depths, the total wind-induced mass transport, integrated over this layer, is 90° to the right of the wind. Therefore, a horizontal surface divergence must occur wherever a coastline is found on the left of the wind. The width of the frictional boundary layer at the coast depends on the horizontal viscosity, and is given by $D_H = n(2\mu_H/f)^{1/2}$ (Tomczak, 1972).

The Ekman transport is given by

$$M_x = \tau_y / f \quad (3)$$

$$M_y = -\tau_x / f. \quad (4)$$

The relation between Ekman transport and wind stress is independent of ρ_w and the vertical friction coefficient and f is the Coriolis parameter ($f = 2\omega \sin\varphi$). Once the wind stress has been determined the corresponding offshore transport can be calculated from Ekman transport relations (Smith, 1968). For two similar wind events the same transport will result, but whether upwelling will have a temperature signal in the sea surface depends additionally on the bathymetry and the thermal stratification.

Upwelling as a meso-scale feature is scaled by the internal Rossby radius. It is defined as

$$R_n = c_n / f_n \quad (5)$$

where $n=1, 2, \dots, c_n$'s are the phase and group speed of Kelvin waves and as the thermal stratification varies seasonally depending on changes in heating and wind induced mixing in the Baltic Sea, the baroclinic Rossby radius varies between 1.5–10 km (Fennel et al., 1991, Alenius et al., 2003). Typical scales of upwelling in the Baltic Sea are:

- ✓ vertical motion: 10^{-5} – 10^{-4} ms^{-1} ~ 1–10 m/day;
- ✓ horizontal scales: 10–20 km offshore, 100 km alongshore;
- ✓ temperature change: 1–5 $^\circ\text{C}/\text{day}$;
- ✓ temperature gradient: 1–5 $^\circ\text{C}/\text{km}$;
- ✓ lifetime: several days up to one month.

The principle response of a stratified elongated basin to constant wind in lengthwise direction of the basin can be described as follows (Krauss & Brügge, 1991) expecting that the wind direction is parallel to the coasts:

(i) In the surface layers there is an Ekman transport in cross-wise direction.



(ii) This Ekman transport produces (in northern hemisphere) a sea level rise on the right-hand coast (viewing in wind direction) and a fall on the left-hand side. Furthermore, down-welling occurs on the right-hand side and upwelling on the left-hand side resulting in baroclinic effects of the same sign at both coasts.

(iii) Consequently coastal jets are produced along both coasts parallel to the wind direction and a slow return flow compensates this transport in the central area of the basin.

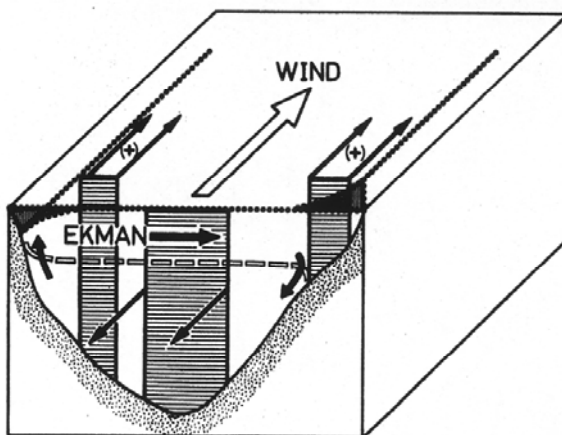
The scheme of this circulation (Fig. 3) can be applied to the different sub-basins of the Baltic Sea. Krauss & Brüggge (1991) demonstrated that upwelling in the Baltic Sea should be regarded as a three-dimensional current system affecting not only the local coast but also the opposite coast and the internal of the basin (Fennel & Sturm, 1992, Fennel & Seifert, 1995). However, the vertical extension of the Ekman compensation below the mixed layer is restricted in the Baltic due to the existence of the halocline normally at a depth of 50–80 m.

4.2. Kelvin waves

Abrupt changes in the alongshore component of the wind stress generate in stratified waters internal Kelvin wave fronts which limit the amplitude of upwelling and give rise to a countercurrent under the thermocline (e.g. Gill & Clarke, 1974). Coastline irregularities generate Kelvin waves in a manner similar to the wind-stress variability (e.g. Crepon et al., 1984). It depends on the shape of the coastline irregularity and the incident angle of the wind whether upwelling will be stabilized or destabilized by propagating Kelvin waves. The generation of Kelvin waves fronts is not only linked to the existence of abrupt discontinuities in the coastline, even continuous variations of the angle of the incident wind on the coasts can initiate Kelvin wave fronts (Crepon et al., 1984, Fennel & Seifert, 1995).

Thus, upwelling areas are related to the shape of the coast, and filaments will be generated at the same locations under similar atmospheric conditions. Even remote areas which are not affected by local upwelling directly will be reached by propagating Kelvin wave fronts.

Fig. 3. Principle response of an elongated basin to constant wind in length direction of the basin, redrawn from Krauss & Brüggge (1991).





4.3. Atmospheric forcing

Coastal upwelling depends on atmospheric forcing: wind speed, direction and duration of the wind events. So, accurate descriptions of the wind, temperature and humidity fields are essential for studying upwelling dynamics. From Ekman's theory, long-shore winds are most effective to generate upwelling.

A measure of the characteristics of the wind suitable to produce upwelling is the wind impulse I (Haapala, 1994).

$$I = \int_0^t \tau dt = \int_0^t C_D \rho_a U_{10}^2 dt \quad (6)$$

where ρ_a is the air density, C_D is the drag coefficient, U_{10} the wind speed at 10 m height and t the wind duration. The occurrence of upwelling depends on the stratification and the strength of the wind impulse. During thermal stratification a $4,000\text{--}9,000 \text{ kgm}^{-1}\text{s}^{-1}$ wind impulse of about 60 h duration is needed to generate upwelling, and when the sea is thermally homogeneous the impulse required is $10,500\text{--}14,000 \text{ kgm}^{-1}\text{s}^{-1}$. This implies that under strongly stratified conditions the wind stress has a direct effect only on the relatively thin water column over the thermocline. Even quite weak winds can lead to upwelling. If the stratification is weak the influence of the wind penetrates distinctly deeper, and more wind energy is needed to produce upwelling (Haapala, 1994). For the Baltic area there exist different general weather conditions which are favorable for upwelling at various coastal areas. Bychkova et al. (1988) identified 22 typical areas in different parts of the Baltic Sea which were favorable for upwelling in relation to 11 different wind conditions (Figs. 4, 5). For example the wind event I (north-easterly wind) is coupled with upwelling regions 3, 5, 6, and 9 while for example case VI (west, south-westerly winds) are coupled with cases 2, 10–20 and 22 (see Bychkova et al., 1988 for details).

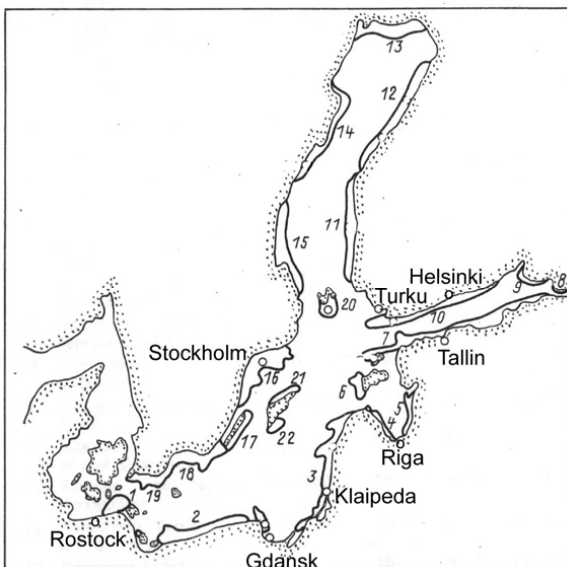


Fig. 4. Main upwelling regions in the Baltic Sea due to corresponding general weather conditions, redrawn from Bychkova et al. (1988).



5. Requirements on future research

To resolve the full spectrum of meso-scale features numerical models should have a horizontal resolution in the order of the internal Rossby radius or even higher. These high resolution models should be validated with high resolution satellite data and hydrographic measurements which provide information not only on the location of upwelling but also on the temporal development and horizontal extent. Thus high resolution hydrographic measurements campaigns are needed to describe the upwelling process mainly due to changes in stratification and mixing of different properties including nutrients. High resolution modeling can then attribute corresponding transports and quantification of the upwelling process including mixing. The combined advances in observational techniques and modeling can help to understand the upwelling process and related implications. The mostly needed research should aim at:

- ✓ quantification of transports and fluxes on-/offshore related to upwelling including coastal jets;
- ✓ contribution to the total mixing and impact on residence times;
- ✓ impact and quantification of changes of the interaction between ocean and atmosphere;
- ✓ documentation of upwelling areas and their probability to occur with respect to specific atmospheric general conditions for the total Baltic Sea;
- ✓ impact of upwelling on bio-geochemical processes and phytoplankton development;
- ✓ impact of climate change on wind fields and related changes in upwelling regions.

A deeper understanding of the upwelling process and its implication on the marine environment will lead to an improvement of the prognosis of the local weather prediction, algae bloom forecasting, transports and mixing of nutrients and harmful substances.

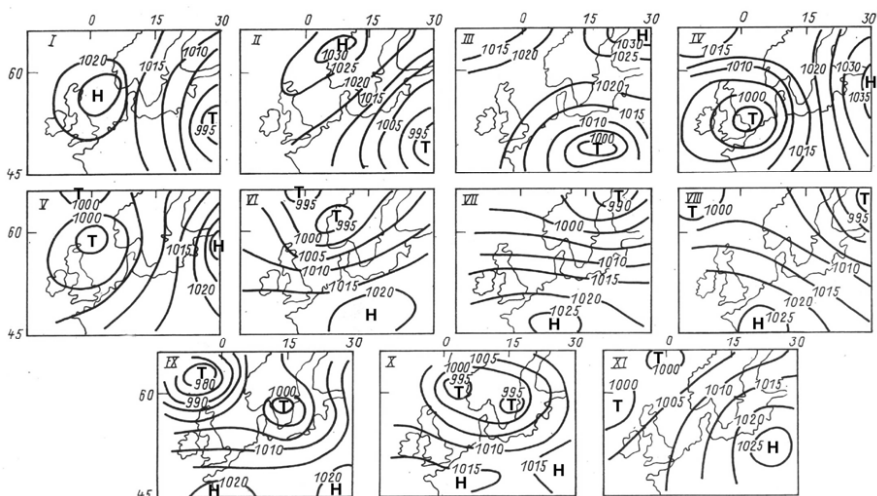


Fig. 5. Typical general weather conditions favoring upwelling in the Baltic Sea, redrawn from Bychkova et al. (1988).



References

- Alenius, P., Nekrasov, A., Myrberg, K. (2003) Variability of the baroclinic Rossby radius in the Gulf of Finland. *Cont. Shelf Res.* **23**:563–573.
- Bychkova, I. & Viktorov, S. (1987) Use of satellite data for Identification and Classification of Upwelling in the Baltic Sea. *Oceanology* **27**(2):158–162.
- Bychkova, I., Viktorov, S., Shumakher, D. (1988) A relationship between the large-scale atmospheric circulation and the origin of coastal upwelling in the Baltic. *Meteorologiya i Gidrologiya* **10**:91–98 (in Russian).
- Crépon, M., Richez, C., Chartier, M. (1984) Effects of coastline geometry on upwelling. *J. Phys. Oceanogr.* **14**(8):1365–1382.
- Ekman, V. (1905) On the influence of the earth's rotation on ocean currents. *Ark. Mat. Astr. Fys.* **2**(11):1–52.
- Fennel, W., Seifert, T., Kayser, B. (1991) Rossby radii and phase speeds in the Baltic Sea. *Cont. Shelf Res.* **11**:23–36.
- Fennel, W. & Seifert, T. (1995) Kelvin wave controlled upwelling in the western Baltic. *J. Marine Systems* **6**:289–300.
- Fennel, W. & Sturm, M. (1992) Dynamics of the western Baltic. *J. Marine Systems* **3**:183–205.
- Gidhagen, L. (1987) Coastal Upwelling in the Baltic Sea—satellite and *in situ* Measurements of Sea-Surface Temperatures indicating Coastal Upwelling. *Estuarine, Coastal and Shelf Science* **24**:449–362.
- Gill, A.E. & Clarke, A.J. (1974) Wind-induced upwelling, coastal currents and sea-level changes. *Deep Sea Research* **21**:325–345.
- Haapala, J. (1994) Upwelling and its Influence on Nutrient Concentration in the Coastal Area of the Hanko Peninsula, Entrance of the Gulf of Finland. *Estuarine, Coastal and Shelf Science* **38**:507–521.
- Hela, I. (1946) Coriolis-voiman vaikutuksesta Suomenlahden hydrografisiin oloihin. *Terra* **2**:52–59.
- (1976) Vertical velocity of the upwelling in the sea. *Societas Scientiarum Fennica, Commentationes Physico-Mathematicae* **46**(1):9–24.
- Horstmann, U. (1983) Distribution patterns of temperature and water colour in the Baltic Sea as recorded in satellite images: Indicators for phytoplankton growth. *Berichte aus dem Institute für Meereskunde an der Universität Kiel*, 106.
- Kahru, M., Håkansson, B., Rud, O. (1995) Distributions of the sea-surface temperature fronts in the Baltic Sea as derived from satellite imagery. *Cont. Shelf Res.* **15**(6):663–679.
- Kononen, K. & Niemi, Å. (1986) Variation in phytoplankton and hydrography in the outer archipelago. *Finnish Marine Research* **253**:35–51.
- Kortum, G. & Lehmann, A. (1997) A. v. Humboldts Forschungsfahrt auf der Ostsee in Sommer 1834. *Schr. Naturwiss. Ver. Schlesw.-Holst.* **67**:45–58.
- Kowalewski, M. & Ostrowski, M. (2005) Coastal up- and downwelling in the southern Baltic. *Oceanologia* **47**(4):453–475.
- Krauss, W. & Brügge, B. (1991) Wind produced water exchange between the deep basins of the Baltic Sea. *J. Phys. Oceanogr.* **21**:373–384.
- Lass, H.-U., Schmidt, T., Seifert, T. (2003) Hiddensee upwelling field measurements and modelling results. *ICES Coop. Res. Rep.* **257**:204–208.
- Lehmann, A. & Myrberg, K. (2008) Upwelling in the Baltic Sea—a review. *J. Marine Syst.* **74** (Suppl. 1):3–12, doi: 10.106/j.jmarsys.2008.02.010



- Niemi, Å. (1979) Blue-green algal blooms and N:P ratio in the Baltic Sea. *Acta Bot. Fennica* **110**:57–61.
- Palmén, E. & Laurila, E. (1938) Über die Einwirkung eines Sturmes auf den hydrographischen Zustand im nördlichen Ostseegebiet. *Soc. Sci. Fenn., Comment. Phys.-Math.* **X(1)**:1–52.
- Siegel, H., Gerth, M., Rudloff, R., Tschersich, G. (1994) Dynamic features in the western Baltic Sea investigated using NOAA-AVHRR data. *Deutsche Hydrographische Zeitschrift* **46(3)**:191–209.
- Sjöblom, V. (1967) Meriveden kumpuaminen ja Porkkalan niemi (Summary: Upwelling of the sea water and the cape of Porkkala). *Suomen Kalatalous* **27**:1–12.
- Smith, R. (1968) Upwelling. *Oceanography Mar. Biol. Ann. Rev.* **6**:11–46.
- Svansson, A. (1975) Interaction between the coastal zone and the open sea. *Merentutkimuslaitoksen Julkaisu* **239**:11–28.
- Thorade, H. (1909) Über die Kalifornischen Meereströmung, Oberflächentemperaturen und Strömungen an der westküste Nordamerikas. *Ann. d. Hydrogr. u. Mar. Meteor.* **37**:17–34, 63–76.
- Tomczak, M. (1972) Problems of physical oceanography in coastal upwelling investigations. *Geoforum* **11**:23–36.
- Walín, G. (1972a) On the hydrographic response to the transient meteorological disturbances in the Baltic Sea. *Tellus* **24**:169–186.
- (1972b) Some observations of temperature fluctuations in the coastal region of the Baltic Sea. *Tellus* **24(3)**:187–198.

Multiparametric in-situ observations in the Gulf of Finland

**Urmas Lips, Inga Lips, Taavi Liblik, Villu Kikas,
Kristi Altoja, Natalja Kuvaldina, Nelli Norit**

Abstract

New observation tools, which enable to measure the fine structure of marine ecological state variables, are significantly improving the existing understanding of the ecosystem functioning and may be applied operationally. We present the multiparametric observations in the Gulf of Finland (Baltic Sea) using an autonomous system installed on board a ferry (autonomous measurement twice a day: time step 20 s, spatial resolution 150 m; weekly sampling), a moored water column profiler (vertical profiling of temperature, salinity and Chl *a* fluorescence with a time step of 3 h) and an ADCP deployed in the gulf, and measurements and water sampling on board a research vessel. An analysis of the collected data together with wind data from the area enabled us to characterise the structure and variability of hydrophysical fields, nutrients and phytoplankton and to relate the observed changes to the forcing and key processes.

Новые средства измерений, позволяющие измерять тонкую структуру параметров морской воды, существенно расширили существующие возможности в понимании функционирования морских экосистем. Они также могут использоваться и для операционных целей. Мы представляем многопараметрические наблюдения в Финском заливе (Балтийское море) с использованием автономных измерительных систем. Одна из них была установлена на борту парома, пересекающего акваторию два раза в день. Измерения проводились каждые 20 с, что соответствовало шагу по пространству порядка 150 м. С помощью заякоренной в стационарной точке буйковой системы проводилось регулярное (каждые 3 ч) вертикальное профилирование характеристик солёности, хлорофилла, флюорисценции и измерение скорости течений с помощью ADCP. В ходе еженедельных

Urmas Lips, Inga Lips, Taavi Liblik, Villu Kikas, Kristi Altoja,
Natalja Kuvaldina, Nelli Norit (✉)
Marine Systems Institute, Tallinn University of Technology, Tallinn, Estonia
e-mail: urmas.lips@phys.sea.ee



рейсов научного судна проводились стационарные наблюдения в точках вдоль трассы парома. Анализ собранных данных вместе с информацией о ветре позволил описать структуру и изменчивость гидрофизических полей, распределения биогенных элементов и фитопланктона, а также выявить ключевые процессы и отклики на внешние воздействия.

1. Introduction

New observation tools introduced within the last 10–20 years, which enable to measure the fine structure of marine ecological state variables, are significantly improving the existing understanding of the ecosystem functioning. Classical observations are performed with low frequency or episodically, the remote sensing methods do not reveal the vertical structure of the water column, i.e. essential phenomena and mechanisms may remain unnoticed. Thus, autonomous *in-situ* observation systems (among them autonomous vertical profilers) with near real-time data delivery play the key role in assessing the state and studying the pelagic ecosystem, especially meso-scale and fine-scale processes/features.

The Gulf of Finland is a stratified and wide estuary with a major fresh water inflow in the eastern end and relatively open water exchange with the Baltic Proper through the gulf's western boundary. Residual circulation in the surface layer consists of an outflow of gulf's waters in the northern part and an inflow of open Baltic Sea waters in the southern part of the gulf. Wind-driven circulation in the Gulf of Finland is highly variable and is characterized by intense meso-scale features—eddies, upwelling/downwelling, coastal and frontal jet currents which can cause significant vertical advection of water masses and substances, e.g. nutrients and phytoplankton.

Upwelling events have been reported to influence the phytoplankton dynamics in the upper layer in summer in the Baltic Sea, including the Gulf of Finland (Vahtera et al., 2005, Nausch et al., 2009, Lips & Lips, 2010). It has been shown both by modelling and direct measurements that the amount phosphate-phosphorus transported into the surface layer by a single coastal upwelling event may be approximately equal to the average total monthly riverine load of phosphorus to the Gulf of Finland (Zhurbas et al., 2008, Lips et al., 2009). One of the main factors influencing the cyanobacteria (especially *Aphanizomenon* spp.) bloom intensity in the Gulf of Finland is the intensity of pre-bloom upwelling events in May–June (Lips & Lips, 2008) and thus, near real time observations of upwelling events and their intensities are a pre-requisite for operational bloom forecasts (Laanemets et al., 2006).

The sub-surface maxima of phytoplankton biomass, among them the relatively deep maxima formed by dinoflagellate *Heterocapsa triquetra* (e.g. Pavelson et al., 1999, Kononen et al., 2003), have been observed in the Gulf of Finland in summer when the upper layer is depleted of nutrients but high reserves of nutrients are available below the seasonal thermocline. In July 2006 the sub-surface Chl *a* maximum layers with thickness varying between 1.5 and 9 m and intensity up to 7.6 $\mu\text{g l}^{-1}$ were observed in the lower part of the seasonal thermocline within the depth range of 14.5 to 35 m (Lips et al., 2010). Nutrient analyses of water samples collected from the thermocline revealed the coincidence of the location of Chl *a* maxima and nutriclines.



However, no estimates of the role of sub-surface maxima in the total primary production during summer months are available yet for the Baltic Sea (Gulf of Finland).

The main aim of the present paper is to show how the high resolution *in-situ* observation systems can be applied to define the role of upwelling events for the development of surface blooms and to define the processes responsible for the formation and maintenance of sub-surface maxima of phytoplankton.

2. Material and methods

We present the results of multiparametric observations conducted in the Gulf of Finland (Baltic Sea) in July–August 2009. The measurement program was designed to map both, the horizontal and vertical distribution of ecological state variables with sufficient resolution, duration and extent. An autonomous measurement system (Ferrybox) installed on board a ferry travelling between Helsinki and Tallinn was used for measurements and sampling in the surface layer. Temperature, salinity and Chl *a* fluorescence were recorder along the ferry route (Fig. 1) twice a day with a time step of 20 s (corresponding approximately to spatial resolution of 150 m) and weekly water sampling at 17 locations was conducted. Water samples were analyzed for Chl *a* content and phytoplankton species composition and biomass.

In order to register the changes in the vertical distribution of temperature, salinity and Chl *a* fluorescence a moored water column profiler was deployed close to the ferry line (Fig. 1) from June 30 to August 28. While Ferrybox data were delivered once a day (after arrival of ferry to Tallinn) the vertical profiles acquired at the buoy station were transmitted after every profiling conducted with a time step of 3 h in the layer from 2 to 50(45) m. An acoustic Doppler current profiler (ADCP) was deployed near the autonomous buoy profiler to register the vertical flow structure in the whole water column (water depth 86 m) since July 23. CTD measurements and water sampling on board a re-

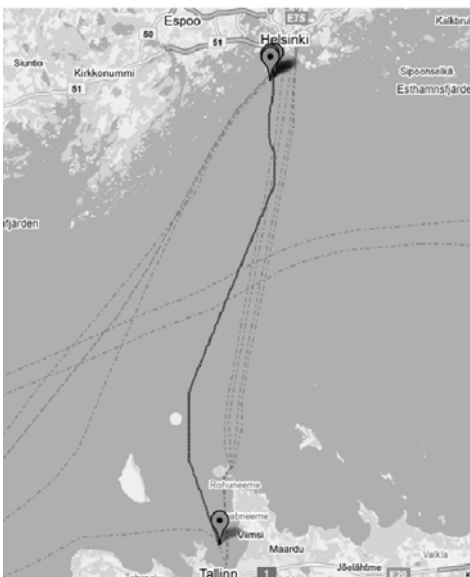


Fig. 1. Ferry route between Tallinn and Helsinki (blue/dark line) and location of autonomous buoy profiler (yellow/light circle) in the Gulf of Finland.



search vessel were performed on July 28 and 31, and August 11–12. Water samples were analyzed for nutrient (PO_4^{3-} and $\text{NO}_2^- + \text{NO}_3^-$) concentrations, Chl *a* content and phytoplankton species composition and biomass. Wind data used in the analysis were obtained from the Kalbådagrund meteorological station (Finnish Meteorological Institute).

3. Results

The observed changes in the horizontal and vertical distribution of temperature and salinity can be related to the changes in the atmospheric forcing. We specified four periods with different wind forcing and related changes in the vertical stratification (Fig. 2). South-easterly winds, which prevailed in the study area from 6 to 13 July, caused an upwelling near the Estonian coast. This event was registered also at the buoy station situated more than 20 km from the southern coast. Westerly-south-westerly winds (prevailing from July 16 until the end of July) caused deepening of the seasonal thermocline. This period was characterized by three-layer flow structure—an inflow was observed in the surface layer, a relatively weak outflow below the thermocline in the intermediate layer and a strong outflow in the near-bottom layer.

Period of weak winds in the beginning of August led to the formation of a warm and shallow surface layer. The flow structure returned to a typical

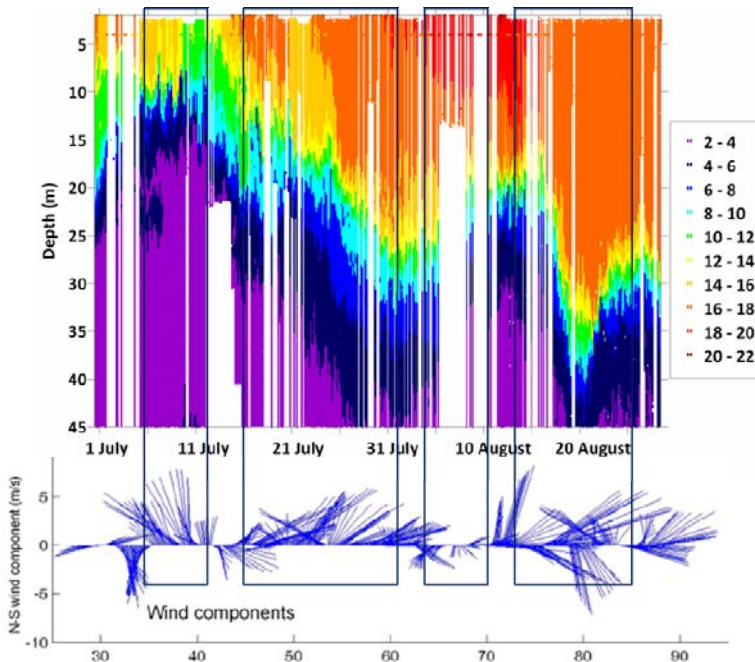


Fig. 2. Changes in the vertical structure of temperature field at the buoy station (upper panel, °C) and time series of wind vectors at the Kalbådagrund meteorological station (numbers on x-axis indicate days starting from June 1) from June 30 to August 28, 2009. Four periods with different wind characteristics are shown as rectangles. Dots at 4 m depth indicate simultaneous Ferrybox data at the closest point to the buoy station.



estuarine circulation pattern with an outflow in the surface and intermediate layers and an inflow in the deeper layers. Strong wind pulses observed in mid August caused barotropic current oscillations in the whole water mass. On August 16–20 a sharp deepening of the seasonal thermocline happened due to the strong winds from westerly directions. A clear two-layer flow structure was established.

In the described periods with different wind forcing and related hydrodynamic processes different phytoplankton groups dominated the community according to the water samples analyses collected in the surface layer. In the first period flagellates were dominating the phytoplankton community in the area of upwelling influence. When deepening of the seasonal thermocline and three layer flow structure were observed, dinoflagellate *Heterocapsa triquetra* became dominant. Warming of the surface layer (and development of stratification) created favourable conditions for cyanobacteria dominance.

In the periods of dominance of flagellates and especially dinoflagellate *H. triquetra* clear vertical migration of phytoplankton was revealed (Fig. 3). Speed of downward migration of the latter species up to 1 m h^{-1} could be estimated. According to the vertical distributions of Brunt-Väisälä frequency the phytoplankton cells did not stop in the layer with the strongest stratification but mostly just a few metres below it. As a rule the current shear was relatively low at the depths where the most intense sub-surface maxima were observed. Sampling on board the research vessel Salme revealed very high abundances of *H. triquetra* in these maxima—for instance on July 28 up to 2.5 million cells per litre were counted in a sample obtained from the 33 m depth.

It has to be noted that during the dominance of cyanobacteria in the beginning of August no remarkable vertical migration of phytoplankton was observed. However a high number of heterotrophic flagellates was often observed at the base (just below) the seasonal thermocline.

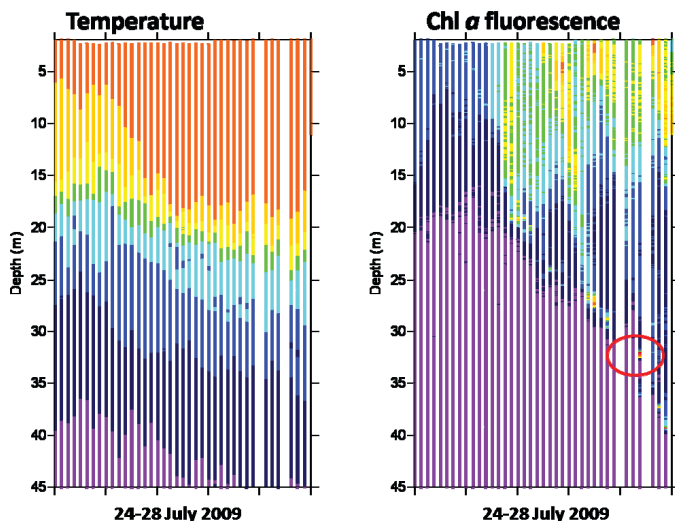


Fig. 3. Changes in the vertical distribution of temperature (left panel, °C) and Chl a fluorescence (right panel, arbitrary units) at the buoy station (July 24–28, 2009). Red oval indicates the maximum Chl a fluorescence value measured on July 28 at 33 m depth.



4. Conclusions

We have observed pronounced hydrodynamic features and related changes in the horizontal and vertical distributions of temperature, salinity and Chl *a* in the Gulf of Finland in July–August 2009. Depending on the wind forcing a three-layer, two-layer or barotropic flow structure (oscillations) was observed. On the basis of high resolution Chl *a* fluorescence recordings different vertical migration patterns of phytoplankton were found. Phytoplankton behaviour depends on species composition (dominating species) but the species dominance seems to be controlled by the physical processes of various scales. High biomass of heterotrophic flagellates is commonly observed close to the base of the seasonal thermocline while very high biomass is formed there under certain conditions by mixotrophic dinoflagellate *Heterocapsa triquetra*.

In order to understand the mechanisms of the formation and maintenance of these layers of deep phytoplankton maxima and their role in the total primary production in the stratified estuaries further studies are needed.

References

- Kononen, K., Huttunen, M., Hällfors, S. et al. (2003) Development of a deep chlorophyll maximum of *Heterocapsa triquetra* Ehrenb. At the entrance to the Gulf of Finland. *Limnol. Oceanogr.* **48**:594–607.
- Laanemets, J., Lilover, M.-J., Raudsepp, U. et al. (2006) A fuzzy logic model to describe the cyanobacteria *Nodularia spumigena* blooms in the Gulf of Finland, Baltic Sea. *Hydrobiologia* **554**:31–45.
- Lips, I. & Lips, U. (2008) Abiotic factors influencing cyanobacterial bloom development in the Gulf of Finland (Baltic Sea). *Hydrobiologia* **614**:133–140.
- (2010) Phytoplankton dynamics affected by the coastal upwelling events in the Gulf of Finland in July–August 2006. *J. Plankton Res.*, doi:10.1093/plankt/fbq049.
- Lips, I., Lips, U., Liblik, T. (2009) Consequences of coastal upwelling events on physical and chemical patterns in the central Gulf of Finland (Baltic Sea). *Cont. Shelf Res.* **29**:1836–1847.
- Lips, U., Lips, I., Liblik, T., Kuvaldina, N. (2010) Processes responsible for the formation and maintenance of sub-surface chlorophyll maxima in the Gulf of Finland. *Estuar. Coast. Shelf Sci.*, doi:10.1016/j.ecss.2010.04.015
- Nausch, M., Nausch, G., Lass, H. U. et al. (2009) Phosphorus input by upwelling in the eastern Gotland Basin (Baltic Sea) in summer and its effects on filamentous cyanobacteria. *Est. Coast. Shelf Sci.* **83**:434–442.
- Pavelson, J., Kononen, K., Laanemets, J. (1999). Chlorophyll distribution patchiness caused by hydrodynamical processes: A case study in the Baltic Sea. *ICES J. Marine Sci.* **56(S)**:87–99.
- Vahtera, E., Laanemets, J., Pavelson, J. et al. (2005) Effect of upwelling on the pelagic environment and bloom-forming cyanobacteria in the western Gulf of Finland, Baltic Sea. *J. Mar. Syst.* **58(1–2)**:67–82.
- Zhurbas, V., Laanemets, J., Vahtera, E. (2008) Modeling of the mesoscale structure of coupled upwelling/downwelling events and related input of nutrients to the upper mixed layer in the Gulf of Finland, Baltic Sea. *J. Geophys. Res.* **113**, C05004, 1–8.

Coastal and local processes

Kai Myrberg

Abstract

Coastal and local processes are very important in the Baltic Sea. Here a discussion is given about the physics of the coastal zone, the area influenced directly by the nearby presence of land and open ocean. Due to the small size of the Baltic Sea, a significant part of it belongs to the coastal zone independently on the exact definition. The treatment included sea level elevation, upwelling, archipelago areas and coastal weather. Also local processes are important, like frontal areas, river plumes and mixing processes. This text is based on the book “Physical Oceanography of the Baltic Sea” (Leppäranta & Myrberg, 2009).

Для Балтийского моря прибрежные и локальные (мезомасштабные) процессы оказываются очень важными. В этой лекции обсуждается физика процессов происходящих в прибрежной зоне — области, находящейся под непосредственным влиянием и суши, и открытого моря. Поскольку размеры Балтийского моря относительно невелики, довольно значительная его часть принадлежит прибрежной зоне (независимо от ее точного определения). Обсуждаются изменение уровня моря, апвеллинг, районы архипелагов и прибрежные погодные условия. Среди локальных процессов важны такие как образование фронтальных зон, речные плюмы и процессы перемешивания. Лекция основана на материалах книги “Physical Oceanography of the Baltic Sea” (Leppäranta & Myrberg, 2009).

1. Coastal zone processes

1.1. Definition of coastal zone

Coastal zones play a specific role in the Baltic Sea, because their extension is relatively large compared with the entire area of the sea. Moreover, the definition of a coastal area or a coastal zone is a complicated task in the Baltic Sea because no such clear topographic feature as the continental shelf in the World Ocean exists. The coastal zone is under intensive physical processes

Kai Myrberg (✉)
Finnish Environment Institute, Marine Research Centre, Helsinki, Finland
e-mail: Kai.Myrberg@ymparisto.fi



and additionally water (material) exchange between the coastal zone and the open sea is remarkable. Here we shall take into consideration several views how to solve this problem, each usable in certain situations. We restrict the definitions mostly to the physical criteria.

The coastal zone locates between the land and the open sea. The width of this zone in the Baltic Sea is the key question. A simple approach is to define the coastal zone to be the area where the water depth is less than a fixed value, say 20 m. This encloses the islands in to the coastal zone, except for a few ones locating in the central basins. The area more shallow than 20 m covers about 25 percent of the total area of the Baltic Sea.

One way to define the coastal zone is the area in offshore direction where the influence of shoreline becomes visible. As an example of that, Lessin & Raudsepp (2007) concluded that the coastal zone is characterized by high fresh-water fluxes, nutrients as well as organic matter from the land together with the availability of light down to the seabed due to the shallow depths. This classification reflects the fact that the coastal zone is highly productive and vulnerable for eutrophication. In winter conditions, a natural boundary of the coastal zone is the fast ice edge, which normally lies near the 10-meter isobath (Leppäranta, 1981).

A theoretical consideration can be taken on the basis of ocean dynamics. According to the characteristic baroclinic Rossby-radius of deformation, the width of the coastal zone is 3–10 km in the Baltic Proper (Fennel et al., 1991) while in the Gulf of Finland it is only 2–4 km (Alenius et al., 2003). This width must be taken from off the archipelagic areas. The offshore extension of the wind-induced upwelling zone can also be employed, its width typically being 10–20 km and the same numbers represent the scale of the frictional influence of the coastline. One potential way to define the coastal zone is the area influenced by the river plume (Lessin & Raudsepp, 2007), but this is not so feasible since the extent could go too far offshore. Using the zone of influence of wind-generated waves on the sea bottom as the definition would limit the coastal zone to depths less than about 20 m.

In applied research it may be necessary to take an administrative point of view to define the coastal zone. The EU Water Framework Directive says that the coastal zone is: “surface water on the landward side of a line every point of which is at distance of one nautical mile on the seaward side from the nearest point of the baseline from which the breadth of territorial waters is measured” (European Commission, 2000). In practice the width of the coastal zone is quite large after this definition because the baseline follows mostly follows the outer archipelago.

1.2. Sea-level

The sea-level variability is influenced by various kinds of factors with varying time-scale, this including meteorological, astronomical and hydrological elements. Relatively rapid land uplift in some parts of the Baltic Sea has lead to long-term drift of the local sea level. The concept of theoretical mean sea-level represents an estimator of the actual mean sea-level and provides a reference level in order to compare sea-levels in different sections and times. It includes the influence of land uplift and eustatic rise of the global mean



sea-level, and therefore the theoretical mean sea-level changes with time. Referring the measured sea-level to this tells whether the actual sea-level is high or low. The frequency spectrum of the sea-level in the Baltic Sea shows periodical as well as irregular variations.

In the periods of 1–24 h sea-level variations are associated with long waves, currents, tides and seiches. Witting (1911) concluded that tides in the Baltic Sea are mostly diurnal (components K_1 and O_1) with amplitudes of about 0.5–2 cm. The semi-diurnal tides (M_2 and S_2) have amplitudes of some 0.5–1.5 cm. The diurnal tides are generated within the Baltic Sea whereas the semi-diurnal tides are partially externally-forced. The amplitudes of tides, currents and waves are small in the Baltic Sea and thus the separation of their signal in the sea-level records might be difficult.

Variations of wind and air pressure cause sea-level variations from periods of about one day to several weeks. The influence of wind is to pile up water, which is particularly strong at the end of bays. Air pressure change by 1 mbar corresponds to about 1 cm in sea-level elevation (barometer effect). Air pressure variations cause thus sea-level variations of about ± 50 cm (Lisitzin, 1974, Carlsson, 1997).

Towards longer periods, annual and semi-annual periods come then. The variations in density of sea water cause sea-level variations in time scales of several months. If e.g. the water density would change by 1 kg/m^3 this would lead to a change of 5 cm in sea-level. The permanent horizontal water density gradient of about slightly less than 10 kg/m^3 between the northern and southern Baltic Sea is reflected as higher sea-level in north than south. On average the sea level declines 35–40 cm from the Bay of Bothnia to the Skagerrak. The active water storage capacity of the Baltic Sea, taken as the difference between monthly maximum and minimum volumes, corresponds to about 1 m thick water layer over the Baltic Sea. Landsort represents the mean Baltic Sea sea-level and it is also the nodal point of a uninodal seiche. The mean sea-level varies according to the water balance as shown in Section 4.1. The large-scale processes causing variability of the NAO-index has also strong effects on the sea-level, this being true especially during December–May period (Johansson et al., 2001). Positive NAO-index means strong westerly winds and consequently increased water transport into the Baltic Sea from the North Sea.

1.3. Coastal weather

Coastal areas have specific weather conditions where both the open sea and the land areas play a role. Here, we discuss some specific key elements of the coastal weather. The coastal weather is a result of the mixture of different factors. Different characteristics of atmospheric stability, wind and moisture distributions between the land and sea may cause specific weather features at coastal areas (convective precipitation, fogs etc.). This is furthermore important in the Baltic Sea where many narrow bays and gulfs exist. The sparsity of meteorological observations in the coastal area and at the open sea has made it difficult to study in detail the specific features of the coastal weather.

The land-sea breeze. The wind conditions in the coastal areas are specific due to the asymmetry of air-sea interaction and surface roughness conditions between land and open sea. A well-know feature at any coastal area is the sea-



breeze, this being true at all coastal areas of the Baltic Sea during the summer time, too. Sea-breeze (or onshore breeze) is formed by increasing temperature differences between the land and water which create a pressure minimum over the land due to its relative warmth and forces higher pressure, cooler air from the sea to move inland.

The sea is warmed by the sun to a greater depth than the land due to its greater specific heat. The sea therefore has a greater capacity for absorbing heat than does the land and so the surface of the sea warms up more slowly than the land's surface. As the temperature of the surface of the land rises, the land heats the air above it. The warm air is less dense and so it rises. This rising air over the land lowers the sea level pressure by about 0.2 percent (about 2 mbar). The cooler air above the sea, now with relatively higher sea level pressure, flows towards the land into the lower pressure, creating a cooler breeze near the coast. The strength of the sea breeze is directly proportional to the temperature difference between the land and the sea. If the environmental wind speed is larger than 8 knots and opposing the direction of a possible sea breeze, the sea breeze is not likely to develop. Sea-breezes occur most often in early- and midsummer during daylight hours when there is a large difference between the temperature of the air over the land and the temperature of the air over the still cold sea.

A sea-breeze front is a weather front created by a sea-breeze, also known as a convergence zone. The cold air from the sea meets the warmer air from the land and creates a boundary like a shallow cold front. When powerful, this front creates cumulus clouds, and if the air is humid and unstable, cumulonimbus clouds, the front can sometimes trigger thunderstorms. At the front, warm air continues to flow upward and cold air continually moves in to replace it and so the front moves progressively inland. Its speed depends on whether it is assisted or hampered by the prevailing wind, and the strength of the thermal contrast between land and sea. At night, the sea-breeze usually vanishes.

At night, the land cools off quicker than the sea due to differences in their specific heat values, which forces the dying of the daytime sea breeze. If the land cools below that of the adjacent sea-surface temperature, the pressure over the water will be lower than that of the land, setting up a land breeze as long as the environmental surface wind pattern is not strong enough to oppose it. If there is sufficient moisture and instability available, the land breeze can cause showers or even thunderstorms, over the water. Overnight thunderstorm development offshore can be a good predictor for the activity on land the following day, as long as there are no expected changes to the weather pattern over the following 12–24 h. The land breeze will die once the land warms up again the next morning.

Specific air-sea interactions. There are a few good examples of the specific weather phenomena which develop over the Baltic Sea due to the asymmetry in thermal and moisture balance over the land and sea. During autumn and early winter, when the sea-surface temperature is higher than atmospheric temperature, a so-called thermal low can be developed due to thermal imbalance between the sea and the land areas. This situation takes place when the overall vertical stability of the large-scale circulation is favourable for cyclone development. In such a situation a thermal low deepens over the sea based on the release of warm and moist air to the atmosphere.



A favourable condition is when onshore winds blow from the cold towards the warm sea. In such a case there is an asymmetry in the vertical heat exchange: over the open sea the atmosphere gains heat and moisture whereas over the land the situation is opposite i.e. horizontal Laplacian of diabatic* heating is non-zero at the coastal area which is an important term to produce vertical motion in addition of thermal advection and vorticity advection. The energy gained from the sea-surface will furthermore weaken the atmospheric stability and the deepening of the low can be rapid, when convective and baroclinic instability interacts. When the low is advected over the land it will rapidly weaken due to the existing horizontally homogeneous vertical heat fluxes. Such a thermal low is often developed in the Bay of Bothnia during autumn coupled with strong wind and heavy precipitation. Such lows also have been observed in other parts of the Baltic Sea.

Another example, where the land-sea interaction plays a key role is the formation of convective snow bands, e.g. over the open Gulf of Finland and at the Swedish east coast. Such features are observed in a cold air mass with neutral atmospheric stability when the geostrophic wind is blowing along the gulf's latitudinal axis. The convective showers can be very intense. The main causes of for the formation of such snow bands over gulfs are related to the differences in thermal and evaporational characteristics between the land and open sea-surface. Also the geometrical configuration of coast is expected to play a crucial role. Due to the small size of the Baltic Sea both the coast of departure and the coast of arrival play an important role.

At the coast of departure the open gulf is triggering the formation of the snow bands. The reason behind the genesis is in thermal difference between the land and sea: land breezes are formed at one or both coasts which result as convergence over the gulf. This in turn cause forced convection, and organised snow bands are formed moving downwind. This takes place even if the nearly parallel coast is lost demonstrating the importance of coastal departure concept. The warm and moist surface may lead to intense growth of the snow bands when they move enough long-time over the sea. When the snow bands approach the coast of arriving, a clear intensification of the snow bands may occur, this depending of the shape of the coastline. A land-breeze circulation may be formed at the coast of departure directed against the mean flow and new convergence zone may be established. An example of this is when the snow bands drift to west to the Swedish coast from Gulf of Finland with the prevailing easterly mean flow. Over the cold land the snow bands quickly disappear due to the lack of moisture and heat supply (Andersson & Nilsson, 1990, Andersson & Gustafsson, 1994).

As an example of a heavy snowstorm caused by such a type of mechanism described here is that one which took place in December 1998 in Gävle, Sweden when 1.4 m of snow fell in a few days (Andersson & Michelson, 1999). The forecasting of such an event is difficult and requires the use of coupled atmosphere-sea models.

Especially during late summer there are situations when often non-forecasted fogs appear at the coastal area. The role of air-sea interaction is very

* $\nabla^2 Q_d$, where Q_d is the diabatic heat flux.



important in such situations. The interesting feature is that the sea can be either warmer or colder than the air above. In warm and moist air mass the triggering mechanism might be a coastal upwelling which causes an abrupt drop of sea-surface temperature. Thus, the relative humidity of the lowest air layer will rapidly increase and finally the air mass temperature equals to the dew point temperature. If the wind is weak, a fog can form rapidly. In such a situation, the coupled air-sea models are needed where the sea-surface temperature is realistically forecasted. Such unpredicted fogs have caused problems for sea navigation.

Another specific feature is the sea smoke which typically occurs during late autumn or early winter. In such a situation the sea-surface temperature is clearly higher than the atmospheric temperature. When the evaporated water vapour from the sea-surface moves upwards, it reaches quickly the dew point temperature and a fog, called as sea smoke is formed. The mechanism is the same as in the case of fog, but the condensation in the upward air motion leads to a fog-like visual impression. Sea fog is typically observed during cold air near the ice boundary or in cracks in the ice.

2. Local processes

2.1. Formation of fronts and river plumes

The large-scale horizontal temperature and salinity patterns are associated with circulation dynamics. The most interesting part of the thermohaline structure of the Baltic Sea are the boundaries between different water masses i.e. areas of large horizontal density gradients. The numerous fronts observed in the Baltic Sea can be formed either between meso-scale circulation patterns or in transition zones between sea areas, e.g. at straits (Alenius et al., 1998). Pavelson (2005) states that the diversity of water masses follows from the estuarine-like character of the Baltic Sea, the circulation in and between the sub-basins and the vigorous modulation by the coastal processes. Fronts can be found in the whole water body, but those formed in the uppermost layer are the most interesting and widely-studied due their implications to biochemical processes. The internal fronts on the other hand play a role in horizontal mixing processes of the deep layers.

There is a large variety of different kinds of fronts in the Baltic Sea. According to Pavelson (1988) the following division can be given: (1) quasi-permanent salinity front at the entrance to the larger gulfs or those related to the general circulation in a certain sub-basin, (2) meso-scale salinity front as the most frequent one found everywhere in the Baltic, (3) temperature front formed more likely by the interplay of water masses of different thermal stratification (a rare phenomenon), (4) density-compensating front with sometimes considerable cross-front temperature and salinity differences (most probable quite rare case) and (5) wind-forced upwelling front in the coastal zones with high temperature differences and gradients.

A good and well-known example of such a dynamic feature is the type 1 quasi-permanent salinity (density) front at the entrance of the Gulf of Finland. Its existence has been confirmed by extensive field studies (see e.g. Pavelson, 2005). The dynamical background of the front can be explained by the



existing cyclonic mean circulation in the Gulf of Finland. The saltier water of the northern Baltic Proper intrudes into the gulf along the Estonian coast whereas the seaward flow of fresher gulf water above the pycnocline occurs at the Finnish coast. The interface of these in- and outflowing waters characterised by different salinity and/or temperature form this quasi-permanent front at the entrance area of the Gulf of Finland. The front is typically oriented in the south-west-north-east direction, i.e. positioned approximately parallel to the bottom slope. The frontal area responds to wind forcing (Pavelson et al., 1997) so that under easterly winds, the denser (saltier) water mass moves offshore. Thus, the front becomes sharp and it is strongly inclined to the sea surface. During the westerly winds, the less dense Gulf of Finland water mass forms a surface layer over the denser water mass creating a secondary pycnocline approximately in the middle of the upper layer. Pavelson et al. (1997) also studied changes in the potential energy (stratification conditions) in the upper layer. These changes are coupled with differential advection induced by along-front wind stress and wind-generated vertical mixing.

There are also other areas (Irbe Strait, Northern Quark etc.) in the Baltic Sea with quasi-permanent or meso-scale salinity fronts (type 1 or 2 front), the most well-known of them being the Danish Straits (Bo Pedersen, 1993). The subject has already partly discussed earlier in Chapter 5 in connection with inflows to the Baltic and in relation to intrusions.

The horizontal temperature field also shows frontal structures (type 5 front). Kahru et al. (1995) found from satellite images that temperature fronts occur predominantly in areas of straight and uniform sloping topography. Major frontal areas exist along the north-western coast of the Gulf of Finland and near the eastern coast of the Sea of Bothnia. The main factors that produce these fronts are: interaction between coastal upwelling and coastal jets, formation of eddies, differential heating and cooling and water exchange between the basins with different water characteristics (advection of cold/warm water). The temperature fronts are further discussed later in this chapter in the connection with upwelling.

There are several large rivers flowing into the Baltic Sea with their plumes extending occasionally several tens of kilometres from the shore. Very little research, however, has been made of these plumes.

2.2. Specific features of archipelago areas

There are a few important archipelago areas in the Baltic Sea: Archipelago Sea, Stockholm, Vaasa, Northern Bay of Bothnia and Belt Sea. The circulation and hydrography of these areas are influenced by the morphology of the island systems, and short spatial scales require very high-resolution measurements. The steering effect of bathymetry and strong friction impose major difficulties into numerical modelling.

The Archipelago Sea is the largest archipelago. It locates between the Gulf of Bothnia and the Gulf of Finland, within Finnish territorial waters. It is characterized by an enormous topographic complexity, including about 25,000 islands. The average water depth is only 19 m and the area is 8,893 km². The total drainage area is about 8,900 km² (of which lakes cover fewer than 2 percent and arable lands 28 percent). The salinity of surface



water varies between 4–6 ‰, depending on the distance of the mainland and river mouths. In the Archipelago Sea the halocline is very weak or absent and the surface layer is stratified by temperature in summer with a thermocline at a depth of 10–20 m, and a deeper, denser and colder layer extending down to the sea-bed. The emergence of the thermocline is a premise for the launch of micro algae production in spring.

There are north-south channels with depths ranging from 30 to 40 m through this sea-area. They form a part of the water exchange system between the Sea of Bothnia and the Gotland Sea. The sill depth towards the Sea of Bothnia is about 18 m. The main route goes through the Kihti Strait. The mean depth of the Sea of Archipelago is less than 20 m, which restricts the inflow of deep waters from the Gotland Sea to the Sea of Bothnia. The area is roughly divided into inner and outer archipelagos, with the outer archipelago consisting mainly of smaller, uninhabited islands. The archipelago covers a roughly triangular area with the towns of Mariehamn, Uusikaupunki and Hanko at the corners.

The Stockholm Archipelago is the largest archipelago of Sweden, and one of the largest ones in the Baltic Sea. It stretches from Stockholm to about 60 km to the east, bordering to the Åland Sea. It consists of approximately 24,000 islands and islets. It mainly follows the coastline of the provinces Södermanland and Uppland. The area is characterised by a mixture of different length scales both in horizontal and vertical directions. There are several kilometres wide basins and with a depth of more than 100 m connected by straits with widths and sill depths clearly less. The surface water has a salinity of about 6 per mille with somewhat higher salinities in the bottom layer. The most pronounced freshwater input is due to Lake Mälaren with an outflow approximately 165 m³/s.

The area is traditionally partitioned into three parts: the inner, the middle and outer archipelago. These areas are forced by different mechanisms: in the inner archipelago the dominating exchange process is estuarine circulation, induced by the marked freshwater discharge and the vertical mixing. In the outer and middle archipelagos the density fluctuations due to Ekman pumping along the Baltic boundary interface produce another type of baroclinic process that clearly dominates. The modelling of such an area is a complicated task and should be carried out by a cascade of models where the local archipelago models gets their open boundary conditions in the east e.g. from a three-dimensional model (see e.g. Engqvist and Andrejev, 2003).

References

- Alenius, P., Myrberg, K., Nekrasov, A. (1998) The physical oceanography of the Gulf of Finland: a review. *Boreal Environment Research* **3**(2):97–125.
- Alenius P., Nekrasov A., Myrberg K. (2003) The baroclinic Rossby-radius in the Gulf of Finland. *Continental Shelf Research* **23**:563–573.
- Andersson, T. & Gustafsson, N. (1994) Coast of Departure and Coast of Arrival: Two Important Concepts for the Formation and Structure of Convective Snowbands over Seas and Lakes. *Monthly Weather Review* **122**:1036–1049.
- Andersson T. & Michelson, D. (1999) The December 1998 snowfall over Sweden as seen by weather radars. *Polarfront* **100/101**:26–33.



- Andersson, T. & Nilsson, S. (1990) Topographically Induced Convective Snowbands over the Baltic Sea and Their Precipitation Distribution. *Weather and Forecasting* **5**:299–312.
- Bo Pedersen, F. (1993) Fronts in the Kattegat: the hydrodynamic regulating factor for biology. *Estuaries* **16**:104–112
- Carlsson, M. (1997) *Sea level and salinity variations in the Baltic Sea. An oceanographic study using historical data.* Department of Oceanography, Gothenburg University (PhD Thesis).
- Engqvist, A. & Andrejev, O. (2003) Water exchange of the Stockholm archipelago: a cascade framework modelling approach. *Journal of Sea Research* **49**:275–294.
- European Union Water Framework Directive, 2000.
- Fennel, W., Seifert, T., Kayser, B. (1991) Rossby radii and phase speeds in the Baltic Sea. *Continental Shelf Research* **11**(1):23–36.
- Johansson, M., Boman, H., Kahma, K. K., Launiainen, J. (2001) Trends in sea level variability in the Baltic Sea. *Boreal Environmental Research* **6**(3):159–179.
- Kahru, M., Håkansson, B., Rud, O. (1995) Distributions of the sea-surface temperature fronts in the Baltic Sea as derived from satellite imagery. *Continental Shelf Research* **15**(6):663–679.
- Leppäranta, M. (1981) On the structure and mechanics of pack ice in the Bothnian Bay. *Finnish Marine Research* **248**:3–86.
- Leppäranta, M. & Myrberg, K. (2009) *The physical Oceanography of the Baltic Sea.* Berlin-Heidelberg-New York: Springer-Verlag,
- Lessin, G. & Raudsepp, U. (2007) Modelling the spatial distribution of phytoplankton and inorganic nitrogen in Narva Bay, southeastern Gulf of Finland, in the biologically active period. *Ecological Modelling* **201**(3–4):348–358.
- Lisitzin, E. (1974) *Sea level changes.* Elsevier oceanography series. Amsterdam: Elsevier.
- Pavelson, J., Laanemets, J., Kononen, K., Nömmann, S. (1997) Quasi-permanent density front at the entrance to the Gulf of Finland: response to wind forcing. *Continental Shelf Research* **17**:253–265.
- Pavelson, J. (2005) *Mesoscale physical processes and related impact on the summer nutrient fields and phytoplankton blooms in the western Gulf of Finland* (PhD Thesis). Tallinn University of Technology.
- Witting, R. (1911) Tidvatten i Östersjön och Finska viken. *Fennia* **29**(2):84.

Short period variability in the euphotic zone of the north-eastern Black Sea as inferred from combined acoustic and hydrographic surveys

Alexander Ostrovskii

Abstract

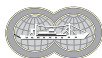
Oceanic moored profiling multiparametric observation technology has been developed recently for various applications in oceanology and marine environmental monitoring. The moored profiler equipped with CTD and acoustic Doppler current meter was successfully tested during the expeditions into the north-eastern Black Sea in 2007–09. By using the profiler a new data on inertial oscillations, submesoscale variability, and vertical exchange (the mean gradient Richardson number, the eddy viscosity and the eddy diffusivity) in waters over the continental slope was obtained. The depth of the seasonal thermocline, the vertical gradient of density driven by temperature distribution and the current velocity gradient in the thermocline as well as the vertical exchange coefficient, all are substantially modulated by inertial oscillations and submesoscale vortices. The acoustic backscatter data were useful for studying daily variability of the ecosystem and its vertical structure. In particular the euphotic zone, the oxycline, and the suboxic zone were identified along with the diurnal migrations of the zooplankton in the top 130 m layer of the Black Sea. The vertical speed of the suspended matter in the anoxic layer deeper than 150 m was also estimated.

В докладе представлены результаты акусто-гидрофизических исследований, проведенных с помощью автоматической заякоренной профилирующей обсерватории, оснащенной измерителями температуры и электропроводности воды, содержания растворенного в воде кислорода, а также скорости морских течений и акустической силы звукорассеивающих слоев. Работы с профилографом были проведены в шельфово-склоновой зоне северо-восточной части Черного моря в 2007–2009 гг. С помощью профилографа удалось получить новые данные об инерционных

Alexander Ostrovskii (✉)

P. P. Shirshov Institute of Oceanology RAS, Moscow, Russia

e-mail: osasha@ocean.ru



колебаниях, субмезомасштабной изменчивости и вертикальном обмене в море. Наблюдения за акустическим рассеиванием позволили исследовать вертикальную структуру черноморской среды и суточную миграцию зоопланктона, а также оценить скорости оседания взвешенных частиц в зоне сероводородного заражения.

1. Introduction

In past few years, several international programs were launched targeting at long-term monitoring, mostly in near real-time, of environmental processes related to the interaction between ocean biogeochemical processes, marine ecosystem, ocean dynamics, and climate. For example, the multisensor oceanographic platforms measuring variables from sea surface to sea floor at chosen locations (9 designated sites and 3 associated sites) are integrated into the observational network by EuroSITES project funded by the EU. Scientific objectives of this project focus on understanding of changes and trends in oceans emerged in response to climate variability. Such programs usually aim at observations in waters deeper than 1,000 m rather than in the continental margin. Meanwhile important boundary zone where coastal waters interact with the open ocean still remains poorly monitored. A new moored profiler Aqualog delivers a solution for in situ measurements of vertical profiles of multiple parameters over continental slope and outer continental shelf.

2. Methods

Aqualog is an observational platform that moves down and up along a mooring line, which is taut vertically between a subsurface flotation and an anchor. The profiler comprises a carrier with a load of modern oceanographic instruments. The sensors include, but are not limited to the FSI Excell 2" Micro CTD probe, the Nortek Aquadopp-3D current meter, and the AANDERAA fast Oxygen Optode 4,330 F. The acoustic Doppler current meter is a horizontal beam single frequency 2 MHz instrument remotely sensing the water volume in the range of about 0.5–2 m from the profiler with a sampling frequency of 23 Hz. When the carrier is moving with the speed of 0.1 m/s the vertical profiles are measured with a vertical resolution of 0.05 m for pressure, conductivity and temperature, 0.3 m for acoustic backscatter signal and horizontal current speed and 0.8 m for dissolved oxygen.

The moored multisensor profiler has a number of advantages which are briefly summarized below. Unlike conventional mooring where the equipment is placed on fixed depths, Aqualog conducts continuous measurements of vertical profiles applicable for assessing both integral and differential characteristics of the ocean fine structure. By combining pressure, conductivity, temperature, and horizontal current velocity data it is possible to evaluate vertical mixing. The joint analysis of dissolved oxygen data and the strength of the acoustic backscatter signal give a better understanding of the variability of the marine ecosystem vertical structure at multiple time scales.

The acoustic Doppler current observations by Aquadopp-3D mounted on the profiler are superior to those done by a conventional ADCP. Unlike the traditional ADCP approach where (i) a longer working range is achieved by



the price of poorer vertical resolution (e.g., 644-meter vertical profile is binned at 24-meter cells by the longest range ever 38 kHz ADCP) and (ii) the horizontal span of the beams widens proportionally to the distance from ADCP (e.g., up to 508 m in horizontal at the distance of 700 m by 75 kHz ADCP), Aqualog obtains horizontal current profiles at the above mentioned fixed distance of 0.5–2 m from the profiler with a uniform ocean-fine-structure resolution throughout the full water column from the near-surface layer down into the abyss. The Aquadopp-3D's 2 MHz acoustic remote sensing signal is most sensitive to scatterers of the size of about 0.05–5 mm including lithogenic particles suspended in the water, phytoplankton, and mesozooplankton. If compared to conventional long range ADCPs (38–150 kHz), which signals are more sensitive to certain larger scatterers, so the instruments may occasionally misestimate the swimming nekton species for current fluctuations, the Aqualog current profile data should have higher signal-to-noise ratio.

The profiler oceanographic sensors are rigid, high-precision and stable giving the opportunity to make an extended survey of the ocean. So far the typical depth range of Aqualog's profiling was 5–1,000 m. Vertical speed can be set within 0.1 and 0.3 m/s. The pay load consists of at least 3 probes. Weight in the air is 62 kg without sensors or up to 75 kg with sensors. Start and stop by magnetic switch or as preprogrammed. There is LED indication of the system status. The programmable hardware of the profiler allows the user to set an automatic operation algorithm (variable movement speed, time and period of profiling, stops, etc.). The profiler mooring line is made of stainless steel wire or Kevlar™ fiber. The Aqualog has enough resources to profile a water column in the programming regime during several months. The total profiling distance is about 800 km in still waters for a profiler with a lithium battery pack.

3. Results

The Aqualog was successfully tested during the expeditions into the north-eastern Black Sea in 2007–09. By using the Aqualog new data on inertial oscillations, submesoscale variability, and vertical exchange (the mean gradient Richardson number, the eddy viscosity and the eddy diffusivity) in the waters over the continental slope was obtained. The depth of the seasonal thermocline, the vertical gradient of density driven by temperature distribution and the current velocity gradient in the thermocline as well as the vertical exchange coefficient, all are substantially modulated by inertial oscillations and submesoscale vortices. The acoustic backscatter data were useful for studying daily variability of the ecosystem and its vertical structure. In particular the euphotic zone, the oxycline, and the suboxic zone were identified along with



Fig. 1. Aqualog—a new multisensor platform for autonomous vertical profiling in the ocean.



the diel migrations of the zooplankton in the top 130 m layer of the Black Sea. The vertical speed of the suspended matter in the anoxic layer deeper than 150 m was also estimated.

In October 2009, two Aqualog's were moored near the shelf break at the depths of 88 and 270 m west of Gelendzhik bay at the locations of 44°29.75' N 37°59.13' E and 44°29.36' N 37°58.44' E, correspondingly. The first profiler performed descending/ascending cycles in the depth range of 10–82 m every 3 h during October 3–11. The second profiler made repeated round trips between 10 and 240 m every 2 h from the evening of October 4 throughout the noon of October 11.

Very interesting are the depth-time diagrams of the acoustic backscattering at 2MHz during these surveys. The data reveal time varying multilayer structure of the acoustic scattering. At the beginning of the survey, the acoustic backscattering from suspended particles was higher throughout the water column because the suspended-sediments were brought in by the northwestward jet from the littoral. The current profiles obtained by Aqualogs indicated that the northward current speed reached 0.3 m/s in the upper 50 m layer. Noticeably, the satellite remote sensing by ENVISAT imaging spectrometer MERIS showed much larger chlorophyll-a concentration in the jet waters approaching the moorings in October 3.

In 2–3 days, the northwest current moved offshore into the deep basin so that the horizontal transport of the suspended sediments substantially decreased. The towed ADCP survey revealed a new structure in the current field as follows. The southeast countercurrent emerged in the upper 40–50 m layer over the continental shelf region limited by the isobaths of 50 and 100 m. A submesoscale cyclonic eddy was generated between the countercurrent and the coast to the southwest of the Gelendzhik bay.

The submesoscale eddy moved off the coast and appeared near the first mooring around 22 p.m. on October 6. Analysis shows that the eddy occupied the upper layer above pycnocline. The rotational speed of the eddy was about 0.2 m/s. In the next few hours the eddy's eastern front shifted further offshore towards the second mooring. The eddy center appeared right above the upper part of the continental slope early morning of October 8. The eddy water mass had more suspended particles than the surrounding waters. It seems that the water rich in the suspended particles was pulled around the eddy in the clockwise direction forming the spiral curl.

The changes in the current structure were associated with vertical displacements of the thermocline. The thermocline shallowing events were rapid: the isotherms moved upward by several meters in a few hours. Most noticeable shifts occurred between 3 and 6 a.m. early mornings on October 4 and 7. In the former case the depth of the maximum vertical temperature gradient was lifted from 52 to 46 m. By the end of the survey on midday of October 11, the maximum vertical temperature gradient elevated up to 40 m depth while the sea surface temperature gradually decreased from 21.5 to 20.8 °C during the survey.

Measurements of the vertical profiles of the acoustic backscattering at frequency 2 MHz indicated that by the end of the survey the amplitude of the acoustic signal did not exceed 75 percent of its value on October 3–4. The sinking of the particulate matter can be observed in the depth-time dia-



grams of the acoustic backscattering in the anoxic layer where biological scatterers are absent. Accordingly to ship borne castings of Idronaut-320 CTD equipped with fluorimeter, turbidimeter, and dissolved oxygen sensor in October 2009, the marine environmental conditions were as follows: the oxycline was located between 50 and 130 m whereas upper boundary of the sulfide-containing zone slightly fluctuated near the depth of 160 m in the vicinity of the Aqualog mooring sites. In the anoxic layer between 160 and 240 m, the depth-time patterns of the acoustic backscattering suggested that patches having higher concentration of the suspended sediments propagated downward with speed of about 0.002 m/s on October 4–6 and at 0.001 m/s at the end of the survey.

The profiling demonstrated that the acoustic backscattering had multilayer structure. In the upper mixed layer the acoustic backscattering by the lithogenic and biogenic particles, phytoplankton and mesozooplankton was rather uniform with depth. The ship borne castings indicated that the fluorescence of chlorophyll was at maximum value of 2.47 mg/m³ at the depth of 26 m and it quickly decreased to 0.21 mg/m³ downward to 50 m below the sea surface where the highest vertical temperature gradients were observed. The amplitude of the echo signal substantially decreased in 5-m thick core layer of the thermocline. It is noteworthy that local minimum 0.16 mg/m³ of the fluorescence was located at the depth of 52 m. A few meters below there was slight increase in the fluorescence up to 0.25 mg/m³. Then the fluorescence gradually decreased to 0.06 mg/m³ at 63 m. The phytoplankton almost vanished below the thermocline. Hence the phytoplankton did not contribute to the acoustic backscattering in the oxycline.

A strong variation of the sound scatter was observed daily in the oxycline. In day time, the acoustic backscattering strengthened in the layer of 100–130 m from the sea surface. This phenomenon became clearly pronounced since October 7 after the particulate matter brought by the coastal jet on October 3–5 suspended deeper than 150 m. Earlier, Flint (1989) noted patchy accumulations of 3 mass mesozooplankton species *Calanus helgolandicus*, *Sagitta setosa*, and *Pleurobrachia pileus* in the lower part of the oxic layer in autumn. These organisms, which mature species reach 3.5, 8–22, 5–20 mm correspondingly, along with the lithogenic particles and detritus of the size more than 0.05 mm can scatter the acoustic signal at 2 MHz in the oxycline.

The diel migrations of the mesozooplankton were observed at the dawn and sunset. The vertical migrations occur below the pycnocline down to the isopycnal surface of 15.7 sigma-theta units i.e., almost to the hydrogen sulfide zone boundary. The vertical migrations took less than 2 h. During the survey, the maximums of the acoustic backscatter in the lower part of the oxycline were found at 115–125 m below the sea surface where the dissolved oxygen content was 2.1–3.7 mg/l. The maximum depth of the zooplankton sound scattering layers was between 135 and 145 m.

Below the zooplankton sound scattering layers at the depth of 140–145 m there was a local minimum of the acoustic backscattering at 2 MHz.

In the hydrogen sulfide layer the sound scatter was due to suspended sediments including the detritus. An increase of the acoustic backscatter amplitude by 5 percent was observed at the depth of 140–145 m where particle coagulation usually takes place.



4. Summary

Overall, the moored profiler Aqualog is a useful tool for multidisciplinary research of the variability of both biotic and abiotic parameters of the sea environment on time scales from a few hours to several months. A real-time data transmission system with underwater inductive modems and a satellite/radio/cellular-link surface buoy is envisaged for the Aqualog profiler. Autonomous profiling multiparametric observatories of the moored type have great potential for being the key technical means for marine environmental monitoring at the boundary zone between the deep ocean and coastal waters.

Acknowledgements

The author is indebted to Andrey Zatsepin, Vladimir Soloviev, Dmitry Shvoev, and Andrey Tsibulsky, who devoted a lot of their time and efforts into developing the moored profiling technology. Sergey Nizov helped with field experiments. Since 2006 the project was partly supported by Russian Fund for Basic Research's grants 06-05-08092-ofi, 08-05-12046-ofi, 09-05-02120-e_k, and 09-05-13527-ofi_c.

References

- Flint, M. V. (1989) Vertical distribution of the mass zooplankton species in connection with the oxygen field structure. In: *Structure and Production Characteristics of Plankton in the Black Sea*, 187–212. Moscow: Nauka.

Submesoscale Eddies at the Narrow Shelf: Observations at the Black Sea

**Andrey Zatsepin, Viacheslav Kremenetskiy,
Andrey Korzh, Alexander Ostrovskii**

Abstract

Submesoscale eddies (with diameter of 2–8 km) at a narrow Black Sea shelf were investigated in-situ for the first time. The investigation was fulfilled during the autumn seasons of 2006–09 in the coastal zone of Gelendzhik using traditional and modern measuring techniques. Two following physical mechanisms of submesoscale eddies formation and evolution were revealed: (1) horizontal shear instability of alongshore flow; (2) formation of eddies in the regions with concave forms of coastal line due to the flow separation.

Впервые проведено натурное исследование субмезомасштабных вихрей (с диаметром 2–8 км) на узком черноморском шельфе. Работа выполнена в осенние сезоны 2007–2009 гг. в районе г. Геленджика с использованием традиционных и новейших методов гидрофизических наблюдений. Выявлены некоторые физические механизмы образования и эволюции таких вихрей, проведены лабораторные эксперименты по их исследованию.

1. Introduction

The Black Sea is a semi-enclosed basin with very original hydrological structure (Fig. 1) and complicated ecological conditions. Because of limited water exchange with the open basins and the comparatively thin (100–150 m) oxygen-containing (active) layer (due to sharp pycno-halocline that blocks vertical mixing and oxygen supply into the deep layer), the Black Sea ecosystem is extremely sensitive to climatic changes and anthropogenic forcing.

Intensification of anthropogenic stress conditioned by industrial-economic activity on the shore and in the coastal regions results in contamination and eutrophication of the shelf zone and can give rise to changes on the ecosystem

Andrey Zatsepin, Viacheslav Kremenetskiy, Andrey Korzh,
Alexander Ostrovskii (✉)
P. P. Shirshov Institute of Oceanology RAS, Moscow, Russia
e-mail: zatsepin@ocean.ru



level. Because of this, investigation of horizontal mixing processes and water exchange in the Black Sea, including that between the coastal zone and deep sea as a shelf self-cleaning mechanism, is of great importance.

The classical scheme of the Black Sea basin-scale circulation includes the Rim current (RC) cyclonically flowing along the continental slope, as a general element (Fig. 2) (Blatov et al., 1984). Numerous IR and visible satellite images and hydrographic surveys with mesoscale spatial resolution elucidated the fact that horizontal water exchange in the Black Sea as a whole is largely determined by dynamics of mesoscale (20–100 km) anticyclonic eddies as well as their interaction with neighboring cyclonic eddies and the RC (Fig. 2) (Zatsepin et al., 2002, Zatsepin et al., 2003, Zatsepin et al., 2005).

However, the observations fulfilled upon the narrow (less than 10 km) shelf of the north-eastern part of the Black Sea revealed the existence of submesoscale (1–10 km) shelf eddies that are a widespread feature of shelf dynamics and play an important role in cross-shelf water exchange (Fig. 3) (Zatsepin et al., 2010, Aref, 2006). The aim of this report is to describe shortly the results of the shelf eddies *in-situ* investigation and to discuss their generation mechanisms.

2. Data and methods

The study was fulfilled in Gelendzhik area at autumn seasons of 2007–09. Following data, methods and equipment were used:

- (1) NOAA, MODIS-AQUA and MODIS-TERRA satellite information (sea surface temperature, chlorophyll-a, water leaving radiance);
- (2) cross-shelf CTD sections;
- (3) towed ADCP surveys with submesoscale resolution;
- (4) bottom mounted ADCP measurements at selected stations.

3. Results and discussion

Complex hydro-physical observations based on mention above methods and equipment usage were fulfilled in 2006–09 in Gelendzhik region of the north-eastern Black Sea during summer and autumn seasons. Well-pronounced short-term and submesoscale variability of fluid dynamics over the shelf and

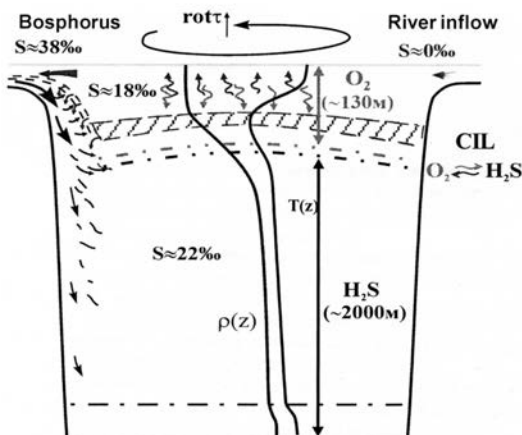


Fig. 1. Hydrologic structure of the Black Sea: CIL—cold intermediate layer, $\rho(z)$ —density profile, $T(z)$ —temperature profile, $O_2 \rightarrow H_2S$ —red/ox zone. The upper boundary of the bottom homogeneous layer is shown by chain line. Corrugated arrows at the upper part indicate the process of winter convective mixing which provides the CIL formation and vertical transport of dissolved oxygen.

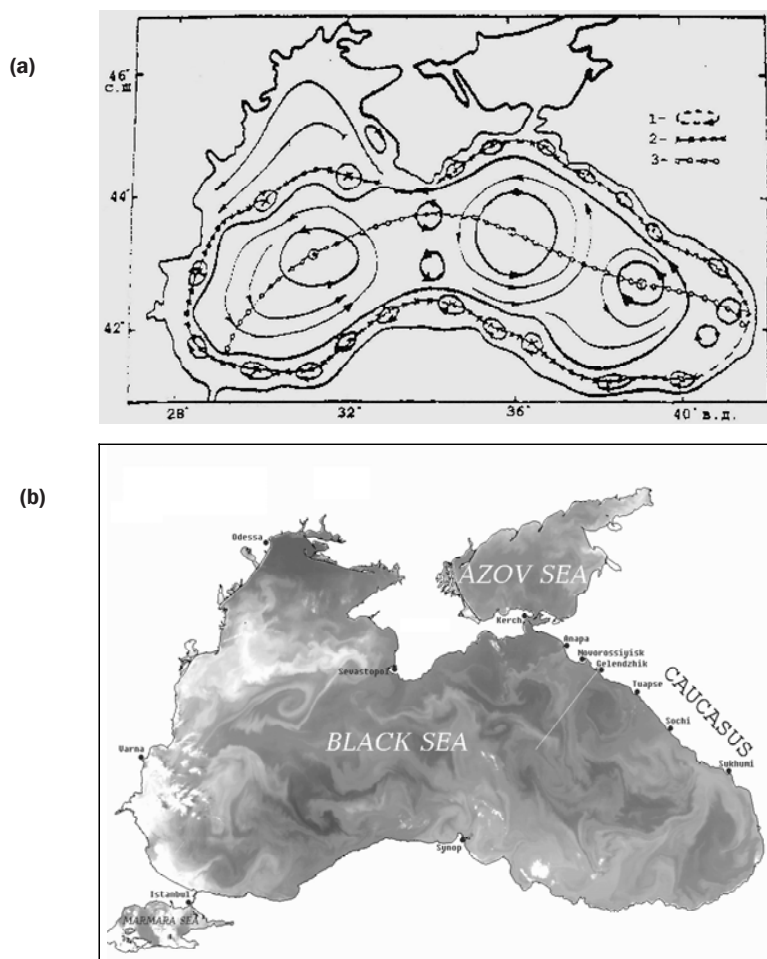


Fig. 2. The Black Sea: (a) scheme of the upper layer circulation: (1) coastal anti-cyclonic eddies; (2) cyclonic Rim current; (3) central flow divergence zone; (b) NOAA satellite image (June 23, 1993, optical band) illustrating high level of mesoscale eddy activity in all areas of the sea.



Fig. 3. Photographic image of mesoscale eddy structures in the Black Sea visualized on the sea surface as a spiral slick structure.



upper part of continental slope was revealed. The dynamics variability was characterized by inconstancy of alongshore and cross-shore velocity components accompanied by intensive cross-shelf water exchange.

General origin of the observed variability was related to the formation and along-shore transfer of submesoscale eddies with diameter about 2–8 km. These shelf eddies were ageostrophic and their life-time normally did not exceed several days. The main energy source for shelf eddies formation was the external circulation—currents over the continental slope. The influence of other factors such as non-stationary and spatially inhomogeneous wind forcing and coastal fresh water run-off on the formation of the shelf eddies was not so obvious. However, we don't exclude that these factors sometimes play an important role for the formation and evolution of submesoscale shelf eddies. This question should be studied in more details in future.

Up to this moment two basic physical mechanisms of sub-mesoscale eddy formation were revealed. The first was the shear instability of the alongshore current. Due to shear instability the cyclonic shelf eddies are generated in the case when the alongshore current over the continental slope has south-eastern direction (Fig. 4a) and anti-cyclonic—in the opposite case (Fig. 4b). The second mechanism was observed only in case of strong external circulation (when alongshore current velocity over the shelf edge exceeded 40–50 cm/s) and resulted in periodic eddy formation in the concave forms of coastal line relief, particularly, behind the cape Idokopas due to basic flow separation. These eddies were shedding periodically to the basic flow. The non-dimensional frequency of this process—Strouhal number, $St=D/UT$ (D —length scale of orographic feature, U —scale of along-shore current velocity, T —time period of eddy formation) was equal to 0.1. Such value ($St=0.1-0.3$) is typical for the periodic eddy formation behind high-drag bodies in laboratory gas and fluid dynamics experiments (Figs. 5, 6) (Elkin, 2010).

A detachment of the shelf eddy from the shore and its inclusion to the along-shore current accompanied by strong shelf-slope water exchange was also revealed.

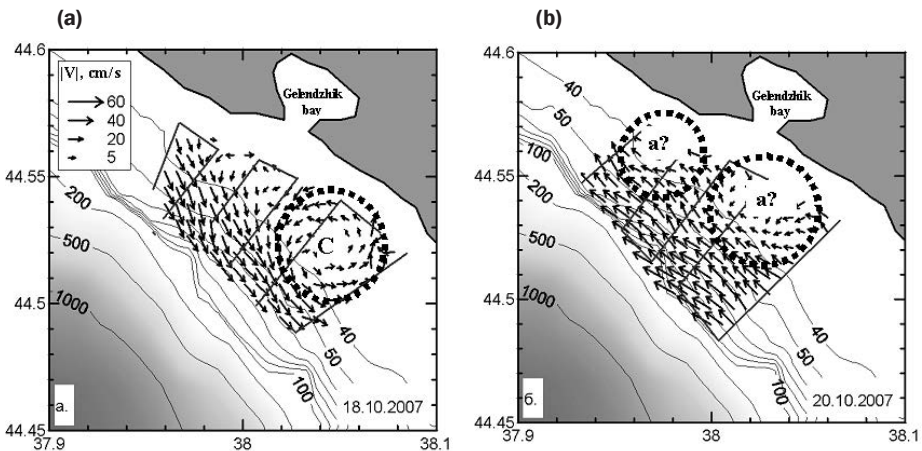


Fig. 4. Horizontal current velocity component over the Gelendzhik shelf: results of towed ADCP surveys: (a) October 18, 2007, 12:27–16:40; (b) October 25, 2007, 09:43–15:47.



Fig. 5. Velocity field in a shelf area near Gelendzhik according to ADCP surveys fulfilled on 28.09.08. Dotted line marks approximately a position of submesoscale anti-cyclonic eddy A1.

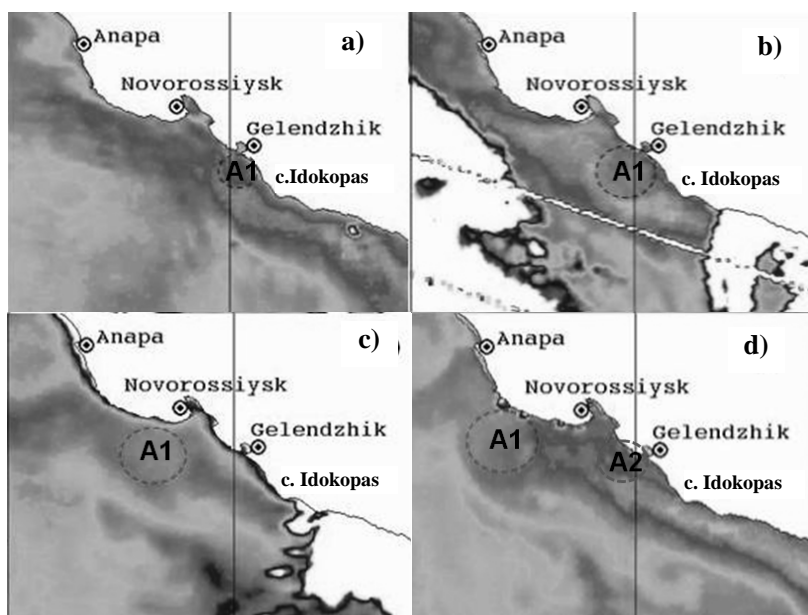
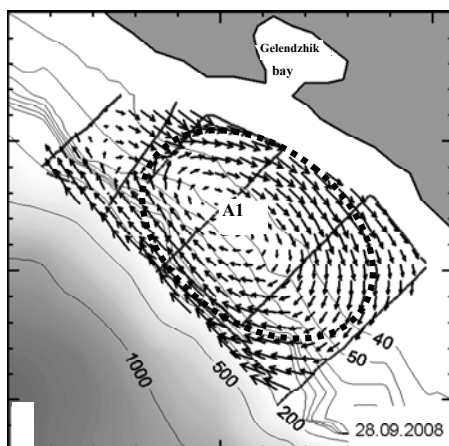


Fig. 6. Evolution of near-shore anti-cyclonic eddies A1 and A2: 28.09.08 06:59 GMT (a), 29.09.08 08:25 GMT (b), 30.09.08, 19:22 GMT (c) and 01.10.08, 09:53 GMT (d). Dotted line—eddy's position and size.

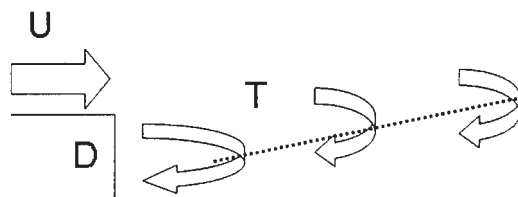


Fig. 7. Scheme of periodic eddy formation in a flow behind high-drag body (a step). D —the step height; U —velocity of the flow upstream the step; T —time period of eddy formation.



The study of the regulations and peculiarities of shelf eddy formation and evolution mechanisms were performed in rotating and non-rotating fluid by means of laboratory experiments. The results of this study are presented and discussed in (Elkin, 2010).

Acknowledgments

The work was supported by the Program of Fundamental Research No. 20 of the Russian Academy of Sciences and the Russian Foundation for Basic Research: grants Nos. 08-05-00183 and 09-05-13527.

References

- Aref, H. (2006) Vortex dynamics of wakes. *Nonlinear Dynamics* 2(4):411–424 (in Russian).
- Elkin, D. M. (2010) Laboratory study of sub-mesoscale eddy formation mechanisms at the narrow Black Sea shelf. *This volume*.
- Blatov, A. S., Bulgakov, N. P., Ivanov, V. A. et al. (1984) *Variability of hydrophysical fields of the Black Sea*. Leningrad: Gidrometeoizdat (in Russian).
- Zatsepin, A. G., Denisov, E. S., Emel'yanov, S. V. et al. (2005) Effect of bottom slope and wind on the near-shore current in a rotating stratified fluid: laboratory modeling for the Black Sea. *Oceanology* 45(Suppl. 1):S13–S26.
- Zatsepin, A. G., Ginzburg, A. I., Kostianoy, A. G. et al. (2003) Observations of Black Sea mesoscale eddies and associated horizontal mixing. *J. Geophys. Res.* 108(C8):2-1–2-27, doi.10.1029/2002JC001390.
- Zatsepin, A. G., Ginzburg, A. I., Kostianoy, A. G. et al. (2002) Variability of water dynamics in the north-eastern Black Sea and its effect on water exchange between near-shore and off-shore parts of the basin. *Oceanology* 42(Suppl. 1):S1–S15.
- Zatsepin, A. G., Kondrashov, A. A., Korzh, A. O. et al. (2010) Sub-mesoscale eddies at the Caucasian Black sea shelf and the mechanisms of their generation. *Oceanology* 50(6) (in press) (in Russian).

Poster presentations

Numerical simulation of density inhomogeneity (“spot”) collapse

Dmitry Ampilogov, Viktor Vasilkin, Denis Maliy

Abstract

It is well known that formation of water volumes denser than the ambient is possible in nearshore sea zones. For instance, it includes the formation of nearshore waters filled with suspended matter during the intense autumn storms. The present work objective is to study the specific features of stratified fluid collapse under the dimensional asymmetry of one of modeling space’s borders.

Хорошо известно, что в прибрежной зоне морей могут формироваться более плотные воды. Например, при интенсивных осенних штормах плотность прибрежных вод может увеличиваться благодаря взмучиванию. Цель данной работы — изучить специфические черты поведения объема стратифицированной жидкости при помощи численного моделирования при пространственной асимметрии одной из границ модельного пространства.

Dmitry Ampilogov, Viktor Vasilkin, Denis Maliy (✉)
Immanuel Kant State University of Russia (UKSUR), Kaliningrad, Russia
e-mail: dimanak74@mail.ru

Changes in hydro-meteorological characteristics for marine coast and lagoons of the South-East Baltic

Boris Chubarenko, Zhanna Stont, Oleg Goushchin

Abstract

10-years data set of hydro-meteorological measurements at the lagoon coasts of the Vistula and Curonian spits (South-East Baltic) shows evident rise of the air and water temperatures with the rates of 0.09–0.15 and 0.07–0.17 °C per year respectively. Statistical distributions of wind speed for three intervals (1992–94, 1998–2000, 2001–04) for the Vistula Lagoon and 5-years period (2004–08) for the open marine oil platform D6 evidence that wind condition become more calmer, repetition of strong and moderate winds is reduced, air pressure is increased. All these allow to formulate hypothesis that trajectories of cyclones crossing the Baltic Sea are changed—they are shifting to North in comparison with previous ordinary ways.

На основе анализа данных 10-летних ежедневных наблюдений температуры воздуха и воды на заливных берегах Вислинской и Куршской кос сделан вывод об их очевидном росте со скоростями 0,09–0,15°С в год для температуры воздуха и 0,07–0,17°С в год для температуры воды. Сравнение статистических распределений для скорости ветра для трех трехлетних периодов (1992–1994, 1998–2000, 2001–2004) для Вислинского залива и за 5 лет (2004–2008) для открытой морской платформы Д-6 показало, что в целом ветровой режим становится спокойнее, уменьшается повторяемость умеренных и сильных ветров. В совокупности с общим повышением значений атмосферного давления над территорией Калининградской области эти изменения в статистике повторяемости различных скоростей ветра позволяют выдвинуть гипотезу об изменении траекторий движения циклонов над Балтикой — смещение на север траекторий движения их центров.

1. Introduction

Hydro-meteorological conditions in the Baltic Sea region are varied in a response to global climate variability and anthropogenic influences as everywhere (Shkolnik et al., 2006, Assessment... 2008). This response is not equal

Boris Chubarenko, Zhanna Stont (✉)

P. P. Shirshov Institute of Oceanology RAS, Atlantic Branch, Kaliningrad, Russia
e-mail: chuboris@mail.ru, ocean_stont@mail.ru

Oleg Goushchin (✉)

Immanuel Kant State University of Russia (UKSUR), Kaliningrad, Russia



for different part of the Baltic Sea region, and local conditions respond to global changes in different ways (Meier, 2002, Graham, 2004). As concern the coastal water bodies as the Curonian and Vistula lagoons, which are of the horizontal scale of 10–100 km, the local conditions are the most driving forces for them (Chubarenko & Chubarenko, 2002).

The aim of the study is to analyse changes in hydro-meteorological conditions exactly in the South-East Baltic during last 10 years.

This analysis was fulfilled on the basis of both, the data collected at the points 1, 2, 4 (Fig. 1) by Atlantic Branch of P.P. Shirshov Institute of Oceanology of Russian Academy of Sciences (ABIORAS, and the data from open sources, as data collected by official agencies are not freely available.

Daily average temperature of air and water (1997–2007) were measured at the lagoon coast of the Vistula Spit (Kosa Village), approximately 1 km southward from the Baltiysk Strait, the single inlet of the Vistula Lagoon; and at the lagoon coast at the central part of the Curonian Spit, the Rybachii Village (points 2 and 4, Fig. 1). Hourly data on water and air temperature, wind and air pressure at the water level (2004–08) were measured at the oil platform D6, located at a distance of approximately 30 km from the shore of the Curonian Spit (point 5, Fig. 1). Therefore, points 2 and 4 characterize conditions at the Vistula and Curonian lagoons respectively, while point 5 characterize marine conditions. Historical data for City of Kaliningrad and Port Pionerskii (points 1 and 3, Fig. 1) were used for comparison.

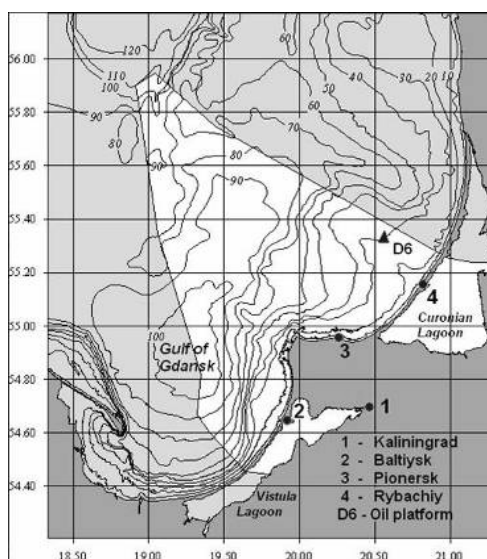
2. Results

2.1. Increase of air and water temperature

Despite some variations from year to year all data show an increase of average air and water temperatures for both Curonian and Vistula lagoons (Figs. 2, 3; Table)—a positive linear trend statistically significant (reliable) for daily data for points 2 and 4 (Table).

Fig. 1. Locations of points of hydrometeorological monitoring which data are used in the paper:

- (1) City of Kaliningrad, the Pregolia River, museum vessel “Vityaz”;
- (2) the Vistula spit, lagoon shore, just near the Vistula Lagoon inlet, Kosa Village of the City of Baltiysk;
- (3) northern coast of the Sambian Peninsula, marine shore, City of Pionersk;
- (4) the Curonian Spit, the Rybachiy Village, lagoon shore;
- (5) open sea, 30 km from the shore, oil platform D6.





Table

Trends for air and water temperatures (1997–2007) at points 2 and 4, characterized the Vistula and Curonian lagoon conditions respectively.

Parameter, location	Averaging scale, period 1997–2007	Trend rate (°C per year)	Student's t-test
Air temperature, Vistula Spit, lagoon shore, Kosa Village (Baltiysk)	Daily-averaged	0.0891 or ~0.09	2.02
	Monthly-averaged	insignificant	0.23
	Yearly-averaged	insignificant	0.48
Air temperature, Curonian Spit lagoon shore, Rybachii Village	Daily-averaged	0.146 or ~0.15	4.79
	Monthly-averaged	insignificant	0.86
	Yearly-averaged	insignificant	0.36
Water temperature, Vistula Spit, lagoon shore, Kosa Village (Baltiysk)	Daily-averaged	0.17374 or ~0.17	4.59
	Monthly-averaged	insignificant	0.36
	Yearly-averaged	insignificant	1.40
Water temperature, Curonian Lagoon, lagoon shore, Rybachii Village	Daily-averaged	0.0719 or ~0.07	2.22
	Monthly-averaged	insignificant	0.70
	Yearly-averaged	insignificant	0.80

There is a big difference in relationship between air and water temperature trends for both lagoons: for the Vistula Lagoon, the rate for water temperature rise is 2 times higher than one for air temperature (0.17 and 0.09 °C per year respectively), but for the Curonian lagoon—*vis versa* (Table). The only one explanation derives from location of sampling points. The point 4 (Curonian Lagoon) is equally far from both main drivers—Klaipeda Strait (the Curonian Lagoon inlet) and Neman River, and therefore may represent purely lagoon conditions, while point 2 (Vistula lagoon) is just in the vicinity of the Baltiysk Strait, the Vistula Lagoon inlet, and, therefore, it is under permanent influence from sea water intrusions.

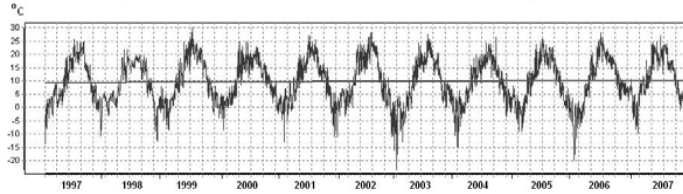
The rate of increase of air temperature for the Curonian Lagoon is approximately 2 times higher than one for the Vistula Lagoon. As these points are rather close to each other, and a general tendency of more rapid increase of the air temperature for northern parts of the Baltic Sea Region (Graham, 2004) couldn't be so pronounced between them, this difference in the rates evidences to influence of local microclimate conditions.

Important to note, that the only trend of daily averaged temperatures should be used for reliable analysis, as trends estimated for monthly- or yearly-averaged temperatures are not statistically significant (reliable). Consequent averaging (from daily-averaged to yearly-averaged data) gives a reduction in the trend rate (Table), and may even lead to possible change of the tendency; e.g., for point 2, the rate for air temperature is higher than that for water temperature in terms of yearly average data, while it should be opposite considering daily averaged data.

Positive trend in air temperature founded for both lagoons was not revealed for the inland station in Kaliningrad (point 1, Fig. 1). Statistical analysis of daily measurements at this point (1996–2008) showed even negative (but statistically non-reliable) trend of -0.01 °C/year.

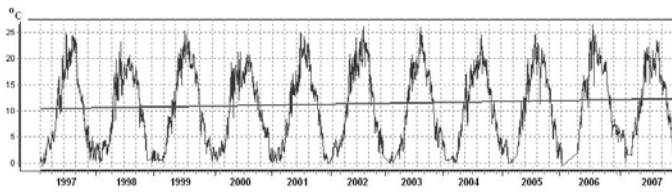


(a) T_a (average daily data), 1997–2007, Kosa Village (Baltiysk), Vistula Spit



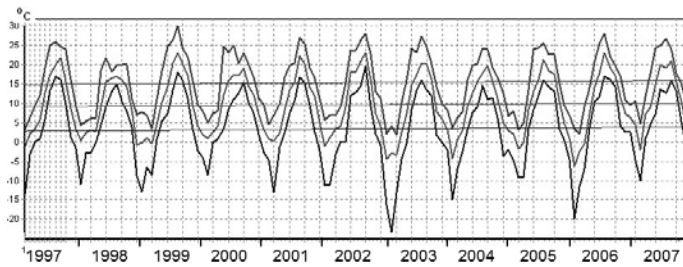
T_a $A_trend=9.18$ $B_trend=0.000244$ $t_student=2.02$

(b) T_w (average daily data), 1997–2007, Kosa Village (Baltiysk), Vistula Spit



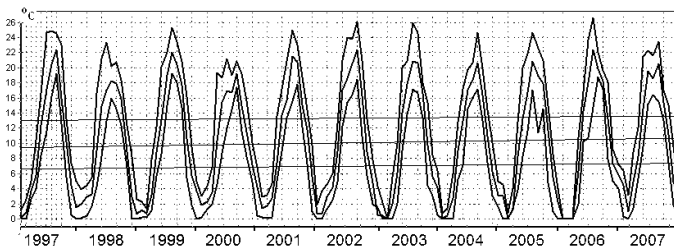
T_w $A_trend=10.37$ $B_trend=0.000476$ $t_student=4.59$

(c) T_a (maximal, average and minimum monthly data), 1997–2007, Kosa Village (Baltiysk), Vistula Spit



T_{a_max} $A_trend=14.80$ $B_trend=0.0077$ $t_student=0.433$
 T_{a_avg} $A_trend=9.09$ $B_trend=0.0074$ $t_student=0.416$
 T_{a_min} $A_trend=2.86$ $B_trend=0.0077$ $t_student=0.363$

(d) T_w (maximal, average and minimum monthly data), 1997–2007, Kosa Village (Baltiysk), Vistula Spit

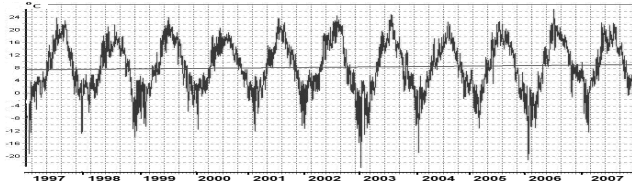


T_{w_max} $A_trend=13.03$ $B_trend=0.0045$ $t_student=0.245$
 T_{w_avg} $A_trend=9.44$ $B_trend=0.0096$ $t_student=0.576$
 T_{w_min} $A_trend=6.61$ $B_trend=0.0058$ $t_student=0.395$

Fig. 2. Time variations of air and water temperature, point 2 (Vistula Lagoon, Kosa Village, Baltiysk), 1997–2007: average daily data of air (a) and water (b) temperature; maximal, average and minimum monthly data of air (c) and water (d) temperatures.

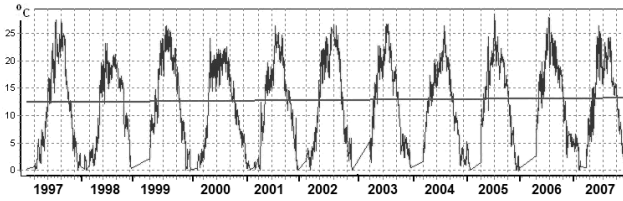


(a) T_a (average daily data), 1997–2007, Rybachiy Village, Curonian Spit



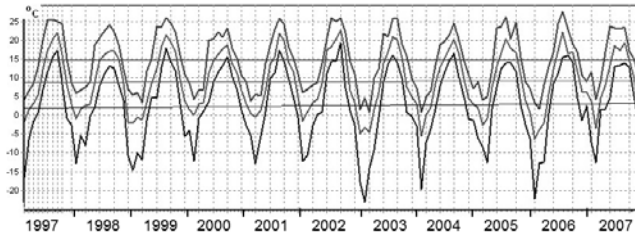
T_a $A_trend=7.32$ $B_trend=0.0004$ $t_student=4.79$

(b) T_w (average daily data), 1997–2007, Rybachiy Village, Curonian Spit



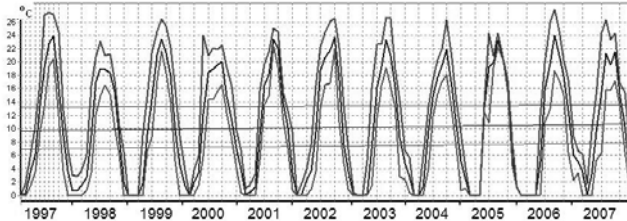
T_w $A_trend=12.23$ $B_trend=0.000197$ $t_student=2.22$

(c) T_a (maximal, average and minimum monthly data), 1997–2007, Rybachiy Village, Curonian Spit



T_{a_max} $A_trend=14.80$ $B_trend=0.0004$ $t_student=0.022$
 T_{a_avg} $A_trend=8.83$ $B_trend=0.0034$ $t_student=0.190$
 T_{a_min} $A_trend=1.96$ $B_trend=0.0091$ $t_student=0.399$

(d) T_w (maximal, average and minimum monthly data), 1997–2007, Rybachiy Village, Curonian Spit



T_{w_max} $A_trend=13.23$ $B_trend=0.0025$ $t_student=0.116$
 T_{w_avg} $A_trend=9.70$ $B_trend=0.0076$ $t_student=0.400$
 T_{w_min} $A_trend=6.97$ $B_trend=0.0066$ $t_student=0.394$

Fig. 3. Time variations of air and water temperature, point 4 (Curonian Lagoon, Rybachii Village), 1997–2007: average daily data of air (a) and water (b) temperature; maximal, average and minimum monthly data of air (c) and water (d) temperatures.



2.2. Wind speed and direction

Data up to 2000, collected within (Gilbert, 2008), showed the negative trend for magnitudes of maximal winds for the South-East Baltic. Comparison of pictograms (Fig. 4) for wind speed probability for three periods (1992–94, 1998–2000, 2001–04) and historical data (1949–88) in Baltiysk, explicitly evidence, that the probability of wind of more than 6 m/sec dropped down after 1994. The data on wind speed in the point 2 (the Vistula Lagoon, 1997–2007) also show permanent and slow reduction of wind, and trends for minimal and maximal temperature are statistically significant (Fig. 5).

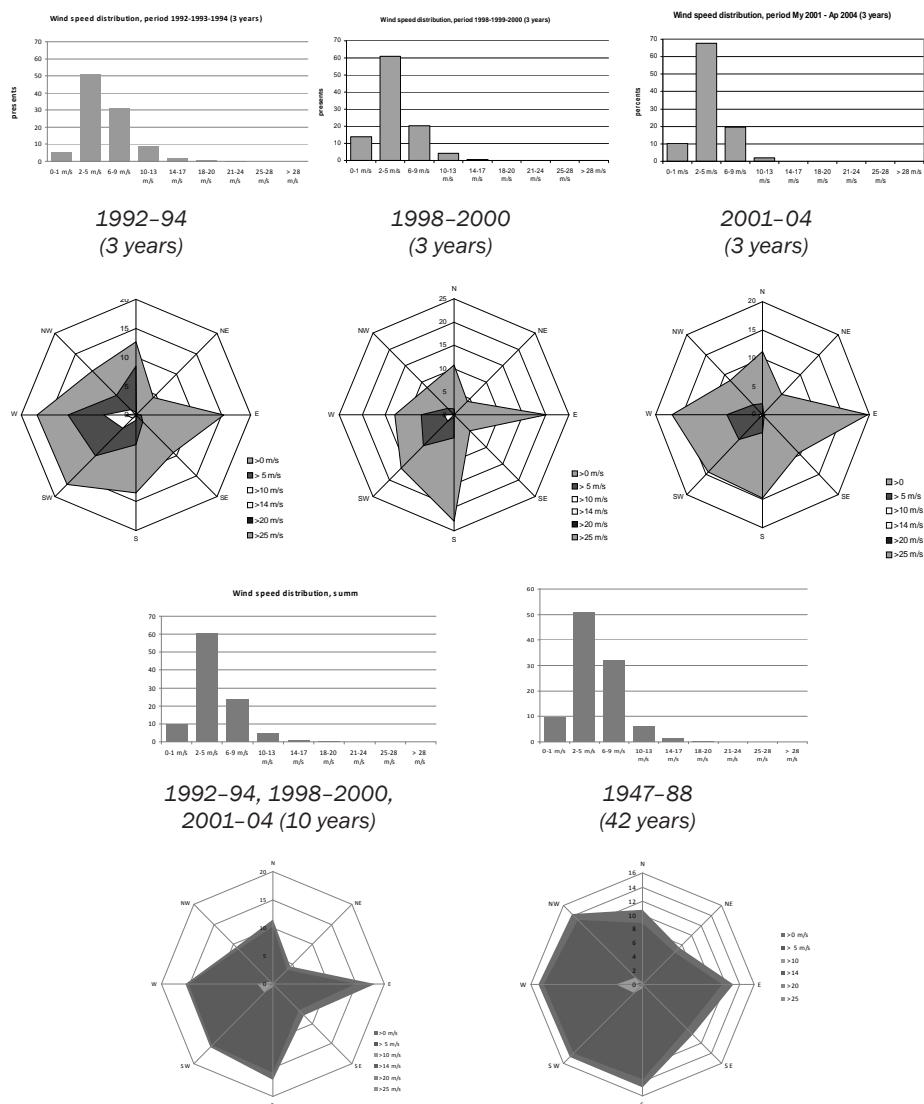


Fig. 4. Wind statistics for three periods (1992–94, 1998–2000, 2001–04), and historical period 1947–88 for the Vistula Lagoon. Rose-in-rose pictograms show consequent statistical distributions of wind directions for all winds, winds higher than 5, 10, 15, 20 and 25 m/s.



Correct estimation of changes in wind direction is not possible, as all coastal points of meteorological measurements at the Russian territory of the South-East Baltic are partly shadowed by buildings or trees. The point of measurements at the oil platform D6 (point 5, Fig. 1) is the most representative one (Fig. 6), but measurements there started only five years ago.

2.3. Changes in air pressure

Time variations of air pressure (referred to a sea water level) at the oil platform D6 in the Baltic Sea has obvious and statistically significant positive (student's t-test equals to 18.77) trend of 0.641 hPa per year for the period 2004–08 (Fig. 7).

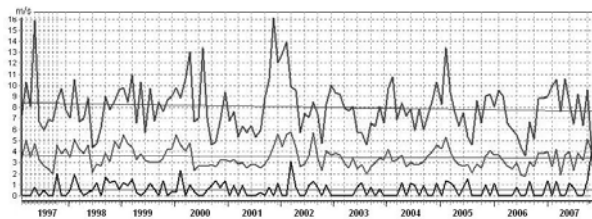
Analysis of hourly air pressure at the oil platform D6, namely, the repetition of three grades of pressure (Az, anti-cyclonic conditions, air pressure greater than 1,015 hPa, Zn, cyclonic conditions, air pressure greater than 1,010 hPa, and GF, and low gradient fields of atmospheric pressure) showed that number of Az-conditions is increased, against reduction of numbers of Zn-conditions.

Both these steady tendencies for an air pressure over the South-East Baltic, as well as reduction of wind speed while wind direction distribution keeps constant, evidence to a change in cyclones trajectories, and we may set up a hypothesis, that cyclone's trajectories shifted to North from their usual corridor.

3. Conclusions

Data collected at the coastal measuring points in the Russian part of the South-East Baltic (1997–2007) show positive trend for daily averaged temperatures of air and water. Such a trend is observed not only in averaged data, but for minimal and maximal values of temperature also, and therefore, the 10-years warming tendency is obvious for the South-East Baltic. Rate of average temperature increase for the Vistula Lagoon equals 0.09 °C per year for the air temperature and 0.17 °C per year for the water temperature; for the Curonian Lagoon respective rates are 0.15 and 0.07 °C per year.

Wind speed, Baltiysk (Vistula Spit), 1997–2007



$W_{min} A_trend=0.553 B_trend=-0.0002 t_student=0.116$
 $W_{avg} A_trend=3.655 B_trend=-0.0019 t_student=0.847$
 $W_{max} A_trend=8.428 B_trend=-0.0060 t_student=1.148$

Fig. 5. Time variations and trends of maximal, average and minimal daily values of a wind velocity, point 2, Vistula Lagoon, Baltiysk, 1997–2007.

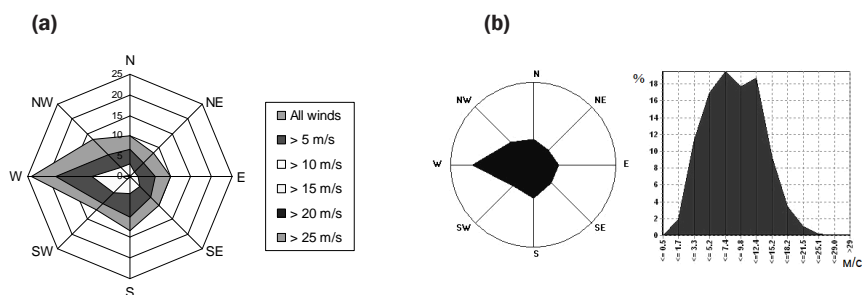
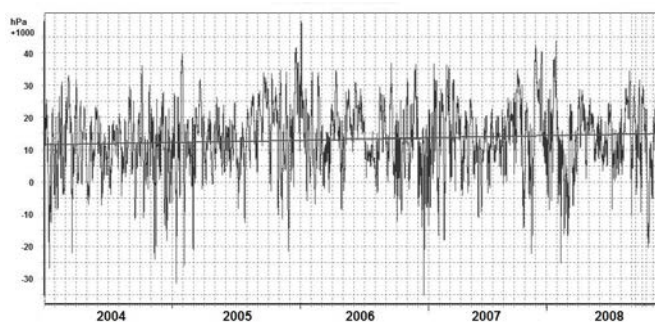


Fig. 6. Consequent wind roses for different wind speed gradations (all winds, wind speed more than 5, 10, 15, 20, 25 m/sec) (a), and statistical distribution of probability for velocity speed of different grades (b) at oil platform D6.



$A_trend=11.484 (+1,000 \text{ hPa})$ $B_trend=0.000077$ $t_student=18.770$.

Fig. 7. Time variations and trend of atmospheric pressure according to automatic hydro-meteorological station, established on oil platform D-6.

Differences in the rates between air and water temperatures for both lagoons is caused by location of measuring points—in the Vistula Lagoon measuring point is close to lagoon inlet (Baltiysk Strait) and under permanent influence of random marine water intrusions, while in the Curonian Lagoon the measuring point is rather far from main drivers—the Neman River delta and lagoon inlet (Klaipeda Strait). The local microclimate influence is very strong at the Curonian Spit, as the rate of air temperature increase is 2 times higher there than for the Vistula Lagoon.

Data for wind speed for three periods (1992–94, 1998–2000, 2001–04) and for the period 1997–2007 evidence about reduction of minimal and maximal wind speeds, and reduction of repeatability of winds of moderate and high speed. Therefore, recent data approved a tendency (which were formulated before on the basis of the data from late 90th) of evolution of wind climate in the South-East Baltic to more calm conditions.

As all coastal measuring points are partly shadowed by buildings or trees, the only representative measurements are executed at the oil platform D6 located 30 km offshore in the Baltic Sea, but regular measurements have started there only 5 years ago.

General negative trend in air pressure, increase of repeatability of anti-cyclonic and low gradient field conditions, as well as wind speed reduction in the South-East Baltic allowed to set up a hypothesis, that trajectories of

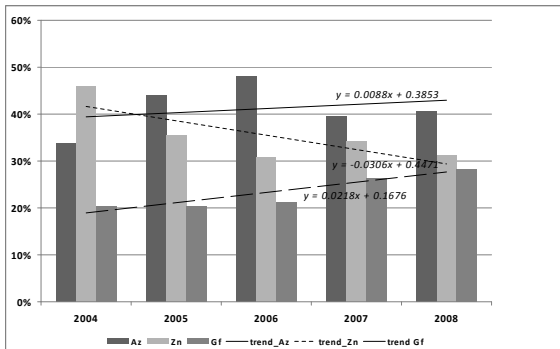


Fig. 8. Repeatability of cyclonic, anti-cyclonic conditions and low gradient field of atmospheric pressure in the South-East Baltic in 2004–08; the linear trends are also shown.

centers of cyclones crossing the Baltic Sea shifted to North from their usual corridor.

In any cases, it is expected that all these trends will be accompanied by positive consequences to marine and lagoon shore dynamics. Reduction of storminess, increase of probability for south strong winds may ensure an intensification of coastal accretion on northern marine shore of the Sambian Peninsula, suffered nowadays from intensive coastal abrasion.

Acknowledgements

This work was partly supported by grants Nos. 08-05-01023 and 08-05-92421 of the Russian Foundation for Basic Research. Data was collected during the measurement programs performed by the Atlantic Branch of P.P. Shirshov Institute at the Museum Vessel “Vityaz” of the Museum of the World Ocean and at the oil-platform D6 of the LUKOIL Company, and authors thank these organizations for substantial support.

References

- Assessment of climate change for the Baltic Sea basin (2008) Berlin, Heidelberg: Springer-Verlag.
- Chubarenko, I. P. & Chubarenko, B. V. (2002) General water dynamics of the Vistula Lagoon. *Environmental and Chemical Physics* **24(4)**:213–217.
- Gilbert, C., ed. (2008) *Sustainable development indicators for integrative coastal zone management of the South-East Baltic*. Gdansk: Drukarnia WL.
- Graham, L. P. (2004) Climate Change Effects on River Flow to the Baltic Sea. *Ambio* **33(4–5)**:235–241.
- Meier, H. E. M. (2002) Regional ocean climate simulations with a 3D ice-ocean model for the Baltic Sea. Part 1: model experiments and results for temperature and salinity. *Climate Dynamics*, DOI 10.1007/s00382-001-0224-6. Springer-Verlag [on-line publication].
- Shkolnik, I. M., Meleshko, V. P., Katkov, V. M. (2006) Probable climate change on both the European part of Russian Federation and adjacent territory up to the end of XXI century: simulation by regional model of “Voejeikov’s GGO”. *Meteorologiya i Gidrologiya* **3**:5–16 (in Russian).

Analysis of thermohaline structure of water in coastal zone of the Baltic Sea and of characteristics of its cold intermediate layer

Natalia Chubarenko, Sergey Shchuka, Irina Chubarenko

Abstract

Analysis of field data on vertical thermohaline structure of waters in the South-East Baltic, obtained in 75 and 78 cruises of r/v “Professor Stockman” (March and July 2006) in frames of “LUKOIL” monitoring program, is presented. Using previously developed formalized criterion, the cold intermediate layer is allocated and its features are described.

Представлен анализ данных экспедиционных исследований НИС «Профессор Штокман» (75-й и 78-й рейсы по программе мониторинга Лукойл, проводившиеся в марте и июле 2006 г.) вертикальной термохалинной структуре юго-восточной части Балтийского моря. На основе разработанного ранее формализованного критерия в вертикальной термохалинной структуре вод в летний период выделен холодный промежуточный слой, характеристики которого подробно описаны.

1. Data and the goal of the analysis

Data of vertical profilings performed in coastal and deep parts of the Gulf of Gdansk (south-eastern Baltic Sea) in March and July 2006 during the 75 and 78 cruises of research vessel “Prof. Stockman” (Report on 75 cruise... 2006, Report on 78 cruise... 2006) was analyzed. The purpose of the analysis was to clarify the thermal structure and examine possible impact of change of the mixing regime while crossing of the temperature of maximum density of water (T_{md}). We compared the characteristics of water observed over the

Natalia Chubarenko (✉)

Moscow Institute of Physics and Technology, Dolgoprudny, Russia;

P. P. Shirshov Institute of Oceanology, Moscow, Russia

Sergey Shchuka (✉)

P. P. Shirshov Institute of Oceanology, Moscow, Russia

Irina Chubarenko (✉)

P. P. Shirshov Institute of Oceanology RAS, Atlantic Branch, Kaliningrad, Russia



coastal underwater slopes of the Gdansk Bay (off the Curonian spit) by the beginning of the period of spring warming—with the characteristics of the cold intermediate layer (CIL) in the summer when it is most clearly manifested in general vertical thermohaline structure of water. The measurements were performed using a standard CTD probe Neil Brown Mark III.

For the comparative analysis the following stations were selected: (i) station No. 12 (55°35' N, 20°2' E) in the deepest part of the south-eastern Baltic Sea (center of the Gulf of Gdansk); depth at this point was about 80 m; and (ii) station No. 7 (55°14' N, 20°53' E) as a coastal station, depth at which was 10–12 m (see Report on 75 cruise... 2006, Report on 78 cruise... 2006).

2. Characteristics of CIL in summer time

In July 2006, after a fairly typical winter, the vertical thermohaline structure of water was also typical: the upper heated layer with the thermocline at a depth of 15 m, then the second (seasonal) thermocline (29 m), CIL, the main pycnocline below 60 m (Fig. 1). The profiles of temperature, salinity and the density anomaly were analyzed in detail, and the Tmd-profile for them was calculated taking into account its dependency on the observed salinity and pressure. The analysis of the characteristics of CIL was presented in the form of detailed tables.

3. Characteristics of water over coastal underwater slopes by the beginning of the spring warming

In order to examine the possibility of penetration into the CIL of coastal waters formed in March, which may have been transported in deep part along the slopes by cascading due to early-spring heating from temperature $T < T_{md}$ (Chubarenko, 2010), the profiles of temperature and density in March in the coastal zone were analyzed, as well as in March and July in the deepwater part.

During the measurements in March 2006 (Report on 75 cruise... 2006) the process of cooling was still going on and the temperature of coastal waters

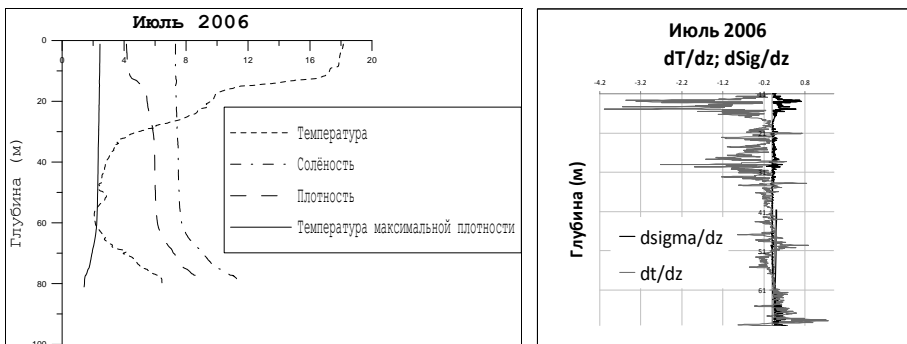


Fig. 1. Vertical profiles of temperature, salinity, density anomaly and Tmd (depending on salinity and pressure) in the deepwater of Gulf of Gdansk (station 12, July 2006) and the corresponding vertical temperature and density gradients.

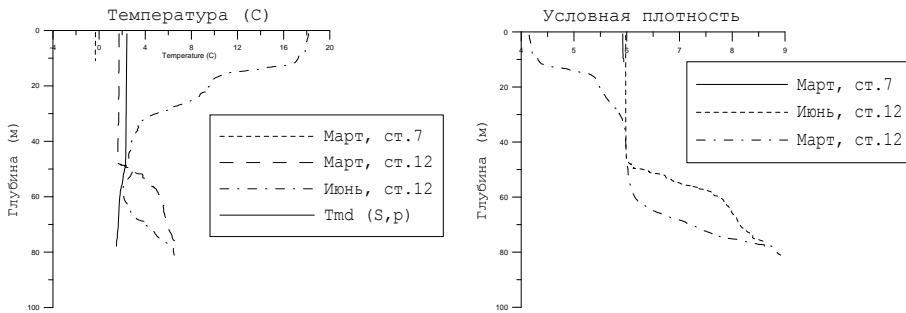


Fig. 2. Deepwater (St. 12) and coastal (St. 7) parts of the south-eastern Baltic Sea in March and July 2006 (according to (Report on 75 cruise... 2006, Report on 78 cruise... 2006)); profiles of water temperature (a) and density anomaly (d).

remained significantly lower ($-0.3\text{ }^{\circ}\text{C}$) than the temperature of surface waters in the open-sea part ($1.7\text{ }^{\circ}\text{C}$), both at the same time confidently below Tmd, amounting to $2.3\text{--}2.5\text{ }^{\circ}\text{C}$ at a given salinity. Thus, the conditions were quite favorable for the possible occurrence of the cascading along coastal underwater slopes with the beginning of the spring warming.

Analysis of the density distribution showed that the density anomaly of coastal waters was 5.9 kg/m^3 in March, which was in the range of the properties of CIL in the deep part of the sea in July: there it varied from 5.14 (at a depth of 15 m) to 7.07 kg/m^3 (at a depth of 67 m); the density anomaly of 5.9 kg/m^3 was observed in deep part at the depths of $31\text{--}34\text{ m}$. At the same time, in the spring the thickness of the upper quasi-homogeneous layer was about 50 m .

4. Conclusions

(1) After a typical winter (2006), water temperature in the upper layers of the Baltic Sea ($40\text{--}60\text{ m}$) is lower than the temperature of maximum density: in 2006 it ranged from -0.3 to $1.7\text{ }^{\circ}\text{C}$. This means that at the beginning of the spring warming from the surface vertical convection occurs. Where convection reaches the bottom (it is about 60 percent of the sea area), the cascading of denser waters with temperature $T < T_{md}$ should arise along the slopes.

(2) The density of coastal waters (according to the analyzed data) fits the range of the properties of CIL: for example, in March 2006, the density anomaly of coastal waters was 5.9 kg/m^3 , and the range of densities within the CIL in the deep part of the sea in July varied from 5.14 to 7.07 kg/m^3 .

(3) With the salinity typical for the upper (more fresh) layer at the given area, coastal waters cannot sink down along the slopes below the level of permanent halo-cline, i.e., they should separate from the slope and propagate further into the deep part of the sea in the intermediate layer. Water with exactly such characteristics is found inside the CIL of Baltic Sea in summer: with $T < T_{md}$ and salinity close to the salinity of the surface layer.

Thus, the comparative analysis confirms the possibility of contribution of early-spring cascading to the formation of CIL of Baltic Sea. Details of this water exchange could be clarified only by special full-scale studies.



Acknowledgements

This work was supported by RFBR, grants Nos. 09-05-90726 mob_st), 10-05-00540a.

References

- Chubarenko, I. P. (2010) Horizontal Convective Water Exchange above a Sloping Bottom: The Mechanism of Its Formation and an Analysis of Its Development. *Okeanologiya* **50(2)**:184–193 (in Russian), *Oceanology* **50(2)**:166–174 (in English).
- Report on 75 cruise of r/v “Professor Stockman”, March 3–9, 2006 (2006) Atlantic Branch of P. P. Shirshov Institute of Oceanology, Kaliningrad (in Russian).
- Report on 78 cruise of r/v “Professor Stockman”, July 1–5, 2006 (2006) Atlantic Branch of P. P. Shirshov Institute of Oceanology, Kaliningrad (in Russian).

Distribution of sea surface temperature in the South-East Baltic by remote sensing and in-situ data

Vsevolod Chugaevich, Elena Sapozhnikova

Abstract

The Sambion shore water was investigated by Atlantic Branch of P. P. Shirshov Institute of Oceanology and Immanuel Kant State University of Russia in 2009. The frontal zones and thermohaline structure were objects of scientific interest. The new high resolution data were obtained during expedition on the sail boat "Ikar". It was compared with satellite data from NOAA and MODIS. The special attention was paid to outflow lagoon waters.

В 2009 г. вдоль побережья Самбийского полуострова сотрудниками кафедры географии океана Российского государственного университета им. И. Канта совместно с Атлантическим отделением Института океанологии им. П. П. Ширшова РАН проводились экспедиционные работы по исследованию фронтальных зон и термохалинной структуры вод. Измерения параметров выполнялись в различных гидрометеорологических условиях с борта катамарана «Икар». Для исследуемого района был получен новый ряд данных высокого пространственного разрешения. Данная работа посвящена изучению распределения температуры поверхностного слоя моря по экспедиционным данным и анализу спутниковых данных в районе взаимодействия морских и заливных вод. Особое внимание уделено анализу языка заливных вод, для которого получены CTD данные высокого пространственного разрешения.

Vsevolod Chugaevich, Elena Sapozhnikova (✉)
Immanuel Kant State University of Russia (UKSUR), Kaliningrad, Russia
e-mail: ocean@kantiana.ru

The temperature front in the rotating fluid: laboratory modeling

Natalya Demchenko, Andrei Zatsepin, Irina Chubarenko

Abstract

This work is devoted to investigation of the warm buoyant jet—“late” stage of the thermal bar phenomenon—in the rotating laboratory basin with a sloping and horizontal bottom. 24 experiments were performed for various specific power supply q (2,574 Wt/m²; 1,313 Wt/m²; 638 Wt/m²); Coriolis parameters $f=0.8, 1.25, 2.5 \text{ s}^{-1}$ and without rotation; for the slope angle $\alpha=39^\circ$ and horizontal bottom. It was pointed out, that the buoyancy flux and the Coriolis parameter are the key factors influencing the radial speed of propagation of the warm buoyant jet over sloping bottom in rotating fluid. Therefore, the main dimensionless parameters, governing this process, are the flux Rayleigh number and the Ekman number. The experiments showed that they are related as $Ra_b = Ek^{-2}$.

Данная работа посвящена исследованию плавучей струи — поздней стадии развития термобара — во вращающейся жидкости. Были выполнены 24 эксперимента для трех параметров удельной мощности подогрева q (2574 Вт/м²; 1313 Вт/м²; 638 Вт/м²); параметров Кориолиса $f=0.8, 1.25, 2.5 \text{ s}^{-1}$ и без вращения; с наклонным ($\alpha=39^\circ$) и горизонтальным дном. Результаты лабораторных экспериментов показали, что на радиальную скорость продвижения теплой плавучей струи при наличии уклона дна во вращающейся жидкости оказывают значительное влияние два фактора: параметр Кориолиса и величина потока плавучести через поверхность. Таким образом, основными безразмерными параметрами могут являться числа Рэля и Экмана. Эксперименты показали, что они связаны соотношением $Ra_b = Ek^{-2}$.

1. Introduction

It is well known, that the bottom topography and the Earth rotation significantly influence the dynamics and structure of the thermal fronts in the freshwater basins and brackish seas. Field observations of the thermally in-

Natalya Demchenko, Irina Chubarenko (✉)

P. P. Shirshov Institute of Oceanology RAS, Atlantic Branch, Kaliningrad, Russia

Andrei Zatsepin (✉)

P. P. Shirshov Institute of Oceanology RAS, Moscow, Russia



duced fronts in the Baltic sea during spring heating have revealed, that large-scale fronts in the southern and central Baltic are aligned with the coasts and isobaths; significant correlation between SST and topography was found (Bychkova et al., 1987). It was corroborated also by an analysis of 9-month time series of infrared imagery in the northern and central Baltic (Kahru et al., 1995). In some regions of the Ladoga Lake non-uniform topography leads to the deceleration of the thermal bar (frontal zone, associated with the temperature of maximum density, $T_{md}=3.98\text{ }^{\circ}\text{C}$) and formation of the “secondary” thermal front, marked by $5\text{ }^{\circ}\text{C}$ -isotherm at the surface, with the very sharp temperature gradients in the upper layers (Naumenko & Karetnikov, 1993).

The main goal of this work is to investigate how the rotation and bottom topography influence the propagation of the thermal bar at its late stage.

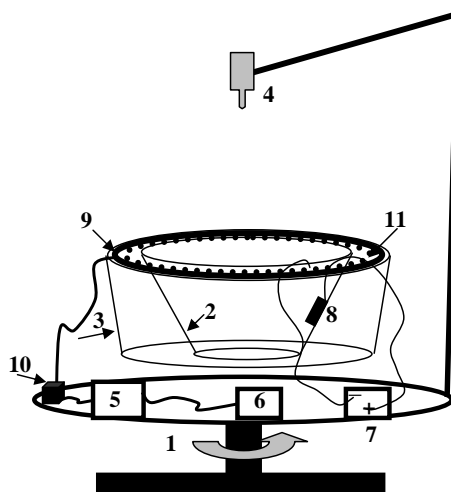
2. Methods

Experiments were performed in a cylindrical tank with radius $R_{tank}=0.3\text{ m}$, mounted on a rotating table. The tank was fitted with false bottom with circular heating isolated cable. The working section of the tank was closed with a model of a slope (slope angle $\alpha=39^{\circ}$) and horizontal bottom, decreasing a whole depth of the tank to 15–16 cm. The tank was filled with fresh distilled water. Experiments were performed (i) with rotation periods of 5, 10, 15 s, what gave the Coriolis parameter, $f=2\Omega$, around 0.8, 1.25, 2.5 s^{-1} respectively, and (ii) without rotation. In order to reproduce the warm buoyant jet, the heating cable was used, which was mounted over top of incline at the depth of 1-cm along the round wall of the tank. Series of experiments were performed using various specific power supply q , Wt/m^2 (0.26; 0.13; 0.06 Wt/m^2). The water temperature was controlled near the wall (depth, $D\sim 1.5\text{ cm}$; distance from the tank wall, $L\sim 2\text{ cm}$), at the middle of the radius ($D\sim 16\text{ cm}$; $L\sim 26\text{ cm}$) and at the center of the tank ($D\sim 27\text{ cm}$; $L\sim 37\text{ cm}$) by 3 verified thermometers. For visualization of the surface currents the water-soluble blue thymol indicator and paper tracers with neutral buoyancy were used.

Initially water temperature in the tank was 1–2 $^{\circ}\text{C}$ below the air temperature; in order to avoid vertical convection ice cubes were put on the free

Fig. 1. Experimental setup.

- (1) rotating table;
- (2) slope;
- (3) tank wall;
- (4) video camera;
- (5) autotransformer;
- (6) ampermeter;
- (7) voltage supply;
- (8) copper plate (anode);
- (9) heating resistance isolated cable;
- (10) outlet;
- (11) nichrome wire (cathode).





surface. At the beginning of each experiment the tank was filled with the fresh distilled water (concentration of thymol indicator was around 25g/65 L of water). Before the beginning of the experiments with rotation, the rotating frame was switched on; the working fluid was brought into rigid-body rotation (rotation rate f). After that the video record was switched on; the electrodes were supplied by the voltage, and the heating cable was initiated as a heater. Due to the electrochemical reaction, water solution near the nichrome wire became alkaline and changed its colour, becoming navy-blue. The paper tracers were put on the free surface in order to allow recalculating its replacement into surface velocity fields. Data processing was performed after the experiments using Tank Field Calculator, Excel and Surfer.

3. Results

3.1. Development of the temperature front in presence of the slope

The laboratory experiments with rotation did show, that the speed of the warm buoyant jet propagation to the middle of the tank depends on rotation rate f : with increasing specific power supply q the jet speed increases (but 1.5–4 times less).

It was pointed out, that in rotating fluid the buoyant jet is forced to the shore by the Coriolis force (Fig. 2); its radial speed is one order less than in non-rotating fluid. Therefore, strong along-shore currents is initiated; the thickness of the thermally active layer increases in comparison with the non-rotating fluid. In presence of the slope, along-shore currents are stable and keep axisymmetric shape during the entire experiment. In non-rotating fluid, the structure of the warm jet as a thread-like due to the convective instability near the heater.

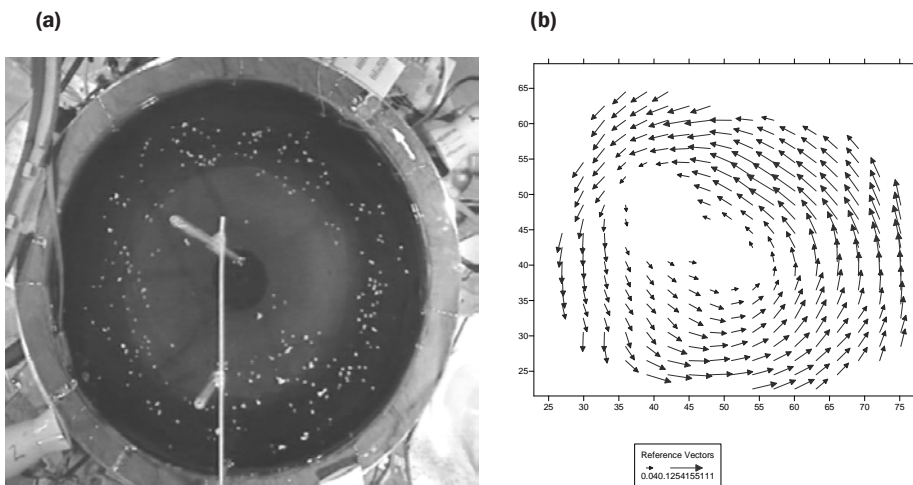


Fig. 2. (a) Photo of warm buoyant jet propagating to the deep part of the tank; (b) velocity field, calculated from paper tracers displacement using Tank Field Calculator program. The time from the beginning of the experiment is 35 min; specific power supply $q=0.26 \text{ Wt/m}^2$.



Results of laboratory experiments did show, that the Coriolis parameter and the buoyancy flux play the key role in the development of the jet, influencing its propagation speed in presence of the slope in rotating fluid. Thus, the main dimensionless parameters governing the process are the (flux) Rayleigh number, $Ra_F = \frac{g\alpha FL^4}{\rho_0 c_p \kappa_T^2 \nu}$ and the Ekman number, $Ek = \frac{\nu}{fL^2}$. Here, g is the acceleration due to gravity, α —thermal expansion coefficient, F —heat flux, L —horizontal length scale, ρ_0 —reference density, c_p —water heat capacity, κ_T —thermal conductivity coefficient, ν —viscosity. The heat flux, F , causes the buoyancy fluxes, $B = \frac{Fag}{\rho c_p}$, into the surface layer. Thus, more convenient is to use for the Rayleigh number the expression $Ra_B = \frac{BL^4}{\kappa_T^2 \nu}$. The dependence $Ra_B = Ek^{-2}$ was obtained, which is in a good agreement with results of Boubnov & Golitsyn (1995) who showed that $Ra_f \sim Ta^{2/3} \sim Ek^{-4/3}$ for the convection in a rotating fluid.

3.2. Development of the temperature front over horizontal bottom

The qualitative results of laboratory experiments without rotation effect did show, that over horizontal bottom in the deep tank (the thickness of the thermal active layer is insignificantly) the along shore currents are unstable and meandering; the quasi-geostrophic eddies are initiated. Therefore, radial propagation speed of the meandering temperature front increases over horizontal bottom in comparison on propagation speed of axisymmetrical buoyant jet over the slope due to the eddy viscosity. This effects are absent in non-rotating fluid with a model of horizontal bottom.

4. Conclusions

(1) Influence of the bottom slope is most significant in the sense that it stabilizes the propagation of the leading edge of the temperature front, preventing for its breaking-up and formation of the quasi-geostrophic eddies. Without the slope, rapid propagation of the coastal waters towards the deep part initiate formation of eddies.

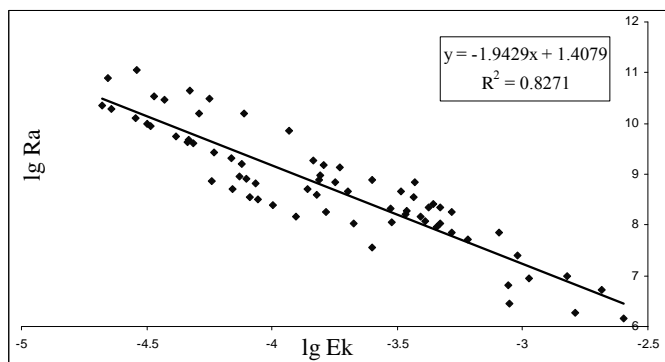


Fig. 3. The flux Rayleigh number as a function of the Ekman number.

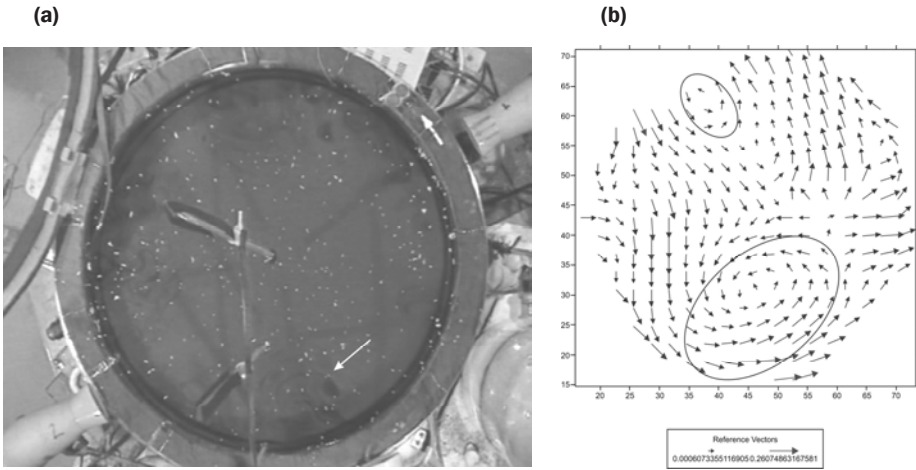


Fig. 4. Warm meandering temperature front in a basin with horizontal bottom at $q=0.26 \text{ Wt/m}^2$ and Coriolis parameter $f=0.8 \text{ s}^{-1}$: (a) photo of the surface; (b) calculated surface velocity field; the quasi-geostrophic eddies are marked by ovals.

(2) The buoyancy flux and Coriolis parameter play the key role for the radial speed of propagation of the warm buoyant jet, therefore, the main dimensionless parameters, governing this process, are the flux Rayleigh number and the Ekman number. The described experiments have demonstrated that they are related as $Ra_B = Ek^{-2}$.

Acknowledgement

This work is supported by RFBR 10-05-90746_mob_st, 10-05-00472a, 10-05-00540a. We would like to express great thanks to leading engineer of laboratory of experimental physics of the ocean (P. P. Shirshov Institute of Oceanology, Moscow) Dmitriy Elkin for his technical assistance.

References

- Boubnov, B. M. & Golitsyn, G. S. (1995) *Convection in rotating fluids*. London: Kluwer Academic Publishers.
- Bychkova, I. A., Viktorov, S. V., Losinsky, V. N. (1987) Structure of coastal fronts of the Baltic Sea from remote sensing data of infra-red range. In: *Proc of the 3rd Congr. of Sov. Oceanogr.* III, 64–65 (in Russian).
- Kahru, M., Hakansson, B., Rud, O. (1995) Distributions of the sea-surface temperature fronts in the Baltic sea as derived from satellite imagery. *Cont. Shelf Res.* **15**(6):663–679.
- Naumenko, M. A. & Karetnikov, S. G. (1993) Using of the IR-information for the study of the Ladoga Lake thermal regime. In: *Earth Investigation from Space*, 69–78 (in Russian).

Laboratory study of sub-mesoscale eddy formation mechanisms at narrow Black Sea shelf

Dmitry Elkin

Abstract

The laboratory investigation of the shelf eddies periodic formation behind the capes in the presence of the alongshore current was fulfilled. The experiments were provided in a cylindrical tank filled with homogeneous or two-layered fluid and displaced on a rotating table. The conditions of eddies periodic formation behind the cape with their subsequent shedding and trapping by the flow were determined. The laboratory results were successfully compared with the natural observations obtained in the survey of 2009 at the Black Sea coastal zone near Gelendzhik.

Проведено лабораторное исследование механизма образования вихрей на шельфе при обтекании течением препятствия в виде мыса с крутым обводом. Эксперименты проводились на вращающейся платформе в цилиндрическом бассейне, заполненном однородной или двухслойной жидкостью. Установлены условия периодического вихреобразования за мысом, последующего отрыва вихрей и их захвата вдольбереговым потоком. Полученные результаты успешно сопоставлены с данными натурных наблюдений, полученными в экспедиции 2009 в прибрежной зоне г. Геленджика.

1. Introduction

The classical scheme of the Black Sea basin-scale circulation includes the Rim current (RC) cyclonically flowing along the continental slope, as a general element (Blatov et al., 1984). Numerous IR and visible satellite images and hydrographic surveys with mesoscale spatial resolution elucidated the fact that horizontal water exchange in the Black Sea as a whole is largely determined by dynamics of mesoscale (20–100 km) anticyclonic eddies as well as their interaction with neighboring cyclonic eddies and the RC (Zatsepin et al., 2002, 2003, 2005).

Dmitry Elkin (✉)

P. P. Shirshov Institute of Oceanology RAS, Moscow, Russia

e-mail: dmelkin@mail.ru



The width of Black Sea shelf in Caucasian region is about 2–10 km. It is essentially smaller than the width of RC, or the diameter of mesoscale eddies in deep-sea zone. So, it is reasonable to consider the narrow Caucasian shelf as a zone where the energy of basinscale and mesoscale current is dissipating. Usually the hydrodynamic dissipation process is associated with formation and distraction of eddies of much smaller scale than the scale of most energetic eddies.

Indeed, the observations fulfilled upon the narrow (less than 10 km) shelf of the north-eastern part of the Black Sea revealed the existence of sub-mesoscale (1–10 km) shelf eddies that are a widespread feature of shelf dynamics and play an important role in cross-shelf water exchange (Zatsepin et al., 2010). The aim of this report is to describe the results of the laboratory experiments directed toward the investigation of shelf eddies generation mechanisms.

Two possible mechanisms of the Black Sea Caucasian shelf eddies were considered. First was the shear instability of the alongshore current. Due to shear instability the cyclonic shelf eddies are generated in the case when the alongshore current over the continental slope has south-eastern direction and anticyclonic—in the opposite case. The second mechanism was observed only in case of strong external circulation and consisted in periodic eddy formation in the concave forms of coastal line relief, particularly, behind the capes due to basic flow separation. These eddies were shedding periodically to the basic flow. The non-dimensional frequency of this process—Strouhal number, $St=D/VT$ (D —lengthscale of orographic feature, V —scale of along-shore current velocity, T —time period of eddy formation) was equal to 0.1. Such value ($St=0.1-0.3$) is typical for the periodic eddy formation behind high-drag bodies in laboratory gas and fluid dynamics experiments (Aref, 2006).

In this paper we would like to describe the results of laboratory investigation of the shelf eddies periodic formation behind the capes in the presence of the alongshore current.

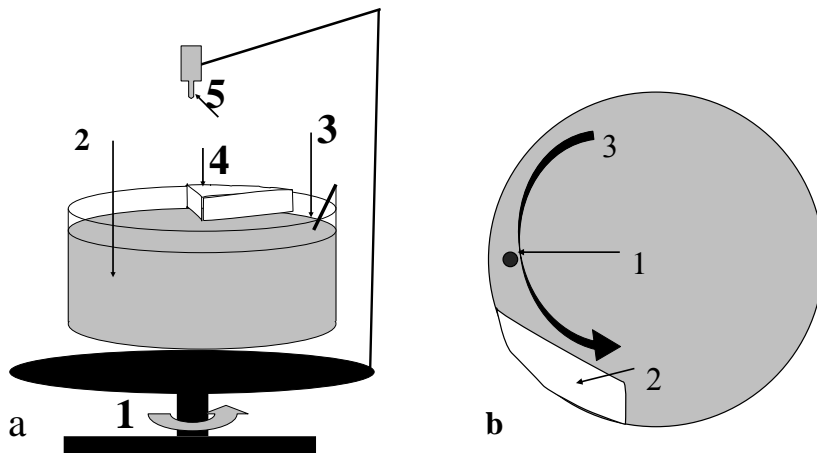


Fig. 1. Scheme of the laboratory set-up (a) side view: (1) rotating platform; (2) circular organic glass tank with homogeneous or two-layered liquid; (3) stick with the manganese crystals; (4) cape; (5) video camera. (b) top view: (1) position of the stick end with the manganese crystals; (2) cape; (3) alongshore flow direction.



2. Experimental set-up

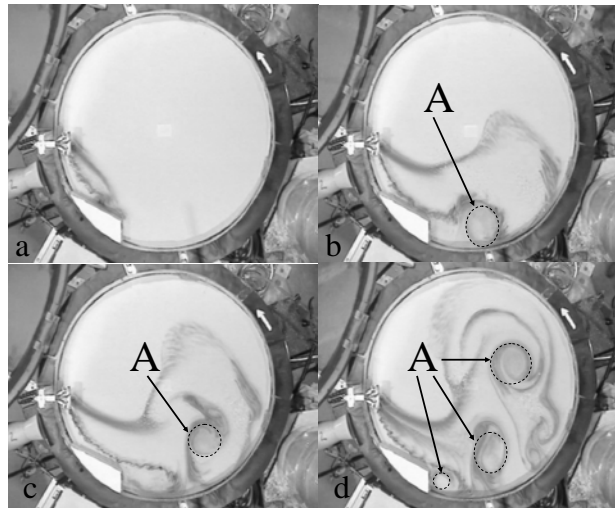
The experimental runs were performed in the cylindrical tank positioned in the center of the rotating platform (Fig. 1a). The tank was filled with homogeneous fluid to the depth of about 5 cm. The cape with a maximal width of about $D=5$ cm was mounted to the entire wall of tank (Figs. 1a, 1b). At the beginning of the experimental run the fluid in the tank was at the state of solid body rotation. The flow oncoming the cape was generated by abrupt deceleration of the platform angular velocity from the value Ω_1 to Ω_2 ($\Omega_2 < \Omega_1$). As a result the cyclonic alongshore current with velocity scale $V_{max} = (\Omega_1 - \Omega_2)R_b$, where R_b is the radius of the tank was formed. Due to the bottom friction this current was decelerating with time. However it was lasting long enough to observe the periodic formation of several eddies behind the cape. A wooden stick with manganese crystals glued to its end was fastened to wall of tank for visualization of current. The end of the stick was located to the upstream of the cape. It was immersed into the fluid just a moment before the decelerating of the platform so the alongshore current was marked by the colored trace (Fig. 2). The process of eddy formation and displacement was recorded from above by video camera mounted at the rotating platform.

3. Results of the experiments

The anticyclonic eddies were generated periodically in the area behind the cape. After generation, diameter of eddy was growing with time while the eddy was moving down the stream and toward the central part of the tank. The new eddy was formed in the same area after the previous one leaved it. We observed the periodic formation of 3–4 eddies during the time of damping of the current due to bottom friction (Fig. 2). Six experimental runs were fulfilled with different Ω_1 and Ω_2 values.

The video data of each experimental run was processed and analyzed. Following dimensional and non-dimensional parameters that characterize the eddy generation and evolution processes were determined: V —flow velocity

Fig. 2. The images from on of experimental runs: (a) $t/T_2=1$ where t —the time counted off the moment of platform rotation decelerating, T_2 —period of platform rotation after the deceleration; (b) $t/T_2=5$ —appearance the first eddy; (c) $t/T_2=6$ —detachment of the first eddy; (d) $t/T_2=9$ —appearance the third eddy. The anticyclonic eddies (A) are contoured by dotted line.





near wall upstream the cape, V_{max} —maximum flow velocity (just after the deceleration of the platform), R —radius of the eddy, V_{or} —orbital velocity of the eddy, V_{tr} —translation velocity of the eddy, l —the distance between the eddy and the cape, and $V(t)/V_{max}$, $R(t)/D$, $V(t)/Df$, $V_{or}(t)/Df$, $V_{or}(t)/V(t)$, $V_{tr}(t)/V(t)$, where $f=2\Omega_2$ —Coriolis parameter. Time dependence of V/V_{max} is shown on Fig. 3. The laboratory data is presented by solid line with dots (measured values). The theoretical estimate based on Ekman spin-up regularities are shown by dotted line.

The dependences of: R/D on V/Df , V_{or}/Df , V_{or}/V , V_{tr}/V on t/T_2 are shown in Figs. 4a–4d correspondingly. The dependence of l on V/f is shown on Fig. 5a. It is impossible to get dimensionless frequency detachment of the eddy over cape Strouhal constant knowing period detachment of the eddy, where V —

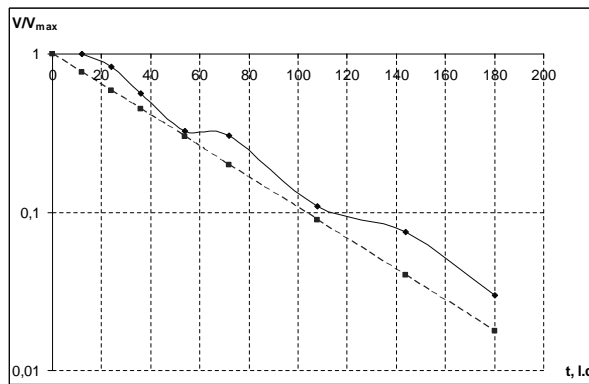


Fig. 3. Time dependence of V/V_{max} . Solid line—laboratory data, dotted line—theoretic estimate.

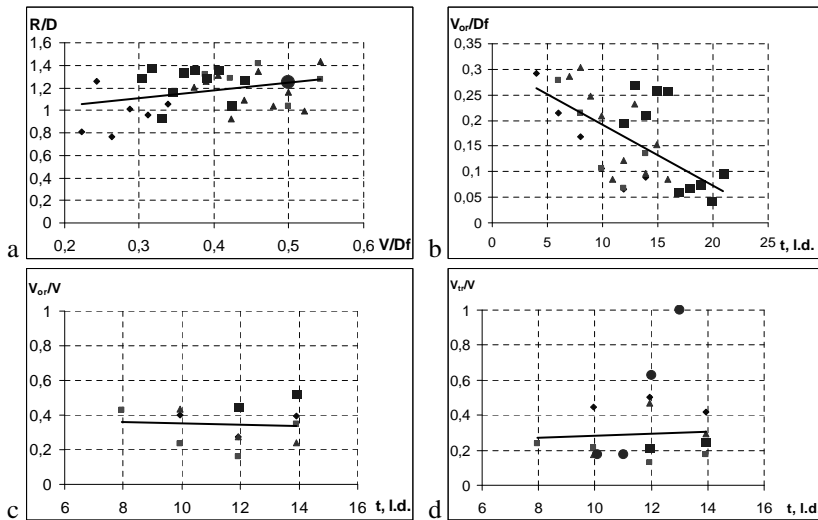


Fig. 4. (a) Dependence R/D from V/Df . (b) Dependence V_{or}/Df from time.

(c) Dependence V_{or}/V from time. (d) Dependence V_{tr}/V from time.

◆ $T_1=5$ s, $T_2=5.9$ s; ■ $T_1=5$ s, $T_2=6.8$ s; ▲ $T_1=10$ s, $T_2=13$ s;

■ $T_1=10$ s, $T_2=20$ s — experiments with homogeneous fluid.

● Natural data, line—trend line.

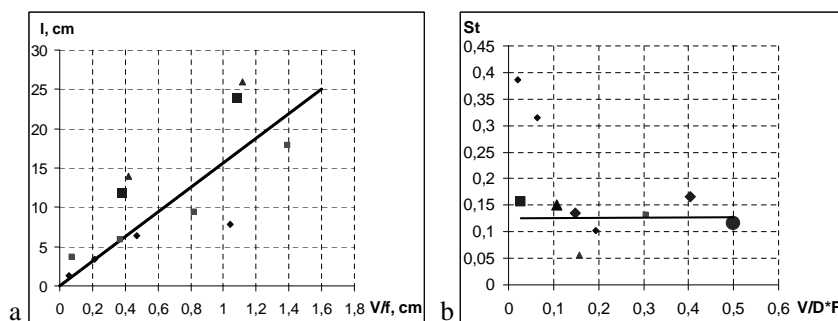


Fig.5. (a) Dependence l from V/f . (b) Dependence of Strouhal constant from V/Df .
 (c) Dependence V_{or}/V from time.
 (d) Dependence V_{tr}/V from time.
 ◆ $T_1=5$ s, $T_2=5.9$ s; ■ $T_1=5$ s, $T_2=6.8$ s; ▲ $T_1=10$ s, $T_2=13$ s; ■ $T_1=10$ s, $T_2=20$ s; ▲ $T_1=5$ s, $T_2=5.4$ s—experiments with homogeneous fluid.
 ● Natural data, line—trend line.

velocity of current in the channel of incident flow, T —period of eddy generation, detachment of one and capture flow capture. The values Strouhal number, $St=D/VT$ on V/Df shown on Fig. 5b. This graph include also the point from natural observation of periodic eddies formation at the Black Sea coastal zone near Gelendzhik. The value of Strouhal number varies from 0.05 to 0.15 in the laboratory experiments. It is counting, that for case of natural observations ($V \approx 40$ cm/s; $D \approx 8$ km; $T \approx 2$ day) $St \approx 0.1$. So the laboratory results are very consistent with the natural observations fulfilled at the Black Sea coastal zone near Gelendzhik.

Acknowledgments

The work was supported by RFBR grants Nos. 08-05-00183, 09-05-13527, 09-05-13574, 09-05-90715.

References

Aref, H. (2006) Vortex dynamics of wakes. *Nonlinear Dynamics* **2(4)**:411–424 (in Russian).

Blatov, A.S., Bulgakov, N.P., Ivanov, V.A. et al. (1984) *Variability of hydrophysical fields of the Black Sea*. Leningrad: Gidrometeoizdat (in Russian).

Zatsepin, A.G., Denisov, E.S., Emel'yanov, S.V. et al. (2005) Effect of bottom slope and wind on the near-shore current in a rotating stratified fluid: laboratory modeling for the Black Sea. *Oceanology* **45**, Suppl. 1:S13–S26.

Zatsepin, A.G., Ginzburg, A.I., Kostianoy, A.G. et al. (2003) Observations of Black Sea mesoscale eddies and associated horizontal mixing. *J. Geophys. Res.* **108(C8)**:2-1–2-27, doi.10.1029/2002JC001390.

Zatsepin, A.G., Ginzburg, A.I., Kostianoy, A.G. et al. (2002) Variability of water dynamics in the north-eastern Black Sea and its effect on water exchange between near-shore and off-shore parts of the basin. *Oceanology* **42**, Suppl. 1:S1–S15 (in Russian).

Zatsepin, A.G., Kondrashov, A.A., Korzh, A.O. et al. (2010) Sub-mesoscale eddies at the Caucasian Black sea shelf and the mechanisms of their generation. *Oceanology* **50(6)**, in press (in Russian).

The horizontal water exchange between coastal zone and open sea in the East and South-East Baltic

Elena Esiukova

Abstract

Temporal variability of horizontal water exchange between coastal zone and open sea within the Baltic Sea was investigated using three-dimensional not hydrostatic hydrodynamic model MIKE3-FlowModel during annual cycle under mean-annual. Horizontal exchange between coastal and off-shore regions through (curvilinear) cross-sections, put along 30-m and 50-m iso-baths, was estimated. The volumetric flow-rate values through stated cross-sections for coastal zones of East and South-East Baltic were researched.

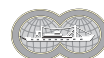
Представлены результаты моделирования динамики вод Балтийского моря на базе трехмерной гидродинамической негидростатической модели MIKE3-FlowModel. На основе проведенных численных экспериментов дана оценка величины горизонтального удельного объемного расхода вод через комплекс вертикальных сечений по изобатам 30 и 50 м в прибрежной зоне Юго-Восточной Балтики. Выявлена внутригодовая изменчивость удельных расходов в районах прибрежного мелководья в Восточной и Юго-Восточной Балтике в течение годового цикла при среднемноголетних внешних условиях.

1. Numerical model and the set-up

Three-dimensional not hydrostatic hydrodynamic model MIKE3-Flow-Model (DHI Water & Environment, <http://www.dhi.dk>) was used to investigate spatial and temporal variability of horizontal water exchange in the Baltic Sea. The model integrates Reynolds-averaged Navier-Stokes equations using rectangular grid and accounting for solar radiation (with day/night variations for the corresponding latitude), turbulent heat exchange with the atmosphere, wind, bottom friction, the Earth rotation, river inflows and water exchange with the North Sea. Equations of conservation are used for water

Elena Esiukova (✉)

P.P. Shirshov Institute of Oceanology RAS, Atlantic Branch, Kaliningrad, Russia
e-mail: elena_esiukova@mail.ru



temperature and salinity; water density is then calculated from temperature, salinity and pressure via Chen-Millero equations. Turbulence was parameterized via Smagorinsky formulation. “Not hydrostatic” approach is based on the so-called artificial compressibility technique (<http://www.dhi.dk>).

Bathymetry of the Baltic Sea is based on data of www.io-warnemuende.de. Numerical regular rectangular grid has 152×306 meshes in horizontal (5×5 km) and 92 layers in vertical (4 m each). Time step of integration was 90 s, what keeps the Courant number close to 1. Overall duration of the simulation was 2 years; data of the second year was analyzed. As initial conditions, mean-annual salinity and temperature fields $T, S(x, y, z)$ were taken for the whole Baltic sea in February in accordance with (Janssen et al., 1999). Open boundary was placed in the Northern Kattegat, where mean-annual salinity and temperature profiles, taken from (Janssen et al., 1999), varied monthly. Water level variations due to tides for the given location were prescribed at the open boundary. External forcing included solar radiation, turbulent heat exchange with the atmosphere, wind, rivers and the Earth rotation. The conditions of solar radiation, including day/night variations, are calculated in the model automatically on the base of latitude/longitude of every particular place. Mean-monthly values for cloudiness are used, averaged over the Baltic area. Turbulent heat exchange with the atmosphere is calculated from air-water temperature difference and wind speed; evaporation/precipitation and ice coverage are not included. Air temperature (2 m above sea level) variable over the sea area follows monthly mean-annual variations (Hydrometeorology and hydrochemistry... 1992). Cloudiness is taken from mean-monthly data (Hydrometeorology and hydrochemistry... 1992). Wind data is the only set taken from real measurements in Visby (in the central part of the Baltic Sea): once a day, for the year 2007 (<http://rp5.ru>). The whole Baltic Sea river runoff is distributed between 21 individual rivers and varies monthly (which preserves mean-annual volume and seasonal variations within the particular basins) (Hydrometeorology and hydrochemistry... 1992, Sea and Coast, 1992).

2. The components of horizontal exchange through the cross-section in the coastal zone in the East and South-East Baltic

Coastal shallow waters in the East and South-East Baltic (by the shore of Latvia, Lithuania, Russia, Poland) have two zones (according to (Janssen et al., 1999)): the underwater bank vault with depths up to 20 m, and the shallow waters outside it. The coastal shallow water from depths 50 m glides to gentle slopes of the depressions with down gradient less 1° . The shallow water topography is evened, also there are the hills and ridges (10–15 m above bottom). The heights of the coastal shallow water constitute the banks (Klaipeda, Vinkov, Mihailov, Sarychev and so on).

The curves shown on Fig. 1 are the cross-sections, put along 30-m and 50-m isobaths. Horizontal exchange between coastal and off-shore regions through the (curvilinear) cross-sections was calculated for four Baltic countries. The isobath 30 m is represented by thin line, the isobath 50 m—by thick line. The components of horizontal exchange through the cross-section in the coastal zone are as follows: Q_+ —flow-rate towards the shore; Q_- —flow-rate



Fig. 1. The South-East Baltic. The isobaths in the coastal zone of Latvia, Lithuania, Russia and Poland.

off-shore; the value $Q=Q_+-Q_-$ represents a flow-rate along the shore (Fig. 2). The Q [km^3/year] is the volumetric flow-rate, normal to the cross-section; Q/L [$\text{m}^3/\text{s}/\text{m}$] $—$ specific volumetric flow-rate.

3. Analysis of the results of the simulation

The analysis of the results of the simulation showed the following magnitudes.

The mean-annual volumetric fluxes through *large-scale* cross-sections, put along 30-m isobath along the shores of Latvia, Lithuania and Russia, have an order of $\sim 150 \text{ km}^3/\text{year}$ in the direction off-shore (Q_- , Fig. 2), but by the shore of Poland they are as big as total river runoff into the sea $\sim 450 \text{ km}^3/\text{year}$. The same situation is in the on-shore direction (Q_+ , Fig. 2). The mean-annual volumetric fluxes through *large-scale* cross-sections, put along 50-m isobath along the shores of Poland and Latvia, are 1.5–1.7 times as big as total annual river runoff into the sea in the direction off-shore, but that along the Lithuanian and Russian shores is 1.4 times less than total river runoff into the sea. The value $Q=Q_+-Q_-$ represents a volumetric flow-rate along the shore (Fig. 2).

The most intense horizontal volumetric flow-rate along the shore for *large-scale* cross-sections ($Q=Q_+-Q_-$), put along 30-m isobath, is observed by the shore of Latvia. It amounts to 5 percent of mean annual river runoff into the sea. The most intense horizontal volumetric flow-rate along the shore for *large-scale* cross-sections, put along 50-m isobath, is found by the shore of Russia and Lithuania. They amount to 10 and 20 percent of total river runoff into the sea, correspondingly (Table). This exchange is suggested to be the result of intense water circulation in the shelf area. Most probable cause of powerful alongshore transport is wind, i.e. the main regime-generative factor. The dominant wind direction in the course of year is W and SW.

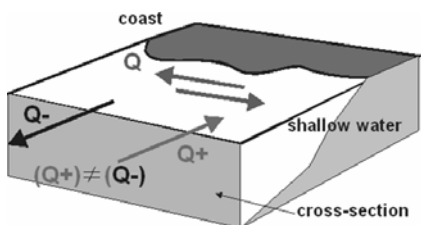


Fig. 2. The components of horizontal exchange through the cross-section in the coastal zone: Q_+ —flow-rate towards the shore; Q_- —flow-rate off-shore; the value $Q=Q_+-Q_-$ represents the volumetric flow-rate along the shore.



Table

The volumetric and specific volumetric flow-rate (the components of horizontal exchange) through cross-sections, put along 30-m and 50-m isobaths.

volumetric flow-rate, 30-m isobath			
coastal zone	Q_- , km ³ /year	Q_+ , km ³ /year	$Q=Q_+-Q_-$, km ³ /year
Poland	452	461	9
Russia (Kaliningrad)	143	140	-3
Lithunia	170	156	-14
Latvia	148	171	23
specific volumetric flow-rate, 30-m isobath			
coastal zone	Q_-/L , m ³ /s/m	Q_+/L , m ³ /s/m	$Q/L=Q_+/L-Q_-/L$, m ³ /s/m
Poland	0.0353	0.0360	0.0007
Russia (Kaliningrad)	0.0362	0.0355	-0.0006
Lithunia	0.0809	0.0743	-0.0066
Latvia	0.0234	0.0270	0.0036
volumetric flow-rate, 50-m isobath			
coastal zone	Q_- , km ³ /year	Q_+ , km ³ /year	$Q=Q_+-Q_-$, km ³ /year
Poland	683	597	-86
Russia (Kaliningrad)	258	753	495
Lithunia	327	432	105
Latvia	765	170	-595
specific volumetric flow-rate, 50-m isobath			
coastal zone	Q_-/L , m ³ /s/m	Q_+/L , m ³ /s/m	$Q/L=Q_+/L-Q_-/L$, m ³ /s/m
Poland	0.0559	0.0488	-0.0070
Russia (Kaliningrad)	0.0612	0.1785	0.1173
Lithunia	0.0844	0.1116	0.0272
Latvia	0.1102	0.0245	-0.0857

The specific volumetric flows for coastal zones of East and South-East Baltic were analyzed in more detail. Seasonal variations of the specific volumetric flow-rates were obtained. For example, by the shore of Russia horizontal exchange between coastal and off-shore regions through the (curvilinear) cross-sections, put along 30-m and 50-m isobaths, did show an obvious seasonal behavior, with maxima during spring and autumn transition periods (Fig. 3). This exchange is suggested to be the result of horizontal convective exchange currents, arising due to differential coastal heating/cooling.

Total specific volumetric flow-rates along the shore for cross-sections ($Q/L=Q_+/L-Q_-/L$), put along 30-m isobath, are ~500 times as small as the maximum specific volumetric flow-rate in the Baltic Sea (amounted to 1.4 m³/s/m, or 46 km³/year/km) (Esiukova, 2009a, 2009b, 2009c). Specific volumetric

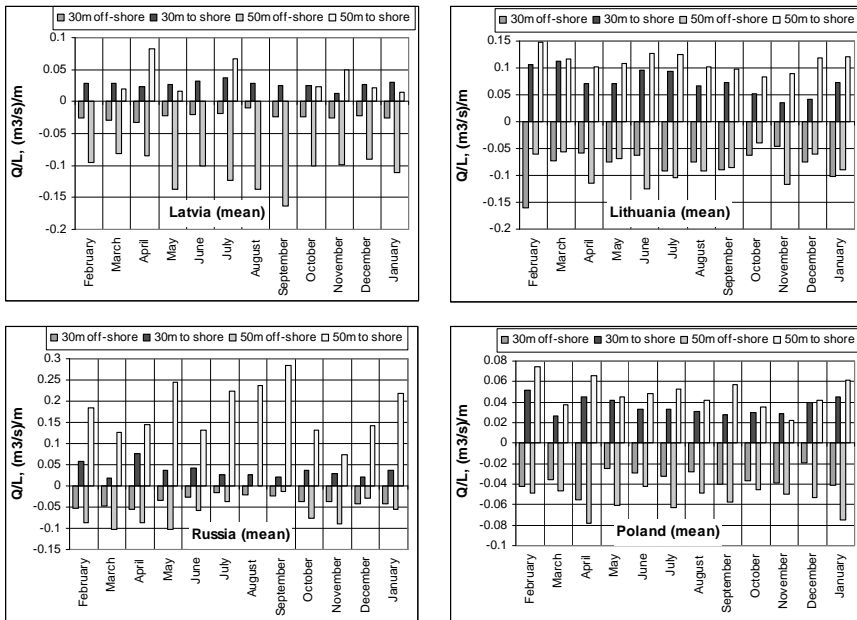


Fig. 3. Specific volumetric flow-rate for coastal zones of Latvia, Lithuania, Russia and Poland. Q_{L} —specific volumetric flow-rate towards the shore, Q_{L} —specific volumetric flow-rate off-shore [$\text{m}^3/\text{s}/\text{m}$].

flow-rates along the shore for cross-sections, put along 50-m isobath, are about 10 percent of the maximum of specific volumetric flow-rate in the Baltic Sea, with its maximum by the shore of Russia.

Acknowledgements

Investigations are supported by RFBR via grants Nos. 10-05-00540, 08-05-01023, 08-05-92421.

References

- Esiukova, E. E. (2009a) *Spatial structure and seasonal variability of horizontal water exchange in the Baltic Sea*. Abstr. of a thesis on comp. academ. degree cand. of geograph. science. Kaliningrad.
- (2009b) *Spatial structure and seasonal variability of horizontal water exchange in the Baltic Sea*. Ph. D. thesis on comp. academ. degree cand. of geograph. science. Kaliningrad.
- (2009c) Spatial structure of Horizontal water exchange within the Baltic Sea: results of numerical modeling. In: *Selected papers of Int. Conf. "Fluxes and structures in fluids"*, Moscow, 23–27 June 2009, 374–379.
- Hydrometeorology and hydrochemistry of the seas of the USSR* (1992) Volume 3: The Baltic Sea. St.Petersburg: Hydrometeoizdat (in Russian).
- Janssen, F., Schrum, C., Backhaus, J. O.A (1999) Climatological Data Set of Temperature and Salinity for the Baltic Sea and the North Sea. *D. Hydrogr. Zeitschrift*. Ergänzungsheft, Suppl. 9.
- Sea and Coast* (1992) The National Atlas of Sweden.
- URL: <http://rp5.ru/> (date of application: 28.05.2008)
- URL: <http://www.io-warnemuende.de> (date of application: 12.07.2007)

Horizontal water exchange through the borders between exclusive economic zones of the Baltic states and sub-basins of the Baltic Sea

Elena Esiukova, Irina Chubarenko, Boris Chubarenko

Abstract

Calculation of volumetric flow-rates through cross-sections between exclusive economic zones of the Baltic states and sub-basins of the Baltic Sea was performed. Three-dimensional non-hydrostatic hydrodynamic numerical model MIKE3-FlowModel was used for that. Volumetric flow-rate through the vertical cross-sections were averaged, so there are described the magnitudes of the horizontal water exchange in the Baltic Sea on the whole, without details. Analysis of water exchange has revealed, that the magnitudes of the mean annual volumetric flux through the borders between exclusive economic zones of the Baltic states are in the range 0.3–28.3 km³/year/km. Largest variations of the resulting water transport from season to season (3–5 times) were found in the south-east part of the Baltic Sea component along the main axis of the sea, and the smallest ones (1.5–2 times)—in the lagoons, component across the main sea axis. In an order of magnitude, mean-annual volumetric fluxes through these sections are several times as big as the total river runoff into the sea. Trans-boundary transport within the Baltic Sea is most extensive in the south-east and central basins. General cyclonic circulation manifested through the resulting trans-boundary transport.

В работе методом численного моделирования проведены оценки интегральных значений переноса вод через границы ИЭЗ государств в Балтийском море. Величины результирующего среднегодового удельного горизонтального расхода вод через границы между ИЭЗ находятся в диапазоне 0.3–28.3 км³/год/км. Наибольшие вариации результирующего переноса вод от сезона к сезону (в 3–5 раз) установлены в юго-восточной части Балтийского моря, вдоль основной оси моря, а наименьшие вариации (в 1,5–2 раза) — в заливах и поперек основной оси моря. Трансграничный перенос в Балтике (через границы ИЭЗ) по объемам сравним и

Elena Esiukova, Irina Chubarenko, Boris Chubarenko (✉)
P. P. Shirshov Institute of Oceanology RAS, Atlantic Branch, Kaliningrad, Russia
e-mail: elena_esiukova@mail.ru



превосходит среднегодовой речной сток в Балтику. Перенос вод в Балтийском море наиболее интенсивно происходит в юго-восточной и центральной частях Балтики. В результирующем трансграничном переносе вод в этих районах прослеживается общее циклоническое направление.

1. Introduction

Aims of this investigation are to evaluate by numerical modelling the quantitative characteristics of values and direction of water exchange through the boundaries within sub-basins of the Baltic Sea and the borders between exclusive economic zones of the Baltic states; to determine the most active transit zones in the Baltic Sea; to estimate integral horizontal water exchange between these zones.

2. Numerical model

Three-dimensional non-hydrostatic hydrodynamic numerical model MIKE3-FlowModel (DHI Water & Environment, <http://www.dhi.dk>) was used for that. Bathymetry field was taken from <http://www.io-warnemuende.de> (Baltic Sea Research Institute, Warnemünde, Germany). Rectangular grid of dimensions of 152×306 cells has a resolution of 5 km in horizontal and 92 levels (4 m each) in vertical. Open boundary is in the North Kattegat. Time step of integration was 90 s, what kept the Courant number close to 1. More detailed information about the numerical model and the set-up see in (Esiukova, 2009a, 2009b, Esiukova & Chubarenko B., 2009, Esiukova & Chubarenko I., 2009).

3. Results

Analysis of volumetric flow-rates through the vertical cross-sections was carried out. Time series (with time step of 90 s during the whole year) of volumetric flow-rate through the set of vertical cross-sections all over the sea was analyzed in order to investigate structure, direction and magnitude of horizontal water exchange within the basin. Integral volumetric flow-rate Q (m^3/s) through the set of vertical cross-sections (normally to them), put along the borders between exclusive economic zones (EEZ) of the Baltic states and sub-basins of the Baltic Sea, was calculated. The line of the EEZ cut the border between sub-basins of the Baltic Sea at the point, which divide the border and line into parts, i.e. *segments*. For one-year period, the values of horizontal water exchange through the *segments* were also calculated (Figs. 1–5).

In an order of magnitude, mean-annual volumetric fluxes through these EEZ (large-scale sections) are similar in quantity and several times as big as the total river runoff into the sea ($\sim 450 \text{ km}^3/\text{year}$). For example, mean annual integral volumetric flow-rate Q across the border from Polish to Russian (Kaliningrad region) economic zone is about $1,900 \text{ km}^3/\text{year}$, from Russian (Kaliningrad region) to Polish economic zone—about $300 \text{ km}^3/\text{year}$; from Russian (Kaliningrad region) to Lithuania economic zone—about $1,700 \text{ km}^3/\text{year}$; from Lithuania to Russia economic zone—about $200 \text{ km}^3/\text{year}$ (Fig. 5).



Fig. 1. Mean annual integral volumetric flow-rates ($Q \text{ km}^3/\text{year}$) between exclusive economic zones (EEZ) and sub-basins in the Bothnian Sea.



Fig. 2. Mean annual integral volumetric flow-rates ($Q \text{ km}^3/\text{year}$) between exclusive economic zones (EEZ) and sub-basins in the Gulf of Finland.

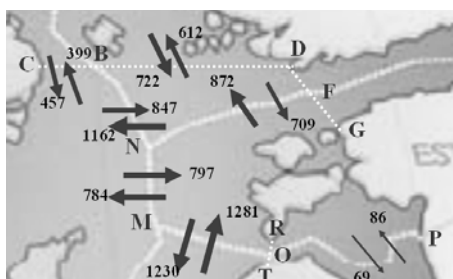


Fig. 3. Mean annual integral volumetric flow-rates ($Q \text{ km}^3/\text{year}$) between exclusive economic zones (EEZ) and sub-basins in the northern part of the Baltic Proper.

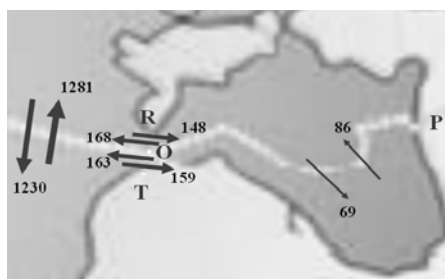


Fig. 4. Mean annual integral volumetric flow-rates ($Q \text{ km}^3/\text{year}$) between exclusive economic zones (EEZ) and sub-basins in the Gulf of Riga.

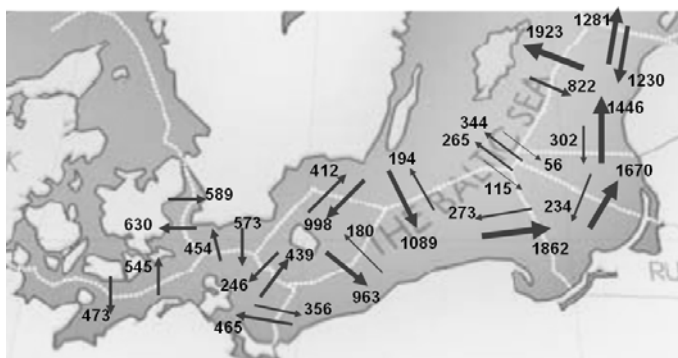


Fig. 5. Mean annual integral volumetric flow-rates ($Q \text{ km}^3/\text{year}$) between exclusive economic zones (EEZ) in the South, South-East and Central parts of the Baltic Proper.

Directions of prevalent water transit are observed in particular regions of the Baltic Sea. For example, there is a mean annual volumetric flux from Polish to Russian (Kaliningrad region) economic zone, from Russian (Kaliningrad region) to Lithuanian economic zone, from Lithuanian to Latvian economic zone and so on (Fig. 6). The most intense mean annual volumetric flux is formed across the border between Polish and Russian (Kaliningrad region)



gest variations (3–5 times) of the resulting water exchange are observed (i) in the South-East Baltic in seasonal time scale and (ii) in the direction along the main sea axis; the smallest seasonal variations are (i) in the gulfs and (ii) across the main sea axis. Intensive horizontal exchange is observed in autumn–winter period: from Lithuanian EEZ to Swedish EEZ, from Polish EEZ to Russian EEZ, from Russian EEZ to Lithuanian EEZ, from the Lithuanian EEZ to Latvian EEZ (from 17 to 50 km³/year/km). In gulfs the biggest specific volumetric flows are 2 km³/year/km in March and seasonal prevalent water transit is absented.

The analysis has revealed that the horizontal water exchange in the Baltic Sea and the resulting trans-boundary water transport through the borders between exclusive economic zones (EEZ) is much more intense than that driven by river inflows. Horizontal water exchange is most active in the South-East and Central Baltic. There is general cyclonic circulation in the resulting trans-boundary water transport in the Baltic Sea.

Volumetric flow-rate through the vertical cross-sections were averaged, so there are described the magnitudes of the horizontal water exchange in the Baltic Sea on the whole, without details. The main conclusion is that general annual horizontal water exchange within the Baltic Sea is much more intense than that driven by river inflows and exchange with the ocean, and is significantly influenced by local wind and convective processes.

Acknowledgements

Investigations are supported by RFBR via grants Nos. 10-05-00540, 08-05-01023 and 08-05-92421.

References

- Esiukova E. E. (2009a) Spatial structure and seasonal variability of horizontal water exchange in the Baltic Sea. Ph. D. thesis, Kaliningrad, 172 pp.
- (2009b) Spatial structure of horizontal water exchange within the Baltic Sea: results of numerical modeling. Selected papers of Int. Conf. “Fluxes and structures in fluids”. Moscow, 23–27 June 2009, 374–379.
- Esiukova E. E. & Chubarenko B. V. (2009) Water exchange through the borders between exclusive economic zones of the Baltic states and sub-basins of the Baltic Sea. In: Truhin, V. I., Pirogov, Y. A., Pokazeev, K. N., eds. *The physical problems of ecology (ecological physics)*, M: MAX Press, 16, 130–140. (in Russian).
- Esiukova E. E. & Chubarenko I. P. (2009) Horizontal water exchange within the Baltic Sea: results of numerical modeling. *The environmental and socio-economic response in the southern Baltic region*. Abstr. Int. Conf. on Climate Change. Szczecin, 35–36.
- URL: <http://www.dhi.dk>
- URL: <http://www.io-warnemuende.de>

Geostrophic currents in the Drake Passage based on the hydrological section in January 2010

Dimitry Fedorov

Abstract

In January 2010, during the scientific expedition of P.P. Shirshov Institute of Oceanology, the hydrological section has been taken across the Drake Passage east to the Hero F.Z. At 54 stations measurements of CTD parameters and current vectors by the immersion Acoustic Doppler Current Profiler (LADCP) and shipboard SADCPC down to the sea bottom were performed.

В январе 2010 г. в рамках очередной экспедиции Института океанологии им. П.П. Ширшова был выполнен гидрологический разрез пролива Дрейка к востоку от хребта в разломе Хиро. Измерения проводились на 54 станциях, на каждой проводилось СТД-зондирование океана до дна и измерения скорости течения погружаемым акустическим профилографом течений (LADCP) и судовым ADCP (SADCPC).

1. Introduction

Southern Ocean is the major component of the climate system of our planet. It connects three other oceans and influences characteristics of the global abyssal water masses. The Drake Passage is one of the places where single section represent currents of the whole region, and repeat observations in the Passage are very important to estimate the average annual transport and deviations. Because of the Drake Passage's high winds (up to 40 mps—world strongest storms) and depths (up to 4,700 m) the geostrophic model can be precisely applied to it and net transport can be calculated in 10–20 percent (Cunningham & Alderson, 2003).

P.P. Shirshov Institute of Oceanology provides many research programs, linked to the Drake Passage. This paper represents one of them—an investigation of the Drake Passage' currents based on the section, made by R/V *Academic Ioffe* in January 2010. The transport and structure of currents are reported and some critical steps for data processing and interpretation are described.

Dimitry Fedorov (✉)
P.P. Shirshov Institute of Oceanology RAS, Moscow, Russia
e-mail: 0013th@gmail.com



2. Data

In January 2010 an expedition to Drake Passage has been taken place by P.P. Shirshov Institute of Oceanology onboard R/V *Academic Ioffe*. During this cruise, a cross-section has been carried out consisted of 54 full depth CTD stations with SADCP and LADCP measurements. The first southern station has been fulfilled on 2010/02/01 at the point of 62.9° S, 62.6° W. The last northern one has been fulfilled on 2010/10/01 at the point of 56.4°S, 67.0°W. The section has 815 km length with two heavy bendings (at Nos. 10, 45) and distances between stations from 4.1 to 20.2 km. The net area of the section is 2,772 km². As specials its worth to note that stations No. 30–45 are taken in the abnormal still weather, and stations No. 36–44 has been caught a vortex clearly visible on height anomalies map (Fig. 8).

In addition the data has been taken from daily MSLA (Maps of Sea Level Anomalies & geostrophic velocity anomalies) and ADT (Absolute Dynamic Topography) on <http://www.aviso.oceanobs.com> to defend interpretations (both sea levels and anomalies).

3. Transport

Geostrophic model is supposed to be highly applicable to the Drake Passage's circumstances: high zonal winds and great depth. It is well known that geostrophic current originates from the balance between pressure and Coriolis forces. In return pressure is controlled by the sea level tilt (Zubov & Mamaev, 1956).

$$\rho_0 \cdot f \cdot u = -\partial p / \partial y, \quad (1)$$

where the Coriolis factor is $f=2 \cdot \omega \cdot \sin(\varphi)$, φ is latitude, $\varphi < 0$ in the Southern Hemisphere, $\omega=7.29 \cdot 10^{-5} \text{s}^{-1}$ is the Earth angular velocity, so $f < 0$ too.

For every known velocity value u_H on the H bottom level, any upper velocity u_z can be easily derived from

$$u_z = u_H + \frac{g}{\rho_0 \cdot f} \cdot \int_H^z \frac{\partial \rho}{\partial y} \cdot dz, \quad (2)$$

where ρ_0 is mean density of the water, g is gravitation constant and u_z is col-linear to the O_x .

The equation above is applied to convert the density field into the relative velocity one. The barotropic component u_H is determined from the ADCP data by fitting baroclinic profiles to the ADCP ones:

$$u_H = \frac{1}{H} \cdot \int_H^0 (u_{ADCP} - (u_z - u_H)) \cdot dz, \quad (3)$$

where $(u_z - u_H)$ is baroclinic velocity component depending of z .

The transport calculation now resolves itself into simple double integral

$$Q = \iint_S u(y, z) \cdot dy \cdot dz, \quad (4)$$

where S is net area of the section.



Several difference schematics have been used during the calculations. The horizontal derivations have been realized through the second-order and the third-order geometry. The first one gives the result for midpoint between stations, the last one—to the points themselves. The advantages and losses of them are discussed in the next chapter.

The vertical integration results from only a simple second-order schema, because of the tiny pressure step ($1/4700=2\cdot 10^{-4}$).

Before the calculations temperature and salinity z -profiles have been smoothed with a Tukey filter. The filter has empirically chosen bases and eliminates the obvious substructure noises.

Table 1

	Transport, Sv	Root mean velocity, cm/s
Net LADCP	165	11.7
Dynamic determined baroclinic velocity through the 2nd-order scheme + LADCP derived barotropic velocity.	164	11.1
Same, but 3rd-order scheme.	164	11.5

The resulted velocity fields are proposed in Figs. 1–3.

Shelf water transport processing is also a non-trivial question and is beyond the scope of this paper. There is only an expectation of the shelf water transport value within assigned 20 percent (Cunningham & Alderson, 2003).

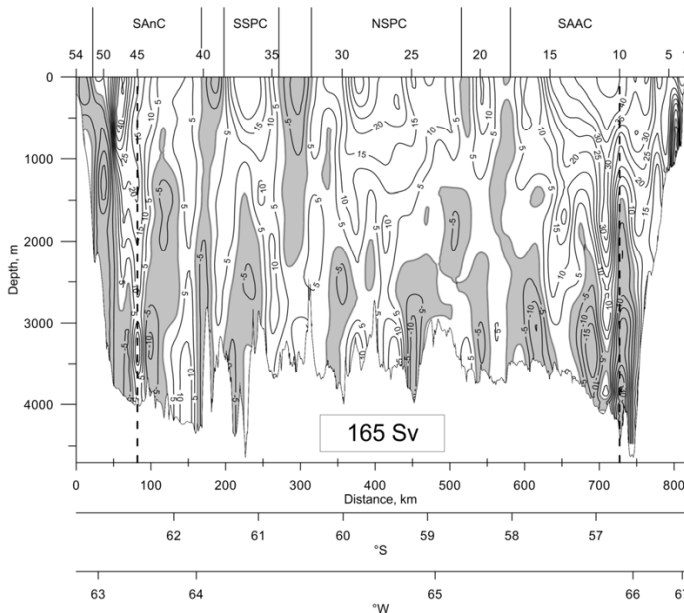


Fig. 1. Net ADCP velocity field (cm/s) over the section across the Drake Passage on January 2–10, 2010. SAAC, NSPC, SSPC and SAnC denote the Subantarctic, two components of the South Polar and the South Antarctic currents. The location and numbers of the CTD stations are shown at the top.

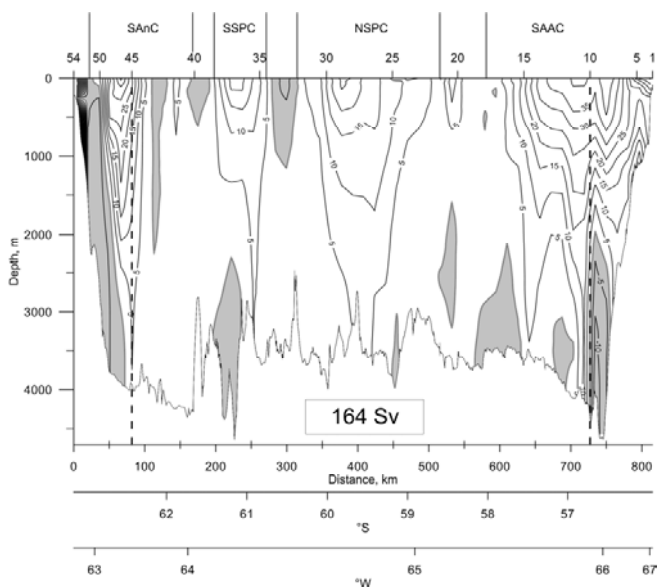


Fig. 2. Geostrophic velocity field (cm/s) over the section across the Drake Passage on January 2–10, 2010. Processed with the 2nd order schema. SAAC, NSPC, SSPC and SAnC denote the Sub-Antarctic, two components of the South Polar and the South Antarctic currents. The location and numbers of the CTD stations are shown at the top.

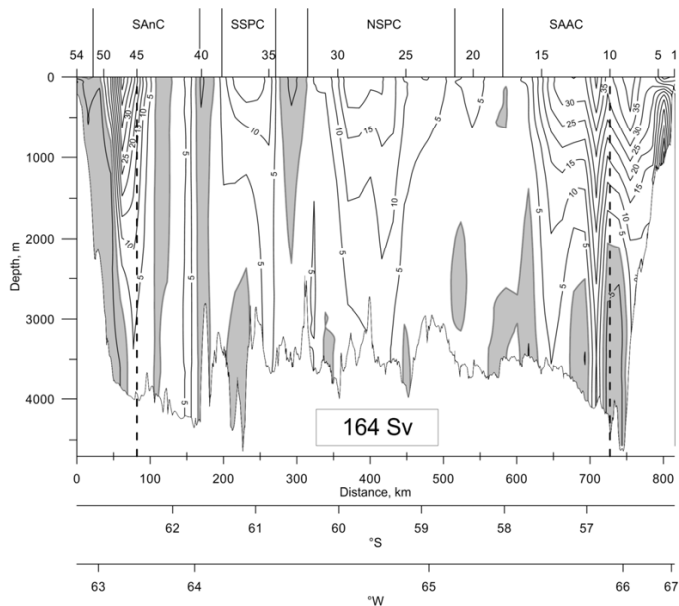


Fig. 3. Geostrophic velocity field (cm/s) over the section across the Drake Passage on January 2–10, 2010. Processed with the 3rd order schema. SAAC, NSPC, SSPC and SAnC denote the Subantarctic, two components of the South Polar and the South Antarctic currents. The location and numbers of the CTD stations are shown at the top.



4. Interpretation

Fig. 1 shows the smoothed net LADCP velocity fields. The ocean surface velocity extrema provide support for the geostrophic current model drawing, at least for the near top levels. Four currents can be separated out there for sure the Sub-Antarctic current (SAAC), two components of the South Polar current (NSPC and SSPC), and the South Antarctic current (SanC). Near bottom there are some countercurrents revealing the bottom-raised maximums. This fact must be explained by recent wind variations and highly dissected bottom relief.

Figs. 2 and 3 present velocity fields calculated with difference schematics. The main point must be noticed is their similarity. This similarity is very important for different schematics. It confirms the validity of station spacing as well as provides the more accurate result. Maximum discrepancies for different schematics are seen near the bending points (Nos. 10, 45), this results from the normal pointing errors in the third-order schema. According to expectation, the second-order schematic provides more detailed results.

The major LADCP errors grow out various external influences (wind, atmosphere pressure, internal waves and etc.). Figs. 4 and 5 show two vivid applications of equation (3). Anyway, the baroclinic component is more exact than the barotropic one (Fig. 6 illustrates the barotropic component differences). The vortex, for example (Fig. 8), adds a contribution to the barotropic component mostly. A crude estimate of the transport error may be recognized

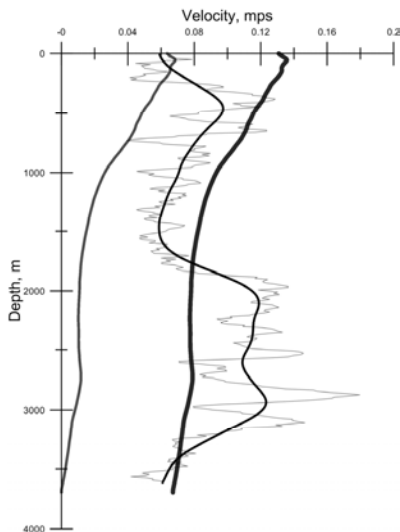


Fig. 4. Vertical distributions of the velocity component (m/s) normal to the section at the station No. 35 (see Figs. 1–3) based on LADCP data (thin line), depth smoothed LADCP data (medium line), and pre-calculated baroclinic geostrophic currents (one of thick ones). East-erly is positive.

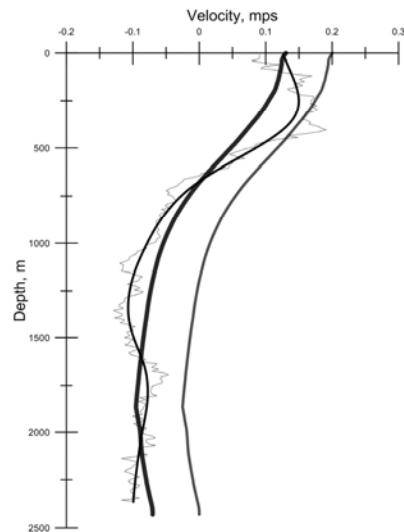


Fig. 5. Vertical distributions of the velocity component (m/s) normal to the section at the station No. 49 (see Figs. 1–3) based on LADCP data (thin line), depth smoothed LADCP data (medium line), and pre-calculated baroclinic geostrophic currents (one of thick ones). East-erly is positive.



as $\epsilon_Q = \frac{Q_{haroltrap}}{Q} = \frac{165-134}{165} = 19\%$. It is matched the previous estimates in a very clear manner.

The satellite measured sea level heights present not very good values for ocean surface velocities. It is because of the great data points spacing (0.3°) and the geoid shape ambiguity. But there is the way the ADT can be really useful with identifying ocean surface currents and confirmation the results. The ADT map is shown on the Fig. 7. The countercurrent at stations Nos. 15–16

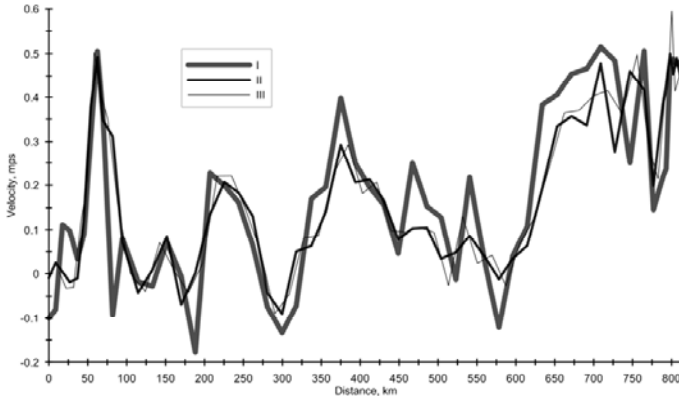


Fig. 6. Ocean surface velocity horizons (mps) derived from the sea level tilt (III), LADCP measurements (II) and resulted geostrophic velocity field (I). Easterly is on top.

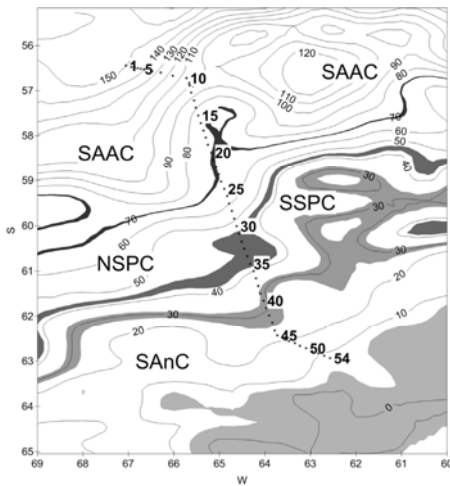


Fig. 7. Dynamic ocean surface level (cm) in the Drake Passage on January 2–10, 2010, on the basis of satellite observations.

(<http://www.aviso.oceanobs.com/NRTMADT> product). SAAC, NSPC, SSPC and SAnC denote the Sub-Antarctic, two components of the South Polar and the South Antarctic currents. The stations are completely indicated.

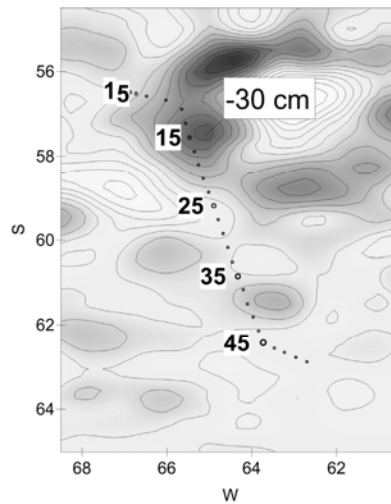


Fig. 8. Sea level anomalies (cm) in the Drake Passage on January 2–10, 2010, on the basis of satellite observations

(<http://www.aviso.oceanobs.com/NRTMSLA> product). SAAC, NSPC, SSPC and SAnC denote the Subantarctic, two components of the South Polar and the South Antarctic currents. The stations are completely indicated. The vortex depth is showed (cm).



now is considered to be the cyclonic meander for certain. An isoline closing should be analyzed as current velocity (Gladyshev et al., 2008) and fits the processed fields strongly (Figs. 1–3).

5. Summary and conclusions

In January 2010 the transport of the Drake Passage was 164 Sv, and there is a considerable difference from early calculated one (Gladyshev et al., 2008). This should be explained by great time spacing of sections, whilst a current evolution goes much faster. Probably, the single one Southern Ocean' cross-section is not sufficient as well to predict the transport value alternation.

Baroclinic-barotropic proportion is one of the most considerable results. This can be used for prediction models providing the net transport value as well. One way or another, this paper is just a small supplementary part of a big investigation.

References were not provided by the author.

Investigations of coastal hydrodynamics features by combining of SAR and SST satellite data

Evgenia Gurova, A. Ivanov

Abstract

Combining use of quasi-synchronous synthetic aperture radar (SAR) images of the sea surface and MODIS sea surface temperature (SST) maps for retrieval information about features of coastal water dynamics and interaction between coastal zone and open sea is applied for the conditions of the South-East Baltic Sea. Good correlation between the SST and SAR signatures of coastal upwelling and river plums in marine coastal waters having different spatial and temporal scales at low winds and sharp temperature gradients is demonstrated.

Обсуждаются возможности совместного использования квазисинхронных радиолокационных изображений (РЛИ) и карт температуры поверхности моря (ТПМ), восстановленных по данным спектрорадиометров MODIS, для исследования динамики прибрежных вод и водообмена между прибрежной зоной и открытым морем в условиях Юго-Восточной Балтики. Показано, что сигнатуры прибрежных апвеллингов и плюмов речных вод различных пространственно-временных масштабов, видимые на РЛИ и в поле ТПМ, в условиях слабого ветра и больших градиентов температуры, хорошо коррелируют друг с другом.

Evgenia Gurova, A. Ivanov (✉)

P. P. Shirshov Institute of Oceanology RAS, Atlantic Branch, Kaliningrad, Russia
e-mail: jessica_geo@mail.ru

Application of nautical X-band radar for measurements of surface currents. Testing. The Black Sea.

Dmitry Ivonin, Viktor Bakhanov, Alexey Ermoshkin,
Viktor Telegin

Abstract

Nautical X-band radar (10 GHz, antenna angular resolution 1.9°) was applied for measurements of surface near-shore currents at the Black Sea. The algorithm developed by Nieto-Borge for extracting sea-state information from the signal of no-coherent nautical radars was applied. Testing measurements of currents were possible for distances up to 4 km off the shore. They showed presence of a current pattern similar to a sub-mesoscale vortex passing the experimental field at the time of measurements.

Навигационный радар СВЧ диапазона (10 ГГц) применен для измерения прибрежных течений на Черном море. Для проведения измерений был реализован алгоритм использования сигнала некогерентного радара, разработанный Ньето-Борже (Nieto-Borge). Алгоритм позволяет обойтись без использования доплеровского сдвига сигнала радара, существенного для когерентных систем. Примененный алгоритм позволяет определять течения в зоне до 5 км от берега. Проведенные тестовые измерения показали в районе измерений наличие некоторой структуры течения похожей на суб-мезомасштабный вихрь, идущий вдоль берега.

1. Introduction

Nautical no-coherent X-band radars (10 GHz) were getting started for the measurements of the sea state and the surface currents in the 90-th of the last century. On their base the commercial radar system WaMos II was de-

Dmitry Ivonin (✉)

P.P. Shirshov Institute of Oceanology RAS, Moscow, Russia
e-mail: ivonin@deom.chph.ras.ru

Viktor Bakhanov, Alexey Ermoshkin (✉)

Institute of Applied Physics RAS, Nizhny Novgorod, Russia
e-mail: bakh@hydro.appl.sci-nnov.ru

Viktor Telegin (✉)

Research Institute of Long-Range Radio, Moscow, Russia
e-mail: telvik@rambler.ru



veloped (Hessner et al., 2003, Nieto-Borge et al. 1999, 2006, Reichert et al., 1999, Vogelzang et al., 2000). WaMos II developers announced possibility to measure the directed spectrum of the sea waves and the surface currents on the base 2 min data accumulation. The minimal radar requirements for wave analysis purposes are (Reichert et al., 1999): (1) a minimum antenna rotation speed of 24 rpm (antenna rotation time <2.5 s); (2) a maximum radar pulse length of 80 ns; (3) a minimum antenna length of 2.44 m. The system operating ranges are between 0.1 to 5 km, depending on the wind speed and the installation height. The minimum wind speed required for measurements is 3 m/s.

The significant wave height measurements by WaMos II were tested successfully many times by the buoy and other independent systems (Hessner et al., 2003, Nieto-Borge et al., 1999, 2006, Reichert et al., 1999, Vogelzang et al., 2000). Sometimes, the surface currents were also measured, mainly when significant tides with current velocities of 3 m/s were observed (Vogelzang et al., 2000). It is worth noting that practically all cited measurements were done at near range from the radar (500–850 m). The only measurement for larger distance (2.7 km) is cited in (Hessner et al., 2003). As to surface currents, the vector velocity fields reconstructed by these systems are unknown by the time.

This work is deduced to testing: 1) the possibilities of the similar nautical radar but with an antenna which has the length 1.2 m (twice less that recommended in (Hessner et al., 2003, Nieto-Borge et al., 1999, 2006; Reichert et al., 1999, Vogelzang et al., 2000)) and, respectively, the angular resolution 1.9° instead of required 0.9° ; 2) possibility to measure the radial component field of the surface current velocity; 3) possibility to measure the vector field (amplitude and direction) of the surface current velocity; 4) study of dependence of such measurements on the aperture of the radar antenna, the distance and the wind conditions (speed and direction).

2. Method

The experiments were carried at the Black Sea, near Gelendzhik (44.576° N, 37.977° E) out in 2006–08 years. The radar FURUNO 1832 with the antenna of the angular resolution 1.9° was used. The radar operated frequency was 9.41 GHz, the pulse length 80 ns (that corresponds to the distance resolution of 12 m). Radar video signal was sampled at frequency 25 MHz (which corresponds to the distance resolution of 6 m) and recorded up to a distance of 6 km. In average, 574 directions were saved for each antenna turn (that corresponds to the formal angle resolution of 0.63°).

The method developed by Nieto-Borge and others (Nieto-Borge et al., 1999, 2006, Reichert et al., 1999, Vogelzang et al., 2000) for measurements of sea wave heights and surface currents was used. The method is based on the assumption that the Bragg backscattering from the gravitational-capillary ripple contributes mainly to the signal. The ripple is modulated by the motion of the longer waves so the latter results in displaying the wave pattern on the radar screen. The method has the following steps:

(1) acquiring a set of radar images for 32 antenna turns (2 min data accumulation);



(2) distinguishing an interesting area of 128 points in radial distance and 32 points on the angle (this corresponds to the area $770 \times 1,050 \text{ m}^2$ at distance 3 km from the radar) and converting this data from the polar coordinates to the Cartesian ones;

(3) 3-d Fourier transform $F_3(k_x, k_y, \omega)$ of the data array of the size (128, 32, 32);

(4) transformation of 3-d Fourier spectrum $F_3(k_x, k_y, \omega)$ into the two dimensional wave number/frequency spectrum $F_2(|k|, \omega)$;

(5) suppressing of the speckle-noise (Hessner et al., 2003) and filtering the signal corresponding to the gravitational sea waves;

(6) determination of the velocity of surface currents.

The signal corresponding to the gravitational sea waves obeys the dispersion relation for these waves

$$\omega = \sqrt{gk} + kU \cos \alpha, \tag{1}$$

here $g=9.8 \text{ m/s}^2$ is the gravitational acceleration, U is the current velocity, α is the angle between the sea wave and the current. The second term reflects the result of the sea waves interaction with the current. It is possible to estimate the radial component $U \cos \alpha$ of the current by evaluating the value of this frequency shift from the base value \sqrt{gk} . In case when a wide-angle sea wave spectrum is observed it is possible to reconstruct not only the radial component but the velocity U and the current direction α themselves. The shift value was estimated by minimizing the integral $I(U, \alpha)$ over the filtered part of the two dimensional frequency-wave number spectrum $F_2(|k|, \omega)$

$$I(U, \alpha) = \int_{k_1}^{k_2} \int_{\omega_1}^{\omega_2} F_2(k, \omega) dk d\omega, \quad \text{where} \quad \begin{cases} k_1 = 0.13 \text{ rad/m}; & k_2 = 0.27 \text{ rad/m} \\ \omega_1 = \sqrt{gk} + kU \cos \alpha - 2n\Delta f \\ \omega_2 = \sqrt{gk} + kU \cos \alpha + 2n\Delta f \\ \Delta f = 0.15 \text{ Hz} \end{cases} \tag{2}$$

3. Results

The data for the following wind conditions was processed: (1) the south-west wind 6 m/s (09/14/2008), (2) the south-west wind 3 m/s (09/12/2008), (3) the west wind 6 m/s (09/11/2008), (4) the north wind (wind from the shore) 10 m/s (07/03/2006). The radar zero direction was oriented to the south (168°). The north wind happened to be inapplicable for current measurement because the wind could not drive waves sufficient for distinguished backscatter signal up to the distance of 4 km from the shore. The results obtained for situations when the wind was blowing from the sea to the shore (September 12 and 14, 2008) are presented below.

First, we examined the 3d spectra $F_3(k_x, k_y, \omega)$. The spatial spectra $F_3(k_x, k_y)$ at distances of 1 km and 4 km at fixed frequencies ω are shown on Fig. 1. It is seen that a rather angle-widen sea wave spectrum about 60° is observed at the distance of 1 km. Meanwhile, a rather narrow angle sea wave spectrum about 15° of waves travelling almost exactly from the radar zero direction is seen at



the distance of 4 km. It is seen that the range of k_y , the spanwise wave numbers to the radar beam, narrows four times while the distance increases from 1 to 4 km. So the observation of the waves coming from other directions than the zero radar direction becomes almost impossible. It is unlikely that at distances from 1 to 4 km from the shore the sea wave spectrum changes significantly. So the difference can be explained mainly by the worse spatial resolution at large distances at directions perpendicular to the beam. In the region of small wave numbers (Fig. 1) the signal caused by other backscatter mechanism different from the Bragg one (modulations by wave tilts, shadowing effects, signal attenuation with distance) is also seen. These parts of the signal were characterized as a speckle-noise in work (Hessner et al., 2003).

The two dimensional wave number/frequency spectra $F_2(|k|, \omega)$ (for corresponding distances of 1 and 4 km) are shown on Fig. 2. There are pronounced peaks at wave numbers 0.13–0.25 rad/m. These values correspond to sea wave lengths from 25 to 50 m. There is a distinguished frequency shift of peak position at Fig. 2a which can be attributed to the current value of 11 cm/s. We proceeded the spectra $F_2(|k|, \omega)$ for distances from 1 to 5 km with the step of 1 km and for angles from -20 to 20° with the step 10° and calculated the radial component of the current. The radial velocity fields reconstructed for September 12 and 14, 2008 are shown on Figs. 3a, 3b. The velocity on Fig. 3a varies from -25 to 25 cm/s. On the next Fig. 3b it varies slightly near 30 cm/s.

The behavior of the radial velocity leads to assumption that a cyclonic vortex 4 km in size was near the radar on September 14, 2008 (the suggested vortex velocities are shown by arrows). Existing of such sub-mesoscale vortices near the Black Sea shore was proved by Zatsepin (Zatsepin et al., 2010) by measuring the current velocity from the ship (Fig. 3d). For comparison we show on Fig. 3c the ERS image of the vortex taken in August 2006.

We also tried to reconstruct the vector velocity field. Nevertheless, it was possible for distances less than 1 km only. The cause was bad spatial resolution spanwise the radar beam at larger distances that resulted in a very narrow range of spanwise wave numbers k_y . The antenna angular resolution $\Delta\varphi$ makes the spanwise wave number resolution $k_y = \pm n/(\Delta\varphi R)$ at the distance R . So, for the antenna aperture $\Delta\varphi = 1.9^\circ$ and the distance of 1 km the real resolution is $k_y = 0.09$ rad/m (i.e. 3 times less than the maximal range at Fig. 1a).

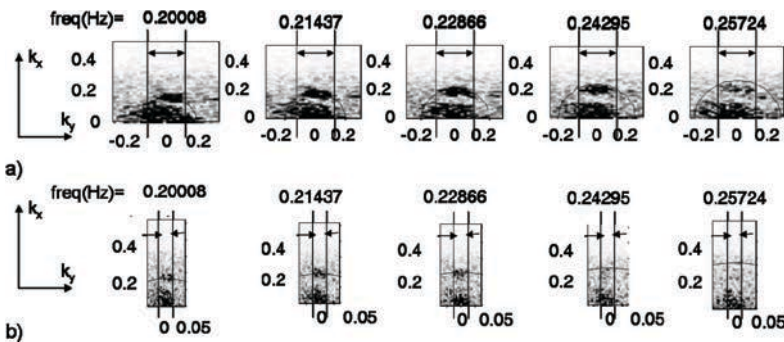


Fig. 1. Spatial spectra $F_3(k_x, k_y)$ at fixed frequencies (September 14, 2008). (a) distance 1 km, (b) 4 km. The black line marks positions of wave vectors determined from the dispersion rela

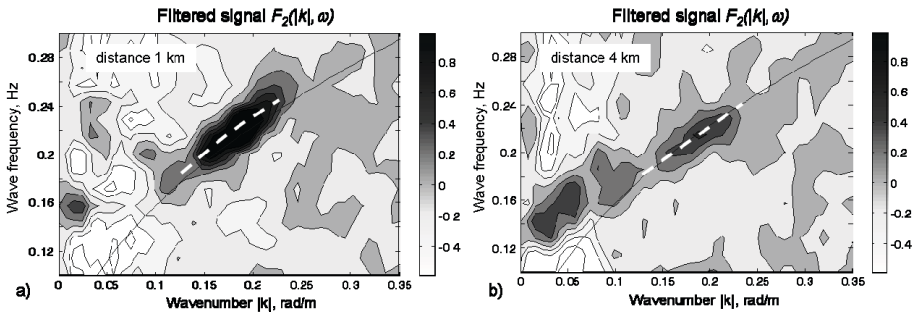


Fig. 2. September 14, 2008 the wind 6 m/s SW. The filtered spectrum (wave number $|k|$ / frequency f), $f = \omega/2\pi$. The signal corresponding to the gravitational sea waves appears in the range from 0.13 to 0.4 rad/m. The dispersion relation (w/o current) shown by the solid line. The dash line marks the peak position.

The real maximal distance R_{max} at which all the range of wave vectors is covered (i.e. all directions) is

$$R_{max} = n / (\Delta\varphi k_{min}) \quad (3)$$

here k_{min} is the minimal wave number necessary for the directed wave spectrum observation (by our estimate $k_{min} \sim 0.18$ rad/m). For our antenna with $\Delta\varphi = 1.9^\circ$ the maximal distance is $R_{max} = 530$ m (for $\Delta\varphi = 0.9^\circ$ $R_{max} = 1,100$ m).

4. Conclusions

Nautical X-band radars with antenna angle resolution worse than 0.9° can register the distinguished signal from the sea waves and measure the surface currents. The limitation on the minimal speed wind is the same (>3 m/s). It was possible to reconstruct the field of the radial component of velocity up to the distance of 4 km for the wind 6 m/s and up to 3 km for the wind 3 m/s when the wind was blowing from the sea to the radar. It was impossible or rather difficult to measure the current when the wind was blowing from other directions (especially, from the shore to the sea).

The worse angle resolution limits the possibility to measure the velocity vector up to distances of 500 m for the antenna aperture 1.9° (1,000 m for the aperture 0.9°). We suppose that for situations when the sea waves travel mainly perpendicular to the shore these distances can be augmented twice or more. Respectively, we believe that these limitations have effect when estimating the directed spectrum of sea waves. It is worth noting that almost all the results for WaMos II testing were at distances less than 1 km. The estimation of the antenna aperture necessary for measurements of the directed wave spectrum and the vector of surface currents up to 5 km is 0.2° (or 10 m length).

The results of velocity measurements on September 14, 2008 demonstrate the possibility to study the dynamics of the near shore currents and structures up to 4 km from the shore by means of nautical X-band radars.

Acknowledgements

This work was supported by the Reasearch Institute of Long-Range Radio (NIIDAR), the Federal program "World ocean", the program "The study of wind waves in the ocean", the research program of RAS "The Fundamental

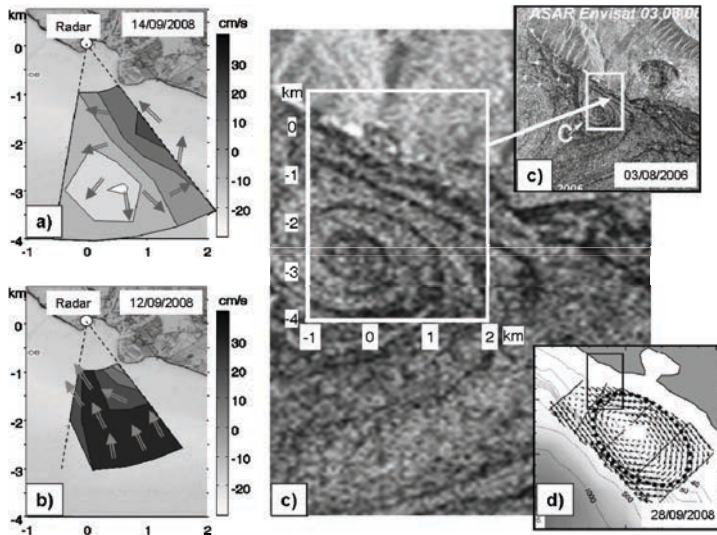


Fig. 3. (a) The radial component of the current velocity (September 14, 2008); (b) September 12, 2008. Arrows mark the behavior of the suggested cyclonic vortex; (c) ERS image of the region of interest with similar vortex August 3, 2006 (cited from (Director's report... 2010), the white rectangle marks the radar coverage zone corresponding to September 2008; (d) The observation of the sub-mesoscale vortex by ADCP measurements from the ship board (September 28, 2008) (Zatsepin et al., 2010); the black rectangle marks the radar zone coverage.

problems of oceanology: physics, geology, biology, ecology” (part: “Theory of monitoring and forecast of the wind driven waves”).

References

- Director's report for 2009 year (2010) P. P. Shirshov Institute of oceanology, April 28, 2010, http://www.ocean.ru/index2.php?option=com_docman&task=doc_view&gid=256&Itemid=78
- Hessner, K. et al. (2003) *Ocean Wave Measurements by X-Band Radar: from Spectral Wave Parameters to Single Wave Detection*, IFREMER Seminar, 2003, <http://www.ifremer.fr/dtmsi/colloques/sec/communications/C03.doc>
- Nieto-Borge, J. C. et al. (2006) Estimation of Ocean Wave Heights from Temporal Sequences of X-Band Marine Radar Images. In: *Proceedings of 14th European Signal Processing Conference (EUSIPCO 2006)*, Florence, Italy, September 4–8, 2006.
- Nieto Borge, J. C. et al. (1999) Estimation of the Significant Wave Height With X-Band Nautical Radars”. *OMAE 99 Proceedings*.
- Reichert, K. et al. (1999) WaMos II: A Radar Based Wave and Current Monitoring System. *ISOPE 99 Proceedings*. Brest, May 1999, Vol. 3.
- Vogelzang, J. et al. (2000) “Wave Height Measurements with Navigation Radar”. *International Archives of Photogrammetry and Remote Sensing*, Vol. XXXIII, Part B7. Amsterdam.
- Zatsepin, A. G. et al. (2010) Sub-mesoscale Vortices on the Caucasus Shelf of the Black Sea and Driven Mechanisms. *Oceanology* (to be published).

One of the mechanisms of simulation of viscous adhesion at the bottom in numerical model of bottom currents

Alexander Kiles0

Abstract

The role of bottom currents in suspended matter transportation is well known (Shepard, 1969). However, as it turned out (Gritsenko & Yurova, 1997), to set the current's velocity at the bottom explicitly to zero is not always correct from physical standpoint. This work objective is to present one of the mechanisms of simulating viscous adhesion at the bottom, built using XZ-model upon the nested grid. Distribution of local velocity and density gradients in along-slope density currents are analyzed and their role in sedimentation is substantiated.

Хорошо известна роль придонных течений в транспорте взвеси (Шепард, 1969). Вместе с тем, как оказалось (Гриценко, Юрова, 1997), явное обнуление скорости на дне не всегда физически корректно. Целью работы является изложение одного из алгоритмов вязкого прилипания на дне при помощи дополнительной модели, встраиваемой в базовую XZ-модель на вложенной сетке. Также выполнен анализ распределений локальных градиентов скорости и плотности для вдольсклоновых плотностных течений и сделано предположение об их возможной роли в процессах седиментации.

1. Introduction

The role of bottom currents in suspended matter transportation is well known. However, as it turned out (Gritsenko & Yurova, 1997), to set the current's velocity at the bottom explicitly to zero is not always correct from physical standpoint. This work objective is to present one of the mechanisms of simulating viscous adhesion at the bottom, built using XZ-model upon the nested grid.

Alexander Kiles0 (✉)

Immanuel Kant State University of Russia (IKSUR), Kaliningrad, Russia

e-mail: aleksandr.kiles0@gmail.com



2. The model

Preliminary calculations suggest that the algorithm offered in work can be free from a part of lacks inherent in base model (Gritsenko & Yurova, 1999). This mechanism of simulation allows, without a significant increase in the size of the main grid to add to base model a viscous mechanism of generation of vorticity at the bottom line, which is essential for analyzing the mechanisms of suspended matter deposition/transportation at the bottom of the ocean. The initial equation system of the model (Gritsenko & Yurova, 1997) took the following form

$$\frac{d\omega}{dt} = \frac{g}{\rho_0} \frac{\partial \rho}{\partial z} + v_T \Delta \omega, \quad \frac{\partial \rho}{\partial t} = D_T \Delta \rho, \quad \Delta \psi = \omega, \quad \frac{\partial c}{\partial t} = D_T \Delta c,$$

where ω —vorticity, ψ —stream function, $g=982 \text{ cm/s}^2$, ρ_0 —fresh water density, ρ —salt water density, $v_T=v_0+c v_{ef}$, $D_T=(Sc)^{-1}v_T$ —coefficients of turbulent viscosity and diffusion respectively, $Sc=2$, $v_{ef}=\sqrt{Re} \cdot v_0$, $Re=u_0 h_0/v_0$, with $t=0-v_{\text{sp}}=0$; C —water mass tracer of the current. The finite-difference equations of the model are constructed using the grid $1,501 \times 501$ ($\Delta x=\Delta z=0.05$). The values of measureable parameters varied in the following range: $\Delta \rho_0$ —from 0.0005 to 0.005 g/cm^3 , h_0 —from 1 to 1,000 cm, u_0 —from 1 to 20 cm/s , v_{ef} —from 0.3 to 5.0 cm^2/s .

Additional model that simulate a viscous adhesion at the bottom was made in two steps. During the first step the boundary layer was calculated for main current with slip and impermeability boundary conditions at the bottom. To the model space was added additional layer in which the boundary layer was calculated by following equations

$$u \frac{\partial u}{\partial x} + v \frac{\partial u}{\partial y} = u_\infty \frac{\partial u_\infty}{\partial x} + v_T \frac{\partial^2 u}{\partial y^2}, \quad \frac{\partial u}{\partial x} + \frac{\partial v}{\partial y} = 0,$$

where u_∞ —velocity at the upper boundary.

Step along Oz axis was reduced in 10 times, step along Ox didn't change. Further evolution of bottom current was calculated using boundary layer.

Fig. 1 shows the distribution of the velocity's horizontal component in the boundary layer for one of the calculated currents. Fig. 2 presents a typical distribution of density for normal regime of propagation of bottom current. Also represented graphs of variability vertical gradient of velocity's horizontal component (Fig. 2b) and horizontal gradient of velocity's vertical component (Fig. 2c). These parameters form conditions for sedimentation processes at

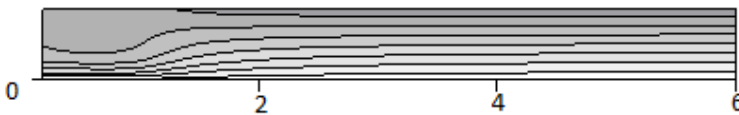


Fig. 1. The distribution of the velocity's horizontal component in the boundary layer for one of the calculated currents. The isoline pass consequently the values of 0, 3, 6, 9, 12, 15, 18. Parameters of the current: grid $1,501 \times 501$, $\Delta \rho_0=0.0001 \text{ g/cm}^3$, $u_0=3 \text{ cm/s}$, $v_{ef}=10^{-1} \text{ cm}^2/\text{s}$, angle of the slope 7° .

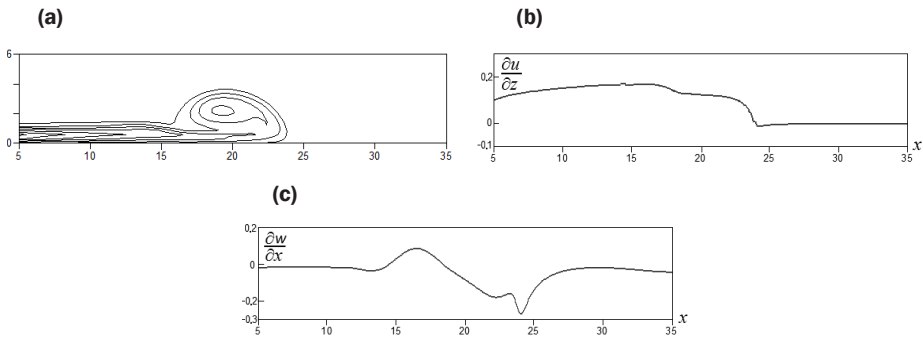


Fig. 2. The distribution of isoline of density values (a) for one of the calculated currents. The isoline of density values pass consequently the values of 0.05; 0.15; 0.25; 0.35; 0.45; 0.55; 0.65; 0.75. The distribution of the vertical gradient of velocity's horizontal component (b) and horizontal gradient of velocity's vertical component along the bottom (c). Parameters of the current: grid $1,501 \times 501$, $\Delta\rho_0 = 0.0001 \text{ g/cm}^3$, $u_0 = 3 \text{ cm/s}$, $\nu_{ef} = 10^{-1} \text{ cm}^2/\text{s}$, angle of the slope 7° .

the bottom. Assessment of the values of the bottom stress was done using traditional method $\tau = \mu \frac{\partial u}{\partial z}$.

Fig. 3 presents perturbations of the tangential interaction of water flow with bottom. Graphs shows that the velocity's gradients along and perpendicular to the bottom at the current's head has sharp jumps, that can facilitate the involvement of sedimentary material and its transportation. It's obvious that their appearance on the background of the viscous boundary layer can significantly enhance the impact of bottom current on the upper layer of sedimentary material and lead to local zones of its erosion.

3. Conclusion

Thus, the analysis of the data array allows to state that such kind of bottom boundary condition can reproduce peculiarities of sediment re-suspension.

Acknowledgements

The work is supported by RFFI via project 09-05-00446a and by Russian Federal Target Program "World Ocean", project 2008-MO-5-09.

References

- Gritsenko, V.A. & Yurova, A.A. (1997) On propagation of bottom gravity current over steep bottom slope. *Okeanologiya* **37(1)**:44–49 (in Russian).
- (1999) On the main phases of detachment of the bottom gravity current from the bottom slope. *Okeanologiya* **39(2)**:187–191 (in Russian).
- Rouch, P. (1980) *Computational Hydromechanics*. Moscow: Mir (in Russian).

About features of autumn cooling of coastal waters in the presence of near-surface currents

Alexandra Korosteleva

Abstract

In work presented the formation of process of cooling coastal waters is studied with regards to presence of near-surface currents. Results of numerical modeling and laboratory experiments are presented.

В работе выполнено исследование формирования процесса выхолаживания прибрежных вод при наличии приповерхностного течения при помощи расчетов на численной модели и лабораторных экспериментов.

Alexandra Korosteleva (✉)
Immanuel Kant State University of Russia (IKSUR), Kaliningrad, Russia
e-mail: sashakrs07@rambler.ru

Analysis of the velocity gradients and suspension transport in bottom flow at slope

Vladimir Kortishko

Abstract

Numerical modeling of the vortex-wave regime of propagation of the bottom gravity current was performed. Velocity and pressure gradients were calculated in order to determine the influence on suspension transport. This regime can be observed at steep slopes—10–15° and more. Nonlinear two dimensional model (Gritchenko & Yurova, 1997) was used. Stratification was provided by means of salinity variations, what is most convenient for comparison with laboratory results. Density iso-lines at the upper boundary of the flow have wave-like shape. Distributions of the modulo of the along-slope velocity component and of the local Richardson number indicate that bottom shear has a quasi-periodical character. Analysis of simulated data has demonstrated that large spatial inhomogeneities in distribution of the gradients are able to provide favorable conditions for bottom re-suspension.

Для определения роли волно-вихревого режима в процессах переноса вещества было проведено компьютерное моделирование и посчитаны градиенты скорости и давления. Данный режим можно наблюдать на склонах дна больше 10 градусов. Использовалась нелинейная 2D модель (Гриценко, Юрова 1997). Для удобства сравнения с лабораторными данными был выбран соленостный механизм стратификации. На изолиниях плотности наблюдался волнообразный характер верхней границы течения. Распределения изолиний модуля градиента вдольсклоновой компоненты скорости течения и локального числа Ричардсона свидетельствуют о квазипериодическом характере касательных взаимодействий потока с дном. Анализ расчетных данных показал, что значительные пространственные неоднородности в распределениях градиентов могут создавать благоприятные условия для ресуспензии донных осадков.

Vladimir Kortishko (✉)
Immanuel Kant State University of Russia (IKSUR), Kaliningrad, Russia
e-mail: Wowtchick@gmail.com



1. Introduction

It is well known fact that bottom gravity currents influence re-suspension and transportation of bottom sediments (e.g. (Gritsenko & Chubarenko, 2003)). The work goal was to investigate peculiarity of velocity gradients distribution and to determine the bottom sediments resuspension conditions for bottom slope density flow propagation in the Wave-Vortex mode. In 2006–07, a new type of density flow spreading was discovered and described in IO RAS experimental oceanology laboratory by A.G. Zatsepin. It was called Wave-Vortex mode (WVM).

2. The model

In this investigation of bottom slope flow thin structure was made on the Gritsenko’s XZ-model data base (Gritsenko & Yurova 1997). The analysis of more than 30 flows data was made. Calculations were made on the grid with 701*621 meshes. Typical scales of model flows was in the range: excess density— $\Delta\rho_0$ —from 0.0001 to 0.001 g/cm³, thickness— h_0 —from 1 to 1,000 cm, velocity— u_0 —from 1 to 10 cm/s, effective viscosity ν_{eff} —from 0.3 to 3.0 cm²/s; bottom slope angle— $\alpha=45^\circ$, at start time linear stratification and non-perturbed fluid was supposed in the model.

3. Results

A Qualitative Classification attempt was made for all the calculated flows. The WVM was observed just in 18 cases of observed flows. 6 different types of the WVM were picked out by qualitative sign of density (current-flow line) contour for different stage of every flow (Figs. 1–6).

- (1) Singular WVM (there is just one vortex, the whole flow breaks down quickly).
- (2) Shoaly WVM (vortexes are not greatly more than other part of the tail).
- (3) Huge WVM (huge roundish vortexes).
- (4) Flat WVM (vortexes are elliptical).
- (5) Freely WVM (inceptive vortex is far from head of flow).
- (6) quasi-WVM (there are just waves without vortexes).

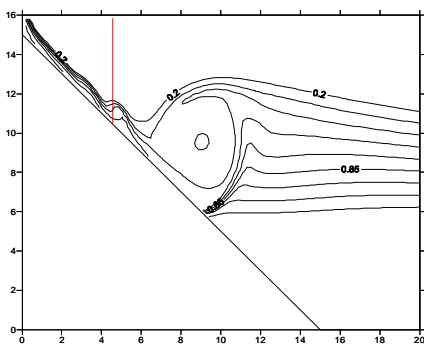


Fig. 1. Typical view of the first flow type.

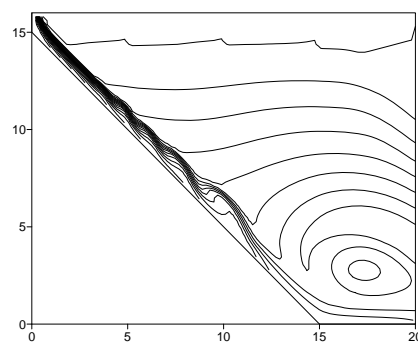


Fig. 2. Typical view of second flow type.

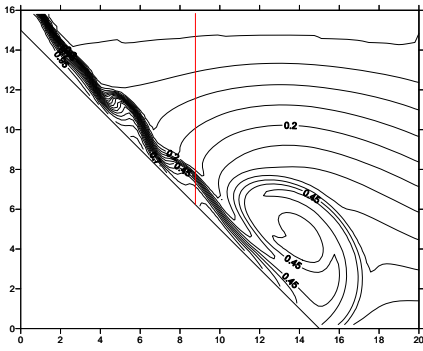


Fig. 3. Typical view of third flow type.

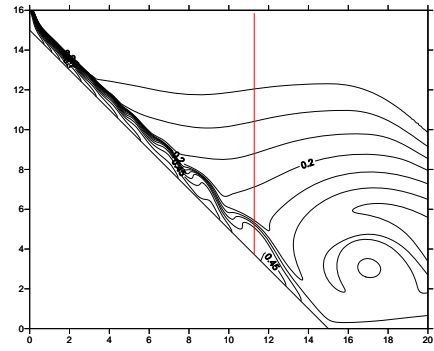


Fig. 4. Typical view of fourth flow type.

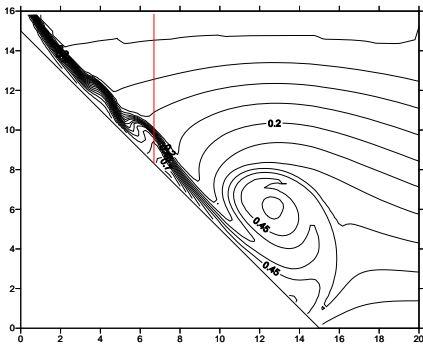


Fig. 5. Typical view of fifth flow type.

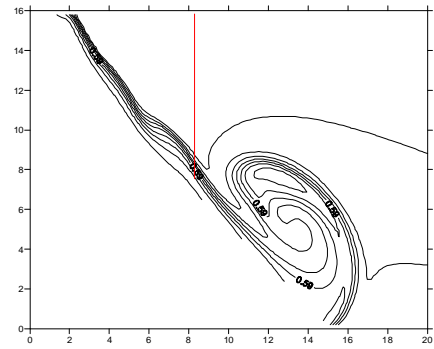


Fig. 6. Typical view of sixth flow type.

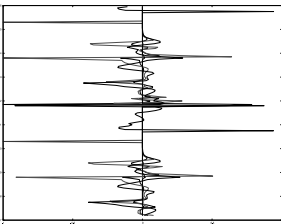


Fig. 7. First type flow velocity profile.

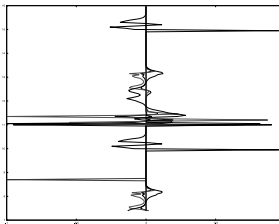


Fig. 8. Second type flow velocity profile.

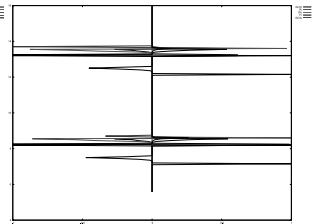


Fig. 9. Third type flow velocity profile.

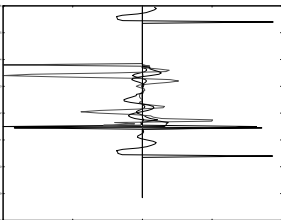


Fig. 10. Fourth type flow velocity profile.

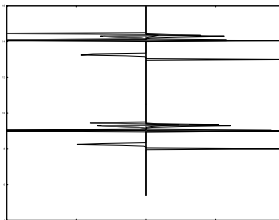


Fig. 11. Fifth type flow velocity profile.

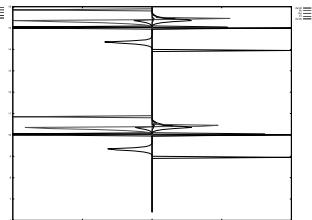


Fig. 12. Sixth type flow velocity profile.



The corresponding vertical profiles of along-slope component of the velocity is presented on Figs. 7–12. Location of the transversal section of them is shown with red line in Figs. 1–6.

An attempt was made to find the general parameter of start conditions. But the attempt had not success. Flows with the same initial condition parameter could be usual in different flow types. There were planed to find a general start conditions class.

The internal structure analysis has shown gradient activity of flows. There are some transversal sections of every flow type sketched below.

4. Conclusions

Classification of Wave-Vortex mode flows was made. Parameters, characterizing internal structure of the flow were obtained. More precise definition of boundary conditions is planned.

Acknowledgments

The work was supported by Russian Foundation for Basic Research, grant No. 09-05-00440a.

References

- Gritsenko, V.A. & Chubarenko, I.P. (2003) One mechanism of bottom sediment weighting. In: *Geology of seas and oceans*. Abstracts of XV International marine geology school, Vol. 2. Moscow: Geosfera (in Russian).
- Gritsenko, V.A. & Yurova, A.A. (1997) About gravity currents spreading on steep slope. *Oceanology* **37**(1):44–49 (in Russian).

Features of the Baltic Sea cold intermediate layer on the base of mean annual data (1952–2005) of IOW

Olga Kozlova

Abstract

Comparative analysis of minimum monthly averaged water temperature at the surface and inside the cold intermediate layer (CIL) all over the Baltic sea area, divided in $1 \times 1^\circ$ squares, was performed using the data base of IOW, published on CD in the appendix to the book “State and Evolution of the Baltic Sea 1952–2005” (Feistel et al., 2008). It is shown, what from totally 80 squares 1×1 of water surface of the sea, in 43 squares (54 percent) the minimum water temperature within CIL is lower, than the minimum water temperature at the surface at the given location. This indicates, that waters of the CIL came to the given area horizontally and are not the remainder of winter-time vertical convection, as it is commonly believed. The criterion of definition of the CIL upper and lower boundaries is suggested; it appeared to be convenient for its description and is useful for understanding of mechanisms of its formation.

В работе представлены результаты сравнительного анализа минимальных среднемесячных температур воды на поверхности и внутри холодного промежуточного слоя (ХПС) Балтийского моря по всей его акватории по одноградусным квадратам. Анализировались данные Института исследований Балтийского моря (IOW), опубликованные на CD в приложении к книге “State and Evolution of the Baltic Sea 1952–2005” (2008). Оказалось, что из 80 квадратов (1×1) акватории Балтийского моря в 43 квадратах (54 %) минимальная температура воды в пределах ХПС ниже, чем минимальная температура на поверхности. Это указывает, что воды ХПС не являются остатком зимней вертикальной конвекции, а распространяются горизонтально. Предложен критерий выделения ХПС для Балтийского моря; он оказался удобен для его описания и полезен для понимания механизмов его формирования.

Olga Kozlova (✉)

P.P. Shirshov Institute of Oceanology RAS, Atlantic Branch, Kaliningrad,
Russia

e-mail: olga_may87@mail.ru



1. Introduction

Intermediate layers of a various origin are formed in many large stratified basins (in the Black sea, the Pacific ocean, Sea of Marmara). Cold intermediate layer (CIL) in the Baltic sea is a seasonal phenomenon; it can be distinctly allocated only in warm seasons in deep-water areas of the sea by its abnormally low temperature at depths of 40–60 m. Due to connection with the Atlantic ocean, deep waters of the Baltic in the central part of the sea have a temperature about 7–8 °C throughout the year, whilst surface water is heated up to 19–22 °C in summer. At the same time, water temperature in intermediate layers is only 2–4 °C from spring to autumn. Even though the existence of intermediate layers is quite a typical feature of large stratified reservoirs at the Earth, the CIL of the Baltic has unique characteristics: no other basin has a cold intermediate layer, water of which is not only colder than the coldest water at the surface at the given place (during winter time), but also has a temperature below the temperature of maximum density (Tmd) (Chubarenko & Demchenko, 2008).

2. Methods

Before to start the analysis of concrete characteristics of the CIL, it is necessary to define it accurately. Though visually it is easy to make, the formal criterion is not developed up to now. With a view of the given research, we will accept the following formal criterion (Chubarenko et al., 2009): we will consider as a cold intermediate layer the layer between levels of maximum negative to maximum positive gradient of a water temperature in vertical, i.e. between thermocline and anti-thermocline (the term of (Prokopov, 2000)). Then, according to this criterion, in May 2005 the CIL was located between horizons of 22.5 and 67.5 m (total thickness 45 m), and in 2006—between 23.5 and 49.5 m (thickness 26 m).

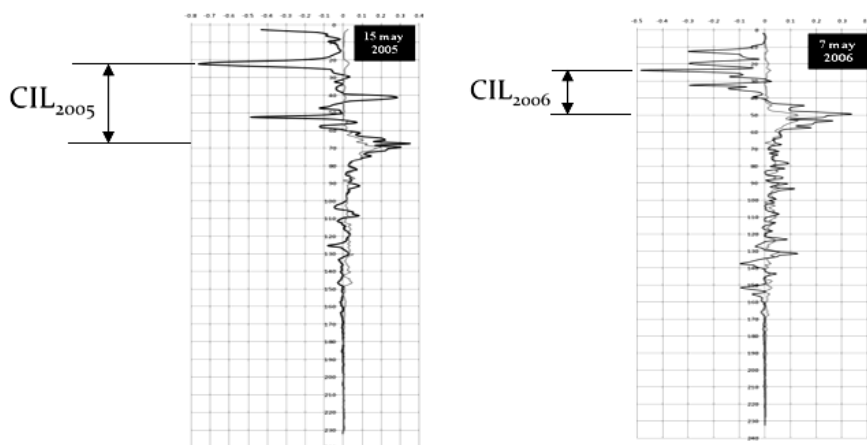


Fig. 1. Vertical gradients of a water temperature and density in the Gotland basin in May 2005 and 2006 (data of IOW monitoring reports; courtesy Dr. R. Feistel). The CIL is defined as a layer between levels of maximum negative and maximum positive gradient of a water temperature in vertical.



3. Results

Analysis of mean annual data, published on CD-disc with the book “State and Evolution of the Baltic Sea 1952–2005” (Feistel et al., 2008), has demonstrated that from about 80 quadrates ($1 \times 1^\circ$) of the Baltic Sea area, in 43 quadrates minimum water temperature within the CIL is lower than the lowest water surface temperature in the course of the year, see Fig. 2. This shows that the CIL contains waters advected horizontally, and this feature seems to be typical, usual thing for the Baltic sea.

In order to find spatial correlations, standard T–S analysis was applied, which showed that the CIL waters might drift from south-western (more saline) rather than from northern areas, since water salinity increases towards the Danish Straits whilst low temperature is commonly found in winter in coastal areas all over the Baltic Sea.

The Baltic CIL contains waters, advected from shallow areas; most probably, they were formed during spring transition of a water temperature in upper layer across the temperature of the maximum density (Chubarenko & Demchenko, 2008).

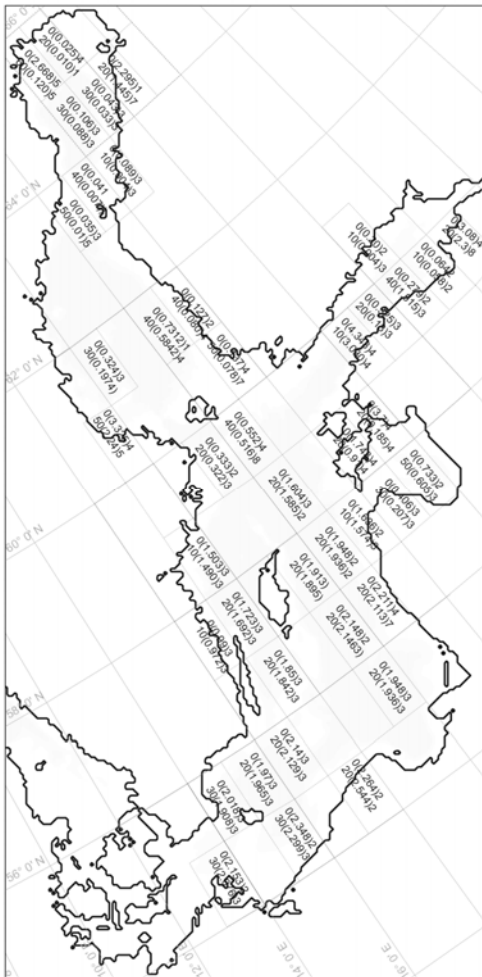


Fig. 2. Mean annual characteristics of the surface and the CIL waters in $1 \times 1^\circ$ quadrants, presented in the format $D(T)M$, where D is the depth, T is minimum water temperature during a year and M is the month when this minimum temperature is observed. This way, the first line in the quadrants shows monthly mean minimum water surface temperature in the given quadrant (which is observed typically in February–March) and the second line gives the depth, minimum water temperature and month of that minimum, characterizing the CIL. Only those quadrants are shown, where minimum water surface temperature is above minimum temperature within the CIL. Data source: “State and Evolution of the Baltic Sea, 1952–2005”, Willey&Sons, 2008.



Analysis of Fig. 2 shows the following. Minimum water temperature in upper layer is well below the temperature of maximum density all over the sea.

Northern part of the Baltic sea. The CIL colder than the surface is well pronounced. Here, *in a coastal parts* at the surface the minimum temperature varies from 0.083 to 2.295 °C and observed (in different quadrants) in March and January, whereas temperature minimum within the CIL is found in different quadrants at different depths: at the depth of 10 m minimum temperature is 0.004 °C in March, at 20 m (at another location)—1.445 °C in July, at 30 m—0.033 °C, again in March.

In deep parts, minimum water temperature at the surface varies from 0.035 to 2.668 °C (observed in different quadrants in March and May), at the depth of 20 m—0.010 °C in January, at 30 m—0.088–0.010 °C, in March and May, at 40 m—0.007–0.120 °C in April and May.

Central Baltic. *In a coastal part* value of temperature at the surface varies from 0.0127 to 3.3250 °C in February and April, and at 40 m—0.080 °C in April; at 50 m—0.078–2.240 °C in July and May.

In a deep part value of temperature at the surface varies from 0.052–1.604 °C in April and March, at 20 m—0.322–1.585 °C in March and February, at 30 m—0.197 °C in April, at 40 m—0.0510–0.584 °C in August and April.

Northwest part of the Baltic sea. *In a coastal part* value of temperature at the surface varies from 0.064–3.08 °C in February and April, at 10 m—0.058–3.030 °C in February and April, at 20 m—0.16–2.3 °C in March and August.

Gotland basin. *In a coastal part* value of minimum temperature at the surface varies from 0.99 to 2.211 °C in March and July, at 10 m—0.72–1.490 °C in March, at 20 m—1.574–2.113 °C in March and July.

In a deep part value of minimum surface temperature varies from 1.604 to 2.211 °C in March and April, at 20 m—1.503–1.936 °C in March.

Southeast part of the Baltic sea. *In a coastal part* value of temperature at the surface varies from 2.154 to 2.264 °C in March and February, at 20 m—2.544 °C in February, at 30 m—2.06 °C in March.

In a deep part value of surface temperature varies from 1.97 to 2.342 °C in March and February, at 20 m—1.965–2.129 °C in March, at 30 m—1.908–2.299 °C in March.

Thus, totally over the entire sea area, minimum temperature within the CIL is observed in the following month: in February (19.5 percent), in March (42.5 percent), in April (21 percent), in May (6.5 percent), in July (6.5 percent), in August (4 percent). Other months with minimum water temperature within the CIL lower than the minimum temperature at the surface are never met. The reason may very well be the shortage of the data (it is necessary to consider other sources as well).

Table summarizes the values of minimum water temperatures in coastal and deep parts of the Baltic sea.

4. Summary and conclusions

The accurate and uniform approach to definition of the Baltic sea cold intermediate layer is suggested. The CIL is considered as the layer between levels of the maximum negative and maximum positive gradient of a water temperature in vertical.



Table

Coastal parts, m	Min/Max T, °C	Month	Parts
0	0.127 / 3.325	February / April	Central Baltic / Central Baltic
10	0.004 / 3.030	March / April	Northern part / Northwest part
20	0.16 / 2.3	March / April	Northwest part / Northwest part
30	0.033 / 2.06	March / March	Northern part / Southeast part
40	0.080	April	Central Baltic
50	0.078 / 2.24	July / May	Central Baltic / Central Baltic
Deep parts, m	Min/Max T, °C	Month	Parts
0	0.035 / 2.6680	March / May	Northern part / Northern part
20	0.01 / 2.129	February / March	Northern part / Southeast part
30	0.088 / 2.299	March / March	Northern part / Southeast part
40	0.007 / 0.584	April / April	Northern part / Central Baltic

The performed analysis of IOW data published on CD-disc with the book “State and Evolution of the Baltic Sea 1952–2005” (Feistel et al., 2008) clearly shows in which months it may be formed.

As follows from mean annual data on water temperature (1952–2002), it is a typical feature that minimum water temperature within the CIL is below minimum local water surface temperature. Thus, typically, the CIL contains waters advected horizontally.

Acknowledgements

Investigations are supported by RFBR via projects 10-05-90754mob_st and 10-05-00540a.

References

- Chubarenko, I. P. & Demchenko, N. Y. (2008). On contribution of horizontal and intra-layer convection to the formation of the Baltic Sea cold intermediate layer. *Ocean Sci. Discuss.* **5**:1–43, <http://www.ocean-sci-discuss.net/5/1/2008/>.
- Chubarenko, I. P., Kozlova, O. I., Sachenko, L. S. (2009) Probable response of the Baltic sea Cold Intermediate Layer to climate warming: field data analysis and numerical modeling. In: *Abstr. Int. Conf. on Climate Change “The environmental and socio-economic response in the southern Baltic region”*, Szczecin, Poland, 25–28 May 2009, 31–32.
- Feistel, R., Naush, G., Wastmund, N., eds. (2008) *State and Evolution of the Baltic Sea, 1952–2005. A Detailed 50-year Survey of Meteorology and Climate, Physics, Chemistry, Biology, and Marine Environment*. J. Wiley & Sons.
- Prokopov, O. I. (2000) Formation of structure of a cold intermediate layer in Black sea. *Meteorol. Hydrol.* **5**:76–85. (in Russian).

Short-term water dynamics variability at the narrow Black Sea shelf

**Viacheslav Kremenetskiy, Andrey Korzh,
Alexander Ostrovskiy, Andrey Zatsepin**

Abstract

Results of field investigations of water dynamics over the Black Sea shelf are presented on the base of high-resolution quasi-instant towed ADCP surveys, conducted in summer time for the period of 2006–09. Sub-mesoscale eddies formation's mechanisms and certain features of their evolution are revealed and discussed.

Представлены результаты натурных исследований динамики вод на шельфе Черного моря по результатам высокоразрешающих квази-мгновенных съемок буксируемым акустическим доплеровским измерителем скоростей течений, выполнявшихся ежегодно в течение нескольких лет (2006–2009). Выявлены некоторые физические механизмы формирования суб-мезомасштабных вихревых структур и особенности их эволюции.

Viacheslav Kremenetskiy, Alexander Ostrovskiy, Andrey Zatsepin (✉)

P. P. Shirshov Institute of Oceanology RAS, Moscow, Russia

e-mail: sk@ocean.ru

Andrey Korzh (✉)

P. P. Shirshov Institute of Oceanology RAS, Atlantic Branch, Kaliningrad, Russia

Longterm high resolutional hydrodynamical model simulation for the Gulf of Finland

Ilja Maljutenko

Abstract

This study is carried out in the frame of BONUS+ research project ECOSUPPORT. The goal of this work is to investigate variability of circulation and temperature-salinity distribution over the time span from 1997 to 2006 in the Gulf of Finland. Highly parallelized 3D hydrodynamical model (GETM) has been set up to perform long-term simulations with spatial grid resolution of 0.5×0.5 nautical miles in the Gulf of Finland. The model resolves the mesoscale phenomena (upwelling/downwelling, filaments/squirts, eddies). The model is forced with lateral boundary data at the entrance to the Gulf of Finland from the larger-scale model for the whole Baltic Sea and atmospheric forcing data is applied from RCAO model output. Temporal development of temperature and salinity, and coastal-offshore exchange in relation to the climate variability will be discussed.

Данное исследование проводится в рамках проекта Bonus и исследовательского проекта Ecosupport. Цель данной работы — исследовать изменчивость циркуляции и распределения температуры и солёности в течение временного промежутка с 1997 по 2006 г. в Финском заливе. Для расчетов была использована трехмерная гидродинамическая модель (GETM) с пространственным разрешением 0,5×0,5 морских миль для Финского залива. Модель разрешает мезомасштабные феномены, такие как апвеллинг/даунвеллинг, филаменты/струи, вихри. Начальные условия на входе в Финский залив были взяты из модельных расчетов для всего Балтийского моря, полученных на сетке с большим пространственным разрешением; метеорологические данные были взяты из расчетов RCAO модели. Изменение во времени температуры и солёности, прибрежного водообмена будет обсуждаться с точки зрения климатических изменений.

Ilja Maljutenko (✉)

Marine Systems Institute at Tallinn University of Technology, Tallinn, Estonia

e-mail: iljamal@gmail.com



1. Introduction

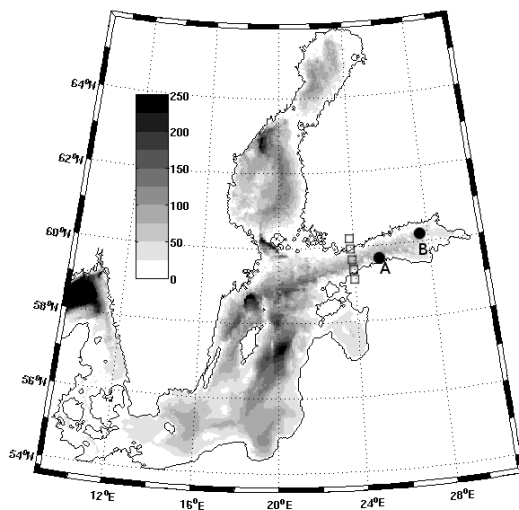
Gulf of Finland (GoF) is often described as water body with very complex hydrography. Buoyancy driven mean cyclonic circulation varies with short term wind forced currents. Discharge of the largest river Neva in the Eastern part of GoF gives its part in seasonal circulation variability and is the main cause for horizontal salinity gradient. Stratification is being described as highly variable both in space and time (Alenius et al., 1998). All of those features makes it very interesting “playground” for scientists to study the estuarine dynamics and coastal processes. Due to wide range of physical processes it is also tough task for numerical models to reproduce exact conditions of events. With advancing computation hardware and models, that are possible to run with parallel tasks, it is possible to scale down both spacial and temporal resolution of processes. Following is first attempt to set up the 10 year simulation and spot the inaccuracies with an intention to improve model performance.

2. Model description

The simulation is done with the General Estuarine Transport Model (GETM). GETM is a fully baroclinic three dimensional hydrodynamic model with the hydrostatic and Boussinesq assumptions (Burchard & Bolding, 2002). Both for momentum and tracers high order advection schemes are applied. For turbulence the module of the General Ocean Turbulence Model is used with k-epsilon model and constant stability functions (Burchard & Bolding, 2001). To hindcast a period from 1997 to 2006, nested grid approach has been used in similar way as described by Andrejev et al. (2004).

For the Baltic Sea setup a 2 nm spherical topography had been interpolated from the study of Seifert et al. (2001) (Fig. 1). The bathymetry has been smoothed over 3 grid steps with moving average filter in order to reduce artificial flows caused by the horizontal pressure gradient errors (Mellor et al., 1998). Also depths deeper than 250 m were adjusted, because of insufficient initial data. The allowed barotropic time step, for stability, was 15 s and

Fig. 1. Topography of the Baltic sea (Seifert et al., 2001). Boundary between models is marked with rectangles. Sites A and B are included.





baroclinic mode is integrated with 300 s. In vertical 25 sigma layers were set. Western open boundary was set to Kattegat strait with artificial shore.

GoF grid was interpolated into 0.5×0.5 nm grid (beginning from 23.5° E) with land adjustment for shallower depths than 1.2 m. In vertical there was same number of sigma layers as in large scale setup. Such grid allowed to make 10 year integration with 10 s barotropic and 250 s baroclinic timestep without stability problems. The lateral boundary was forced with larger scale model output of 20 min interval for elevations and 3 h interval for salinity and temperature.

Three dimensional salinity and temperature initial fields have been adopted from Modular Ocean Model (Pacanowski & Griffies, 1999) simulation for Baltic Sea (1960–2004), using December mean fields for the year 1996. Atmospheric forcing was adopted from RCAO (the Rossby Center Atmosphere Ocean model, (Döscher et al., 2002)) output with 3 h time intervals. Rivers are implemented so that the small rivers are included in the large river runoff. The river data originates from IKZM-Oder project (web 2.). Data is distributed within ECOSUPPORT project partnership (web 1.).

Before January 1997 the model has been warmed up by 2 spin up periods. First to simulate only baroclinic circulation where salinity and temperature forcing has been applied for 10 days. The next 30 days the boundary conditions from larger scale run have been applied. Atmosphere forcing and riverine output has been applied with linear increasing during second spin-up period.

3. Model output

Six hour mean values were chosen to make reasonable output for salinity, temperature and velocity fields. The main aim was to observe model performance to reproduce annual cycle of thermocline and variability of halocline. It also made available to plot mean surface velocity field for the whole period.

For salinity and temperature vertical profiles were chosen at two sites from different parts of GoF. The sites are marked with letters A and B in Fig. 1. A is located at the center of GoF where we can observe model performance in depths below 80 m. According to previous studies rather eastward current dominates there (Andrejev et al., 2004). Site B is located at eastern part of GoF where water column height is ~ 65 m and due to fresh water supply from rivers lower salinity values than at site A occur (Andrejev et al., 2004).

In Fig. 2 transect of 6 h salinity and temperature mean values are plotted. We can see that salinity is annually very variable with decreasing 1.5 psu over 10 year period near bottom. It is also noticeable that salinity stratification is strongly difused after first year summer. After downwelling event in 1997 autumn halocline seems to vanish with losing salinity above 9 psu for the whole next simulation period. Surface salinity peaks varied from 7.5 to 4.5 psu which is probably caused by presence of eddies that are responsible of less saline water transport over the gulf. In average, 15°C waters are reaching ~ 30 m depth in summer months with few exceptions: in years 1997 and 2002 warm water did not reach over 30 m depth. With lower mixing more saline waters were able to develop next winter. In overall we can see similarities between descending warmer water and lower salinity values in bottom.

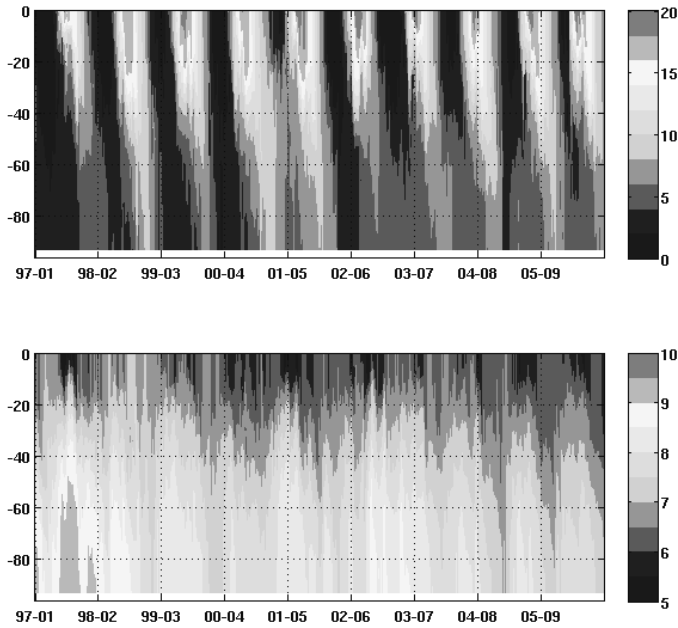


Fig. 2. Temperature ($^{\circ}\text{C}$, upper plot) and salinity (psu, lower plot) time slices at site A.

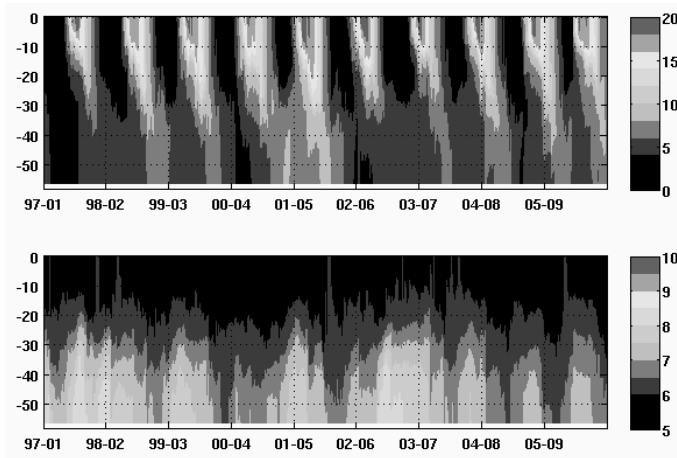


Fig. 3. Same as in Fig. 2 but for site B.

Site B reveals similar processes going on temporally in Fig. 3. In vertical direction we can see that salinity of 4–5 psu is dominant in the upper 15 m layer. Deeper it has annual variability coherent with convective entrainment of warmer water from above. Salinity bottom maximums over 8 psu appears only in the first year and after calm 2002 year summer, where mixing was moderate compared to other years. Trend towards less saline water is not so obvious due to 2002 year winter peak. Bottom temperature in average was around 5 $^{\circ}\text{C}$ with autumn maximum around 9 $^{\circ}\text{C}$. It is also visible that both salinity and temperature variability is lower than on site A.

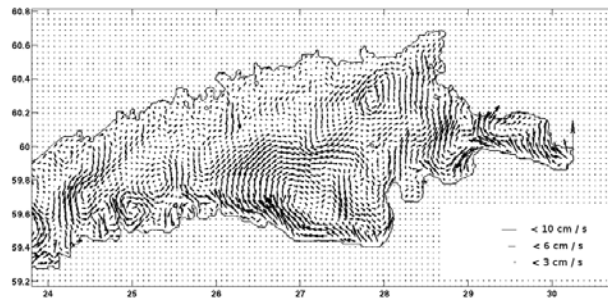


Fig. 4. Average surface (0–1 m) circulation for the GoF in cm/s. Every 4th vector is plotted.

Surface currents in GoF are mainly wind driven where rivers in east gulf also have their contribution (Alenius et al., 1998). Average mean surface circulation in Fig. 4 shows that more persistent surface currents are located near southern coast of the GoF. Near the coast of Finland westward currents can be clearly distinguished only around 28° N. Model produced strong westward outflow from river Narva. In the center of GoF persistent eastward flow exists that also agrees with mean wind stress direction. Due to large river output from Neva and Earth rotation currents turn northward (Alenius et al., 1998) where they get affected by high eddy activity and form unstable flow in the west direction toward the exit of the GoF.

4. Conclusion

Figures show that overall seasonal hydrographic characteristics were reproduced. Vertical timeseries of salinity and temperature revealed high yearly variability. Over the period the salinity tends to have trend towards less saline conditions near the bottom while on surface riverine output and boundary conditions are important. Vertical mixing plays the key role to stratification, therefore vertical turbulence model should be revised. Persistent unusual Narva bay surface circulation (comparing to that in (Andrejev et al., 2004)) maybe caused by incorrect river output or too strong current in center of GoF. Following validation work should reveal how good the agreement between the model and measured data is. For next model runs it is necessary to get rid of artificial shore near Kattegat that might improve bottom inflows of more saline water. Within the framework of ECOSUPPORT project new, more accurate, river output will be applied.

References

- Alenius, P., Myrberg, K., Nekrasov, A. (1998) The physical oceanography of the Gulf of Finland: a review. *Boreal Environ. Res.* **3(2)**:97–125.
- Andrejev, O., Myrberg, K., Alenius, P., Lundberg, P.A. (2004) Mean circulation and water exchange in the Gulf of Finland—a study based on three-dimensional modeling. *Boreal Environ Res.* **9(1)**:1–16.
- Burchard, H. & Bolding, K. (2001) Comparative analysis of four second-moment turbulence closure models for the oceanic mixed layer. *J. Phys. Oceanogr.* **31**: 1943–1968.



- Burchard, H. & Bolding, K. (2002) *GETM—a general estuarine transport model*. Scientific documentation, Tech. Rep. EUR 20253 EN, European Commission.
- Mellor, G. L., Ezer, T., Oey, L.-Y. (1998) Sigma coordinate pressure gradient errors and the seamount problem. *Journal of Atmospheric and Oceanic Technology* **15**: 1122–1131.
- Döscher, R., Willén, U., Jones, C. et al. (2002) The development of the regional coupled ocean-atmosphere model RCAO. *Boreal Env. Res.* **7**:183–192.
- Pacanowski, R. C. & Griffies, S. M. (1999) *The MOM 3 Manual*. Geophysical Fluid Dynamics laboratory/NOAA, Princeton, USA, p. 680.
- Seifert, T., Tauber, F., Kayser, B. (2001) A high resolution spherical grid topography of the Baltic Sea, revised edition. *Baltic Sea Science Congress*, 25–29 November 2001, Post. No. 147.
- URL: <http://www.baltex-research.eu/ecosupport/> (13.04.2010)—Ecosupport home page.
- URL: <http://www.ikzm-oder.de> (13.04.2010)—IKZM–ODER project home page.

Investigation of evolution of a gravity current with constant inflow on a horizontal bottom (laboratory experiment)

Sergey Nizov

Abstract

Laboratory experiments on two-dimensional gravity current with constant inflow in ten-meters long tank of Atlantic Branch of IO RAS are fulfilled. The initial values of density (salinity) difference between the inflowing fluid and the fluid in the tank as well as the inflow rate were varying from one experimental run to another. The dependences of the translation velocity on the density current head and the rate of salinity change in it as a function of traveling distance and basic parameters of experiment are established. An applicability of the obtained laboratory results to the natural density currents is discussed.

Проведены лабораторные эксперименты по изучению закономерностей распространения двумерного плотностного течения с постоянным притоком (расходом) в десятиметровом лотке АО ИОРАН. Исследование проводилось при различных начальных значениях перепада плотности (солености) и расхода, варьировавшихся от опыта к опыту. Получены зависимости скорости распространения головы плотностного течения, а также изменения его солености от расстояния от источника и от определяющих параметров эксперимента. Обсуждается применимость полученных данных к природным плотностным течениям.

1. Introduction

There are many examples in the oceans and seas when dense water spreads over the slope or horizontal bottom. For example, Mediterranean water enters the Atlantic through the deep part of the Gibraltar Strait, rushes down the continental slope, separates from the bottom and extends further within the corresponding isopycnic layer. Another example, North Sea water penetrates into the Baltic Sea as bottom gravity flows, which are distributed along a hori-

Sergey Nizov (✉)

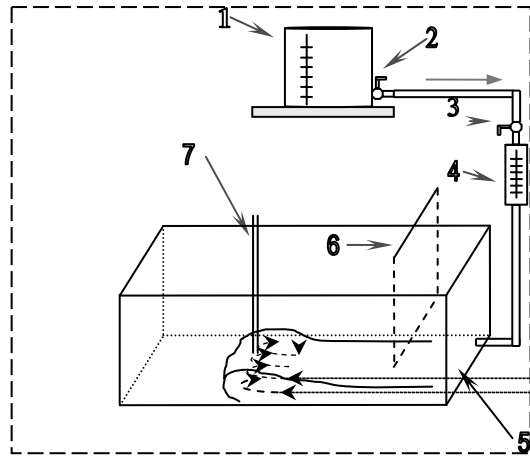
P. P. Shirshov Institute of Oceanology RAS, Moscow, Russia

e-mail: nizov@ocean.ru



Fig. 1. Scheme of the laboratory model.

- (1) Mariott discharge bottle with dense dyed water;
- (2) close tap;
- (3) tuning tap;
- (4) discharge grid;
- (5) small tank;
- (6) vertical flat plate;
- (7) probe for water sampling.



zontal bottom or slope (Gritsenko, 2001). This process is one of the important mechanisms of mass and oxygen exchange between shelf and deep sea.

There a lot of works that studied the density currents upon the slope but some aspects of their structure and dynamics as well as their interaction with the ambient fluid are still not clear. Ocean gravity currents can be divided into 2 groups—those which are influenced by the Earth rotation and those which are not. First group of the gravity currents should be modeled in the rotating fluid and another group doesn't need it. In this work we observe second case without effect of the Coriolis force.

2. Methods and results

The main goal of the work is to study different physical regimes (dynamical modes) of the density current in the homogeneous surrounding fluid and to find critical parameters that control salinity exchange between gravity current and surrounding fluid.

Basic parameters of the model are:

- ✓ q , [cm^2/s]—discharge of the source (over the length of the source); variation range 2–8 [cm^2/s];
- ✓ $g' = (\delta\rho/\rho)g$, [cm^2/s]—reduced gravity force acceleration, where g —gravity force acceleration; variation range 0.2–6 cm/s^2 ;
- ✓ ν , [cm^2/s]—kinematics viscosity of the fluid;

Using the above three parameters one can combine two governing non-dimensional parameters—Froude, $Fr_c = u_c/(g'h)^{1/2}$ and Reynolds $Re_c = u_c h/\nu$ numbers, where u —velocity of the frontal part of the gravity current.

In frame of this work the eighteen experiments with different combinations of q and g' parameters were fulfilled. Each experiment began from the filling of the main tank (10 m length) with homogeneous fresh water. Then we filled the small tank with dense dyed water from Mariott discharge bottle. Temperature in the main tank and Mariott discharge bottle were equal. After that we set required flow rate through discharge grid (by tuning tap). When all preparations were finished, the vertical flat plate was lifted up for 5 cm and dense water under gravity force drug spread over the bottom. Water samples

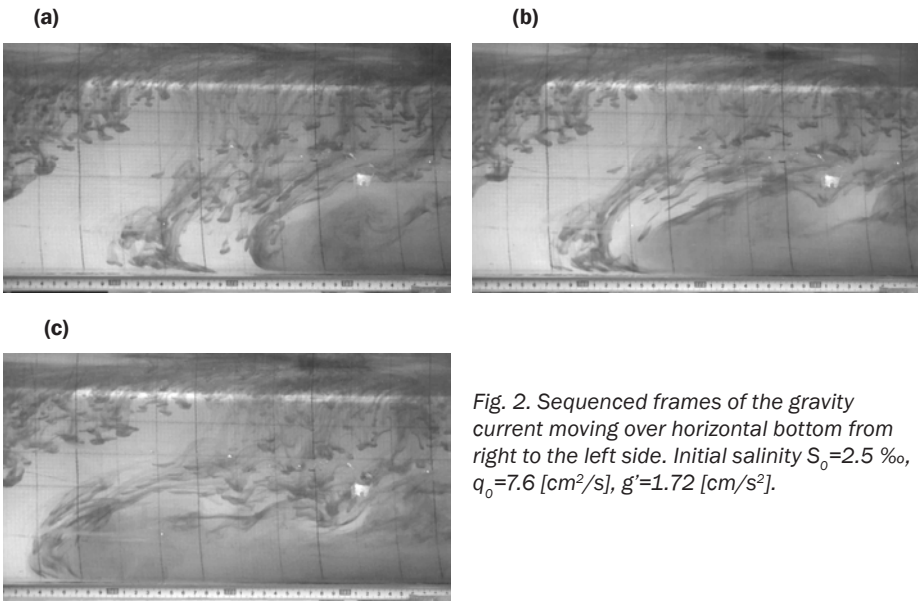


Fig. 2. Sequenced frames of the gravity current moving over horizontal bottom from right to the left side. Initial salinity $S_0=2.5\text{ ‰}$, $q_0=7.6\text{ [cm}^2/\text{s]}$, $g'=1.72\text{ [cm/s}^2]$.

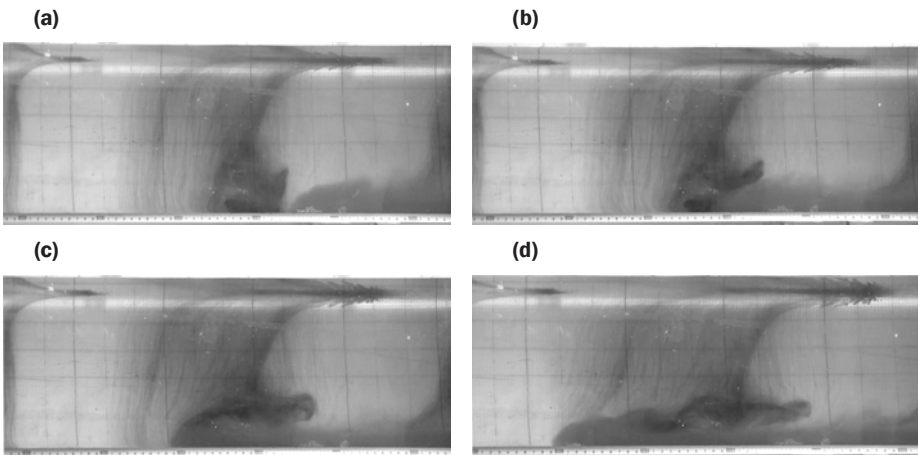


Fig. 3. Sequenced frames of the gravity current moving over horizontal bottom from right to the left side. Initial salinity $S_0=12.5\text{ ‰}$, $q_0=1.7\text{ [cm}^2/\text{s]}$, $g'=6.7\text{ [cm/s}^2]$.

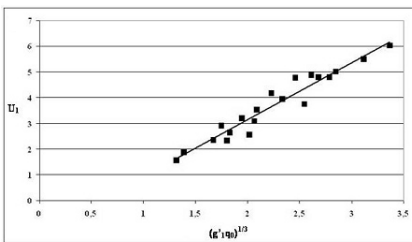


Fig. 4. Dependence of frontal velocity U_1 on $(g'_1 q_0)^{1/3}$.

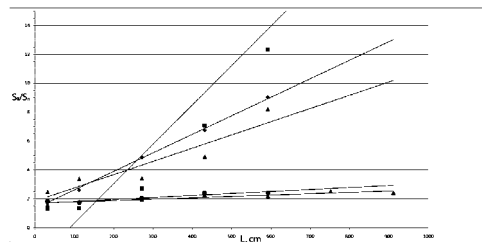


Fig. 5. Dependences of S_0/S_n on L . S_0 —initial salinity; S_n —salinity samples that takes every 1.5 m.



from the head of the gravity current were taken across equal distance. For further data processing the video filming of all experiments were made.

Surrounding fluid was involved into the flow differently in frontal and tail parts of the gravity current, and frontal part was more intensive at that. Velocity measurements let us conclude that the tail part spreads faster than frontal part, so the “body” of the current injects salt water continuously to the “head” of the current.

A sequence of snapshots of the gravity current moving on horizontal bottom with small value of g' parameter is shown on the Fig. 2. Manganese crystals behind the head demonstrate the process of surround fluid involving to the back part of the head. In case of bigger salinity difference (Fig. 3) the gravity current is thinner in frontal part but spreads faster.

Previous experiments with homogeneous water in the tank with sloping bottom revealed the relation for the flow head's spreading velocity $U=C(g'q_0)^{1/3}$ (Fig. 4). In these experiments, though, U , g' and q_0 were constant along the whole tank. In the long tank with horizontal bottom we have a different situation: even with $q_0=\text{const}$ g' is changing along the flow that causes the corresponding change of U .

Flow head water samples processing let us to derive the rate of salinity change in the flow head as a function of traveling distance (Fig. 5). It shows that the salinity at the end of the laboratory tank decreases by 6–8 times in case of a big initial salinity S_0 and only by 1–2 times in case of a small initial salinity S_0 .

3. Conclusions

The laboratory model for the density current investigations was created to simulate different physical modes of the dense water spreading on horizontal bottom.

Dependence of the flow frontal velocity from the basic parameters of the model was obtained. It can be described as a friction and drag forces balance.

The dependences of the translation velocity of the density current head and the rate of salinity change in it as a function of traveling distance and basic parameters of experiment are revealed.

Acknowledgements

Investigations are supported by RFBR, project No. 10-05-00728mob_st.

References

Gritsenko, V.A. (2001) Bottom gravity flow in the ocean. *Earth Sciences* 1:64–70.

Analysis of temporal variability of measured and modelled vertical distributions of salinity and temperature in the Gulf of Finland during 10-year period

Jelena Passenko, Gennadi Lessin, Ilja Maljutenko

Abstract

The Gulf of Finland is the sub-basin of the Baltic Sea seriously affected by the effects of eutrophication. Accurate representation of distributions and variability of hydrophysical parameters is necessary for correct simulations of biogeochemical variables. General Estuarine Transport Model (GETM) was used for modeling hydrophysical fields of the Gulf during the period from 1997 to 2006. Long-term measurement data from HELCOM monitoring stations LL12, LL7 and LL3a, representing western, central and eastern parts of the Gulf, respectively, were used for GETM model verification.

Финский залив, являющийся суббассейном Балтийского моря, подвергается серьезной эвтрофикации. Точное представление распределения и изменчивости гидрофизических полей необходимо для корректного воспроизведения биохимических параметров. Для моделирования гидрофизических полей, характерных для Финского залива в период с 1997 по 2006 г., была использована Общая Эстуарная Транспортная Модель (GETM). Для верификации данной модели были использованы многолетние натурные измерения, проводимые в рамках HELCOM, на станциях мониторинга LL12, LL7 и LL3a, находящихся в западной, центральной и восточной частях Финского залива.

1. Introduction

The Baltic Sea is one of the largest brackish water areas in the world. It has very limited water exchange with the open ocean via the narrow and shallow Danish Sounds, and is characterised by a significant fresh water surplus due to river runoffs. This leads to a two-layer salinity stratification which plays an important role for the physical processes (Andrejev et al., 2004a).

Jelena Passenko, Gennadi Lessin, Ilja Maljutenko (✉)
Marine Systems Institute at Tallinn University of Technology, Tallinn, Estonia
e-mail: jelena@phys.sea.ee



The Gulf of Finland is a sub-basin located in the north-eastern area of the Baltic Sea. It is a complicated hydrographic region, having saline water input from the Baltic Proper in the west and a large fresh water input from the rivers in the east (Andrejev et al., 2004b, Inkala & Myrberg, 2002). Salinity increases from east to west and from north to south. The surface salinity typically varies from 5–7 ‰ in the western Gulf of Finland (the Hanko–Osmussaari line at the mouth of the Gulf) to about 0–3 ‰ in the east (Neva Bay) (Alenius et al., 1998, Mälkki & Tamsalu, 1985). Bottom salinity in the western Gulf of Finland can typically reach values of 8–9 ‰. In the eastern Gulf of Finland and in the eastern part of the central Gulf of Finland, there is no permanent halocline. In the western Gulf of Finland a permanent halocline exists throughout the year between depths of 60–80 m (Alenius et al., 1998).

Annual variations in the sea-surface temperature are large in the Gulf of Finland. Seasonal thermocline usually forms at the beginning of May and starts eroding by the end of August due to cooling of the surface waters (Andrejev et al., 2004a). Thermocline is usually situated at a depth of 10–15 m and is at its strongest in July–August when the temperature difference between the warm upper and the cold intermediate layer below the thermocline lies in the range of 12–20 °C (Vahtera et al., 2005).

The Gulf of Finland is seriously affected by eutrophication. General Estuarine Transport Model (GETM) was used for modeling hydrophysical fields of the Gulf during the period from 1997 to 2005. Long-term measurement data from HELCOM monitoring stations LL12, LL7 and LL3a, representing western, central and eastern parts of the Gulf, respectively, were used for GETM model verification.

The results of the hydrodynamic modeling are important input information for ecosystem modeling, in which of the hydrodynamic parameters: salinity and temperature have variations which play the most important role in ecosystems. An accurately simulated salinity field is to some extent a proof that the transport of passive biochemical tracers can also be simulated correctly. Biological processes are often functions of sea temperature, which has to be predicted accurately by the hydrodynamic model. For these reasons, the model studies and the verification of the model results concentrate on investigating salinity and temperature variations.

2. Methods

GETM (Burchard et al., 2004) with the turbulence module of the General Ocean Turbulence Model (Umlauf & Burchard, 2005) has been used for the present numerical study. GETM has been successfully applied to several coastal, shelf sea and limnic scenarios, e.g. for turbulent flows in the Wadden Sea (Stanev et al., 2003), for dynamics in the North Sea (Stips et al., 2004), for plume study in the Arkona Basin (Burchard et al., 2005). In present study the whole Baltic Sea was modeled with a special focus to the Gulf of Finland. GETM model set up and detailed description is given by Maljutenko (Maljutenko, 2010).

Observational data used for model validation on salinity and temperature originate from three intensively sampled HELCOM monitoring stations (LL12, LL7 and LL3a) in the Gulf Finland (Fig. 1).

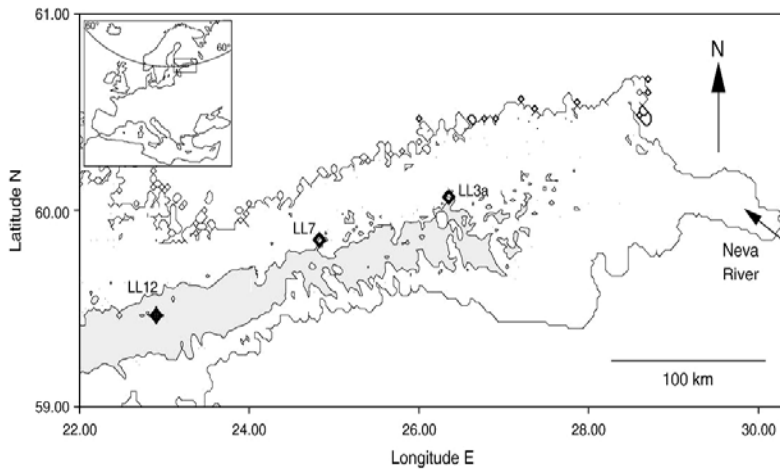


Fig. 1. Locations of hydrographic stations LL12 (59° 28.0' 22° 54.0'), LL7 (59° 51.0' 24° 49.6') and LL3A (60°04.0' 26°20.9') in the Gulf of Finland.

In all stations maximum sea surface temperature were observed in August. The highest sea surface temperature (22.25 °C) was recorded in August 2002 at station LL3a. Salinity at stations LL12 and LL7 (around 10 PSU) does not show much difference but at the shallower eastern site (station LL3a) salinity is around 7.5 PSU.

3. Results

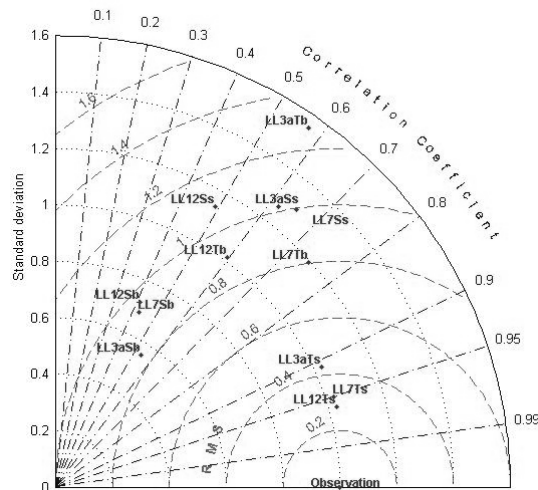
The usual way to validate model is to determine whether its behavior resembles the observed data. In most cases, plots showing that some pattern of observed variation is reasonably well reproduced by the model are used for model verification (Taylor, 2001). Nowadays more complex models are used and they need more detailed and complex statistical analysis. In recent years a Taylor diagram is used for summarizing the rate of correspondence between simulated and observed fields. On the diagram the correlation coefficient and the root-mean-square difference between the two fields, along with the ratio of the standard deviations of the two patterns, are all indicated by a single point on a two dimensional plot (Jolliff et al., 2009). Taylor diagram provide to get quick summary of the degree of patterns correspondence and allow seeing how well model simulates natural pattern.

For statistical analysis the surface temperature and salinity have been given the values at a depth of 5 m, and the bottom salinity and temperature are the corresponding values at the lowest depth (about 60 m) at which measurements were carried out.

On Fig. 2 the comparison of simulated data to observed data are presented. Simulated salinity and temperature that agree well with observations lie nearest the point marked "observation" on the x-axis, besides they have low RMS errors and high correlation. From Fig. 2 it is clearly seen, that simulated near surface temperature at stations LL7 and LL12 agree best with observations, they have about the same RMS(0.3) error and Correlation coefficient (0.95). Near surface temperature at station LL3A is also very well simulated by the



Fig. 2. Comparison of simulated data to observed data from HELCOM monitoring stations LL12, LL7 and LL3a. The parameters are temperature (T) and salinity (S). Small letters s and b indicate surface and bottom values, respectively. Observations are presented by 1.



model. Near surface salinity is better reproduced at stations LL3A and LL7 because comparing with LL12 they have higher correlation coefficient (0.6) and lower RMS (1.0). Near bottom temperature showed best results at station LL7 (correlation=0.75, RMS=0.8), and the poorest performance of the model is at station LL3A, while model has variations that are larger than observed for about 2 °C. Near bottom salinity in all three stations have quite low correlation coefficient and lower correlation deviation compared to observation.

4. Conclusion

In this study the Taylor diagram was used to analyze temperature and salinity in the Gulf of Finland during the period 1997–2005. Modeled surface temperature showed good agreement with observed data in all three stations. Seasonal cycles in upper layer were reproduced well by the model. Salinity is overestimated by the model for about 1 PSU, which explains lower correlation with observations.

Acknowledgments

This work is carried out as a part of an international project “ECOSUPPORT-Advanced tool for scenarios of the Baltic ECOsystem to SUPPORT decision making” funded by BONUS+ Interreg IV.

References

- Alenius, P., Myrberg, K., Nekrasov, A. (1998) The physical oceanography of the Gulf of Finland: a review. *Boreal Environmental Research* 3:97–125.
- Andrejev, O., Myrberg, K., Alenius, P., Lundberg, P. (2004a) Mean circulation and water exchange in Gulf of Finland—a study based on three dimensional modelling. *Boreal Environment Research* 9:1–16.
- Andrejev, O., Myrberg K., Lundberg P.A. (2004b) Age and renewal time of water masses in a semi-enclosed basin—application to the Gulf of Finland. *Tellus* 56A:548–558.



- Burchard, H., Bolding, K., Villarreal, M. R. (2004). Three-dimensional modelling of estuarine turbidity maxima in a tidal estuary. *Ocean Dynamics* **54**:250–265.
- Burchard, H., Lass, H., Mohrholz, V. et al. (2005). Dynamics of medium-intensity dense water plumes in the Arkona Sea, Western Baltic Sea. *Ocean Dynamics* **55**:391–402.
- Inkala, A. & Myrberg, K. (2002) Comparison of hydrodynamical models of the Gulf of Finland in 1995: a case study. *Environmental Modelling and Software* **17**(3):237–250.
- Jolliff, J. K., Kindle, J. C., Shulman, I. et al. (2009). Summary diagrams for coupled hydrodynamic-ecosystem model skill assessment. *Journal of Marine Systems* **76**:64–82.
- Maljutenko, I. (2010) *Longterm high resolutional hydrodynamical model simulation of the Gulf of Finland*.
- Mälkki, P. & Tamsalu, R. (1985) Physical features of the Baltic Sea. *Finnish Marine Research* **252**:110.
- Stanev, E. V., Wolff, J.-O., Burchard, H. et al. (2003). On the circulation in the East Frisian Wadden Sea: numerical modelling and data analysis. *Ocean Dynamics* **53**:27–51.
- Stips, A., Pohlmann, T., Bolding, K., Burchard, H. (2004). Simulating the temporal and spatial dynamics of the North Sea using the new model GETM (General Estuarine Transport Model). *Ocean Dynamics* **54**:266–283.
- Taylor, K. E. (2001). Summarising multiple aspects of model performance in a single diagram. *Journal of Geophysical Research* **106**(D7):7183–7192.
- Umlauf, L. & Burchard, H. (2005). Second-order turbulence models for geophysical boundary layers. A review of recent work. *Continental Shelf Research* **25**:795–827.
- Vahtera, E., Laanemets, J., Pavelson J. et al. (2005) Effect of upwelling on the pelagic environment and bloom-forming cyanobacteria in the western Gulf of Finland, Baltic Sea. *Journal of Marine Systems* **58**(1–2):67–82.

The analysis of mixing and entrainment processes for downslope density currents using Baines' approach

Anna Shishova

Abstract

Downslope density currents play a significant role in vertical water exchange in near-shore zones of oceans. Entrainment and mixing processes at the density currents' interface has been described by many authors (e.g., Barenblatt, Benjamin, Britter & Linden, Simpson, Turner, Holyer & Huppert, Baines), however further understanding is still required.

Известно, что вдольсклоновые плотностные течения играют заметную роль в вертикальном водообмене в прибрежных зонах морей. Процессы вовлечения и перемешивания для плотностных течений были описаны многими авторами (Баренблатт, Benjamin, Britter и Linden, Simpson, Simpson, Turner, Holyer & Huppert, Baines), однако полноты понимания достигнуть не удалось.

Anna Shishova (✉)
Immanuel Kant State University of Russia (IKSUR), Kaliningrad, Russia
e-mail: lwish.grant@gmail.com

Propagation of the denser water on the bottom slope in the stratified fluid

David Sikharulidze

Abstract

This article deals with the problem of the gravity currents on a uniform slope. The work is based on a series of experiments which are aimed at modeling a gravity current in the different environmental conditions, such as homogeneous, two-layered and linearly stratified surrounding fluid.

В данной работе рассматриваются плотностные течения на наклонном дне. В основе работы лежит серия экспериментов, которые были нацелены на то, чтобы промоделировать плотностное течение в различных средах: однородной по плотности, двухслойно стратифицированной жидкости и жидкости с линейной стратификацией.

Propagation and sinking of dense water on the sloping bottom is a vital part of the water exchange of the shelf zone, lagoons, internal basins with open sea, also it takes a major role in ventilation of the deep waters. Near-bottom gravity currents participate in a general process of the sediment transport from the coastal zone of the sea to its deeper part.

The gravity currents in seas and oceans can be divided into two groups on the scale basis. The first one is relatively large-scale and quasi-stationary currents. Their thickness is significantly higher than the Ekman's scale, and the time of living is much longer than the inertial period.

The second group is short-period and/or small-scales gravity currents. Their time of living is less than the inertial period and their characteristic thickness doesn't exceed the Ekman's scale. The Earth's rotation are insignificant for the dynamic of such currents. A suspension current can be observed as a good example of the gravity currents of the second type. Suspended and as a result of this, denser water rapidly falls down on the sloping bottom and the skating force is one of the major factors influencing the dynamics of the current, as well as the processes of the vortical suspension and gravitational

David Sikharulidze (✉)
P.P. Shirshov Institute of Oceanology RAS, Moscow, Russia
e-mail: david2006s@rambler.ru



settling of solid phase particles. The current's dynamics also depend on bottom friction and/or turbulent drawing of the surrounding water.

The methods of the theoretical and laboratory modeling are of vital importance because of the obvious difficulties in the near-bottom gravity currents research in the marine conditions. Thanks to these methods we are able to study the basic physics of this phenomenon and interpret the data from separate and irregular field observations, as well as quantitative estimation of the characteristics of the near-bottom gravity currents.

Previously a series of experiments have been conducted by A. G. Zatsepin, V. A. Gritsenko, V. V. Kremenetskiy, S. G. Poyarkov, O. Yu. Stroganov—laboratory and numerical studies of the dense water spreading along the sloping bottom; by A. V. Gusev, V. Yu. Liapidevskii, A. G. Zatsepin, S. S. Nizov—dynamics of downslope gravity currents in stratified fluid. Their goal was to model the gravity current in the homogeneous and two-layered surrounding fluid. For the homogeneous environment we can specify three different modes of dynamic gravity currents:

(1) Laminar mode (Fig. 1). This mode is characterized by low Re and Fr absence of the water drawing. Dynamics of the gravity current is defined by the balance of the skating force and the viscous bottom friction. $g'sina = v\partial^2u/\partial z^2 \approx vU/h^2 = vU^3/q^2$; $h = q/U$. Result: $U \approx (g'q^2sina/v)^{1/3}$, where q is a flow rate, g' the reduced gravity and a the bottom slope.

(2) Quasi-laminar mode with the “head” (Fig. 2). This mode is characterized by low Re , $Fr \approx 1$ and minor drawing, which can be neglected at the first approach. The dynamics of the gravity current is defined by the balance of the skating force and the drag of the ambient fluid in the “head”. $g'sina = 1/2\partial u^2/\partial x \approx 1/2U^3/q$; $x \approx h = q/U$. Result: $U \approx (2g'qsina)^{1/3}$, where q is a flow rate, g' the reduced gravity and a the bottom slope.

(3) Turbulent mode with “head” (Fig. 3). This mode is characterized by quite high Re and $Fr \approx 1$, and significant drawing. The height of the “head” reaches the peak value and the moving force is determined by the pressure gradient. But the drag of the ambient fluid balances the moving force. The “head” is continually fed by the fluid of the gravity current which is flowing in it. $1/2\partial u^2/\partial x = g'\partial h/\partial x$; $1/2U^3/q \approx g'$. Result: $U \approx (2g'q)^{1/3}$, where q is a flow rate, g' the reduced gravity.

Laboratory experiments showed that three different modes of bottom gravity currents “behavior” take place in the two-layered fluid (as well as in the

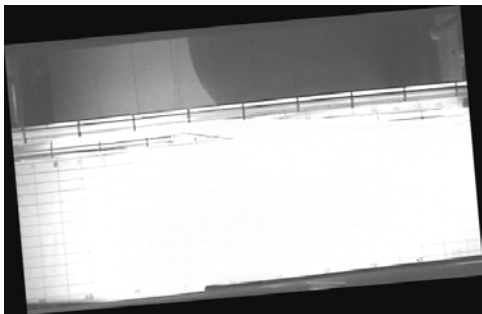


Fig. 1. Laminar mode.

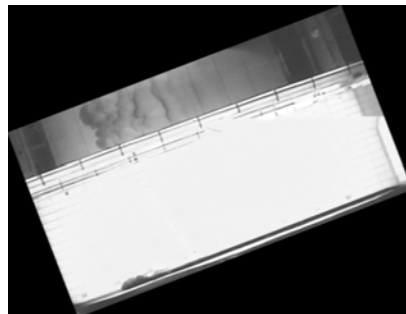


Fig. 2. Quasi-laminar mode

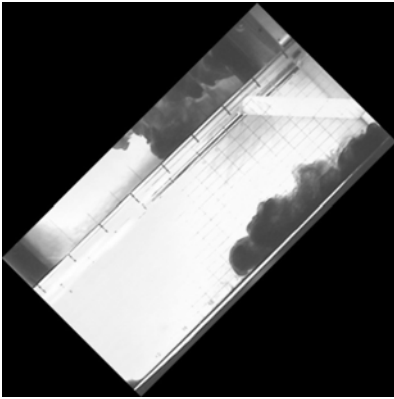


Fig. 3. Turbulent mode.

homogenous fluid). Let us give several designations: S_0 —the gravity current initial salinity, S_1 —the upper-layer salinity, S_2 —the lower-layer salinity. In the first mode ($S_0 \gg S_2$) the gravity current “does not notice” the pycnocline and retains its bottom nature. In the second mode ($S_1 < S_0 < S_2$) the initial gravity current comes off the bottom and transforms into the clearly intrusive and propagates in the pycnocline zone. The third mode ($S_0 > S_2$) is the most interesting and complicated. The gravity current “splits” into two parts during the interaction with the pycnocline. The former intrudes into the

pycnocline, and the latter continues to move along the bottom slope (Fig. 4).

The main purpose of this work is to conduct the series of the similar experiments, modeling the gravity currents in the linearly stratified fluid. Prior experiments results showed that the gravity currents in the linearly stratified ambient fluid are significantly different from the ones in the homogeneous and two-layered fluids.

It was discovered that the gravity current draws the surrounding less density fluid. Consequently less density fluid gets under the denser fluid, what results in the vertical convective mixing. The upper part of the gravity currents participates in that process. The products of mixing separate from the gravity current and intrude into the ambient fluid (quasi-isopycnic intrusion). As a result of this the gravity current rapidly loses its mass and does not spread so deeply as it comes from the estimations based on the initial gravity current density and the parameters of the stratification (Fig. 5). However, in order to estimate and parametrize mentioned above effects of interaction between the gravity current and the surrounding medium, we need additional experimental research which will be conducted in the planned future work.

References

- Alavian, V. (1986) Behaviour of density currents on an incline. *J. Hydraul. Engng. ASCE* **112**:27–42.
- Batchelor, G. (1967) *An introduction to Fluid Dynamics*. Cambridge University Press.
- Britter, R. & Linden, P. (1980) The motion of the front of a gravity current traveling down an incline. *J. Fluid Mech.* **99**:531–543.
- Gusev, A.V., Liapidevskii, V.Yu., Zatsepin, A.G., Nizov, S.S. (2006) Dynamics of downslope gravity currents in stratified fluid. In: Chashechkin, Yu.D., Baydulov, V.G., eds. *Fluxes and structures in fluids. Selected papers*, 155–159. Moscow: IPM RAS.
- Zatsepin, A.G., Gritsenko, V.A., Kremenetskiy, V.V. et al. (2005) Laboratory and numerical studies of the dense water spreading along the sloping bottom. *Oceanology* **45**(1):5–15.

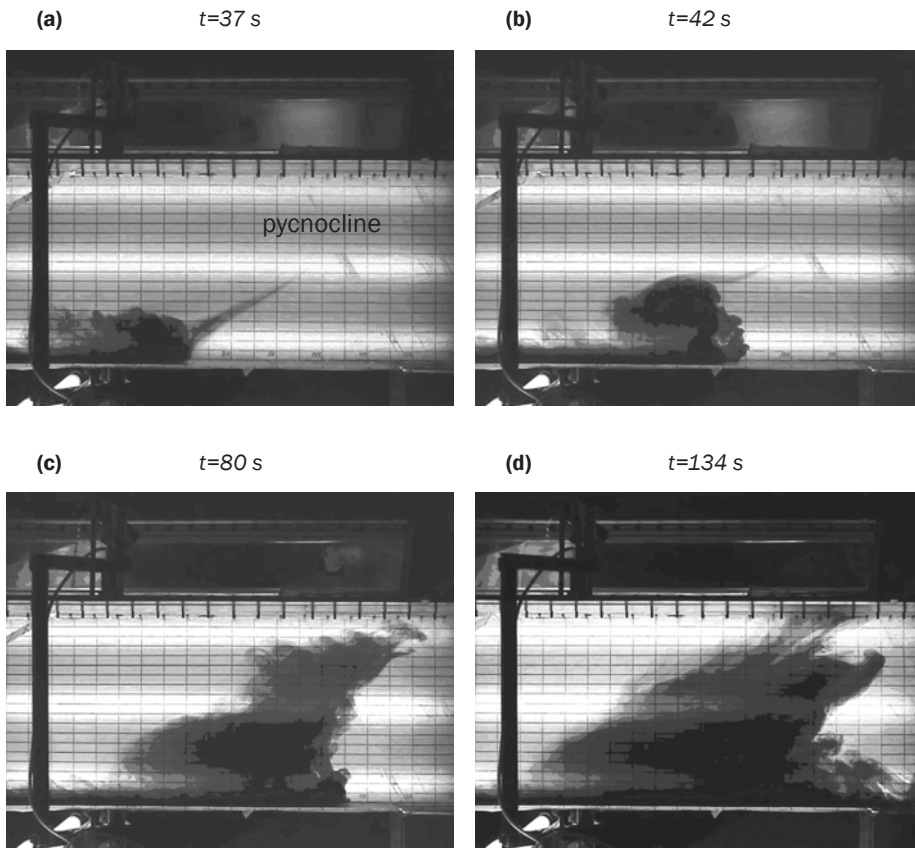


Fig. 4. Propagation of the gravity current in the two-layered fluid with time.
Parameters: $\alpha=30^\circ$, $S_1=2\text{‰}$, $S_2=4\text{‰}$, $S_0=6\text{‰}$.

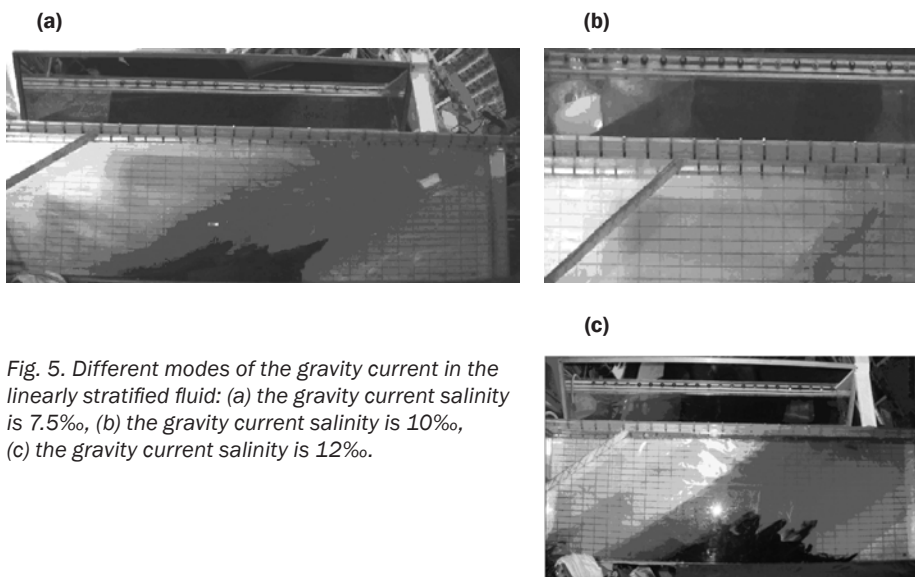


Fig. 5. Different modes of the gravity current in the linearly stratified fluid: (a) the gravity current salinity is 7.5‰ , (b) the gravity current salinity is 10‰ , (c) the gravity current salinity is 12‰ .

Structure and dynamics of coastal waters near the Kaliningrad region according to measurements of recent MSU expedition

Ksenia Silvestrova

Abstract

During the expedition of Moscow State University in August 2009 temperature, salinity, turbidity and current velocity were measured. The measurements were made by the CTD YSI 6600 and acoustic current meter FSI 2D ACM. 6 sections include CTD-data and echo sounder data within nearshore 12-miles zone. Analysis of the created database allows to describe the thermohaline structure and dynamics of coastal waters near the Sambian Peninsula.

Исследование выполнено на основе данных экспедиции МГУ. Проведены измерения температуры, солености, мутности, скоростей течений на различных горизонтах (в 12-мильной зоне). По результатам обработки получены: вертикальные распределения на разрезах температуры, солености, плотности и схема поверхностных течений.

Ksenia Silvestrova (✉)

M. V. Lomonosov Moscow State University, Moscow, Russia

e-mail: ksberry@mail.ru

Estimation of oil pollution at the Oil Stones production site in the Caspian Sea using synthetic aperture radar images

Anastasia Sineva

Abstract

In latest years problem of water pollution become the actual one. The most convenient way to monitor the sea surface condition is cosmic radiolocation. In current work the method of handling satellites datasets and oil pollution identification is showed on example of deposit Oil stones.

В настоящее время проблема загрязнения акваторий является особенно актуальной. Наиболее подходящим способом мониторинга состояния поверхности морей является космическая радиолокация. В данной работе на примере месторождения Нефтяные камни показана методика обработки спутниковых данных и определения параметров загрязнений.

In current years problem of water pollution by oil become the actual one both at ecological and economical standpoint. In the costal zones on sea surface oil films of anthropogenic pollution (crude oil, petroleum products, surface-active substances, etc.) can be frequently seen. It exerts pernicious influence on flora and fauna of the coastal zones and disturbs physical-chemical-biological processes in the ocean-atmosphere system, effects on social processes, and results in large financial losses in tourist business.

The most convenient way to monitor the sea surface conditions is imaging with spaceborne radars. Synthetic aperture radars (SAR) provide high spatial resolution allowing quite precise detection of location and square of oil spills. In addition imaging radars allow to receive an all-weather image, which is independent of time of the day, sun illumination, any hydrometeorological and cloudy conditions.

In this paper some results of radar monitoring of the Oil Stones production site in the Middle Caspian Sea with emphasize on detected oil spill characteristics are presented and briefly discussed. This oilfield is located 42 km east of the Absheron Peninsula and it is the easternmost industrial settlement

Anastasia Sineva (✉)
Moscow Institute of Physics and Technologies, Moscow, Russia
e-mail: sinastasia@gmail.com



in Azerbaijan. This site is located on the metal racks, built in 1949 in connection with the beginning of oil production from the seabed around the bank called Black Stones. Oil Stones are surrounded by stone reefs. There are banks, submarine and surface rocks among them. Here are the derricks united with flyovers, on which the village of oil workers placed. The most probable origin of the oil pollution in the area of “Oil Stones” belonging to the Oil-and-Gas Production Department of Azerbaijan is chronic leaking from outdated production systems and pipelines (The Sea of Problems, 2001). In connection with the constant leaks at this and other areas, the Baku Bay is one of the most polluted water areas in the world. The, so-called dead zone, is formed there. The thickness of bottom sediments contaminated with oil (in which concentration of toxic substances exceeds the maximum in 100 times) is 8–10 m (The Sea of Problems, 2001). Almost every day, the vast area is covered by oil films that prevents dissolution of oxygen in the water and detrimental effect on the marine flora and fauna. According to the (The Sea of Problems, 2001), the surface film can cover up to 200–800 km² in around the area of “Oil Stones”, and daily industrial losses of petroleum are estimated to be up to 500–700 tonnes.

The concentration of oil surface film is often enough to change the physical properties of the sea surface (see, e.g., (Ivanov, 2007)). Oil films actively suppress centimeter and decimeter surface waves (ripples). They also prevent wave generation at weak wind, and therefore smoothed areas (so-called slicks) appear on the sea surface. The normalized radar cross section (NRCS or σ_0 ; quantity normalized on unit area, which characterize radar backscatter) of slicks is significantly lower than σ_0 of the surrounding water. Therefore the slick having the low NRCS values is represented in SAR image as a dark spot.

An oil spill on the sea surface can be characterized by the contrast (K) or the ratio of the absolute values of NRCS of the spot and the NRCS of the clear surface:

$$K = \frac{\sigma_w}{\sigma_s} \approx \frac{\eta_s}{\eta_w} = f(k_0, \omega, \gamma, \rho, \nu \dots);$$

Here σ_s and σ_w are the NRCS (in dB) of spot and clear surface, η_s and η_w —coefficients of viscous damping in the oil spill and outside, k_0 and

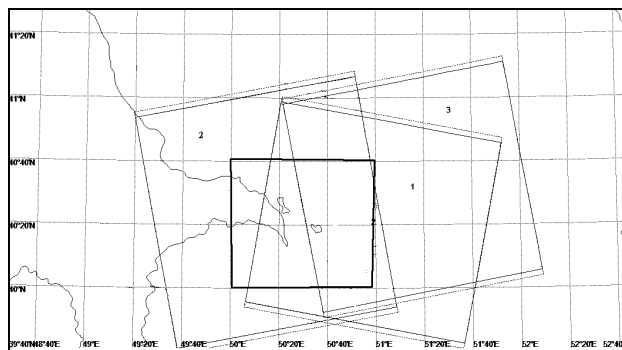


Fig. 1. Coverage by the Radarsat-2 SAR images of Oil Stones production site in June 2009.



ω —wave number and angular frequency of surface waves, γ —surface tension, ρ —density, ν —the coefficient of dynamic viscosity. Contrast can also be calculated from the SAR image as the ratio of the NRCSs of dark oil spill and grey background.

Radarsat-2 SAR images of the satellite (Wide mode) were obtained within the program “Scientific Opportunity and Research” (SOAR), project No. 648 “Oil slicks in Radarsat-2 SAR multi-polarization images”. The Wide mode products are images with nominal pixel spacing 12.5×12.5 m and swath width of 150 km (details are available at: http://www.radarsat2.info/product/RS-2_Product_Details.pdf). Images were delivered as standard processed SGX-products from the MDA Corporation (www.mda.com).

Though SAR as a tool of remote surface monitoring is indispensable in radiolocation it fails to solve the problem of identification and measurements of oil characteristics (for example, thickness and volume of spills). To determine the density of petroleum products the data from other satellites or indirect methods are necessary.

As a result of work important processing and analysis of three satellite SAR-images has been performed. The results of the work are presented in Table.

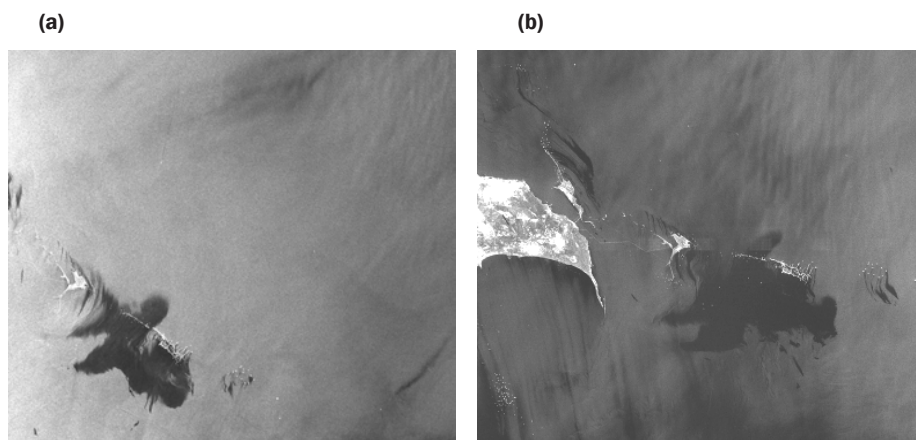


Fig. 2. Subscenes of the Radarsat-2 SAR images, acquired in Wide mode (W2) and showing the Oil Stones production site on: (a) July 11, 2009 14:29 UTC (wind 2–3 m/s); (b) July 12, 2009 02:19 43 UTC (wind speed 2–3 m/s). © CSA/MDA.

Fig. 3. Subscene of the Radarsat-2 SAR image (W2) and showing the Oil Stones production site on July 28, 2009 14:33 UTC (wind speed 8–10 m/s). © CSA/MDA.





Table

The results of processing of the SAR images

Date	Time, UTC	Polarization	Wind speed, m/s	Oil spill area, km ²	Min and max estimates of oil spill volumes, tonnes
11.07.2009	14:29:40	VV	2–3	384.0	115.2÷1920.0
12.07.2009	02:43:04	VV	2–3	568.5	170.5÷2842.5
28.07.2009	14:33:49	VV	8–10	38.7	11.6÷193.5

The first SAR images were taken at weak wind, the last one at wind 8–10 m/s. As seen on the images, low wind conditions promote the oil spreading over the wide sea area, which results in formation of large oil spills. Strong wind also prevents this process and doesn't allow the oil to spread over long distances. In weak wind conditions the spill areas increases up to 400–500 km², indicating sufficiently intense chronic oil pollution.

Oil spill contrasts varied from 9.5–10 (July 11, 2009) to 5.5 dB (July 28, 2009). Image analysis showed that the areas with the greatest contrast are mainly located in close proximity to pollution sources—oil rigs and platforms. That leads to the consideration that such areas can be covered by fresh oil with high activity index than the areas with lower values of contrast.

The minimum and maximum estimates of the amount of oil spills can be obtained indirectly on the basis of the techniques developed in (Bonn Agreement, 2004) under the assumption that the oil films at the Oil Stones are likely to have thickness of 0.30 to $5.0 \cdot 10^{-3}$ mm (300–5,000 kg per 1 km²). This way the min and max estimates were calculated, and they are also given in Table. Evidently these estimates better correspond to the real facts, than the estimates by Boev & Matveev (2005). According to independent sources, the volumes of oil spilled in the sea at the “Oil Stones” production site range from 100 to 700 tonnes per day.

References

- Boev, A. G. & Matveev, A. Ya. (2005) The amount estimation of oil pollutants in the oil-producing area “Oil Stones” in the Caspian Sea using multifrequency radar data. *Radiophysics and Radioastronomy* **10(2)**:178–188 (in Russian).
- Bonn Agreement (2004) Aerial Surveillance Handbook 25.
- Ivanov, A. Yu. (2007) Slicks and film signatures on spaceborne radar images. *Issledovanie Zemli iz Kosmosa* **3**:73–96 (in Russian).
- The Sea of Problems* (2001) An Experience of System Research in the Caspian Region. Moscow (in Russian).

High resolution bathymetry for Gulf of Finland

Rolf Värvi

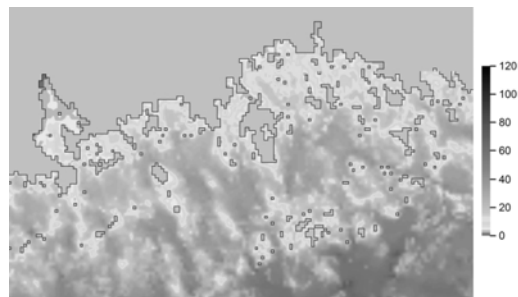
Abstract

Gridded bathymetric information is widely used in scientific research and practical projects, for example, in constructing circulation models, water level forecast, wave modelling, etc. The bathymetry has been specifically made for the international scientific project “Baltic Way”. This project targets to the practical use of a certain structure of the currents in the Gulf of Finland for protection of the coastal ecosystem.

Информация о батиметрии широко используется в научных и коммерческих проектах, например, для построения циркуляционных моделей, мониторинга уровня воды, моделировании волн и т. п. Данная батиметрия была сделана для международного проекта «Балтийский путь». Целью этого проекта является исследование структур течений в Финском заливе с целью практического использования для защиты прибрежных экосистем.

While the existing 1-mile bathymetric grid more or less adequately reflects certain Gulf of Finland areas where the typical size of bed forms is a few kilometres (such as south of Narva Bay, Keibu Bay aperture section), it significantly distorts the appearance of smaller bays, small islands, capes and smaller underwater landforms. The $\frac{1}{4}$ -mile grid realistically depicts most underwater

Fig. 1. Area near Kotka (fragment from Gulf of Finland bathymetry).



Rolf Värvi (✉)

Institute of Cybernetics at Tallinn University of Technology, Tallinn, Estonia

e-mail: Rolfv2rv@hotmail.com



landforms in the sections of the maps referenced. This depth grid is used in calculations of currents for the Gulf of Finland in the international project “Baltic Way” where it will replace the too coarse 1-mile gridded bathymetric information.

The grid was based on Estonian and Finland sea maps in a scale of 1:50,000. The sea maps have been divided into $\frac{1}{4}$ -mile squares, and the average depth has been calculated for each square. The resulting gridded bathymetry has been put to digital form. The quality of the grid has been checked on basis of computer-generated depth maps.

An analytic approach to description of the dissipative effects in 3+1 dimensions

Valerian Yurov

Abstract

Dissipation plays an important role in coastal water dynamics. Its effects are commonly described via the one-dimensional Burgers equation. We construct Lax pairs for a more reasonable 3+1 dimensional integrable generalization of the Burgers equation. A procedure for generation of exact solutions of this equation is developed, using a class of discrete symmetries of the Darboux transformation type. In the one-dimensional limit, these symmetries reduce to the Cole-Hopf substitution for the Burgers equation. It is discussed how the technique can be used to construct exact solutions for higher-dimensional evolution partial differential equations in a broader context.

Диссипация играет важную роль в динамике прибрежных вод. Её влияние обычно описывается одномерным уравнением Бургера. Мы составили пары Лакса для более подходящего 3+1-мерного обобщённого интегрируемого аналога уравнения Бургера. Предложена процедура получения точного решения этого уравнения с использованием класса дискретных симметрий типа преобразования Дарбу. В одномерном пределе, эти симметрии сводятся к подстановке Коула-Хопфа для уравнения Бургера. Обсуждается, как этот метод может быть использован в более широком смысле для получения точного решения уравнений в частных производных для более высокой размерности.

1. Introduction

An integrability of nonlinear PDEs is closely related (though not equivalent) to existence of $[L, A]$, or Lax pairs. It turns out that for any $d \geq 1$ and *any* nonlinear scalar evolution equation

Valerian Yurov (✉)
University of Missouri, Columbia, MO, USA
Immanuel Kant State University of Russia (IKSUR), Kaliningrad, Russia
e-mail: vayt37@mail.missouri.edu



$$u_t = F[u] \quad (1)$$

where $F[u]$ is a finite algebraic expression containing u and its space derivatives, there exists an $[L, A]$ pair.

We're going to restrict ourselves to a special case when $F[u]$ is such that the first order terms in the A -equation will be altogether eliminated. Moreover, we will deal with $d=3$, namely with the following 3+1 dimensional representative of the family (1):

$$u_t + a_1(u_x^2 - u_{xx}) + a_2(u_z^2 - u_{zz}) + b_1(u_x u_y - u_{xy}) + b_2(u_x u_z - u_{xz}) - \rho u_x - \mu u_y - \lambda u_z = 0, \quad (2)$$

where $u = u(x, y, z, t)$ and the rest of the parameters are constants.

In the 1+1 dimensional limit, equation (2) reduces to the dissipative Burgers equation. Indeed, imposing a one-dimensional reduction, letting $\rho = 0$ and defining the quantity

$$\xi(x, t) = u_x(x, t), \quad (3)$$

we obtain

$$\xi_t - a_1 \xi_{xx} + 2a_1 \xi \xi_x = 0. \quad (4)$$

Hence, equation (2) can be viewed as a special non-isotropic three-dimensional extension of the Burgers equation.

Our main result is the following theorem.

2. The theorem

Let $u(x, y, z, t)$ be a particular solution of equation (2) and $\psi = \psi(x, y, z, t)$ satisfy the following linear equation:

$$\begin{aligned} \psi_t = & a_1 \psi_{xx} + a_2 \psi_{zz} + b_1 \psi_{xy} + b_2 \psi_{xz} + (\rho - 2a_1 u_x - b_2 u_z - b_1 u_y) \psi_x + \\ & + (\mu - b_1 u_x) \psi_y + (\lambda - 2a_2 u_z - b_2 u_x) \psi_z \end{aligned} \quad (5)$$

Then any $\tilde{u}_{klm} = \tilde{u}_{klm}(x, y, z, t)$ defined as

$$\begin{aligned} \tilde{u}_{klm} = & u - \log((\partial_x - u_x)^k (\partial_y - u_y)^l (\partial_z - u_z)^m \psi) = \\ = & u - \log(L_x^k [u] L_y^l [u] L_z^m [u] \psi), \end{aligned} \quad (6)$$

for some $(k, l, m) \in Z_+^3$, is also a solution of equation (2).

Above, Z_+ denotes non-negative integers; Z_{++} further stands for positive integers.

Successive iteration of (6) results in the following corollary.

Corollary. Let, $\{\psi_i\}$, $i=1, \dots, N$ be a set of particular solutions of the A -equation (5). Given a potential \mathbf{u} satisfying equation (2), new solutions of this equation can be generated as follows:



$$\tilde{u} = u - \log \left(\prod_{i=1}^N L_x^{k_i}[u] L_y^{l_i}[u] L_z^{m_i}[u] \psi_i \right), \tag{7}$$

where $(k_i, l_i, m_i) \in Z_+^3$.

The proof of the Theorem is based on a corresponding Lax pair, some parameters of which have been assigned zero values.

Note, that if we set $u = u(x, t)$ in (6) and use it with $u \equiv 0, k = 1$, then after differentiation with respect to x , the expression (6) results in the Cole-Hopf substitution.

3. Construction of the exact solutions

Now let us use the Theorem to construct some exact solutions of equation (2) on the vacuum background $u \equiv 0$, under assumption that $\mu = \lambda = Q = 0$ (this assumption makes (2) more similar to the Burgers equation and thus more interesting from the physical point of view).

Example 1. One immediate solution to equation (5) is

$$\begin{aligned} \psi(x, y, z, t) = & c_1 e^{\alpha(a_1 + \beta b_1)t} \cosh(ax + \beta y) + \\ & + c_2 e^{(a_1 a_2 + a_2 b_2 + a b b_2)t} \cosh(ax + by) + c_3 e^{a_2 c t} \cosh(cz), \end{aligned} \tag{8}$$

where $\alpha, \beta, a, a_1, a_2, b, b_1, b_2, c, c_1, c_2, c_3$ are some real constants. Let us choose them such that

$$\beta = -\frac{\alpha a_1}{b_1}, \quad b = -\frac{a}{2a_2} \left(b_2 \pm \sqrt{b_2^2 - 4a_1 a_2} \right). \tag{9}$$

Substituting (8) into (6), we compute the quantity \tilde{u}_{klm} . Further differentiating it with respect to x and choosing $k = l = m = 0$, we obtain a solution w to equation (2) as follows:

$$w(x, y, z, t) = -\frac{ac_1 \sinh(ax + \beta y) + ac_2 \sinh(ax + bz)}{c_1 \cosh(ax + \beta y) + c_2 \cosh(ax + bz) + c_3 e^{a_2 c t} \cosh(cz)}. \tag{10}$$

Example 2. Another solution of the Lax pair equations would be

$$\psi(x, y, z, t) = a^2 x^2 + b^2 y^2 + c^2 z^2 + 2(a_1 a^2 + a_2 c^2)t + s^2, \tag{11}$$

where a, a_1, a_2, b, c, s are some real constants. In the same vein as in the previous example, we obtain

$$\psi(x, y, z, t) = \frac{2a^2 x}{a^2 x^2 + b^2 y^2 + c^2 z^2 + 2(a_1 a^2 + a_2 c^2)t + s^2}. \tag{12}$$

an exact solution of equation (2). Does this solution have a physical meaning? Apparently it describes a rationally localized impulse, vanishing as $t \rightarrow +\infty$. To ensure that it is non-singular for $t \geq 0$, one should impose the inequality $a_2 \geq -a^2 a_1 / c^2$ on the coefficients. In the case $a_2 = -a^2 a_1 / c^2$, the solution becomes stationary.



References

- Ablowitz, M.J. & Segur, H. (1981) Harvey Solitons and the inverse scattering transform. *SIAM Studies in Applied Mathematics* **4**. Philadelphia, PA: Society for Industrial and Applied Mathematics (SIAM).
- Burgers, J.M. (1974) *The nonlinear diffusion equation*. Massachusetts: D. Reidel.
- Cole, J.D. (1951) On a quasi-linear parabolic equation occurring in aerodynamics. *Quart. Appl. Math.* **9**:225–236.
- Crum, M.M. (1955) Associated Sturm-Liouville systems. *Quart. J. Math. Oxford Ser. (2)* **6**: 121–127.
- Frisch, J. Bec. (2001) “Burgulence”. *Turbulence: nouveaux aspects/New trends in turbulence* (Les Houches, 2000), 341–383. EDP Sci., Les Ulis.
- Gesztesy, F. & Holden, H. (2000) The Cole-Hopf and Miura transformations revisited. *Mathematical physics and stochastic analysis (Lisbon, 1998)*, 198–214. NJ: World Sci. Publishing, River Edge.
- Haselwandter, C. & Vvedensky, D.D. (2002) Fluctuations in the lattice gas for Burgers’ equation. *J. Phys. A* **35**, 41:L579–L584.
- Hopf, E. (1950) The partial differential equation $u_t + uu_x = u_{xx}$. *Comm. Pure Appl. Math.* **3**:201–230.
- Leble, S.B., Salle, M.A., Yurov, A.V. (1992) Darboux transforms for Davey-Stewartson equations and solitons in multidimensions. *Inverse problems* **4**:207–218.
- Matveev, V.B., Salle, M.A., Darboux (1991) *Transformation and Solitons*. Berlin–Heidelberg: Springer Verlag.
- Newell, A.C. (1985) Solitons in mathematics and physics. *CBMS-NSF Regional Conference Series in Applied Mathematics*, **48**. Philadelphia, PA: Society for Industrial and Applied Mathematics (SIAM).
- Peebles, P.J.E. (1993) *Principles of Physical Cosmology*. Princeton University Press.
- Sakovich, S.Yu. (1988) On the Thomas equation. *J. Phys. A* **21**:L1123–L1126.
- Yurov, A.V. (1999) BLP dissipative structures in the plane. *Phys. Letters A* **262**, 6:445–452.

Physics of spreading of a gravity current on a slanting bottom of the ocean with involving in current solid particles of dredge

Ivan Zavyalov

Abstract

The goal of this work is investigation of the features of gravity current spreading near ocean's bottom with mass exchange between the current and solid particles of dredge. It was shown that the velocity of gravity current is constant. A new hypothesis about the equality between gravitation force and the force created by involving in motion of solid particles of dredge was proposed. This hypothesis was verified by experiment.

В данной работе изучались особенности распространения взвесенесущих потоков вдоль дна, при условии вовлечения в движение донных осадков. В ходе данной работы было установлено, что скорость распространения подобного потока остается постоянной. Была предложена гипотеза о том, что сила тяжести, действующая на поток, компенсируется реактивной силой, связанной с вовлечением в движение донных осадков. Данная гипотеза была подтверждена экспериментально.

1. Theoretical part

Descent and development of gravitational flow can be represented in the following way: the area of moving mass near bottom escapes from the flow. Let's call it "precursor". Then precursor began to grow at the expense of involving in motion detritus. The growth of the main mass ceases. The main mass loses contact with the precursor and drops down on bottom Fig. 1.

Consider the second Newton's law for the whole flow

$$\frac{d}{dt} \iiint_V \rho \vec{u} dV = +g \sin \alpha \iiint_V \delta \rho dV - \iint_S \mu \left(\frac{\partial u}{\partial n} \right) dS - \iint_S u_n u_{p_{en}} dS,$$

(\vec{u} , ρ and V —velocity, density and volume of dredge carrying flow, g is free fall acceleration, $\sin \alpha$ —sine of bottom angulation, μ —viscosity number, u_n —

Ivan Zavyalov (✉)

Moscow Institute for Physics and Technology, Dolgoprudny, Russia

e-mail: Ivenzz@mail.ru

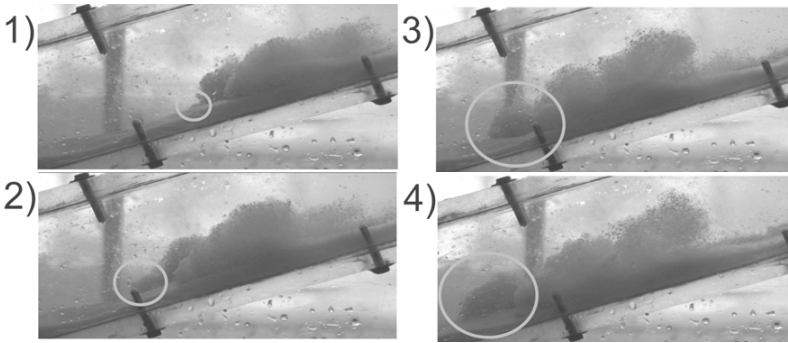


Fig. 1. The main mass loses contact with the precursor and drops down on bottom.

velocity of particles of bottom and the external water directed perpendicular to the flow or the velocity of involving in motion detritus and the medium water. ρ_{en} —the average density of detritus and medium water, involving in motion with the flow). In right-hand side of equation the first term is gravity, second term is the force of viscous friction between the bottom and external water and the third term is connected with involving in motion the detritus.

As well as the velocity of motion is constant and the size of dredge carrying flow does not change in scales of deviation from the middle value the part

$$\frac{d}{dt} \iiint_V \rho \vec{u} dV = 0.$$

As we could see from the results of other scientists the viscosity force, which connected with the viscous friction with bottom, is much more bigger than the force of friction with medium water

$$0 = +g \sin \alpha \iiint_V \delta \rho dV - \iint_{S_b} \mu \left(\frac{\partial u}{\partial n} \right)_{z=0} dS - \iint_S u_n u \rho_{en} dS,$$

the S_b is the square of the bottom.

The part $\iint_S u_n u \rho_{en} dS$ can be divided into two parts, the first is connected with involving in motion the detritus, the second is connected with external water.

$$\iint_S u_n u \rho_{en} dS = \iint_{S_b} u_n u \rho_b dS + \iint_{S \setminus S_b} u_n u \rho_w dS,$$

ρ_b is the average density of detritus (including the water in detritus), ρ_w —the density of the external water. According to the different observations over the gravity flow involving in motion the external liquid occurs from the back part of the head of the flow by force of torsion vortex. But in present experiments exactly in this area occurs the escape of redundant mass of the flow. It means that we can neglect the part connected with the involving the external water.

Obtain

$$0 = +g \sin \alpha \iiint_V \delta \rho dV - \iint_{S_b} \mu \left(\frac{\partial u}{\partial n} \right)_{z=0} dS - \iint_{S_b} u_n u \rho_b dS.$$



The entire impetus, which is lost on friction with detritus turns into impetus of detritus. In case the interaction with the firm bottom is absent and there is only interaction with the detritus we can conclude then there is no friction and only the transmission of impetus from the flow to the detritus is presented. Then we can neglect the $\iint_{S_b} \mu \left(\frac{\partial u}{\partial n} \right)_{z=0} dS$.

Then

$$g \sin \alpha \iiint_V \delta \rho dV = \iint_S u_n u \rho_b dS.$$

Then we expected that the density of the flow is constant at the whole volume. The typical geometric sizes are substituted for volume.

$$g \sin \alpha \delta \rho (Lhl) = u_n u \rho_b Ll,$$

$gh \delta \rho \sin \alpha = u_n u \rho_b$ —this formula stands for the equality of gravity and the jet force connected with involving in motion the detritus.

$$hg \frac{\delta \rho}{\rho} u \sin \alpha = u_n u^2 \frac{\rho_b}{\rho},$$

$$\frac{u^2}{gh \frac{\delta \rho}{\rho}} = \frac{u \sin \alpha}{u_n} \frac{\rho}{\rho_b}.$$

Then receive:

$$Fr^2 = \frac{u}{u_n} \frac{\rho}{\rho_b} \sin \alpha.$$

In our case we can consider that $\rho \approx \rho_b$, then

$$Fr^2 = \frac{u}{u_n} \sin \alpha.$$

2. Experimental part

2.1. Installation

Experimental installation consisted of the transparent channel with square cross-section with side 81 mm. This channel can be established with different angulations from 10 till 30 degrees. The motion of the flow was registered with camera Canon EOS 1D. It made 4 frames per second. Powdered polystyrene was distributed in the uniform layer on the bottom. For organization the convergence of gravity flow in the top part of channel, which was leakproofly separated from the medium water, the huge amount of powdered polystyrene was situated. When cylinder was sharply pushed up the redundant mass began to move along the slope involving in motion polystyrene, which recumbent on the bottom.

2.2. Experimental results

The velocity of development of the front of this flow remains constant during the whole motion. And the measuring inaccuracy of this flow does not exceed 2 percent. The plots of dependence between the front and time are presented at Fig. 2.

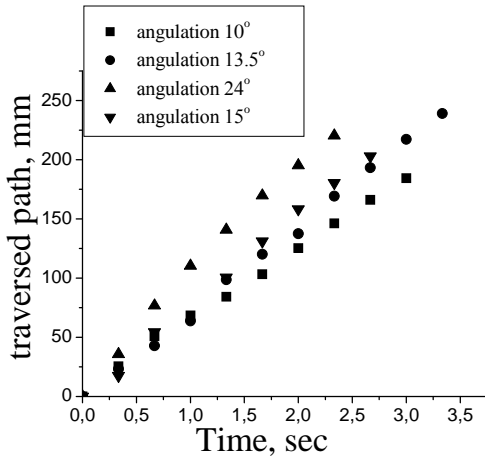


Fig. 2. The plots of dependence between the front and time.

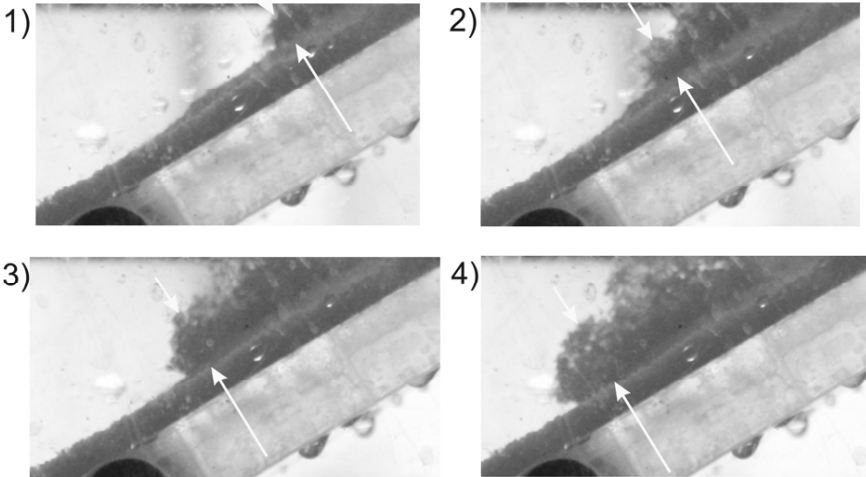


Fig. 3. The examples of successive frames of tongue.

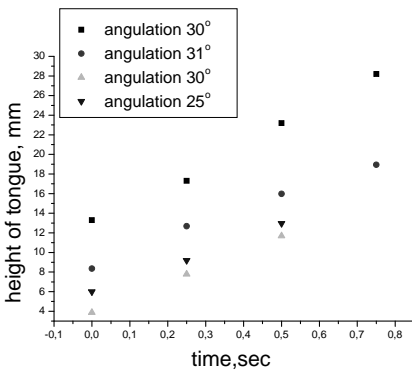


Fig. 4. The plot about the dependence of tongue velocity and time.

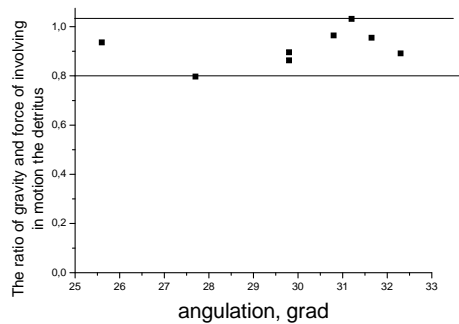
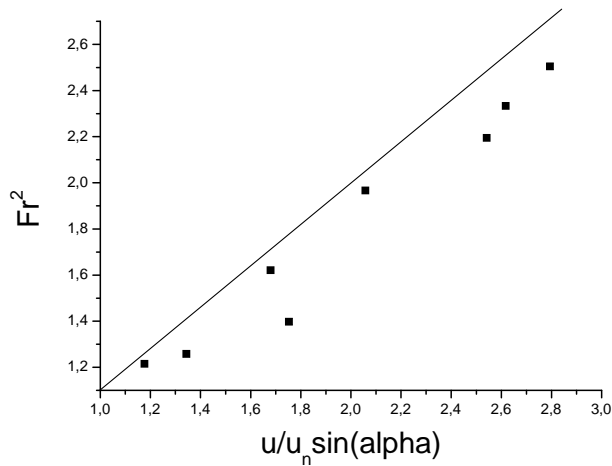


Fig. 5. The ratio of gravity and force of involving in motion the detritus.



Fig. 6. The plot of dependence of the Froude number on $\frac{u}{u_n} \sin \alpha$.



For the obtained frames we can estimate the growth of tongue which runs forward. This velocity could be considered as the velocity of involving in motion the detritus, designated as u_n in theoretical part. The examples of successive frames of tongue see at Fig. 3. The plot about the dependence of tongue velocity and time see at Fig. 4. From the results presented in plots we can see, that the velocity of involving the detritus can be considered as constant. The ratio of gravity and force of involving in motion the detritus are presented on plot at Fig. 5. The plot of dependence of the Froude number on $\frac{u}{u_n} \sin \alpha$ see at Fig. 6.

3. Resume

(1) Qualitatively, the descent of this flow can be presented in following way: the part from the mass in near bottom layer is selected, and then this part runs forward from the common mass, we call it the precursor. Then by means of involving the detritus precursor begin to grow and the growth rate of the main mass decreases. Then the former main mass leaves the increased precursor and falls on the bottom. And from the newly formed mass runs forward the new precursor.

(2) The velocity of motion of dredge carrying flow with taking into account of near bottom dredge with an error less than 2 percent is constant: it neither increase nor decrease without any dependence on angle.

(3) During this work under the conditions of the experiment the hypothesis about the equality of gravity and the jet force, which appears because of involving in motion the detritus, was confirmed.

Научное издание

Proceedings of the 2nd International Conference (school) on
DYNAMICS OF COASTAL ZONE OF NON-TIDAL SEAS

Baltiysk (Kaliningrad Oblast), 26–30 June 2010

Подписано в печать 17.06.2010 г.
Формат 70x108 ¹/16. Усл. печ. л. 35,8.
Тираж 250 экз.

Издательство «Терра Балтика»
236029, г. Калининград, ул. Гаражная, 2-Б, 208